

**21st Conference on
Computer and IT Applications in the Maritime Industries**

COMPIT'22

Pontignano, 21-23 June 2022

**21st International Conference on
Computer and IT Applications in the Maritime Industries**

COMPIT'22

Pontignano, 21-23 June 2022

Edited by Volker Bertram

21st International Conference on Computer and IT Applications in the Maritime Industries, Pontignano, 21-23 June 2022, Hamburg, Hamburg University of Technology, 2022

© Technische Universität Hamburg-Harburg
Schriftenreihe Schiffbau
Schwarzenbergstraße 95c
D-21073 Hamburg
<http://www.tuhh.de/vss>



Sponsored by



tutech.de



www.krs.co.kr



www.prostep.com

SIEMENS

www.siemens.com/marine



b



FRIENDSHIP SYSTEMS

www.friendship-systems.com



www.blommaritime.com



www.cadmatic.com



www.numeca.de



www.napa.fi

HANSA

INTERNATIONAL MARITIME JOURNAL

<https://hansa-online.de/>



<https://www.rina.org.uk/>

Index

Maurits van den Boogaard, Giacomo Alessi, Benoit Mallol, Dirk Wunsch, Nathan Clero, Dario Amadori, Charles Hirsch, Luca Zampieri, Thomas Hildebrandt <i>Accelerating Marine Propeller Development in Early Design Stages Using Machine Learning</i>	7
Tracy Plowman, Ulrich Bernhardt <i>Digital Transformation in Maritime Trainings in COVID-19 Times</i>	16
Simone Tani, Francesco Ruscio, Matteo Bresciani, Riccardo Costanzi, Andrea Caiti <i>Visual Inspection of Underwater Structures using an AUV: A Preliminary Simulative Evaluation</i>	24
Wilfried Abels, Leif-Erik Gorris <i>Using a Bridge Simulator for Hybrid Coupling of Manoeuvring and Engine Simulations</i>	34
Yasuo Ichinose, Tomoyuki Taniguchi <i>A Hull Form Design System Suitable for Machine Learning That Integrates Deformation, Data Structure, and Analysis</i>	43
Lars Lindegaard Mikkelsen, Simon Stochholm <i>Transparent Charge Plans for Battery Driven Ferries Using an Intelligent Multi-Agent Software System – A Case Study</i>	53
Simon Stochholm, Lars Lindegaard Mikkelsen <i>Clustering Variations within Ferry Operational Patterns by applying Unsupervised Machine Learning - A Case Study</i>	63
Kaan Terün, Austin A. Kana, Rommert Dekker <i>Assessing Alternative Fuel Types for Ultra Large Container Vessels in Face of Uncertainty</i>	76
Tycho Brug, Jasper van der Waa, Valentina Maccatrozzo, Hans van den Broek <i>Dynamic Task Allocation Algorithms within Intelligent Operator Support Concepts for Shore Control Centres</i>	95
Peter Burggräf, Tobias Adlon, Moritz Beyer, Niklas Schäfer, Judith Fulterer <i>Enabling Individual Part Production Planning in Shipbuilding: Machine-Learning-Assisted Prediction of Production Times</i>	110
Marco Bibuli, Angelo Odetti, Massimo Caccia, Claudia Presicci, Roberta Ferretti, Simona Aracri <i>Networked Robots and IoT: Real Time Data Acquisition at its Finest</i>	120
Rodrigo Perez Fernandez <i>Smart Technologies for Improving Design Tools</i>	131
Kohei Matsuo, Shuhei Fujimoto, Masahito Takezawa <i>Application of Augmented Reality Technology to Manufacturing in Shipbuilding</i>	137
Wisam Jabary, Florian Sprenger, Lutz Kleinsorge, Hauke Baumfalk, Simon Mewes, Jens Neugebauer, Changqing Jiang, Ould el Moctar <i>Development of a Unified Data Model to Improve Ship Operational Performance Analyses</i>	153

Stefan Harries, Fabian Thies, Simon Hauschulz, Jochen Marzi, Scott Gatchell <i>Comparing Hydrodynamics of Original and Remodeled Hull Forms and Appendages for Digital Twins</i>	169
Thomas DeNucci, Daniel Brahan <i>A Digital Twin for the Formulation of Ice Accretion on Vessels</i>	187
Jon S. Dæhlen, Endre Sandvik, Ulrik Jørgensen <i>Model Predictive Approach for Realistic Operational Decisions in Sea Passage Simulation</i>	201
Erik Stensrud, Kristian Klausen <i>Another Step towards Remote Inspections of Maritime Vessels using Tailored Inspection Drones Instrumented with Computer Vision</i>	212
Andrea Serani, Matteo Diez <i>Super-Parametrizing CAD Models for Efficient Shape Optimization via Parametric Model Embedding</i>	221
Muhammad Mukti, Rachel Pawling, David Andrews <i>Development of an Early-Stage Design Tool for Rapid of Distributed Ship Service Systems Modelling in Paramarine – A Submarine Case Study</i>	231
Ørnulf Jan Rødseth, Marianne Hagaseth <i>Developments toward a Common Maritime ICT architecture</i>	249
Myeong-Jo Son, Tapio Seppälä, Jani Merikanto, Ove Aae, Ole Christian Astrup <i>Utilization of OCX as Part of 3D Model Based Approval in Ship Design Process</i>	258
Philip Bronkhorst, Roy de Winter, Thijs Velner, Austin A. Kana <i>Enhancing Offshore Service Vessel Concept Design by Involving Seakeeping - Developing a Framework to Efficiently Design High-Performance Offshore Service Vessel Concepts</i>	273
Stephan Procee <i>Human Machine Interface for Ships with Wind-Assisted Propulsion</i>	288
Alexander Pinskiy <i>Autonomous Shipping in Real Conditions: The Practical Experience</i>	299
Pauline R. Bellingmo, Brian Murray, Ulrik Jørgensen, Armin Pobitzer, Svein P. Berge, Ole G. Rørhus <i>Evaluation of Ship Energy Models and Route Optimization</i>	311
Ahmed Elzalabany, Vincent Settler, Robert Rost, Hermann Lödding <i>Digitalization of Maritime Commissioning: A System for Automatic Content Creation and Augmented Reality-based Commissioning Execution</i>	323
Carsten Zerbst, Ulrike Lutz, Alexander Danetzky <i>Concept to Reality: Implementing a Digital Twin for Ship Production</i>	336
Arijana Milat, Darko Frank <i>Quick Patch Design and Repair Planning Using Software Tool for Carbon-Reinforced Epoxy Type of Repairs for Ship Structures</i>	343

Marianne Hagaseth, Ørnulf Jan Rødseth, Per Håkon Meland, Egil Wille, Brian Murray, Pia Meling <i>Methodology for Approval of Autonomous Ship System CONOPS</i>	352
Andrea Orlandi, Andrea Cappugi, Riccardo Mari, Francesco Pasi, Alberto Ortolani <i>Meteorological Navigation by an ECDIS-Like System: Discussing the Algorithms and Demonstrating the Functionalities for Conventional Propulsion and for Sail-assisted Ships</i>	367
Marius Blom, Gauthier Stonestreet <i>Exploiting Digital Point Clouds in Design E3D</i>	382
Luisa Mancarella, Francesca Calabrese, Marco Cataldo, Gabriele Serafino, Luigi Paiano, Luca Carlino, Angelo Cirigliano, Nicola Leonardi, Emanuele Sansebastiano, Luca Sebastiani <i>A Novel Integrated Multi-System Approach for Situational Awareness in Maritime Environ- ment</i>	387
Madalina Florean, Verónica Alonso de los Ríos, Juan Prieto, Ludmila Seppälä <i>Standalone Intelligent General Arrangement Tool for Holistic Basic Design</i>	403
Henrique Gaspar <i>Open and Collaborative Ship Design</i>	416
Jan Bitomsky, Alexander Danetzky, Carsten Zerbst <i>OCX Revisited: The New Data Exchange Standard?</i>	429
Carsten Genschorek, Tim Holzki <i>Using Deep Reinforcement Learning for Energy Efficient Automatized Berthing Maneuvers in Inland Navigation</i>	437
Antoine Rouhan, Richard Audoire, Baldassare Messina <i>A Modular Ship Design, Construction and Pre-Approval Approach</i>	446
List of authors	
Call for Paper for next year	

Accelerating Marine Propeller Development in Early Design Stages Using Machine Learning

Maurits van den Boogaard, NUMECA-Cadence, Brussels/Belgium, boogaard@cadence.com

Giacomo Alessi, NUMECA-Cadence, Brussels/Belgium

Benoit Mallol, NUMECA-Cadence, Brussels/Belgium

Dirk Wunsch, NUMECA-Cadence, Brussels/Belgium

Nathan Clero, NUMECA-Cadence, Brussels/Belgium

Dario Amadori, NUMECA-Cadence, Brussels/Belgium

Charles Hirsch, NUMECA-Cadence, Brussels/Belgium

Luca Zampieri, Neural Concept, Lausanne/Switzerland

Thomas Hildebrandt, NUMECA Ingenieurbüro, Altdorf/Germany, thomas.hildebrandt@numeca.de

Abstract

This paper presents a machine learning approach to accelerate the design of marine propellers. For open-water propeller characteristics, neural nets are trained to predict both integral quantities of open-water performance curves and local field values of velocities and pressures on two-dimensional planes for Wageningen B-Series propellers. The average difference between the predicted and CFD-obtained values remained below 1.5% for integrated quantities (thrust, torque, efficiency). The quasi-instantaneous response of a trained neural net may accelerate propeller design significantly.

1. Introduction

With the increase in computational power, machine learning offers new opportunities for accelerating the marine engineer's workflow during the initial design phases. Taking the example of open-water calculations, which tend to have high relative computational costs, the application of a machine learning algorithm like a Geodesic Convolutional Neural Network (GCNN) to such computations is shown in this paper to be promising and could allow increasing productivity in the initial design process by orders of magnitude. The goal of this study is therefore to describe the approach and discuss the results of applying a GCNN to open-water computations using geometries following the design of the Wageningen B-series propeller family and explore the productivity gains that can be achieved by applying artificial intelligence to marine CFD results.

2. Methodology

2.1. Geometry generation and verification using CFD

The Wageningen B-series propeller series was chosen as the 'parent' series for the design of experiments (DoE). Propellers in this series are described by four parameters: the diameter D , the expanded area ratio EAR , the number of blades Z , and the propeller pitch P . If the diameter is kept constant ($D = 1$ m), the geometry is fully described by EAR , Z and P . The propellers were modelled using Rhino 3D in combination with Grasshopper along with a proprietary Python code containing the sectional geometry description based on the definitions described in *Kuiper (1992)*. The two-dimensional sections were developed into three-dimensional blades using NURBS.

Van Oossanen and Oosterveld (1975) developed the description of open-water performance curves valid for any Wageningen B-series propeller based on regression analysis of earlier model tests performed at the Maritime Research Institute in the Netherlands (MARIN). The original description of the thrust and torque coefficient curves is valid at a Reynolds number of 2,000,000. These regression curves were subsequently compared to CFD (Computational Fluid Dynamics) results for a selected number of propellers and operating conditions to verify that the created propeller geometries yielded the expected results corresponding to the Wageningen B-series.

The results indicated that thrust and torque predictions coming from CFD were within 5% of the regression-based prediction for a wide range of advance ratios J .

Very high advance ratios, where propellers generate close to zero thrust, showed lower accuracy which was already expected based on previous experience. At low values of J , the propeller is acting in bollard pull conditions and this was identified as a less interesting condition to include as most ships only spend very little amount of time operating in these conditions. Therefore, the allowed range of J values was determined by first calculating the theoretical range of positive thrust (first quadrant propeller operation) for each propeller in the design set. Subsequently, the bottom 10% was discarded to avoid bollard pull conditions and the maximum allowed J value was chosen halfway between the point of maximum efficiency and the J value corresponding to thrust breakdown, to avoid inaccuracies of the CFD solver close to the point where $K_t = 0$. This is visualized in Fig.1.

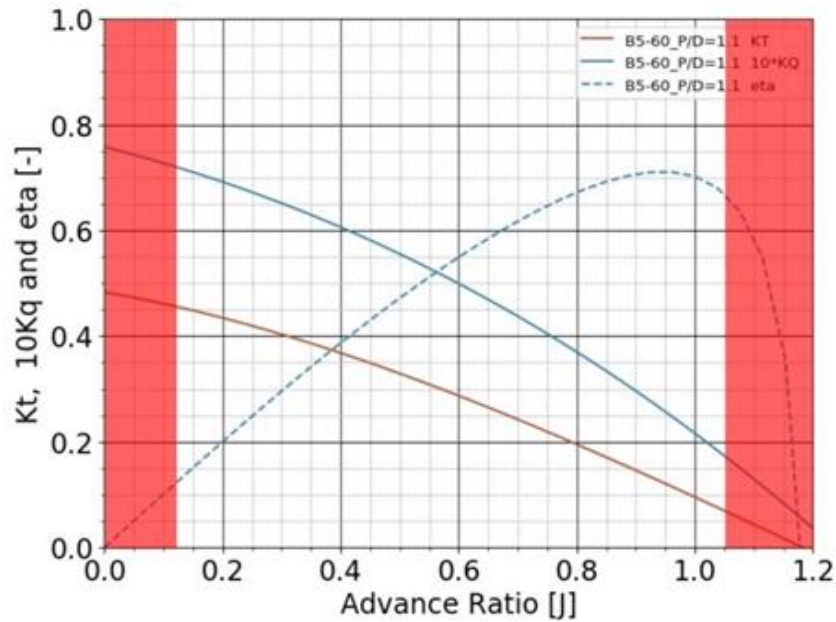


Fig.1: Indication of excluded values of J (in red) in the open-water performance curve for the Wageningen B5-60 propeller with $P/D=1.1$.

2.2. Design of Experiments (DoE)

The nature of machine learning requires the generation of large amounts of data obtained, in this case, from many similar propellers and operating conditions. The propeller geometries (parametrized as the Wageningen B-Series) and operating conditions must be chosen randomly by what is called the design of experiments (DoE). The DoE was managed using FINE™/Design3D. The CAD files of the propellers were generated using Rhino 3D in combination with Grasshopper, followed by an export as STL using a proprietary tool. As the process needed to be fully automated, the different patches (e.g. leading edge) were identified automatically with this tool if the number of blades was maintained equal. This created a constraint for the creation of the DoE: the design space had to be created for each blade number separately.

The design space for each blade number could therefore be defined by the geometrical parameters EAR and P (as D and Z are fixed) and by the operational parameter: the advance ratio J . The parametric ranges of the Wageningen B-Series were used for EAR and P (through the pitch-diameter ratio). The number of blades was varied between 2 and 7. Given the J value limits described in Fig.1, the J value in the DoE was a normalized range with values between 0 and 1, corresponding to the minimum and maximum of the propeller-specific allowed range, respectively. The normalized values were converted to the actual J values when setting up the computations. The Latinized CVT and Inherited LHS (for additional samples) methods were used to sample randomly across the design

space for each blade number. A total of 271 STL files was created, each corresponding to a single propeller operating at a specific advance ratio J .

2.3. Mesh generation

The meshes were generated with OMNISTM/Hexpress using the surface-to-volume (S2V) technique. This methodology ensures superior mesh quality on curved surfaces like propeller blades, but also a more constant viscous layer height enveloping the blades, compared to the more common volume-to-surface approach. Leading and trailing edges as well as the area around the blade tip were more finely discretized compared to the blade surface. This can be seen in the mesh close-ups in Figs.2 and 3.

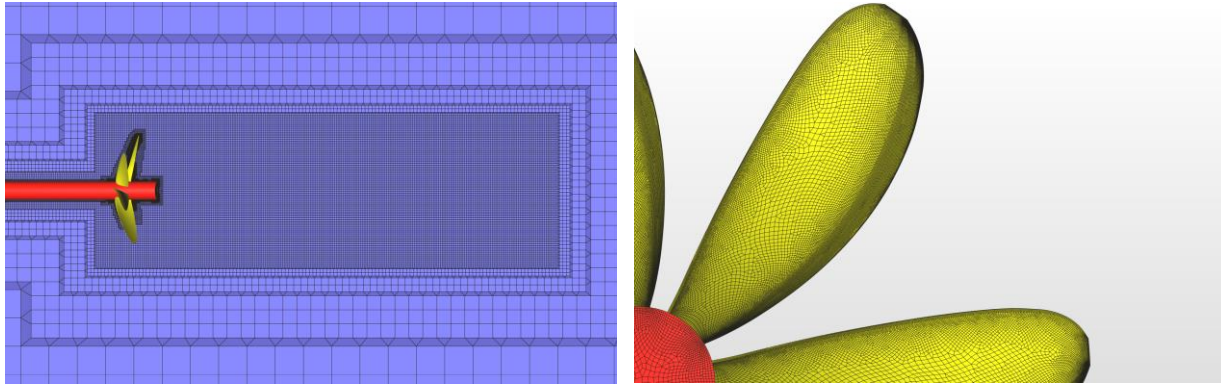


Fig.2: Mesh far field (left) and blade surfaces (right) for Wageningen B7-59 and $P/D=1.25$

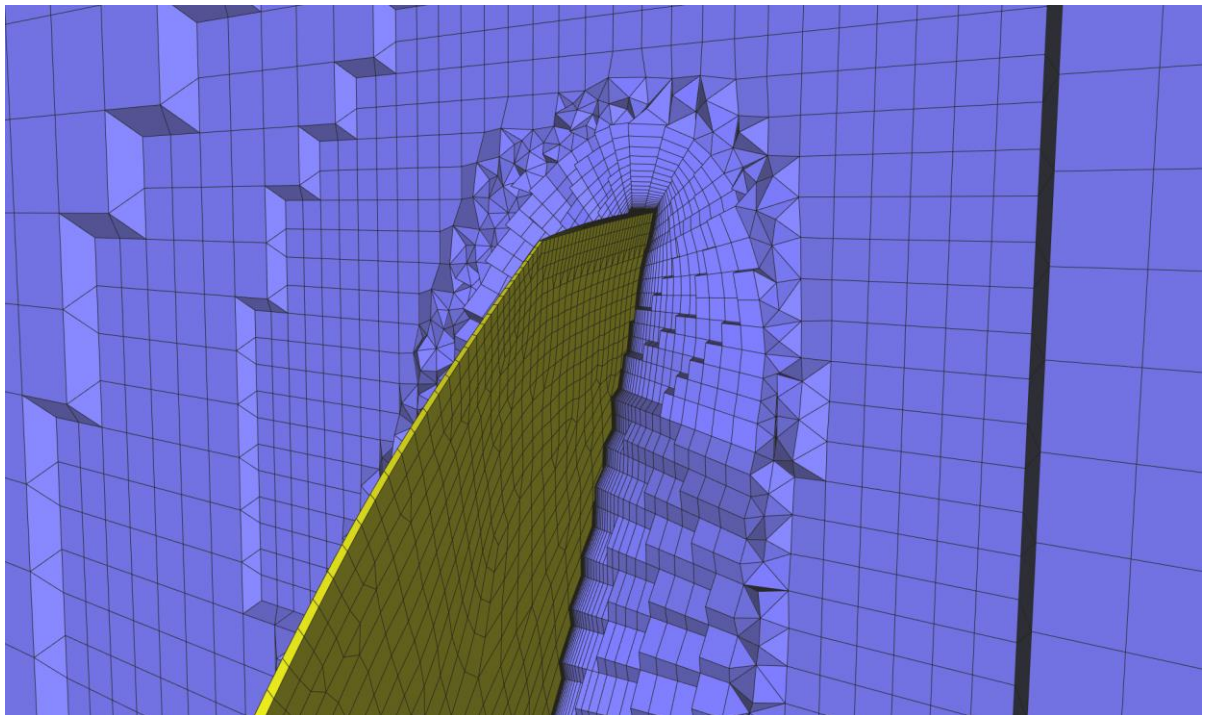


Fig.3: Mesh close-up with viscous layers for Wageningen B7-59 and $P/D=1.25$

Viscous layers were inserted with a first layer thickness defined by $y^+=1$ (and Reynolds number of 2,000,000), Fig.3. Preliminary results were compared between using a y^+ value of 1 and 0.1, but no significant differences were found in the prediction of thrust and torque between both approaches. Given the lower cell count using $y^+=1$, this higher value was used for all meshes. The wake behind the propeller was additionally refined until 4 diameters behind the propeller location to enable an accurate calculation of the flow behind the propeller. The total number of cells for all different propellers ranged from 25 to 35 million cells. The meshing procedure was completely automated with the use of Python.

2.4. Computational details

As the model tests at the basis of the regression curves were performed at Reynolds number of 2,000,000, all computations were set up such that the Reynolds number (based on reference velocity and propeller radius) was kept as close as possible to this value. The reference velocity u_{ref} for propeller was defined as:

$$u_{ref} = \sqrt{u_{x,\infty}^2 + (0.7R\omega)^2}, \quad (1)$$

where $u_{x,\infty}$ is the inflow velocity in the far field in [m/s], R is the propeller radius in [m], and ω is the propeller rotational speed in [rad/s]. Additionally, the advance ratio of the propeller J is defined as:

$$J = u_{x,\infty} / 2nR, \quad (2)$$

where n is the rotational speed in [rps]. n can be converted to ω as $\omega = 2\pi n$.

The goal was to obtain a fixed value of propeller rotation rate n across computations so that only the inflow velocity needed to be varied to simulate different values of J , as the Reynolds number is much more sensitive to changes in the propeller rotation speed than to the inflow velocity (as $\omega^2 \gg u_{x,\infty}^2$) through Eq.(1).

After initially fixing the rotational speed $n = 1.97418$ rps (by fixing ω , see below) and the Reynolds number $Re = 2e6$, the value of $u_{x,\infty}$ could be determined for a target J value using:

$$u_{x,\infty} = J \cdot (2nR) \quad (3)$$

The value of ω was determined from the definitions of Re and u_{ref} as:

$$\omega = \nu Re / R \cdot \sqrt{1 / R^2 \left(\frac{J_0^2}{\pi^2} + 0.7^2 \right)}, \quad (4)$$

where $J_0 = 0.7$, but this can be set to any realistic value.

The k- ω SST model, *Menter (1994)*, was used as a turbulence model. The model was chosen after comparison with the SSG EARSM model of *Speziale et al. (1991)* and the SST 2003 formulation by *Menter et al. (2003)*, with and without transition modeling (using the γ -model of *Menter et al. (2015)*). The original SST model showed the best agreement with the regression-based predictions. The propeller was accelerated from stand-still in an unsteady simulation and the rotating-frame method (also known as multiple reference frame method) was used to reduce the computational cost. Second-order discretization methods were used for the time, momentum and turbulence equations.

All computations were set up using the C-Wizard and run using FINETM/Marine version 10.1 on a Linux-based HPC cluster using 96 CPU cores (2x Intel Xeon Platinum CLX-9242 48C). As the total number of time steps was fixed and equal for every computation, the total runtime of each computation was between 2 and 3 h (clock time) depending on the mesh density. Only propellers for which thrust convergence was reached within a 1% tolerance of the average were included in the training sets for the neural network. The average was calculated over the last 30% of time steps.

2.5. Machine learning algorithm

For the presented study, a deep learning approach was used, implemented in the form of a geodesic

convolutional neural network (GCNN). Such a neural network is trained on a large amount of training data obtained from CFD computations. The data can be in the form of integral values or field data plotted on two-dimensional and three-dimensional surfaces. Using a geodesic convolutional neural network is ideal for CFD computations because it does not require equidistant data points in the original data (i.e. CFD output) and accepts surface manifolds as input data. A thorough description of the underlying theory can be found in *Baqué et al. (2018)*.

Of the initial number of 271 computations, 239 yielded converged results based on the previously defined criteria. The computations were subsequently divided into two sets using a 90-10 split; 90% of the computation formed the training set, while 10% of the computations were designated as the validation set to test the model.

Two sets of inputs for the neural network can be distinguished. First, data needs to be provided only for the training data set, consisting of the converged values of the thrust coefficient K_t , torque coefficient K_q and open-water efficiency η (the “integrated quantities”) as well as the field quantities. The field quantities consist of the nondimensional axial velocity u'_x in the propeller wake and the pressure coefficient C_p on the propeller blades. Both are defined as:

$$u'_x = u_x / u_{x,\infty} \quad \text{and} \quad C_p = p / \frac{1}{2} \rho u_{ref}^2 \quad (5)$$

The field quantities were saved as surface CGNS data, while the integrated quantities were saved in comma-separated value files. A support grid needed to be constructed to represent the field quantities for the GCNN.

The second set of data needs to be provided for both the training and the exploitation of the model, and consisted of the STL definition of the blade geometry and the advance ratio J . For the research described in this paper, the geometry parameters pitch P , number of blades Z and the expanded area ratio EAR were explicitly provided to the neural network. However, the GCNN can learn straight from the provided STL without this explicit input, which can be exploited in future applications.

The GCNN was trained for approximately 240 thousand iterations, whereby at each iteration, the model is trained on results from a single propeller geometry. This means that the model training enters a new epoch every 239 iterations (i.e. equal to the number of propellers in the training set). The total training time of the neural network is 65 h on a single GPU (Nvidia Tesla V100). Once the model has been trained, it takes roughly 0.3 s to interrogate the model and another 19.7 seconds to represent the data visually. This brings the total to 20 s that are needed to obtain a full performance curve and corresponding velocity and pressure fields for a new propeller geometry.

3. Results-

The results for the integrated quantities and field quantities can be discussed using, on the one hand, the R^2 -metric and on the other by checking differences between the AI prediction and the CFD result using the L_1 -norm. The former relates to an entire set of samples (i.e. the training and the validation set), while the latter can be done on a sample-by-sample basis. The R^2 -metric of the training and validation sets is the main indicator for conclusions regarding predictability and generality of the trained model. The R^2 - and L_1 -norms are defined as:

$$R^2 = 1 - \frac{\sum (\phi_{CFD} - \phi_{AI})^2}{\sum (\phi_{CFD} - \overline{\phi_{CFD}})^2} \quad \text{and} \quad L_1 = \phi_{CFD} - \phi_{AI}, \quad (6)$$

where $\overline{\phi_{CFD}}$ indicates the average of all CFD values and ϕ_{CFD} and ϕ_{AI} denote respectively the CFD value and prediction by the GCNN. From Eq.(6) follows that if $R^2=1$, the predicted result exactly equals the CFD result for the entire set, while if $L_1=0$, there are no differences for a specific sample

between the AI prediction and the CFD result.

3.1. Integrated quantities

The values of R^2 in Fig.3 are very close to 1, indicating very good predictability of the model. The line of the validation set is very close to the line of the training set, indicating that the model generalizes well, i.e. it not only predicts K_t , K_q and η well on already seen data (training set), but also on unseen data (validation set). Table I shows the averaged sample-by-sample error (the difference between the AI prediction and the CFD result) for all three integrated quantities. The averaged error is at most 1.5% for all three quantities, and as such of the same order of magnitude of the modeling error usually accepted in CFD.

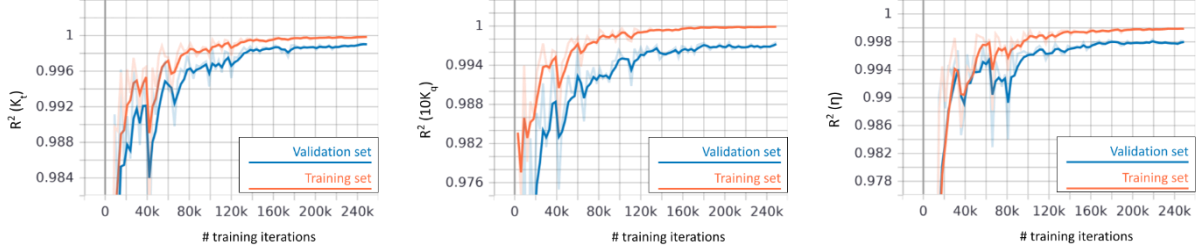


Fig.3: Evolution of R^2 in function of the number of training iterations for K_t , $10K_q$ and η

Table I: Averaged sample-by sample error for integrated quantities

Quantity	Error $ \phi_{AI} - \phi_{CFD} $
K_t	1.21%
$10K_q$	1.48%
η	1.50%

3.2. Field quantities

The R^2 value for the field quantities u'_x and C_p is slightly lower than for the integrated quantities, as visualized in Fig.4. The R^2 value of the velocity field prediction on the validation set stagnates after the first 80,000 iterations around $R^2 = 0.94$. The value is slightly higher at $R^2 = 0.98$ for the pressure. Given the proximity to $R^2 = 1$ for both quantities and for both sets, it can be concluded that also for the field quantities, the currently trained model generalizes and predicts the solution well. The stagnation of the R^2 value in the case of u'_x indicates that there may be an input-data related issue. This issue is addressed in more detail below.

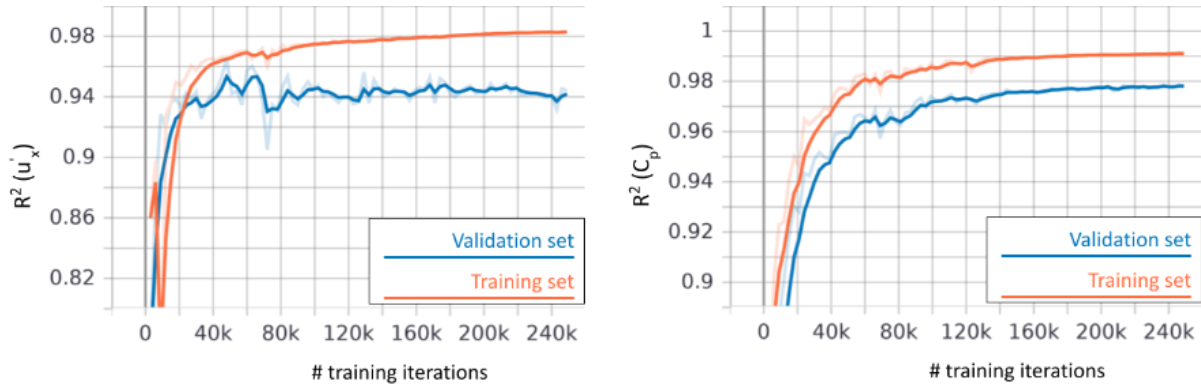


Fig.4: Evolution of R^2 in function of the number of training iterations for u'_x and C_p

Fig.5 shows the best samples for the pressure coefficient of the 7-bladed and 3-bladed Wageningen B-Series propellers that were tested. These were selected from the validation set and represented thus unseen data for the model. While the overall value of L_1 is very low, especially on the blade surfaces,

particularly the 7-bladed propeller displays slightly larger differences of around 5-8% between CFD and AI results closer to the tip.

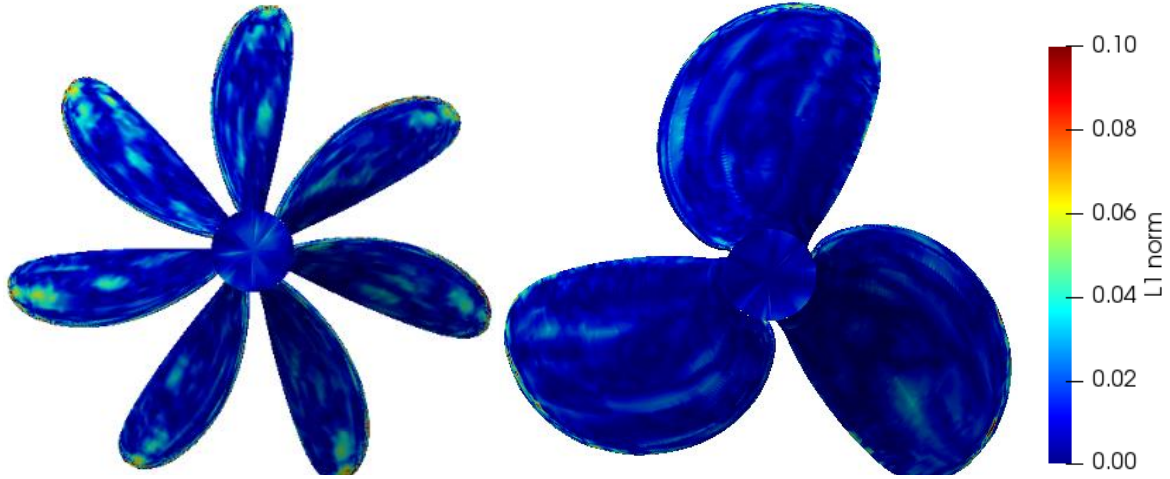


Fig.5: Value of L_1 norm on best samples of 7-bladed and 3-bladed Wageningen B-Series propellers

The plots in Fig.6 comparing the axial velocity field at the different indicated stations A through E also show local differences in the order of a few percent. Results are given for the same 7-bladed propeller as in Fig.5. Differences are largest around the radial location of maximal thrust (i.e. $0.7R$). This difference may be due to unsteadiness of the flow field, present for some of the samples. It is probable that this is connected to the stagnating and relatively lower value of the R^2 metric for the u'_x velocity field.

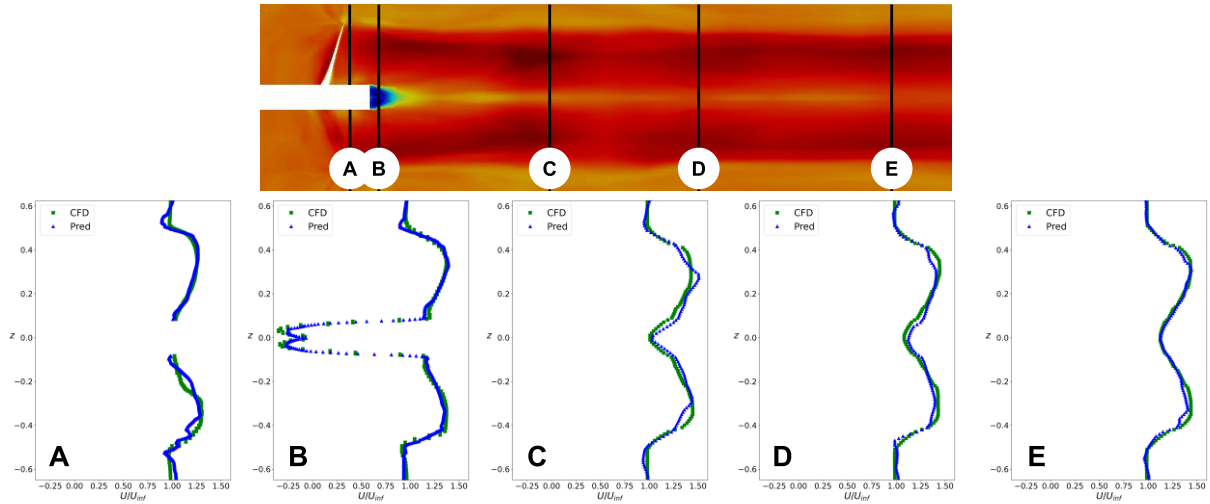


Fig.6: Nondimensional axial velocity field u'_x compared at different stations indicated above

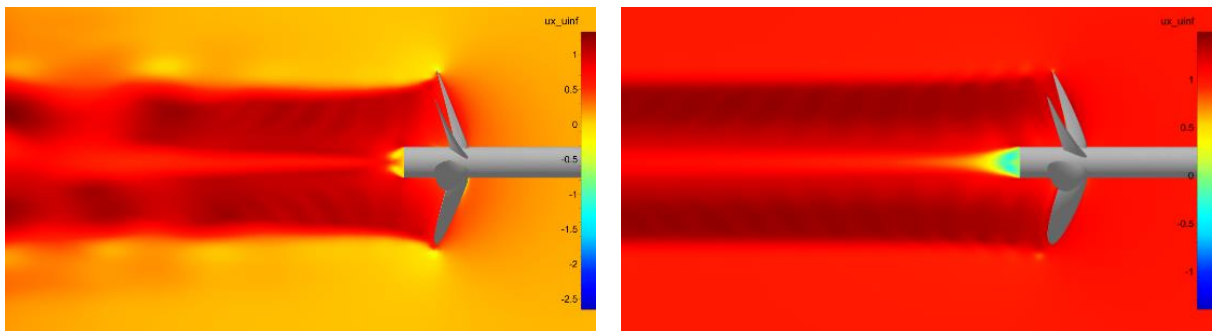


Fig.7: Unsteadiness in wake for low J values (left) compared to expected steady wake result (right)

The earlier mentioned unsteadiness relates to the nature of the input for the machine learning algorithm. Given that the GCNN is trained based on field values, ideally those field values should represent a steady solution. If some of the results are unsteady, this perturbs the training of the GCNN. Unsteadiness in the wake of the propeller was found for some of the samples used to train the model, see Fig.7. The unsteadiness was found for low values of J and follows from the longer time needed for the flow to stabilize at low inflow speeds. Given that the unsteadiness is linked to the transient solution, the computations should have run approximately twice as long in order to obtain only fully steady fields for all propellers and operating conditions.

4. Conclusion

A working application of machine learning to a marine propeller has been demonstrated, where a geodesic convolutional neural network (GCNN) has been trained to predict both the integral quantities of an open-water performance curve and local field values of velocity and pressure on two-dimensional planes for Wageningen B-Series propellers. The GCNN was trained on 239 samples, of which 90% constituted the training set and the remainder the validation set.

The values of the R^2 metric were almost equal to 1 for the integrated quantities K_t , K_q and η on both training and validation sets, indicating a very good prediction and generalization capability of the trained model for propellers in the Wageningen B-Series regarding integrated quantities. The average difference between the predicted and CFD-obtained value remained below 1.5% for all three integrated quantities. The local field quantities of nondimensional wake velocity u'_x and C_p showed slightly lower R^2 values of respectively 0.94 and 0.98 for the validation set. While capabilities of the model to predict the local flow fields and its generalizability can be qualified as good, improvement is possible.

Unsteadiness in the flow field was identified for several cases with low advance ratios, perturbing the training of the GCNN and reducing the accuracy of the prediction for the u'_x field values. This underlines the importance of careful data selection prior to feeding the data to the GCNN as well as the requirement of understanding the present limitations of neural networks in dealing with unsteady data.

It was shown that when proper care is taken in data selection and computation parameters, machine learning can, in fact, enhance productivity for marine engineers in the initial design process of propellers by orders of magnitude. This is possible due to a drastic reduction in interrogation time from more than 200 CPU-hours per operating point in CFD to 20 s for an entire performance curve using a machine learning approach.

A logical next step is testing the presented concept on resistance and self-propulsion applications.

References

- BAQUÉ, P.; REMELLI, E.; FLEURET, F.; FUA, P. (2018), *Geodesic convolutional shape optimization*, 35th Int. Conf. Machine Learning, Stockholm, pp.472-481, <https://fleuret.org/papers/baque-et-al-icml2018.pdf>
- KUIPER, G. (1992), *The Wageningen propeller series*, MARIN, Wageningen, <https://www.scribd.com/document/402540817/The-Wageningen-Propeller-Series-G-Kuiper>
- MENTER, F.R. (1994), *Two-equation eddy-viscosity turbulence models for engineering applications*, AIAA Journal 32(8), pp.1598-1605, <https://pdfs.semanticscholar.org/7671/2e2e2063bf33133f10fad4d3ff648b3acd6e.pdf>
- MENTER, F.R.; KUNTZ, M.; LANGTRY, R. (2003), *Ten years of industrial experience with the SST turbulence model*, Turbulence, Heat and Mass Transfer 4(1), pp.625-632, <https://www.researchgate.net/publication/254499381>

[net/profile/Florian-Menter/publication/228742295 Ten years of industrial experience with the SST turbulence model/links/0046353c6330b1c0a4000000/Ten-years-of-industrial-experience-with-the-SST-turbulence-model.pdf](https://www.researchgate.net/profile/Florian-Menter/publication/228742295_Ten_years_of_industrial_experience_with_the_SST_turbulence_model/links/0046353c6330b1c0a4000000/Ten-years-of-industrial-experience-with-the-SST-turbulence-model.pdf)

MENTER, F.R.; SMIRNOV, P.E.; LIU, T.; AVANCHA, R. (2015), *A one-equation local correlation-based transition model*, Flow, Turbulence and Combustion 95(4), pp.583-619

OOSTERVELD, M.W.C.; VAN OOSSANEN, P. (1975), *Further computer-analyzed data of the Wageningen B-screw series*, Int. Shipbuilding Progress 22(251), pp.251-262, <http://citeseerx.ist.psu.edu/viewdoc/download?doi=10.1.1.460.2869&rep=rep1&type=pdf>

SPEZIALE, C.G.; SARKAR, S.; GATSKI, T.B. (1991), *Modelling the pressure-strain correlation of turbulence: an invariant dynamical systems approach*, J. Fluid Mech. 227, pp.245-272, [https://www.researchgate.net/profile/T-Gatski/publication/23820839 Modelling the pressure-strain correlation of turbulence - An invariant dynamical systems approach/links/55db599608aed6a199ac5e32/Modelling-the-pressure-strain-correlation-of-turbulence-An-invariant-dynamical-systems-approach.pdf](https://www.researchgate.net/profile/T-Gatski/publication/23820839_Modelling_the_pressure-strain_correlation_of_turbulence_-_An_invariant_dynamical_systems_approach/links/55db599608aed6a199ac5e32/Modelling-the-pressure-strain-correlation-of-turbulence-An-invariant-dynamical-systems-approach.pdf)

Digital Transformation in Maritime Trainings in COVID-19 Times

Tracy Plowman, DNV, Hamburg/Germany, tracy.plowman@dnv.com
Ulrich Bernhardt, DNV, Hamburg/Germany, ulrich.bernhardt@dnv.com

Abstract

The paper describes DNV's maritime training department's journey in converting predominantly traditional classroom training to digital alternatives. Motivation, objectives and (sometimes surprising) experience of the digital transformation in our training activities are described. Virtual classroom delivery via MS Teams and self-paced e-learning via Rise 360 have evolved as key vehicles to convey our training content in COVID-19 times.

1. Introduction

1.1. Disruption as a chance

Teaching environments and techniques have changed since the COVID-19 pandemic, Fig.1. Whether we liked it or not, the training community had to embrace digital, remote forms of training rapidly. Post-graduate training in industry and academic training were affected similarly. The first response to the lock-down of physical classrooms was employing ad-hoc measures such as presenting PowerPoint lectures in videoconferences. But at the same time, a more fundamental discussion has started on how to provide quality training digitally in the medium-term and long-term perspective. The COVID-19 disruption turned into a chance to redesign and modernize our training portfolio for more agile and cost-effective delivery modes.



Fig.1: Training before COVID-19 (left) and during COVID-19 (right)

1.2. Management considerations

Classification Societies are big on rules and regulations. Training is no exception. Plan approval engineers and surveyors need proof of appropriate qualification to perform certain tasks. Without a record of such a qualification (= participation in a training), a surveyor may not perform the task and a customer may have to wait or go to a different port to get his required survey in time. This system had been challenging already in pre-COVID-19 times, as surveyors around the globe needed to be trained, with highly qualified trainers usually located in the DNV headquarters of Hamburg and Høvik, and training demand often coming in at short notice and for small numbers of trainees. COVID-19 brought essentially a shut-down on travel outside your own country, and temporarily also a ban on face-to-face meetings and classroom training.

The latent management strategy for a digital transformation of traditional classroom training turned in this situation into a pressing necessity for action. The key requirement was a rapid solution for delivering

training remotely. COVID-19 brought a massive boom for remote communication tools like MS Teams and Zoom, as they addressed the need for face-to-face meetings without physical meetings, in private applications, in schools and universities, and in the business world. The existing infrastructure for 1-to-1 chats and business meetings just needed to be enhanced with a few more features to address specific training needs, such as enabling small-group work in (digitally) secluded environments, so-called break-out rooms.

We reviewed a variety of competing options for live online training, including [MS Teams](#), [Zoom](#), [GoTo-Training](#), [Webex](#), and [Adobe Connect](#). Zoom was best in functionality, but it had initial cyber-security issues when used without due attention. MS Teams had initially inferior functionality, but features similar to Zoom have been added making it a comparably useful tool. We now use MS Teams and Zoom in our trainings, where the choice often depends on what the trainer or host is more familiar with.

Looking at the required development effort as a short-term priority and the saving potential compared to traditional classroom training, Fig.2, it became quickly apparent that live online training via videoconferencing and self-paced e-learning were the obvious choices for our training courses. Most now employ a blend of these two training solutions.

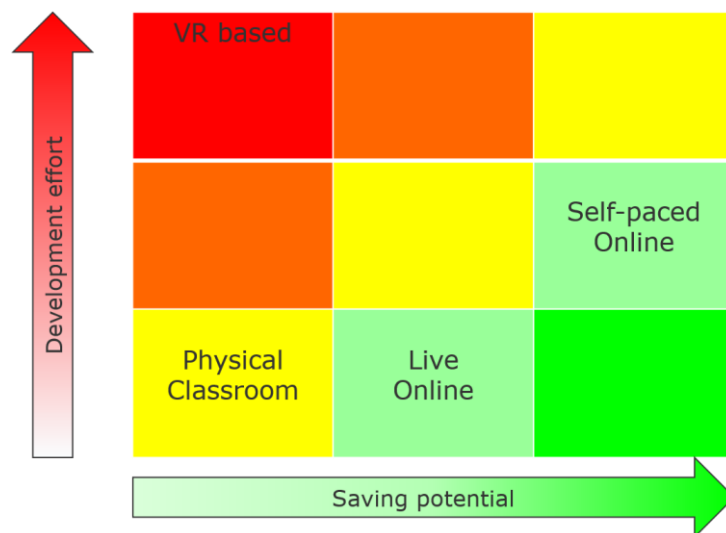


Fig.2: Live online training is an attractive option – at least in the short term

Software solutions for developing self-paced online training have been improving steadily over the years. Our decision to move from Articulate's [Storyline](#) to [Rise](#) brought down development times and costs significantly, while at the same time improving trainee satisfaction with the “look and feel” of the end products. We use self-paced online training based on Rise predominantly for the following applications:

- resource libraries with reading material (pdf files or hyperlinks) and videos, often referencing to publicly available sources, such as IMO websites
- assessment tests, mainly in the form of multiple-choice tests, for self-assessment as well as formal assessment for compliance purposes
- secondary topics, such as fringe applications or historical background knowledge

We use live online training for the following purposes:

- Kick-off and closure of trainings
- Question & Answer sessions
- Short group activities
- Material that needs live commentary of trainers and is most likely to spark interactivity such as questions from trainees with fast response from trainer

The next chapter will discuss the considered choices for digital training solutions in more detail, always within the context of the COVID-19 constraints.

2. Key vehicles

The first task in converting classroom training to digital training solutions was generally a review of what could be rapidly converted to e-learning, e.g. quizzes, libraries with reference material (pdf and hyperlinks), and background information. Such a partial conversion to e-learning gave well-received breaks from live online presentations via videoconferencing.

2.1. Virtual classroom (VC) via videoconferencing

In the training community, we refer to live online training via videoconferencing as “Virtual Classroom”, Fig.3. Unlike business videoconferencing, the training options of MS Teams and Zoom offer some additional features, such as digital breakaway rooms allowing smaller subsets of the trainee group to discuss a task in private with possibility of the trainer entering each sub-group virtually.

As with classroom trainings, there are good Virtual Classroom trainings and bad ones. Bad ones are of the format “you look at PowerPoint slides while the expert drones on”. Participants often zone out, doing other things like checking their emails, passively absorbing the audio, and tuning back into the training occasionally. The good ones are relatively focused on what the trainee really needs to know with clear take-home messages and strong user interaction.

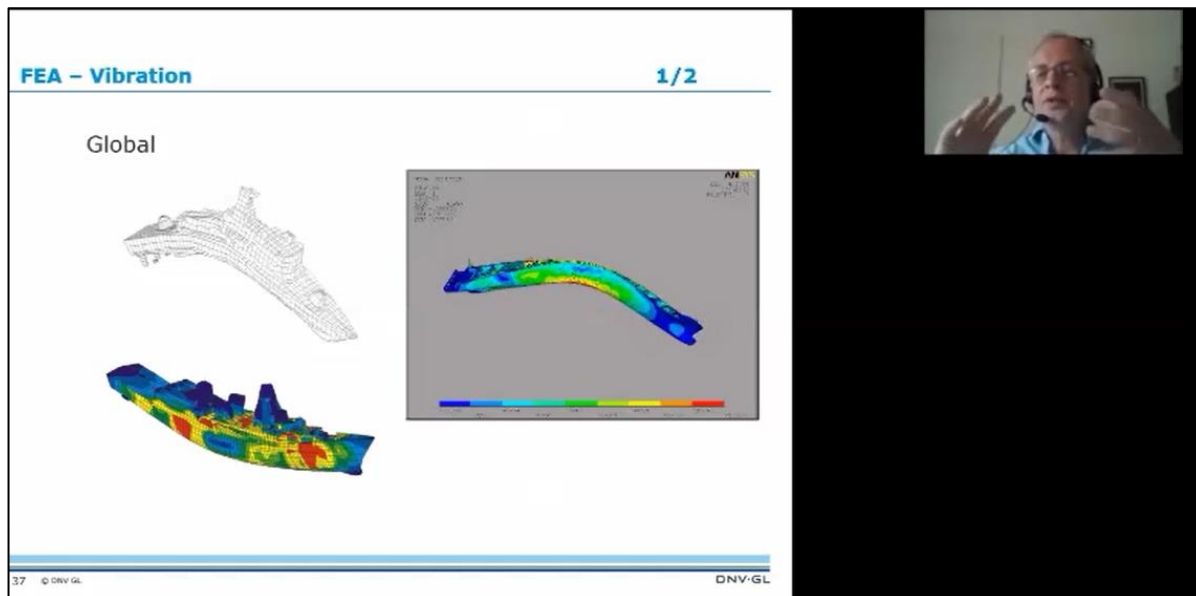


Fig.3: Virtual Classroom training

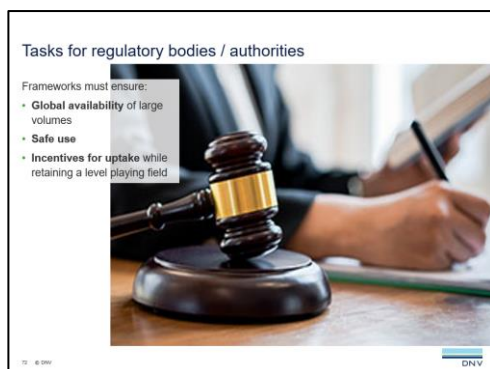


Fig.4: Typical virtual classroom slide

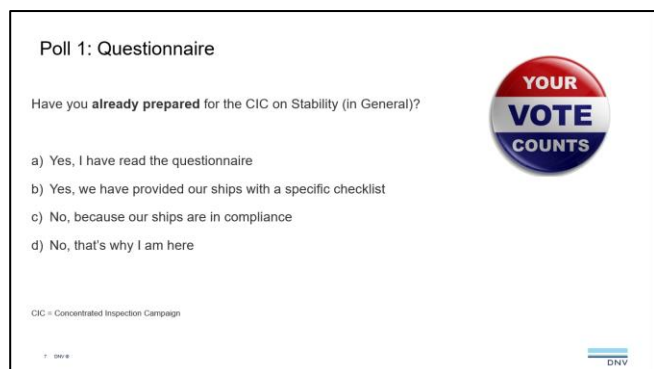


Fig.5: “Polls” stimulate audience to think

Presentation material generally needs some reworking for online delivery, cutting down on reading text, making it more visual, and introducing more interactive elements, e.g. asking questions to participants instead of stating facts to them (“What do you estimate to be...” or “Who of you has already heard of...”), Fig.4. After ~10 minutes speaking time, an interactive element, e.g. as shown Fig.5, should stimulate the audience to refocus on the topic. Otherwise, the temptation to multi-task (i.e. read incoming emails, etc.) becomes overwhelming for most people.

Overall, the experience is that Virtual Classroom training is more tiring than traditional classroom training, possibly due to reduced audio and visual resolution. To address this issue, we generally reduce conventional full days in classrooms to half-days online while doubling the course duration in calendar days.

Multitasking for trainers is more difficult in Virtual Classroom environments. Besides training delivery, typical trainer tasks are:

- Answering questions from participants. Besides dedicated Q&A sessions, there are typical questions or comments from participants as the training material is presented. In Virtual Classrooms, it has worked best for us to use the chat function for this purpose. Sometimes, a second person is needed to monitor and address chats; sometimes, it works well for the trainer to address chats/comments during breaks.
- Monitoring nonverbal feedback from audience to assess whether the audience is bored, confused, lacking understanding, disagreeing, etc. Webcam images are often too small for us to perform these tasks, and in some cases, trainees switch off cameras either for privacy or bandwidth reasons. This makes more frequent formalized feedback, e.g. in the form of mini-quizzes, even more important in Virtual Classroom training.

2.2. E-learning

E-learning is just one of our tools, albeit a powerful and useful one if properly employed. A key risk with any self-paced learning is that the trainee does not study. And self-paced learning generally has less impact than classroom training where individual feedback is possible and where trainees generally have a higher attention rate.

E-learning courses employ a wide range of training elements to avoid fatigue: text, images, short videos, hyperlinks, interactive elements (click, drag-and drop, mouse-over pop-ups), assessments (usually in the form of multiple-choice quiz), etc. In principle, all good advice for designing PowerPoint presentations for classroom training also applies to designing e-learning courses. The typical e-learning feature of supplying information on demand allows us to declutter slides with faster progress for those who don't need higher information detail.

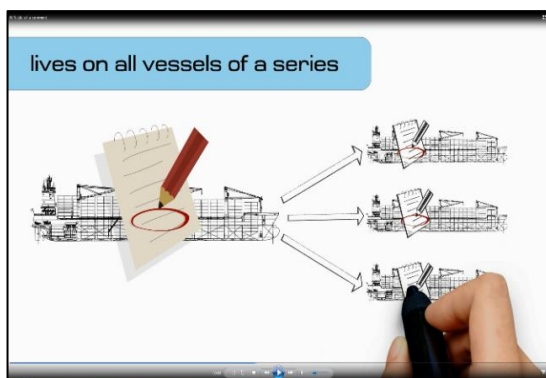


Fig.4: Still from short, embedded video



Fig.5: Video recording of lecture

Videos are frequently used in e-learning, varying from small add-on videos embedded in a flow of training storyline, Fig.4, to longer recorded presentations kept in video libraries, Fig.5. Used in moderation and mainly for drill-down topics of interest to fewer trainees, such videos can be an effective and cost-efficient way to develop trainings.

Similarly, there can be pdf attachments for reading material, e.g. for lecture notes, further recommended reading, reference material, Fig.6, instructions for activities, etc.

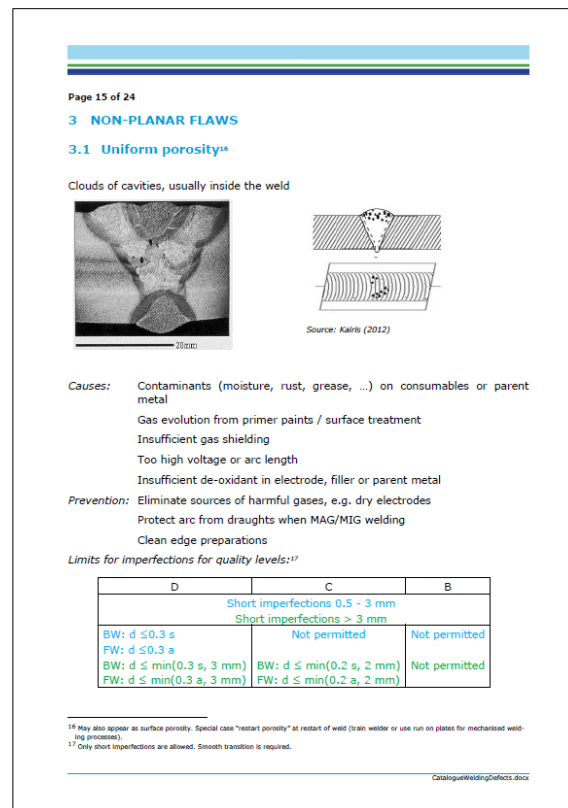


Fig.6: Typical reference knowledge in pdf

3. Selected projects

The basic approach outlined above has been applied to a large part of our course portfolio, both for internal training courses and external courses of the DNV maritime academy, <https://www.dnv.com/maritime/maritime-academy/index.html>. In the following, we use examples of an internal training course, an external course, and a course that is offered both for internal staff and customers.

3.1. MOU in operation

The course provides the required minimum theoretical basis for general surveyors of Mobile Offshore Units (MOUs). The course was initially a 3-day classroom course. Approximately 60% of the course material was converted to e-learning, Fig.7. Several PowerPoint lectures were converted to e-learning, including some interactive elements (e.g. "flip the card to see the correct answer"), reference material was put in a pdf online library, and the learning success was assessed by an automatic online multiple-choice test.

The conversion took approximately 120 h over a duration of 2 months, with subject matter expert and digital training developer working closely together on creating the blended learning. See Figs. 8 and 9 for examples of how the basic philosophy was put into practice, with Virtual Classroom presentation slides being strongly visual and light on text, Fig.8, and occasional polls or similar interactive elements, Fig.9.

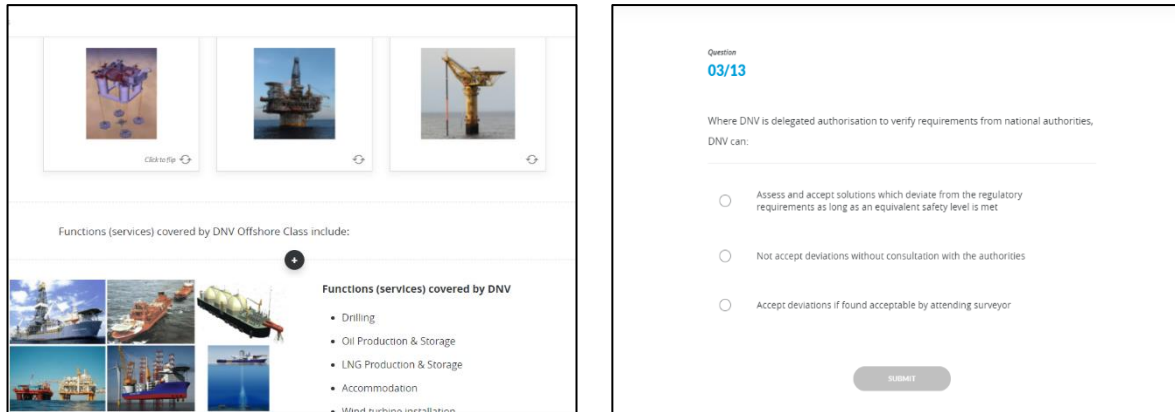


Fig.7: Parts of e-learning; material presented (left) and quiz (right)



Fig.8: Slide in Virtual Classroom

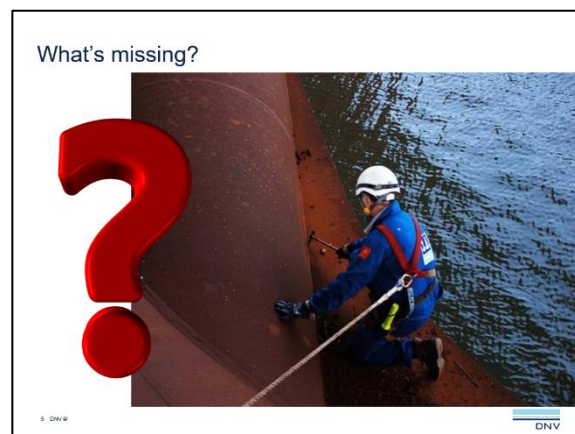


Fig.9: Question to participants in VC

3.2. Energy Efficiency in a Nutshell

This course came in response to the strong industry focus on energy efficiency, in the wake of rising fuel prices after IMO's 2020 Global Sulphur Cap, e.g. <https://www.ics-shipping.org/current-issue/2020-global-sulphur-cap/>, and IMO's announcement to make energy efficiency measures in design (EEXI) and operation (CII) mandatory for the existing fleet in service starting from 2023.

The course consists of two half-days, which are interspersed with Virtual Classroom and e-learning modules. The format allows delivery of the course for different time zones, either Europe and East-Asia, or Europe and the Americas. Fig.10 shows examples from the e-learning, Figs.11 and 12 Virtual Classroom presentation slides.



Fig.10: Parts of e-learning; material presented (left) and recorded video (right)

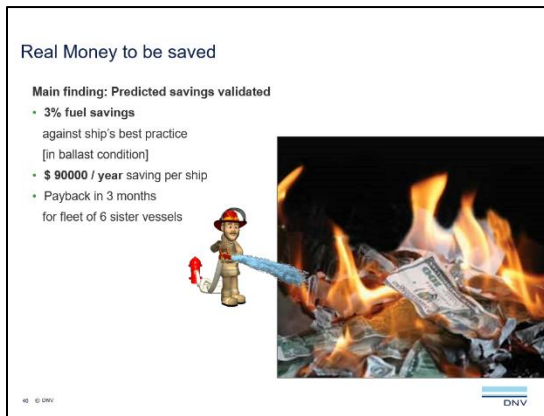


Fig.11: Slide in Virtual Classroom



Fig.12: Question to participants in VC

3.3. Understanding Digital Transformation

“Digital transformation” or “digitalization” have become very popular marketing terms or buzzwords in the maritime world. We perceived a wide-spread need in the industry (including our own company) to come to terms with the “digital new-age” jargon, focusing on the capabilities, but even more so limitations of the key technologies, including Artificial Intelligence, Virtual & Augmented Reality, Digital Twins, and Autonomous Ships. The course was to offer value and be accessible for everyone in the hierarchy, (almost) “from cleaning woman to CEO”. The response was to develop a blended course, with two half-days of Virtual Classroom, Figs.13 and 14, and approximately a day’s worth of four e-learning modules plus a library of pdf reading material and videos, Fig.15, where colleagues from DNV and external experts offered drill-down lectures on selected topics, e.g. hull optimization using high-fidelity Digital Twins in High-Performance Computing, Fig.16.



Fig.13: Slide in Virtual Classroom

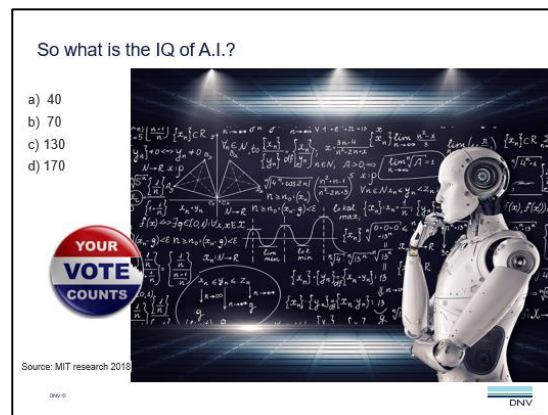


Fig.14: Poll in Virtual Classroom

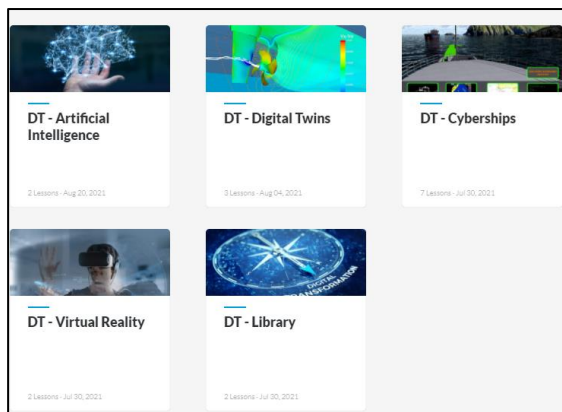


Fig.15: Menu of e-learning modules incl. library

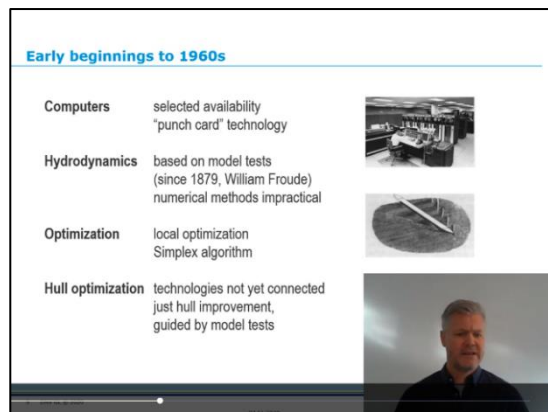


Fig.16: Guest lecture video from library

4. Conclusions

The COVID-19 situation has forced us to adopt digital training options, whether we wanted or not. Not all options worked well. We learnt some lessons and we keep learning. Focussing on key elements and doing them well is one of those lessons for successful digital training development.

For content, the key to success is the same as for traditional training: Make it relevant, make it short, make it fun. No media is per se evil, and no media is per se perfect.

Acknowledgements

We thank our colleagues in the developer team in the MCLA (Maritime Competence Learning & Academy) department for their support, especially Volker Bertram for his assistance in writing this paper.

Visual Inspection of Underwater Structures using an AUV: A Preliminary Simulative Evaluation

Simone Tani, University of Pisa, Pisa/Italy, simone.tani@ing.unipi.it
Francesco Ruscio, University of Pisa, Pisa/Italy, francesco.ruscio@phd.unipi.it
Matteo Bresciani, University of Pisa, Pisa/Italy, matteo.bresciani@phd.unipi.it
Riccardo Costanzi, University of Pisa, Pisa/Italy, riccardo.costanzi@unipi.it
Andrea Caiti, University of Pisa, Pisa/Italy, andrea.caiti@unipi.it

Abstract

This work addresses the problem of underwater structures inspection using an Autonomous Underwater Vehicle (AUV) proposing a strategy which exploits a stereo vision system and a range sensor to compute orientation and distance of the vehicle with respect to the target. The relative orientation is refined within an Extended Kalman Filter (EKF) using an inertial unit as input. Then, a control system is employed to maintain a desired configuration of the robot during the whole mission. The developed system has been tested in a realistic simulated environment, performing surveys of two structures: a sequence of walls and a cylindrical pylon.

1. Introduction

The visual inspection of underwater structures represents a fundamental operation which needs to be periodically executed to ensure the structural integrity of the system. The early identification of structural degradation, such as corrosion, leaks, or cracks, allows to effectively schedule maintenance operations, thus reducing risks and costs. Divers are typically employed to perform inspections of subsea structures, which are time-consuming and dangerous tasks for human operators. More recently, Remotely Operated Vehicles (ROVs) have been utilised to conduct inspection operations, e.g. *Mai et al. (2016)* and *Choi et al. (2017)*. Exploiting ROVs allows to improve the safety of the mission and to reduce its costs, but it requires a trained operating crew, and it has some limitations on the mobility and operating range due to the communication cable.

To overcome such limitations, Autonomous Underwater Vehicles (AUVs) have been proposed for inspection activities. Indeed, AUVs can perform routine tasks autonomously and do not have connection cables which limits their movements. Thanks to recent technological advances, AUVs have the potential to automatise inspection tasks of subsea facilities, bringing several benefits, *McLeod and Jacobson (2011)*, such as reduced cost of operations, increased safety, and faster inspection. This would result in a reduction of the interval between inspections, thereby improving integrity assessment of subsea assets and reducing the risk of asset failure.

Preliminary work concerning autonomous inspection was presented in 2001 in *Foresti (2001)*. Since then, AUVs have been proposed to perform inspection tasks of different underwater assets, ranging from underwater constructions to floating objects like vessels or offshore working platforms. Examples of inspection applications include harbour facilities, *Jacobi (2015)*, offshore drilling and pumping platforms, offshore wind park foundations, *Kleiser and Woock (2020)*, reservoir dams, *Ridao et al. (2010)* and ship hulls, *Hong et al. (2019)*. All these systems need regular inspection, mainly for maintenance purposes and to check structural defects, like corrosion or malfunctions.

The main challenges to accomplish visual inspection, within the aforementioned applications, are represented by the autonomous manoeuvring in complex environments and operating in short distance to the inspected object. To this aim, AUVs are usually equipped with exteroceptive devices such as optical sensors (cameras) or acoustic sensors (sonars, echo-sounders, etc.), which allow perceiving the surrounding environment and avoid possible obstacles.

With this purpose, this paper proposes a strategy which allows an AUV, equipped with exteroceptive

devices, to inspect underwater structures remaining always at a predefined safety distance and maintaining an orientation orthogonal to the inspected surface. In particular, the observations coming from a stereo vision system are processed to compute the orientation of the vehicle with respect to the surveyed surface. An Extended Kalman Filter (EKF) is employed to refine the orientation information using measurements coming from an inertial unit. Such information is then fused with range measurements provided by an acoustic sensor to determine the normal distance of the vehicle from the surface. These estimates are finally exploited by a control system to maintain the desired configuration of the AUV during the whole mission.

The proposed algorithm is based solely on the real-time perception of the target, and it does not require any a priori knowledge of the surrounding underwater environment to accomplish the mission.

Several tests have been executed in a simulative environment to assess the performance of the developed strategy and its possible criticalities. In particular, the structures analysed during the simulations are the following: a surface composed of four planar walls with different orientations and a cylindrical pylon.

2. Methodology

The strategy proposed to perform the inspection task aims at maintaining both a predefined safety distance to the structure and the vehicle orientation that guarantees the orthogonality between the principal optical axes of the stereo camera and the examined surface. The first condition results in the possibility to execute, in cases of malfunctions, some safety manoeuvres to avoid collisions with the target and it is important to ensure an adequate framing of the scanned surface. On the other hand, an orientation orthogonal to the inspected surface allows to achieve a proper reconstruction and mapping of the target, since with this configuration the image planes result to be parallel to the surface itself.

To this end, the following assumptions have been made:

- Images from the stereo vision system are properly calibrated and rectified, *Dhond and Aggarwal (1989)*. This allows to project images into a common image plane, thus facilitating the research of corresponding features between couples of images.
- The portion of the inspected surface, framed by the stereo camera, is assumed to be locally planar. This is reasonable because the target structures analysed within this work have a reduced curvature compared to the distance from which the surface is framed.
- The roll angle of the vehicle with respect to the target is neglected within the proposed strategy since it is assumed that the AUV has a frontal vision system and its rotation around the surge axis is controlled to the null value.

The reference systems considered within this work are depicted in Fig.1. According to the third assumption, the orientation of the AUV relative to the surface of the inspected target can be described by the tuple (θ, ψ) , representing the pitch angle and the yaw angle to the surface, respectively. The range between the AUV and the surface is instead represented by the normal distance $dist_{norm}$, which is intended as the distance between the vehicle and the scanned surface along the orthogonal direction to the surface itself. The objective of the proposed strategy is hence to control the values of the two angular variables to zero and the normal distance to a predefined reference value. Based on the turbidity conditions of the water, the reference value must be properly chosen as a compromise between robot safety and satisfying framing.

With this aim, images recorded by the stereo vision system are processed to extract the orientation of the vehicle relative to the inspected target. To obtain such result, a relative attitude estimation algorithm has been implemented, which consists of three phases: features extraction and stereo matching, 3D point cloud generation and relative orientation computation.

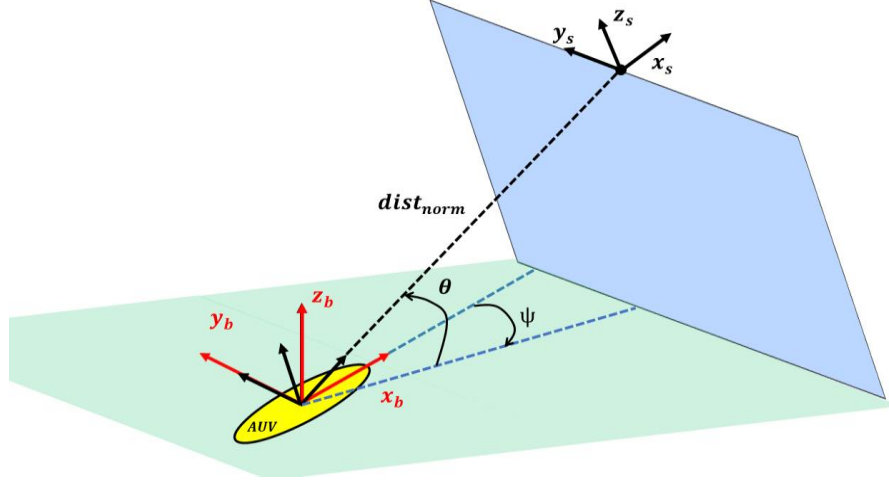


Fig.1: Representation of the AUV's body reference system $\{b\}$ and the surface reference system $\{s\}$ considered within this work

In the first stage, image processing techniques are applied to process the information available from the two cameras. The most informative pixels in the images are extracted exploiting the Speeded Up Robust Features (SURF) algorithm, *Bay et al. (2006)*, which is commonly used to detect features in underwater images, as it represents a good compromise between the number of features extracted and the computational cost of the extraction process. The SURF algorithm provides as output a descriptor vector for each detected feature, which is used to find correspondences between features in the left and right images.

The second phase of the algorithm aims at reconstructing the 3D scene associated to the current couple of images. To this end, the assumption of rectified images, together with a pinhole camera model, allows to define the geometric relationship between a 2D point in the image plane and a 3D point in the Camera reference system as described in *Dhond and Aggarwal (1989)*.

The obtained 3D point cloud representing the framed scene is then exploited, in the third phase, to extract the orientation of the vehicle relative to the inspected surface. However, due to intrinsic deficiencies during the feature detection and matching algorithm, some wrong correspondences can occur. Such mismatches determine errors (outliers) in the 3D location of their correspondent 2D points. Aiming to delete the outliers and extract the best possible orientation estimate, the third stage of the method also involves the application of a Random Sample Consensus (RANSAC) algorithm, *Fischler and Bolles (1981)*, which represents one of the most common algorithms to get a mathematical model from a dataset containing outliers. In this specific work, RANSAC algorithm is adopted to compute the best fitting plane of the 3D point cloud, retrieving all the 3D points whose distance from the plane is smaller than a predefined threshold (inliers). Then, according to *Chung et al. (2017)*, the planar model used within the RANSAC algorithm allows to compute the pitch angle θ and the yaw angle ψ defining the orientation of the vehicle with respect to the inspected target.

Such orientation is used as observation in an EKF, which exploits also measurements provided by an inertial unit as input. This step allows to provide more frequent data and to refine the orientation estimate $(\hat{\theta}, \hat{\psi})$. Afterwards, the range measurement provided by an acoustic sensor is projected exploiting the filter estimate to obtain the normal distance $dist_{norm}$ between the vehicle and the target. The relative orientation and distance information are lastly used by the robot's control system to correct its pose, restoring the desired configuration. To accomplish the inspection tasks described in Section 3, the vehicle has also to maintain a constant lateral speed and a constant depth. However, details about the control of depth and lateral speed are beyond the scope of this work.

Fig.2 shows the proposed approach as a blocks scheme, where the various steps composing the vision-based estimation algorithm are depicted in green, the EKF in orange, and the control system in blue.

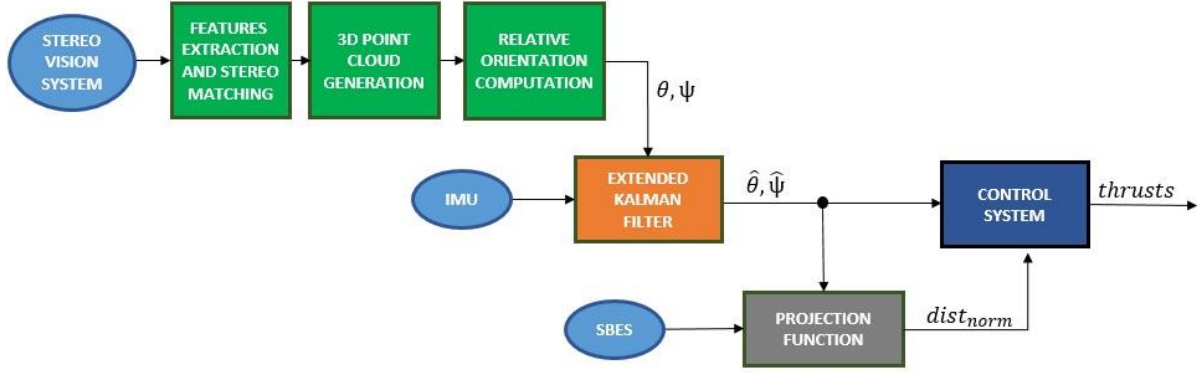


Fig.2: Structure of the developed motion control system

3. Evaluation in virtual environment

In preparation of future field application, the simulation of the mission to carry out results to be of crucial importance. In fact, it allows to plan strategies, to predict the behaviour of the vehicle when subjected to different types of disturbances and malfunctions and to evaluate the possible results that would be obtained in a real scenario. With this purpose, the proposed strategy has been tested in a simulative environment. In particular, the framework exploited in this work is Unmanned Underwater Vehicle (UUV) Simulator, *Manhaes et al. (2016)*, which is a package containing the implementation of Gazebo plugins and ROS nodes, allowing the simulation of unmanned underwater vehicles such as ROVs and AUVs.

The vehicle used as reference for the simulation is a Zeno AUV, *Gelli et al. (2018)*, property of the CrossLab, an interdisciplinary laboratory of the Department of Information Engineering of the University of Pisa. The AUV, shown in Fig.3, has a propulsion system composed of 8 thrusters, which have been arranged to actively control all the six degrees of freedom. Moreover, it is equipped with two frontal cameras, Inertial Measurement Unit (IMU), Single-Beam Echo-Sounder (SBES) mounted between the two cameras, depth, and GPS sensors. The high manoeuvrability and the on-board sensors make the Zeno AUV suitable for inspection operations.

To make the simulated vehicle's behaviour as consistent as possible with the real one, the AUV Zeno model was properly replicated within the UUV Simulator. Then, customised structures have been inserted within the simulated environment to reproduce a common scenario of underwater structures inspection, as described in the following section.



Fig.3: Zeno AUV

3.1. Simulative scenarios

The structures chosen to test the developed system are a sequence of walls and a cylindrical pylon. Concerning the first target, the model used for the tests proposed within this work is composed of a set of four planar surfaces with different orientations properly assembled. This kind of structure represents the first step for the validation of the proposed approach since it clearly satisfies the planar assumption. Fig.4 shows the vehicle during the scanning task of one of the surfaces.



Fig.4: Planar surfaces model in UUV Simulator

Instead, the cylindrical pylon, which has a radius of 8 m, has been used to simulate the inspection of the typical supporting structure of offshore platforms. This has been done with the aim to investigate the performance of the algorithm on structures characterised by more complex shapes. Fig.5 reports the pylon model in the simulative environment.

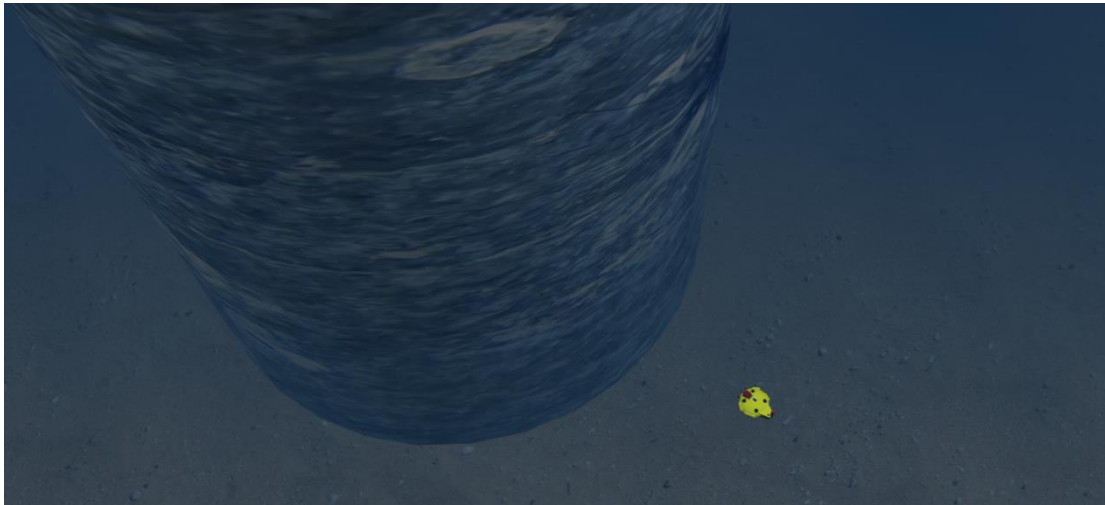


Fig.5: Pylon model in UUV Simulator

Figs.4 and 5 show that a texture has been attached to the two models, so that the surfaces to examine can be representative of real underwater structures. Moreover, changing the characteristics parameters of the default marine environment, it has been possible to reproduce a turbidity condition which could be reasonable for typical inspection missions of underwater structures. This is particularly important to assess the feasibility of the vision-based estimation algorithm.

3.2. Simulative results

This section reports the results achieved during the simulations carried out to inspect the aforementioned surfaces. The reference inspection trajectory consists in a lateral motion at constant depth, during which the vehicle must maintain the orthogonality with respect to the inspected target. This results in a trajectory that is parallel to the surface, aiming to guarantee an accurate coverage of the target at a specific depth value and it represents the first step towards a full coverage trajectory, such as typical lawn mower paths.

3.2.1. Planar surfaces inspection

The inspection mission of the sequence of planar surfaces is composed of two different phases. During the first one, which has a duration of 60 s, the vehicle executes a preliminary correction of its normal distance and relative orientation with respect to the target, also reaching the desired depth reference. The inspection of the target is conducted during the second phase, in which the vehicle was supposed to maintain a normal distance of 3 m from the target structure. Fig.6 shows the trajectory performed by the AUV utilising the proposed motion control system (in magenta) and the reference trajectory (in blue), expressed in a North-East reference frame.

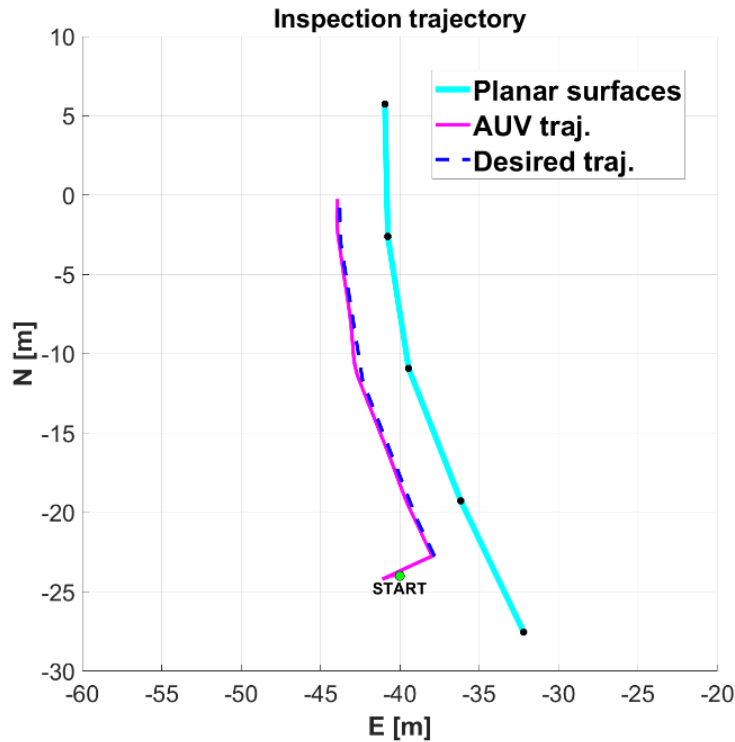


Fig.6: Planar surfaces inspection: vehicle trajectory

Fig.7 shows the errors between the estimate of the yaw and pitch angles respect to the surface and their null reference value. The error peaks, visible in the trend of the yaw estimate, are the direct consequence of the presence of edges between two consecutive faces of the model under inspection. During this transition, the relative orientation estimates suffer from variations, since the two cameras are framing different surfaces. Thus, the planar surface assumption is not valid in those points, producing higher estimation errors. However, the vehicle can correct its orientation, restoring the desired configuration, as shown by the fact that the yaw estimate tends to the null value between two consecutive peaks.

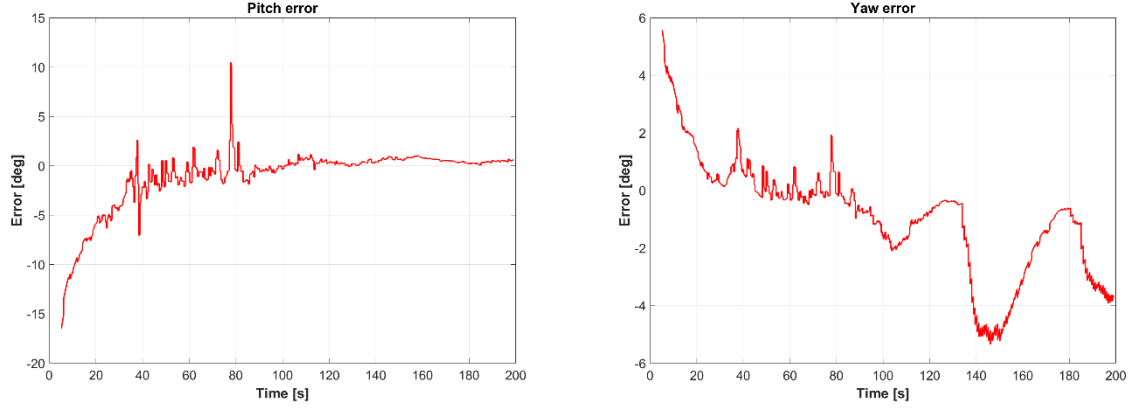


Fig.7: Trend of the relative orientation estimate errors

The normal distance error, which represents the difference between the desired normal distance and the one estimated by the proposed algorithm, converges to the null value, once the initial phase of adjustments ends, as shown in Fig.8. The presence of small ridges in the trend of the error is again due to the transition from one face of the structure to the next, since it generates higher error in the orientation estimate exploited for the distance projection.

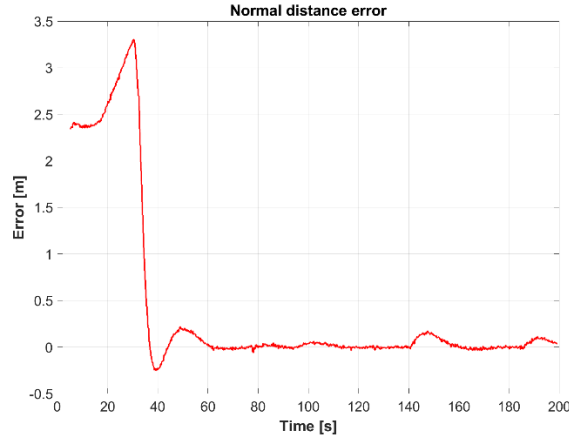


Fig.8: Normal distance error

3.2.2. Pylon inspection

This mission consists in the visual survey of a quarter of a pylon. During the first 150 s the vehicle executes a preliminary correction of its normal distance and relative orientation with respect to the target, also reaching the desired depth reference. Then, the inspection of the target is performed, in which the vehicle was supposed to maintain a normal distance of 5 m from the pylon surface. Fig.9 shows the trajectory performed by the AUV utilising the proposed motion control system (in magenta) and the reference trajectory (in blue), expressed in a North-East reference frame.

The errors between the relative orientation estimate and the null value are represented in Fig.10. Since the proposed algorithm is based on the planar fitting assumption, it is logical to expect larger estimation errors in the case of cylindrical surfaces because of the curvature of the structure. However, since the distance between the vehicle and the target should be 5 m for visibility reasons, the hypothesis of local planarity is still valid, and the errors result to be limited. Fig. 11 shows the normal distance error. After a short transient of ~ 50 s, the error converges to the null value. Once the inspection phase has begun, fluctuations with zero mean value are visible. These are related to the action of the control system which must simultaneously control orientation, normal distance, and depth of the vehicle. Nonetheless, as suggested by Fig.9, the proposed strategy is effective in replicating the curvature of the pylon.

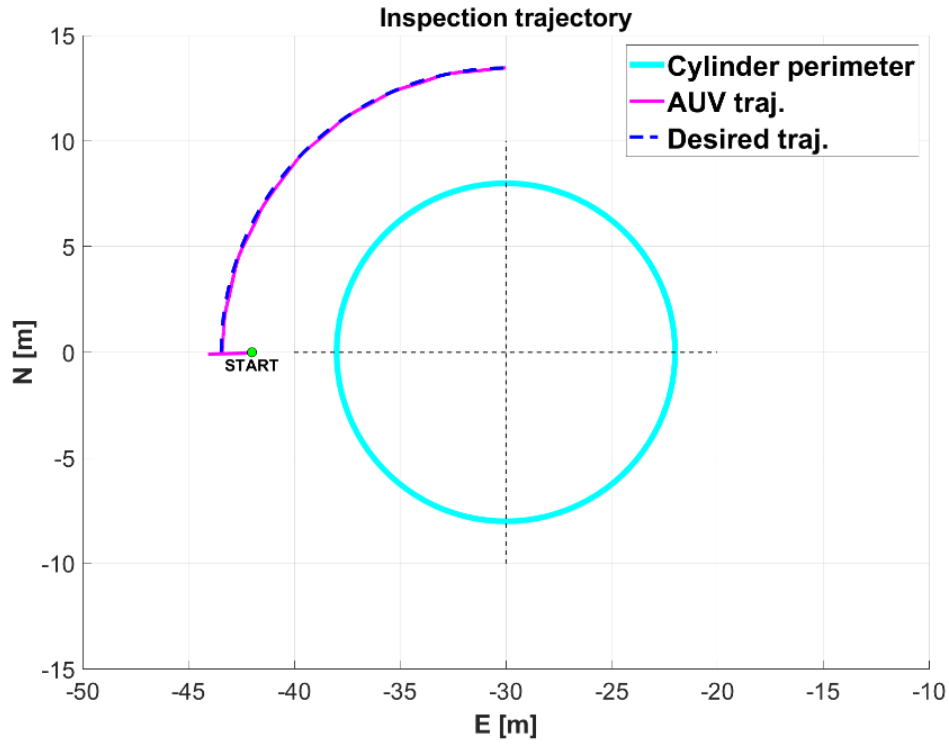


Fig.9: Pylon inspection: vehicle trajectory

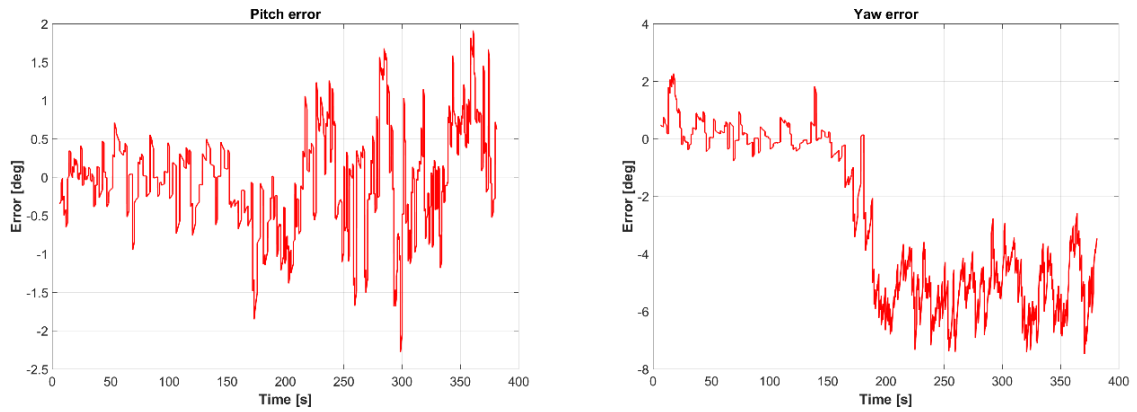


Fig.10: Trend of the relative orientation estimate errors

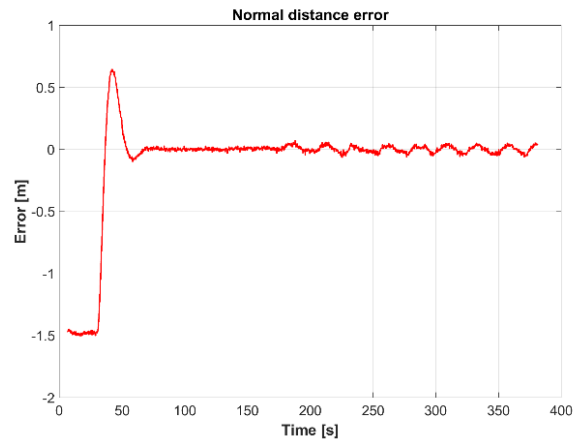


Fig.11: Depth and normal distance errors

4. Conclusions and future work

This work proposes a strategy for the employment of AUVs in underwater structures inspections without an a priori knowledge of the target shape. The developed system, based on observations from optical and acoustic payload, allows the vehicle to correct its relative orientation and normal distance with respect to the target to guarantee an adequate mapping and reconstruction of the inspected surface.

The performance of the developed system, in terms of estimation errors, have been evaluated on two different structures through simulations in a virtual marine environment. The obtained results show that the use of the developed strategy allows to perform the desired mission while maintaining the relative orientation and normal distance errors limited.

The performance of the developed system is strongly affected by visibility conditions of the underwater working scenario. Since many underwater structures are typically built far away from the coast, visibility conditions should not be too much prohibitive for exploiting the proposed system. However, not always a good visibility of the target is available, and an excessive water turbidity could jeopardise the mission with the risk of collision between the robot and the working environment. In this case, in addition to the proposed inspection technique, it is a good idea to exploit acoustic sensors which are not influenced by visibility conditions.

To improve the proposed approach, some aspects will need a further investigation. For example, different techniques for features fitting can be employed, maybe removing the planar surface assumption, so as to obtain reliable estimates even for more complex shapes. This could be useful for cylindrical structures, such as pylons.

The short-term objective is to test the developed system during at-sea experiments in a real marine scenario. To do so, we will implement a stereo visual odometry algorithm which allows to extract an estimate of the vehicle speed exploiting the video stream, thus enabling the control of the lateral speed of the AUV. Moreover, a technique for creating georeferenced mosaic will be developed, so as to proceed with the reconstruction of the inspected surface which represents the final goal of the work.

References

- BAY, H.; TUYTELAARS, T.; VAN GOOL, L. (2006), *SURF: Speeded up robust features*, Computer Vision - ECCV 2006, pp. 404-417
- CHOI, J.; LEE, Y.; KIM, T.; JUNG, J.; CHOI, H. (2017), *Development of a ROV for visual inspection of harbor structures*, IEEE Underwater Technology (UT), pp.1-4
- CHUNG, D.; HONG, S.; KIM, J. (2017), *Underwater pose estimation relative to planar hull surface using stereo vision*, IEEE Underwater Technology (UT), pp. 1-4
- DHOND, U. R.; AGGARWAL, J.K. (1989), *Structure from stereo - A review*, IEEE Trans. Systems, Man, and Cybernetics 19/6, pp.1489-1510
- FISCHLER, M.A.; BOLLES, R.C. (1981), *Random sample consensus: a paradigm for model fitting with applications to image analysis and automated cartography*, Communications of the ACM 24/6, pp.381-395
- FORESTI, G.L. (2001), *Visual inspection of sea bottom structures by an autonomous underwater vehicle*, IEEE Trans. Systems, Man, and Cybernetics, Part B (Cybernetics) 31/5, pp.691-705
- FOSSEN, T.I. (2002), *Marine control systems: guidance, navigation and control of ships, rigs and underwater vehicles*, Marine Cybernetics, Trondheim

- GELLI, J.; MESCHINI, A.; MONNI, N.; PAGLIAI, M.; RIDOLFI, A.; MARINI, L.; ALLOTTA, B. (2018), *Development and Design of a Compact Autonomous Underwater Vehicle: Zeno AUV*, IFAC-PapersOnLine 51/29, pp.20-25
- HONG, S.; CHUNG, D.; KIM, J.; KIM, Y.; KIM, A.; YOON, H.K. (2019), *In-water visual ship hull inspection using a hover-capable underwater vehicle with stereo vision*, J. Field Robotics 36/3, pp.531-546
- JACOBI, M. (2015), *Autonomous inspection of underwater structures*, Robotics and Autonomous Systems 67, pp.80-86
- KLEISER, D.; WOOCK, P. (2020), *Towards Automated Structural Health Monitoring for Offshore Wind Piles*, Global Oceans 2020: Singapore – U.S. Gulf Coast
- MAI, C.; PEDERSEN, S.; HANSEN, L.; JEPSEN, L.K.; YANG, Z. (2016), *Subsea infrastructure inspection: A review study*, IEEE Int. Conf. Underwater System Technology: Theory and Applications (USYS), pp.71-76
- McLEOD, D.; JACOBSON, J. (2011), *Autonomous UUV inspection — Revolutionizing undersea inspection*, Oceans'11 MTS/IEEE, Kona, pp.1-4
- MANHAES, M.M.M.; SCHERER, S.A.; VOSS, M.; DOUAT, L.R.; RAUSCHENBACH, T. (2016), *UUV simulator: A gazebo-based package for underwater intervention and multi-robot simulation*, Oceans 2016 MTS/IEEE, Monterey
- RIDAO, P.; CARRERAS, M.; RIBAS, D.; GARCIA, D. (2010), *Visual Inspection of Hydroelectric Dams Using an Autonomous Underwater Vehicle*, J. Field Robotics 27/6, pp.759-778

Using a Bridge Simulator for Hybrid Coupling of Manoeuvring and Engine Simulations

Wilfried Abels, Hamburg University of Technology (TUHH), Hamburg/Germany, w.abels@tuhh.de
Leif-Erik Gorris, Hamburg Port Authority AöR, Leif-Erik.Gorris@hpa.hamburg.de

Abstract

This paper shows how the problem of coupling different software systems was solved within the project "Gas Engine Performance". The task was to investigate how the engines and electrical system behave in detail under realistic manoeuvring conditions of a ship. For this purpose, a bridge simulator was used, which allows to perform manoeuvres in real-time with a "look and feel" as nautical personnel are used to. For this, it was necessary to couple software systems as different as a purely Unix-based manoeuvring tool, with a Windows-based Simulink software and the Unity-based VR-Engine. The paper describes how synchronization of parallel running systems with different time scales is handled and how the physical coupling of the bridge simulator is done with tools that were originally planned as desktop-only applications.

1. Introduction

The complexity of technical systems increases more and more. Especially in the field of naval architecture, it is important, to consider the interaction of all parts of the complete systems. Additionally, increasing requirements in environmental protection results in high development pressure. This paper is based on the project "Gas Engine Performance" as described in Wirz (2020). This project shows how technical problems become more and more to the point where the holistic interactions of the onboard installed systems are more and more relevant. That means, many questions of a single technical system like the power engine, the propeller and rudder can not be optimized alone. To optimize a single system, it is important to know how are the demands of the complete system. Within the mentioned project the task was to analyse how the gas engine will interact with the ship during manoeuvring.

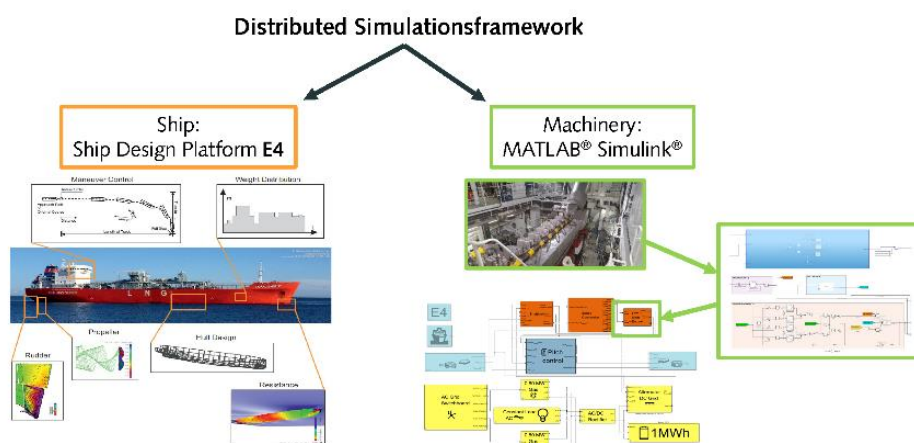


Fig.1: Simulation Framework, Jannsen (2020)

Therefore, it was necessary to have a system simulation of the gas engine and the ship. Both simulation techniques have been already available and a lot of research has been conducted on each of them respectively. The manoeuvring behaviour of a ship has been already developed and validated over the years, Haack (2006).

On the other hand, drive train engine simulations are also state of the art for new engine designs. Many of the utilized programs and models are proprietary which leads to a significant challenge with the

development of a generically applicable holistic simulation. Many of these simulation tools have been developed for a specific component and are often developed in a closed software environment. The coupling of proprietary models with the software of other component manufacturers is a relatively new concept and a “go-to” open-source solution has not yet been established.

Such a situation has been at the start point of the mentioned project. The TUHH “Department of Marine Engineering” has already done many investigations in the field of gas engines and the “Institute of Ship Design and Ship Safety” has done its developments in the field of ship design and manoeuvring. In principle, most features have been already developed. The ship design tool E4, *Krüger (2003)*, is a tool for the manoeuvring behaviour of a dedicated ship. The behaviour of a ship with the natural maritime environment can be simulated. In the same way, there are many simulation tools available for the behaviour of a gas engine in different use cases. But these tools have been developed for completely different tasks and in different software environments.

The ship design tool E4 has been developed in a Unix environment in FORTRAN. On the other hand, the complete engine simulation has been done within a Simulink environment based on Windows operating systems. This means that it is nearly impossible to integrate such tools directly into one monolithic system. A further challenge was that the time steps needed for the single simulation tools are completely different. The manoeuvring tool calculates with ten time-steps in a second, while the engine simulation needs much more time-steps per second to analyse the internal behaviour of an engine. An additional requirement was to have a real-time simulation controlled by a physical ship bridge. A human should steer the ship to have the possibility to simulate the behaviour of ship and engine in a quasi "real" environment with the human factor and not only through standardised automatic driving manoeuvres. These constraints result in the problem to build an interface structure that allows connecting all these parts of ship simulation, engine simulation and the hardware of the ship bridge.

To solve these boundaries a dedicated communication server has been implemented. This server handles the communication interfaces to the single parts of the simulation network. The communication during the simulation is handled by a classical TCP/IP connection between the single simulation tools and the communication server. This approach allows every tool to use its own environment.

2. The simulation network

To solve the problem of coordination of such different tools a central server has been implemented (the light green box in Fig.2). This server has the task to handle all the information which has been exchanged during every time step. Therefore, every tool has been upgraded with a TCP/IP interface that connected the single tool with the simulation server.

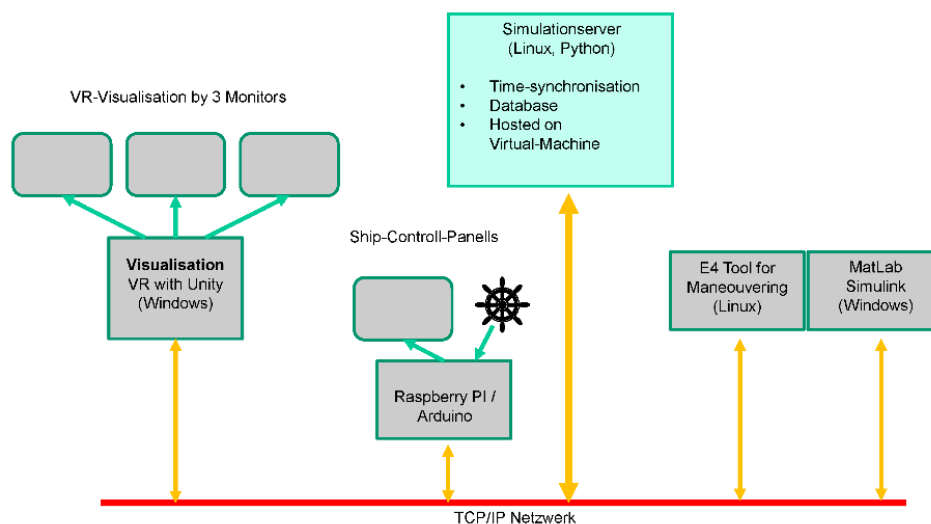


Fig.2: Simulation network set-up

The changes by the single tools have been very small. The main task was to do an additional subroutine call within the main loop of the simulation to exchange the information of the actual time-step. The numerical part of the software has not been changed. By this approach, it was possible to connect the different tools to a complex system for a mission simulation. In contrast to other bridge simulators, it is possible to do a manoeuvring simulation within a bridge simulator already during the design process. A classical bridge simulator needs its own data model which is generated exclusively for this bridge. Often a bridge simulator is only used after the ship has been already built and the behaviour of the real ship is known. In such a case you can use the bridge simulator for crew training. But it would be helpful to use such a bridge simulator already during the design stage of a ship.

In this design stage, it is necessary to do fast changes to a design. You have no resources to implement a complex model for an external bridge simulator. Our approach of coupling the specific design tools allows the direct integration of a human-controlled bridge. It is not necessary anymore to generate an adapted data model for the bridge simulator. The numerical manoeuvring kernel is the same as used during the design process. This approach has the advantage that changes are directly available within a nautical simulation with the bridge.

The consequences of specific design changes can be tested directly. For example, the used rudder of a ship should be changed. As fast as you have generated a new configuration for your project you can use the bridge simulator to get a feeling for the impact on the manoeuvring behaviour of the ship.

2.1. The simulation server

The simulation server is a network-based server implemented in Python. The task is to establish a connection to every part of the simulation network. This server handles the exchange of information and controls time synchronisation. The communication protocol is based on a TCP/IP socket where textual commands are sent and received. In principle, the communication can be controlled and debugged by a terminal-based connection like the classical Unix-tool “telnet”.

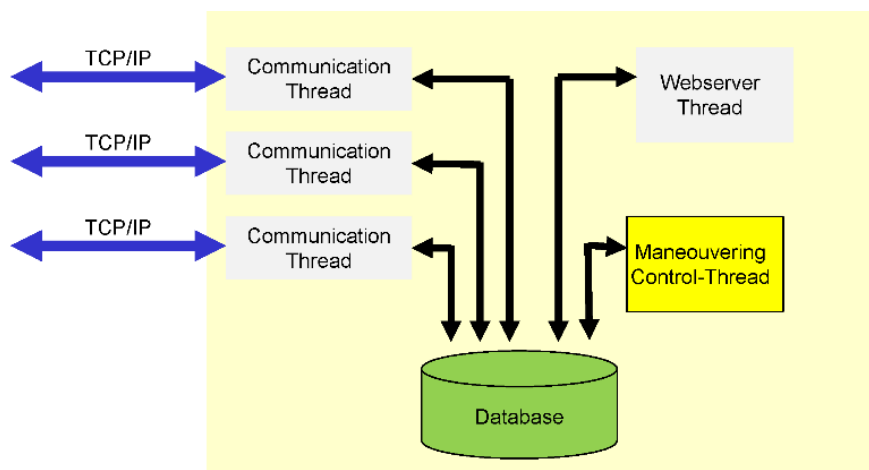
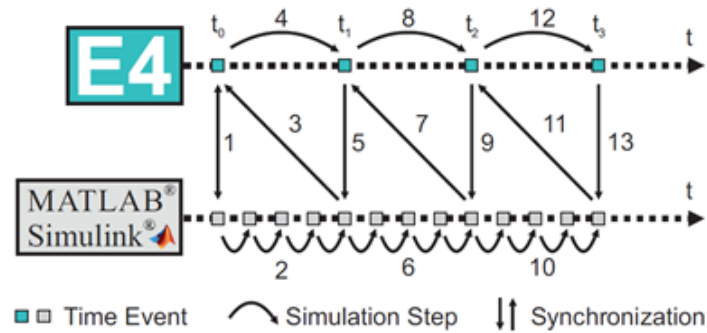


Fig.3: Structure of the simulation server

The server is a multi-threaded application for parallel communication with every separated simulation tool. Additionally, separated threads control a building web server and a central thread for controlling the manoeuvring simulation. The database is used to store all necessary state information. The machinery simulation needs ship information like propeller torque and power setpoint. Otherwise, the manoeuvring simulation depends on the actual train speed to calculate the thrust and velocity of the ship. A problem is that both simulation parts need different time scales for simulation. The machinery needs much faster time steps than the manoeuvring simulation. The mean value engine calculations for instance utilize different step sizes ranging from 10 Hz to 2000 Hz depending on the component composition.

The synchronization is handled by a token that is passed between the simulation tools. The calculation token is passed back only if enough time steps have passed that a further step for the inert ship behaviour has been reached, Fig.4. Parallel to this token passing, the simulation server has implemented a streaming function, used to communicate with the visualisation server. The server streams continuously a dataset of the ship-state (position, velocity, ...). In contrast to the numerical simulation of the interaction between ship and machinery, the visualisation needs no exact time synchronisation. Time variations of a few milliseconds are not noticeable for a human being who controls the ship. For a human being, it is much more important to perceive a smooth visualisation of the ship movement.



HyProS synchronization procedure

Fig.4: Simulation Framework, Jannsen (2020)

The last tool for the simulation network is the physical bridge and the input interfaces which resemble a real bridge setup. The bridge shown in Fig.5 was already available from a previous project. The bridge has been old and a repair has been necessary anyway. Therefore, we have been concentrated on the reuse of the mechanical control devices. On basis of a Raspberry Pi and Arduino board for an analogue-digital converter, we have captured directly the electronic signals from the control devices. The Raspberry Pi allows us to control the hardware devices and to implement the network connection to the simulation server. The state of all used control devices is propagated with 10 Hz to the database of the simulation server.

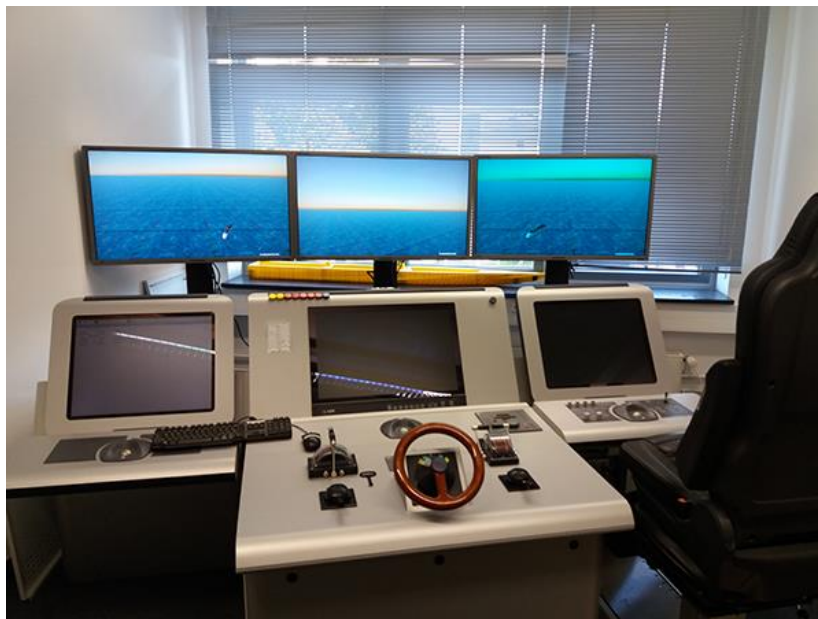


Fig.5: Bridge hardware used

During every simulation step, the manoeuvring tool gets the actual state of the bridge from that database and adapts the course of the simulated ship manoeuvre. At the end of a time step the actual ship state is propagated back to the simulation server and the visualisation can update the VR view from the bridge.

2.2. Ship design tool E4

The E4 ships design software has been already developed over many years and is proven in praxis on different yards; *Krüger (2003)*; *Krüger and Haack (2004)*. Over the years the software has continuously developed and validated. The focus was to build a software framework for ship design, where many different types of numerical methods have been developed and integrated into one system. This framework supports the ship designer, especially during the early design. The E4 software is not a monolithic software application. It consists of a set of many different tools working on the same project database. This concept has allowed different engineers and scientists to include their own knowledge in the E4 framework by developing a special method.

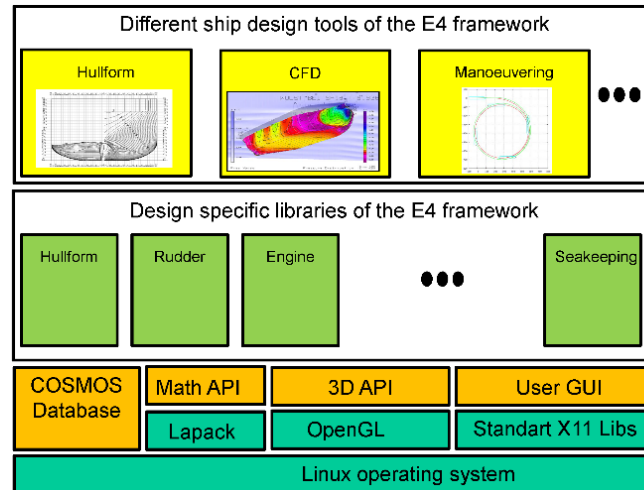


Fig.6: E4 ship design tool box

The E4 framework has already a manoeuvring method that is used for the analysis of the manoeuvring capability of a ship design already during the early design. Standard IMO manoeuvres like a turning circle or zig-zag manoeuvres are implemented and validated with build ships.

The aim to use a bridge simulator already during the early design is old and different investigation has been done already. *Abels and Greitsch (2008)* explain how this E4 framework has been used to couple the bridge simulator from FORCE Technology. Although this approach has shown that usage of a bridge simulator is possible during the early design, many problems have been still there. Even if it was possible to generate a data model for the used bridge simulator without using trial-trip data, the process of generating a ship model was not very comfortable. The main problem of two different numerical manoeuvring kernels have been still present and the behaviour of the ship within the bridge simulator is not the same as calculated by the ship designer.

This problem could be now solved. Since different manoeuvring cores are no longer used, there are no differences between the construction of a ship and manoeuvring on the bridge simulator. Further there is no effort anymore for conversion the data models from one simulator to another.

As explained, the manoeuvring has already implemented different types of standard IMO manoeuvres. To couple this tool with an external bridge the implemented auto-pilot has only been deactivated. Instead of the auto-pilot, the control instructions are now loaded from the database of the simulation server which gets the information from the Raspberry Pi of the physical bridge.

2.3. The Maneuvre and Drive-Train Simulation

The commercial and private ships utilize a broad set of different components in the drive train to power the propeller and generate sufficient thrust. A schematic drivetrain configuration of a gas tanker vessel

is presented in Fig.6. The propeller is driven via a propeller shaft at relatively low revolutions which is connected to a reduction gearbox (black box). The gearbox often has multiple connected shafts and can merge or divide power upstream or downstream for a wide range of possible devices or components. In this specific example, the other components are an electric machine (left) and a combustion engine on the right. The electric machine is connected to the electric grid with three combustion-engine-driven generator sets (“G”).

This example of a single-engine and single propeller configuration is one of the simpler configurations possible, more advanced concepts often utilize multiple interconnected drive trains, battery hybrid concepts or gas turbines. If one keeps in mind that usually almost every component is built and provided by a different manufacturer, the early design and dimensioning stage bears quite a challenge. Especially because very few information or simulation models are available before signing legally binding procurement contracts.

However, the performance of the full system is of great interest for the dimensioning and design, because fundamental design decisions (i.e. one or two engines, hybrid or conventional, 6 or 8 cylinder combustion engines,...) have a large impact on follow-up design decisions regarding the propeller and steering gear and the compartmentation. Some early dimensioning decisions are hardly reversible at a later stage.

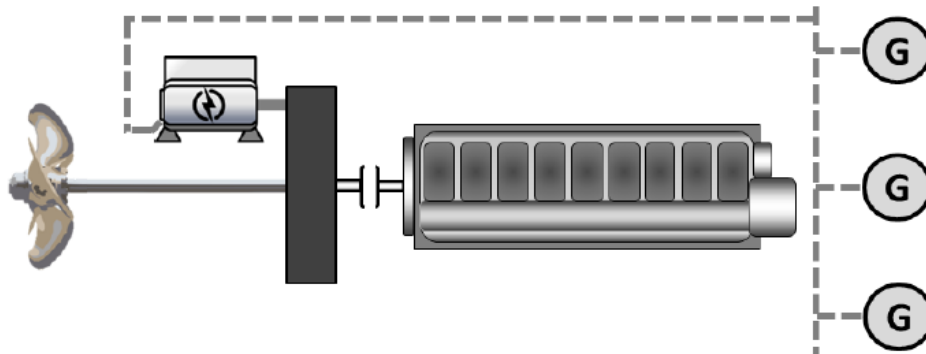


Fig.6: Drive train example

The endeavour of finding an optimal solution for the complex multi-variant design problem is tackled with a holistic full system simulation approach that utilizes a library of generic machinery component models, which are pre-tuned and represent a broad range of commercially available ones. While setting the scope on the early design stage the modular approach allows changing each model with a more detailed one once they are available.

Another benefit of the full system simulation becomes apparent if the ship's specification requires not only a matched design speed but also the ability to master complex manoeuvring situations: By connecting the machinery and the ship's hydrodynamical simulation via the TCP interface, the system "Ship" is digitally represented in full and the ability to withstand the manoeuvring specifications can be tested virtually. If utilized correctly, the system allows for a dimensioning and design of multiple technical systems now tailor-made for the unique manoeuvring specification.

The missing component to complete the three domains (ship, machinery and the human) is added by the VR visualization and the physical bridge simulator.

2.4. The virtual-reality visualisation with Unity™

For the visualisation of the view from the ship bridge, the Unity engine on a windows system was used. The Unity engine is a powerful framework for virtual reality (VR) development. This framework is based on the computer language C# and allows the engineer to implement complex VR scenarios. The framework offers all functionality for the visualisation of three-dimensional objects within a VR

environment. Texture mapping, the positioning of lights and the handling of different viewpoints is already available. The engineer has only to implement the behaviour of objects within such a VR scenario.

The visualisation has been implemented on a dedicated computer which has the only task to generate the real-time view out of the windows of the bridge, which are realized by three displays, Fig.7. One main task was to synchronize the visualisation with the numerical simulation. The numerical tools are synchronized by the simulation server exactly for every time step. The server uses a real-time clock for controlling the single tools in a way that one simulated second is also one real-time signal.

The visualisation engine has its own time scale. The main time scale for the visualisation is the frame rate of the graphic card. During every frame rate, the Unity engine has to generate the view for all three monitors of the bridge. This frame rate is independent of the simulation server. The important information for the visualization is the actual state of the ship. This information is sent by a continuous data stream from the server. Every data set has its timestamp which identifies the exact time. But this timestamp is always a bit in the past.

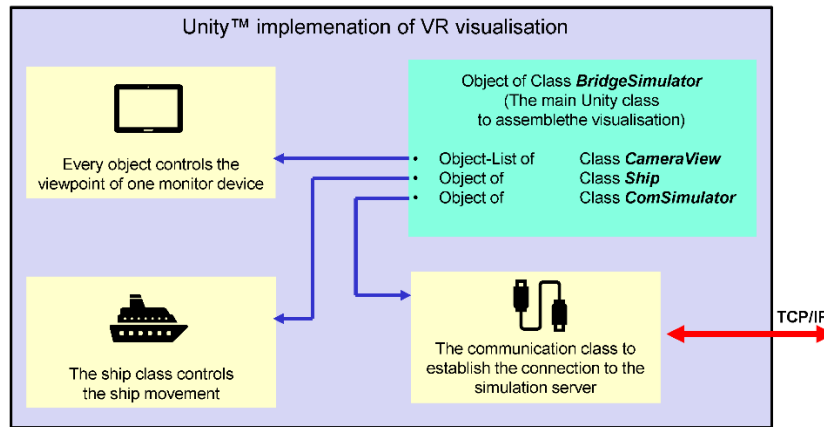


Fig.6: Structure of Unity Model

The latency is not big. The communication over TCP/IP is very fast. Therefore, this is no big problem especially since all parts of the simulation network are connected by a fast network with low latency. But there is a latency between the simulation and the visualization server. Further, the interval between two data packages is 10 Hz. But for a smooth view of the visualisation, the graphic card uses a frame rate above 50 Hz. If the visualisation would use the state information directly, the visualisation of the ship movement would be very bumpy and the user has no feeling of being on a “real” bridge. Therefore, it was necessary to interpolate the movement of the ship between the received data with separated time stamps from the past and the actual time of the visualization process. At the moment a simple linear extrapolation has been implemented for the movement of the ship:

$$\vec{x}_{actual} = \vec{x}_{last} + \frac{\vec{x}_{last} - \vec{x}_{last-1}}{t_{last} - t_{last-1}} \cdot (t_{actual} - t_{last-1})$$

This linear approach is not perfect because \vec{x}_{last} , \vec{x}_{last-1} , t_{last} , t_{last-1} changes every time a new data package is received. This means a small buckling still appears. But the movement of a ship is normally slow enough that this buckling is mostly not observable. Nevertheless, this is a point where the algorithm should be improved in the future.

3. The usage of the simulation network

After all these tools have been integrated a distributed simulation network is available where different types of simulations are possible. A primary advantage is to configure different types of simulation.

Because all tools are standalone modules, they can be used if necessary, but they can be deactivated if not needed. For example, the complete engine simulation is a very resource-intensive simulation. For a pure nautical manoeuvre simulation, it is often not important to know exactly the behaviour is within the engine.

The normal usage of the simulator network is to do a simulation in real-time. But this is not a must. The time steps are forced by the central simulation server. The time steps can be synchronized with real-time. If a particular situation is to be analysed in detail and the models used are so complex that hardware resources do not allow them to be calculated in real-time, the simulation can be slowed down. On the other hand, it could be useful to speed up the simulation time for example in a case where no detailed engine simulation is necessary and someone is only interested in a classical turning circle controlled by an autopilot. In such a case the simulation can run much faster than in real-time.

Most of the modules can be activated or not. For example, the bridge controls implemented by the Raspberry Pi can be used in the same way as the build-in autopilot of the manoeuvring method of the E4 design tool. In the same way, the engine simulation can be used to do detailed analyses regarding the engine behaviour during a nautical manoeuvre. But if the behaviour of the ship is in the focus of a simulation, the engine can be often adapted by a model with less complexity. By this modular concept, it is possible to use the simulation tools in that context a design engineer needs them. During the early design, the tool can be used as all other design tools. It can be used as a standalone tool on the desktop computer of the engineer. On the other hand, it is possible to do a distributed system simulation with the usage of the physical bridge.

4. Summary

The coupling of tools over the border of different software systems like Unix and Windows systems is not easy, because the porting of software is mostly a difficult or impossible approach. Nevertheless, it is more and more necessary to do technical system analyses where no single software system is available which can represent all important subsystems.

This paper has shown a project where the coupling of different types of such tools has been solved by implementing an additional network layer for the communication on a TCP/IP connection. Independent from the software environment of the needed tools a central server has been implemented to establish a continuous data exchange to every tool. This server allows data exchange and synchronisation of the simulation loop between the tools.

By this approach, it was possible to realize a system simulation during the early design of a ship project. The Unix based ship manoeuvring tool could be coupled with a detailed engine simulation based on a Windows MatLab/Simulink tool. Additionally, a coupling with a physical bridge and a Unity-based VR visualisation has been integrated. By doing this, it is now possible to do a human-controlled bridge simulator for nautical manoeuvres during the early design. The approach of open network communication is open for further developments. To connect new functionality can be realized by upgrading tools with a small TCP/IP interface.

References

- ABELS, W.; GREITSCH, L. (2008), *Using a Bridge Simulator during the Early Design-Stage to Evaluate Manoeuvrability*, 7th Conf. Computer and IT Applications in the Maritime Industries (COMPIT), Liège
- HAACK, T. (2006), *Simulation des Manövrierverhaltens von Schiffen unter besonderer Berücksichtigung der Antriebsanlage*, Dissertation, Hamburg University of Technology, Hamburg
- JANNSEN, L.E. (2020) *Development of a Simulation Environment for Hybrid Propulsion Drive Trains*, 39th Int. Conf. Ocean, Offshore & Arctic Engineering, Fort Lauderdale

KRÜGER, S. (2003), *The Role of IT in Shipbuilding*, 2nd Conf. Computer and IT Applications in the Maritime Industries (COMPIT), Hamburg

KRÜGER, S.; HAACK, T. (2004), *Design of propulsion control systems based on the simulation of nautical manoeuvres*, 9th Symp. on Practical Design of Ships and Other Floating Structures (PRADS), Lübeck-Travemünde

WIRZ, F. (2020), *Optimization of the transient performance of gas-driven ship propulsion plants*, FVV-Informationstagung 2020, Würzburg, pp.131-162

A Hull Form Design System Suitable for Machine Learning That Integrates Deformation, Data Structure, and Analysis

Yasuo Ichinose, National Maritime Research Institute, Tokyo/Japan, ichinose@m.mpat.go.jp
Tomoyuki Taniguchi, National Maritime Research Institute, Tokyo/Japan, taniguchi-t@m.mpat.go.jp

Abstract

This paper proposes an integrated design method using machine learning based on a database of structured grids on hull surfaces. Machine learning requires a high-quality, large database, therefore the learning database should be created and stored efficiently and preferably automatically. In addition, the data format should be flexible so that a designer can incorporate a hull form manually made in CAD. This paper demonstrates a design example of a machine learning design method using the Imaged Hull surface Representation method and the Convolutional Neural Network and discusses the effectiveness of this method in ship design.

1. Introduction

There has been a growing interest in hull form design because of the increase in fuel costs due to the use of alternative fuels in the near future and the recent rising oil prices caused by imbalance in supply and demand. What is required for hull form design in next generation is faster and more efficient design method, and automation of hull form design that does not rely on tacit knowledge.

The current mainstream of hull design is Simulation Based Design (SBD), which generally consists of three design systems: performance evaluation tool, shape deformation tool, and optimization tool, e.g. *ITTC (2008)*. For each of the three optimization tools, detailed research is being conducted. From a practical standpoint, particular emphasis has been placed on the problem of speeding up the design process. For example, *Kandasamy et al. (2011)* proposed a method called multi-fidelity optimization, which combines potential-based Computational Fluid Dynamics (CFD) (low-fidelity) and Reynolds averaged Navier Stokes (RaNS)-based CFD (high-fidelity). In this method, global optimization with a wide design space is first performed by potential-based CFD, and then detailed hull form optimization with a narrow design space is performed by RaNS-based CFD based on the results of global optimization. In this way, potential-based CFD and RaNS-based CFD are used alone or in combination as performance evaluation tools in SBD. However, it is still a challenge to design optimal hull form with practical computation time.

On the other hand, as an effort to formalize tacit knowledge, a lot of efforts has been put into applying machine learning techniques to ship design. In early 2000, *Matsumura and Ura (1998)* applied Artificial Neural Network (ANN) technique to predict wave making resistance from the input parameters of ship length, width, Froude number. Following this, *Kanai (2000)*, *Mesbahi and Bertram (2000)*, *Bertram and Mesbahi (2004)* and *Mason et al. (2005)* presented some models to predict calm-water propulsive performances using ANNs. These ANNs handle only up to 10 input parameters of principal dimensions that cannot represent complex three-dimensional hull forms. *Radojcic and Kalajdzic (2017)* proposed an ANN model to estimate resistance and trim based on the systematic generated hull form database, and *Margari et al. (2018)* also modeled another series tank-test results. Although the ANN technique has been advanced in the last 20 years, input parameters of these models are still dimensional information of ship, such as lengthbeam ratio, slenderness ratio, longitudinal center of gravity (LCG). *Kazemi et al. (2021)* designed a stepped planing craft using ANN trained by CFD database, which can estimate resistance from loading weight, LCG position, step type and step position. In this model, some local shape parameters began to be applied that is easy to parameterize in the hull form. *Cepowski (2020)* applied an ANN to estimate added resistance by means of ship's principal dimensions, block coefficient and Froude number. However, these machine learning methods are limited in the number of input parameters and have not yet been able to capture the detailed local shape of hull form.

To attempt to capture the local shape of hull form by machine learning, *Ichinose and Taniguchi (2021)* proposed wake field prediction method by Imaged Hull surface Representation method (IHR). The limitation of input parameters of machine learning is caused by overfitting problem in conventional neural networks. Convolutional Neural Network (CNN) widely used for image analysis contribute to solve the problems and enable to increase input parameters and capture detail shape of hull form. The IHR utilizes a structured grid on the hull surface to represent a hull with more than 20,000 data and is suitable for learning data of CNN that can overwhelm the overfitting problem. This CNN model can predict wake field on the propeller plane with acceptable accuracy for hull form and propeller design. Based on the IHR, it may be possible to formalize the relationship between the detailed shape of the three-dimensional phase of the hull form, the propulsive performance, and the flow field by analyzing the hull form database not only with the flow field but also with the propulsive performance using machine learning.

This paper proposes a hull form design method based on machine learning as one of the design methods that contribute to reducing the time and the automation of hull form design. This method is characterized by the fact that this design method directly constructs a hull form database from the structural grid of the hull surface in Computational Fluid Dynamics (CFD) and integrates this database into all of the shape deformation, CFD evaluation, and machine learning operations. In the deformation, hull form blending enables deformation with a high degree of freedom and easy incorporation of past existing hull forms. In addition, CFD calculations are faster than those on unstructured grids, which is necessary for database (DB). Furthermore, in machine learning, the application of the CNN method has made it possible to represent the hull form with a much larger number of data points than before, thereby improving the estimation accuracy and extending it to the detailed hull form, which was previously limited to the selection of the principal dimensions. This paper also demonstrates a design example of the machine learning design method using the IHR and the CNN and discusses the effectiveness of this method in ship design.

2. Overview of the proposal design method

The present design method has been developed as an effort to formalize tacit knowledge of designers by analyzing a pre-prepared RaNS-based CFD hull form database using IHR as the basic technology through machine learning. This design system is a hull form design system suitable for machine learning that integrates deformation, data structure, and analysis.

In order to use machine learning methods in practical design, it is necessary to increase the hull form database intermittently in daily design practice. In conventional SBD, as in Fig. 1, most hull form data produced in optimization process has been deleted except the one for final product after a design process completed. The few hull form data survived in former studies is used as initial hull forms for the next design process, while almost all other hull forms are discarded. This hinders the implementation of ship design based on machine learning, which requires a large amount of training data.

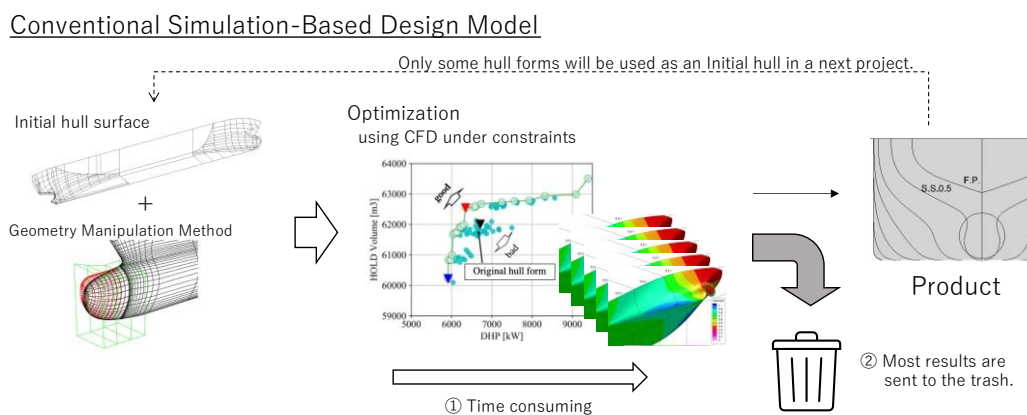


Fig.1: Challenges in conventional simulation-based design model

In a hull design method based on machine learning, it is necessary to have a mechanism to increase the hull database efficiently in daily design. For this, the following factors need to be considered.

- Data structure: how to make a database
- Database analysis methods: differences in analysis methods depending on data structure

The proposal design method employs the Imaged Hull surface Representation (IHR) as data structure on database, which has equivalent data structure to the structured grid on the hull surface in CFD. This data structure of database has following two advantages for creating database. First, as for CFD simulation, the calculation time of the structural grids tends to be shorter than that of the unstructured grids so that the database can be generated efficiently, since the third-order interpolation of the influx term enables reducing the number of grids and shortens the calculation time, *Ohashi et al. (2019)*. In addition, the use of an overset grid can also consider energy-saving devices. Second, to create various hull forms automatically, Adaptability of hull form deformation methods is essential for the data structure of hull form. Since the hull surface is treated as a point group in the IHR, various methods such as the *Lackenby (1950)* method, Free Form Deformation, *Sederberg and Parry (1986)*, *Peri and Campana (2008)*, and hull form blending (morphing) create a new hull form by mixing a plurality of hull forms can be easily adapted. Furthermore, the use of segmented meshes provides the flexibility for designers to incorporate hand-made CAD hull forms into the database.

The hull form blending method is a method of generating a hull form from some basic hull forms. When the N -th basic hull forms are represented by resolvable discrete surface points (\vec{P}_i) – e.g., grid points on hull surface in CFD –, new hull form (\vec{P}) is obtained by the operation of Eq. (1) in the hull form blending method like Fig.2.

$$\vec{P} = \sum_{i=0}^N a_i \vec{P}_i \quad (1)$$

where $\sum_{i=0}^N a_i = 1$

When N is 2, two-hull ship blending can be realized by the following equation:

$$a_1 = \alpha, a_2 = (1 - \alpha) \quad (2)$$

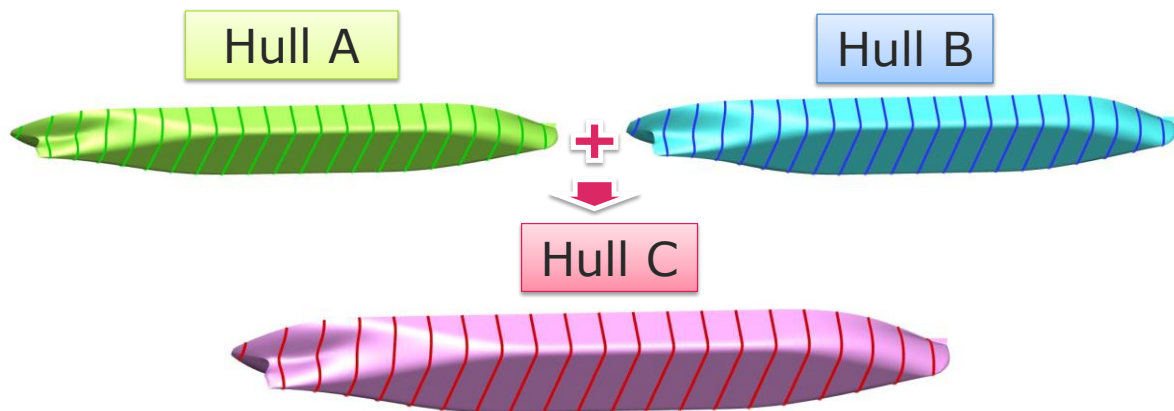


Fig.2: Image of hull form blending (morphing)

By adopting specific hull forms that designers manually create with some intention as basic hull, the hull form blending method enable to visualize the changes of propulsive performance and flow fields and help us recognize the relation between hull form and performance, *Ichinose et al. (2017)*.

The present design method adopts the CNN as a database analysis method to predict propulsive performance like wave-making resistance, form factor, and self-propulsion factor, and estimate flow field around ship aiming to preventing acoustic noise or vibration generated by revolution of a propeller. Although the CNN prediction method can handle unparametrized hull form database, parametrized hull form database help designer to understand the nature of physical phenomena by visualizing the performance distribution in design space. In the present method, hull form blending method is applied for organizing unparametrized data to be parametrized and visualized as shown in Fig.3. This will contribute to understand the characteristics of hull form and propulsive performance and contribute to the formalization of tacit knowledge of designers.

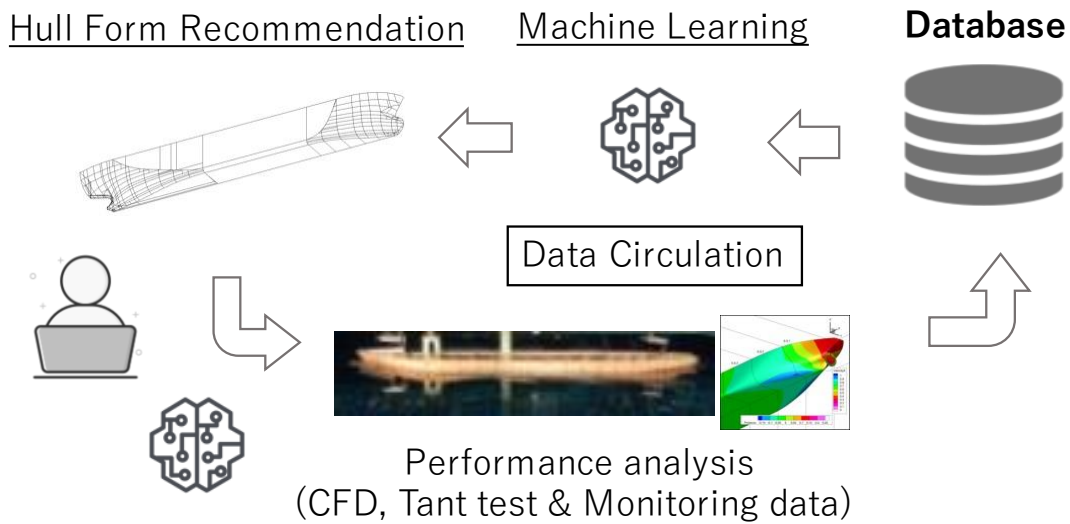


Fig.3: Data flow in the present design system with machine learning

3. Data structure of hull form database

For the data structure of the database, the IHR based on the structured-hull-surface grid is adopted to use for analysis in CNN. The IHR has several additional advantages as a data structure in database creation and storage. Machine learning requires a high-quality, large database, therefore the learning database should be created and stored efficiently and preferably automatically and should also be flexible so that a designer can incorporate a hull form manually made in CAD. In this regard, the utilization of the structured hull surface grid is invaluable as the data structure of the learning database.

Fig.4 shows an overview of the IHR. The main point of the representation is the two-dimensional grid format of the hull surface. A structured grid based CFD format has the same structure as the image data. The image data are represented by three primary colors (cyan, magenta and yellow) on the vertical (i) and horizontal (j) pixels. The hull-form structured grid is also expressed as $i \times j$ structure data with (x, y, z) coordinates, which have the same data structure as the three primary colors in the image data.

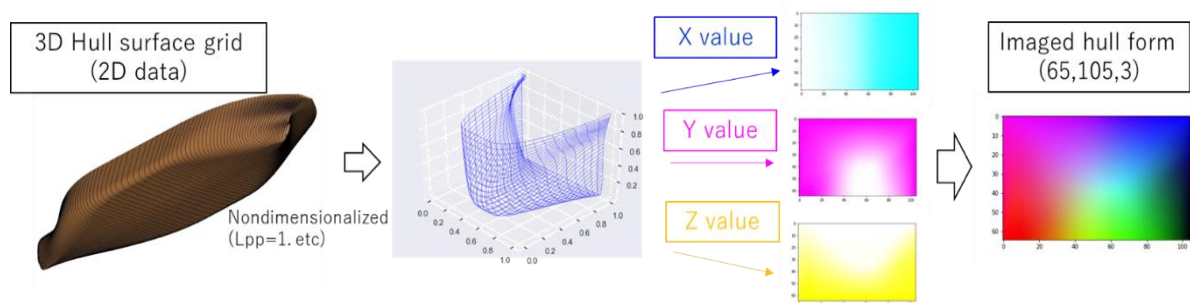


Fig.4: Imaged Hull surface Representation method

For ANNs, this representation has two advantages over the conventional parametric hull-form representation method. First, this representation has a higher degree of freedom in hull-form expression than do conventional hull-form representations based on hull parameters. The proposed method can practically describe any curved surface with no limitations. Second, data augmentation can be achieved by placing different grids on the same hull form. In general, the number of CFD results is often limited, but machine learning needs large amounts of training data. Given that the number of grids of the database is sufficient and the CFD calculation result converges to the correct value even if the grid arrangement is changed, the proposed method can use data augmented by creating multiple grids with different hull surface grids from a single CFD calculation result.

4. Database analysis methods

Taniguchi and Ichinose (2020) presented the wake field prediction method utilizing Convolutional Neural Network. The present method extends this architecture to prediction of propulsive performance components predict propulsive performance like wave-making resistance, form factor, and self-propulsion factor.

The architecture of the proposed CNN that predicts each propulsive performance components is shown in Fig.5. This model is built this model referencing the Generative Adversarial Networks (GAN) model proposed by *Radford et al. (2016)* and adjusting the convolution layer and filter size to applied to our hull surface data. In Fig.4, the rectified linear unit activation function (ReLU) is a commonly used activation function in CNNs, and batch normalization (BN) is a technique for standardizing data to accelerate neural network training. In this architecture, the imaged hull-form data of the input data is on the left-side of the figure, and the model generates the value of the stern wake flow on the right-side. The first three processes in this model imply convolution operations to extract the high-level feature of each hull form, and the dense processes indicate fully connected layers to learn non-linear combination of the high-level features as represented by the output of the convolutional layers. The proposed CNN was coded using Keras, <https://github.com/fchollet/keras>.

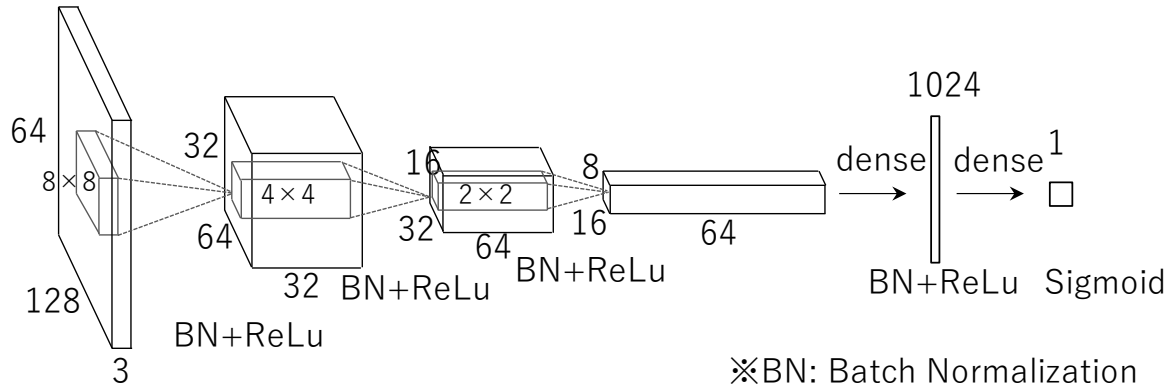


Fig.5: CNN architecture of present prediction

In the training of this CNN model, mean square errors (*MSE*) of each of the flow velocity is applied to the loss function; *MSE* is defined by Eq. (3).

$$MSE = \frac{1}{n} \sum_{i=0}^{n-1} (y_i - \hat{y}_i)^2 \quad (3)$$

where y_i are the ground truth values, \hat{y}_i predicted values of each hull form, and n the number of data available for the training. As the solver of optimization to reduce the loss function in the training, Adam method, *Kingma and Ba (2015)*, is applied in the present research. The learning rate is 2×10^{-4} in the referenced paper, *Radford et al. (2016)*, but because the number of images available for

learning is limited, the learning rate of the present paper is set to 1×10^{-6} through trial and error observing the loss function of training and validation data.

Based on this method, hull form recommendation in Fig.2 can be realized in the following two ways. First, this machine learning model replaces CFD tool in conventional Simulation Based Design (SBD) methods. That enables reduction of the design time to fit within a practical design time, since the average prediction speed of the machine learning model is more than 100,000 times faster than that of RaNS based CFD, *Ichinose and Taniguchi (2021)*. The other unique method is to find the hull form from the ideal wake flow by solving the inverse problem of predicting the wake field from the hull form. *Ichinose and Tahara (2019)* proposed a wake design system using hull form database for ESD design as shown in Fig.6. The system analyzes the pre-built hull form and flow field database using a combination of the nearest neighbor method and the hull form blending method and obtains the specific shape of the hull form that realizes the desired wake flow as the output of the system. Ichinose demonstrated the design a hull form with a suitable companion current for ESD and achieved output power reduction with ESD in a tank test by the system.

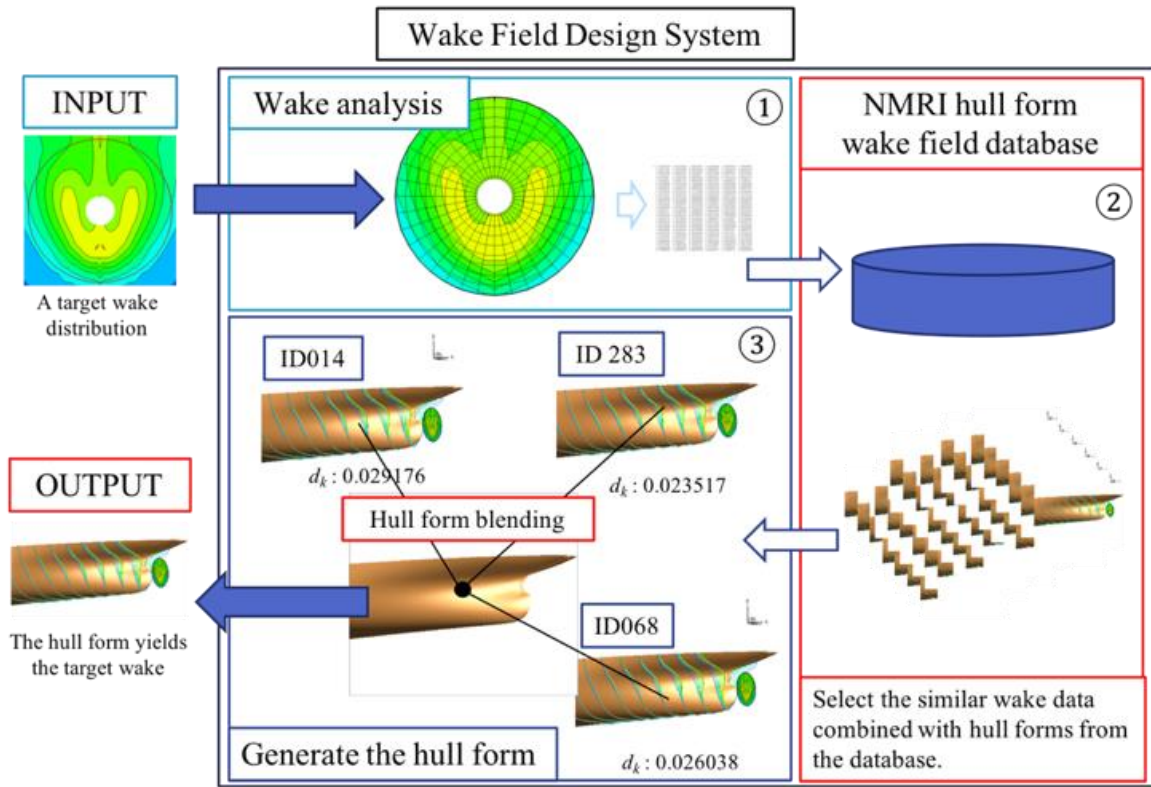


Fig.6: The overview of a wake field design system, *Ichinose and Tahara (2019)*

4. Results

This chapter demonstrates the effectiveness of the present method by conducting a trial prediction and design. The dataset of the present study is the domestic 749 GT dataset, which contains 2,730 hull forms and double-model resistances, which is solved by the three-dimensional incompressible Reynolds averaged Navier Stokes (RaNS) equation. An in-house structured CFD solver, NAGISA, *Ohashi et al. (2019)*, was employed to solve the discretized RaNS equation with one-equation turbulent model, modified Spalart-Allmaras (MSA). This solver and turbulence model are normally used for hull form design at NMRI to estimate model-scale flow field. The calculation grids of basic hull forms without any appendages at full loads and even keels were generated with HO topology, 0.9 million cells in half side ($i \times j \times k = 174 \times 64 \times 80$) at model scale. On the center plane of the hull, a symmetry condition is assigned, and the result is mirrored after the calculation. The minimum spacing normal to wall is set to be $y^+ < 1.0$ for constant $R_\eta = 1.0 \times 10^7$. The effect of free surface is considered to

be small and ignored in all cases. An investigation on grid uncertainty for this calculative configuration was carried out in the previous study, *Ichinose and Tahara (2019)*, and we judged that the present grids have the same acceptable uncertainty level as in this research. The main dimensions of this dataset are presented in Table I; only the aft part (from S.S. 3.0 to the aft end) is deformed, Fig.7.

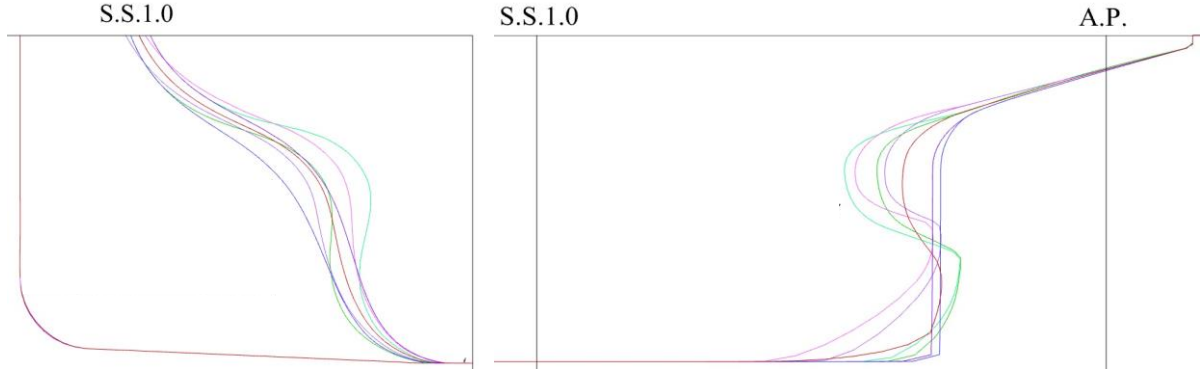


Fig.7: Examples of frame lines at S.S. 1.0 and aft profiles of hull forms in the dataset

Table I: Main dimensions of the 749 GT general cargo dataset

Ship length: L_{PP}	79.0 m
Ship Breadth: B	13.0 m
Design Draft: d	4.7 m
Block coefficient: C_B	0.72

The 2,730 CFD dataset mentioned here is randomly divide by two components: training set, and test set. The 20% of all 2,730 dataset (564) is held out as test set which is used to provide an unbiased evaluation on a final model. The other 80% (2,184) data is used for training of the present CNN model to determine the parameters, this set is called training set.

The training set is used for training of the present CNN model, and it takes about 10 minutes for 2,000 epochs using a computer equipped as follows: CPU: AMD EPYC 7302P (16 Core, 3Ghz) $\times 1$; GPU: NVIDIA RTX3090 24GB Memory GPU $\times 2$. In the training, the training set (2,184) is divided further as 90% (1,966) training data and 10% (218) validation data, randomly. This validation data is used to predict the response of the fitted model which is trained by the training data.

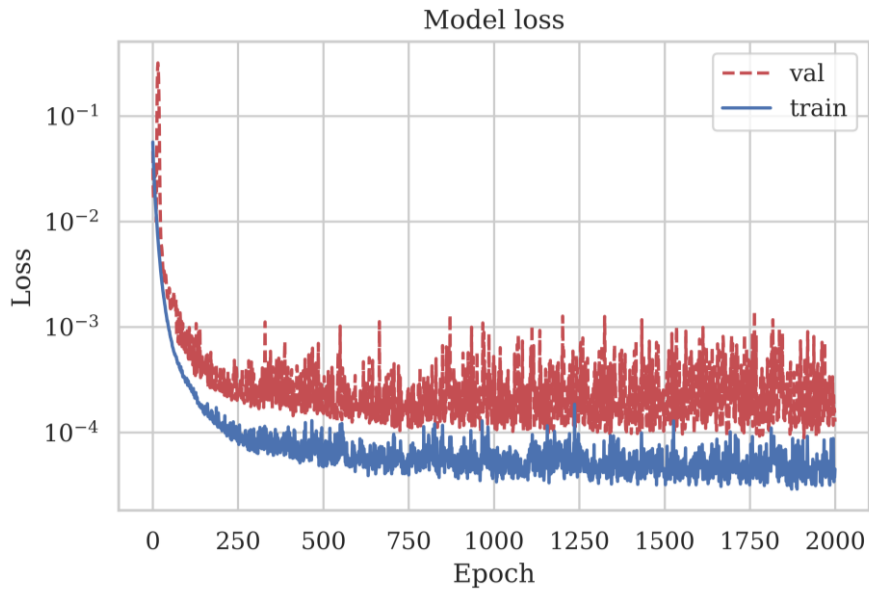


Fig.8: Loss function convergence history for proposed CNN

Fig.8 shows a convergence history for the loss function of the proposed CNN. The abscissa represents epochs, which is the number of times all the training vectors are used once to update the weights, the ordinate represents the loss function value, and *train* and *val* present historical training and validation data, respectively. The convergence history shows that overfitting did not occur with the proposed CNN on this training data.

Fig.9 reveals the distribution of the variance of the prediction resistance results of the present model, the distribution of the prediction results of the present model for test set (564). The graph indicates that the difference between the prediction results and test set is almost entirely within the range of $\pm 0.25\%$, which is sufficiently acceptable for practical design.

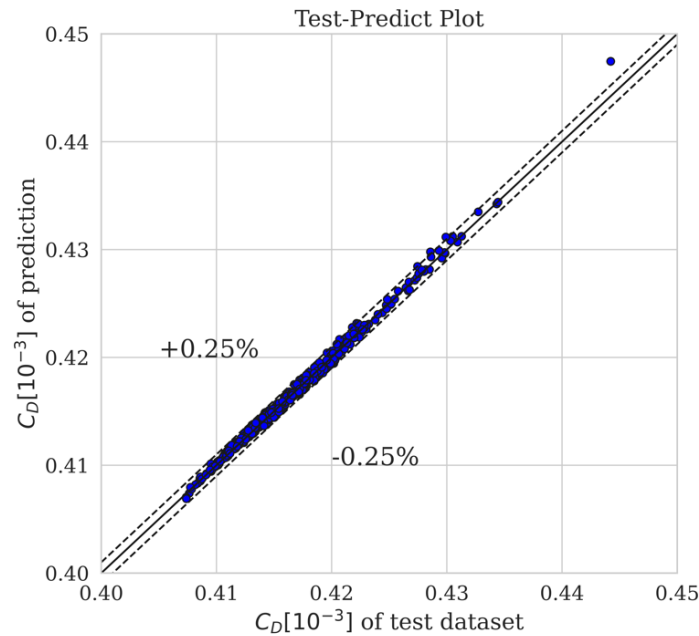


Fig.9: Distribution of the prediction results of resistance for test datasets

Fig.10 shows the histogram of the difference between test data and a predicted value for the test set. The difference is normalized by minimum and maximum values of all datasets and presents in percentage expression. The standard deviation is 0.008 and most of the test data is placed within 0.02.

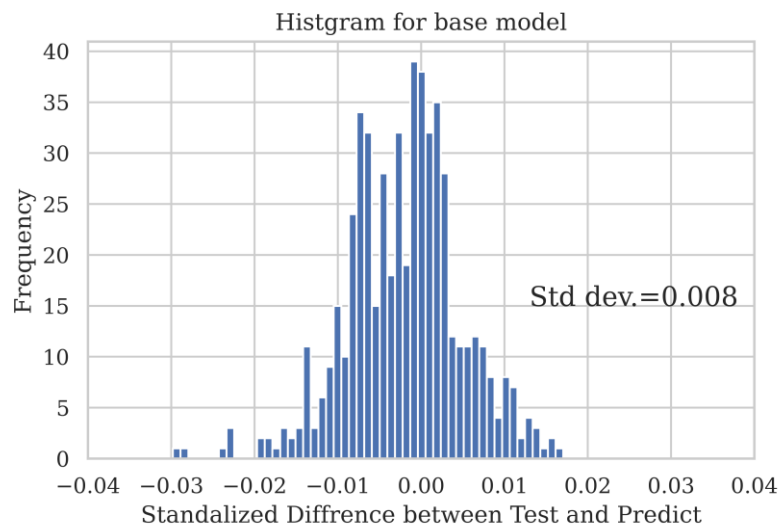


Fig.10: Histogram of difference between test and predict value of resistance

The average estimation speed for each hull form prediction is approximately 0.001 seconds, which is more than 100,000 times faster than are physics-based simulations, which require approximately an hour for each prediction. It will be necessary to determine whether this model can be adapted to other performance parameters, such as the self-propulsion factors, and how general and accurate it is, by accumulating more data.

5. Concluding Remarks

This paper proposed a hull form design method based on machine learning as one of the design methods that contribute to reducing the time and the automation of hull form design. This method is characterized by the fact that this design method directly constructs a hull form database from the structural grid of the hull surface in CFD and integrates this database into all of the shape deformation, CFD evaluation, and machine learning operations. In the deformation, hull form blending enables deformation with a high degree of freedom and easy incorporation of past existing hull forms. In addition, CFD calculations are faster than those on unstructured grids, which is necessary for DB. Furthermore, in machine learning, the application of the CNN method has made it possible to represent the hull form with a much larger number of data points than before, thereby improving the estimation accuracy and extending it to the detailed hull form, which was previously limited to the selection of the principal dimensions.

The demonstration of the present method shows that the model can predict resistance within $\pm 0.25\%$ for the domestic 749 GT dataset.

Acknowledgements

This work was partially supported by JSPS KAKENHI Grant Number 20K04954.

References

- BERTRAM, V.; MESBAHI, E. (2004), *Estimating Resistance and Power of Fast Monohulls Employing Artificial Neural Nets*, 4th HIPER Conf., Rome, <http://data.hiper-conf.info/Hiper2004/Rome.pdf>
- CEPOWSKI, T. (2020), *The prediction of ship added resistance at the preliminary design stage by the use of an artificial neural network*, Ocean Eng. 195, <https://www.sciencedirect.com/science/article/pii/S0029801819307772>
- ICHINOSE, Y.; TAHARA, Y. (2019), *A wake field design system utilizing a database analysis to enhance the performance of energy saving devices and propeller*, J. Marine Science Technology 24, pp.1119-1133, <https://link.springer.com/content/pdf/10.1007/s00773-018-0611-x.pdf>
- ICHINOSE, Y.; TAHARA, T.; KUME, K. (2017), *A construction and evaluation of hull form database for domestic vessels with regulation on gross tonnage—development of a prototype for 749 GT-type domestic general cargos*, (in Japanese), J. Japan Soc. Naval. Arch. Ocean. Eng. 26, pp.51-62
- ICHINOSE, Y.; TANIGUCHI, T. (2021) *A curved surface representation method for convolutional neural network of wake field prediction*, J. Marine Science and Technology <https://doi.org/10.1007/s00773-021-00857-3>
- ITTC (2008), *Final report and recommendations to the 25th ITTC*, Resistance Committee, 25th Int. Towing Tank Conf., Fukuoka
- KANAI, K. (2000), *Application of the Neural Network to Estimate of Ship's Propulsive Performance and Hull Form Optimization*, (in Japanese) Trans. West-Japan Society of Naval Architects 99, pp.1-1

- KANDASAMY, M.; PERI, D.; OOI, S. K.; CARRICA, P.; STERN, F.; CAMPANA, E. F.; COTE, O. P.; MacDONALD, N. (2011), *Multi-fidelity optimization of a high-speed foil-assisted semi-planing catamaran for low wake*, J. Marine Science and Technology 16/2, pp.143-156
- KAZEMI, H.; DOUSTDAR, M.M.; NAJAFI, A.; NOWRUZI, H.; AMERI, M.J. (2021), *Hydrodynamic Performance Prediction of Stepped Planing Craft Using CFD and ANNs*, J. Marine Science and Application 20, pp.67-84
- KINGMA, D.P.; BA, J. (2015), *Adam: a method for stochastic optimization*, CoRR, [1412.6980v3.pdf \(arxiv.org\)](https://arxiv.org/abs/1412.6980v3)
- LACKENBY, H. (1950), *On the systematic geometrical variation of ship form*, Trans. RINA 92, pp. 289-316
- MARGARI, V.; KANELLOPOULOU, A.; ZARAPHONITIS, G. (2018), *On the use of Artificial Neural Networks for the calm water resistance prediction of MARAD Systematic Series' hull forms*, Ocean Eng. 165, pp.528-537, <https://www.sciencedirect.com/science/article/pii/S002980181830876X>
- MASON, A.; COUSER, P.; MASON, G.; SMITH, C.R.; KONSKY, B.R. von (2005), *Optimisation of Vessel Resistance using Genetic Algorithms and Artificial Neural Networks*, 4th COMPIT Conf., Hamburg, http://data.hiper-conf.info/compit2005_hamburg.pdf
- MATUMURA, T.; URA, T. (1998), *Preliminary Planning of Ship Hull Form based on Artificial Neural Networks (1st Report) -Estimation of Wave Making Resistance for High-Speed Ships*, (in Japanese), J. Society of Naval Architects of Japan 183, pp.91-100
- MESBAHI, E.; BERTRAM, V. (2000), *Empirical design formulae using artificial neural nets*, 1st COMPIT Conf., Potsdam, pp.292-301, http://data.hiper-conf.info/compit2000_potsdam.pdf
- OHASHI, K.; HINO, T.; KOBAYASHI, H.; ONODERA, N.; SAKAMOTO, N. (2019), *Development of a structured overset Navier–Stokes solver with a moving grid and full multigrid method*, J. Marine Science and Technology 24, pp.884-901, <https://doi.org/10.1007/s00773-018-0594-7>
- PERI, D.; CAMPANA, E.F. (2008), *Variable Fidelity and Surrogate Modeling in Simulation-Based Design*, 27th Symp. Naval Hydrodynamics, Seoul
- RADFORD, A.; METZAND, L.; CHINTALA, S. (2016), *Unsupervised Representation Learning with Deep Convolutional Generative Adversarial Networks*, 4th Int. Conf. Learning Representations, San Juan
- RADOJCIC, D.; KALAJDZIC, M. (2017), *Resistance and Trim Modeling of Naples Hard Chine Systematic Series*, Int. J. Small Craft Technology 160, pp.31-41
- SEDERBERG, T.W.; PARRY, S.R. (1986), *Free-form deformation of solid geometric models*, SIGGRAPH Computer Graphics 20/4, pp.151–160
- TANIGUCHI, T; ICHINOSE, Y. (2020), *Hull form design support tool based on machine learning*, 19th COMPIT Conf., Pontignano, pp.89-97, http://data.hiper-conf.info/compit2020_pontignano.pdf

Transparent Charge Plans for Battery Driven Ferries Using an Intelligent Multi-Agent Software System – A Case Study

Lars Lindegaard Mikkelsen, UCL University College, Odense/Denmark, lk1m@ucl.dk

Simon Stochholm, UCL University College, Odense/Denmark, sist@ucl.dk

Abstract

To support energy-efficient charging and to extend battery lifetime, an intelligent multi-agent software system is proposed and tested with operational data from the two ferries M/F Langeland and M/F Lolland. The study also includes two land-based Energy Storage Systems. The software architecture consists of a multi-context multi-agent system and the paper proposes a mapping of the physical assets into the software domain. The system provides loosely coupled agents, which allows agents to be introduced, changed or removed in a running system without reconfiguration needed. Transparency is obtained as the individual agents will show how well the objectives are fulfilled and it is possible to trace decision paths across the system.

1. Introduction

As described in *Mikkelsen and Stochholm (2021)* in Denmark there is a broad political agreement on achieving a 70% reduction in CO₂ emissions by 2030, and by 2050 Denmark should be climate neutral. The 2030 goal is described in a climate program [Danish Ministry of Climate, Energy and Utilities (2021)]. The main sustainable energy sources in Denmark are wind and the import of hydro power from Norway and Sweden. Solar power is also used, but it covers less than 3% of electrical energy by 2020. One of many areas in the 2030 program is the electrification of ferry operations. Domestic ferries contribute with a CO₂ emission of 72.000 tons per year. The combination of cost-efficient operation, energy management, ensuring safety margins, and battery preservation will be a new operational topic when retrofitting existing ferries with batteries.

The focus for this paper is energy support software for battery and hybrid operations i.e. the ferries are fully battery powered with backup from the existing diesel generator sets i.e. propulsion, auxiliary systems and heating (heat pumps). It is also demonstrated how to configure a multi-context multi-agent system and generate charging plans to maximize energy efficiency, cost, and battery lifetime based on *Mikkelsen (2013)*.

The two sister ferries “M/F Langeland” and “M/F Lolland” are built in 2012 as diesel-electrical and they are sailing on the route Langelandslinjen between the port of Spodsbjerg on the island Langeland and Tårs on the island Lolland in Denmark. The ferry “M/F Langeland” in its new colors depicted in Fig.1, <https://www.soefart.dk/>, has provided data for the case study described in sections 3 and 5. The two ferries were designed with void space for a later LNG conversion. This space can be used for an eventual Battery ESS (Energy storage system).



Fig.1: “M/F Langeland”

1.1 Project status

The retrofitting of the two ferries with batteries is still in the exploration and scoping process. There are still a number of major open issues:

- Business case and new business models
- Auto berthing
- Owner of the electrical infrastructure 60 kV or ESS in the harbors
- ESSs in the harbors used to stabilize the grid as running reserve
- How should the hybrid-mode be used?
- How to accelerate the transition from fossil fuel to electrical power based on available green electrical energy
- When can the ferries be operated 100 % with green power?

Fig.2 depicts the two most promising charging options. A direct connection to a 60 kV system, which requires a new 5-10 km 60 kV cables or an ESS connected to the existing 10 kV grid in the harbor.

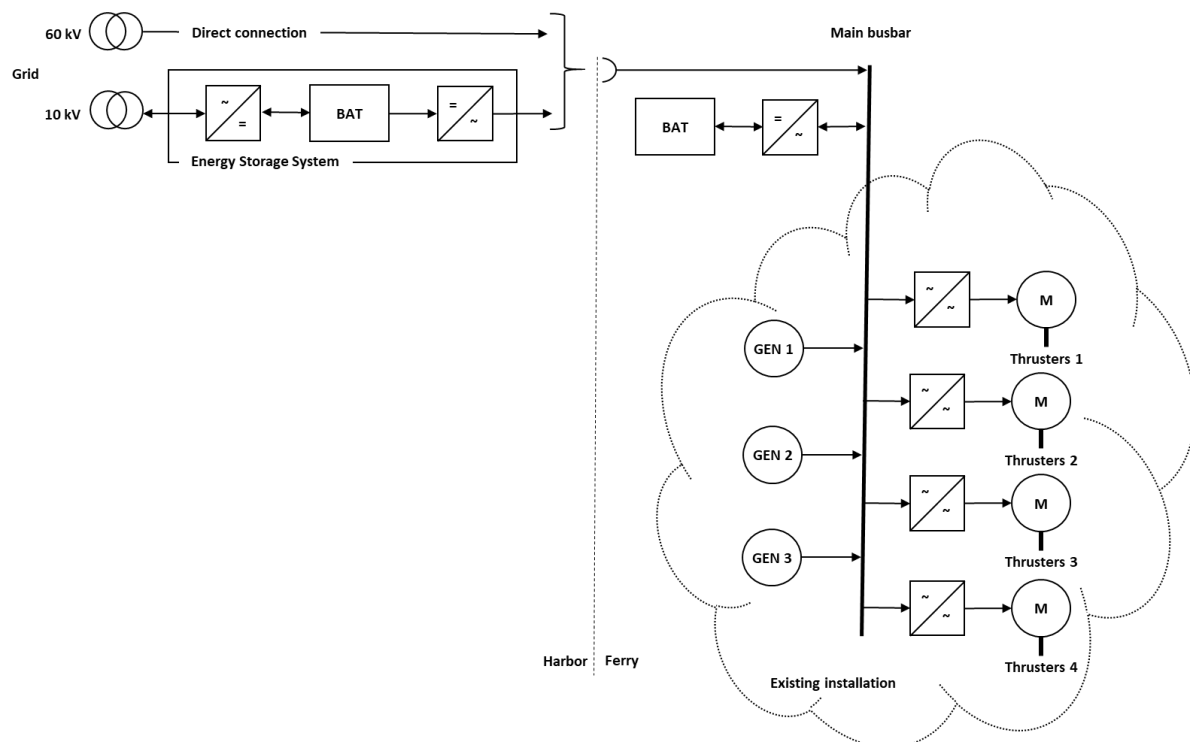


Fig.2: Electrical shore connection

1.1.1 Business case and new business models

The project is driven by a business case approach without too much focus on redefining the business model. There are many uncertainties to be considered when creating a reliable business case in the transition process going from black (fossil fuel) to sustainable green energy (Wind, Hydro, Solar, etc.) The retrofit project uses the existing electrical infrastructure onboard the ferries, as this will reduce the installation cost and make the approval process more straightforward. This should mitigate the main risk and ease the approval process. A backup solution is also in place by leaving a number of the diesel generator-sets in place.

A number of new business models arise when introducing batteries like selling the battery capacity as a grid reserve, selling green energy to the customers when charging their cars or trucks in the harbor or during the crossing.

Some of the issues which make a retrofit project complicated are the number of stakeholders as authorities, owners, ferry operators, and customers who are both private and business, yard, battery (ESS), auto charge connector, auto berthing system, energy suppliers etc. The combination of cost-efficient operation, energy management, ensuring safety margins, and battery preservation will require new ecosystems to gain the full economic and environmental potential when upgrading the ferries with batteries. Further digitalization is also needed

1.1.2 Auto berthing

A number of unstructured interviews have been executed as a follow up on the findings in *Mikkelsen and Stochholm (2021)* with regards to auto berthing. An auto berthing system is by the crew seen as an important safety improvement. It will potentially reduce human fatigue sailing in poor weather conditions. It was also important for the crew that manual berthing should still be trained on a daily basis to ensure enough routine. After additional analyses and the new interviews, it is a recommendation to install an auto berthing system to achieve the expected safety improvement and stable berthing, ensuring maximum time to charge. The installation of auto berthing systems is a prerequisite in the simulations and generation of charge plans and operational mode plans presented in chapter 5.

1.2 Organization

The rest of this paper is organized into the following sections: section 2 describes the mapping of a physical system to multi-context, multi-layered, multi-agent software system, section 3 covers the mapping of the Langelandslinjen, section 4 describes the solver implementation, section 5 shows a simulated charge plan example and finally section 6 covers the conclusion and future work.

2. Mapping a physical system to a multi-context, multi-layered, multi-agent software system

In this section the process of mapping a complex physical system to a multi-layered multi-agent software system is described. There are multiple software models and processes which can be used to design and implement a system that is well structured and easy to extend and maintain, but there is a gap when introducing multi-agents in a multi-layered multi-context system. In this paper we propose a generic software framework and demonstrate a configuration tool

The first steps in the process are to identify a system and the main subsystems in the physical world i.e. the system could be the crossing, where subsystems are the harbors and ferries. A system defines a context with multiple subsystems and optimizations across. A company can have many independent systems e.g. Molslinjen is the operator of several different crossings.

The next steps are to identify groups of operational tasks and operational requirements. These tasks can be organized into layers and contexts. The layers are used to arrange the concerns in the relation to their impact and focus i.e. long-term strategic goals in the range of days; tactical in the range of hours; and execution layer in real-time. In this case study the timespan is mostly in the range: strategic (days/weeks), tactical(days/hours) and execution (hours/minutes).

Most likely, the identified tasks and operational requirements need to be split into minor parts and be formulated as the concept of a concern in the problem domain and as software agent in the solution domain. The concerns can be divided into two groups: hard and soft. The hard concerns are restricting the solution space and need to be fulfilled at all times, whereas the soft concerns are flexible to utilize the elasticity in the solution space. As hard concerns constrain the solution space, they should only be used when required. The soft concerns can be used more freely so long as the number and focus are balanced to avoid unintentionally biasing the results.

The concerns can be grouped into contexts and thereby improve scalability, as each concern group can be solved independently i.e. it is possible to run the system in a distributed multi-threaded

environment. It will also improve overview for the users, as it will be possible to show results at a context level.

Fig.3 depicts the multi-layered framework consisting of a system with multiple subsystems. There is no limit in the depth of systems of systems, but in this project three levels are chosen to balance the need for overview and detailed insight.

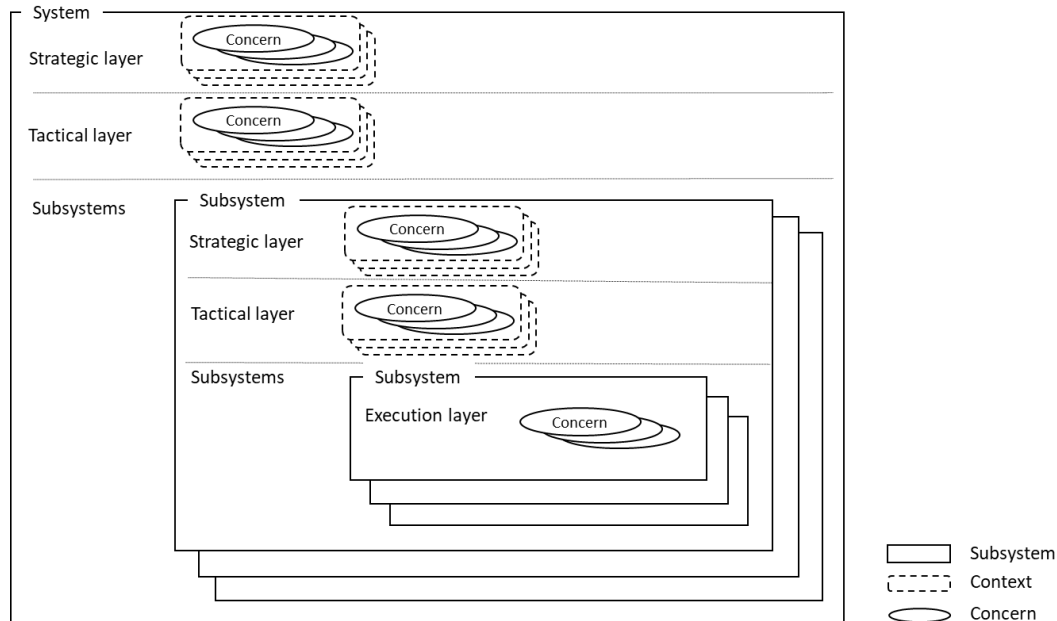


Fig.3: Model

At level three, only the execution layer is active, as the strategic and tactical decisions are handled at level one and two.

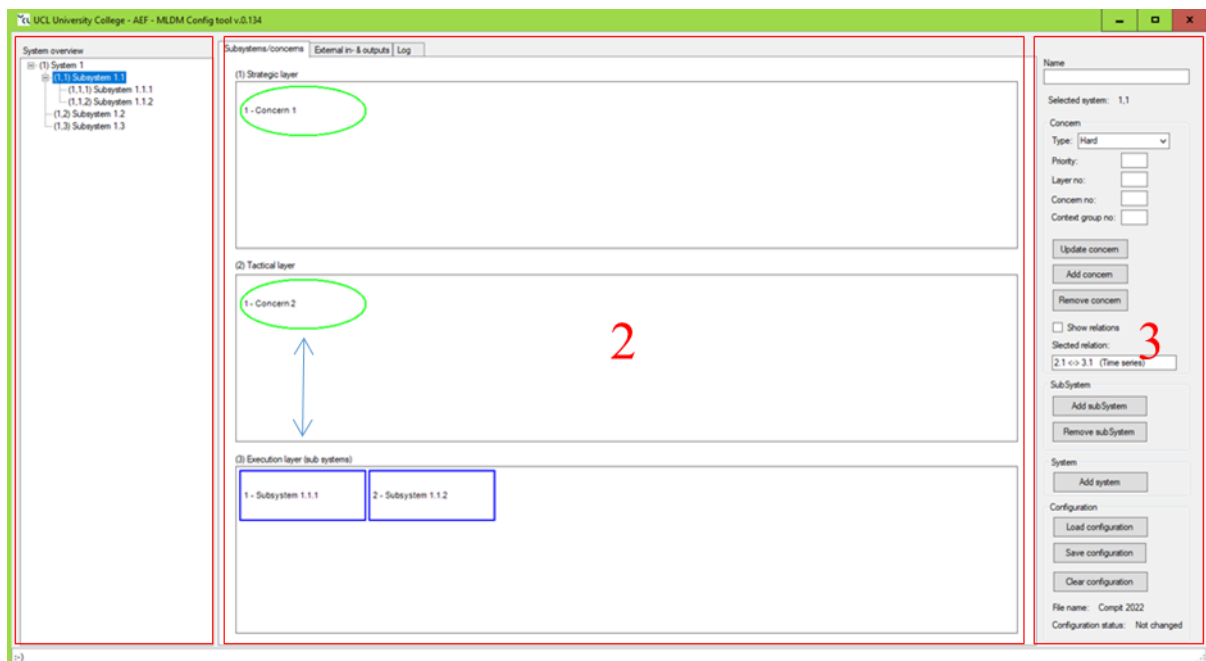


Fig.4: Configuration tool

Fig.4 depicts the newly developed configuration tool and it is split into three areas:

- 1) System overview
- 2) Details: Layers, relations, concerns, External in- & outputs and system log
- 3) Configuration interface

Area 1: System overview

As mentioned in the previous section, it is chosen to use depth of three levels and this is reflected in this version of the tool. The number in the parentheses indicates position in the hierarchy and is used in the configuration section of the tool.

Area 2: Overview

The area contains three tabs:

- I) “Subsystems/concerns”: In the overview area the context (system/subsystem) selected in the tree menu is shown. Concerns are represented as green ovals and the blue boxes at the execution layer indicate that these are subsystems and can be unfolded. The relation between concerns and subsystems are shown by arrows. They can be directional (up or down) or bi-directional.
- II) “External in- & outputs” can be added to a table linking the external inputs to the concerns where they are used. The outputs are linked to a context or a layer.
- III) In “Log” all transactions can be found.

Area 3: Configuration

The configuration area is organized with the most used functions at the top i.e. configurations of concerns and at the bottom clear, load and save options are located. The relations, shown as arrows, can be hidden by un-checking the “Show relations” checkbox. The syntax of the text representation of the relations is [“concern/subsystem no/external source”] [“->” “<-“ “<->”] [“concern/subsystem no”] ([“data type: time series, analog, digital”]) e.g. “2.2 <-> 3.1 (time series)” If the configuration is changed a save popup menu is shown at the closing of the program. The configuration is stored in json format, so it can be used and edited outside the configuration tool. A new project can be started by clearing the tool and adding a new system. The next steps are to add subsystems and concerns.

3. Mapping “Langelandslinjen” into the new software framework

In this section the process of mapping Langelandslinjen into the new software framework is demonstrated in detail. Fig.5 shows the system on an open sea map, <https://map.openseamap.org/>, with the traffic layer activated.



Fig.5: Langelandslinjen assets shown in an Open sea map

The Langelandslinjen system consists of the following physical assets:

- the two ports: Harbor 1 “Spodsbjerg” and Harbor 2 “Tårs”
- the two ferries: Ferry 1 “M/F Lolland” and Ferry 2 “M/F Langeland”.

The same system could also be modelled as depicted in Fig.6. This could create an overview of physical assets shown in Fig.5 and with an option to add the missing subsystems. It is important to choose a modelling granularity so that future users can identify and understand the link to the real world, but not lose the overview by too many details. As described previously a level of three is chosen to meet the balance i.e. level 1: a system “Langelandslinjen”, level 2: main assets (ports + ferries) and level 3 main subsystems.

The following abbreviations are used in Fig.6:

- ESS: Energy Storage System
- AUX: Auxiliary systems
- T: Azimuth thrusters
- GEN: Diesel electrical generator sets
- Berth: Berth including car ramp and mooring system

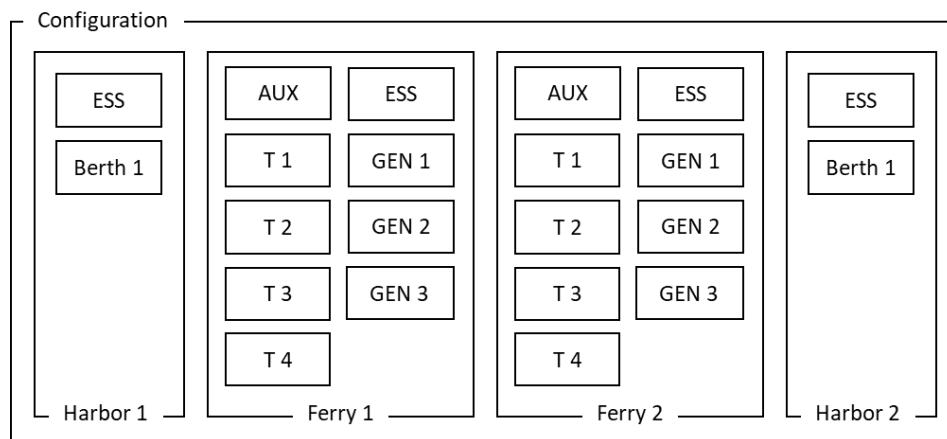


Fig.6: Physical systems and subsystems

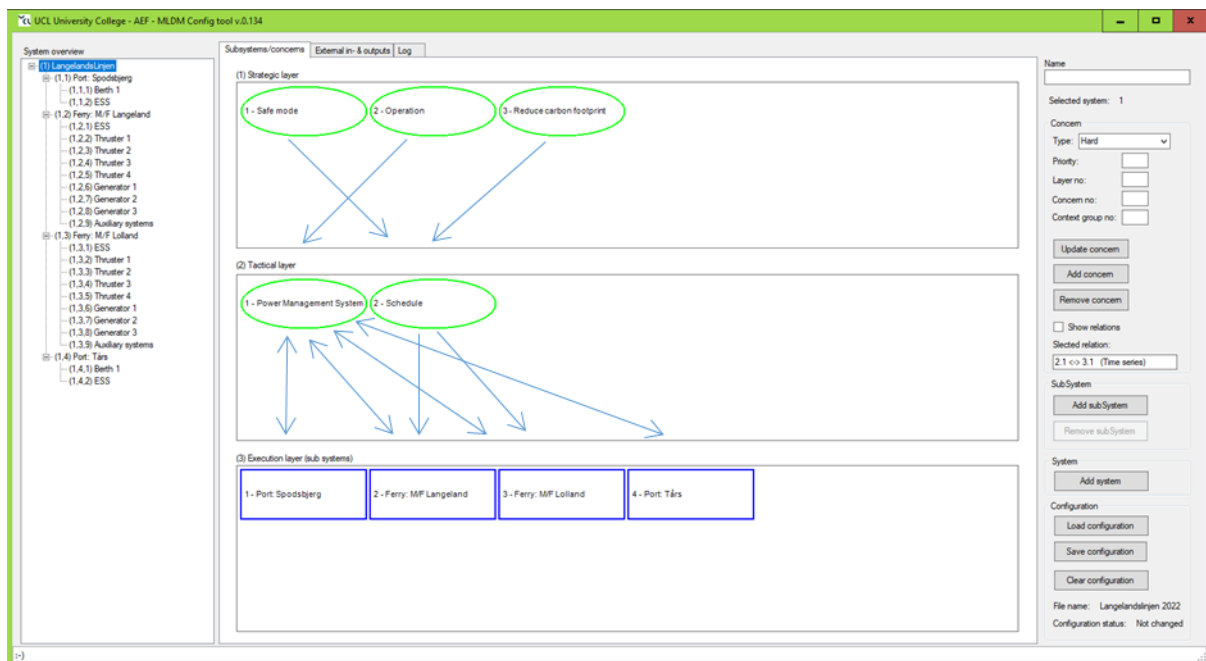


Fig.7: Configuration tool

When comparing the model system with the actual configuration two generators are removed from each of the ferries. ESSs are added in the harbors and onboard the ferries. Today only one of two berths in harbors can be used for operation and therefore only one is shown.

Using the configuration tool the system can be modelled and concerns, relations, In-/outputs can be added. Fig.7 shows in the “System overview” area the complete Langelandslinjen system and examples of concerns and relations in the “Details area”.

4. Solver implementation

With regards to the solver implementation - work is still in progress. The current solver version is based on a mediator agent using a genetic algorithm (GA) as proposed in *Mikkelsen (2013)*. As the layers are connected and solutions at one layer have the potential to change solutions on layers over and under, there is a risk of destabilizing, as seen in cascade control loops. To improve the system stability all underlying layers are solved at a 5-10 higher rate.

The role of the mediators is to handle interactions with multiple concerns, by collecting prestate information, control the GA search and providing poststate information by updating outputs. The solving process is as follows and the flow is shown in Fig.8:

1. Initialization where inputs and the latest solution are read.
2. Generates a population of solutions. The best solution from last run is always included in the population to speed up the negation process.
3. Search for the best solution based on accepted solution, priority and how the objectives of the concern are fulfilled (expressed as fitness) i.e. all accepted solutions are sorted by priority of concern. For each priority, the solutions are sorted by average fitness. The 50% best solutions are selected.
4. The process is terminated if:
 - no improvement is observed
 - time is elapsed
 - the number of fixed cycles is reached.
5. If terminated go to step seven else the best half of the population is kept.
6. Generate new population based on: random, crossover and mutations.
7. Go to step 3.
8. Update outputs with the new solution

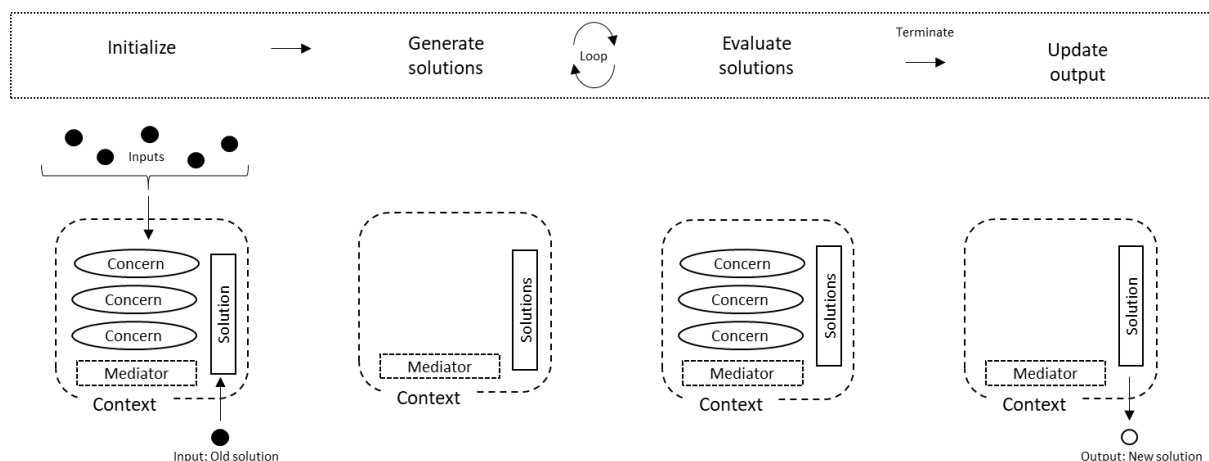


Fig.8: GA solving process

The fitness value is the percentage to which the proposal fulfils the concern’s objectives. If the GA search has not converged towards a solution at the end of the period of control, the algorithm repeats the search process. The search process is said to have converged, and a satisfying solution found,

when no proposal is any better than a previous proposal. When no satisfying solution could be found, the entailment relation of the control context is broken. Broken entailments are typically observed by allocation conflicts over shared resources e.g. power. Many of these resource allocation conflicts among concerns can be handled by adjusting priorities, but it is important that any change in priority is thoroughly considered and tested, as unintended behaviors could occur.

One of the options of showing the results - currently being tested - is color-coding the concerns based on their fitness. The goal is to have as high fitness as possible and the stakeholders i.e. crew and management need to react when the total fitness gets close to 80%. The colors indicate the fitness (cost function) in the range from 0-100 % and the orange color is offset from 50% to 80%, as shown in Fig.9. Otherwise the green will be dominant and it will be hard to distinguish in the normal operation range.

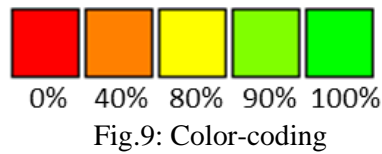


Fig.9: Color-coding

5. Generate charge plans operation mode plans

As the battery retrofit project is still not decided on, this section will focus on a single ferry with the expected hybrid configuration with three diesel generators and with battery ESS in the harbors.

The example of different charge plans generated are only simulation based on historical weather and operational data.

Fig.10 depicts wind and anonymized energy data. The energy data is shown in the percentage of the maximal energy used at 1100 hours day 16. As seen at the early hours of day 9 there is high energy consumption in one direction and a much lower in the other showing the difference despite relatively calm weather conditions. Energy data from day 9 is used as input for the following example.

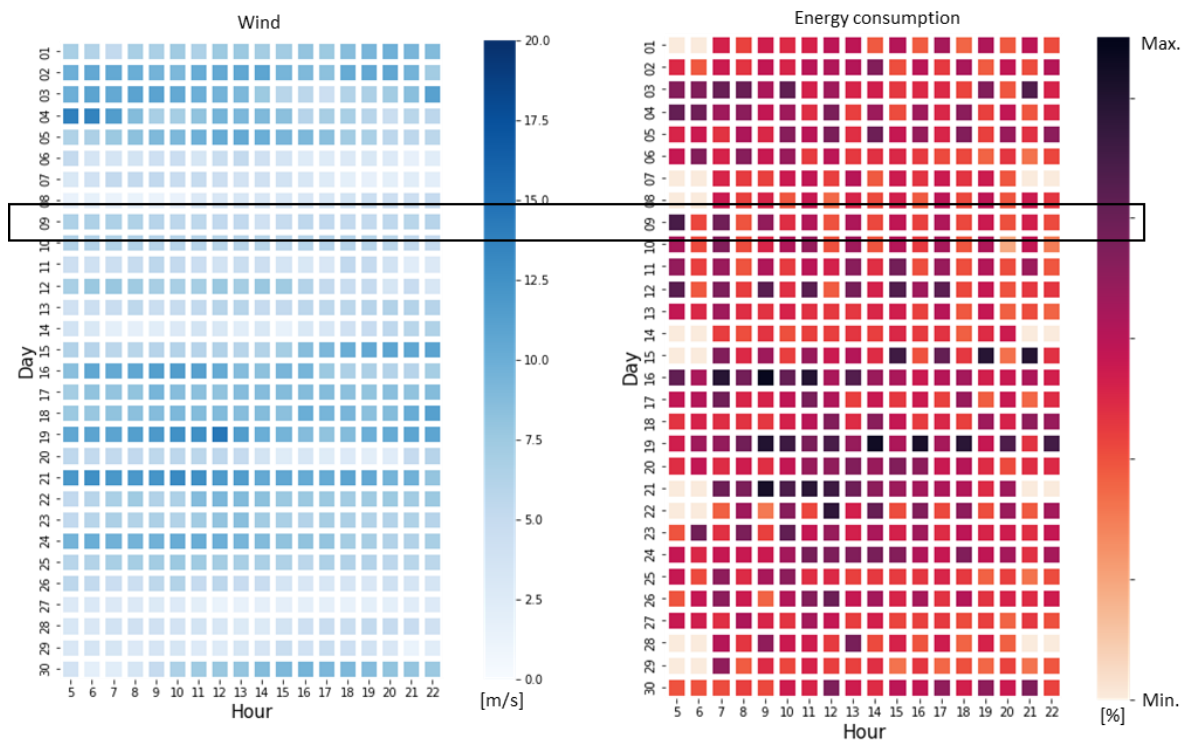


Fig.10: Historical wind and anonymized energy data

Fig.11 shows charge energy needed based on three strategies:

- a charge profile “0 % drop in SoC (State of Charge)” (blue) requires the same amount as used.
- a charge profile based on a calculated average i.e. same amount of energy charged all day (red).
- a “Max. 20 % drop in SoC” (green) approach SoC during the day is shown.

The same information shown, as the drop in SoC, can be seen in Fig.12.

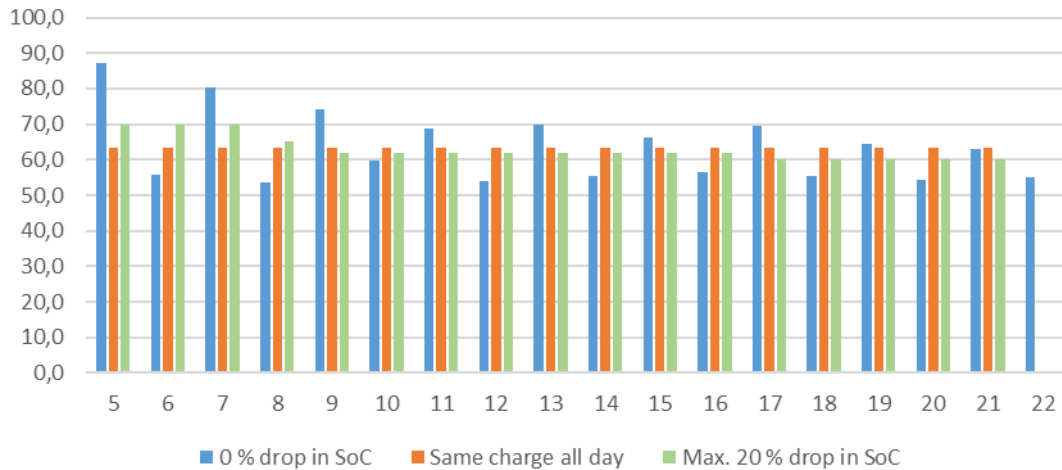


Fig.11: Charge examples

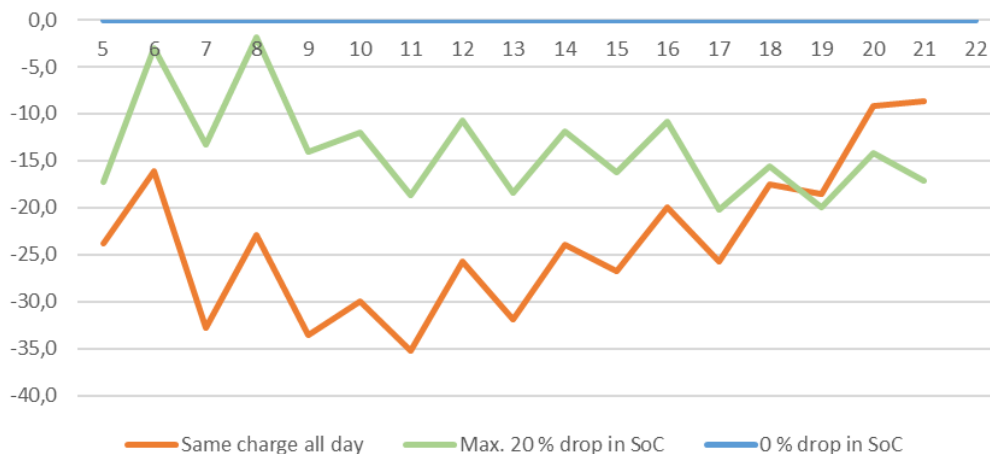


Fig.12: Drop in SoC

The interviews with the crew reveal that at the same range anxiety as when introducing electrical cars. Molslinjen has a focus on the change in culture needed and plans extensive training programs. As discussed with the crew of Langelandslinjen all these detailed pieces of information are not beneficial in the daily operation, but transparency is still a top priority to avoid the system being a black box out of the crew’s reach and responsibility. The result of the initial test shows a simple and intuitive interface with the option to drill down into the details requested. To support this a simplified operational plan is shown per day and split into three modes: Battery, Hybrid and Fossil fuel. From the overview it is possible to drill down into the underlying concerns and thereby full transparency is provided. It is possible to select an hour and see solutions and the fitness of the individual concerns. It is proposed to update the plans (forecasts) during the crossing.

Fig.13 shows the simple output tested. The operation mode is represented as either Electrical, Hybrid or Diesel. If an interaction is required the hour will be marked yellow as seen at 1800 hours. From this operation mode overview there is a direct link to the underlying decision support system.

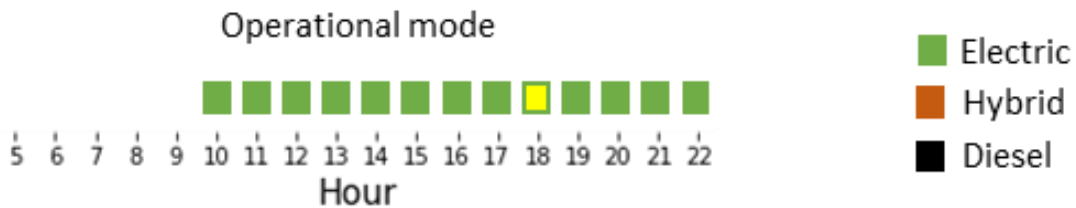


Fig.13: Operation mode

6. Conclusion and future work

In this paper a generic mapping of a physical energy system into a multi-system multi-layered multi-context multi-agent system is proposed. The introduction of a distributed role of responsibility makes the system open for change without the need to re-test the complete system. It is important to address the formulated concerns to avoid bias or misbehaviors. It is also important to avoid constraining the solution space by adding either too restrictive, too many or both concerns.

As a part of the shift to battery operation an auto-berthing system is recommended to increase safety and optimize time to charge.

Transparent charge plans are important in the transition from fossil fuel to battery operation to mitigate range anxiety. The users should have the opportunity to look into the details, but the normal operational GUI should focus on a very simple version.

Focus of the future work at Langelandslinjen will be:

- Distributed systems
- Dynamic update of mediator algorithms
- Improved use of ML predictions to update concern models
- Development of tools to create new business models when retro-fitting ferries with batteries
- Eye-tracking experiments to better understand the use of information available

Acknowledgements

The authors would like to thank the crew and employees from the ferry company Molslinjen A/S for participating and for sharing valuable information about operating the ferries.

References

MIKKELSEN, L.L. (2013), *Vertical Integration of Multi-Layered Decision Making In Offshore Oil & Gas Production*, SDU, Denmark

MIKKELSEN, L.L.; STOCHHOLM, S. (2021), *The Need for an Updated Energy Decision Support System Framework when Retrofitting Ferries with Batteries - A Case Study*, COMPIT Conf., Mülheim, pp.130-140, http://data.hiper-conf.info/compit2021_muelheim.pdf

Clustering Variations within Ferry Operational Patterns by applying Unsupervised Machine Learning - A Case Study

Simon Stochholm, UCL University College, Odense/Denmark, sist@ucl.dk

Lars Lindegaard Mikkelsen, UCL University College, Odense/Denmark, lk1m@ucl.dk

Abstract

This paper investigates the process of applying unsupervised machine learning on operational data from ferry M/F Langeland. Previous unsupervised machine learning studies have, inter alia, focused on energy emission patterns in buildings through the application of transfer learning; encoding of time series to images; convolutional autoencoders; and clustering algorithms. This study follows a very similar approach into the field of ferry operational patterns, with the primary focus of identifying differences within maneuvering patterns. The findings unequivocally show that it is possible to identify such patterns, albeit inconsistencies exist which are almost certainly due to external factors.

1. Introduction

Unsupervised machine learning is a fascinating technology. The whole idea of machines figuring out patterns without any human intervention is simply exhilarating, and the more unsupervised the process is, the more it feels like the machines are actually making decisions on their own. Simultaneously to the feel of AIs supporting humans, there is the added benefit of being able to applicate the methodology to new domains. It is a lot easier to apply unsupervised machine learning to new areas of interest as opposed to supervised machine learning, where data needs to be labeled beforehand. So an advance within unsupervised machine learning on ferry operational patterns might be applicable to other operational patterns e.g. the landing styles of pilots, which is why we have chosen this approach.

In Mikkelsen and Stochholm (2021), we described the current political requirement in Denmark regarding reduction of CO₂ emissions. The goal is to have CO₂ emissions reduced by 70% in 2030, and by 2050 Denmark should be climate neutral. We proposed an updated energy decision support system framework for retrofitted batteries, which relies on several different approaches for prolonging harboring time so as to increase time for charging of batteries while docking. One approach to prolong harboring time, is to see if studying operational patterns, such as maneuvering, brings any valuable information into the question of energy consumption. However, the main purpose of this study is to see if we are able to positively identify differences within operational ferry patterns and in particular maneuvering patterns. Just like every single person has his or her own particular way of walking, so the hypothesis here is that every master has his or her own (or at least a shared but delimited) way of operating the ferry. Therefore, if we can positively identify operational styles, knowledge hereof can be applied to other domains as well, however, the study is very limited in its scope and serves only as a case study. In order to avoid too much bias, the present study is completely blinded. We have no knowledge of who is operating the ferry at any time, nor how many different masters have been involved in operating the ferry during the examined time period, and nor do we aspire to know, since the purpose of this study is not to identify any one particular person, but simply to identify and cluster the specific maneuvering patterns that naturally emerge while operating a ferry.

2. Data collection

Over the last four years (2018-2021) Langelandslinjen has gathered data from roughly 18,000+ ferry crossings between Spodsbjerg and Tårn in Denmark. The data gathered includes energy consumption on the four thrusters of each ferry; angles of the thrusters; coordinates of each crossing; wind speed and wind direction; and much more which we will not consider here as it is less relevant to our endeavor.

In order to identify ferry operational patterns we have firstly split all crossings of the ferry M/F Langeland into modes and sections, as can be seen in figure 1 below. The modes are termed Harboring, Maneuvering and Passage respectively, whereas the sections are designated numbers 1 through 4, and serve to give us a way to refer to direction and mode simultaneously. Since maneuvering is both an inbound and outbound action the four sections make it possible to refer to the maneuvering in question. For instance, maneuvering mode in section 1 is the inbound maneuvering toward Spodsbjerg while maneuvering mode in section 3 is the outbound maneuvering from Spodsbjerg.

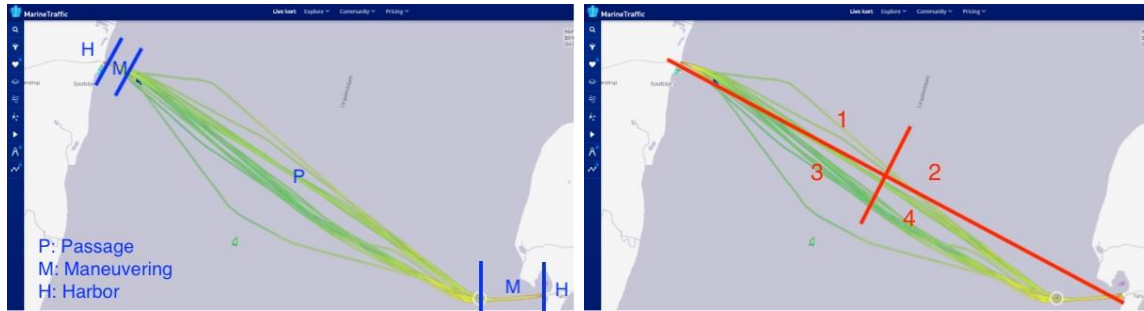


Fig.1: Different modes (left) and sections of crossings (right)

In the present study we focused only on operational patterns within maneuverings in section 1, i.e. maneuverings towards Spodsbjerg. This decision is based on several factors. Firstly, wind conditions will most likely be opposite when considering both directions. Second, a speed limit has been imposed in section 4 due to the presence of another harbor straight north of the ferry route and this affects how maneuvering is conducted; and finally, the sailing channel in section 4 is straighter and has less depth than that of section 1, all of which might skew results if compared uncritically. The reason we only consider maneuvering toward the harbor and not out of the harbor is because we are interested in patterns that can potentially lead to high charging times while the ferry is harboring. The data we examined came from a randomly chosen month within the four years of data available, but has been anonymized, regarding dates and energy, in consideration of business critical elements. The dataset was originally unlabeled, i.e. there was no indication of when the ferry was harboring or which of the modes it was in at a given time. Several attempts were made to label the dataset according to the three modes discussed above, but ultimately we decided to simply go with coordinates as most precise indicator of modes. The labelling is used merely to extract the coordinate sections we are interested in.

2.1. Data considerations

Several steps and considerations are necessary in order to utilize the datasets we have been given access to. These considerations will be expanded upon below through a concrete example.

2.1.1. First step: Interpolation

We collected the datasets as separate csv-files through calls to a private web api. Since the data was not adjoined from the beginning, the first task was to concatenate all sets on common time stamps.

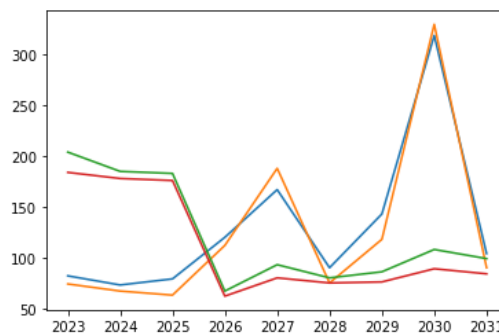


Fig.2: A maneuvering in section 1, thrust on the y-axis and time in 15 second intervals on the x-axis

However, since the coordinate dataset available to us only had a resolution of 30 s, while the thrust dataset had a resolution of 15 s, coordinates have been interpolated in order to achieve the highest possible resolution. Afterwards we adjoined the coordinate dataset to the thrust dataset. Fig.2 shows selected maneuvering from section 1 (extracted on the basis of coordinates) after interpolation.

2.1.2. Second step: Timeboxing

In order to achieve our goal of comparing patterns, it is very important that we can align the samples somehow. Using coordinates to delimit our modes causes a comparison problem, since times will vary between maneuverings and this again will skew results. In order to accommodate this issue we decided to timebox the maneuverings by creating a 10-min window which runs from five minutes prior to, as well as five minutes past, the moment where the ferry crosses the specific coordinate which indicates going from passage mode to maneuvering mode. This results in a graph like that in Fig.3. It is now possible to see the end of passage mode as well as the beginning of harboring mode.



Fig.3: Same as Fig.2, but in a 10-min time frame

2.1.3. Third step: Thruster angles

Even though this graph is now comparable to other graphs due to equality in the time domain, it actually does not tell us much about the operational pattern, or rather, it is a visually incorrect way of displaying the data. In the above graph, braking is visualized by thrust moving toward zero on the y-axis, but this would only be true of thrusters that are in line with the heading of the ferry. If the thrusters are turned 180° while at first, in line with the heading, thrust will still be high, but will affect the ferry with an opposite force. In order to truly compare operational patterns, we therefore have to take the angle of the thrusters into consideration. However, sometimes the ferry itself is turned around 180°, so the physical direction of the ferry is opposite that of the heading of the ferry, in which case we must first multiply the thrusters by negative one in order to know whether the thrust should be counted as positive or negative. Therefore, in order to achieve the most correct visualization for comparison, we can apply the cosine function to the angle of the thruster in radians, times the value of the thrust in order to get a curve which more accurately shows the pattern of the master's maneuvering. Also, as can be seen from the figure above, the thrusters are always moving in pairs, and so we might as well simply add them to together, to create a simpler and clearer plot. Applying these changes will result in the following figure.

$$thrust = \cos\left(angle * \frac{\pi}{180}\right) * combined\ thrust\ value$$

Now the image is much clearer and indicative of the operational pattern. We can see that the steep spike at around 2030 on the x-axis in Fig.3 is actually a downward moving force rather than an upward moving force in Fig.4, which means that the master decided to take advantage of the ferry's

momentum in order to brake. Be aware that the value is around negative 600 on the y-axis and not around negative 300 because we added the values of the paired thrusters together.

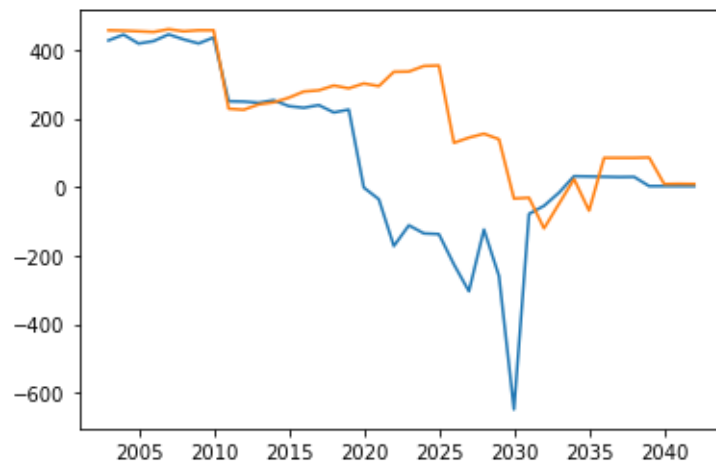


Fig.4: Same as Fig.3, where the angle of the thrusters have been taking into consideration.

2.2. Considerations regarding unsupervised learning

Some considerations regarding the use of unsupervised learning also need to be addressed. First of all, when applying unsupervised learning, we can never be absolutely sure what the result is actually showing us. As the method is unsupervised, no human is involved in the process, which is why it is important to limit as many known factors as possible. In this study we apply two types of unsupervised machine learning. First we apply a convolutional autoencoder which is considered to be self-learning, and afterwards we apply a clustering algorithm called K-means clustering, which will attempt to cluster the results by similarity. The algorithms will be described in more detail in section 3.

2.3. Errors and biases

As mentioned, we decided to label the data by the use of coordinates in order to know which mode the ferry is in at a given time, however, using this approach we could potentially wrongly identify a new crossing, if, for instance, the ferry bounces back and forth inside the harbor, or due to inaccurate coordinate logging and the frequency of a logging. Thus a lot of time has been spent on cleaning the data by removing outliers or interpolating missing values in the datasets. We will discuss the specific types of errors next.

Here is a short overview of the different kinds of errors we have come across in the dataset:

1. There are doubles in the data
2. There are times where the loggers have not been working properly
 - a. Coordinate loggers:
 - I. The coordinate loggers are stuck at a coordinate through a longer period of time
 - II. The coordinates are changing, but never past the specific coordinate where the harbor is located.
 - b. Thruster loggers:
 - I. Loggers are stuck at 0 or 1 through longer periods of time despite movement in the coordinates.
 - II. A single thruster is not being logged through a longer period of time which makes it seem like the engine has been shut off
 - III. Engines are not turned off at arrival in the harbor, which makes it seem like the ferry is still in passage or maneuvering mode

We have applied the following solutions to mitigate the errors in the dataset:

1. Doubles have been handled by simply sorting the dataset and only choosing unique elements. This solved the problem.
2. In situations where coordinate loggers have been stuck, we could have estimated the correct coordinate, but chose to remove those parts of the dataset instead and not examine any patterns in that particular time period.
3. In situations where thruster loggers are stuck, we duplicated the value from the logger it is bound to, as thrusters move in pairs, this should suffice as a fair approximation. At no time are all loggers stuck at the same time, so it is reasonable to always make this approximation. We have not used thrust to determine the different modes, and only focused on the maneuvering mode this study, so this should not be an issue for the current study.

Other biases include the time of year and time of day. It is much lighter in Denmark during the summer than in the wintertime, and hence we would expect masters having a harder time maneuvering the ferry in the winter and around dusk and dawn due to lack of eyesight. We also have to consider the amount of wind or other weather conditions like high tide or rough sea, as this may affect the master's ability to navigate the ferry, e.g. backwind could potentially be the cause of lower energy consumption.

In the present case, we have not been able to get historical data for sea currents and tide, but only for wind conditions, and even these have not been taken into consideration. This however could be explored further in the future. It is also important to keep in mind, that on every round trip the ferry is controlled by two different masters that swap seats depending on the direction the ferry is heading. If for some reason one master gets delayed - say if numerous vehicles need to embark - then this delay could cascade through the rest of the day, and hereby limit the possible time for harboring. This again could potentially cause the masters not to turn the thrusters off in the harbor, since it takes time and energy to turn them on again. All of this will most likely affect the maneuvering style when the masters are in a hurry.

3. Methodology

3.1. Time series and autoencoders

To view ferry crossings as energy consumption on the thrusters over time, makes them inherently time series. There are many different ways to approach time series problems, but in our case we are particularly interested in exploring how we can cluster the different maneuverings according to some common measure, and to reveal information about said maneuverings. Deep learning has previously, been applied to the extraction of implicit features of time series, and according to *Richard et al. (2020)* using a convolutional autoencoder should allow us to extract meaningful features, reduce the dimension of data and lead to an improvement of the subsequent clustering. A convolutional autoencoder is a type of neural network architecture which attempts to create an output which is identical to the input. The idea is, that through several convolutions, whereby the input gradually gets smaller through each layer, the network is able to learn the inner representation of the data and produce a non-linear latent space which contains a simple representation of the input from which we are still able to recreate the output. Fig.5 provides a diagram of such a convolutional autoencoder, produced by *Kucharski et al. (2020)*.

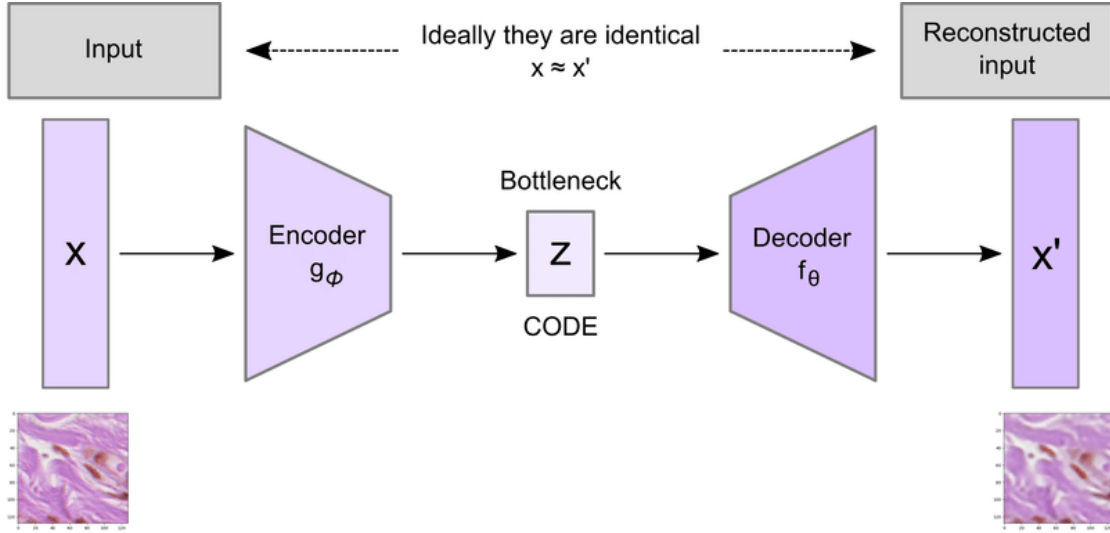


Fig.5: Diagram of a convolutional autoencoder

3.2. GAFs and MTFs

In order to move from a time series diagram of thrust to the actual representation the diagram contains, *Wang et al. (2015)* came up with the idea of converting time series into Gramian Angular Fields (GAFs) and Markov Transition Fields (MTF) thereby keeping the inherent information intact while accentuating specific features of the time series per se, e.g. the shifts in high and low values over time. In simple terms, GAFs encode time series into images by taking cartesian values from a one-dimensional sequence and mapping them to a two dimensional matrix by computing the polar coordinates, and thereby preserving the temporal correlation. GAFs can result in two different images (GASF and GADF) by computing the cosine of the sum of the angles; or the sine of the difference of the angles respectively. MTFs on the other hand preserve details in the temporal range by discretizing the sequence into bins and computing the transition probability of each point in the sequence moving from one bin to another. And finally it spreads out the transition matrix to a field in order to reduce the loss of temporal information. This gives us three images which, in each their own way, encompass some features of the time series while at the same functioning as a two-dimensional representation that can be fed into an autoencoder. The result of such a process can be seen below. Ever since *Wang et al's* first attempt of applying GAFs and MTFs on time series, it has almost become the de facto standard for classification of time series, due to the great results this approach has shown.

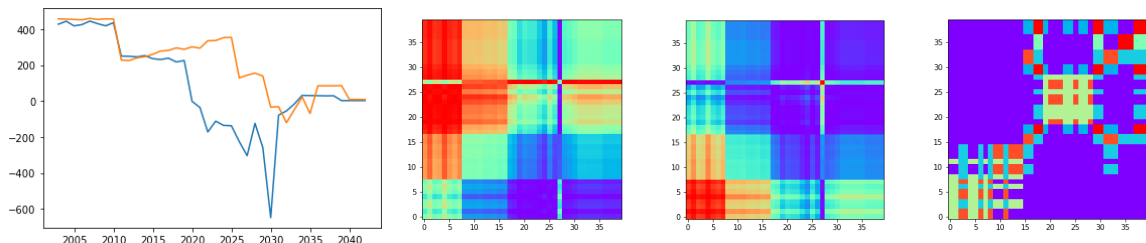


Fig.6: Encoding time series as GAFs and MTF

When looking at the time series graph in Fig.6, one might notice that the data in the graph is not normalized. This is not a real problem however, since we normalize the data before applying MTF, GADS and GASF, and so the time series graph only serves illustrative purposes.

Yang et al. (2019) have taken the same approach as *Richard et al. (2020)*, but instead of feeding the time series as vectors into the convolutional autoencoder, they have decided to encode the time series as images by applying GAFs as well as MTF as suggested by *Wang et al. (2015)*, and concatenate these into one bigger image as shown in Fig.7.

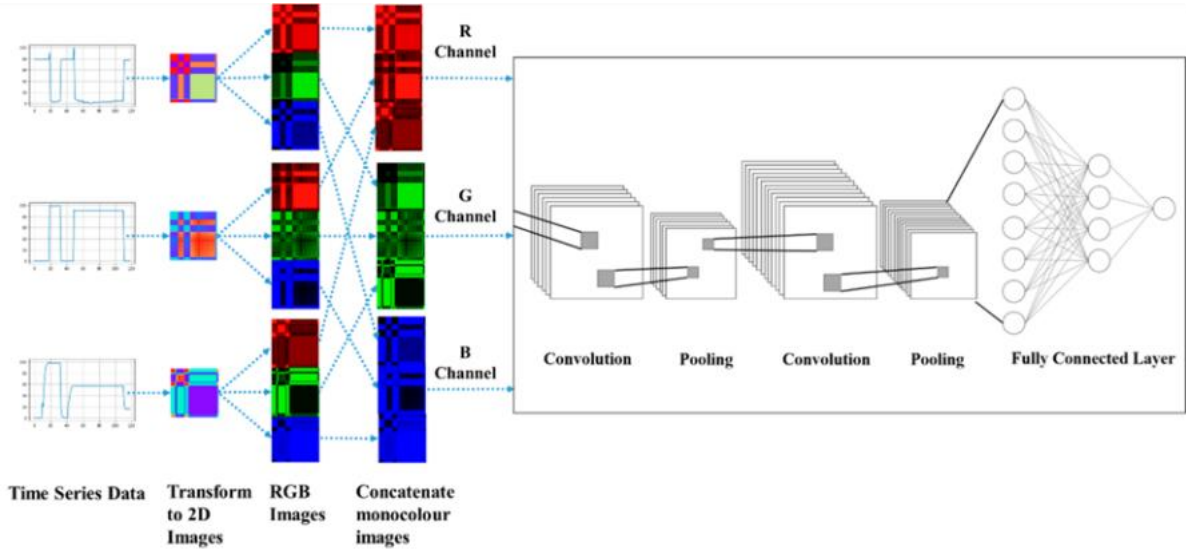


Fig.7: Concept of the concatenating method with red, green, and blue (RGB) images, if three time series are considered

Yang et al (2019) thereby achieve a complete two-dimensional image which encompasses both the temporal correlation as well as the temporal range. In the present study, we also decided to follow the method for concatenations of GAFs and MTF proposed by *Yang et al. (2019)*. However, since all neural network architectures we are aware of are made for square images and our concatenated images are rectangular, we had to construct an architecture of our own, which can be seen below.

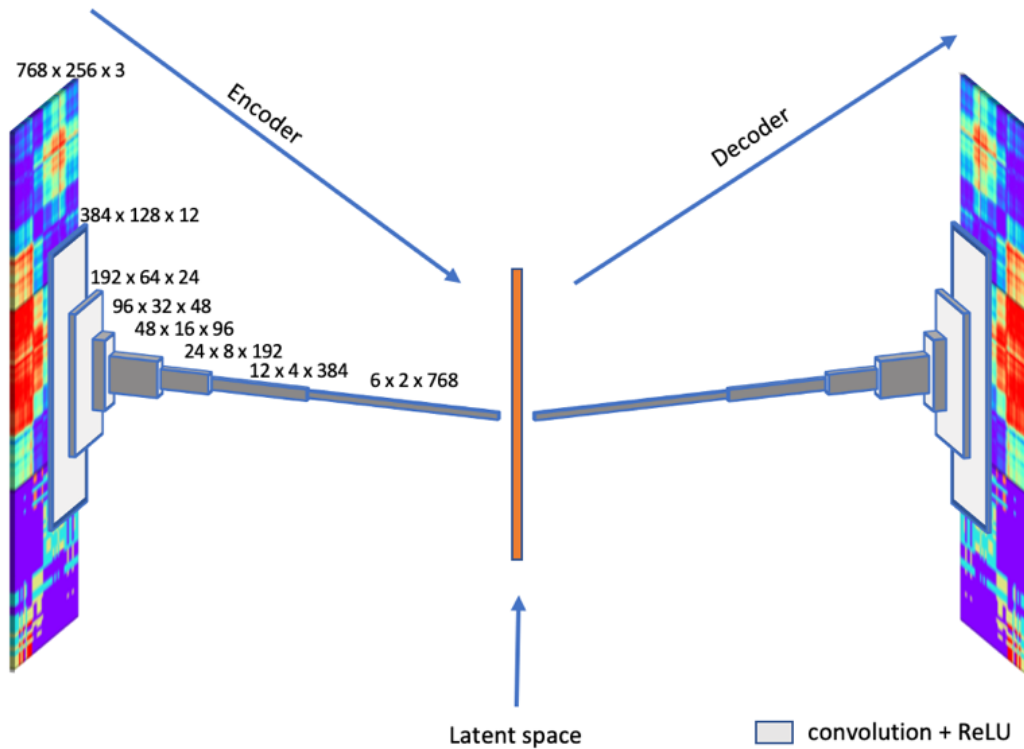


Fig.8: Our convolutional autoencoder network architecture

The architecture is very simple. Dimensions can be read directly off the diagram, and every convolution is followed by a ReLU activation function. We use a 4 by 4 kernel, and a padding of 1 in every convolution, whereby the resulting layer is a quarter of the size of the one before it - in regard to

height and width - but the size of the channels is equally bigger. Moreover, for training we used a learning rate of 0.01, and the initial weights have come about through transfer learning, i.e. by applying the weights from the famous ImageNet - *Deng et al. (2009)* before training. Once we reach the end of the encoding network, we flatten the result and apply Principal Component Analysis (PCA) on it (see Section 3.4). One other difference compared to Yang et al.'s setup, is that our network expects three dimensions to begin with, as this is standard for convolutional neural networks when working with color images, and so there is no need to split the image into red, green and blue explicitly, since all color images are already stored this way on the computer and are loaded in as tensors with three dimensions that represent width, height and color channels. Moreover we decided to more or less follow the proposed end-to-end architecture of *Ulyanin et al. (2019)*, which suggests first encoding the images as GAFs and MTFs, then extracting features through a convolutional autoencoder and also restore the image in order to check the quality of the neural network architecture, and finally clustering the images from the latent spaces. *Ulyanin et al (2019)* apply the binary cross-entropy algorithm to measure the loss during training, but suggest the use of mean squared error instead. We have chosen to go with the latter.

3.3 Training

During training we checked the quality of the autoencoder as suggested by *Ulyanin et al. (2019)* by visualizing how closely it mimics the original input. In the diagram below the input image is on the left, and the expected output image on the far right, while the autoencoders attempt at recreating the image is shown in the middle. We trained for 40 epochs - additional training did not seem to add significant benefit.

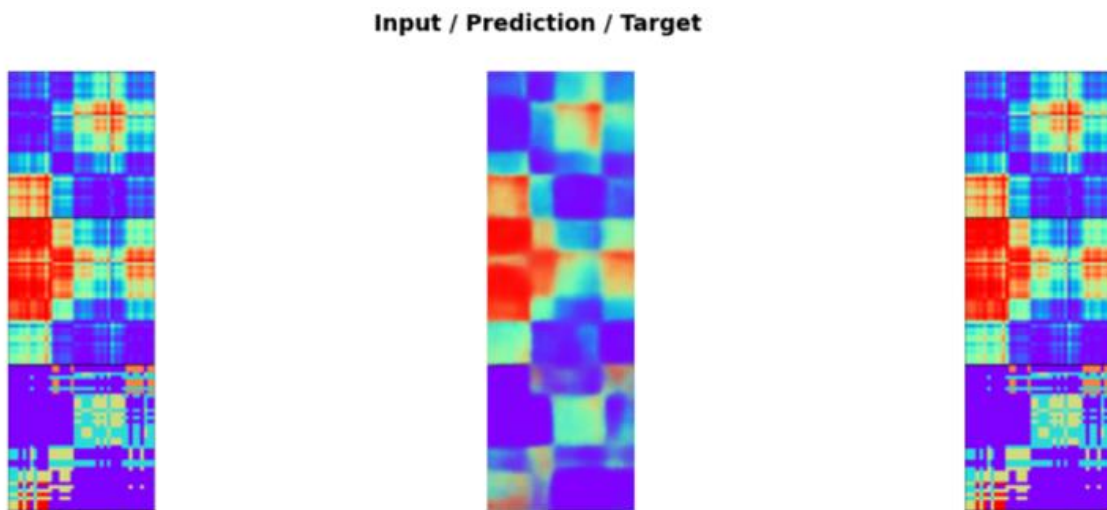


Fig.9: Actual result from training of the convolutional autoencoder

The autoencoder has indeed captured enough information to recreate an image which is fairly similar to the input, which means we can rest assured, that it has captured the essence of the time series, even though this step can surely be improved. Suggestions for future work can be found in Section 6.

3.4 PCA and Clustering

After the autoencoder had done its job, we took each latent space, flattened it, and applied PCA on it. The purpose of applying PCA is to have as few dimensions as possible for the clustering algorithm to work with as this will improve the result. The latent space is of itself non-linear in essence, but by applying PCA we approach a more linear result, through eigenvectors, while keeping the most important dimensions intact. For the clustering, we decided to use a K-Means clustering algorithm even though many others could have been applied, but K-Means is probably the most commonly applied algorithm, so for comparative reasons, and in order to keep the case study as simple as possible, we

chose said algorithm. K-Means requires us to provide it with a number of expected clusters of which to divide the latent spaces into. Since the clusters we hope to find are maneuvering patterns of one or more masters, and we don't know how many masters operate the ferry during a month, we decided to use three common ways of deciding the numbers K s to cluster by. We applied the elbow method, the silhouette method and the Davies Bouldin (DB) index method. The DB index method also explains the amount of K s that best differentiates between the clusters. The number of components defined in the PCA greatly affects the results of the aforementioned methods. Since we want to reduce the number of dimension as much as possible while retaining as much variance as possible, we decided to go with 40 components for the PCA which is able to represent 95% of the data.

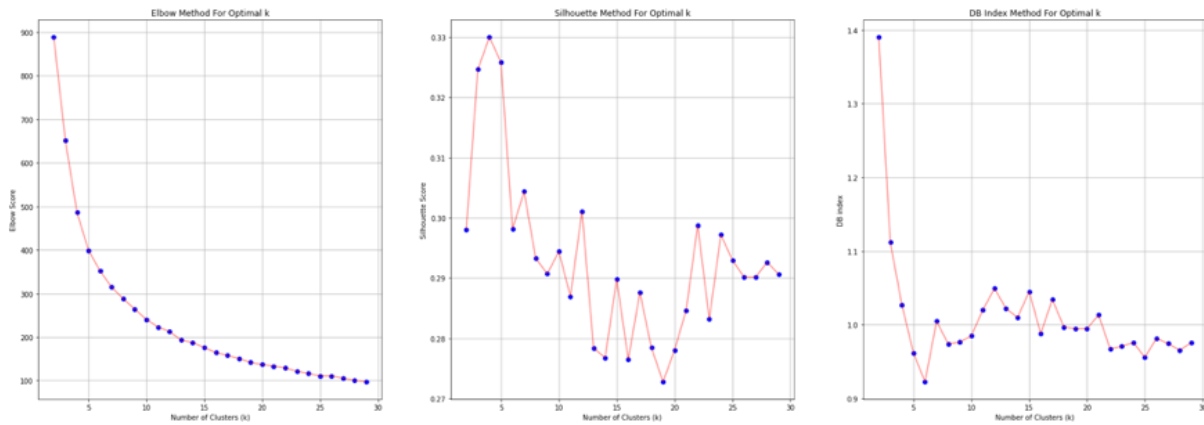


Fig.10: Different methods of finding the right number of clusters

The three diagrams above show the three different methods for finding the best number of K s for K-Means. They are not completely in accord, but there is a clear tendency. The elbow method above shows a preference for a K around 5-10, the silhouette method prefers 4 clusters, while the Davies Bouldin Index method prefers 6 clusters. So in order to find a compromise we decided to go with 5 clusters, which we numbered 0 through 4.

3.5 Comparing clusters

Below is an image of snippets from two clusters (cluster 1 and 2) that are a result of our work. It is fairly obvious to the naked eye, why the autoencoder chose to group these images. The leftmost pair (cluster 1) has a wavier edge around the red fragment whereas the rightmost pair (cluster 2) has a more rectangular red fragment which is surrounded by green squares. This again gives us some reassurance of believing in the chosen approach.

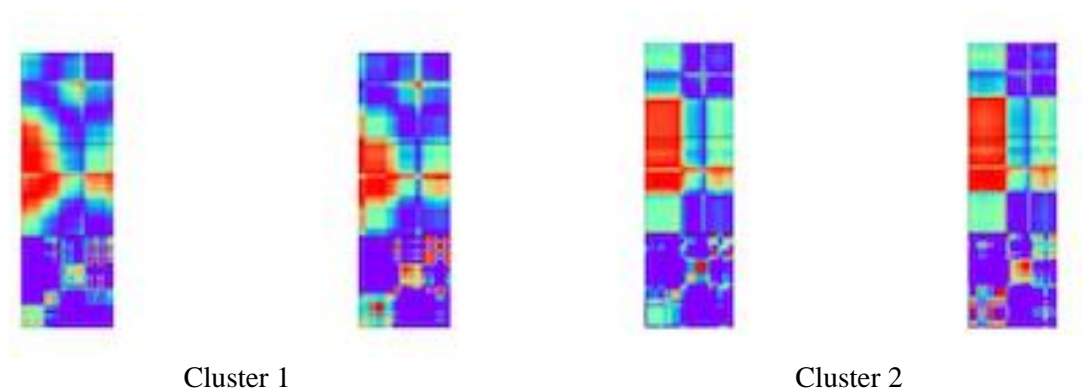


Fig.11: Two clusters compared

4. Results

In the diagrams below, which are supposed to simulate a shift schedule for the masters, we have visualized how the clusters are distributed over the course of a month. The diagrams are to be understood the following way: Each color is a cluster and all clusters with the same color have the same number as well. So for instance, in the first diagram, cluster 0 is blue and cluster 1 is turquoise. The colors cannot be transferred directly to the other diagrams as more clusters require more colors, and so the colors do not represent the same clusters across the diagrams. White fields indicate no crossing since the ferry is not operating at that particular time. The diagram on the left has 5 clusters, the diagram in the middle has 10 clusters, and the diagram on the right has 20 clusters, and while there are some similarities between the diagrams, as soon as we go above five clusters the pattern is not so clear any longer. And so it is quite obvious from the below diagrams that nothing is gained by clustering by more than five, as this will only result in confusion. This, however, is exactly what we expected based on the results of Fig.10.

Each cluster should represent a certain maneuvering style, and since the same cluster number appears in successive crossings, it seems likely that we have, at least to some extent, identified the way the master operates the ship during maneuvering mode. However, since we do not know who actually operated the ferry, nor how many people master the ferry over the course of a month, the cluster numbers could represent more than one person's personal maneuvering style. According to the ferry company a regular shift is from 11 in the morning to 23 in the evening and again the next morning from 5 to 11. However, since we only look at section 1 crossings, merely even hours are shown in the diagram. The hour shown is when the ferry left the harbor in Tårs, and so a shift beginning at 5 in Spodsbjerg will include the hours 6,8 and 10 as departures from Tårs. At 11 the ferry will once again be in Spodsbjerg, and a new master will take over the operation of the ferry. The new master will then have a shift from 11 in the morning to 23 in the evening (shown in the diagram as hours 12,14,16,18,20 and 22), and continue his shift the next morning from 5 to 11 (6-10 inclusive).

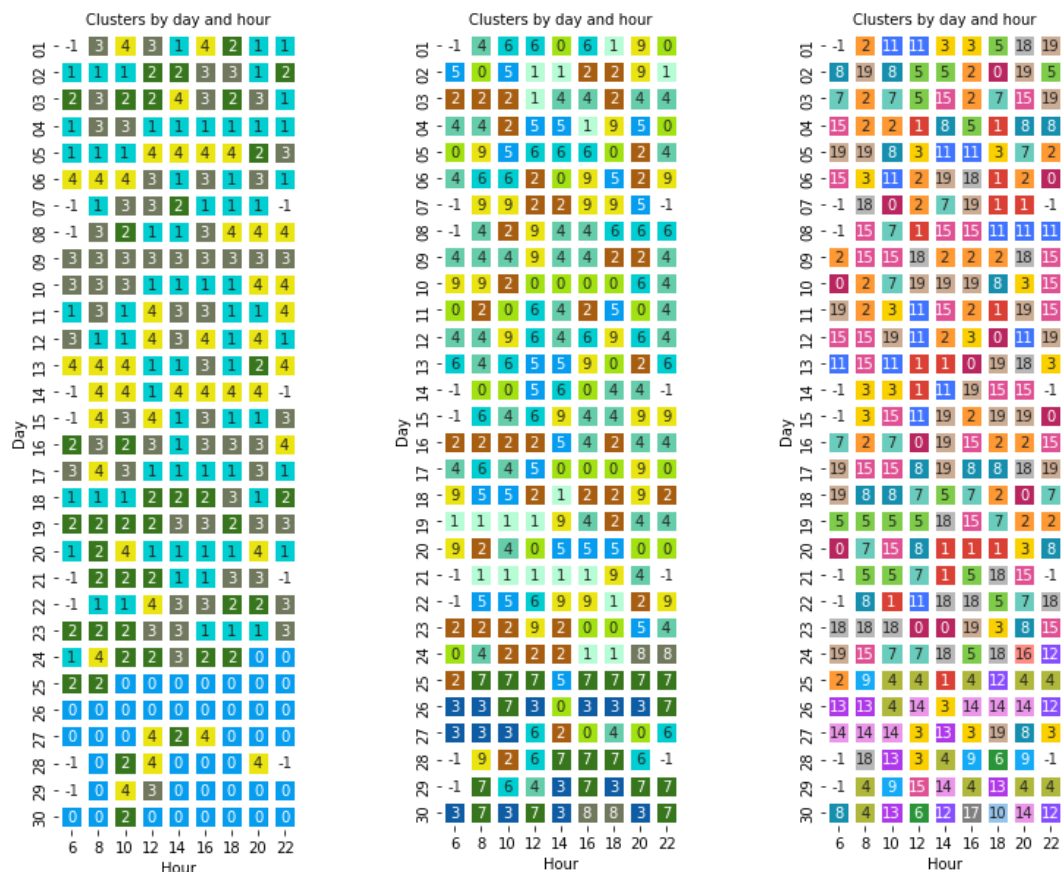


Fig.12: An attempt at clustering the maneuvering style of the masters as a simulated shift schedule

4.1. Observations

We made the following observations by considering the first of the three diagrams in Fig.12: Day 4-5 (the turquoise blocks) is what we would consider to be a complete shift, as it starts at 12 on day 4 and continues until 10 the next day inclusive. This is in line with what we know, from the ferry company, constitutes a regular shift. Likewise day 5 to 6 shows a similar pattern except for the hours 20 and 22. Day 10 looks promising as well, but day 9 starts too early. Day 13 is yet again looking promising, but again the day before (day 12) only shows remnants of a complete shift. And finally day 17-18 is also an almost perfect shift. Apparently, days 24 to 29 are quite different from the rest of the month as this is almost entirely its own cluster. Whether this indicates that the same person was working a lot toward the end of the month we do not know, it could also simply indicate that the weather or traffic was very different in that period. There also seems to be some kind of tendency for our model to wrongly identify the evenings. It is rare that the last two crossings have been grouped into the same cluster. This could be an indication of nighttime approaching and therefore lower visibility, but this would have to be explored further.

4.2. A closer look at the maneuverings

We can furthermore zoom in on the series on day 5-6 and see if we can spot any kinds of trends and dissimilarities between the clusters to see wherein the differences lie.

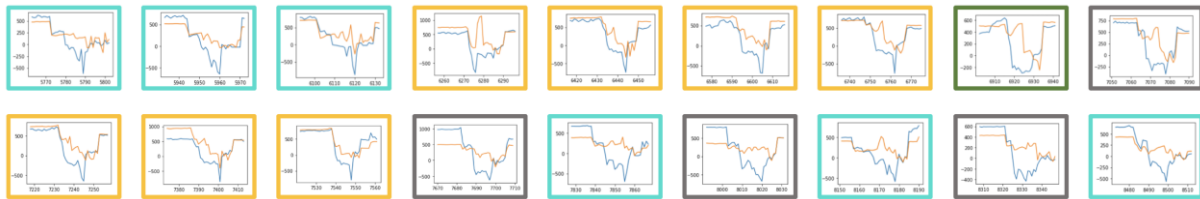


Fig.13: A zoom view of day 5 and 6 colored by cluster

The diagram above shows a zoomed in view of day 5 and 6 from Fig.12. The border colors indicate which cluster each plot belongs to. The first three plots (all in turquoise) belong to the same cluster, namely cluster 1. They are all very similar in style, all cover about the same speed range and the thruster pairs follow each other fairly well in the passage part of the plots. They also all have a double downward peak about two thirds of the way into the plot, but they don't match up too well with the other turquoise plots. The yellow plots are also very similar in style except for the first one, which has a high upward peak in the middle section of the plot, and the sixth yellow plot has a gap between the thruster pairs and one pair comes in at around 1000 rather than 500. Rather than having a double downward peak the yellow plots all have more of a slack and then a downward peak. Since the braking in the first yellow plot is premature compared to the other yellow plots, it is likely the cause of some external factor such as a small fishing boat crossing the track of the ferry, forcing the master into an untimely deceleration, thus having to speed up afterwards in order to get back on track. The green cluster ought to have been yellow based on what we know of the shift schedule, but it is quite obvious why the clustering algorithm has chosen not to include this plot with the yellow plots as it looks very different, however the green plot is actually very similar to the dark gray plot right after it.

When looking at line two (day 6) beginning with three yellow plots, we would expect a different master to take over after those three maneuverings as there should be a shift here. And it is actually quite clear that the style changes significantly. The master taking over uses a much broader speed range, has a bigger gap between thrusters in the passage mode, and the braking isn't so much done as peaks, but rather stays down for a longer period of time. Ultimately, the dark gray and turquoise plots on day 6 probably belong to the same master, and should not be related to the turquoise plots on day 5.

5. Conclusion

We have shown that through small amounts of preprocessing on ferry operational datasets, such as interpolation of coordinates, and manipulating thrust values according to the angle of thrusters; unsupervised machine learning can most certainly be applied to operational ferry patterns in order to identify the maneuvering style, and may even be applicable to yet other similar scenarios as well. Whether the maneuvering style identified is caused by weather conditions, personal preference, or a mixture thereof is still not absolutely clear, however, we do see patterns that point toward personal preference, since abrupt shifts occur in the maneuvering style when one master ends his shift and another begins. It seems very likely that we could further improve our model and achieve even better results by considering more external factors. This may even be improved to the point where each master has his or her own footprint.

5.1. Future work

In order to achieve better results, the neural network functioning as an autoencoder could be changed to a sparse autoencoder or a variational autoencoder, as research has indicated this could improve progress. Other clustering algorithms could be applied as well, to see if data can be even better separated. Grad-cam, see *Zhou et al. (2016)*, could be applied to visualize more of what is going on inside the network, and other measures could be applied to the neural network such as batch normalization. Furthermore, external parameters such as tide, currents and wind could be taken into consideration as well as comparing only similar times of day.

By identifying maneuvering patterns we could further look into why the patterns emerge. If we can identify the correlation between the patterns and some credible causes, we may be able to make decision on that basis. If for instance it turns out, certain patterns emerge because of low visibility conditions, then these situations would be candidates for automatic berthing. One could also envision that the passage mode would show differences within style, and maybe this affects fuel consumption. In that case it would be effectful to install a so-called ghost rider application on the ferry, which for instance, through the use of augmented reality, could show the most fuel-efficient operation the masters can attempt to follow.

References

- DENG, J.; DONG, W.; SOCHER, R.; LI, L.J.; LI, K.; FEI-FEI, L. (2009), *Imagenet: A large-scale hierarchical image database*, IEEE Conf. Computer Vision and Pattern Recognition, pp.248-255
- KUCHARSKI, D.; KŁECZEK, P.; JAWOREK-KORJAKOWSKA, J.; DYDUCH, G.; GORGON, M. (2020), *Semi-Supervised Nests of Melanocytes Segmentation Method Using Convolutional Autoencoders*, Sensors 20/6, 1546, <https://www.mdpi.com/1424-8220/20/6/1546/pdf>
- MIKKELSEN, L.; STOCHHOLM, S. (2021), *The Need for an Updated Energy Decision Support System Framework when Retrofitting Ferries with Batteries – a case study*, COMPIT Conf., Mülheim, pp.130-140, http://data.hiper-conf.info/compit2021_muelheim.pdf
- RICHARD, G.; GROSSIN, B.; GERMAINE, G.; HÉBRAIL, G.; MOLINER, A. (2020), *Autoencoder-based time series clustering with energy applications*, Conf. Apprentissage Automatique, <https://arxiv.org/pdf/2002.03624.pdf>
- ULYANIN, S.; VAZQUEZ-CANTELI, J.R.; NAGY, Z. (2019), *Feature Extraction and Clustering of Building Energy Profiles Encoded as Images*, 16th IBPSA Conf., Rome, pp.2998-3005, http://www.ibpsa.org/proceedings/BS2019/BS2019_210896.pdf

WANG, Z.; OATES, T. (2015), *Encoding Time Series as Images for Visual Inspection and Classification Using Tiled Convolutional Neural Networks*, Computer Science and Electrical Engineering Department University of Maryland Baltimore County

YANG, C.L.; CHENG, Z.X.; YANG, C.Y. (2019), *Sensor Classification Using Convolutional Neural Network by Encoding Multivariate Time Series as Two-Dimensional Colored Images*, Department of Industrial Management, National Taiwan University of Science and Technology.

ZHOU, B., KHOSLA, A., LAPEDRIZA, A., OLIVA, A. and TORRALBA, A. (2016). *Learning Deep Features for Discriminative Localization*, CVPR 2921-2929.

Assessing Alternative Fuel Types for Ultra Large Container Vessels in Face of Uncertainty

Kaan Terün, TU Delft, Delft/The Netherlands, kaanterun@gmail.com

Austin A. Kana, TU Delft, Delft/The Netherlands, a.a.kana@tudelft.nl

Rommert Dekker, Erasmus University, Rotterdam/The Netherlands, rdekker@ese.eur.nl

Abstract

This paper proposes the use of an approach inspired by Robust Decision Making (RDM) to make a comparison between cleaner alternative fuels for ultra large container vessels (ULCV), while taking economic and regulatory uncertainties into account. A parametric design tool for ULCVs with different alternative fuels in combination with an approach inspired by RDM has been developed for modelling the involved uncertainties. The proposed approach provides new insights into the performance of the designs under various scenarios, such as the effect of fuel choice on the operational aspects and the limitations of the designs.

1. Introduction

International treaties such as the Kyoto Protocol and the Paris Agreement encourage countries and international organizations to tackle global warming. The International Maritime Organization (IMO) has the responsibility for limiting greenhouse gasses in the maritime sector, *United Nations (1998)*. IMO forecasts that CO₂ emissions produced by ships could rise by 90 to 130% by the year 2050 if no measures are taken now, *Faber et al. (2020)*. IMO aims to reduce GHG emissions by 50% by 2050 and CO₂ emissions by 40% by 2030, and by 70% by 2050 (all compared to 2008).

Ships are responsible for roughly 2.8% of anthropogenic CO₂ emissions, globally, *Faber et al. (2020)*. Container ships are the most polluting ship type, as they account for 23% of CO₂ produced by ships, i.e., 0.5% of global CO₂ emissions, *Olmer et al. (2017)*. Amongst container ship classes it is not possible to distinguish a particularly pollutant class, but it can be seen that ULCVs are the fastest sailing and fastest growing class, *Olmer et al. (2017)*, *Faber et al. (2020)*. Since ULCVs are the class of the future and usually the flagships of the big shipping companies, it should be asked how ULCVs should be designed, such that their emissions can be reduced. There are different definitions for what an ULCV is, but this paper considers any container ship which can carry more than 14,000 TEU an ULCV, similar to other sources, *Probst (2016)*, *Tas (2018)*, *MAN (2016)*. Additionally, various types of fuels are also considered.

IMO has introduced the Energy Efficiency Design Index (EEDI) to reduce emissions by making newly built ships more efficient. The required EEDI is lowered in phases. Phase 3, which will start in 2025, will require ships to reduce their EEDI by 30% relative to the reference set by IMO. IMO has also introduced a voluntary measure, the Energy Efficiency Operational Index (EEOI). Both indexes indicate how energy efficient a ship is. The EEDI does it with focus on the design, while the EEOI does it with focus on the operations. As a result, EEDI will indicate the potential of a ship, but EEOI will indicate a more realistic operational performance compared to EEDI. IMO plans to introduce new phases for EEDI as defined by IMO's Marine Environment Protection Committee, but it is unclear when and how these phases will be changed. There are also sovereign states which plan to introduce additional policies, such as Germany who prepares to introduce CO₂ price of 25 Euros per ton in 2021 and gradually increase this, *Bundesregierung Deutschland (2019)*.

Beyond regulatory uncertainties there are also technical and economic uncertainties. It is uncertain how fast technologies that could help reduce emissions will be developed or how different economic parameters, which influence the performance of ships will change over time. Det Norske Veritas - Germanischer Lloyd (DNV GL) states that the upcoming period will contain drastic changes and a lot of uncertainties for ships. *DNV GL (2017)* proposes the term "carbon robust ships" for ships that can

stay profitable under any decarbonization scenario and underlines the importance of robustness. This only emphasizes the requirement of handling the involved uncertainties in an adequate manner.

There are different possibilities for reducing emissions: through policies *Psaraftis (2019)*, operational changes, and emission abatement technologies, *Schwartz et al. (2020)*, *van den Berg (2018)*, *Mander, (2017)*. Another option is to switch to alternative fuels; fuels that have a lower carbon content compared to heavy fuel oil (HFO) and are therefore “cleaner”. Implementing alternative fuel types in container ships will affect their design and price, as they require different storage facilities. Research in this field has been conducted for different fuel types, *Adachi et al. (2014)*, *de Vries (2019)*, *Ammar (2019)*. These articles concentrate on one specific fuel type. Some make comparisons between different fuel types, but only focus on one aspect such as emissions, *Gilbert et al. (2018)*, *Bicer and Dincer (2018)*. *Deniz and Zincir (2016)* make a thorough comparison between fuel types, based on 12 criteria, but do not take future uncertainty into account nor adaptations to it.

This paper proposes an approach inspired by Robust Decision Making (RDM) as a valuable method for assessing alternative fuel types for ULCVs, while also taking regulatory and economic uncertainty into account. RDM has been applied in various subjects, such as mitigation of river flooding, *Kwakkel et al. (2016)*, management of an aircraft fleet, *Moallemi et al. (2020)*, deciding on retrofitting or decommissioning old nuclear reactors, *Perrier (2018)*, and others. But as far as the authors’ knowledge, it has not yet been used for subjects regarding ship design. RDM was chosen as the most suitable method for this subject based on the level of uncertainties, the emphasis on robustness, and the possibility to evaluate based on multiple criteria. Based on this method an approach was developed which applies certain steps of RDM.

This approach could be used by ship owners and operators who have to decide what kind of ship they want to invest in and operate in the future or even by policymakers who wish to see how effective new policies may be. The approach gives an integrated view on the outcome of the fuel choice for ULCVs by combining a new parametric design tool specific for ULCVs with an economic model and RDM steps. The parametric design tool is tailored specifically for assessing sizing implications of ULCVs from using alternative fuels. It indicates the effect of fuel choice on the operational aspects, the results due to these, and their limitations. The method intends to define price limits for additional costs which arise due to the implementation of alternative fuels, such that they are economically feasible. We do not claim to include all aspects in the fuel type comparison as that is outside the scope of this paper. However, the integrated nature of the proposed method does show advantages in incorporating many of the interrelated aspects of the problem. Fig.1. shows the general overview of the approach.

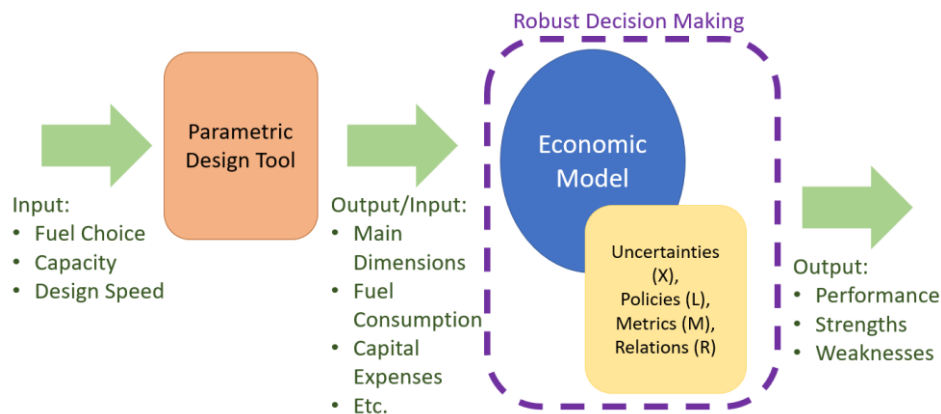


Fig.1: Overview of the approach

2. Alternative Fuel Types

ULCVs can be made more efficient by adapting new energy saving technologies or by changing the way they operate. These changes either depend on technological development or require substantial changes to existing operations. One way to reduce emissions with existing technologies and operations

is switching to alternative fuels. Alternative fuels can be used in existing internal combustion engines but need to be used in a dual fuel configuration as they require a pilot fuel for ignition *ABS (2019)*, *MAN (2018)*. Possible alternatives for dual fuel use are: liquefied petroleum gas (LPG), liquefied natural gas (LNG), methanol, hydrogen, and ammonia *DNV GL (2019)*.

Table I shows a comparison of some properties of these fuel types. The majority requires to be cooled down and/or kept under pressure for storage. Fuels such as LNG or hydrogen will require adaptations of cryogenic technologies. While this has not yet been widely implemented, first implementations show that it is feasible *Ovcina (2021)*. Nonetheless, alternative fuel types require much more storage space than conventional HFO. This will have an effect on the design of ULCVs, if implemented. The additional facilities required for storage will also affect the purchase price of the vessels. Estimating these additional costs is difficult as ships using these fuels are uncommon. The last column of Table I shows the potential reduction in tank-to-wake (TTW) CO₂ emissions for the same output of energy, compared to HFO. While other emissions, such as NO_x and SO_x are also important, this research focused primarily on CO₂ because of the timely IMO goals concerning CO₂ emissions.

Table I: Comparison of different fuel types, adapted from *ABS (2019)*

Fuel Type	Boiling Point [°C] (at 1 bar)	Tank Volume for Equal Amount of Energy (Compared to HFO)	CO ₂ , kg CO ₂ /kWh Reduction (Compared to HFO)
HFO	300-700	1	0%
LNG	-162	3-4	26%
LPG	-26.2	3	15.6%
Methanol	65	2.5	11
Hydrogen (Liquefied)	-253	4-5	100%
Ammonia	-33	2.5	100%

To reduce emissions effectively, well-to-wake (WTW) emissions should be considered but for the purpose of this article only TTW emissions were considered. This is because IMO uses EEOI as metric for regulations and EEOI only considers TTW emissions. Fuels such as hydrogen and ammonia could become even better alternatives in combination with other technologies like fuel cells. However, these types of technologies require further development to be implemented at large scale.

3. Handling Uncertainty

The uncertainties involved in the choice of fuel for ULCVs can be divided in 3 categories; technical, regulatory, and economic. Technical uncertainties concern the development of new, game-changing technologies, such as fuel cells, batteries, etc. It is uncertain when technological breakthroughs in these technologies are going to happen, which would have big potentials in reducing emissions. There are also uncertainties about possible regulatory measures which could be taken by IMO or sovereign states. The introduction of policies enforcing speed limits or bunker levies are being discussed, *Psaraftis (2019)*. It is unclear which type of policy and with what conditions these would be introduced. Fuel prices, trade demand, and other aspects related to markets form the economic uncertainties. These affect how profitable ships are and also affect the willingness of ship owners to invest in cleaner ships.

The combination of all of these uncertainties makes it very difficult to make an accurate forecast of the future. Beyond this, it also puts pressure on the design quality of ships. ULCVs that are going to be built have to survive this upcoming turbulent period. If these uncertainties are not taken into account while designing ULCVs, the probability that they survive will be less. This is why a method for uncertainty modelling is required.

Economic and regulatory uncertainties were the primary uncertainties examined in this study. Decisions related to the next fleet of ULCVs need to be made on a short time frame, and the development of other propulsion technologies will require a longer time horizon to become feasible. Thus, technical

uncertainties have been excluded since economic and regulatory uncertainties provide substantial longer-term uncertainties for ULCVs. Technical uncertainties could be taken into account in future research. To this end, only internal combustion engines have been considered.

3.1. Uncertainty Modelling

There are different methods available for modelling uncertainties, but it is important to choose the right method for the problem that one is trying to solve. Requirements for the method have to be defined to make the right choice. Firstly, the level of uncertainty, which is being handled, must be established. For this purpose, the taxonomy of *Marchau et al. (2019)* has been used.

The lowest level of uncertainty is complete certainty, a situation where everything is known precisely. Level 1 uncertainty is the situation where there is a slight uncertainty but there is no need or necessity to measure the magnitude of uncertainty. Level 2 uncertainty is when there are few future scenarios, which can be predicted or a probabilistic model can be developed for a representation of the situation. Level 3 uncertainty represents the situation when there are more possible future outcomes, but it is not possible to assign any probabilities to them. Level 4 uncertainty is the deepest level of recognized uncertainty. It is divided in two: the ability to put limits for possible futures exist (4a) and the only knowledge there is, is the knowledge of the unknown (4b). Beyond this level is total ignorance.

The level of uncertainty for this study is assumed to be higher than 2, because there are many uncertainties involved and assigning probabilities to them is believed to be very difficult, due to the complexity of the subject (Nonetheless, it has been attempted in *Kana and Harrison (2017)*, *Zwaginga et al. (2021)*). This means that neither deterministic nor stochastic models can be options. On the other hand, there is a general understanding of possible futures and how certain aspects function. Therefore, the level of uncertainty is smaller than 4b. Thus, the level of uncertainty for this subject should be 3 or 4a.

The aim should be robustness. This can also be supported with the taxonomy of *Doerry and Koenig (2017)*. When requirements are fixed, it is possible to optimize a design. However, when requirements change there are two possible design strategies. One can have a fixed design, which is robust and can survive in many circumstances or a flexible design, which is modular and can adapt to the circumstances. Both are valid approaches, but flexibility would mean that the ship is adapted to the changing circumstances, which in this case would require retrofitting.

Table II: Overview of considered methods, based on *Moallemi et al. (2020)*

Method	Level of Uncertainty	Evaluation	Aim	Sources
Real Option Analysis (ROA)	2	Profits	Profitability	<i>Bowman and Moskowitz (2001)</i>
Engineering Option Analysis (EOA)	3	Multiple Criteria	Flexibility	<i>de Neufville and Smet (2019)</i>
Info-Gap Theory (IG)	4b	Multiple Criteria	Robustness & Opportuneness	<i>Ben-Haim (2019)</i>
Robust Decision Making (RDM)	4a	Multiple Criteria	Robustness	<i>Lempert (2019)</i> , <i>Moallemi et al. (2020)</i>
Many Objective Robust Decision Making (MORDM)	4a (probability distribution for parameters)	Multiple criteria	Optimality	<i>Kasprzyk et al. (2013)</i>
Epoch-Era Analysis (EEA)	3	Multiple criteria	Robustness / optimality	<i>Gaspar et al. (2012)</i> , <i>Moallemi et al. (2020)</i>
Markov Decision Process (MDP)	2	Multiple criteria	Flexibility	<i>Kana et al. (2015)</i> , <i>Niese and Singer (2013)</i>

Retrofits for ships are always expensive and in a market as competitive as container shipping it could become problematic. Thus robustness is believed to be a better and safer approach. Similarly, *DNV GL (2017)* proposes “carbon-robust ships” for the same reasons.

Furthermore, the method should make it possible to make evaluation based on multiple criteria. Considering these requirements, a selection of methods have been considered, *Marchau et al. (2019)*. These methods and how they fulfil the defined requirements can be seen in Table II.

Based on Table II, it can be seen that only Robust Decision Making (RDM) and Epoch-Era Analysis (EEA) fulfil the defined requirements. The main difference between these methods is the level of uncertainty. *Moallemi et al. (2020)* have compared both methods by applying them to the same problem and analyzing the results. They show that the level of uncertainty within RDM is higher, as with RDM there is no probability assigned to the scenarios. EEA, on the other hand, deals with uncertainties with known probability distributions (level 2 uncertainty) or when there is a limited amount of possible futures (level 3 uncertainty). In the second case, probabilities are not assigned, but the developer still defines the rules for epoch transitions. This inadvertently creates epochs which the developer believes are plausible, so the outcome heavily depends on his judgement *Gaspar et al. (2012)*. RDM, in contrast, uses scenarios to stress test concepts to define in which circumstances the concept fails, succeeds, or otherwise performs. By comparing all the options, it identifies the most robust option. RDM has been chosen as the most suitable method as it handles a level of uncertainty which is adequate for this subject. The method is capable of making an evaluation based on multiple criteria and aims for robustness, which was deemed critical for this subject. The details of RDM are discussed in Section 5.

What differs RDM from other methods are also the unique insights that it provides. While other approaches typically only vary one parameter at a time, RDM is able to handle the variation of multiple parameters. This gives a better understanding of the outcome over a wider range of possible futures. Furthermore, RDM aims to reduce the effect of over-confident assumptions of designs by providing a better comprehension on why and how concepts fail, *Lempert (2019)*.

4. Parametric Design Tool

An approach based on RDM makes it possible to take uncertainty into account and make a comparison between different designs. As the aim of this study is to make a comparison between ships that use different alternative fuels, a manner of creating designs for ULCVs depending on the choice of fuel is required. Because of this a parametric design tool for ULCVs was developed which generates preliminary designs for ULCVs and calculates all relevant properties, such as main dimensions, engine size, fuel consumption, tank size, etc.

The parametric design tool requires 3 main inputs: capacity in TEU, design speed in knots, and fuel choice. These parameters were chosen as they are believed to have the biggest influence on a ship’s design. Other metrics such as TEUs/DWT or USD/TEU could also have been used, but these are not as tangible as the chosen ones. By using these inputs it was possible to develop a parametric design tool that determines ship dimension which are used to calculate resistance, power, engine size, etc. with common methods. This would not be possible with the above-mentioned ratios. Information regarding the design of ULCVs is not widely accessible. To gain a better understanding of ULCV design, a ship database, *Clarksons Research (2020)*, available pictures of ULCVs and information regarding ULCVs from various sources were used. The following observations were made:

- (i) The general arrangement of ULCVs differs from smaller container vessels. Smaller container vessels have their deckhouse at the aft, above the engine room. ULCVs, on the other hand, usually have the deckhouse at ca. 2/3 of length upfront, while the engine room is in the aft of the vessel, with the funnels also at this position.
- (ii) Regardless of the length of the ship, there are usually 4 bays behind the funnels.

- (iii) The fifth bay from the stern, i.e. the bay in front of the funnels, is above the engine room. Thus, there is less space below deck for this bay, similarly as the last 4 bays.
- (iv) The midship section of the ship is the part that gets longer as the length of the ship increases, the bow (first 4 bays) and stern sections (last 5 bays) of the ship do not change.
- (v) The stack height in the first 4 bays is less due to the regulation regarding the navigation bridge visibility, which states that “The view of the sea surface from the conning position shall not be obscured by more than two ship lengths, or 500 m, whichever is the less...” *IMO (1999)*.
- (vi) Below deck there are 2 rows less than above deck.
- (vii) Even though from a regulatory perspective the distance between the forward perpendicular and the collision bulkhead could be as short as 7 m, *DNV-GL (2020)*, all ULCVs have a much longer bow, usually around 20-25 m.
- (viii) The bays which are affected by the narrowness/form of the hull are the first 4 and last 5 bays. The bays in the midship section are not affected.
- (ix) The deckhouse has a horizontal length of ca. 15 m.
- (x) The horizontal length of the funnels varies between 6 to 15 m, depending on the size of the ship.
- (xi) 87% of ULCVs have a draft of 16 ± 0.5 m.

Based on these observations, some assumptions were made. The draft of all ULCVs is 16 m. The ship can be divided in 3 sections: the aft (last 5 bays), the midship, and the bow (first 4 bays). The aft and bow section of ULCVs do not change, the main change occurs in the midship when ships become longer. It has been assumed that below deck there are always 12 tiers and above deck 11, *Probst (2016)*. Taking these into account, Table III shows the relation between capacity and hull shape.

Table III: Matrix used to calculate the capacity

	Last 5 bays	Midship	Bays 3&4	Bays 1&2
Tiers Above Deck	11	11	10	9
Above Deck	100%	100%	100%	100%
Below Deck	40%	100%	80%	60%

The parametric tool determines the optimal combination of number of bays and rows based on this matrix, such that the total capacity is closest and greater than the given input for capacity. The number of bays and rows are used to calculate the main dimensions of the ship. Subsequently, the resistance is calculated with the Holtrop & Mennen Method, *Holtrop and Mennen (1982)*, according to the design speed. Propeller matching and power calculations are done as proposed by *Klein Woud and Stapersma (2002)*. Wageningen B-series for 4-bladed fixed pitch propellers were used for matching. Engines which were taken as reference had a maximum rotations per minute (RPM) of 80 RPM, which make it possible to match the most efficient propeller without the need of a gearbox. This ensures that the propulsion plant is as efficient as possible. For the engine selection, engines of MAN were used, which has two-stroke diesel engines up to 82,440 kW. It has been assumed that there is an engine margin of 10% and a sea margin of 15%.

$$SFOC = -6.392 \cdot 10^{-5} \cdot SMCR^3 + 0.017 \cdot SMCR^2 - 1.396 \cdot SMCR + 187.175 \left[\frac{g}{kW_h} \right] \text{ Eq. 1}$$

Fuel consumption can be estimated with methods such as described by *Graf von Westarp (2020)*, but such methods require specific speed and fuel consumption of vessels. As such data was unavailable the fuel consumption of these engines was approximated as seen in Eq.(1), which is based on the information given by the manufacturer *MAN (2020a)*. The equation describes the specific fuel oil consumption (SFOC) as a function of specified maximum continuous rating (SMCR), which can be calculated for each required power. The specific pilot oil consumption (SPOC) and specific gas consumption (SGC) for each fuel type has been calculated as described by *MAN [2018]*. For this purpose, Eq.(1), the lower calorific values (LCV), and required pilot fuel ratios, as seen in Table IV, have been used. Table IV also shows the values of specific CO₂ emissions, i.e., the CO₂ produced for burning each fuel, which has been used to determine the TTW emissions of each ship. For the consumption, auxiliary loads were neglected as roughly 80% of energy demand on a container ship comes from the propulsion plant, *Aijjou et al. (2019)*, *Faber et al. (2020)*.

Table IV: Properties of the different fuel types

Fuel Type	Lower Calorific Value [kJ/kg]	Required Pilot Fuel	Specific CO ₂ Emissions [kg CO ₂ / kg fuel]
HFO	42,700	0.0%	3.11 <i>Toolbox (2009)</i>
LNG	48,600	1.5%	2.75 <i>Toolbox (2009)</i>
LPG	46,000	3.0% <i>MAN (2020a)</i>	3.01 <i>Toolbox (2009)</i>
Methanol	19,900	5.0% <i>MAN (2020a)</i>	1.37 <i>Toolbox (2009)</i>
Hydrogen	120,000	3.0%	0
Ammonia	18,600	5.0%	0

The information regarding fuel consumption and the information from Table I were used to calculate the required tank volume. The fuel capacity of a ship is based on the business strategy of the shipping company. It was assumed that the ship should be able to sail 2.5 times the length of its route, at design speed. This would ensure that during a round tour the ship can fuel at the port with the lowest prices, as operational costs mainly consist of fuel costs. The space underneath the deckhouse has been assigned for the fuel tank. From Table I it can be understood that alternative fuels require more volume compared to conventional fuels. Therefore, if the assigned volume is insufficient, a combination of lengthening the ship and converting cargo space to tank space is done. As the cross-sectional area is known it is possible to calculate the length of the fuel tank. Depending on the difference between the required length of the tank and the length of the deckhouse, a combination of lengthening the ship and converting some cargo space to fuel tanks is done. The beam or draft could also have been adjusted to accommodate the extra volume, but these dimensions are limited by ports and the Suez Canal. Therefore, the length has been chosen as it was less limiting. The changes which are done depending on the different situations are in Table V. An example of the consequences for a ship with 24 rows has been demonstrated in the third column. As seen, this procedure ensures that there is sufficient space for the fuel tank, without making drastic changes to the main properties of the ship.

Table V: Lengthening process depending on the length difference

Situation	Consequence	Change in TEU for a vessel with 24 rows
$\Delta L \leq 0$	Nothing	No change
$0 < \Delta L \leq 3$	The ship is made 3m longer	No change
$3 < \Delta L \leq 6.1$	Half of a bay under the deck is added to the fuel tank	262 TEUs less
$6.1 < \Delta L \leq 12.2$	A whole bay under the deck is added to the fuel tank	524 TEUs less
$12.2 < \Delta L \leq 18.3$	The ship is lengthened by 1 bay, i.e., 14.6m(including the additional bulkhead), and 1.5 bays under the deck and a bulkhead are added to the fuel tank	266 TEUs more
$18.3 < \Delta L \leq 26.8$	The ship is lengthened by 1 bay, i.e., 14.6m(including the additional bulkhead), and 2 bays under the deck and a bulkhead are added to the fuel tank	4 TEUs more
$26.8 < \Delta L \leq 32.9$	The ship is lengthened by 1 bay, i.e., 14.6m(including the additional bulkhead), and 2.5 bays under the deck and a bulkhead are added to the fuel tank	258 TEUs less
$32.9 < \Delta L \leq 41.4$	The ship is lengthened by 1 bay, i.e., 14.6m(including the additional bulkhead), and 3 bays under the deck and a bulkhead are added to the fuel tank	520 TEUs less

Data of existing ULCVs, *Clarksons Research (2020)*, which use conventional fuel (HFO) were used to determine the relation between TEUs and purchase price (PP) in Eq.(2). This relation can be used for ULCVs using HFO and having capacity 14,000 to 28,000 TEUs, with an R² value of 0.8354. Estimations for alternative fuels were not possible, as ships using these fuels either do not exist yet or are scarce. ULCVs that use alternative fuels will be more expensive, as they require additional storage facilities. These additional costs are not included in the estimate. A statement regarding the price limits of these additional costs such that vessels are still economically feasible is provided in Section 5.

$$PP = -2.108 \cdot 10^{-7} \cdot n_{teu}^2 + 12.436 \cdot 10^{-3} \cdot n_{teu} - 21.203 \text{ [USD]} \text{ Eq. 2}$$

The PP of each ship was calculated accordingly. A ship which has been lengthened by the process described above will be more expensive compared to original form. To account for this effect, the PP was calculated with the total amount of TEUs and the TEUs which were converted to fuel tanks during the process. Only in the case that the ship is lengthened by 3 m, is there no effect. As the effect of lengthening an ULCV (which is min. 360 m long) by 3 m on the PP is negligible, the difference is smaller than 1%. Furthermore, it is assumed that the cost of financing will affect the capital expenses of a ship, but as it is assumed to influence all ship concepts equally it will not change the conclusion of this paper. For this reason, it was not taken into the scope of this study.

5. Approach to Uncertainty

RDM as a method searches for the most robust strategy/design by running a myriad of scenarios, comparing its performances and hereby identifies vulnerabilities, *Moallemi et al. (2020)*. The method can be divided into 4 steps:

- (i) The first step is defining the key uncertainties concerning the studied system, the designs, and objectives. Usually, the XLMR framework is used in a participatory process to specify the exogenous uncertainties (X), policy levers (L), metrics (M), and relationships (R), *Lempert et al. 2013*).
- (ii) In the second step the performances of the different designs are assessed indifferent scenarios, according to the defined uncertainties.
- (iii) The third step is to search for conditions in which the options show vulnerabilities.
- (iv) In the fourth step trade-off analyses are made, where the performances are compared according to the objectives. The process can be stopped here or turned into an iterative process by starting again at the first step with the newly acquired knowledge with the pursuit of finding a more robust design, *Kwakkel et al. (2016)*.

RDM differs from other methods as it does not assign probabilities to different scenarios but simulates many scenarios and compares the outcome of all. The probability of one scenario occurring is not relevant, rather the performance in all scenarios is. RDM looks under which circumstances one design prospers or fails. By looking at the number of scenarios in which one design outperforms another, it decides which design is more robust. This study differs from the original RDM as it does not strictly execute the third step of the method and has simplified the scenario construction.

RDM seems similar to multi-objective optimization but there are clear differences. While multi-objective optimization is interested in the Pareto optimal front of the results, RDM is concerned with all results. RDM is not only interested in the strengths of each design but also in their weaknesses. Furthermore, it aims to find the reason why the design is strong or weak in some scenarios.

The XLMR framework, *Lempert et al. (2013)*, was used to form the basis of the method. Freight rate, fuel prices, and fullness, i.e., a parameter which indicates how full the ship is or the ratio between available cargo space and used cargo space, were implemented as exogenous uncertainties (X). Two policy options (L) were tested: speed limits, which would limit the maximum speed that ships could sail, and carbon taxes, which would tax ships based on the TTW CO₂ emissions they produce. These are not the only possible policies, but the most prominent ones which was the reason why they were chosen for this study. The implementation date of these policies is also a variable. The EEOI and net present value (NPV) were used as metrics (M). The EEOI is calculated using Eq.(3), where $m_{CO_2,i}$ is the mass of CO₂ produced on trip i , $m_{cargo,i}$ is the number of TEUs carried on trip i , and D_i is the distance travelled on trip i . The EEOI indicates how the vessel performs in terms of CO₂ emissions, so the lower the better. The NPV has been used as an indicator for profitability and is calculated with Eq.(4), where t indicates the year, t_{life} the lifetime of the ship, $Cashflow_t$ the cash flow in year t , and r the discount rate. The cash flow in year 0 is the negative PP which is paid at the start, in the upcoming years it is the profit as seen in Eq.(6). In the last year, additional to the profit, the ship is sold at scrap value which was assumed to be 10% of the PP. An illustrative example has been given in the Appendix.

$$EEOI = \frac{\sum_i m_{CO_2,i}}{\sum_i (m_{cargo,i} \cdot D_i)} [CO_2 \text{ kg}/(TEU \cdot nm)] \text{ Eq. 3}$$

$$NPV = \sum_{t=0}^{t_{life}} \frac{Cashflow_t}{(1+r)^t} [USD] \text{ Eq. 4}$$

A simple economic model (R) has been developed, inspired by existing models, *Corbett et al. (2009)*, *Mulder and Dekker (2014)*, to determine the relation between the above-mentioned parameters and to simulate the operations of the ULCVs over time. The main assumption for this is that the ship operators maximize annual profits, as seen in Eq.(6). Profits are a function of speed, v , and number of trips, z (made in one year), where c_{fuel} is fuel costs, f_{port} is port fees, *Port of Rotterdam (2020)*, f_{canal} is canal fees for the Suez Canal, *Suez Canal Authority (2015)*, f_{cargo} is cargo handling fees, and c_{fix} is fixed costs. The fuel costs c_{fuel} have been calculated as in Eq.(5), where P_{fuel} is the fuel price, P_{pilot} the price of the pilot fuel (i.e., HFO), D the traveled distance (i.e., the distance between Shanghai and Rotterdam), $P(v)$ the power as a function of speed, and $cons(v)$ the fuel consumption as a function of speed, which is the adapted version of Eq.(1).

$$c_{fuel}(v, z) = z \cdot \left(\left(P_{fuel} \cdot cons_{fuel}(v) + P_{pilot} \cdot cons_{pilot}(v) \right) \cdot \frac{D}{v} \cdot P(v) \right) [USD] \text{ Eq. 5}$$

The fixed costs are determined by the costs made for the crew, the administration, insurance and the rest (i.e., stores, repairs, maintenance, etc.). Information regarding these costs are not widely available. *Watson (1998)* gives detailed estimation methods, but as his work is from 1998 the estimates were adjusted according to inflation which occurred between then and 2019, which is 56.8%. Based on different ULCVs, *RINA (2015,2016,2017)*, it was assumed that, regardless the size, ULCVs have a crew of 30, consisting of 10 officers and 20 ratings. Based on this, the fixed costs of a ship, with similar main dimensions as in Case I and II, were estimated as roughly 6.8 million USD.

$$\pi(v, z) = (Income(z) - c_{fuel}(v, z) - z \cdot (f_{port} + f_{canal} + f_{cargo})) \cdot z - c_{fix} \text{ Eq. 6}$$

Income is calculated as seen in Eq.(7), where r_f is the freight rate, δ fullness, and n_{TEU} the ship's total capacity. The factor in front of δ has been implemented to reflect the trade deficit between China and the European Union (EU). Due to this imbalance ships bring more goods to Europe than to China. In 2019, EU's export to China were roughly 55% of their imports, *Eurostat (2020)*. The factor represents the average of the fullness in both traveling directions.

$$Income(z) = z \cdot r_f \cdot \left(\frac{1 + 0.55}{2} \cdot \delta \right) \cdot n_{TEU} [USD] \text{ Eq. 7}$$

The number of trips and speed is optimized for maximum annual profits for each ship. The number of trips was restricted to be an integer, as shipping lines want to have weekly calls at ports. Speed, on the other hand, is a real number. The results from this optimization are used for calculating the EEOI and NPV of each ship over its lifetime, i.e., 25 years. For this optimization a Python tool called GEKKO has been utilized, which is an open-source optimization software for mixed-integer and differential algebraic equations. GEKKO allows users to define optimization models and automatically solves the given model for a given objective function. It is built on a selection of different non-linear solvers which perform the actual optimization, *Beal et al. (2018)*. For the purpose of this research APOPT was used. This information was taken as a basis for creating scenarios. In total 7 parameters were chosen, Table VI. For each parameter a base value has been taken, based on available data from the year 2019, and has been varied around this value.

Fuel prices fluctuate over longer periods. The prices of some fuels can show similar trends as their means of production are related. This makes modelling fuel prices a difficult topic, which was also why it was deemed beyond the scope of this study. As a simplification, fuel prices were taken constant over the years. If a fuel price model should be available, it could be added to the model in future studies. Nonetheless, as it will have a critical effect on the outcomes, this parameter was varied more than the other parameters.

The base value for the different fuel types can be seen in Table VII. HFO, LPG, LNG, and methanol have established open markets. For these fuels, the prices from August 2019 were taken as base prices. Hydrogen and ammonia, on the other hand, do not yet have established markets, which makes it more

difficult to indicate base prices. As ammonia's main contemporary usage is as a fertilizer, the price for this was used. Hydrogen's price heavily depends on the way of its production. The most common way of production at the moment is through natural gas, without any carbon capture, therefore the base price was determined accordingly.

For scenario creation, we assumed that both policies would not coexist. Through all possible combinations of all parameters and their different values, in addition to the scenarios without policies, a total of 855 scenarios were created.

Table VI: Values of the parameters, which are used for scenario creation

Parameter	Symbol	Values	Unit
Freight Rate	r_f	600, 700, 800	\$ / TEU
Fullness	δ	0.6, 0.7, 0.8	-
Fuel Price Adapter	P_{fuel}	50%, 80%, 100%, 120%, 150% of P_{fuel}	\$ / tonne
Carbon Tax	P_{CO2}	25, 45, 65	\$ / tonne
Start Time for CO2 Policy	$t_{p,CO2}$	2, 5, 10	years
Speed Limit	v_{limit}	16, 18, 20	kn
Start Time for Speed Policy	$t_{p,v}$	2, 5, 10	years

Table VII: Base values for fuel price adapters

Fuel Type	Price [\$/t]	Source
HFO (VLSFO)	500.5	<i>Ship & Bunker (2020)</i>
LPG	253.3	<i>Statista (2019)</i>
LNG	362.8	<i>IEA (2020)</i>
Methanol	346.5	<i>Methanex (2020)</i>
Hydrogen	1,650.0	<i>Mulder et al. (2019)</i>
Ammonia	235.0	<i>Markit (2020)</i>

6. Results

Two case studies were done. For each case, the parametric design tool was used to generate designs for each fuel type, such that they can be tested. The same 855 scenarios were simulated for both cases.

6.1. Case I

For Case I, it was decided to look at ULCVs with roughly 25,000 TEU as this will be most likely the next ULCV class. The most common design speed amongst ULCVS is 23 kn, *Clarksons Research (2020)*, which was chosen as the design speed. These ships sail on the route Shanghai-Rotterdam (through the Suez Canal). The main properties of the ships that have been generated by the parametric design tool are provided in Table VIII.

Table VIII: Main properties of the compared ships in Case I

Fuel Type	Length [m]	Beam [m]	Draft [m]	Capacity [TEU]	GT	PP [M \$]	Power [kW]
HFO	414	61	16	24,900	249,104	157.75	82,440
LPG	414	61	16	24,352	249,104	156.63	82,440
LNG	429	61	16	25,450	259,543	158.75	82,440
Methanol	414	61	16	24,626	249,104	157.20	82,440
Hydrogen	429	61	16	25,176	259,543	158.27	82,440
Ammonia	414	61	16	24,626	249,104	157.20	82,440

The results for all ships have been visualized in Fig.2. On the left side of the graph, highlighted in red, hydrogen and ammonia ships can be seen. These are non-carbon fuels, therefore the only TTW CO₂ emissions that they produce comes from the pilot fuel. Ammonia requires slightly more pilot fuel

compared to hydrogen, the effect of this can also be seen as hydrogen has generally a smaller EEOI. The hydrocarbon fuels can be seen on the right side of the graph. The EEOI of the hydrocarbon fuels is one order of magnitude higher than the EEOI of the non-carbon fuels.

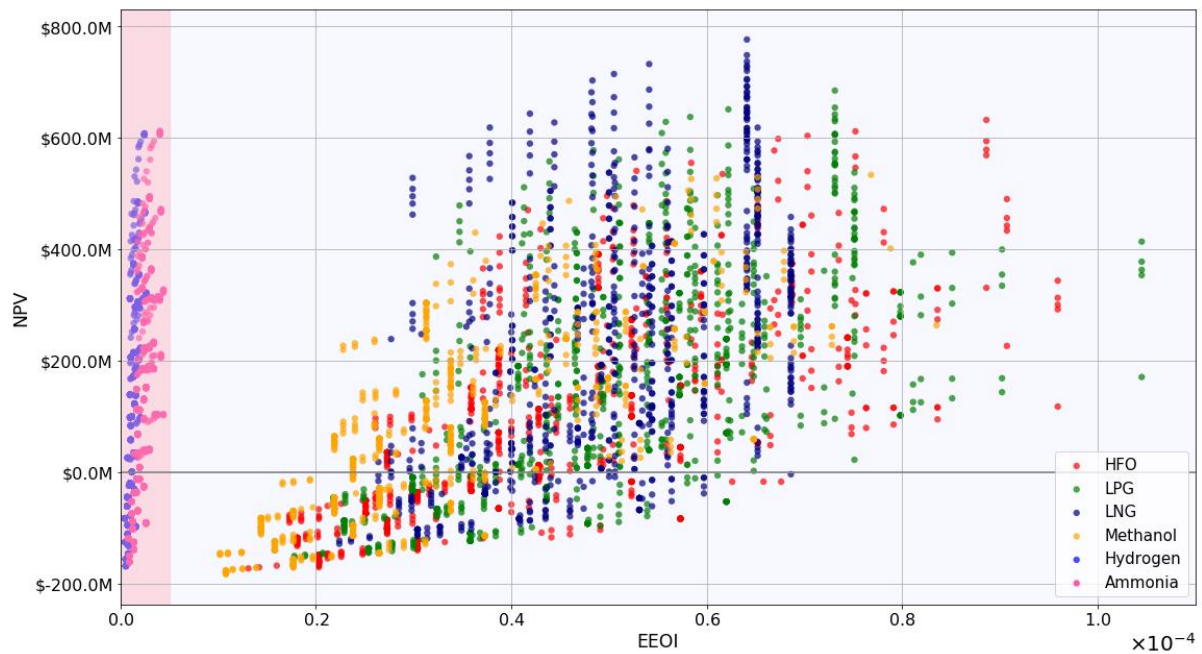


Fig.2: Results of all ships in Case I, non-carbon fuels have been highlighted

The NPVs of all ships have been plotted as box plots in Fig.3. LNG and LPG outperform the other options. It was explained above that the PP for all ships were calculated the same, even though ships which use alternative fuels are more expensive due to their additional storage facilities. As PP are paid at the beginning of an investment, any difference that should occur due to the use of alternative fuels does not require to be discounted. This means that it is possible to come to a conclusion regarding the possible difference by comparing the NPVs of the different ships. Based on the medians, as long as the extra costs, which result from the additional fuel storage facilities, for LNG are not greater than 136 million USD, LNG would be as profitable as HFO. For LPG this is 58 million USD. The situation is more critical for methanol, hydrogen, and ammonia. The price difference between a methanol using ship and a conventional one is minimal, as a conventional ship can be converted to a methanol using ship with small adjustments, *ABS (2019)*. Even though the NPVs of hydrogen and ammonia are similar to HFO, high extra costs due to additional facilities would mean that they would become unprofitable investments in the majority of the scenarios.

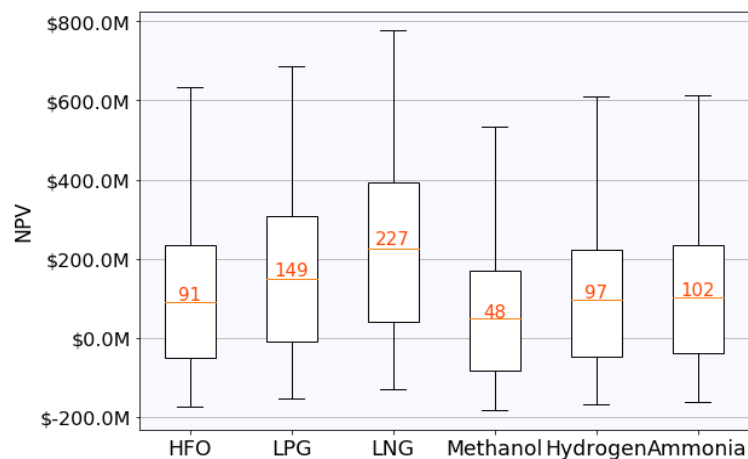


Fig.3: Box plots of NPV of all ships in Case I

Fig.4 shows the EEOIs of the hydrocarbon fuels. HFO has a lower EEOI than LPG and LNG, which might be unexpected. In this model each ship optimizes their operations to the circumstances in each scenario. Therefore, the operations of each ship are different. The results show that a conventional ship sails much slower than LPG or LNG because it has a higher fuel price. As LPG and LNG only have slightly lower specific CO₂ emissions, they emit more CO₂ and have higher EEOIs. This is a unique insight attributed to the approach presented in this paper, as most approaches typically assume that different fuel types will still operate the same way, *Adachi et al. (2014)*, *Ammar (2019)*. As this approach showcases that if ships adapt their behaviour to the circumstances, it will affect the outcome, which might seem unexpected in some cases. The fuel prices, which were used for HFO, are of Very Low Sulfur Fuel Oil (VLSFO) as ships are required to use this HFO due to the new regulations by *IMO (2020)*. Ships can only use other types of HFOs, such as IFO380, if they have a scrubber. Due to the high fuel prices, it is more profitable to sail slower. If the simulations are run for IFO380, implemented with a base value of 297.5 USD/t, *Ship & Bunker (2020)*, the ship sails faster and has a higher EEOI than all other alternatives, so price difference and sailing speed have considerable effects. Strictly speaking, VLSFO cannot be considered as “conventional”, therefore comparing VLSFO to alternative fuels would be unfair. For this reason, a hypothetical comparison has been done with IFO380. If a comparison is made based on the EEOI median of each fuel type, VLSFO will have a reduction of 28%, LPG 17.3%, LNG 14.9%, methanol 47.4%, hydrogen 98%, and ammonia 96.2%.

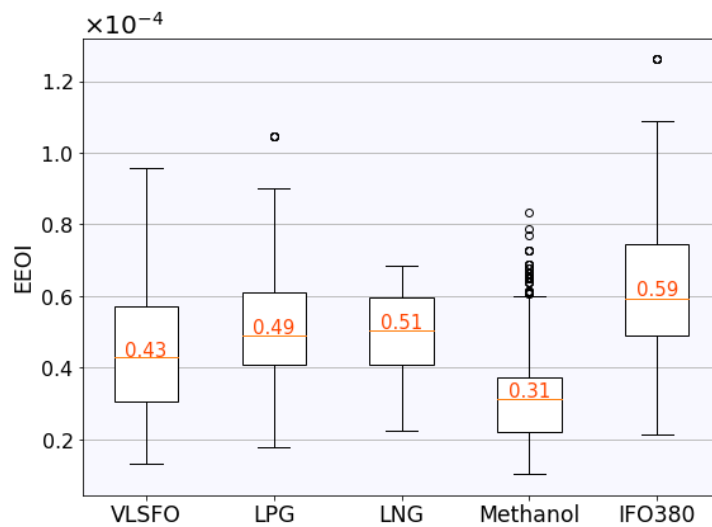


Fig.4: Box plots of EEOI of ships using hydrocarbon fuels in Case I

Detailed analysis of the NPV results shows that methanol, hydrogen and ammonia are also affected by high fuel prices. In the scenarios with lower fuel prices, it has been observed that all ships operate at higher speeds and have higher EEOI and NPVs. Methanol's performance would become similar to VLSFO's in this case, while it would have a slightly higher NPV. Hydrogen and ammonia would have similar NPVs to LPG but would still have an EEOI one order of magnitude lower.

Table IX: Biggest reductions due to policies in Case I

		HFO	LPG	LNG	Methanol	Hydrogen	Ammonia
NPV	Reduction	43.9%	36.9%	30.3%	48.7%	11.1%	12.4%
	Policy	Carbon Tax	Carbon Tax	Carbon Tax	Carbon Tax	Speed Limit	Speed Limit
EEOI	Reduction	26.5%	31.6%	38.1%	21.4%	15.1%	18.7%
	Policy	Carbon Tax	Speed Limit	Speed Limit	Carbon Tax	Speed Limit	Speed Limit

The biggest reductions for each fuel type due to policies are shown in Table IX. These are the most severe policies for each type, i.e., the highest carbon tax or speed limit which is implemented after 2 years. The effectiveness of the policy types depends on the fuel. The highest reduction in NPV was caused by carbon taxes for the hydrocarbons. Non-carbon fuels were not affected by carbon taxes as their emissions are so low. Speed limits caused the highest reductions in NPV and EEOI for the non-

carbons. The highest reduction in EEOI for LNG and LPG were also caused by speed limits, as they sail at higher speeds. For HFO and methanol the highest reduction in EEOI were caused by carbon taxes, on the other hand. Analyses like these can be used by policymakers to test the effectiveness of different policies.

6.2. Case II

For Case II, a different strategy was examined. If more or harsher regulations are expected, it could be beneficial to have ships with lower design speeds. For this purpose, ships with a capacity of roughly 25,000 TEU but with a design speed of 18 kn were generated using the parametric design tool. The resulting ships can be seen in Table X. Compared to Case I, these ships are roughly the same size but have a much smaller engine. Nonetheless, the PP in both cases is roughly the same due to the manner how the PP is estimated. The estimation only takes the number of TEUs into account. Taking the smaller engines into account, the PP should be lower than those in Case I.

Fig.5 shows the NPVs of all ships. The overall picture has not changed compared to Case I but the NPVs of LNG and LPG have decreased. As these ships cannot sail as fast as in Case I, they achieve fewer annual trips which leads to lower profits. In this case the extra costs for LPG should not exceed roughly 63 million USD and for LNG 97 million USD. The situation for methanol, hydrogen and ammonia is the same as in Case I.

Table X: Main properties of the compared ships in Case II

Fuel Type	Length [m]	Beam [m]	Draft [m]	Capacity [TEU]	GT	PP [M \$]	Power [kW]
HFO	406	61	16	24,900	249,104	157.75	41,220
LPG	409	61	16	24,900	254,234	157.75	41,220
LNG	406	61	16	24,626	249,104	157.20	41,220
Methanol	406	61	16	24,900	249,104	157.75	41,220
Hydrogen	406	61	16	24,352	249,104	157.60	41,220
Ammonia	406	61	16	24,900	249,104	157.75	41,220

As in Case I, the EEOIs of the hydrocarbon fuels have been plotted together with IFO380 as seen in Fig.6. Compared to Case I, the interquartile ranges have become narrower. The interquartile range of LPG is 66% narrower, LNG 63%, VLSFO 23%, methanol 1%, hydrogen 18%, and ammonia 28%. The reason for this is the fact that these ships are not affected by policies such as the speed limits of 20 and 18 kn. Based on the medians, compared to IFO380 VLSFO has a reduction of 13.8% in EEOI, LPG 19.4%, LNG 24%, methanol 37.6%, hydrogen 97.6%, and ammonia 95.4%.

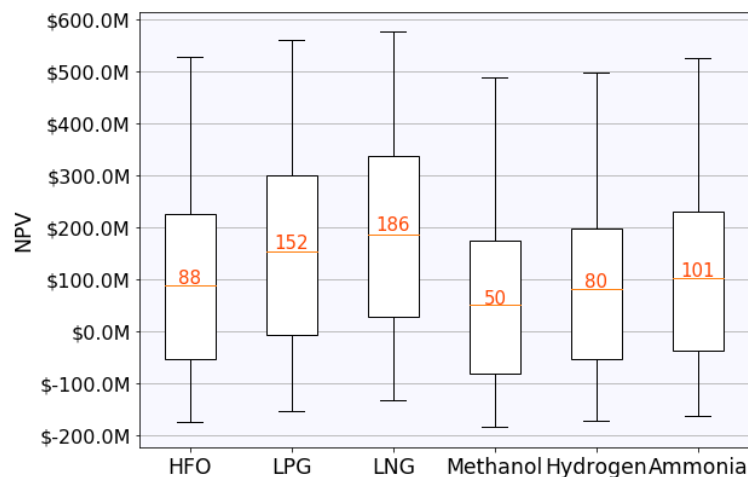


Fig.5: Box plots of NPV of all ships in Case II

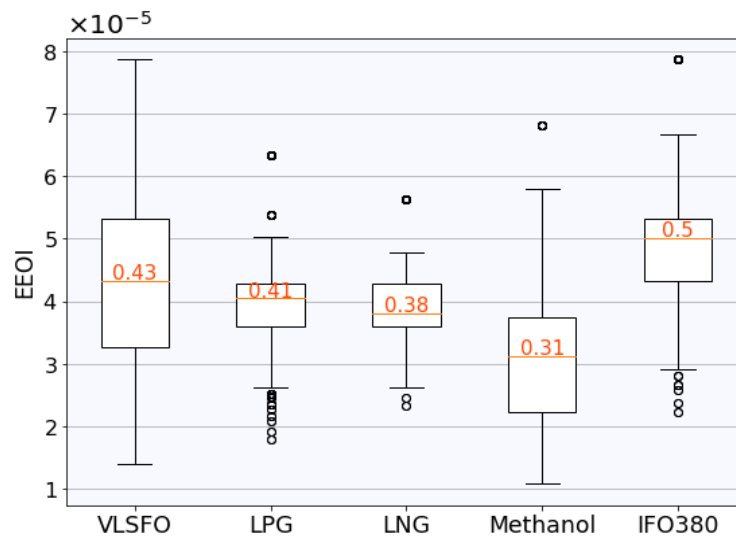


Fig.6: Box plots of EEOI of ships using hydrocarbon fuels in Case II

Also in this case, detailed analysis of the results shows that the fuel prices have a considerable effect on the outcomes. With a freight rate of 600 USD per TEU most ships always have a negative NPV, which is also true for Case I. The ships cannot be profitable below this freight rate. Additional scenarios were simulated to determine the critical value for fullness. Most ships are not profitable if fullness is 0.4 or lower, Table XI. This provides insights into the limitations of designs.

Table XI: Percentage of scenarios with negative NPVs depending on fullness in Case II

Fuel Type	Fullness δ					
	0.3	0.4	0.5	0.6	0.7	0.8
HFO	100%	95%	67%	50%	33%	28%
LPG	100%	85%	59%	35%	30%	16%
LNG	100%	72%	51%	33%	24%	3%
Methanol	100%	100%	81%	57%	40%	30%
Hydrogen	100%	93%	73%	53%	33%	27%
Ammonia	100%	93%	67%	47%	33%	27%

Table XII shows the biggest reductions due to policies. Compared to Case I, the reductions are lower. Thus these ships are less affected by the policies than the ships in Case I. Another difference is that the biggest reduction in EEOI for LPG is caused by the carbon tax instead of the speed limit.

Table XII: Biggest reductions due to policies in Case II

		HFO	LPG	LNG	Methanol	Hydrogen	Ammonia
NPV	Reduction	42.4%	30.3%	24.9%	46.8%	5.9%	5.9%
	Policy	Carbon Tax	Carbon Tax	Carbon Tax	Carbon Tax	Speed Limit	Speed Limit
EEOI	Reduction	19.7%	13.1%	15.7%	14.9%	7.0%	8.4%
	Policy	Carbon Tax	Carbon Tax	Speed Limit	Carbon Tax	Speed Limit	Speed Limit

7. Conclusion

This study showed the benefits of a comprehensive approach for ULCV design under uncertainty. The future of ULCVs is overshadowed by regulatory and economic uncertainties. Ships will be required to reduce their emissions, while being able to make profits. This will require robust designs, which can survive a variety of possible future scenarios.

LPG, LNG, methanol, hydrogen, and ammonia are alternatives to conventional fuels, which have the potential of reducing CO₂ emissions. Alternative fuels require more space and are linked to higher

capital costs as they require additional storage installations. A parametric design tool for ULCVs has been developed, which shows the effect of the implementation of each alternative fuel on the design of an ULCV.

An approach inspired by RDM was used to assess ULCVs with different fuel types under economic uncertainties, i.e., freight rate, fullness, and fuel prices, and different policy options, i.e. speed limits and carbon taxes. The main difference between this approach and RDM is the scenario construction and discovery, which has been simplified. An economic model was developed for this purpose. The integration of the parametric design tool and used methodology creates a new approach which delivers valuable insights. The approach shows how designs adapt their operations to the circumstances (e.g., lower speeds in case of higher fuel prices). Ships using LNG and LPG generally sail faster due to relatively lower fuel costs which result in more profits but also higher emissions. The approach also indicates the factors which limit the performances. For example, it has been seen that if fullness is 0.4 or lower ships cannot make profits.

Results show that LNG and LPG are the most robust alternative to conventional fuels, as long as additional fuel tank costs do not exceed 100-140 million USD for LNG and 60-65 million USD for LPG. If these price limits should be exceeded, they would become less profitable than conventional ULCVs, which would make them less economically feasible. Methanol could become a strong contender if fuel prices for methanol would become cheaper. Hydrogen and ammonia practically eliminate CO₂ emissions but would become unprofitable options with additional fuel tank costs. Compared to IFO380, VLSFO would give a reduction of 14-28% in EEOI, LPG by 17-19%, LNG by 15-24%, methanol by 38-47%, hydrogen by 98% and finally, ammonia by 96%.

Acknowledgements

This work was performed as part of the MSc thesis for the lead author, Kaan Terün. The thesis was performed in Marine Technology at Delft University of Technology and the authors would like to acknowledge both Delft University of Technology and Erasmus University Rotterdam for their support of this research.

References

- ABS, (2019), *Setting the course to low carbon shipping*, American Bureau of Shipping
- ADACHI, M.; KOSAKA, H.; FUKUDA, T.; OHASHI, S.; HARUMI, K. (2014), *Economic analysis of trans-ocean LNG-fueled container ship*, J. Marine Science and Technology 19(4), pp.470-478
- AIJOU, A.; BAHATTI, L.; RAIHANI, A. (2019), *Study on container ship energy consumption*, Energy and Sustainability 2021, pp. 25-36
- AMMAR, N.R. (2019), *An environmental and economic analysis of methanol fuel for a cellular container ship*, Transportation Research Part D: Transport and Environment 69, pp.66-76
- BEAL, L.; HILL, D.; MARTIN, R.; HEDENGREN, J. (2018), *GEKKO Optimization Suite. Processes*, <http://www.mdpi.com/2227-9717/6/8/106>
- BEN-HAIM, Y. (2019), *Info-gap decision theory*, Decision Making under Deep Uncertainty: From Theory to Practice, pp.93-115
- BICER, Y.; DINCER, I. (2018), *Environmental impact categories of hydrogen and ammonia driven transoceanic maritime vehicles: A comparative evaluation*, Int. J. Hydrogen Energy 43(9), pp.4583-4596
- BOWMAN, E. H.; MOSKOWITZ, G.T. (2001), *Real Options Analysis and Strategic Decision Making*,

Organization Science 12(6), pp.772-777

BUNDESREGIERUNG DEUTSCHLAND (2019), *Foundations in place for CO2 pricing*, <https://www.bundesregierung.de/breg-en/issues/nationaler-emissionshandel-1685054>

CLARKSONS RESEARCH (2020), World fleet register

CORBETT, J.J.; WANG, H.; WINEBRAKE, J.J. (2009), *The effectiveness and costs of speed reductions on emissions from international shipping*, Transportation Research Part D: Transport and Environment 14(8), pp.593-598

DE NEUFVILLE, R.; SMET, K. (2019), *Engineering options analysis*, Decision Making under Deep Uncertainty: From Theory to Practice, pp.117-132

DE VRIES, N. (2019), *Safe and effective application of ammonia as a marine fuel*, Master's thesis, TU Delft, <http://resolver.tudelft.nl/uuid:be8cbe0a-28ec-4bd9-8ad0-648de04649b8>

DENIZ, C.; ZINCIR, B. (2016), *Environmental and economical assessment of alternative marine fuels*, J. Cleaner Production 113, pp.438-449

DNV GL (2017), *A global and regional forecast of the energy transition to 2050*, Energy Transition Outlook 2017

DNV GL (2019), *Assessment of selected alternative fuels and technologies*, DNV GL, Hovik

DNV GL (2020), *DNV GL rules for classification: Ships*, DNV GL, Hovik

DOERRY, N.; KOENIG, P. (2017), *Modularity and Adaptability in Future U.S. Navy Ship Designs*, Mecon, pp.1-9

EUROSTAT (2020), *China-EU trade in goods: €164 billion deficit in 2019*

FABER, J.; HANAYAMA, S.; ZHANG, S.; PEREDA, P.; COMER, B.; HAUERHOF, E.; VAN DER LOEFF, W.S.; SMITH, T.; ZHANG, Y.; KOSAKA, H.; ADACHI, M.; BONELLO, J.M.; GALBRAITH, C.; GONG, Z.; HIRATA, K.; HUMMELS, D.; KLEIJN, A.; LEE, D.S.; LIU, Y.; LUCCHESI, A.; MAO, X.; MURAOKA, E.; OSIPOVA, L.; QIAN, H.; RUTHERFORD, D.; DE LA FUENTE, S.S.; YUAN, H.; PERICO, C.V.; WU, L.; SUN, D.; YOO, D.H.; XING, H. (2020), *Fourth IMO GHG study 2014*, Int. Maritime Org., London

GASPAR, H.M.; ERIKSTAD, S.O.; ROSS, A.M. (2012), *Handling temporal complexity in the design of non-transport ships using Epoch-Era Analysis*, Int. J. Maritime Eng. 154(PART A3), pp.109-119

GILBERT, P.; WALSH, C.; TRAUT, M.; KESIEME, U.; PAZOUKI, K.; MURPHY, A. (2017), *Assessment of full life-cycle air emissions of alternative shipping fuels*, J. Cleaner Production 172, pp.855-866

GRAF VON WESTARP, A. (2020), *A new model for the calculation of the bunker fuel speed–consumption relation*, Ocean Eng. 204:107262

HOLTROP, J.; MENNEN, G.G.J. (1982), *An approximate power prediction method*, Int. Shipbuilding Progress

IEA (2020), *LNG import prices in selected countries, 2010-2019*

IMO (2020), *Sulphur 2020 – cutting sulphur oxide emissions*, Int. Maritime Org., London

IMO (1999), *SOLAS: International Convention for the Safety of Life at Sea, 1974*, Resolutions of the 1997 SOLAS Conference Relating to Bulk Carrier Safety, Int. Maritime Org., London

KANA, A.; KNIGHT, J.T.; SYPNIEWSKI, M.J.; SINGER, D.J. (2015), *A Markov Decision Process Framework for Analyzing LNG as Fuel in the Face of Uncertainty*, Int. Marine Design Conf. 2, pp.297-308

KANA, A.A.; HARRISON, B.M. (2016), *A Monte Carlo approach to the ship-centric Markov decision process for analyzing decisions over converting a containership to LNG power*, Ocean Eng. 130, pp.40-48

KASPRZYK, J.R.; NATARAJ, S.; REED, P.M.; LEMPERT, R.J. (2013), *Many objective robust decision making for complex environmental systems undergoing change*, Environmental Modelling and Software

KLEIN WOOD, H.; STAPERSMA, D. (2002), *Design of Propulsion and Electric Power Generation Systems*, IMarEST, London

KWAKKEL, J.H.; HAASNOOT, M.; WALKER, W.E. (2016), *Comparing Robust Decision-Making and Dynamic Adaptive Policy Pathways for modelbased decision support under deep uncertainty*, Environmental Modelling and Software 86, pp.168-183

LEMPERT, R.J. (2019), *Robust decision making*, Decision Making under Deep Uncertainty: From Theory to Practice, pp.23-51

LEMPERT, R.J.; KALRA, N.; PEYRAUD, S.; MAO, Z.; TAN, S.B.; CIRA, D.; LOTSCH, A. (2013), *Ensuring Robust Flood Risk Management in Ho Chi Minh City*, World Bank 1, pp.1-63

MAN (2016), *Propulsion trends in container vessels*, MAN Diesel & Turbo

MAN (2018), *MAN B&W G95ME-C9.5*, MAN Diesel & Turbo

MAN (2020a), *CEAS engine calculation*, <https://marine.man-es.com/two-stroke/ceas>

MAN (2020b), *HFO*, <https://powerplants.man-es.com/fuels/hfo>

MANDER, M. (2017), *Slow steaming and a new dawn for wind propulsion: A multilevel analysis of two low carbon shipping transitions*, Marine Policy 75, pp.210-216

MARCHAU, V.A.W.J.; WALKER, W.E.; BLOEMEN, P.J.T.M.; POPPER, S.W. (2019), *Introduction*, In Decision Making under Deep Uncertainty: From Theory to Practice, pp.1-20

IHS Markit (2020), *Ammonia fertilizer market and price analysis*, <https://agribusiness.ihsmarkit.com/sectors/fertilizers/ammonia.html>

METHANEX (2020), *Historical methanex posted price*

MOALLEMI, E.A.; ELSAWAH, S.; RYAN, M.J. (2020), *Robust decision making and Epoch–Era analysis: A comparison of two robustness frameworks for decision-making under uncertainty*, Technological Forecasting and Social Change

MULDER, J.; DEKKER, R. (2014), *Methods for strategic liner shipping network design*, European Journal of Operational Research 235(2), pp.367-377

- MULDER, M.; PEREY, P.; MORAGA, J.L. (2019), *Outlook for a Dutch hydrogen market*, Policy Papers 5
- NIESE, N.D.; SINGER, D.J. (2013), *Strategic life cycle decision-making for the management of complex Systems subject to uncertain environmental policy*, Ocean Eng. 72, pp.365-374
- OLMER, N.; COMER, B.; ROY, B.; MAO, X.; RUTHERFORD, D. (2017), *Greenhouse gas emissions from global shipping, 2013–2015*, Int. Council on Clean Transportation
- OVCINA, J. (2021), *World's 1st ULCV LNG-conversion completed*, Offshore Energy
- PERRIER, Q. (2018), *The second French nuclear bet*, Energy Economics 74, pp.858-877
- PORT OF ROTTERDAM (2020), General terms and conditions
- PROBST, J.O. (2016), *Pump up the volume*, DNV GL, Hovik
- PSARAFTIS, H.N. (2019), *Speed optimization versus speed reduction: Are speed limits better than a bunker levy?*, Maritime Economics & Logistics 21, pp.524-542
- RINA (2015), *Significant Ships of 2014*, RINA, London
- RINA (2016), *Significant Ships of 2015*, RINA, London
- RINA (2017), *Significant Ships of 2016*, RINA, London
- SCHWARTZ, H.; GUSTAFSSON, M.; SPOHR, J. (2020), *Emission abatement in shipping – is it possible to reduce carbon dioxide emissions profitably?*, J. Cleaner Production 254:120069
- SHIP & BUNKER (2020), *Rotterdam bunker prices*, <https://shipandbunker.com/prices/emea/nwe/nl-rtm-rotterdam#VLSFO>
- STATISTA (2019), *Liquefied petroleum gas (LPG) price in the Netherlands from 2009 to 2019 (in euro cents per liter)*
- SUEZ CANAL AUTHORITY (2015), *Rules of Navigation*, Al Tamsah
- TAS, Z. (2018), *The advantages and disadvantages of ultra-large container ships*, <https://www.morethanshipping.com/advantages-disadvantages-ultra-large-container-ships/>
- TOOLBOX (2009), *Combustion of fuels - carbon dioxide emission*, https://www.engineeringtoolbox.com/co2-emission-fuels-d_1085.html
- UNITED NATIONS, (1998), *Kyoto protocol to the united nations framework convention on climate change*, <https://unfccc.int/resource/docs/convkp/kpeng.pdf>
- VAN DEN BERG, S. (2018), *Low carbon shipping: A decision support tool for the implementation of co2 reducing measures*, <http://resolver.tudelft.nl/uuid:b758d9f7-63a0-4ba0-ba97-d7345f46a38e>
- WATSON, D.G.M. (1998), *Chapter 19 operational economics*, Practical Ship Design Vol.1, pp.491-510
- ZWAGINGA, J.; STROO, K.; KANA, A. (2021), *Exploring market uncertainty in early ship design*, Int. J. Naval Architecture and Ocean Eng. 13, pp.352-366

Appendix

To clarify the XLMR framework an illustrative example will be shown. For this purpose, one scenario for an ULCV with 24,352 TEU and LPG as fuel will be handled. The properties of this ship have been generated by the parametric design tool and the main dimensions can be found in 8.

The exogenous uncertainties (X) are the freight rate, fullness, and fuel price. For the purpose of this example the freight rate will be 700 USD/TEU, the fullness 0.7, and the fuel price 362.8 USD/t. The policy lever (L) will be a carbon tax of 45 USD/CO₂t, which will be implemented after 5 years. As described in the article, the metrics (M) are the NPV and the EEOI of the ULCV. Finally, the relations (R) are the described economic model.

The model calculates the fixed and variable costs. The fixed costs for this ship are roughly 6.8 million USD per year. The variable costs are canal fees for each passing of the Suez Canal, port fees for each port visit, and cargo handling fees for each loading and unloading at each port. In this case, the canal fees are roughly 883,000 USD per transit and the port fees and cargo handling fees together 4.83 million USD per port visit. Additional to these, there are also fuel costs which are a function of speed, as seen in Eq.(5). These values are used to find the optimal speed with which the maximum NPV can be achieved.

The model first optimizes the speed for the first 5 years in which there is no policy. In this case the optimal speed is 18.09 knots, which generates a yearly cash flow of roughly 16.3 million USD. The model then optimizes for the years with the implemented policy and finds that the optimal speed is 15.44 knots, which generates a yearly cash flow of about 13.4 million USD. With the purchase price of 156.6 million USD, the yearly cash flows, and the scrap value of 29 million USD the NPV is calculated, which is 127.8 million USD. On the other hand, the CO₂ emissions per trip are calculated based on fuel consumption and the specific CO₂ emissions from Table I. This is used to calculate the EEOI which is done by taking the average of the EEOI of all trips. In this case the EEOI is $4.66 \cdot 10^{-5}$.

Dynamic Task Allocation Algorithms within Intelligent Operator Support Concepts for Shore Control Centres

Tycho Brug, TNO, Soesterberg/The Netherlands, tycho.brug@tno.nl

Jasper van der Waa, TNO, Soesterberg/The Netherlands, jasper.vanderwaa@tno.nl

Valentina Maccatrozzo, TNO, Soesterberg/The Netherlands, valentina.maccatrozzo@tno.nl

Hans van den Broek, TNO, Soesterberg/The Netherlands, hans.vandenbroek@tno.nl

Abstract

This paper presents a dynamic task allocation algorithm. Its function is to dynamically allocate the supervision of tasks of many autonomous operations to suited operators. The proposed algorithm accounts for the workload capacity of an operator and a balanced work distribution over all operators. We propose an iterative deepening depth-first search algorithm to find the optimal allocation. Through a series of simulated experiments, we show how our proposed algorithm results in a versatile method that can distribute a series of complex operations to operators effectively, both in terms of computational effectiveness as well as workload distribution.

1. Introduction

This paper presents a dynamic task allocation algorithm within an Intelligent Operator Support System for Shore Control Centres in the context of the MOSES EU-project, <https://moses-h2020.eu/>. The MOSES project is one of three research and innovation projects within the Horizon 2020 program that contributes to more automation and autonomy in Europe's short sea logistics. This project illustrates and contributes to the rapidly growing application of Artificial Intelligent and Autonomous Systems in the maritime industry. This paper addresses one of MOSES' innovations: that of an Intelligent Operator Support System (IOSS).

The growing capability of autonomous systems and their application results in a paradigm shift from manual labour towards (remote) supervisory control. With supervisory control an operator is responsible for an autonomous operation (e.g., autonomous sailing, autonomous loading/unloading of containers, etc.). IOSS is a software component for Shore Control Centres (SCC) housing such operators. The goal of this software is to offer support to each operator by offering several vital functions such as aiding in situational awareness, assessing future risks and allocating operations to the right operator.

We envision a SCC capable of ensuring the safe and efficient completion of a large number of autonomous operations with relatively few operators. In this SCC a handful of operators should be capable of supervising several hundreds of such operations in a single shift. The assignment of the operator to the right operation can be done manually. However, this would mean strenuous, error prone, work, which additionally might be infeasible as the number of operators and operations grows. To illustrate this point further, *Van den Broek et al. (2020)* stated that "The way forward to mitigate work overload is (...) to establish an adaptive workload balancing approach among several Shore Control operators to deal with workload fluctuations in a dynamic way (p.6)". IOSS aims to offer this functionality; to dynamically allocate the required supervision task of an autonomous operation to the operator suited for that task. We refer to this function to as Dynamic Task Allocation.

The dynamic task allocation algorithm should take in account several factors that influence the workload of the individual operators and a balanced allocation of the operations over the operators. To achieve this optimization of allocation of work, a measure on quality of the allocation should be developed. Next to that, the amount of possible ways to allocate work over operators grows exponentially with more operations and operators. Calculating all possible assignments (brute-force) gets impossible very quickly. Thus, it should be considered how to optimize the task allocation among all possible options within reasonable time. For this we utilized an easily interpretable and scalable algorithm; Iterative Deepening Depth First Search (IDDFS), *Korf(1985)*. We adapted this algorithm for task allocation

so that it can dynamically re-assign operations when (a) new operations requiring supervision become available, (b) the situation changes significantly requiring an operator with a different expertise, or (c) the operator does not agree with a certain task assignment.

In this work we show how our proposed dynamic task distribution algorithm results in a versatile method that can distribute a series of complex operations to operators effectively, both in terms of computational effectiveness as well as workload distribution. We do this through a series of simulated experiments. In addition, we discuss the limitations of our algorithm as well as potential topics of future research.

Our paper describes in more detail:

- The proposed algorithm and the associated cost function that is being optimized.
- The results of several experiments to show the workings, effectiveness, stability and constraints of the algorithm.
- An in-depth discussion on the usefulness of this approach, its limitations and future research.

2. Methods

2.1. General

We base the allocation of operations to operators on the expected workload. As operators should not be overloaded with too much work or have too little work, *Neerincx (2003)*. In either case the quality of the “work” reduces. Since this work entails the supervision of autonomous operations and potential interventions, a reduced work quality poses a risk for the efficiency and safety of the operation. Below we describe how we model this workload as a function of operator expertise and operation difficulty. We also present a straightforward additive model for supervising simultaneous operations. This workload model enables the allocation of operations of various complexities while balancing the workload over all operators accounting for their expertise.

We first assume that any operation o is static in time. This means each operation has a given start time $t_{o,start}$, and a given duration d_o , which cannot be shifted in time. Each operation is composed of multiple tasks, with each a default workload $w_o(t)$, expressed as a baseline percentage of capacity for an operator. Tasks are linked to each other and sequential in a given operation. Therefore the operations are allocated, and not the single tasks. This is because switching between multiple contexts is distracting for an operator and will thus be less effective or safe. Tasks within operations might be: leaving/approaching berth, port departure/approach, sea passage and container handling. This results in that the workload per operation varies over time. For example, the first task could be “port approach” in the first half hour of the operation, requiring 50% of capacity of an operator to supervise. A second task “container handling” would take the next hour of the operation, requiring 100% capacity of an operator.

Each operation is assigned a difficulty s_o . The difficulty is compared to the expertise e_p of an operator p , to get to the actual workload $w_{o,p}(t)$ for that operation and operator at that time:

$$w_{o,p}(t) = \begin{cases} w_o(t), & e_p \geq s_o \\ w_o(t) \cdot \left(\frac{s_o}{e_p}\right), & e_p < s_o \end{cases}$$

This results in the adjusted workload $w_{o,p}(t)$ that increases linearly if operator expertise is lower than operation difficulty, and does so proportionally to the ratio between the two. It remains the default workload if the expertise is equal or higher than the difficulty of the operation. This models that a less experienced operator requires additional capacity to supervise a difficult operation. For instance, a complex operation due to environmental conditions causes a high workload for a junior operator whereas the same operation requires nothing extra from a senior operator.

We initially assume an arbitrary allocation of operations over operators. In any given allocation, each assigned operation takes some of the available capacity of an operator at that time. The required capacity is equivalent to the workload it takes for that operator to supervise that operation as described above. We assume that an operator's workload at any given time t is equal to the sum of all the workload associated to each operator that operator supervises at that time, as adjusted based on the operator's expertise and operation's difficulty. Imagine operations 1, 2 and 3 are assigned to operator 1. For that given operator 1, the workload becomes:

$$w_{p=1}(t) = w_{o=1,p=1}(t) + w_{o=2,p=1}(t) + w_{o=3,p=1}(t)$$

The mean workload of that operator then becomes:

$$\bar{w}_p = \frac{1}{N} \sum_{t=1}^N \sum_{o \in O} w_{o,p}(t)$$

Where N is an arbitrary finite amount of discrete time steps used in a given time window. For example N could represent an eight-hour shift and t a fifteen-minute interval during that shift. O represents the operations assign to operator p .

2.2. Cost function

To determine the “goodness” of any given allocation, we consider:

- Capacity of an operator: The full (unused) capacity of the operator is set to 100%. If $w_p(t)$ is larger than the capacity (at any point in time), the work distribution is unfeasible and should not be considered.
- Fair work distribution over all operators: For this we consider the following cost attributes:
 - Average mean workload: $\bar{w} = \frac{1}{M} \sum_{p=1}^M \bar{w}_p$
Where M is the number of operators. The distribution of work where the average mean workload is lowest, is the distribution where all operations are supervised by operators with an expertise level equal to or higher than the difficulty of the operations.
 - Standard deviation of mean workload: $\sigma_w = \sqrt{\frac{1}{M} \sum_{p=1}^M (\bar{w}_p - \bar{w})^2}$.
The standard deviation of mean workload increases when a small number of operators get assigned relatively more work than others. Optimizing towards a low σ_w will thus result in an allocation where each operator has a similar mean workload.
 - Average time in a critical workload zone: $\bar{c}_w = \frac{1}{MN} \sum_{p=1}^M \sum_{t=1}^N w_p(t) > 0.85$.
We define the critical workload zone as a point in time where a given operator works above 85% of its capacity; $w_p(t) > 0.85$. By minimizing the average amount of time the operators work above this threshold, we aim to overcome cognitive overload for operators, *Neerincx et al. (2003)*.
 - Ability for the operator to take a break: \bar{b}_w .
We set \bar{b}_w to be the average amount of hours that operators work for more than 4 hours straight without a break (i.e., a period of at least one hour where $w_p(t) = 0$). By optimizing \bar{b}_w , we penalize allocations where operators need to work for a long time without getting a break.

We want to find the work allocation where $w_p(t)$ is never higher than 100% (for all operators and all points in time) and where the cost C is lowest:

$$C = \alpha \bar{w} + \beta \sigma_w + \gamma \bar{c}_w + \delta \bar{b}_w$$

Here α, β, γ and δ are weights to give priority to the above stated constraints. This additive cost function takes several notions of workload into account and can easily be extended to include more.

2.2. Optimization

For cases with a low number of operators and a low number of operations, it is possible to calculate all possible allocations and find the absolute minimum (brute-force method). However, with an increasing amount of operations and operators, the amount of possible allocations grows exponentially and quickly becomes unfeasible. We therefore implemented an Iterative deepening depth-first search (IDDFS) algorithm, *Korf (1985)*. This algorithm randomly orders the operations, and then assigns each operation in turn to the best fitting operator (using the cost function above to determine which). This continues until all operations are allocated, as shown in Fig.1 **Error! Reference source not found..** This optimization algorithm does have a risk on landing on a local minimum, as the order of operations does not necessarily give the best overall fit.

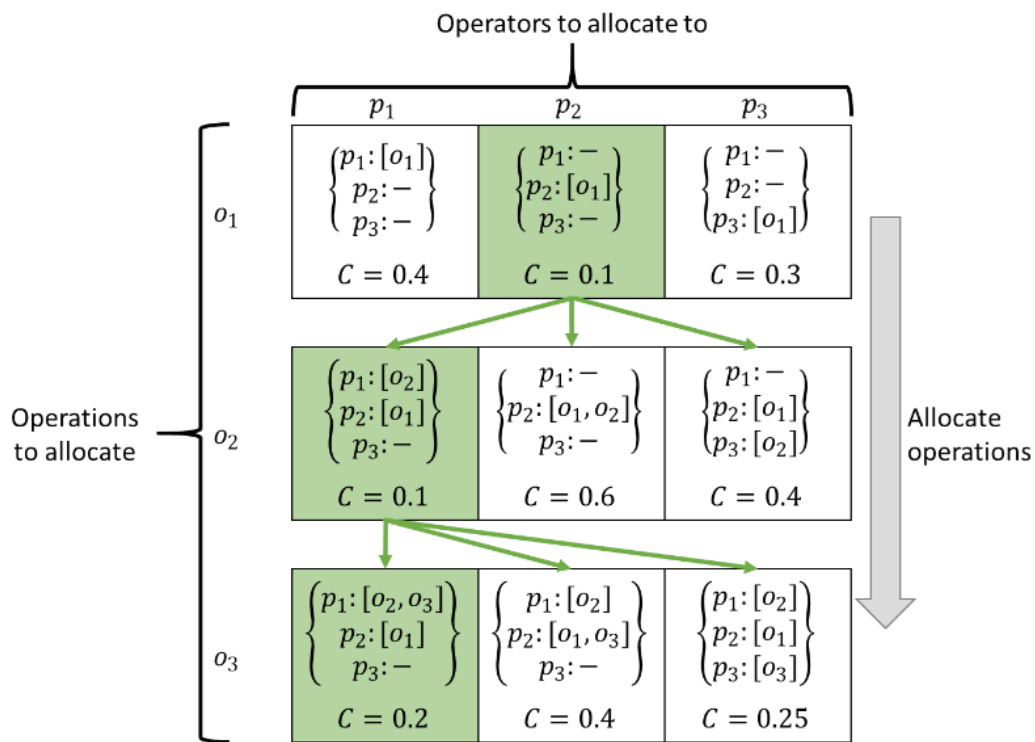


Fig.1: Illustration of IDDFS algorithm

In the example in **Error! Reference source not found.**, the optimization could for instance get to a lower cost if it first assigns operation 3, then 1 and finally 2, in comparison to the displayed order. Therefore, the IDDFS algorithm is run with several repetitions, each time with a different order of assigning operations. This results in an algorithm that is less prone to land in a local minimum, but still needs a significantly less calculations than the brute-force method to get to a result.

2.3. Dynamic allocation

New operations can come in and existing ones can be delayed or cancelled. Each time a potential better allocation might be possible. However, making changes to an already existing allocation is not always preferred. Operators might have already prepared for the given allocation (e.g., read documentation about a certain operation, scheduled their break, etc). Therefore it is preferred to get to a new optimal planning, while making as little changes compared to the previous planning. This is implemented by assigning an additional cost to any changes required. We denote this cost as $\varepsilon \times \Delta o$, where Δo is the

amount of operations that is shifted from one operator to another. This is multiplied by a weight ε . This is then added to the cost C' of the new allocation. By adding this additional cost, the algorithm tries to stay as close to the current plan as possible, as it will only swap operations between operators if it means a change in cost is acceptable. More formally; a change is only implemented if $|C - C'| > \varepsilon \times \Delta o$.

2.4. Implementation

The dynamic task allocation algorithm is implemented and simulated in Python 3.7, *Van Rossum and Drake (2009)*, and run using the PyCharm 2020.3.3 IDE, <https://www.jetbrains.com/pycharm/>. Experiments were run on a HP Elitebook 830 (running Microsoft Windows version 10) with an Intel Core i5 processor running at 1.60 GHz using 8.00 GB of RAM.

3. Results

3.1. Basic functionality

3.1.1. Scenario 1: Simple case

We start off with a simple case with six operations that need to be allocated (as depicted in Table I). These six operations need to be allocated over three operators. These three operators have a respective expertise level e_p of 1, 2 and 3.

Table I: Simple case with 6 (non-overlapping) operations

o	$t_{o,start}$	s_o	Work profile
1	0:00	1	30% (0-1h) 60% (1-2h)
2	1:00	2	30% (0-1h) 60% (1-2h)
3	2:00	3	30% (0-1h) 60% (1-2h)
4	4:00	1	30% (0-1h) 60% (1-2h)
5	5:00	2	30% (0-1h) 60% (1-2h)
6	6:00	3	30% (0-1h) 60% (1-2h)

For the cost function, the following weights are set: $\alpha = 1$, $\beta = 1$, $\gamma = 1$, $\delta = 4$. As this simple case has a relatively low number of calculations needed to calculate all possible allocations ($3^6=729$ possibilities), we start off using only the brute-force method for optimization. The brute-force algorithm comes up with the following best allocation after calculating the costs for all possible allocations ($C = 0.225$, Fig.2): $p_1: [o_1, o_4]$, $p_2: [o_2, o_5]$, $p_3: [o_3, o_6]$.

In this optimal plan:

- None of the operators' maximum capacity is reached.
- Each operator is assigned with the operations that suits their expertise level which minimizes the average mean workload (\bar{w}) over the operators.
- The work is allocated over operators, resulting in two operations being assigned to each operator, which minimizes the standard deviation of mean workload (σ_w)
- None of the operators work in their critical workload zone ($\bar{c}_w = 0$),
- Each operator has enough opportunity to take breaks ($\bar{b}_w = 0$)

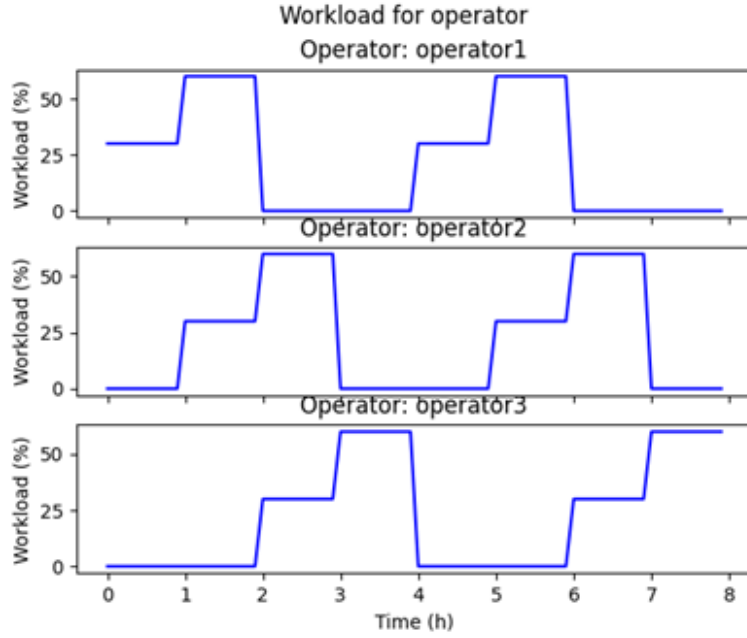


Fig.2: Simple case: workload per operator over time. Every increase (initially 30%, then 60%) signifies one allocated operation. In this specific case all operations are evenly distributed over operators and time.

3.1.2. Scenario 2: Extended simple case – difficulty increased

We now increase the difficulty of the first operation from one to two, i.e.; $s_0 = 2$. The others remain at the same difficulty. The brute-force algorithm comes up with the following best allocation ($C = 0.34$, Fig.3): $p_1: [o_4]$, $p_2: [o_2, o_5]$, $p_3: [o_1, o_3, o_6]$.

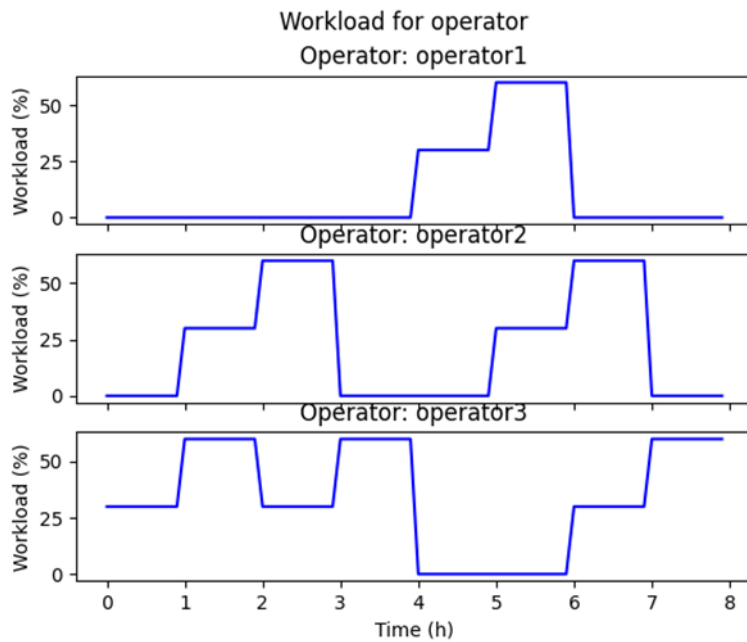


Fig.3: Simple case where operations vary in their difficulty. The more difficult operations are assigned to the third operator. This results in a reasonable workload for the third operator and the first operator having a fairly low overall workload.

The outcome might be counter-intuitive, as the third operator seems to get a substantial part of all the work. However, if the first operation would still be supervised by the first operator, the plan would

become unfeasible. As the difficulty is twice as high than the expertise of the first operator, it would take that operator too much capacity to perform ($60\% \times 2 = 120\%$). Both the second and third operator could perform the task, however, if the second operator does so, he/she would have to work in the critical workload zone ($> 85\%$) as the first and second operations overlap partially. This would still result in a feasible plan, but with a higher cost ($C = 0.38$, an increase of 0.04).

3.1.3. Scenario 3: Extended simple case – overlapping operations

In this scenario we change the timing of the third operation to also start at $t_{o,start} = 6$ (similar to the sixth operation). The other operations remain the same as in the first scenario. The brute-force algorithm comes up with the following best allocation ($C = 0.36$, Fig.4): $p_1: [o_1, o_4]$, $p_2: [o_2, o_3]$, $p_3: [o_5, o_6]$.

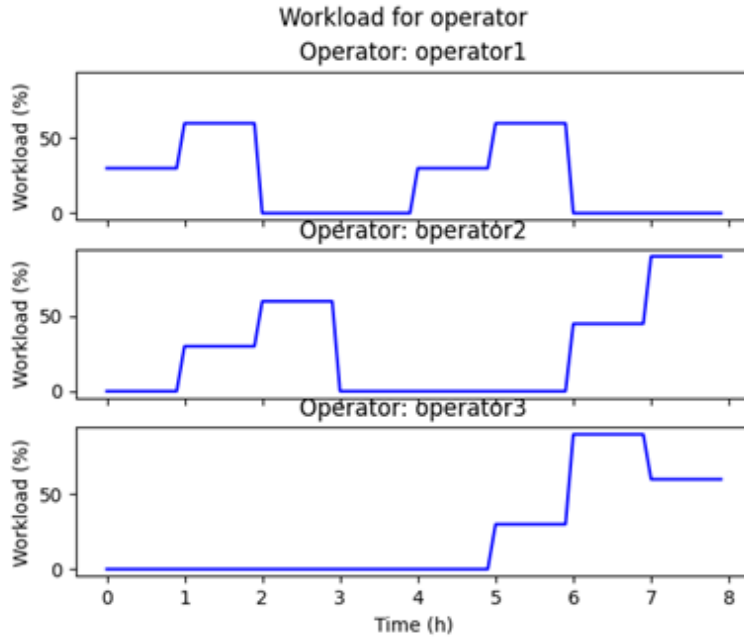


Fig.4: Simple case with overlapping operations, workload per operator over time. Due to the overlapping nature of the operations, the second operator takes on a difficult operation to prevent the third operator being overloaded.

It is unfeasible for the third operator to still supervise the third and sixth operation. They fully overlap, which requires more workload capacity than a single operator has available. The algorithm therefore finds a new optimal solution, in which the second operator takes over o_3 from the third operator, and the third operator takes up o_5 from the second operator. The plan has a higher cost than the outcome of scenario 1.

4. Scenario 4: Extended simple case – high difficulty

Next, let us increase the difficulty of all operations to $s_o = 3$. Again, the rest of the operations are kept the same as the first scenario. The brute-force algorithm comes up with the following best allocation ($C = 0.62$, Fig.5): $p_1: -$, $p_2: [o_2, o_4]$, $p_3: [o_1, o_3, o_5, o_6]$.

Due to all operations having a difficulty value of 3, the first operator is unable to supervise any of the operations (as the peak would cross the capacity of this first operator by quite some margin). The second operator is able to take on operations, but suffers a penalty (1.5x) and is thus not able to handle overlap in operations. This requires the third operator to take on several additional operations.

An alternative plan would be for the second operator to take on o_6 from the third operator. This results in a slightly worse plan ($C = 0.66$). The reason for the increase in cost is twofold:

1. The average mean workload increases as this is lowest when operators supervise operations that fit their expertise level.
2. The standard deviation of mean workload increases. This is due to the fact that the difference in mean workload between the second operator and the third operator actually increases in this scenario, due to higher workload caused by the second operator when taking on a task that has a higher difficulty.

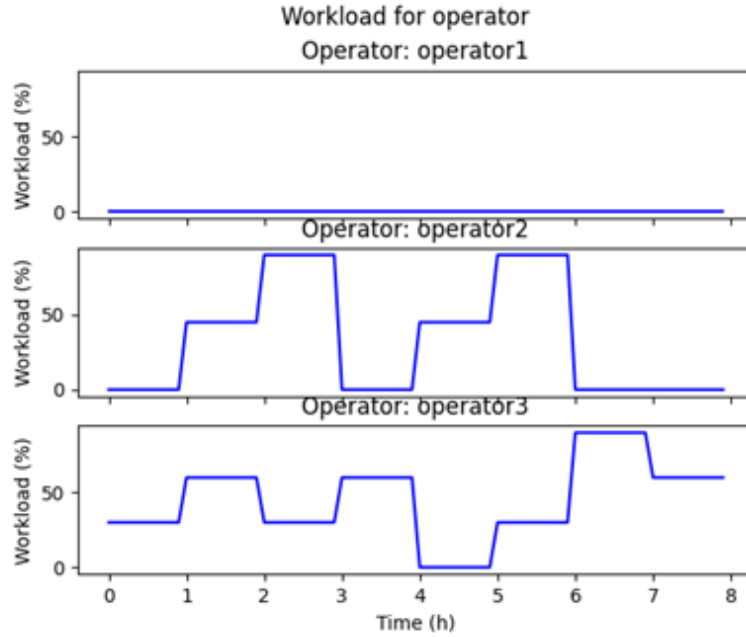


Fig.5: Simple case where all operations are difficult. Most operations are allocated to the third most experienced operator to reduce the average workload. The first operator is not able to take on any operations due to lack of experience.

An even more extreme scenario would be that the third operator takes on all operations. This would still result in a feasible plan, however with a very high cost ($C = 2.1$). Although the average mean workload decreases, this effect is overruled by the high standard deviation of mean workload and mostly because of the fact that the third operator will not be able to have a break (this is highly punished in the current cost function where $\delta = 4$).

3.1.5. Scenario 5: Extended simple case – adding an operation

As a final example, a new operation (o_7 , see Table II) is added to the list. The operation has a difficulty value of 3 and a high workload. The brute-force algorithm is unable to find a feasible allocation (meaning none of all possible allocations is possible). The best, and fairly reasonable, it finds within this time is (see Fig.6); $p_1: [o_1, o_4]$, $p_2: [o_2, o_5, o_6]$, $p_3: [o_3, o_7]$.

Table II: Additional operation

o	$t_{o,start}$	s_o	Work profile
7	6:00	3	50% (0-1h) 100% (1-2h)

Due to the high workload and difficulty of o_7 , only the third operator can supervise this operation without crossing the capacity threshold. Additionally, the third operator is no longer able to pick up any operations that overlap o_7 . This is why the second operator has to supervise o_6 .

Because of the 1.5x penalty due the difficulty of o_6 , and due to the overlap with o_5 , the threshold for the second operator is crossed (105%). This makes even the best plan unfeasible

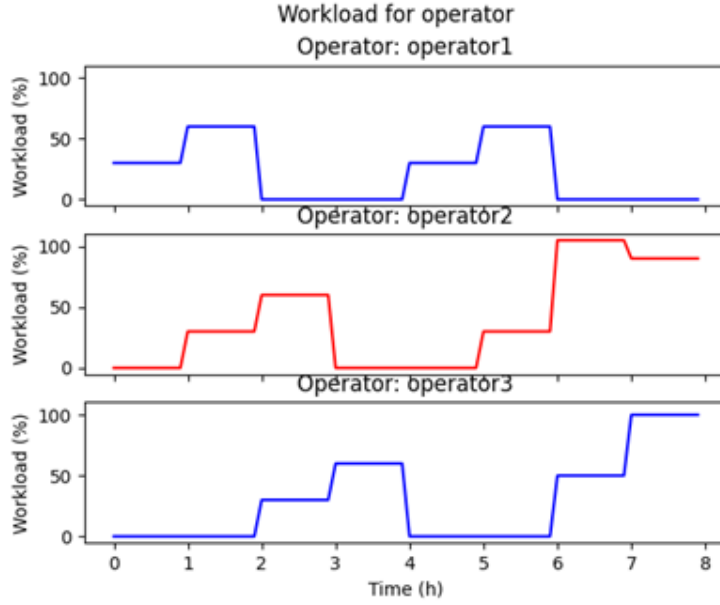


Fig.6: Simple case with an additional operation. In this scenario, no feasible allocation is possible. Even in the most optimal allocation, the second operator gets a too high workload (105%).

3.2. Moderate scenario

Next, we consider a more moderate scenario, in which three operators supervise twelve operations, Table III. The three operators have a respective expertise level e_p of 6, 3 and 2.5. Wherein the simple scenarios, it was still quite possible to get to the best allocation by hand, for this moderate scenario it already proves to be unfeasible to do so. The first step is to use the brute-force method for optimization. With three operators and twelve operations there are $3^{12} = 531.441$ possibilities. On a standard laptop (see 2.4 Implementation) this takes around 5-6 minutes to evaluate. This shows the limitation of the brute-force method. Due to the exponential nature of the number of possibilities, more operation or operators would make this type of optimization unfeasible. The brute-force algorithm finds the following optimal allocation ($C = 1.15$, Fig.7): $p_1: [o_4, o_{10}, o_7, o_9]$, $p_2: [o_{11}, o_8, o_{12}, o_2]$, $p_3: [o_1, o_5, o_3, o_6]$.

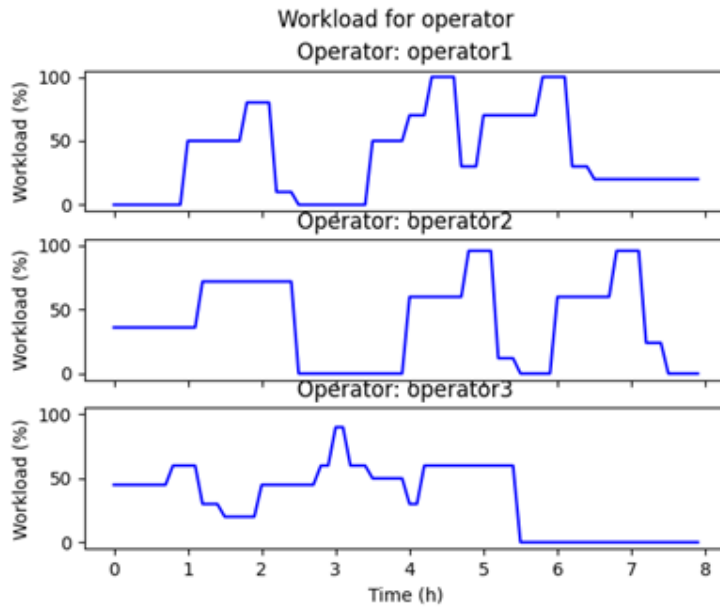


Fig.7: Optimal allocation for the moderate example scenario. In this allocation all operations are evenly distributed over operators and time.

Table III: Moderate scenario

o	$t_{o,start}$	s_o	Work profile
1	0:00	3	25% (0-0:45h) 40% (0:45-1:15h) 10% (1:15-1:30h)
2	0:00	3	30% (0 - 1:15h) 60% (1:15-2:30h)
3	0:00	3	20% (0-4h)
4	1:00	3	50% (0-0:45h) 80% (0:45-1:15h) 10% (1:15-1:30h)
5	2:00	3	25% (0-0:45h) 40% (0:45-1:15h) 10% (1:15-1:30h)
6	3:00	2.5	30% (0 - 1:15h) 60% (1:15-2:30h)
7	3:30	2.5	50% (0-0:45h) 80% (0:45-1:15h) 10% (1:15-1:30h)
8	4:00	3	50% (0-0:45h) 80% (0:45-1:15h) 10% (1:15-1:30h)
9	4:00	6	20% (0-4h)
10	5:00	6	50% (0-0:45h) 80% (0:45-1:15h) 10% (1:15-1:30h)
11	6:00	3	25% (0-0:45h) 40% (0:45-1:15h) 10% (1:15-1:30h)
12	6:00	3	25% (0-0:45h) 40% (0:45-1:15h) 10% (1:15-1:30h)

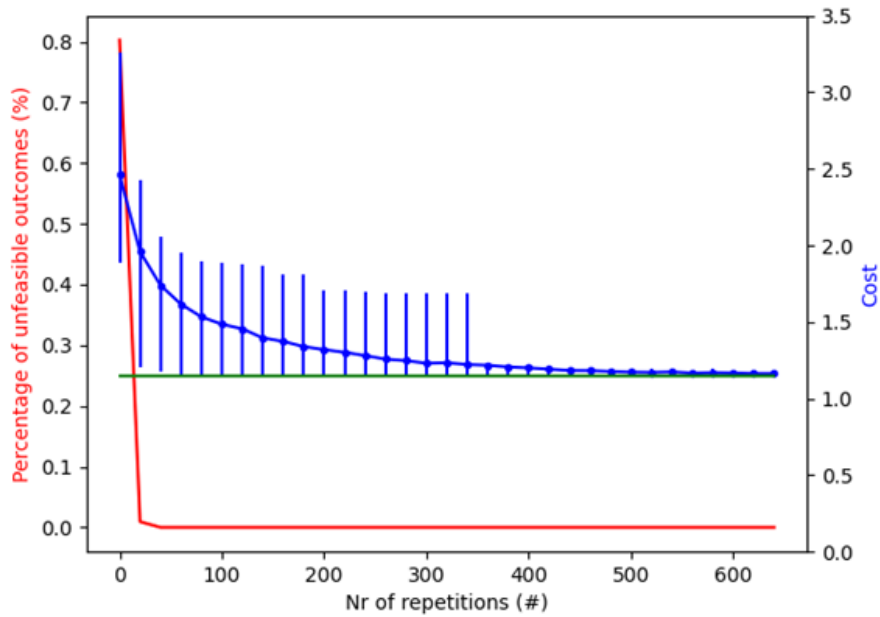


Fig.8: Cost outcome of IDDFS related to number of repetitions. Red: percentage of unfeasible outcomes related to number of repetitions. Blue: average cost of the found solution (10%-90% quartile with vertical lines). Green: global minimum (as found by brute-force method)

We can also use the IDDFS optimization algorithm to get to an approximation of the best allocation of work. For the IDDFS, the amount of repetitions is related to how close we can get to the optimal allocation at the cost of more computation time. The brute-force method will always find this optimal allocation, but only if all possible combinations are evaluated. With IDDFS we are guaranteed to find better solutions over time, whereas cutting off the brute-force method after an incomplete number of evaluations is too random to guarantee a serious outcome.

Fig.8 shows the relation between number of repetitions of the IDDFS and the average outcome (in blue). This was obtained by running the IDDFS 1500 times for each number of sampled repetitions, and analysing the results. We did so to get a reliable average on the IDDFS' performance for each sampled number of repetitions. With a low number of repetitions (< 20), the IDDFS is (in most cases) unable to find the optimal allocation, and has a high percentage of outcomes where the optimizer is not even able to find a feasible outcome at all (as indicated with the red line in Fig.8). Between 20-340 repetitions, the IDDFS method almost always finds a feasible solution, but often does not find the most optimal solution. With 340-560 repetitions, the IDDFS often finds the most optimal solution, and with > 560 repetitions (badly visible in Fig.8), the algorithm is almost guaranteed to find the best possible solution.

In the moderate scenario, even with 560 repetitions, the IDDFS is still much more efficient than the brute-force algorithm. Where the brute-force algorithm requires an exponentially increasing number of cost evaluations (p^o , in this case 531.441 evaluations), the IDDFS requires $\text{repetitions} \times p \times o$, which in this specific case is $560 \times 3 \times 12 = 20.160$ evaluations. As both optimization algorithms themselves require an arbitrary amount of calculation power compared to the cost evaluations, the IDDFS with 560 repetitions is still much faster (about 10 seconds compared to 5-6 minutes on a standard laptop). Simply put, IDDFS performs in linear time ($O(n) = n$) whereas the brute-force method performs in exponential time ($O(n) = c^n$).

This shows the strength of using the IDDFS compared to the brute-force method of optimization. Both are able to find the global minimum, but the IDDFS method is able to get to the result much faster. Next to that, the IDDFS is scalable. Due to the exponential nature of the brute-force method, it becomes unusable in realistic settings. As the IDDFS performs in linear time, it scales quite well with more operators and operations in realistic future shore control centres. The disadvantage is that the amount or repetitions required to get to the global minimum reliably is case specific, which makes it a difficult parameter to determine without an analysis such as shown in Fig.8.

3.3. Complex scenario

Lastly, we look at a much more complex scenario, in which six operators supervise sixteen operations and two new operations come along after a first allocation has been computed, Table IV. We aim to illustrate the adaptive nature of our approach under complex and dynamic settings.

The six operators have an expertise level e_p of 6 (two highly experienced operators), 3 (three fairly experienced operators) and 2.5 (one least experienced operator). This complex scenario cannot be solved by a brute-force approach. This approach would take 2.8×10^{12} evaluations which would take more than 65 years to evaluate with a standard laptop.

To get a sense on how many evaluations we need for the IDDFS optimization algorithm, we can again run the IDDFS 1500 times for each number of repetition, and analyse the results, Fig.9. This shows that the IDDFS algorithm can reliably get to the likely global minimum if we use more than 350 repetitions.

The IDDFS requires in this case $350 \times 6 \times 16 = 33.600$ computations which takes 15 to 25 seconds.

One of the best solutions is ($C = 0.29$, Fig.10): p_1 ($e_p = 6$): [o_6, o_8, o_{13}], p_2 ($e_p = 6$): [o_{14}, o_7], p_3 ($e_p = 2.5$): [o_1, o_2], p_4 ($e_p = 3$): [o_4, o_3, o_{12}], p_5 ($e_p = 3$): [o_{16}, o_{11}, o_9], p_6 ($e_p = 3$): [o_5, o_{15}, o_{10}].

Table IV: Complex example. (Changes will be implemented after the initial allocations (in red))

o	t _{o,start}	s _o	Work profile
1	0:00	1	20% (0-4h)
2	0:00	3	20% (0-4h)
3	0:00 (3:00)	3 (6)	25% (0-0:45h) 40% (0:45-1:15h) 10% (1:15-1:30h)
4	0:00	3	25% (0-0:45h) 40% (0:45-1:15h) 10% (1:15-1:30h)
5	1:00	3	50% (0-0:45h) 80% (0:45-1:15h) 10% (1:15-1:30h)
6	2:00	3	25% (0-0:45h) 40% (0:45-1:15h) 10% (1:15-1:30h)
7	2:00	6	50% (0-0:45h) 80% (0:45-1:15h) 10% (1:15-1:30h)
8	2:00	6	25% (0-0:45h) 40% (0:45-1:15h) 10% (1:15-1:30h)
9	2:00	3	50% (0-0:45h) 80% (0:45-1:15h) 10% (1:15-1:30h)
10	3:30	3	50% (0-0:45h) 80% (0:45-1:15h) 10% (1:15-1:30h)
11	3:30	2.5	50% (0-0:45h) 80% (0:45-1:15h) 10% (1:15-1:30h)
12	4:00	6	20% (0-4h)
13	4:00	3	50% (0-0:45h) 80% (0:45-1:15h) 10% (1:15-1:30h)
14	5:00	6	50% (0-0:45h) 80% (0:45-1:15h) 10% (1:15-1:30h)
15	6:00	3	25% (0-0:45h) 40% (0:45-1:15h) 10% (1:15-1:30h)
16	6:00	3	50% (0-0:45h) 80% (0:45-1:15h) 10% (1:15-1:30h))
17	4:00	6	20% (0-4h)
18	4:30	3	25% (0-0:45h) 40% (0:45-1:15h) 10% (1:15-1:30h)

In this case, multiple optimal allocations exist. This is due to the fact multiple operators have the same expertise level and several operations are identical, making their allocations interchangeable to those operators. The IDDFS method finds an allocation for which all operators have (about) the same workload, experienced operators take on the more difficult tasks and all operators can take a break at least once every four hours.

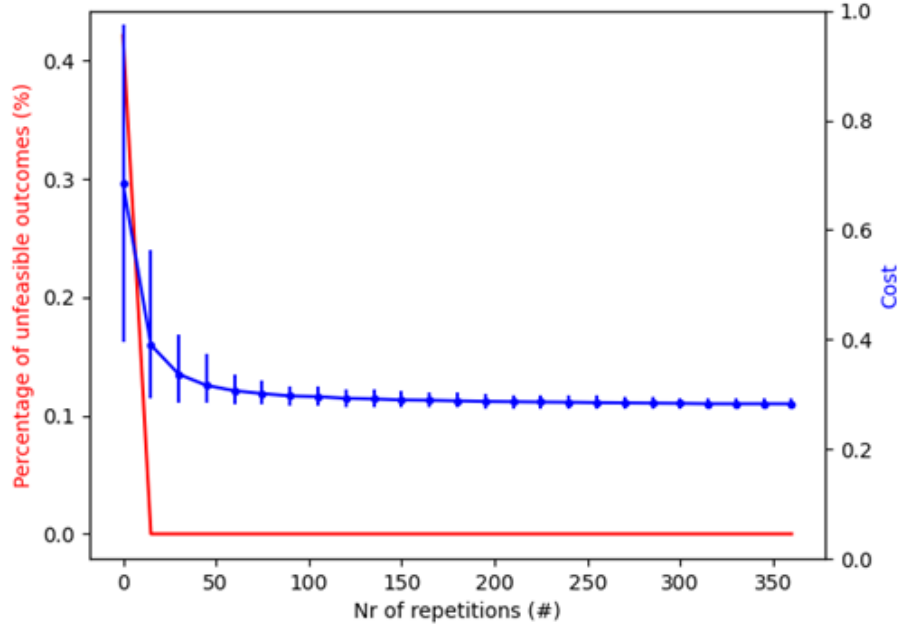


Fig.9: Cost outcome of IDDFS related to the amount of repetitions. Red: percentage of unfeasible outcomes in relation to number of repetitions. Blue: Average cost of the found solution (10%-90% quartile with vertical lines).

We now assume that during the shift, two additional operations connect to the shore control centre (o_{17} and o_{18}). Similarly, we assume a sensor malfunctions during o_3 , and it is delayed until 3:00. This also causes the operation to become much more difficult as redundancy is not guaranteed any longer (s_0 : $3 \rightarrow 6$).

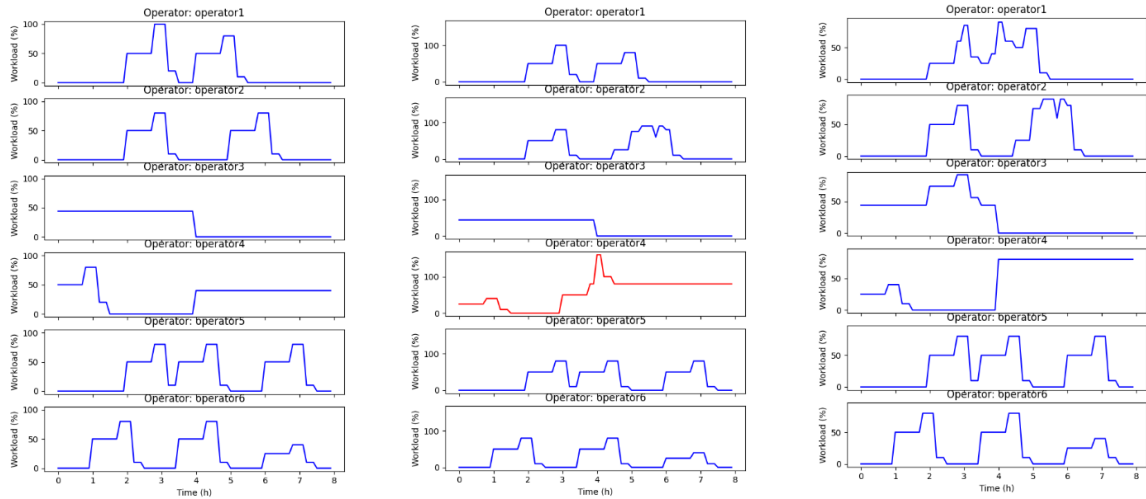


Fig.10: Workload for complex example. Left: Workload before the operations are changed. Middle: Workload after operations are naively allocated without optimization, showing overload for fourth operator. Right: After allocating the new and changed operations and re-optimizing the existing allocations.

The order of events is as follows: 1) o_{17} is added, 2) o_{18} is added, 3) the sensor malfunctions for o_3 . Imagine we naively add o_{17} and o_{18} to the operators which keeps the cost as low as possible. Also, we will not re-allocate o_3 and keep it under fourth operator's supervision. No further optimisation is performed. This results in the following planning, Fig.10: p_1 ($e_p = 6$): [o_6, o_8, o_{13}], p_2 ($e_p = 6$): [o_{14}, o_7, o_{18}], p_3 ($e_p = 2.5$): [o_1, o_2], p_4 ($e_p = 3$): [o_4, o_3, o_{12}, o_{17}], p_5 ($e_p = 3$): [o_{16}, o_{11}, o_9], p_6 ($e_p = 3$): [o_5, o_{15}, o_{10}].

This planning is now unfeasible (thus: it does not get a regular score). The fourth operators gets o_{17} assigned, whereas o_{18} is assigned to the second operator. Though if time progresses and the sensor malfunctions during o_3 , its difficulty spikes and so does its workload for the fourth operator. Who, with the extra assignment of o_{17} , has now more work than it can handle. This creates an unreasonable dangerous situation.

Luckily, with the IDDFS method we can not only naively allocated new operations, but we can do so while performing (minimal) changes to an already existing allocation. In other words, we can dynamically allocate new operations in an optimised way that minimizes operator workload as much as possible. In the above-described case, the method finds a more optimised allocation that requires only two reallocations; as the new operation o_{17} is allocated to the fourth operator p_4 , its previously assigned operation o_3 (the one who will suffer a sensor malfunction) is allocated to the first operator p_1 . Furthermore, the operation o_6 which was allocated to this first operator p_1 is now allocated to the third operator p_3 . These changes create more room for the fourth operator to take on the new operation o_{17} with a minor reallocation needed to prevent other operators to become overloaded with work. Note that where in the original optimisation the method favoured the least experienced operator p_3 , it now makes use of time this operator still has free to take on other work. The complete allocation is as now as follows ($C = 0.39$, see Fig. 10): p_1 ($e_p = 6$): [o_8, o_{13}, o_3], p_2 ($e_p = 6$): [o_{14}, o_7, o_{18}], p_3 ($e_p = 2.5$): [o_1, o_2, o_6], p_4 ($e_p = 3$): [o_4, o_{12}, o_{17}], p_5 ($e_p = 3$): [o_{16}, o_{11}, o_9], p_6 ($e_p = 3$): [o_5, o_{15}, o_{10}].

This plan is feasible, and has a score much closer to the initial score (increase of 0.1 in cost, opposed to an unfeasible plan before optimization). Coincidentally, the score is even close to the likely optimal solution if the proposed changes were known from the beginning ($C = 0.38$). In some cases, a significantly better plan can be found if we fully re-optimize, however, this would also mean the allocation of each operator would change completely, and as a consequence confuse them. The proposed method hence includes a penalty for each change to remedy this.

3.4. Discussion

The proposed cost function is an approximation of reality. The workload of supervising one or more operations might be hard to define as a predetermined percentage. In addition, modelling an operator's expertise or operation's complexity in a single score, can be too simplistic. However, we argue that a fully realistic model of workload is not required to achieve a dynamic allocation of autonomous operations. Ideally, a rigorous evaluation of the workload model is required, although this is hampered by the simple fact that shore control centres where operators supervise autonomous vessels is still an unachieved future. Therefore, the proposed algorithm is an initial step towards dynamic task allocation, but will need to be adapted, evaluated and optimized on more realistic scenarios.

Part of this future work is a way to elicit cost variables and their weights. Currently, the cost variables modelled given common insights from the human factors research field and their weights chosen through intuition to get logical results. A first future step thus could be to more adequately model these variables and their weights. For instance, it needs to be determined how much more (or less) important it is for an operator to have a break versus having a high peak intensity during work. Such knowledge should be elicited from human factors experts with a particular shore control centre in mind, and subsequently evaluated with the operators of such a centre.

The parameter of sampled repetitions is a difficult parameter to set. It determines the likelihood that the IDDFS method finds the optimal allocation, however how many repetitions are required is difficult to estimate beforehand. A representative example of operators and operations can be analysed, as was done in Figs.8 and 9. However, such analysis relies on the brute-force method to find the optimal allocation first. Which in turn requires a potential unfeasible amount of time, preventing such an analysis for realistic scenarios. Future work might aim at presenting different analysis methods or make us of unparameterized algorithmic alternatives to IDDFS.

4. Conclusion

This work proposed a way to allocate autonomous operations within the maritime domain to operators for supervision. The proposed method is intended to automate the safe and effective allocation of such operations in a shore control centre. We argued that human factor knowledge on optimal workload distribution should form the core of such an allocation. Several example scenarios with increasing complexity were presented and analysed.

The results show that the proposed dynamic task allocation algorithm can distribute operations over operators in a way that optimizes the workload following human factors knowledge. The first illustrative example scenario showed that the resulting allocations are logical and meaningful. The moderate example scenario showed that the algorithm can produce feasible solutions when manual allocation is difficult or impossible. We also shown that this scenario can be solved by a brute-force algorithm, but becomes quickly unfeasible due to the time required to find an optimal allocation. The used Iterative Deepening Depth First Search (IDDFS) algorithm however is much more scalable and can, with enough sampled repetitions, find the global optimum. However, given the nature of IDDFS as a heuristic search algorithm, we can never be assured that what seems optimal is indeed so. However, it is likely that a near-optimal allocation is still very much sufficient to enable a few operators to effectively supervise many more operations. Lastly, the complex example scenario showed that the IDDFS implementation is still robust for an increasing number of operations and operators. Next to that, it shows that the dynamic allocation makes the algorithm robust against changes that arise after any previously made allocation.

To conclude, the IDDFS algorithm combined with a cost function capturing human factors knowledge about workload, seems to be a promising technology to facilitate shore control centres where few operators supervise many autonomous operations. This work takes a first step towards automating task allocation in shore control centres. The MOSES EU project is working towards getting closer to this goal.

Acknowledgements

This research has been conducted as part of MOSES project, which has received funding from the European Union's Horizon 2020 Research and Innovation Program under Grant agreement No. 861678.

References

- KORF, R.E. (1985), *Depth-first iterative-deepening: An optimal admissible tree search*, Artificial Intelligence 27(1), pp.97-109
- NEERINCX, M.A. (2003), *Cognitive task load design: model, methods and examples*, Handbook of Cognitive Task Design, Ch.13, Lawrence Erlbaum Associates, pp.283-305
- NEERINCX, M.A.; DOBBELSTEEN, G.J.H. VAN DEN; GROOTJEN, M.; VEENENDAAL, J. VAN (2003), *Assessing cognitive load distributions for envisioned task allocations and support functions*, 13th Int. Ship Control Systems Symposium (SCSS), Orlando
- VAN DEN BROEK, J.; GRIFFIOEN, J.R.; VAN DER DRIFT, M. (2020), *Meaningful Human Control in Autonomous Shipping: An Overview*, IOP Conference Series: Materials Science and Engineering 929(1), <https://doi.org/10.1088/1757-899X/929/1/012008>
- VAN ROSSUM, G.; DRAKE, F. L. (2009), *Python 3 Reference Manual*, CreateSpace

Enabling Individual Part Production Planning in Shipbuilding: Machine-Learning-Assisted Prediction of Production Times

Peter Burggräf, Tobias Adlon, Moritz Beyer, Niklas Schäfer, Judith Fulterer,
RWTH Aachen University, Aachen/Germany, n.schaefer@wzl.rwth-aachen.de

Abstract

This paper presents a procedure model that allows for a data-based prediction of production times by using machine-learning-assisted correlation analysis. We derived this model by adapting related work in other industries to the requirements that we defined based on current challenges to maritime production planning and control. Production times in section construction can be forecasted with comprehensible calculation formulas derived from little training data. Finally, the outlined approach offers shipyards aiming to advance their production planning a comprehensive overview on the associated potentials and challenges.

1. Introduction

European shipyards largely manufacture premium products such as yachts, research vessels, and cruise ships. In specialty shipbuilding as a niche market, the shipyards experience increased competitive pressure. According to Wandt (2014), this pressure forces shipyards to focus on cost-optimized manufacturing processes, typically seeking to improve production planning and control. As these ships are produced as one-of-a-kind, production planners face a low information density and can base their production plan only on similar previous shipbuilding projects. The planning outcome heavily depends on their experience, resulting in imprecise and non-transparent decision-making processes. Close synchronization of design and manufacturing further inhibits the detailing of production plans. Typically, planning experts estimate the required effort for work packages and their corresponding work steps. The granularity of planning does not exceed the work steps that are scheduled on a daily basis, as described by Czarnietzki (2008) and Sikorra et al. (2016). Shop floor management must therefore compensate for the resulting insufficient planning depth with short-term planning adjustments. However, calculated resource planning methods that schedule the production steps of individual parts and assembly groups offer a novel approach.

To allow for this more detailed planning approach, i.e. individual part production planning, the product structure including current changes to the design is the basis for the production plan. The product structure features all parts with their assembly structure for all sections and is used to generate the work break down structure. The work breakdown structure is the collection of all required production activities as well as constraints to their production sequence. For example, flame cutting metal sheets precedes the activity of tacking an individual assembly group that is followed by the respective welding activity. Next, the activity times need to be set, which are given by process-specific production times. The resulting network plan is scheduled into the production plan using algorithms such as heuristics. During the execution of the production plans, live acquired feedback from the manufacturing and assembly processes is linked to the production activities to detect delays. By proposing changes to the production plans, the system supports planners to minimize possible disruptions. In any case, critical deviations from the plan need to be handled on the shop floor, but can be incorporated again to calculate an alternative production plan.

The methodology for this approach was developed and is currently being implemented in a digital twin for production planning in shipbuilding, focusing on section construction. It is under development for a German shipyard in the ProProS research project, as already presented by Zerbst (2021). The digital twin as well as similar methods employing individual part production require a sufficiently accurate forecast of the production times. Due to the large number of parts considered, an automated data-based prediction of these production times is essential for industrial application.

2. Problem definition and objective

The guiding research question of this paper is how the production times for the use in individual part production planning can be predicted. The selection of suitable data-based techniques and their specific applicability for a software-assisted automation is of special concern. Additionally, a comprehensive overview shall be given for the integration into production planning to guide shipyards seeking to adapt this approach.

We aim to answer the research questions by developing a procedure model as a framework addressing the characteristics of specialty shipbuilding and offering a company-independent applicability. The underlying requirements stem mainly from the adaption of current approaches in the prediction of production times to the specifics of individual part production planning. Firstly, the general production process needs to be thoroughly understood to tailor the prediction of production times to the specific production activities. The prediction itself is to be based on expert knowledge supported by historical production data, which is typically characterized by heterogeneous structure, semantics and detail. As a result, this input requires sufficient preparation for utilisation as training data. Originally, *Öztürk et al. (2006)* successfully applied methods from machine learning to predict manufacturing lead times. More recently, *Lingitz et al. (2018)* employed regression algorithms to improve the prediction accuracy in a case study in the semiconductor industry. *Schuh et al. (2019)* compared the application of various machine-learning techniques in the prediction of transition times. However, as *Burggräf et al. (2020)* also pointed out in their review, almost exclusively order data as well as the status of production are used for the prediction of lead times for the total order. Similarly, existing research focuses on workshop production structures as a whole, where production times for individual production activities are not examined. Thus, we adapt these approaches to application in individual part production planning of maritime systems, particularly specialty shipbuilding.

3. Presentation of the procedure model

Following a methodology for data-based prediction and planning of order-specific transition times by *Sauermann (2020)*, we propose the procedure model adapted to the requirements of individual part production planning in shipbuilding. Fig.1 illustrates the model; its components are detailed in the following sub-chapters.

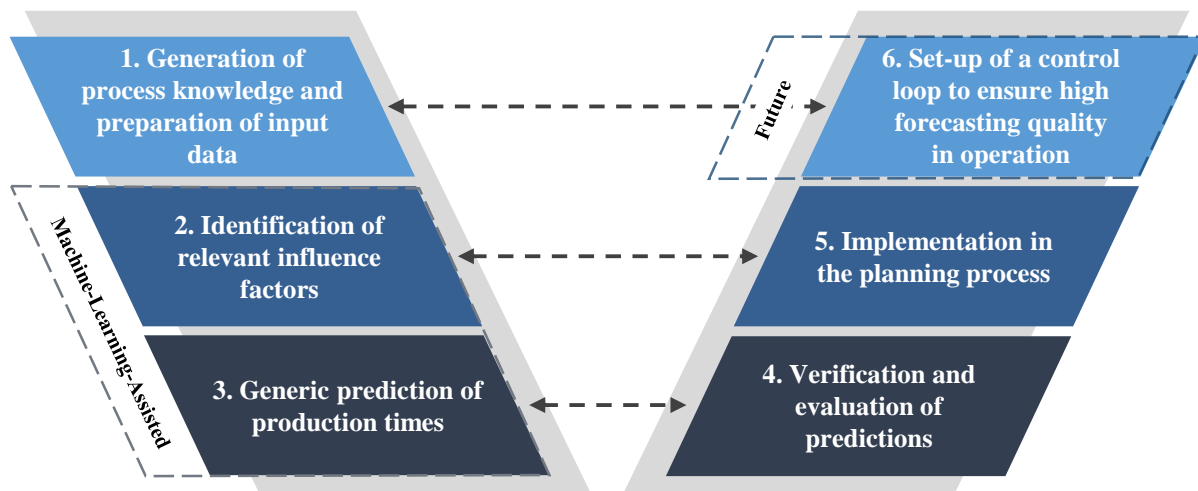


Fig.1: Six-component procedure model for the prediction of production times in the context of individual part production planning

3.1. Generation of process knowledge and preparation of input data

Prior to the actual prediction, the application environment needs to be analysed. Primarily, the production process is recorded in a system-oriented production model that defines the production activities and their production sequences. Including the transportation activities, the overall material flow through the shipyard is mapped out. Production planning and control tasks should be linked to this model as well. To generate common process knowledge, the model can be graphically represented using different modelling languages, such as BPMN (Business Process Model and Notation). Then, the parts and assembly groups from the product structure are converted to the work break down structure, which defines the necessary production activities for each component type. Different component types such as single parts (sheets and profiles, with or without deformation) or assembly groups (of panels or construction elements) relate to different production activities. Setting the prediction scope, the production activities are selected, for which the production times shall be predicted.

For use in maritime production planning and control, these production times are understood as net lead times that are defined by the time span between the start and the end of a production activity. Therefore, this includes in addition to the main process time, the setup time, down time and recovery time, while additional demurrage time is not considered. Transportation activities are defined as a special type of production activity.

For the data preparation, possible influence factors from the product structure, such as a part's height or the number of profiles for a panel, are collected for all examined components. Forming the training data, historical production times of the relevant production activities are then linked to these components. The prepared database is checked for completeness and consistency, while errors are removed to attain machine-readable data.

3.2. Identification of relevant influence factors

The influence factors, which are the component characteristics from the product structure, are investigated for every type of production activity. Either by manual selection or via machine-learning-assisted feature selection, the relevant influence factors need to be identified. This selection reduces the number of input parameters, which in case of increased data amounts can improve computing performances. The manual selection is based on expert knowledge and does not necessarily need training data. However, if available, the selection can be supported by graphs showing the relation of the influence factor to the production times, which are either extracted from real production data or estimated for individual components. This selection process can be facilitated by data mining, which – according to *Mannila (1996)* – taps into methods from machine learning and statistics to extract knowledge from the data, i.e. in this case the influence of component characteristics on the production times. Software solutions for these tasks are available to the user, such as the data science toolkit “Orange” or platform “RapidMiner”. For the feature selection, common methods rank the set of influence factors in their relevance. *Kacprzyk et al. (2006)* suggest the wrapper method that uses a learning algorithm to select the features on basis of their prediction accuracy.

We hypothesise that a small number of influence factors can predict production times with high accuracy. As *Weidemann and Sender (2014)* showed, high correlation of single component characteristics to the production times can be found for specific production activities. For example, the process times of flame cutting correlate to the component weights and the number of cuts per sheet. In fact, the process times for flame cutting as a typical capacity bottleneck are precisely quantified in current production planning. Specialized nesting tools arrange the needed cuts on the sheets and estimate the process time with the sum of the cutting lengths. Nevertheless, we expect that the production times of other production activities can be calculated using different influence factors. For example, the number of profiles in panel construction or the mass of an assembly group in flame straightening could enable similar calculations – without relying on the development of more complicated production process models.

3.3. Generic prediction of production times

The combination of relevant influence factors as input parameters to calculate the production time predictions for the production activities as output parameters forms the prediction model. At its core, the prediction model is composed of to-be-defined mathematical formulas. Since the prediction model can be viewed in terms of these parameters without explaining its inner workings, the prediction model is seen as a black box. Fig.2 illustrates this concept from the perspective of the overall procedure.

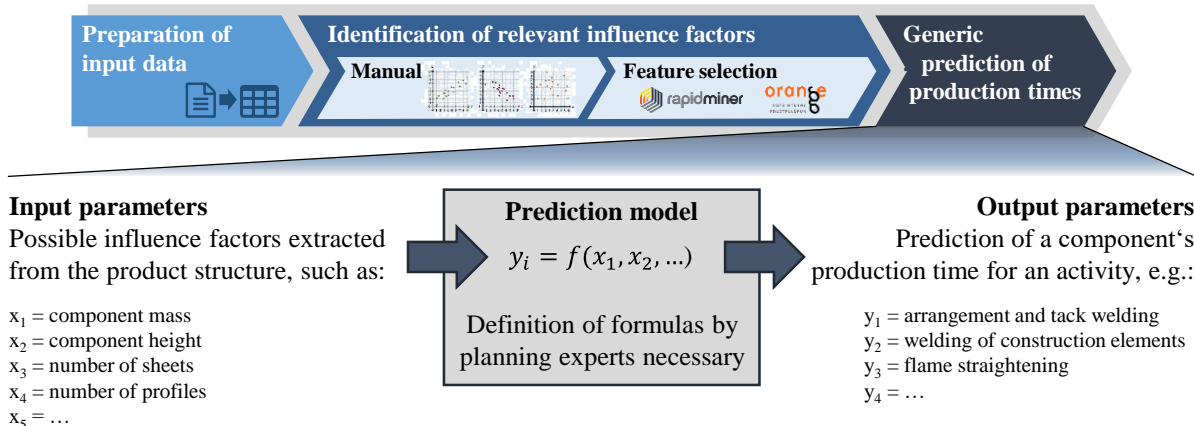


Fig.2: Setup of the prediction model as a "black box"

The production-activity-specific formulas in the prediction model need to be defined by planning experts. To add to their expertise, statistical analysis and computational agents can assist them. In comparison to the identification of influence factors, where patterns in the input data are discovered with data mining, forecasting requires statements about future data sets. Accordingly, supervised machine-learning techniques, as explained by *Alpaydin (2009)* as well as *Russel and Norvig (2010)* offer a solution. Since the output parameters of the prediction model are continuous variables, the application of a regression tree as a decision tree for each type of production activity seems most suitable. *Schuh et al. (2019)* already proved this approach effective in the prediction of transition times. On the other hand, the formulation as a classification problem is thinkable, if the possible predictions are split into distinct time intervals. Several methods for the splitting are available, such as equal-frequency binning with training data split equally into the categories or equal-width binning with fixed time intervals. Depending on the quality of the training data however, the computationally developed formulas might need further adjusting by the planning experts. For example, manual boundaries would be helpful to prevent statistical outliers. In general, assistance by machine learning can be efficient, but eventually the planning experts confirm or define adaptations to the final formulas.

3.4. Verification and evaluation of individual predictions

In the fourth step, individual predicted production times for exemplary components are calculated with the prediction model to check the results for plausibility. Different selections of influence factors and different methods for the generation of the prediction formulas are compared by calculating their prediction accuracy. Ideally, a second training data set is used for this purpose. Higher prediction accuracies indicate a better identification of influence factors and their usage in the prediction formulas. These steps should be performed in an iterative process to achieve a sufficient prediction accuracy.

3.5. Implementation in the planning process

In the case of individual part production planning, the prediction model complements the generation of the work break down structure. The implementation allows for a direct calculation of the predicted production times with the influence factors extracted from the product structure. As a result, the planned production activities can then be scheduled in the production plan using algorithms such as heuristics.

3.6. Set-up of a control loop

In an advanced implementation, a control loop is established to ensure a high prediction accuracy. In the long term, real production acquisition data is combined with the relevant expert knowledge to retrain and improve the prediction model regularly. An expected challenge is the stable control of the feedback loop created, as a new prediction model results in changes in production planning that in turn affect the production feedback data as training data.

4. Application of the model and resulting findings

We validate the model by application in panel production and section construction at a German shipyard. Accompanied with the product breakdown structure including part-individual and assembly-group-specific product characteristics, four specific sections with each 800-3,000 parts are linked with the corresponding time data sources.

The shipyard's application environment had already been analysed in the preceding project work. With the material flow sketched between the different production activities linked to the production planning and control tasks, an extract is shown in Fig.3. This process knowledge is subsequently transformed into the process structure.

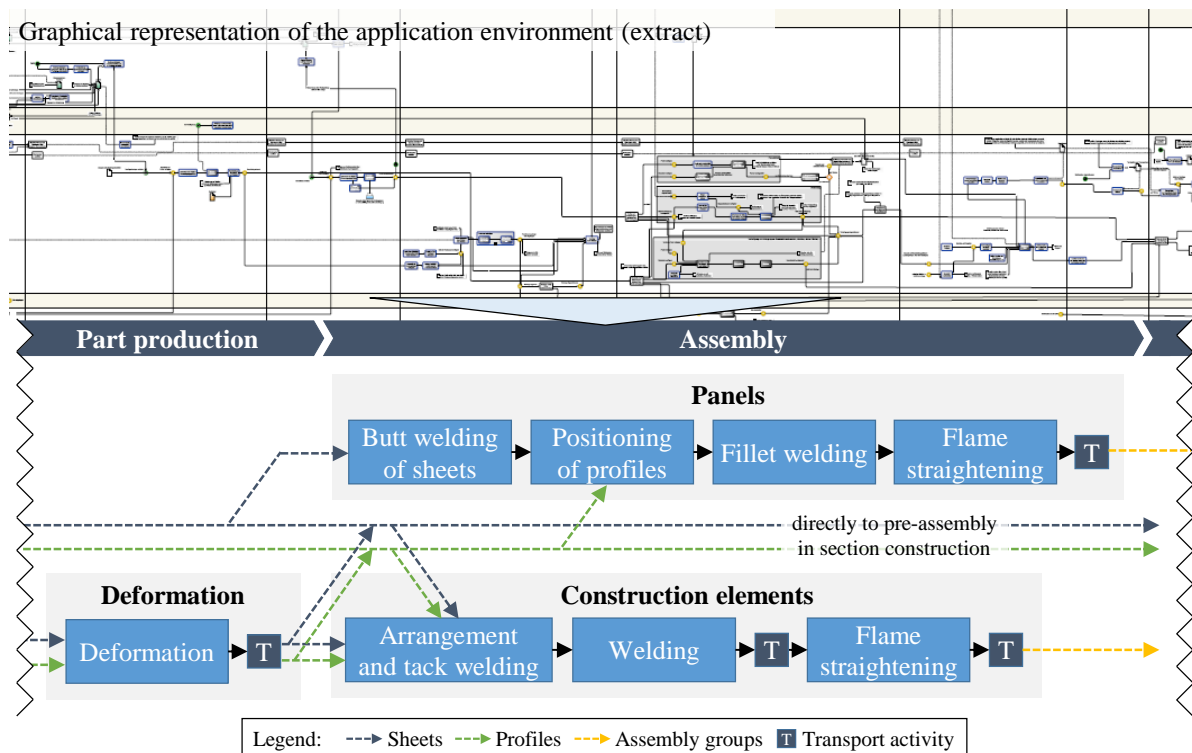


Fig.3: Extraction of the process structure, featuring the application-relevant production activities, from the recorded production and planning processes at the shipyard's application environment

The process structure connects all application-relevant production activities. For example, after profile cutting (not shown in Fig.3) or deformation, a profile to be used for the assembly of a panel would be positioned on already butt-welded sheets. Afterwards, the profiles are welded to the sheets using the fillet welding process, followed by the flame straightening of the panel that is then transported to be used in the section construction (also not shown in Fig.3). Hence, this process structure serves as a template for a component's associated production activities. The transport activities are included in the process structure, but are discounted in the following application. During the preparation of input data, the time data sources are mapped to these production activities.

In the first attempt, production time estimates from several production workers are used as a time data source. For the production activities of panel and construction element assembly, several assembly groups are selected for estimation. Indicating the complexity of the production operations, a group of foremen gave estimates for the required production times based on the production drawings including the components' weights and heights. For the assembly of the construction elements, the relation of the weight and the number of profiles to the estimated production times is exemplary shown in Fig.4. In an initial analysis, statements are made about the relevance of influence factors. For example, the estimations for the welding times correlate well with the assembly groups' component weight.

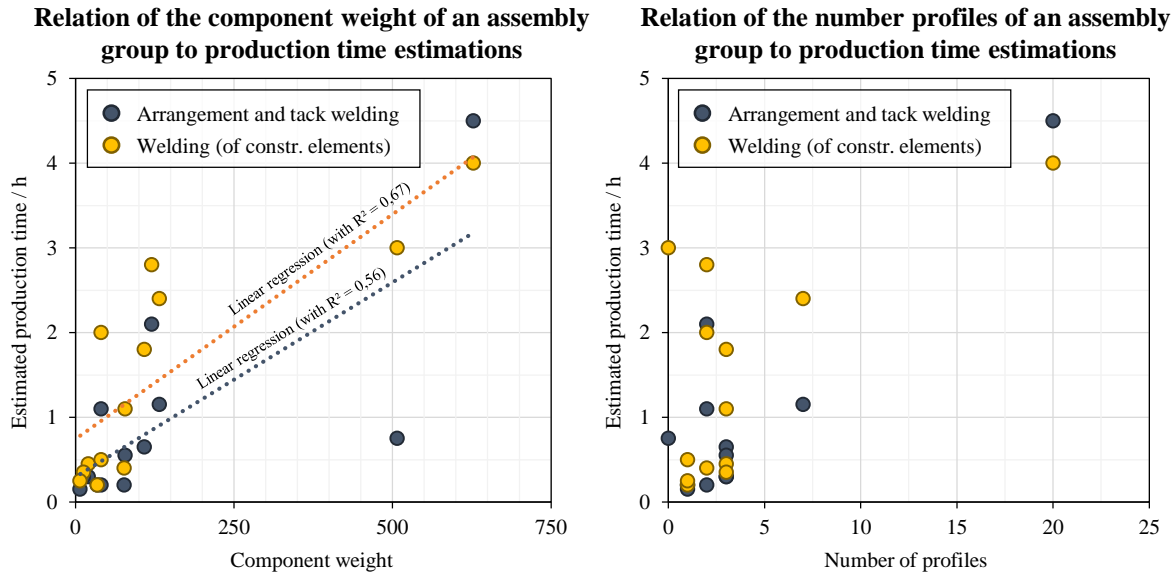


Fig.4: Two exemplary charts to visually analyse the relevance of influence factors in two production activities (arrangement and tack welding; welding) in the assembly of construction elements

The influence factors are identified and following the prediction model is determined in the next step. With help of the machine-learning-assisted feature selection, the relevance of the influence factors is investigated. For each production activity, all statistically significant ($p\text{-value} \leq 5\%$) factors are selected, as shown in Fig.5 exemplary for the assembly of construction elements.

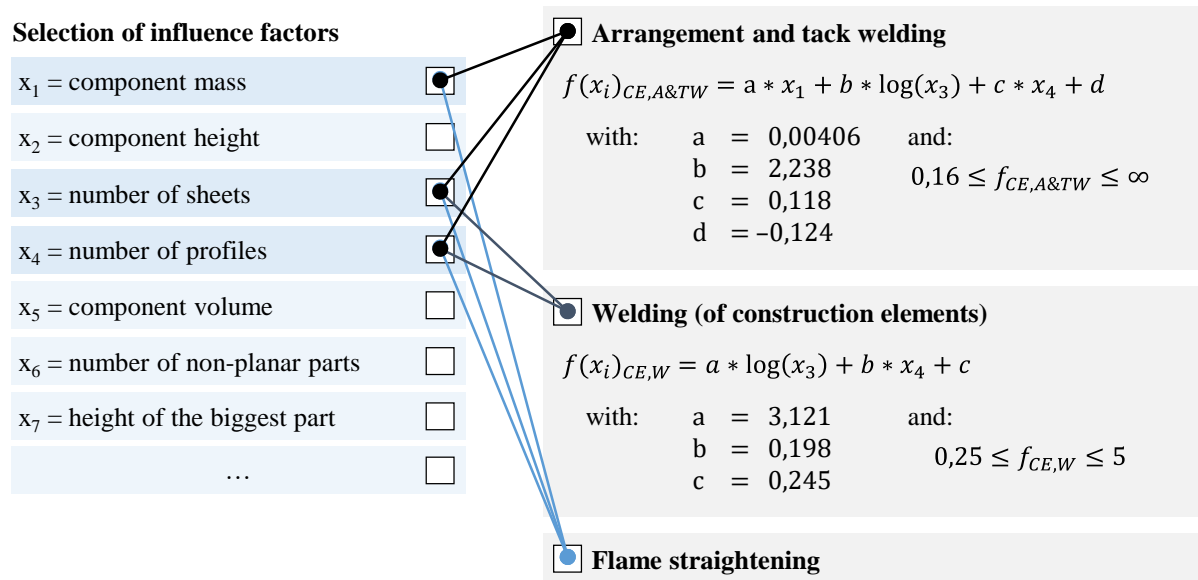


Fig.5: Feature selection for each production activity in the assembly of construction elements and presentation of formulas for the prediction model

In the assembly of construction elements as well as panels, the only significant influence factors are the assembly group's component mass, the number of sheets and the number of profiles. In case of the welding of construction elements, only the number of sheets and the number of profiles can be identified among the available influence factors. For all other production activities, the component weight was found to be most relevant. The formulas of the prediction model, which are shown in Fig.5 for two production activities, are determined using regression analysis. Finally, boundaries for the formulas are manually set. The result are straightforward and comprehensible calculation formulas. However, a major limitation in the application and comparison of different machine-learning techniques is the small amount of time estimations available. Furthermore, this prediction model is based on an estimated data set, which brings about more subjectivity than real production data acquisition.

For the verification of the prediction model, exemplary calculations are performed for assembly groups that were not estimated before. Fig.6 demonstrates the usage for the three production activities in the assembly of a construction element for an individual assembly group. Based on its characteristics, i.e. number of sheets and profiles as well as the overall weight, the production times are predicted.

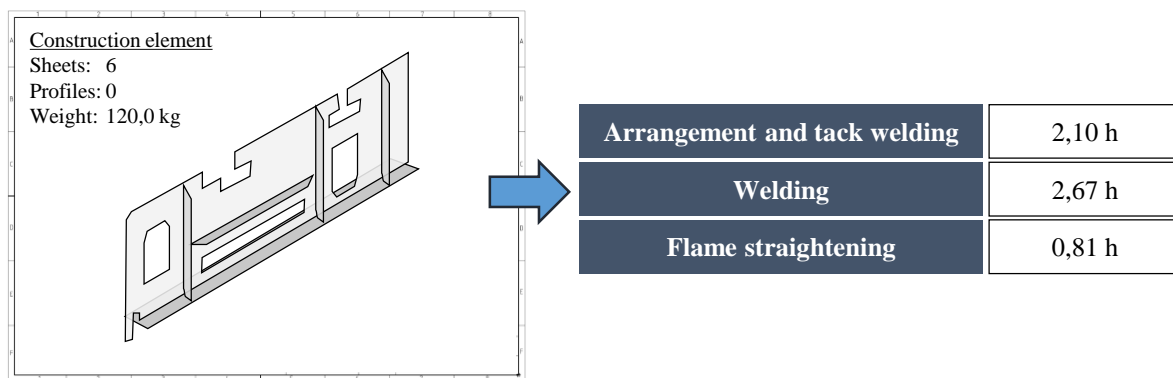


Fig.6: Production time predictions for an exemplary construction element

Analogously, for an exemplary panel, the production times are predicted using the same prediction model, but with different formulas employed, as the associated production activities for a profile differ. Since this panel consists only of one sheet, no butt-welding is required. For the remaining three production activities, the production times are predicted as shown in Fig.7.

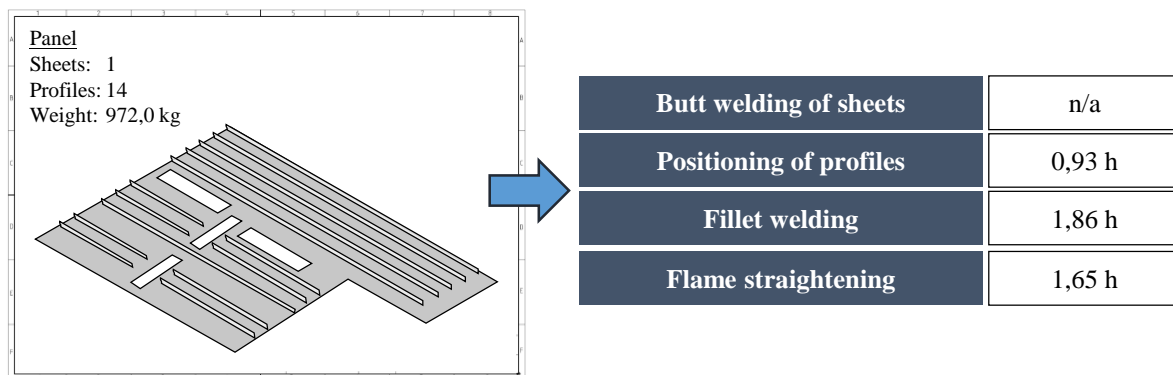


Fig.7: Production time predictions for an exemplary panel

At the time of application, the operating data acquisition at the shipyard did not capture the actual production times for the individual parts of the examined sections. As a result, the predictions are only validated subjectively by the production workers. Differences between manually estimated production times and the automatically predicted production times were not differentiable by a knowledgeable worker. Therefore, the prediction model can already reproduce the estimation efforts of the foremen, even with the little training data available in this attempt.

However, the operating data acquisition captures the sum of all logged working hours per type of production activity and section. Therefore, the sum of the predicted production times is comparable. Fig.8 shows that comparison exemplary for two of the four considered sections. In general, the deviation between the predicted and the actual hours is case-specific and generally rated very low. For example, the sum of predicted production times for the welding of construction elements is for both sections less than 10% from the actual logged hours. Significantly higher logged working hours for the arrangement and tack welding in construction element assembly of section A are partly explained by real occurred production disruptions. Also systematic errors, either consistently under- or overestimating the production times, can be identified. For example, the arrangement and tack welding of construction elements might also be underestimated. Similarly, it seems that the production times for flame straightening in the panel production are overestimated. These deviations can then be manually corrected in the calculation formulas. Overall, even with little training data a promising forecasting quality is achievable.

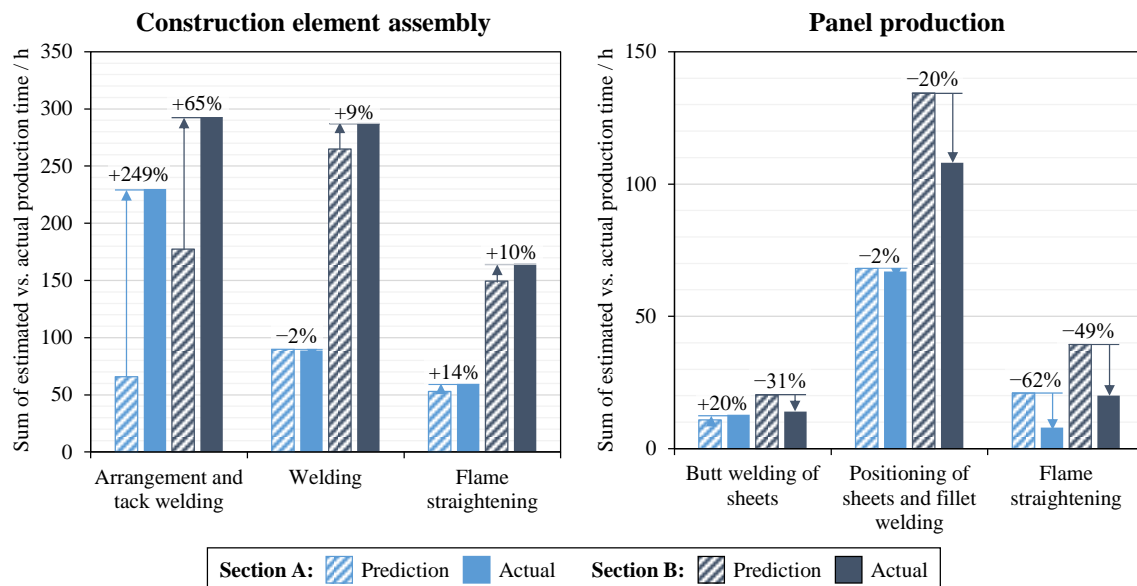


Fig.8: Comparison of sum of predicted production times to actual logged working hours

In a deeper analysis in predictions of individual components' production times, deviations to the actually observed times are revealed. The underlying cause are innate fluctuations in daily production that cannot be considered in the prediction model. However, these fluctuations cancel each other out over the days.

In another attempt, production time stamps from the newly extended data acquisition system at the shipyard are used as another time data source. However, major challenges are encountered in the preparation of input data. As the new acquisition method is currently in ramp-up, the collected time stamps are not yet fully reliable. Nonetheless, parallel processing of production activities at single workstations and regular planned interruptions as well as disruptions are common. This blends the production times with demurrage times that are not to be considered. As a result, an extraction of production times is not possible at this moment, and thus constitutes an object of future research. Therefore, a detailed comparison of different data acquisition methods on prediction accuracy is currently unresolved.

The derived formulas are already implemented into the digital twin for production planning that is being developed in the ProProS research project. This allows for the scheduling of production plans as described in the methodology for individual part production planning in Chapter 1. However, as the demonstrators' development is still ongoing, validation in live production planning and the set-up of the control loop for continuous improvement of forecasting quality are part of future research.

5. Discussion

The main contribution of this paper is the adaption of general approaches to production time prediction to the requirements of individual part production planning in specialty shipbuilding. Outlined in the procedure model, the necessary steps to achieving high forecasting quality are detailed and demonstrated in application. Hence, we offer shipyards seeking to detail their production planning process down to the individual part level a comprehensive overview on this approach.

The possibilities of machine-learning techniques for the identification of influence factors and the determination of the prediction model are explained. However, due to little available training data available at this moment, its potentials were not fully harnessed in application. As a result, the comparison of employing different data analysis methods is still lacking. On the other hand, it is revealed in the evaluation by production workers and by comparison to summed production times that the good forecasting qualities are already achievable. For this purpose, the procedure model constitutes a solid framework for further research. Its investigation continues through the implementation into continuous planning processes to allow for validation in live or simulated production. An open question is which forecasting quality is required to empower individual part production planning. Therefore, we study in future research the ProProS demonstrator software, which implements production planning with real-time capabilities as defined by *Burggräf et al. (2021)* for shipbuilding production systems.

Several entry points for future improvements can be highlighted. The incorporation of further real operation data, which requires shipyards to implement the necessary data acquisition systems, helps to improve the formulas in the prediction model. With more training data available, the applied methods will uncover additional relationships to increase the number of influence factors while improving forecasting quality. The current output parameters of predicted production times can be complemented by personnel and machine requirements to the specific production activity. Finally, the approach is extensible to other planning tasks, e.g. in outfitting, and to other planning levels, e.g. to predict the required production time for a work package or section in a project phase when the work break down structure is not yet available. With the help of feature engineering, more potential influence factors can be created through expert knowledge, which are then available to the prediction model. This will lead to the formation of an advanced analytics platform, opening up possibilities for extended use-cases, e.g. in risk analysis to identify critical production activities.

6. Conclusion

The proposed procedure model demonstrates a systematic approach to predict production times in shipbuilding. This forms the basis for production planning to the level of single production activities of individual parts and assembly groups. In this context, the characteristics of assembly in the construction of maritime systems provide a relevant use-case for machine-learning-assisted forecasting.

Acknowledgements

We would like to thank everyone working in the ProProS project consortium for their contributions, above all Carsten Zerbst, Jan Bitomsky and Nils Sonnenberg from PROSTEP AG along with Heiko Buchholz and Bernhard Urban from Fr. Lürssen Werft.

Funded by the Federal Ministry of Economics and Technology (Germany, BMWi) in the research project ProProS "Proaktive Produktionssteuerung für die Produktion maritimer Systeme" (grant number 03SX492B).

References

ALPAYDIN, E. (2009), *Introduction to machine learning*, 2nd edition, Adaptive Computation and Machine Learning series, MIT Press

- BURGGRÄF, P.; ADLON, T.; MÜLLER, K.; VIERSchILLING, S.; MINDERJAHN, R.; SCHÄFER, N. (2021), *Echtzeitfähigkeit in der schiffbaulichen Fertigung: Zielgerichtete Digitalisierung der Produktionssteuerung und -planung*, wt Werkstatttechnik online 04/21, pp.217-221
- BURGGRÄF, P.; WAGNER, J.; KOKE, B.; STEINBERG, F. (2020), *Approaches for the Prediction of Lead Times in an Engineer to Order Environment—A Systematic Review*, IEEE Access .8, pp.142434-142445
- CZARNIETZKI, R. (2008), *Entwicklung rechnerunterstützter Methoden zur Belegungsplanung auf einer Kompaktwerft und deren Anwendung zur Untersuchung ausgewählter Fertigungsreihenfolgen bei der Paneel- und Sektionsfertigung*, Dissertation, Rostock
- KACPRZYK, J.; GUNN, S.; GUYON, I.; NIKRAVESH, M.; ZADEH, L.A. (2006), *Feature Extraction: Foundations and Applications*, Springer
- LINGITZ, L.; GALLINA, V.; ANSARI, F.; GYULAI, D.; PFEIFFER, A.; SIHN, W.; MONOSTORI, L. (2018), *Lead time prediction using machine learning algorithms: A case study by a semiconductor manufacturer*, 51st CIRP Conf. on Manuf. Sys., Procedia CIRP 72, pp.1051-1056
- MANNILA, H. (1996), *Data mining: machine learning, statistics, and databases*, 8th Int. Conf. Scientific and Statistical Data Base Management, pp.2-9
- ÖZTÜRK, A.; KAYALIGIL, S.; ÖZDEMIREL, N.E. (2006), *Manufacturing lead time estimation using data mining*, European J. Operational Research 173, pp.683-700
- RUSSELL, S.; NORVIG, P. (2010), *Artificial intelligence. A modern approach*, 3rd ed., Prentice-Hall
- SAUERMAN, F.C. (2020), *Databased prediction and planning of order-specific transition times*, Dissertation, RWTH Aachen
- SCHUH, G.; PROTE, J.P.; HÜNNEKES, P.; SAUERMAN, F.C.; STRATMANN, L. (2019), *Impact of Modeling Production Knowledge for a Data Based Prediction of Transition Times*, Advances in Production Management Systems, Springer, pp.341-348
- SIKORRA, J.N.; FRIEDEWALD, A.; LÖDDING, H. (2016), *Early estimation of work contents for planning the one-of-a-kind production by the example of shipbuilding*, MATEC Web of Conferences 77, pp.1025
- WANDT, R. (2014), *Modellgestützte Fertigungssteuerung in der Unikatfertigung am Beispiel des Schiffbaus*, Dissertation, TU Hamburg
- WEIDEMANN, B.; SENDER, J. (2014), *Produktivitätskennzahlen in der Fabrikplanung*, Zeitschrift für wirtschaftlichen Fabrikbetrieb (ZWF) 109, pp.113-116
- ZERBST, C. (2021), *Deming Cycle Enabled: A Digital Twin for Ship Production*, 20th Int. Conf. Computer and IT Appl. Maritime Ind., Mülheim, pp.122-129

Networked Robots and IoT: Real Time Data Acquisition at its Finest

Marco Bibuli, CNR-INM, Genova/Italy, marco.bibuli@cnr.it

Angelo Odetti, CNR-INM, Genova/Italy, angelo.odetti@cnr.it

Massimo Caccia, CNR-INM, Genova/Italy, massimo.caccia@cnr.it

Claudia Presicci, CNR-INM, Genova/Italy, claudia.presicci@inm.cnr.it

Roberta Ferretti, CNR-INM, Genova/Italy, roberta.ferretti@cnr.it

Simona Aracri, CNR-INM, Genova/Italy, simona.aracri@cnr.it

Abstract

Rapid environmental assessment is crucial to promptly understand and intervene in extreme situations. It is also key to a technologically-advanced management of coastal and offshore infrastructure. Autonomous marine vehicles are essential to enable rapid environmental assessment in remote and harsh areas, such as the wave dominated air-sea interface, turbulent waters, mountain lakes, and other similar scenarios. Enabling autonomous monitoring in extreme environments is also important, because it allows the safeguarding of personnel, who can access the vehicles remotely, avoiding putting themselves in harm's way. Stability, dexterity and modularity are the called for features in order to create an optimum autonomous platform. These characteristics combine well in the design of SWAMP, a catamaran ASV with a double-ended hull, made of lightweight foam, with a large payload and four azimuth thrusters. SWAMP, with heterogeneous sensing devices, embraces the Internet of Things (IoT), enabling precise and instantaneous data access, providing the experimental evidence of the reliability and operational capability enhancement given by autonomous and fully connected robotic systems.

1. Introduction

The goal of a precise and almost instantaneous environmental assessment has nowadays become a vital need. The application set spans from environmental monitoring (coastal observation and profile evolution tracking), combined water-air quality and pollutant detection, harbour patrolling, environmental protection (as the detection of rivers' flow rate to prevent flooding).

Environmental monitoring and protection procedures provides well consolidated methodologies and guidelines to carry out the operations and collect data in a consistent way, enabling also historical time-series studies. The numerous European directives of recent years, such as the Water Framework Directive *WFD* (2000) and Marine Strategy Framework Directive *MSFD* (2008) to name a few, demonstrate the importance and centrality of the issue. These water quality management strategies require an integrated approach, which is able to cover all steps of water quality monitoring programs *Behmel et al. (2016)* for different types of marine resources. The geographic areas where water meets the land, including a variety of environments like swamps, bogs and marshes, rivers, lakes, shallow coastal areas are fundamental to study hydro-geological evolution of the environment and also measure the anthropogenic impacts on ecosystems *Odetti et al. (2020)*. Analogous importance covers the marine protected areas (MPAs), distinctive spaces protected by law due to their unique characteristics, such as being the habitat of endangered marine species *Molina-Molina et al. (2021)*. These areas, so important for the management of water resources and for the study of anthropogenic impacts on ecosystems, are particularly critical from a monitoring point of view and require the development of dedicated and innovative technologies *Bibuli et al. (2021)*, *Kurowski et al. (2019)*.

In the last 20 years, robotic technology has provided impressive advancement in the methodologies for effective data gathering and environmental modelling. The ultimate objective for an efficient employment of robotic tools is to provide the capability of instantaneous availability of the data to achieve the rapid environmental assessment goal.

Glancing at the current technological readiness, it is reasonable to state that the technological capability is mature to provide the needed framework. In particular, two main contributions allow the development of such super-rapid sampling frameworks: i) robotic platforms characterized by extreme autonomous capabilities; ii) heterogeneous sampling devices connected through Internet, well known as Internet of Things (IoT).

Adaptation in space and time of the sensing nodes, and the flexibility in handling different sensing platforms can provide to the system the ability to quickly respond to the rapid changes in the environment, as well as to promptly respond to evolving stakeholder and end-user requirements *Mariani et al. (2021)*. This also enables the ability to perform adaptive monitoring of the environment, even in complex situations. Examples of new robotic-based procedures for monitoring port water, together with the design of adaptive guidance strategies for water sampling, innovative tools for sediment sampling, and adaptation of prototype robotic vehicles are described in *Caccia et al. (2019)*.

This work reports the development of a new concept of Autonomous Surface Vehicle devoted to extreme environment monitoring, and the integration of reduced size heterogeneous sampling devices. The main methodological advancement lies on the immediate availability of the gathered data, by means of a fully connected system exploiting mobile networks and providing remote use of the system.

2. The Robotic Platform

SWAMP is a full-electric Catamaran 1.23 m long with a design breadth of 1.1 m by adopting a sliding structure the breadth is variable between 0.7 m and 1.25 m. The hull height is 0.4 m and the vehicle with the structure and the antennas is 1.1 m high. SWAMP lightweight is 38 kg with a draft of 0.1 m, the standard maximum payload is 20 kg with a consequent maximum design draft of 0.14 m but the reserve of buoyancy of SWAMP allows to embark up to 60 kg with a draft of 0.22 m. The small dimensions of the vehicle, Fig.1, comply with the idea of a reduced logistics. The hull shape is inspired by the double-ended Wigley series but with a flat bottom. The double-ended hull form and the propulsion layout is characterised by equally efficient sailing ahead and astern with the possibility of manoeuvring in narrow spaces, Longitudinal centre of buoyancy LCB is centered mid-hull and the hull has large B/T ratios. The hull configuration shape was chosen both for hosting four Pump-Jet azimuth thrusters expressly designed and studied for this project and to create an innovative structure that also avoids the presence of sharp edges on the hull bottom. Indeed one of the main peculiar aspects of SWAMP is the use of light, soft and impact-survival flexible structure made with a sandwich of soft closed-cell HDPE foam, HDPE plates and pultruded bars. With this design SWAMP is a completely modular vehicle that can be dismounted and transported to be remounted in various possible configurations. This flexible design allows to host various types of tools, thrusters, control systems, samplers and sensors.

Also for this reason for the propulsion the choice has fallen on the design of a modular propulsion unit based on Pump-Jet that can be easily installed on the vehicle. Such a solution allows also to remove, if necessary, some of the thrusters and/or substitute them with sensors, tools or even other thrust units. Using four azimuth thrusters gives SWAMP the controllability that is required for high quality surveys. The Pump-Jet thrusters were built in the CNR-INM labs and tested at various angles and with different configurations. A deeper description of the vehicle is reported in *Bibuli et al. (2020)*.

One of the main peculiarities of SWAMP consists in the fact that each hull is conceived to be a single vehicle with its propulsion, navigation, guidance and control (NGC) and power system from the battery. Each monohull results to be an ASV and, thanks to the azimuth thrusters, is highly controllable. Moreover the intelligent core of each vehicle controls the monohull but is able to take over the control of the entire vehicle in the event of failure of the other core. This possibility is guaranteed by the existence of a Wi-Fi-based communication architecture.

The software architecture of SWAMP is based on Commercial off-the shelf components. As

mentioned before one of the main hardware innovations introduced in SWAMP is the elimination of most of the possible wiring reducing the number of wires to just the power connections. The basic NGC package of each hull is composed by an IMU and a GPS. The communication is created by one communication module each hull that provides a communication framework for both its same hull and for the other hull's modules when its work is required.

Specific measuring devices are installed on-board the platform, such as a Micron Echologger Single-Beam Echo Sounder (SBES) for bathymetric sampling and a Velodyne LIDAR for 360° 3D ranging and reconstruction.

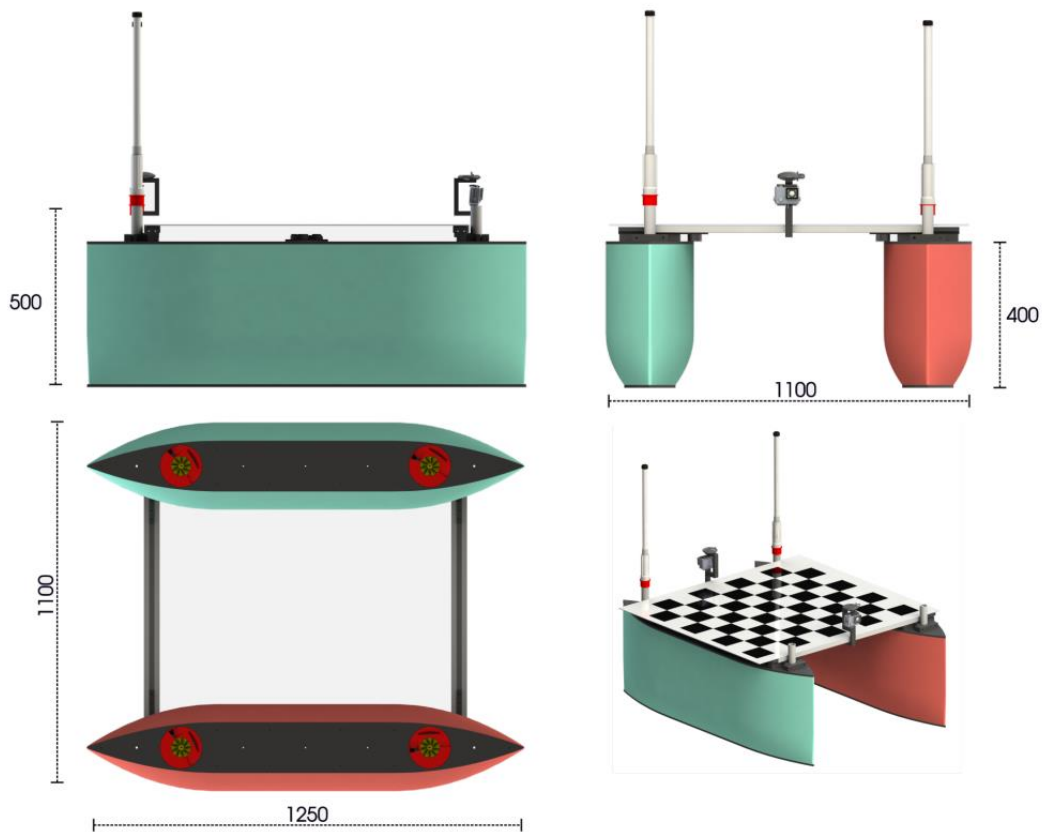


Fig.1: Vehicle general layout with measures

3. Control, Guidance and Planning of the Operations

The effectiveness of a marine robotic platform is strongly bond to its autonomy level, meaning from a mission execution perspective the capability of executing a predefined set of planned operation and providing at the same time an adaptation to unexpected occurrences, as well as to its performance related to the motion accuracy and efficiency in the operative scenario.

The SWAMP ASV operates thanks to a modular and scalable control architecture, allowing from direct piloting handling of the platform up to complete autonomous sequence of actions. Such feature allows the employment of the ASV in a wide span of diverse scenarios, with the chance of adapting the robot capabilities to the specific mission requirements.

3.1. Navigation, guidance and control

Basic autonomous capabilities are provided via the three following modules:

- **Navigation:** refers to the determination, at a given time, of the vehicle's location and velocity (known as the “state vector”) as well as its attitude. It is based on the aggregation and filtering of data generated by the diverse (also redundant) proprioceptive sensors installed on board the robot. By merging data relative to position (GPS for surface vessels or acoustic measurements for underwater vehicles), velocity (obtained by GPS or Doppler Velocity Loggers) and attitude (usually sensed by gyro-compasses), the navigation module provides the most accurate motion information and, if a dynamic-kinematic model is known, an expected forecast of near-future state of the vehicle can be generated.
- **Control:** this module is responsible of the generation of suitable actuation signals in such a way to ensure the execution of commanded motion actions (e.g. moving forward, steering, etc.). A proper mapping from the intended motion command and actuation configuration has to be ensured – this is quite simple for fixed-direction motors in traditional marine robots, but the SWAMP ASV, being characterized by the presence of azimuth motors requires an intelligent management of the thruster. In fact, a one-direction orientation of all the thrusters can be set for maximizing the speed during long-range transitions, while a tetrahedral configuration can be set for precise positioning and holding. The configuration change policy requires advanced techniques capable of adapting towards the specific operative requirements.
- **Guidance:** the module manages the determination of the desired path of travel (the “trajectory”) from the vehicle's current location to a designated target, as well as desired changes in velocity, rotation and acceleration for following that path. The SWAMP architecture actually provides a set of guidance systems implementing the basic point-to-point motion management, up to more complex geo-referenced path-tracking, allowing the execution of custom motion in complex environments.

3.2. Mission planning and monitoring

A complementary part needed to guarantee the full autonomy of a robotic platform is the mission planning and monitoring module. Such part of the architecture is responsible for the mission specification design, in terms of required actions to carry out and objectives to achieve (planning phase), and the supervision of the operations in order to overcome unexpected occurrences, unforeseen conditions or failures (execution phase).

The SWAMP control architectures allow planning the path tracking execution, e.g. parallel transect motion over the area of interest, selecting the operational modes required by the specific mission, giving the possibility to the human operator to interact with the overall system and to intervene in case of unplanned actions to be undertaken. This autonomous operating mode allows the human operator to focus on the specific mission objectives (e.g. the data acquisition), thus reducing the overall workload. Fig.2 reports an illustrative mission log, where the vehicle is commanded to navigate a predefined transect pattern; it can be noticed a manual intervention with the vehicle turning around a spot of interest.

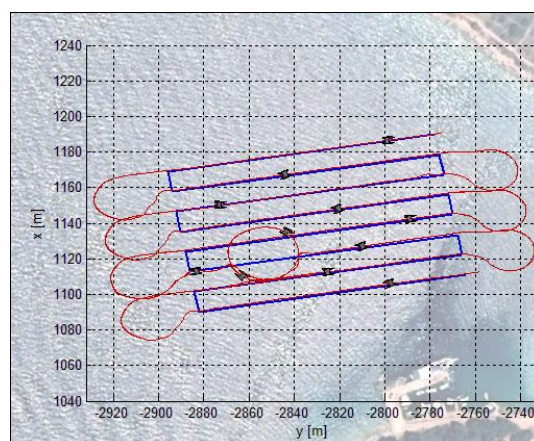


Fig.2: Example of autonomous sampling mission

4. Connected Devices and Remote Data Access

The continuous spread of connection availability and low-cost/reduced-size technological components have strongly contributed to the rise of the so called “Internet of Things” (IoT). The development of marine robotic platforms has surely taken advantage of such technological progress, allowing to render remote the access to autonomous agents made available for specific tasks.

Nowadays, the robotic platforms are intended as parts of integrated systems acting as accessible tools or services, capable of providing reliable information related to the scenario they are operating in. The operational capabilities of robots are now totally different with respect to ones of 10 years ago: once the mission objectives are set and the reliability is consolidated, the autonomous operations can be then triggered and monitored remotely using internet or mobile based software applications, allowing to instantly access the collected data making them available for post-processing or sharing. This revolutionary way of operating robots avoids the presence of local expert operators, with the only need of a maintenance operator in case some major failure arises.

The possibility of customizing the software applications allows to pre-set the allowed operations, providing specific services, also without a specific technical knowledge from the remote user. The centralization of the data lays at the base of the architecture design: the overall system is intended as a set of computing modules, each one providing specific functionalities (e.g. actuation, sensor reading, navigation/guidance task, safety procedures, etc.), publishing the data generated by the module itself and subscribing to information of interest provided by other modules. Thanks to this data-centric design of the control architecture, each module is completely independent from the others (both in the design and execution phases) and shares only the published/subscribed data, avoiding direct communication links, execution time synchronization, knowledge of other modules’ functionalities.

The data sharing infrastructure is based on the MQTT protocol, <https://mqtt.org/>: “MQTT is a Client Server publish/subscribe messaging transport protocol. It is light-weight, open, simple, and designed so as to be easy to implement. These characteristics make it ideal for use in many situations, including constrained environments such as for communication in Machine to Machine (M2M) and Internet of Things (IoT) contexts where a small code footprint is required and/or network bandwidth is at a premium.” In simple terms, MQTT provides a server (called ‘Broker’ in MQTT terminology) which manages the published data and the connection of different clients (intended as any module or agent that wants to publish or subscribe to one or more data). MQTT does not impose any data format, so that developers can design their custom data profile, and provide development libraries in different programming languages, so that each module can be developed independently.

MQTT is a win-win choice for the architecture development because: i) on the robot development side, it accelerates the prototyping of diverse module and their subsequent integration; ii) on the user side, it allows a direct access to all the data, giving the chance to develop specific application for piloting, monitoring data, perform real-time processing, store and aggregate information.

As a final remark, given the accessibility of data and reliability of remote connections, the choice of such a framework easily provides a “world-wide” access to the robotic platform thus improving the exploitation index of the robotic tool.

5. Experimental Validation

Thanks to its characteristics, the SWAMP ASV can be effectively exploited for observation, monitoring and sampling activities in harsh environments and remote sites.

A remarkable result has been obtained during a river sampling campaign, carried out in November 2019 in Liguria (Italy), with the goal of a precise and high-resolution bathymetric mapping of specific areas of interest of the Roja River.

The operational survey, commissioned by GTER s.r.l. Company, took place in the area of West Liguria Region (North Italy) not far from the Italy-France border, where the Roja river flows. Its source is located in the Ligurian Alps, from where it runs southward flowing into the Ligurian sea in the area of Ventimiglia city. The work was commissioned by the Regional Authorities to provide an assessment of the river state, as well as an estimation of the river capacity in case of heavy rains to prevent floodings. The Ligurian region is a hotspot for flash flooding, a consequence of the regional morphology, climate change and anthropization of the area.

Two areas of interest were the objective of the survey: the mouth of the river in and a northern area. The first part of the bathymetric data acquisition campaign focused on the mouth of the Roja river in Ventimiglia, Fig.3 (left), the figure shows the area under investigation. This area is characterized by shallow, calm, waters (from a few tens of centimeters to 4 m depth), with no particular evidence of currents that could hinder the data acquisition. Fig.3 (right) reports the river-bottom range data collected in the Airole area (a Northern suburban area) that is characterized by currents, small rapids and surfacing rocks that make the survey challenging also for personnel.



Fig.3: Range measurements gathered along the Roja river (Liguria, Italy)



Fig.4: Hand transportation of the SWAMP ASV on the path to the Roja river (Liguria, Italy)

The area is only accessible by a small walking path crossing the forest, thus the employment of boats is denied. The small size, reduced weight and modular structure of the ASV allowed an easy transportation and deployment from the riverbank, Fig.4. Once in the water, the ASV was able to navigate in turbulent waters, as well as capable of moving close to the riverbanks and rocks, collecting a dense measurement set. The survey operation in the Airole area took about 2 h.

In 2021 an extensive bathymetric campaign has been carried out on the Gorzente Lakes, again in Liguria region. The lakes complex is a local resource for both potable water and energy production, thus highlighting the importance of periodic surveys for water quality measurements and infrastructure monitoring.

The sampling has been carried out over an area enclosed between two shores of one lake of about 200 x 100 square meters. The adverse meteorological conditions (strong winds with gusts) required the survey to be executed in a semi-automatic way, relying on the auto-speed and auto-heading controls, in order to counteract the drift caused by the wind.

The obtained result is a detailed depth gradient map, Fig.5; the bathymetric profile ranges from the shore level down to about 15 m. The trajectory of the ASV is superimposed to the bathymetric map (red line) and it is possible to notice that, thanks to the navigation capability of the platform in extreme shallow water, the vehicle can perform the sampling also at the very edge of the shoreline.

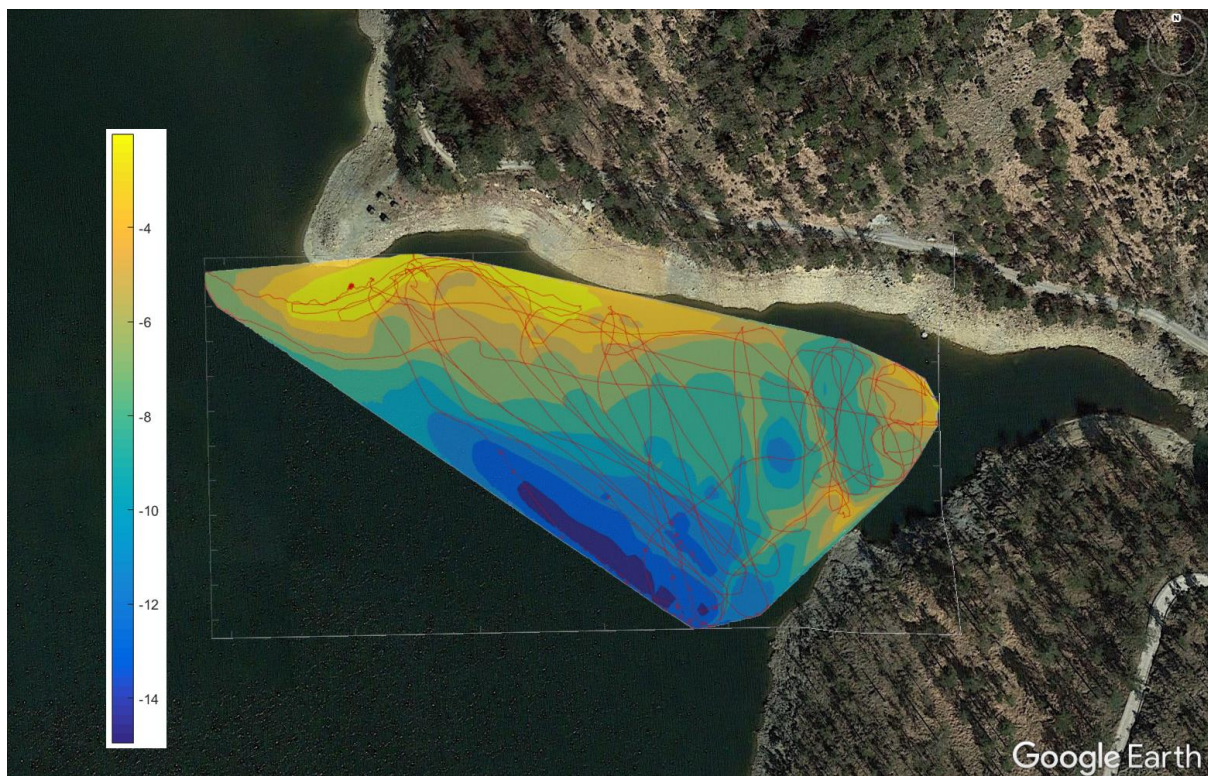


Fig.5: Bathymetric sampling on the Gorzente Lakes (Liguria, Italy)

The operation was completed in about 2 hours and half, collecting around 92.000 measurements; as quick post-processing phase is than needed to verify/filter the data and to compute the interpolation to obtain the bathymetric map. A 3D representation of the depth profile is reported in Fig.6.

An ongoing project in collaboration with the University of Genova (Italy) is focused on the integration of additional photogrammetric information gathered by means of an aerial drone, with the aim of creating a full-coverage 3D reconstruction of the area of interest, with data gathered from the aerial level for dry land mapping and bathymetric samples acquired from the sea-surface layer. A result of this combined modelling is reported in Fig.7 (left), where photogrammetric data of the shoreline is

combined with the bathymetric profile; the 3D model can be used to evaluate the capacity of the reservoir in order to predict the variation with respect to meteorological events such as heavy rains, Fig.7 (right).

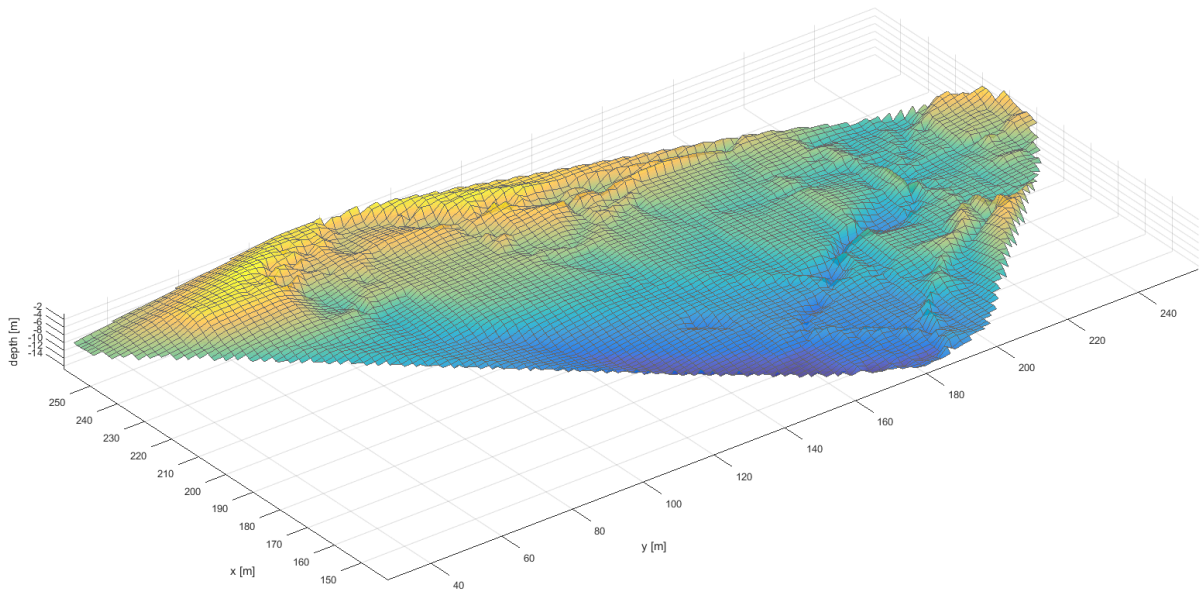


Fig.6: Depth profile in the sampled area of the Gorzente Lakes (Liguria, Italy)

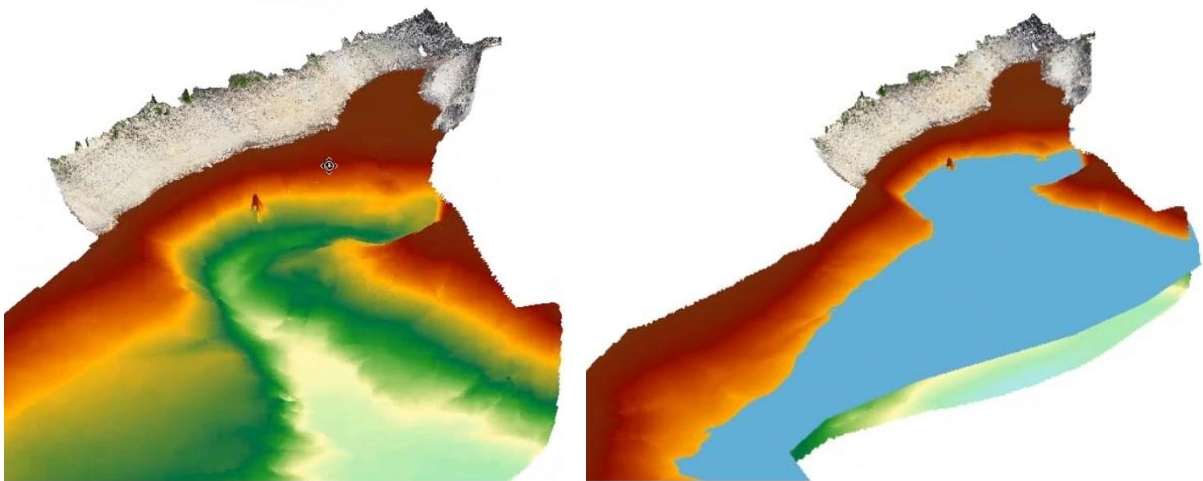


Fig.7: Combined photogrammetric and bathymetric 3D reconstruction (left) of the sampled area of the Gorzente Lakes (Liguria, Italy) and water capacity simulation (right)

Another bathymetric sampling has been carried out in the coastal area of Biograd na Moru (Croatia); in this occasion a more methodological sampling, relying on fully automated procedures provided by the robotic vehicle, was carried out. Fig.8 depicts the motion of the ASV along predefined parallel transects. The coloured bathymetric map is then obtained, modelling the sea-bottom slope, which ranges from about 2 m to 4 m. The methodology proved that the bathymetric campaign can be carried out in an autonomous way making the data real-time available for final users.

Moreover, during the same campaign, a set of complementary data has been gathered by means of the installation of a LIDAR sensor on-board the ASV; a scanning data gathering is reported in Fig.9, showing the coastal line close to the bathymetric sampling area.

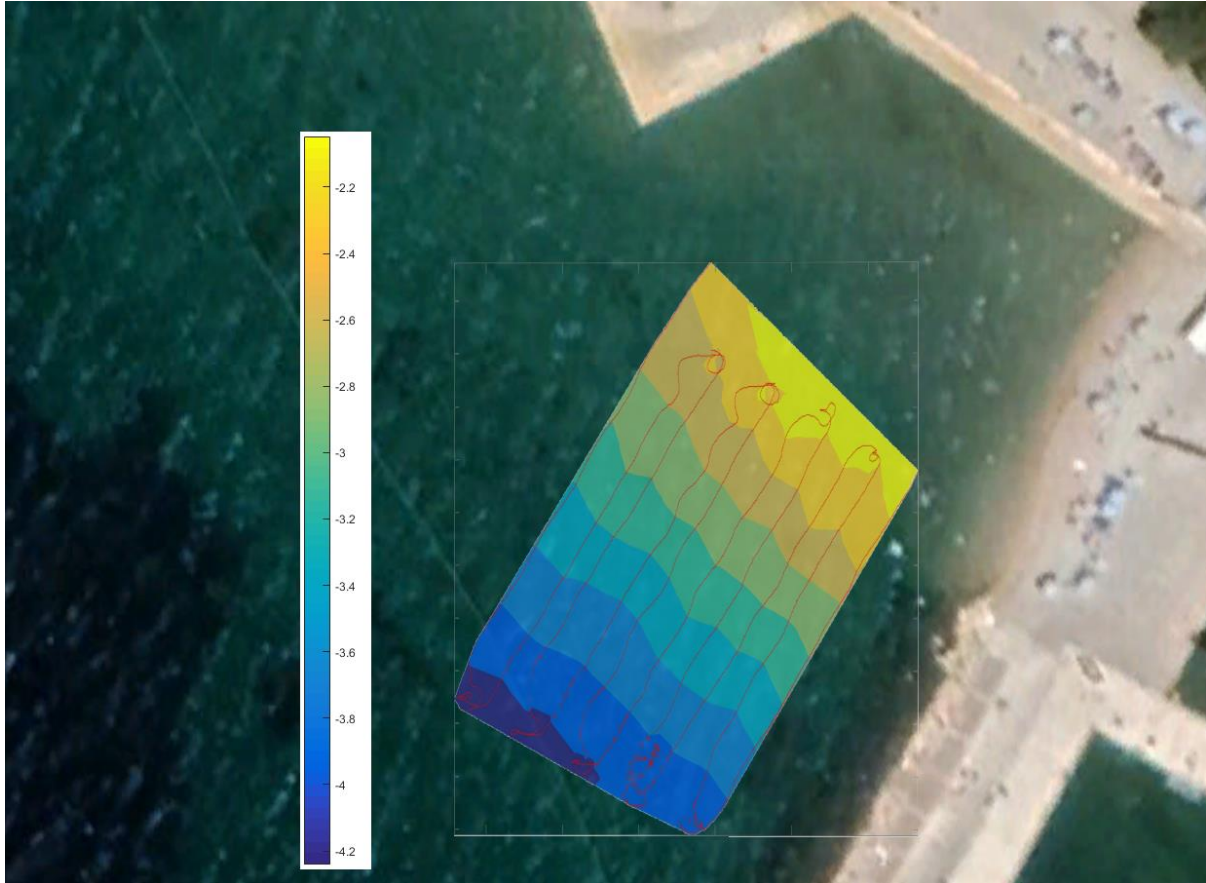


Fig.8: Bathymetric sampling in Biograd na Moru (Croatia)

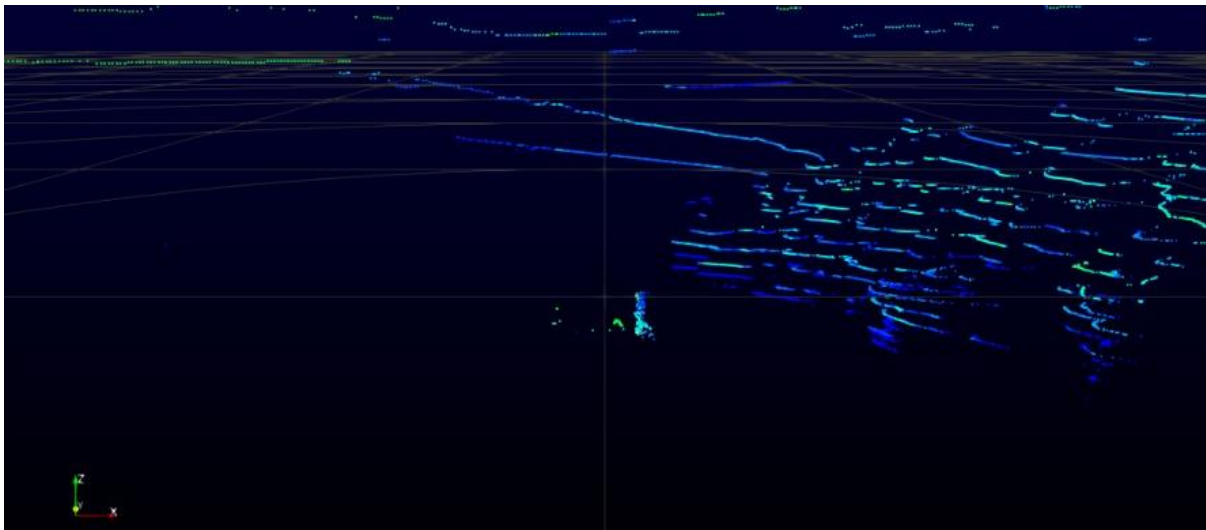


Fig.9: Coastal lines profile captured by the LIDAR sensor (Biograd na Moru, Croatia)

6. Conclusions

The work demonstrates the feasibility and reliability of remote robotic tools and services that currently, thanks to technological advancement and communication infrastructures, can be effectively employed for extensive environmental assessment also in harsh operative scenarios.

The result obtained so far is already a starting point for future developments, aiming in particular at the implementation of cooperative multi-layer systems where different robotic platforms (aerial,

surface and waterborne) can be employed to gather a comprehensive knowledge out the scenario of interest.

As stated in the previous section, a constant development effort will be devoted for the improvement of the combined photogrammetry/bathymetry reconstruction, enhancing the water layer with the employment of a Multi-Beam Echo Sounder (MBES) device.

On the surface layer, the integration of LIDAR information will enhance the quality of the 3D scenario modelling, bridging the gap between aerial measurements and in-water sounding.

A further objective is also to develop proper end-user mobile interfaces in order to simplify the interaction with the robotic tools and services and to provide easy-to-use information.

Acknowledgments

This work is supported by the EU EMFF “Blue-RoSES” Project (g.a.: 863619) and the EU INTERREG “Innovamare” Project.

References

- BEHMEL, S.; DAMOUR, M.; LUDWIG, R.; RODRIGUEZ, M.J. (2016), *Water quality monitoring strategies — A review and future perspectives*, Science of The Total Environment 571, pp.1312-1329, <https://doi.org/10.1016/j.scitotenv.2016.06.235>
- BIBULI, M.; BRUZZONE, G.; CACCIA, M.; CERVELLERA, C.; FERRETTI, R.; GAGGERO, M.; ODETTI, A.; ZEREIK, E.; VIVIANI, M.; ALTOSOLE, M. (2020), *Evolution of Autonomous Surface Vehicles*, 19th COMPIT Conf., Pontignano
- BIBULI, M.; FERRETTI, R.; ODETTI, A.; COSSO, T. (2021), *River Survey Evolution by means of Autonomous Surface Vehicles*, 2021 Int. Workshop on Metrology for the Sea; Learning to Measure Sea Health Parameters (MetroSea), pp.412-417
- CACCIA, M.; FERRETTI, R.; ODETTI, A.; BRUZZONE, G.; SPAGNUOLO, M.; MORTARA, M.; BERRETTA, S.; CABIDDU, D.; PITTALUGA, S.; ZUCCOLINI, M.V.; BRIGNONE, L. (2019), *Robotics and adaptive sampling techniques for harbor waters monitoring: the MATRAC-ACP project*, OCEANS 2019, Marseille
- KUROWSKI, M.; THAL, J.; DAMERIUS, R.; KORTE, H.; JEINSCH, T. (2019), *Automated survey in very shallow water using an unmanned surface vehicle*, IFAC-PapersOnLine 52.21, pp.146-151, <https://www.sciencedirect.com/science/article/pii/S2405896319321834>
- MARIANI, P.; BACHMAYER, R.; KOSTA, S.; PIETROSEMOLI, E.; ARDELAN, M.V.; CONNELLY, D.P.; DELORY, E.; PEARLMAN, J.S.; PETIHAKIS, G.; THOMPSON, F.; CRISE, A. (2021), *Collaborative automation and IoT technologies for coastal ocean observing systems*, Frontiers in Marine Science, <https://www.frontiersin.org/articles/10.3389/fmars.2021.647368/full>
- MSFD (2008), *Directive 2008/56/EC of the European Parliament and of the Council of 17 June 2008 establishing a framework for community action in the field of marine environmental policy*, Marine Strategy Framework Directive
- MOLINA-MOLINA, J.C.; SALHAOUI, M.; GUERRERO-GONZALEZ, A.; ARIQUA, M. (2021), *Autonomous Marine Robot Based on AI Recognition for Permanent Surveillance in Marine Protected Areas*, Sensors 2021, <https://doi.org/10.3390/s21082664>

ODETTI, A.; BRUZZONE, G.; BIBULI, M.; FERRETTI, R.; ZEREIK, E.; CACCIA, M. (2020), *An innovative ASV for the monitoring of anthropogenic pressure on Wetlands*, EGU General Assembly 2020

WFD (2000), *Directive 2000/60/EC of the European Parliament and of the Council of 23 October 2000 Establishing a Framework for Community Action in the Field of Water Policy*, OJ L 327, European Union

Smart Technologies for Improving Design Tools

Rodrigo Perez Fernandez, Siemens Digital Industries Software, Madrid/Spain

rodrigo.fernandez@siemens.es

Abstract

Smart technologies have arisen on the context of the fourth industrial revolution. Applying these to ship design becomes a matter of analysing carefully, finding the best technologies for each specific process in order to provide value to the end-to-end process. Even so, there is an underlying difficulty to find areas of application in the Marine Industry, as a result of stationary design and production processes achieved by this industry. In this paper, different approaches for applying disruptive technologies will be evaluated, aiming to highlight the advantages that these provide on different phases of the life cycle of the ship.

1. State of the art

Nowadays, smart technologies are widely common topics. The question is do we really understand everything implied in the term? In reality, these are formed by a fusion of multiple technologies that sharing the same ambition: digital transformation. Nevertheless, the peculiarities and differences found in them require a subtle and delicate analysis in order to establish how they can be applied to each specific industry.

Technologies considered as crucial in this industrial revolution are currently being secured. In particular, the Marine Industry is being forced to enter in this atmosphere of change, following a slow and uncertain adjustment process absolutely needed for their survival. The key at this point is choosing the right strategy and the best way to measure your success on it.

An additional difficulty at this very moment for companies is to keep their strategies intact in spite of the great uncertainty that COVID-19 has brought to our lives. Although methodology may change, strategies must be consistent and straightforward in order to succeed. To evaluate our strategies for the digital transformation, we need to evaluate the correct *Key Performance Indicators*, particular to each process or business. Among the most valuable *Key Performance Indicators*, profit making, and good practices are key.

According to *McKinsey (2018)*, less than 30% of the companies embarked on this innovative process succeed. Focusing on expectations, there is a 45% chance to obtain less profit than expected, *McKinsey (2019)*. Therefore, in the sense of digital transformation on a company, how we implant the technologies is as important as the technologies itself.

According to the same report, using agile processes and constituting clear priorities are two of the main factors to really influence a digital transformation. Using *Minimum Viable Products* with these practices can help companies achieve real success, by providing real results in short time. Selecting the right *Minimum Viable Products* is decisive to achieve clarity in this fog of digital transformation. As the profits of the marine industry are usually not high, investments and risks are not taken lightly. Therefore, in this new technological hype, a deep understanding of the technologies and how to apply them is indispensable in this particular sector, in order to avoid mistakes and money waste.

According to *Lloyd's Register (2015)*, QinetiQ and Southampton University, technologies such as Artificial Intelligence, Machine Learning and Data Analytics are highlighted for the short term in the Marine Industry.

To address the foundations for the implementation of smart technologies in the ship design industry, the following section explains the state of the art of some of these technologies.

Fig.1 shows the general understanding of different technologies and the relation among them:

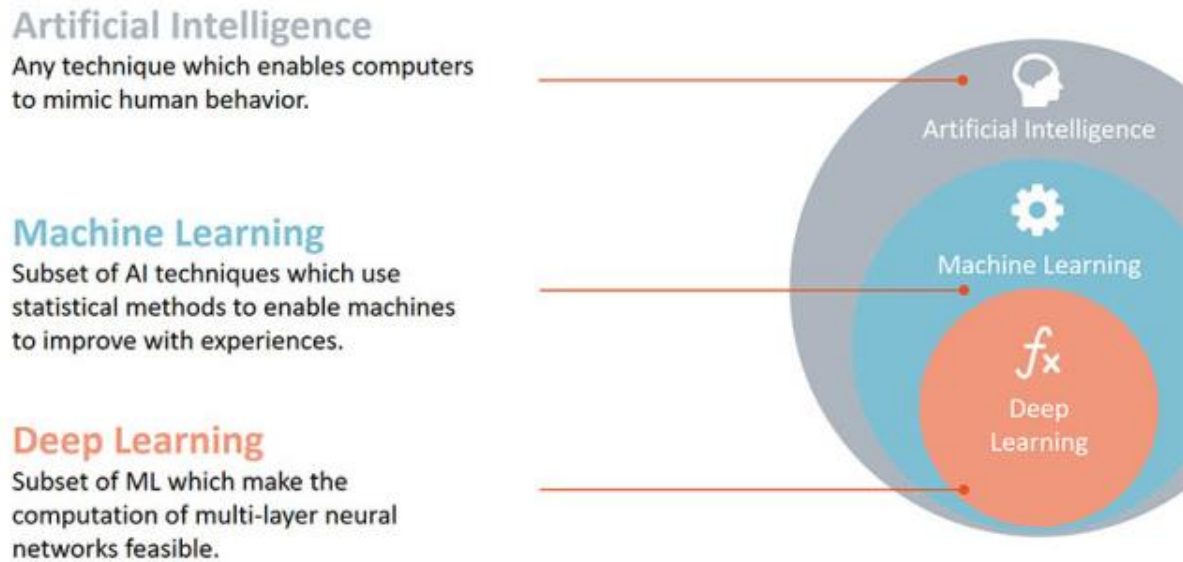


Fig.1: Artificial Intelligence Techniques, *Mierswa (2017)*

Despite being born as the idea of creating machines capable of simulate human behaviour, Artificial Intelligence has evolved to comprise multiple mathematic techniques used in computing and essential to create this “intelligent” machines, sharing a great number of concepts with data science, *Muñoz and Pérez (2019)*.

Data Analytics, also called Data Mining, is the discipline dedicated to analysing data to establish relations and provide conclusions. The extraction and preparation of data are included in this field of study.

Machine Learning allows the extraction of patterns from a data set. There are different types of analysis on this field, such as data clustering, support vector machines, association rule learning, Bayes algorithms, and all other algorithms included in Deep Learning.

Fig.2 explains in detail the different components of Machine Learning:

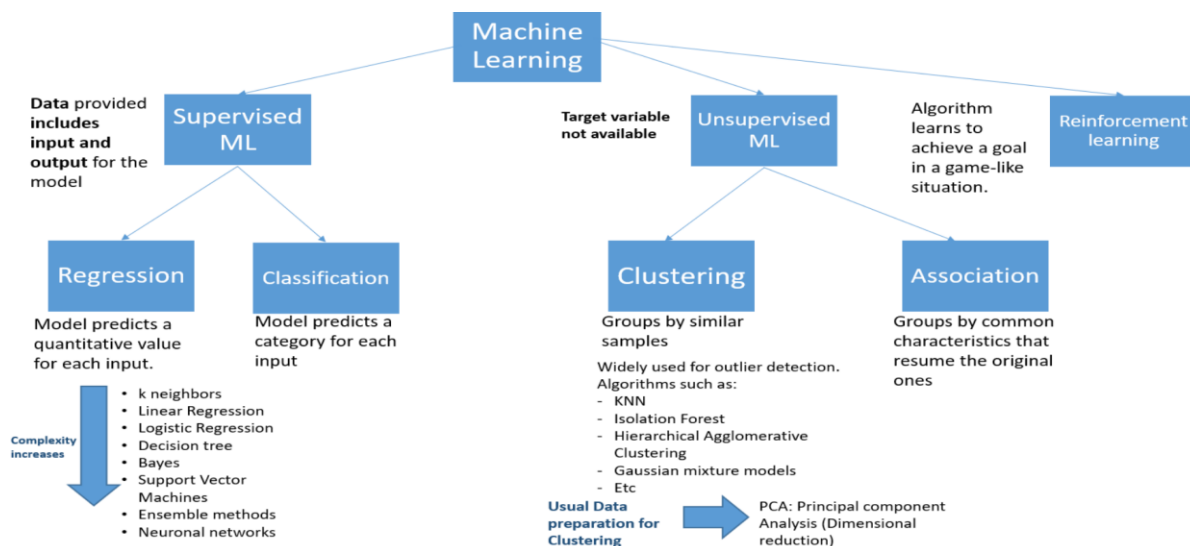


Fig.2: Machine Learning Components, *Ramirez (2020)*

In simple words, Machine Learning is the evolvement of ruled based systems, being able to distinguish among spare and valid data, as well as inferring new rules not formerly programmed. An interesting fact is that over the last five years, Machine Learning studies have focused on Data Learning, high complexity algorithms that simulate human thinking. Therefore, this last sector of Artificial Intelligence is still a matter of study and debate.

2. Concepts to be considered

Machine Learning techniques can be used to determine the quality of CAD/CAM/CAE design. The question is what technique is the best for each purpose? To provide a better understanding on the topic, the following paragraphs explain with more detail the differences among Machine Learning categories.

Machine Learning concept is divided into three categories: Supervised Learning, Unsupervised Learning and Reinforcement Learning.

Supervised Learning is a technique that, knowing the characteristic of the input data, provides an algorithm capable of establishing relations and identifying similar data. I.e. this system relates input and output parameters.

Most problems considered in this category are classification or regression issues. Therefore, this type of Machine Learning is the most used now. For example, a Supervised Learning algorithm can be trained to distinguish pictures of animals. If it is trained to recognize elephants, when showing a picture, the system will be able to tell if the animal contained is an elephant or not by obtaining characteristic elements from the data. Of course, the more data provided, the better the training. To train this algorithm we just must provide a range of data and supervise the learning. In other words, the process would be like teaching a child to distinguish between photographs of dogs and cats.

In this specific area, the term training compounds the process to provide labelled data to the algorithm, making adjustments on it depending on the predictions it is providing, Fig.3.

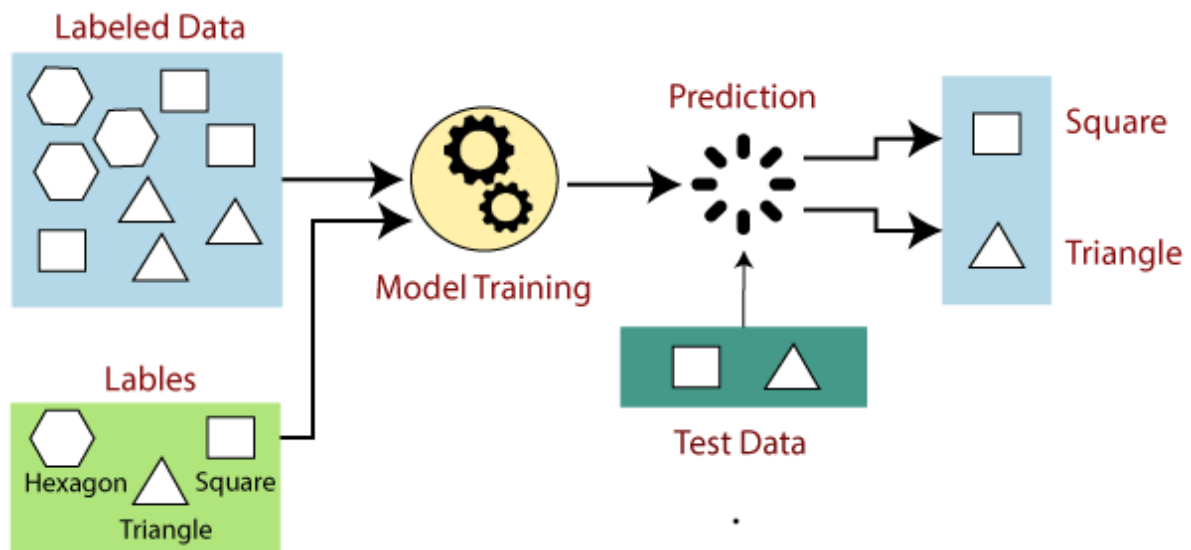


Fig. 3: Diagram of Supervised Learning Machine Learning, *Kranthi (2020)*

On the other hand, *Unsupervised Learning* does not have information about the categories or characteristics of the data but uses the algorithm to extract common features and group the input data in different groups or clusters. An example of this would be an algorithm capable of groping different animals in groups based on the common features it can find in them, Fig.4.

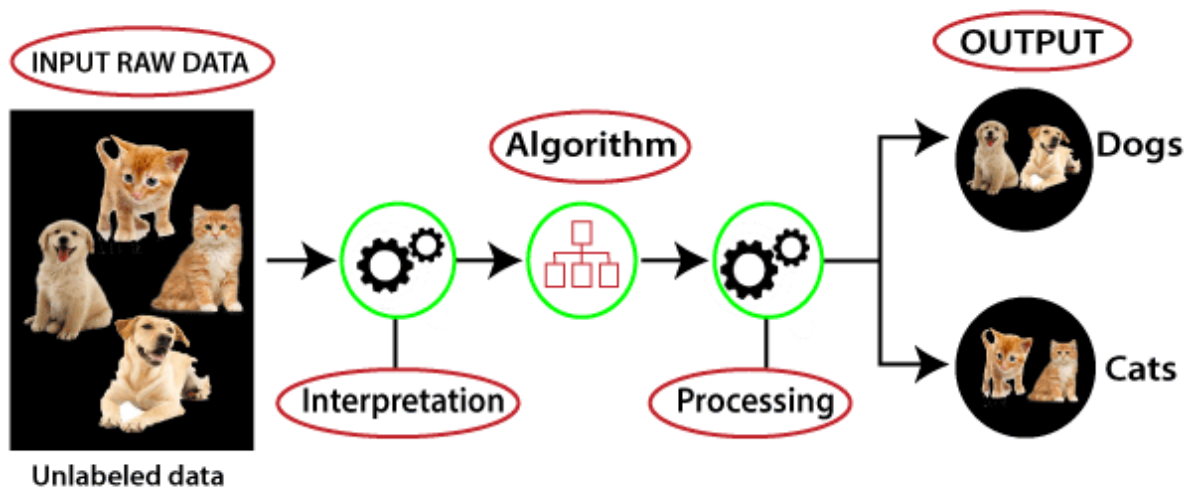


Fig.4: Diagram of Unsupervised Learning Machine Learning, *Kranthi (2020)*

Finally, Reinforcement Learning is characterised by the fact that the algorithm is updated through a continuous trial-error and reward-reward analysis, seeking the optimization of the latter concept to find the optimal combination for certain external conditions, Fig.5.

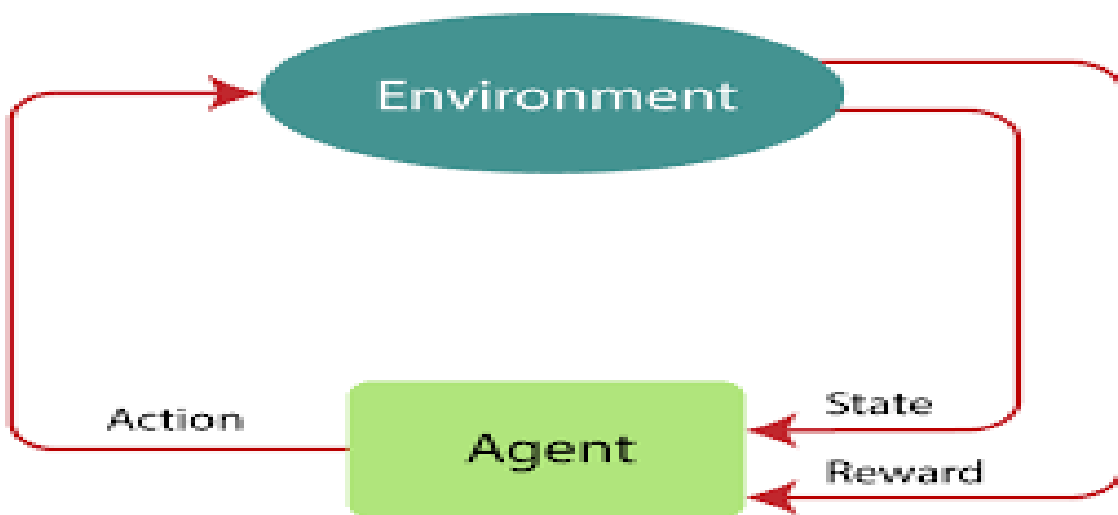


Fig.5: Diagram of Reinforcement Learning Machine Learning, *Kranthi (2020)*

3. How to apply Machine Learning to ship design

The application of this technologies to ship design requires the identification of use cases in which added value is provided to the design process. Having this in mind, these can be used for multiple activities: standardization of objects or designs, automation of repeating tasks, standardization of design, identification of anomalies, design validation, etc.

The key element for all this is data. Although can we used any type of data? The answer is no. This data must be accessible, in great amounts and organized, otherwise the results will get with these technologies will not be valid.

Particularly, for the marine industry, we have found that generic data will not be of much use for the design of particular shipyards or technical offices want to do. On the other hand, shipyards and technical

offices do not usually share specific data of a design, since it is what gives them value and allows them to differentiate themselves from each other. This leads us to conclude that to use Artificial Intelligence technologies, the shipyard, office or naval designer, will need to create their own algorithms based on their own data.

Having all these factors in mind, in Siemens we have developed a tool called FORAN Insights, which takes advantage of having FORAN's powerful relational and accessible database and is capable of analysing the data and extracting anomalies among it. The results of such powerful tool can be used in different stages of the life cycle of the ship, assuring fewer errors, timesaving, and a wider standardization.

In order to develop this Minimum Viable Products, Siemens has found key having experts both in data science and ship design, in order to find benefit to processes and select the best Machine Learning techniques for each problem.

We must keep in mind that *Machine Learning* is a complex science, often mistakenly applied to any process. The reality, however, is that many processes acclaimed under this term are merely classical frequency studies or simple optimization problems, where there is no technology other than classic arithmetic. Due to this fact, to obtain algorithms that provide valid results, it is key to have a professional data analyst or technical profiles that can distinguish between different technologies and the best way to apply them.

4. Connectivity of design and construction systems

Along the production process, the communication between the shipyard and the design office is constant and both must have updated information about the product and its building phase. At this stage, very interesting and increasingly achievable new technologies appear. Each of the assembly plans must be consultable from the workshop. The assemblies will have indelibly printed Quick Response (QR) codes that uniquely identify each of the elements but can also incorporate identification or access to the assembly drawings. Even more, video sequences could be made to show how this assembly should be built, and mobile devices shall read the QR code, and they will access to the building video. CAD/CAM/CAE systems that have virtual reality solutions can perform these assembly sequences, record them, and store them as part of the assembly information as it was done with the drawings. Workers may consult simultaneously or alternatively this set of information. This information circulates in the own network of the shipyard that is a network of its own. However, it is necessary to ensure that the information has the appropriate level of confidentiality. For this, it will be necessary to provide security certificates to devices so that only those who have the appropriate level of security can access the corresponding information. This is of the most importance in military building, but it is also interesting to preserve the shipyard's own knowledge in its area of its privacy.

The different parts to be mounted, not only can incorporate their QR codes with the information described above, but also can incorporate RFID or other location devices. These well-placed and secured devices will allow them to be located in the assembly line, which will allow the controllers to know their finishing condition and therefore the progress of the construction. Obviously, these devices must have characteristics different from the simple RFID tags of the products existing in the stores. They must be sufficient robust and have enough scope so that they can be detected in the workshop area of the assembly line. This information serves not only to know the progress of the construction but also to support the management of materials and the necessary purchases

5. Conclusion and next steps

Digital transformation requires adequate strategies to identify the added value obtained and compare it to the investments made. Moreover, in the current uncertainty we are living, particularly focusing on the shipbuilding business, a strategy that shows good results is to start with small projects that have sufficient viability to be evaluated without large investments (Minimum Viable Products). It has been

widely proved that this approach can provide good results, even exceeding expectations, without compromising too much on risks or investment. The key for success is to clearly define objectives and the profits we wish to obtain, as well as identifying the correct technologies to apply.

In the field of ship design, as we have shown before in this article, it is possible to use Machine Learning to identify anomalies on different parts of the lifecycle of the project. Thanks to FORAN Insights, an Minimum Viable Products developed by Siemens, shipyards and technical offices could benefit enormously by reducing design errors by detecting outlier parts on design phases. It also makes it possible to optimize the resources used, by ensuring the highest possible standardization of parts, standardizing materials and manufacturing, which results in the reduction of design and construction costs.

As next steps, this Minimum Viable Products may be further developed, improving the parameters that allow users to identify and delimit the standard groups of parts. Also, this must be further integrated with the FORAN, allowing automatic and real-time detection to warn users of these possible anomalies.

Furthermore, the incorporation of visual tools for the presentation of results facilitates the work of engineers for decision making. These tools are complemented by dashboards that must be adapted and personalized depending on the users or the shipyard needs.

Future smart ships and yards must be connected, or they will not be smart. The connection of smart devices within a smart ship or yard must be human controlled. The control should start from the design tools (CAD/CAM/CAE) because they control the shipbuilding process from the early stages of the design up to the final production. The set of design tools, product lifecycle management and device must be interconnected among them and will be the platform for the smart ships and yards connected. The information shared must be managed by the human along the whole lifecycle of the ship and the yard (workshops, docks, berths...), starting from the beginning of the initial design. This need requires the CAD/CAM/CAE tools to be prepared with specific characteristics to handle that information. This new ecosystem, opened, incorporating the new trend of technology but adapted to the specific environment of shipbuilding will be the future of shipbuilding.

References

- KRANTHI, K. (2020). *Types of Machine Learning*. <https://www.quora.com/q/mlforeveryone/TYPES-OF-MACHINE-LEARNING>
- LLOYD'S REGISTER (2015), *Global Marine Technology Trends 2030*, Lloyd's Register, QinetiQ and University of Southampton.
- McKINSEY (2018), *Unlocking success in digital transformations*, McKinsey & Company
- McKINSEY (2019), *Digital Transformation: Improving the odds of success*, McKinsey & Company
- MIERSWA, I. (2017). *What is Artificial Intelligence, Machine Learning and Deep Learning?*. <https://ingomierswa.com/2017/04/19/what-is-artificial-intelligence-machine-learning-and-deep-learning/>
- MUÑOZ, J.A.; PÉREZ, R. (2019), *La integración de la Inteligencia Artificial en los procesos y metodologías de diseño naval*, Ingeniería Naval 978, pp.74-84
- RAMIREZ, A.; PÉREZ, R. ; MUÑOZ, J.A. (2020). *Application of Smart Technologies to ship design*. Smart Ship Technology, London

Application of Augmented Reality Technology to Manufacturing in Shipbuilding

Kohei Matsuo, National Maritime Research Institute, Tokyo/Japan, kohei@m.mpat.go.jp
Shuhei Fujimoto, National Maritime Research Institute, Tokyo/Japan, fujimoto@m.mpat.go.jp
Masahito Takezawa, National Maritime Research Institute, Tokyo/Japan, takezawa-m@m.mpat.go.jp

Abstract

This paper concerns the application of Augmented Reality (AR) technology to manufacturing in shipbuilding. First, functions derived from AR technology are comprehensively organized especially for manufacturing in shipbuilding. And, three concrete AR applications that support sheet metal forming work, welding work, and piping installation work are developed to evaluate the functions. After describing the three AR applications developments, the demonstration experiments at a shipyard or a laboratory are explained. Verification of effects on productivity improvement by AR and extraction of technical issues are done for the application of AR technology to manufacturing in shipbuilding through the development of AR applications and the demonstration experiments.

1. Introduction

Augmented Reality (AR) is a promising technology to close a gap between the real and digital worlds by superimposing digital information on the image of real objects or environments. It could improve individual abilities to obtain information, make decisions, and execute required tasks and will transform how companies serve customers, train employees, design and create products, and manage their value chains including shipbuilding.

Shipbuilding industry has a difficulty of its information management, as it is characterized as a small batch production, hand working dependent, and generally ship production starts before a ship is not fully designated and planned. Therefore, AR technology is expected to improve the information management in shipbuilding. The authors carried out fundamental research to verify possibilities and technical issues to apply AR technology to manufacturing in shipbuilding.

To summarise the position of this paper, it starts from literature survey related to the application of AR technology to shipbuilding. Fraga-Lamas et al. considered the basic architecture and hardware used of AR system after comprehensively summarizing the use cases of AR technology to shipbuilding, *Fraga-Lamas et al. (2018)*, *Blanco-Novoa et al. (2018)*, *Fernández-Caramés et al. (2018)*. There are also studies on concrete AR application developments assuming a specific shipbuilding process. For example, AR application that supports pipe layout at shop floor, *Olbrich et al. (2011)*, AR application superimposing a 3D CAD model on actual hull blocks in hull assembly, *Kim et al. (2018)*, and a 3D design drawing visualization system where a 3D model is superimposed on a 2D paper drawing, *Oh et al. (2014)*, *Oh et al. (2015)* can be seen. These R&D focus on proposal of system architecture of AR applications and these prototype developments. On the other hand, there are not many evaluations or considerations on how these AR applications work in actual shipbuilding. This paper considers the technical issues concerning the deployment of AR technology to shipbuilding through the demonstration experiments.

2. Issues in shipbuilding manufacturing and applicable functions of AR technology

Shipbuilding industry has difficulties in its information management. Issues of information management at manufacturing in shipbuilding are summarized as follows:

- Information on manufacturing products is scarce. Detailed work instructions are not usually outputted when manufacturing individual blocks or outfittings. For this reason, workers have to decide work procedure by their own judgment, and their work is not necessarily performed

in an optimum way. There are also variations in the quality of worker.

- Information gathering and information sharing during manufacturing are insufficient. Also, there is no infrastructure to communicate in a manufacturing site. For this reason, situations of workers, products and facilities (cranes, dolly, etc.) are not recorded or shared. As a result, the production management (schedule management, cost management) is inadequate.
- Methods for effectively communicating complicated information are inadequate. Workers themselves need to understand complicated information from paper drawings, which leads to time loss and reading mistakes.

With AR technology, there is a possibility that above issues on information management may be improved, which lead to improving productivity in shipbuilding. Following improvements are expected by enhancing information management:

- Individual work support: To raise the work efficiency of worker.
- Production management: To conduct accurate schedule management, cost management, and asset management.
- Quality management: To accurately control the product quality while manufacturing and to eliminate reworking caused by quality problems.

Functions of AR technology for shipbuilding are summarized to improve above issues of information management in shipbuilding. The primary function of AR technology is to superimpose a virtual image on a real object on the same display of a portable device. In addition, introduction of such devices to a shop floor makes it possible to record work or to communicate remotely. Therefore, general functions of AR are categorized as follows, *Porter and Heppelmann (2017)*:

- Provide digital information;
- Record and capture information on real space;
- Exchange information and communicate.

These general functions permit following concrete functions of AR to manufacturing in shipbuilding:

- Provide digital information - It is a primary function of AR and supports workers' perception by superimposing digital information on real space. In addition, it is possible to provide information with rich expression such as animations, or provide on-demand information that displays information by appropriately switching it according to situations. It is also possible to send necessary information timely to workers.
- Record and capture information on real space - The information acquisition is available by adding sensors such as camera or IC recorder to AR devices. By carrying an AR device in a shop floor, it is possible to record workers' behavior by image or voice.
- Exchange information and communicate - AR devices are generally available to communicate through Wi-Fi network. Each worker carries an AR device, an information network is established in the shipyard. This enables horizontal information sharing at shipyards in real time.

Specific functions for manufacturing in shipbuilding are listed in Table I corresponding to each general function of AR technology.

Fig.1 summarizes how AR technology contributes to productivity improvement in shipbuilding from the viewpoint of information management and functions derived from AR.

Table I: Specialized functions for shipbuilding manufacturing by general functions of AR technology

General functions of AR technology		Specialized functions for shipbuilding by AR technology
Provide digital information	✓ Superimpose digital information on real space	✓ Superimpose step-by-step work instructions
	✓ Deliver push-based information	✓ Superimpose images of inside or back of bulkheads or partitions
	✓ Enhance information expression by rich visualization	✓ Superimpose images of products after completion
Record and capture information on real space	✓ Acquire information quantitatively, automatically, and comprehensively	✓ Push information (properties, status etc.) on materials or products
	✓ Acquire various kinds of data (image, sound, position, environmental data, etc.)	✓ Push information (properties, operating status, quantity of supplies, error message, etc.) on factory equipment
		✓ Push information or alert (no-entry zone, amount of dust etc.) on safety and surrounding environment
Exchange information and communicate	✓ Construct information communication network	✓ Push information or alert (body temperature, heart rate, dehydration, fatigue, etc.) on health condition of workers
	✓ Enhance communication by rich expression	✓ Push information on production management (schedule, delay etc.)
	✓ Communicate without physical and spatial constraints	✓ Push information on destinations and storage locations
Interact with machine	✓ Interact with machine	✓ Display work instructions or manuals on demand of workers
		✓ Substitute AR for markings on plates
		✓ Record a series of work by workers
Record and capture information on real space	✓ Acquire information quantitatively, automatically, and comprehensively	✓ Record surrounding environment or the state of space
	✓ Acquire various kinds of data (image, sound, position, environmental data, etc.)	✓ Record states of products under or after work (assembling, welding, painting etc.)
		✓ Recognize products by computer vision and check the shape or the mounting condition
Exchange information and communicate	✓ Construct information communication network	✓ Communicate real-time and interactively from shop floor
	✓ Enhance communication by rich expression	✓ Report/Register work status and work results in real time
	✓ Communicate without physical and spatial constraints	✓ Add annotation directly to products
Interact with machine	✓ Interact with machine	✓ Receive work assistance from veterans outside shipyards
		✓ Make an on-demand interface of shipbuilding facilities

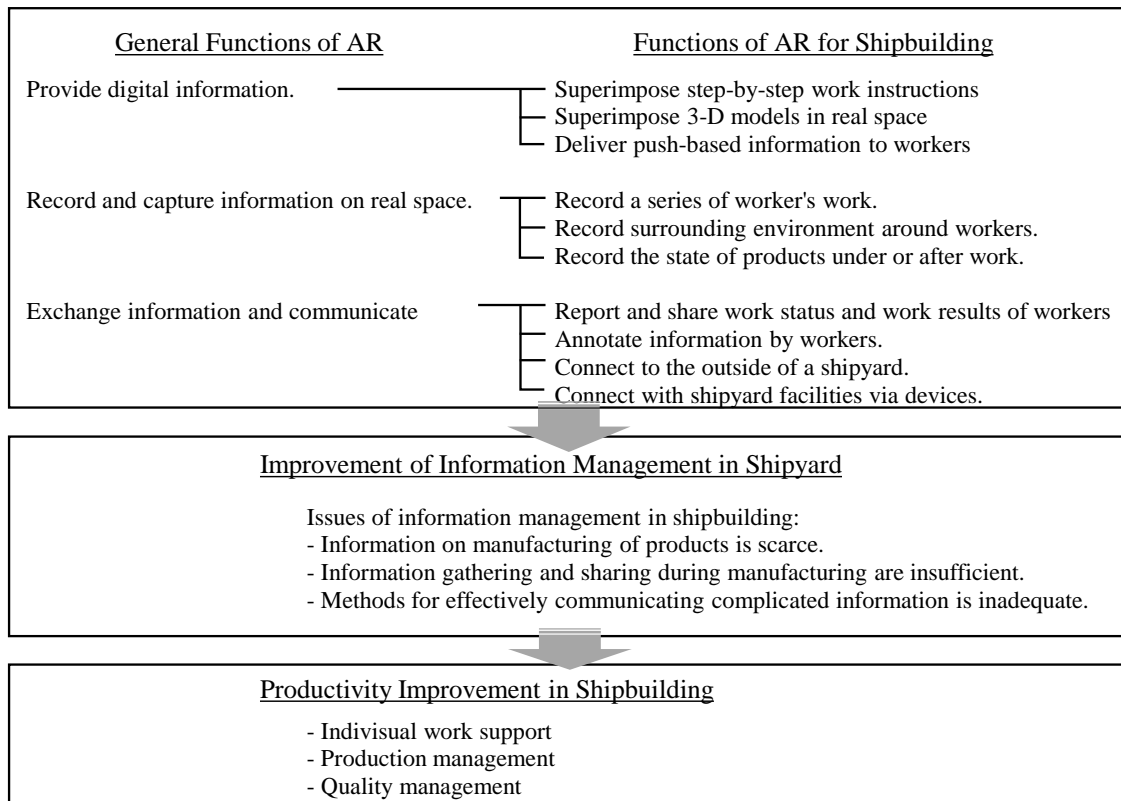


Fig.1: Relation between productivity improvement and AR functions

3. Implementation of AR applications for demonstration experiments

In order to evaluate functions summarized in Section 2 and confirm technical issues when deploying AR technology to actual shipbuilding factory, three concrete AR applications are developed, and demonstration experiments are conducted.

3.1. AR application for sheet metal forming work

3.1.1. Sheet metal forming work in shipbuilding

The sheet metal forming works can be regarded as a typical example of a skilled work operation in shipbuilding because of following reasons as illustrated in Fig.2:

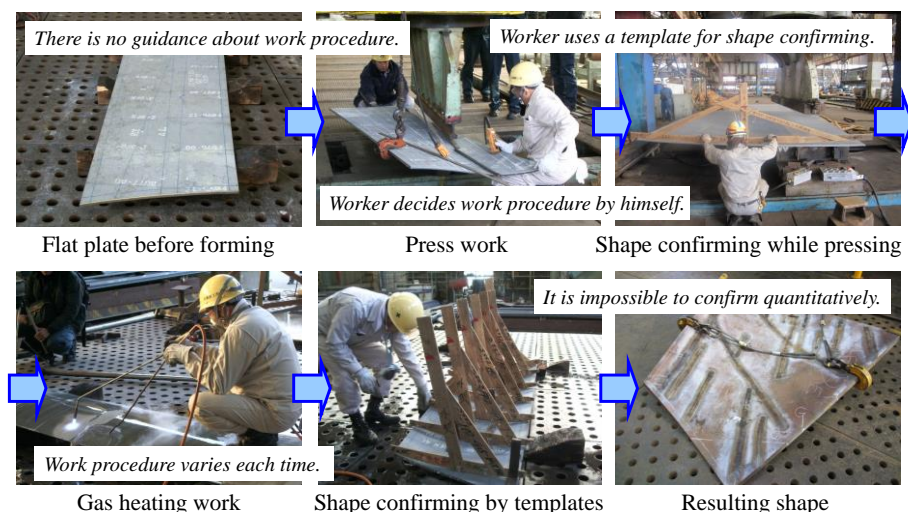


Fig.2: Sheet metal forming work in Japanese shipyards and its difficulties.

- Difficulty in imagining an accurate 3D shape
- Difficulty in judging a geometric forming procedure
- Difficulty in processing to an objective surface
- Difficulty in confirming a shape by traditional way

3.1.2. Functions and requirements of AR application for sheet metal forming work

To facilitate complex tasks as described in the previous section, AR technologies support workers by providing intuitive information in real time. Following functions of an AR application for sheet metal forming work are proposed:

- Provision of the 3D image of a sheet metal plate for intuitive imagination
- Provision of step-by-step work instructions
- Support for confirmation of the complete shape without templates

On the other hand, the requirements for the AR application practically used at shipbuilding factories are as follows:

- To be able to provide proper information for sheet metal forming to workers
- To be stable with respect to AR visualization in shipbuilding factories
- To be able to guide workers with practically sufficient performance (time to display information, etc.)

3.1.3. Implementation of AR application for sheet metal forming work

The workflow with the support of the AR application and the system configuration of the AR application is described in this section, *Matsuo et al. (2013)*.

- Workflow with support of the AR application

The main feature of the AR application scenarios is to provide capability to see information directly on a sheet metal plate in real world through a mobile device.

Fig.3 shows workflow of sheet metal forming work with the support of the AR application. Concerning how to operate the AR application along the workflow, assumed procedure of sheet metal forming work with AR is as follows:

- When workers need to verify the present shape of a sheet metal plate;
- Workers activate the AR application and select the sheet metal plate (I). The application loads data of the target shape (II);
- In order to evaluate the current shape of the sheet metal plate, workers operate a laser scanning system to measure the shape of the sheet metal plate (III). Point cloud data processing for laser scanning data is conducted in a dedicated system (IV);
- The current shape obtained by measurement and the target shape are compared (V), (VI). The distance error from the target shape can be checked by displaying through AR directly on the plate according to the color map or the numerical value (VII);
- If the current shape is not within a tolerance, additional sheet metal forming work is required. The additional work instructions are calculated and superimposed on the plate directly (VIII);
- Workers repeat the above until the shape is completed.

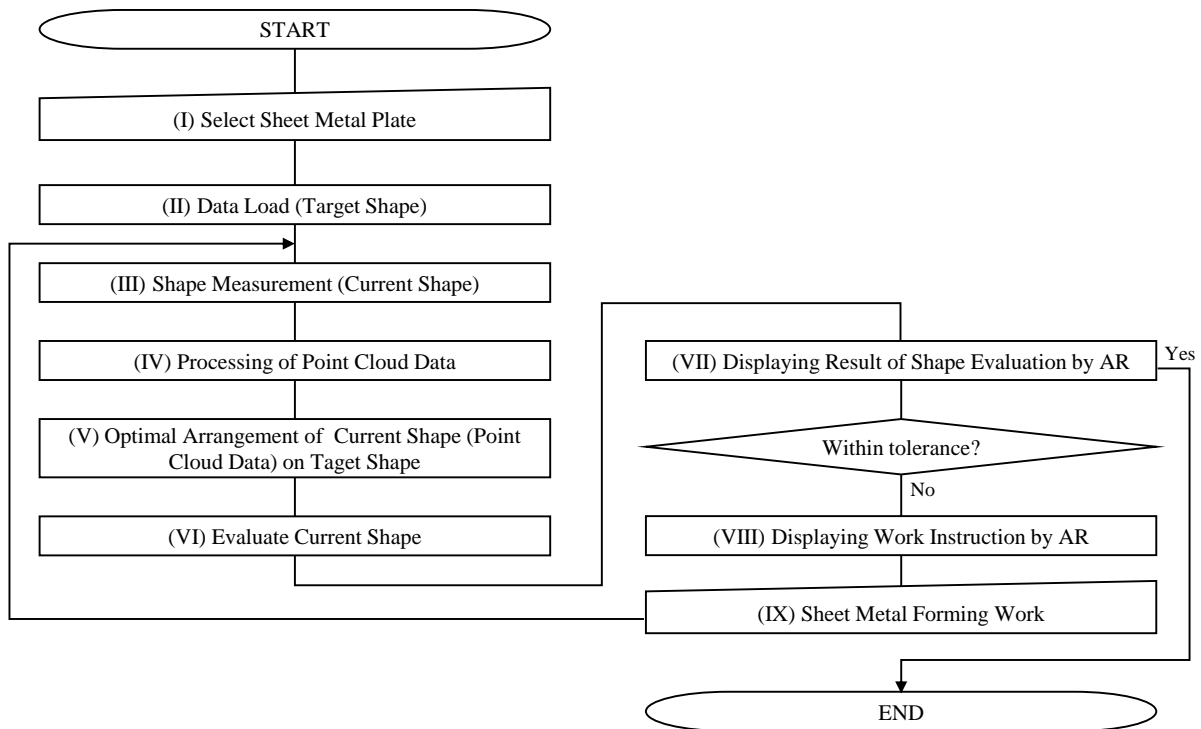


Fig.3: Work flow of sheet metal forming work with of the AR application

- System configuration of the AR application

The AR application developed in this study corresponds to the part after (VII) in Fig.3. The parts related from (I) to (VI) are independent from the AR application.

The AR system is connected to the system dedicated for calculation of step-by-step work instruction for sheet metal forming works. The system analyses sheet metal forming works by a geometric approach that uses a set of lines of curvature on a curved surface, *Matsuo and Matsuoka (2010)*, *Matsuo et al. (2013)*, *Matsuo and Takezawa (2019)*. Basic idea to calculate work instructions is to find the processing line so that lines of curvature of the current shape approaches those of the target shape.

In the AR application, a marker is put on a sheet metal plate. This marker is dedicated to identify the position and the orientation of the sheet metal plate. The AR application generates a coordinate system which has the origin at the centre of the marker and the Z axis perpendicular to the marker. By transforming a coordinate system of a 3D model to coincide with the coordinate system generated by the marker, it makes possible to display 3D CG objects of 3D models in accordance with the real space.

3.1.4. Consideration through the Demonstration

Through the demonstration experiment at a shipyard, Fig.4, the AR application is evaluated from the viewpoint of its application to shipbuilding.

- Evaluation as AR system operated in shipyards

Following remarks including technical issues toward practical use arise as a system for shipbuilding:

- It was possible to superimpose digital information on the entire sheet metal plate. The superimposition was stable, and it was possible to superimpose from any angle.

- It was confirmed that superimposition became unstable because the marker appeared smaller or the viewing angle to the marker became smaller when the distance to the plate was increased. It was found that the size of a marker should be appropriately selected according to a display area. In case of superimposition for large size of sheet metal plate, it is necessary to arrange several markers on a plate.
 - When a marker is placed on a sheet metal plate with a deep curve, it was confirmed that the recognition accuracy and stability decline. It was found necessary to consider the deformation of a marker along a curved surface.
 - A distance error of a few cm for superimposing occurred at the edge of the plate farthest from the marker. According to workers who joined this experiment, this error was not a critical problem in practical application, as manual work by worker cannot deal with precise work instructions.
 - Paper markers turned out to be inappropriate as gas heating and discharge water on a plate were conducted. Measures such as NC marking of marker are necessary. It is also necessary to set markers on both sides as sheet metal forming is done both on the front and back of a plate.
 - Regarding digital information for shape evaluation, the workers appreciated that they were easy to recognize and effective since the contents were directly superimposed on a plate and these can be freely switched.
 - On the other hand, it was found that there was a difficulty to transfer the information displayed in the screen of a tablet PC onto an actual plate. Therefore, it was inconvenience of comparing the screen and the actual plate several times.
 - It took about 10 minutes to check the shape measurement by AR including the time for laser scanning. This time length was not a big problem at the initial stage of sheet metal forming work because the time for shape confirmation is relatively small compared with time for sheet metal forming work. On the other hand, the time for the shape measurement in this experiment was evaluated as inconvenient from the workers at the latter stage of sheet metal forming work, as it required to check the shape for every correction work.
 - Some kinds of a holding device to fix the tablet PC was needed so that the workers could use their hands freely. Hands-free AR technology using smart glasses or projection mapping is expected in the future.
- Evaluation in terms of productivity improvement

Through the interviews with the managers and the workers at the shipyard, the contributions to productivity improvement are summarized as follows:

- Individual work support: Workforce productivity will improve as error locations or additional work instructions can be found intuitively by information directly superimposed on a plate. Workforce productivity will also improve by being able to receive optimal work instructions through AR.
- A quantitative shape confirmation for the entire area of a plate is possible. This removes constraint to use traditional templates, and contributes to save time and cost to use templates. Work time will be further shortened by speeding up laser scanning in the future.
- Production management: Work instructions by AR contribute to optimize and stabilize work time of sheet metal forming. To realize optimal scheduling and reasonable production management can be expected.
- Quality management: Work instructions by AR and quantitative shape confirmation contribute to stabilize and improve the quality of sheet metal forming work. It also contributes to quality traceability.

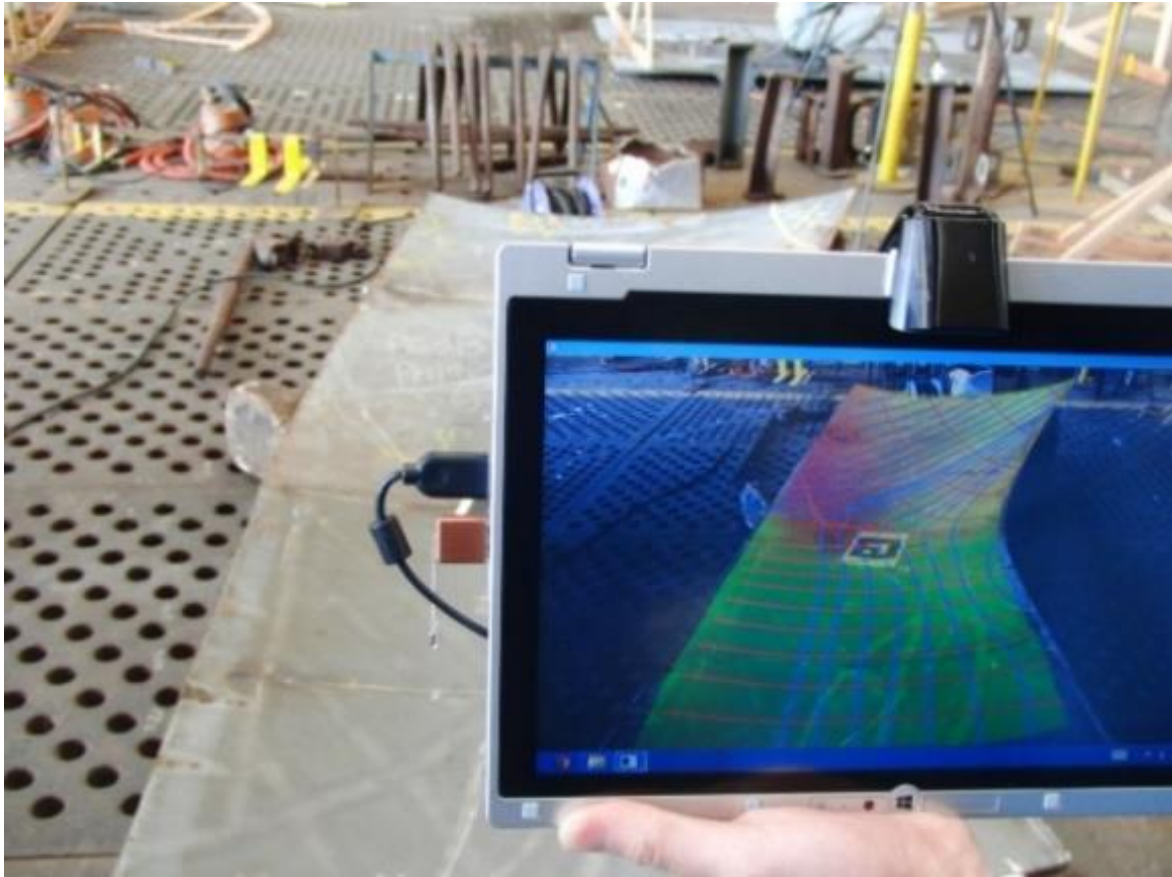


Fig.4: Snapshot of AR visualization

3.2. AR application for welding work

3.2.1. Welding work in shipbuilding

A welding specification is determined beforehand in design department in order to guarantee the sufficient strength of a structure. The workers must perform welding work according to welding specifications. Normally, welding specifications are indicated in paper drawings at shop floor. However, welding specifications on paper drawings have following difficulties:

- The content of 2D drawing is complicated. It consumes time to collate the corresponding part in drawings, especially when the structure is complicated.
- Specific symbols are used to represent welding specifications. These expressions vary from shipyards, and they are not in common, which leads to reading difficulties and mistakes.
- In some shipyards, managers sometimes write or mark welding specifications in advance for each welding line in order to avoid extra work and mistakes when reading paper drawings for welding workers.
- Welding works are scattered throughout shipyards, and production management and quality management are not done for each welding line.

3.2.2. Functions and requirements of AR application for welding work

Desired functions of the AR application are as follows to solve these difficulties:

- Superimpose welding lines on actual blocks, and intuitively inform the workers of welding locations
- Display welding specifications for each welding line

- Workers can input and register various kinds of information (start / end of welding work, memo, photographs, video, etc.) for each welding line from shop floor.

Requirements of the AR application to realize these functions are as follows:

- To be able to superimpose welding lines for complex structures
- To be able to prepare necessary information of welding specifications and import it into AR application
- To be able to perform sufficient operation in specific environment in shipyards

3.2.3. Implementation of AR application for welding work

The work flow with support of the AR application and the system configuration of the AR application is described in this section, *Matsuo (2017)*.

- Workflow with support of the AR application

The main characteristic of the AR application is to provide capability to see welding information directly on a block through a mobile device. Fig.5 shows the workflow of welding work with the AR application. The expected procedure of welding work with AR is as follows:

- A worker moves to the front of a block to be subjected to welding work. Then, start the AR application on a tablet PC;
- Once the worker selects a target block on the application (I), data on the block is downloaded (II) and the 3D model is displayed;
- The worker turns on the camera mode and point the tablet PC to the target block. The 3D model is superimposed on the actual block (III);
- If the worker touches a welding line in the 3D model (IV), the welding specification for the welding line is displayed on a window (V);
- The worker registers the work start on the welding line when starting the welding work (VI). The worker also registers the work completion in the same way after welding (VIII);
- The worker takes pictures of the weld line (IX). If there are somethings to notice, the worker attaches a note in the application. The worker transfers them to a server (X);
- The line manager checks the work progress and pictures of a welding line from an office.

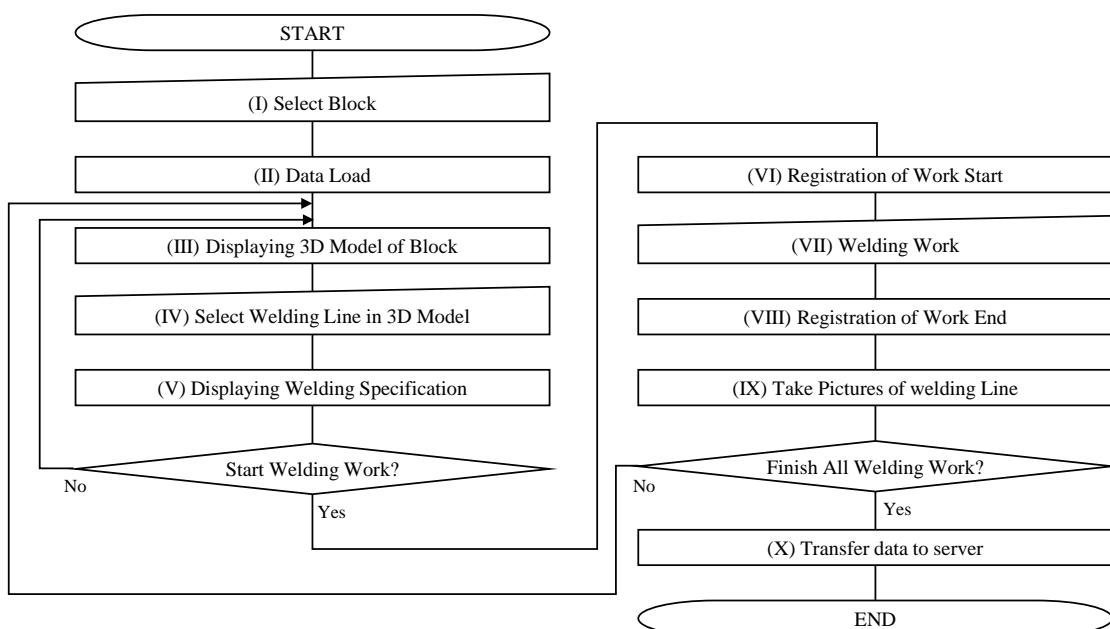


Fig.5: Workflow of welding work with support of the AR application

- System configuration of the AR application

The AR application has been developed as a client server type WEB application. By entering the designated address and connecting a server on an Internet browser, the AR application can be used from any device. The application uses the JavaScript library for implementation of the AR functions.

As a basic flow of information, the information on blocks and welding lines defined in 3D CAD is exported to the AR application at first. The information is superimposed on the actual block and displayed on the AR application. Once the welding line is selected, the welding specification is displayed on the window. The start time and the end time of welding for each welding line are registered by workers from shop floor.

The application uses markers to recognize blocks on site. The same coordinate system as the coordinate system in CAD is defined on site by recognizing a marker, and 3D models defined in CAD are displayed coinciding with the block on a screen. The application supports block recognition using multiple markers. As long as one of the markers is recognized, the same coordinate system in the CAD system can be generated in the real space, and a 3D model can be displayed.

3.2.4. Consideration through the Demonstration

Through the demonstration experiment at a laboratory, Fig.6, the AR application is evaluated from the viewpoint of its application to shipbuilding.

- Evaluation as AR system operated in shipyards

The following remarks including technical issues toward practical use arise as a system for shipbuilding:

- 3D CAD models can be superimposed on the actual hull block. In order to superimpose from all directions on a 3D block, it is necessary to set a marker on each face.
- The distance error of the superimposing position was on the order of several cm. Misunderstanding the position of the actual welding line did not occur under this error, and it is evaluated as sufficient performance as the position confirmation of welding lines.
- In case of a large size of blocks or situations such as welding lines are scattered when structure of a block is complicated, it is necessary to place markers everywhere.
- The welding specification can be confirmed by just touching the welding line on the display, and it is possible to intuitively confirm the welding specification of each welding line. The status whether unfinished or finished can be found intuitively as welding lines are distinguished by color.
- It is able to take pictures of the weld line after the welding with the application. Substitutions of visual inspection for welding lines are expected by using these pictures.
- It is found that there is no extra work to register working status for each welding line because of easy operation by the AR application.
- In addition to 3D CAD models of blocks, it is necessary to prepare welding specifications of each welding line in advance. This will be a burden for the design department.
- It is found inconvenient to use a tablet PC for the AR because the workers have to hold the tablet PC every time. Smooth operation can be expected by the utilization of smart glasses.
- Wi-Fi environment makes it possible to share real-time information.

- Evaluation in terms of productivity improvement

Through the demonstration, the AR application is expected to contribute to following productivity improvement:

- Individual work support: It was confirmed that welding locations and welding specifications can be found intuitively without using drawings. This eliminates time loss and errors caused by misreading drawings. Workers can input and register work results from shop floor through the application. It is not necessary to report work after the end of dairy work, and they can use this time for welding work.
- Production management: By registering work start and end times for each welding line and aggregating them, it is possible to measure work time on a welding line and manage work progress. Work time and photo quality control can be used to quantitatively grasp the skills of workers.
- Quality management: Shipyards can record photos of welding lines and notes on problems related to welding for each welding line and use them for quality control. It can also contribute to quality traceability.

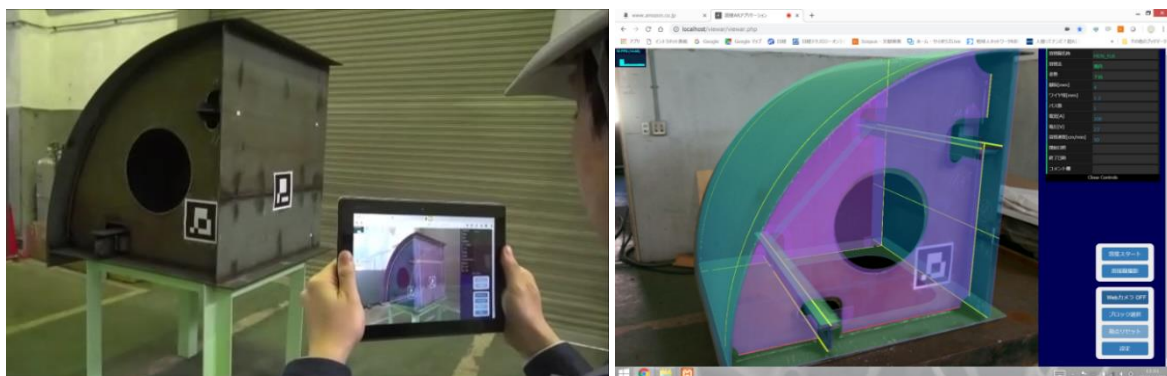


Fig.6: Snapshot of the demonstration experiment

3.3. AR application for pipe installation work

3.3.1. Outfitting work in shipbuilding

There exists an enormous amount of outfitting works in shipyards. Those outfitting works are mainly conducted with hand working, and are usually based on referring to 2D paper drawings. Although the workers must identify a pipe with its correspondence in drawings to clarify where it must be outfitted, there exist some difficulties described below:

- As there are enormous amounts of pipes needed to be outfitted, it is difficult to identify these with correspondence in drawing papers.
- 2D drawings are sometimes too complicated to understand. It consumes time just to find objective pipes in drawing papers.
- There is no additional information on drawings except fundamental ones such as pipe ID numbers and their locations. The workers have to decide the work procedure such as the order of outfitting and so on by themselves.
- Especially in case of small pipes, there is sometimes only a piping diagram which indicates connection and relationship of pipes and machinery, but also no pipe arrangement drawing which explicitly provides their locational information.

3.3.2. Functions and requirements of AR application for pipe installation work

In order to solve these difficulties, the AR application is expected to support pipe installation work.

Desired functions of the application are as follows:

- Refer to corresponding drawings on the pipe by easy operation (one-touch operation).
- Superimpose 3D models of pipes at installation points, and intuitively inform the workers of the installation location.
- The workers can input and register various kinds of information (start / end of installation work, memo, photographs, video, etc.) for each pipe from shop floor.
- The workers can leave messages on their work directly onto real space.

Following requirements are required for the AR application in order to realize these functions in shipyards:

- To be able to identify target pipes from among a large number of pipes
- To be able to superimpose the positions of pipes inside ships or blocks
- To be able to import 3D models, attribute information and related drawings of pipe into AR application
- To be able to perform sufficient operation in shop floor

3.3.3. Implementation of AR application for pipe installation work

The work flow with support of the AR application and the system configuration of the AR application is described in this section, *Matsuo (2015)*, *Matsuo (2016)*

- Workflow with support of the AR application

The main characteristic of the AR application is to provide capability to see pipe information directly on a ship or a block on site through a mobile device. Fig.7 shows the workflow of the pipe installation work with support of the AR application. The expected procedure of pipe installation work with AR is as follows:

- Workers bring a tablet PC or smart phone to the shop floor. Then they start the AR application.
- The AR function starts after the workers select a suitable option (Ship No., worker's name, etc.) from a pull-down menu (I), (II).
- Once a smart device is set to the marker which is on a pipe (III), information windows are displayed to show basic information on the corresponding pipe (IV).
- The workers can directly see the several drawings on the pipe by touching icons on the display (V-I).
- The workers also can see the virtual pipe which is installed in a ship or a block through AR (V-II).
- At the start of installing work for a pipe, the workers register the start of work through the AR application (VII). Register in the same way when the work is completed (VIII).
- When all the installing work is completed, workers upload the work report to a server (X).

- System configuration of the AR application

The AR application was developed using an existing package program, PLEMIA Maintenance Viewer V2 (MV 2), <http://www.fujitsu.com/jp/solutions/industry/manufacturing/monozukuri-total-support/products/plm-software/plemia/mviewer/>, provided by Fujitsu. GUI and AR related functions are provided by MV 2 and customized for the application. Functions related to AR are included in MV 2.

As a basic flow of information, 3D models and their attribute information of pipes defined in 3D CAD are exported to the AR application. Once users select a pipe, information on the pipe

is displayed on a screen. Also, the installation position of the pipe can be superimposed on the inside of a ship or in a block with AR. The start time and the end time of the installation work for each pipe are inputted and registered by the workers.

There are two types of markers in the application. One is for pipe identification and is directly attached on the corresponding pipe. The AR application realizes the objective pipe by analyzing the marker on the respective pipes. As the marker is related with corresponding information for the pipe, the general information on the pipe arise, when the workers put the tablet PC or the smart phone to the objective pipe. Another one is for locational identification and is attached in a designated point of a ship or a block. The position (X,Y,Z) in the coordinate system defined in the CAD model is registered to the marker, the same coordinate system as the CAD model can be generated in the real space, and the model defined by CAD can be superimposed in the real space.

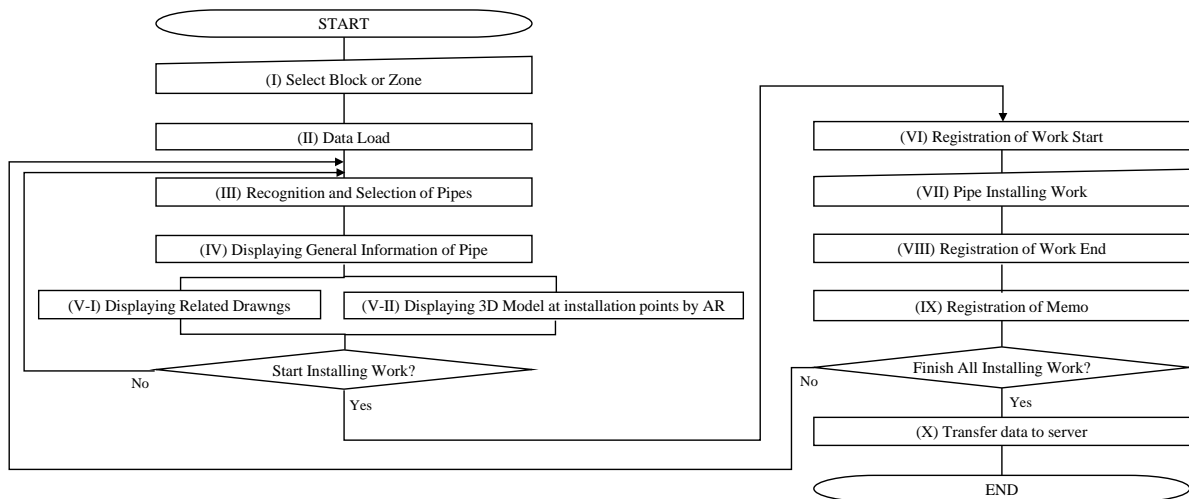


Fig.7: Work flow of pipe installation with support of the AR application

3.3.4. Consideration through the Demonstration

Through the demonstration experiment at a shipyard, Fig.8, the AR application is evaluated from the viewpoint of its application to shipbuilding.

- Evaluation as AR system operated in shipyards

Following remarks including technical problems toward practical use arise as a system for shipbuilding:

- It is confirmed that 3D CAD models of pipes can be superimposed and displayed in accordance with its installation position in a ship. In order to superimpose on every area in a ship, it is necessary to set several markers at each place.
- The distance error of the superimposing position was about several cm in the experiment. This accuracy is reasonable to check the installing position of the pipe for the workers.
- Good operability can be confirmed by one touch operation to make selections. The application collects information on the work status of each worker. This procedure does not increase extra work, as workers input and register their work status with smooth operation by the application.
- In addition to 3D models of the pipes, it is necessary to prepare various information on individual pipe in advance. It became possible to automatically create and import data for AR application by defining the data structure of the AR application and developing the interface with CAD. There is a demand from shipyards that it is desirable to plan the order of pipe installation in advance and to instruct it by AR.

- Although a tablet PC was used for AR in the experiment, it was inconvenient because it was necessary to hold the tablet PC every time. The utilization of smart glasses is promising.
- Markers were affixed to each pipe in the experiment to recognize individual pipes. It is difficult to prepare all the markers for a huge number of pipes.
- Evaluation in terms of productivity improvement

Through the demonstration, the AR application is expected to contribute to following productivity improvement:

- Individual work support: It is confirmed that workers can intuitively find the installation position of the pipes without using drawings. This eliminates time loss and errors due to misreading drawings. Workers can enter and register work results on the spot through the application. This eliminates dairy work reports after the end of the whole work, and they can use this time for installation work. There is a comment from a shipyard that it can contribute to further work efficiency by instructing the optimum installation order of pipes.
- Production management: By registering work start and end times for each pipe and aggregating them, it becomes possible to measure work time for each pipe and manage work progress. As shipyards usually manage their outfitting work by a unit of lot which is composed of several pipes, production management will be improved by management of each pipe unit.
- Quality management: Work management for each pipe improves the forgetting piping installation.

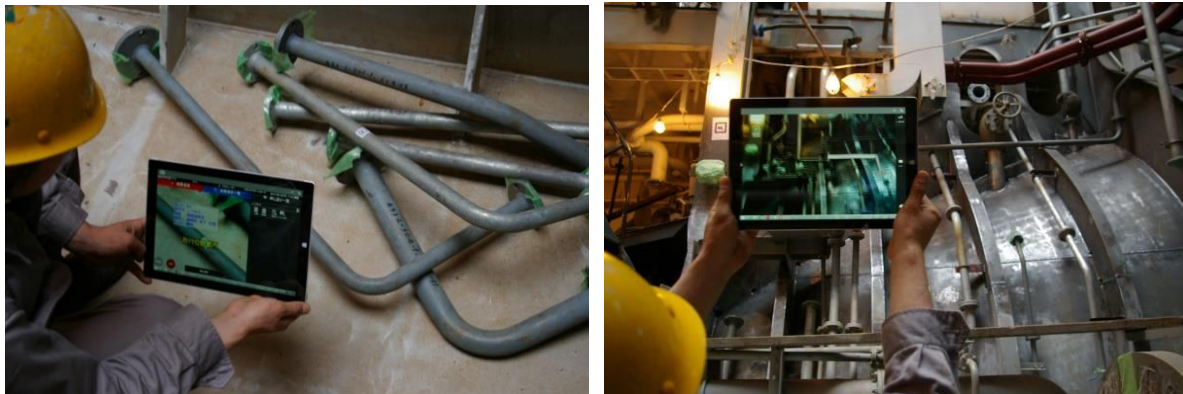


Fig.8: Snapshot of AR visualization in the demonstration experiment

4. Conclusion

In this paper, application of AR technology to manufacturing in shipbuilding is investigated, especially focusing on technical issues and effects for productivity improvement when using AR applications on shipbuilding. These studies were conducted through demonstration experiments using AR applications which have been developed. Through demonstration experiments, followings were found about application of AR technology to shipbuilding:

- It is effective to superimpose drawing information or 3D models on actual products. This eliminates time and mistakes caused by misreading drawings. On the other hand, preparing the production information to superimpose on AR preliminarily is crucial.
- In the case of marker recognition, superimposition on actual objects can be carried out relatively easily and stably in shipyards. However, in case of huge structures, complicated structures, and structures with many places where display parts are scattered, it is necessary to set a considerable number of markers for AR. Marker-less tracking is expected to be introduced.

- The positional accuracy required for superposition depends on the applications. In the case where there is not much problem for practical use even if the position accuracy is relatively coarse, it is easy to deploy AR applications.
- Smart glasses or projection mapping are highly expected to use in order to realize a hands-free AR for shipbuilding.

References

BLANCO-NOVOA, Ó.; FERNÁNDEZ-CARAMÉS, T.M.; FRAGA-LAMAS, P.; VILAR-MONTESINOS, M.A. (2018), *A Practical Evaluation of Commercial Industrial Augmented Reality Systems in an Industry 4.0 Shipyard*, IEEE Access 2018 6, pp.8201-8218

FERNÁNDEZ-CARAMÉS, T.M.; FRAGA-LAMAS, P.; SUÁREZ-ALBELA, M.; VILAR-MONTESINOS, M.A. (2018), *A Fog Computing and Cloudlet Based Augmented Reality System for the Industry 4.0 Shipyard*, Sensors 18/6

FRAGA-LAMAS, P.; FERNÁNDEZ-CARAMÉS, T.M.; BLANCO-NOVOA, Ó.; VILAR-MONTESINOS, M.A. (2018), *A Review on Industrial Augmented Reality Systems for the Industry 4.0 Shipyard*, IEEE Access 2018 6, pp.13358-13375

KIM, D.; PARK, J.; KO, K. (2018), *Development of an AR based method for augmentation of 3D CAD data onto a real ship block image*, Computer-Aided Design 98, pp.1-11

MATSUO, K.; ROTHENBURG, U.; STARK, R. (2013), *Application of AR Technologies to Sheet Metal Forming in Shipbuilding*, Smart Product Engineering, pp.937-945

MATSUO, K. (2013), *Demonstration of AR application for sheet metal forming works in shipyard*, Int. Conf. Computer Applications in Shipbuilding Vol.2, pp.167-170

MATSUO, K.; MATSUOKA, K. (2010), *Development of New System for Developing Curved Shell Plates of Ships*, Trans. Japan Society of Mechanical Eng. 76/771, pp.2797-2802

MATSUO, K.; FUJIMOTO, S.; SHIMADA, M.; NAKAGAKI, N.; SUGAWARA, A. (2013), *Development and Practical Introduction of a Support System for a Cold Bending Work in Shipyard*, Conf. Practical Design of Ships and other Floating Structures (PRADS)

MATSUO, K.; TAKEZAWA, M. (2019), *Development of Work Support System of Press Work for Sheet Metal Forming*, Int. Conf. Computer Applications in Shipbuilding (ICCAS), pp.24-26

MATSUO, K. (2017), *On the AR application to support a welding work in shipyards*, Conf. Japan Society of Naval Architects and Ocean Engineers 25, pp.189-190

MATSUO, K. (2015), *AR application development for pipe installing assistance*, Int. Conf. Computer Applications in Shipbuilding Vol.1, pp.127-130

MATSUO K (2016), *Augmented Reality Assistance for Outfitting Works in Shipbuilding*, COMPIT Conf., pp.234-239

OH, Y.; PARK, K.; KIM, E. (2014), *Mobile Augmented Reality System for Design Drawing Visualization*, 16th Int. Conf. Advanced Communication Technology (ICACT), pp.1296-3000

OH, Y.; PARK, K.; KIM, E. (2015), *Efficient 3D Design Drawing Visualization Based on Mobile Augmented Reality*, 17th Int. Conf. Advanced Communication Technology (ICACT), pp.569-573

OLBRICH, M.; WUEST, H.; RIESS, P.; BOCKHOLT, U. (2011), *Augmented reality pipe layout*

planning in the shipbuilding industry, 10th IEEE Int. Symp. Mixed and Augmented Reality

PORTER, M.; HEPPELMANN, J. (2017), *Why Every Organization Needs an Augmented Reality Strategy*, Harvard Business Review November–December Issue

Development of a Unified Data Model to Improve Ship Operational Performance Analyses

Wisam Jabary, University of Rostock, Rostock/Germany, wisam.jabary@uni-rostock.de
Florian Sprenger, University of Rostock, Rostock/Germany, florian.sprenger@uni-rostock.de
Lutz Kleinsorge, Mecklenburger Metallguss GmbH, kleinsorge@mmg-propeller.de
Hauke Baumfalk, Mecklenburger Metallguss GmbH, baumfalk@mmg-propeller.de
Simon Mewes, University of Duisburg-Essen, Duisburg/Germany, simon.mewes@uni-due.de
Jens Neugebauer, University of Duisburg-Essen, Duisburg/Germany, jens.neugebauer@uni-due.de
Changqing Jiang, University of Duisburg-Essen, Duisburg/Germany, changqing.jiang@uni-due.de
Ould el Moctar, University of Duisburg-Essen, Duisburg/Germany, ould.el-moctar@uni-due.de

Abstract

The reliable evaluation of ship operational performance requires the analysis of extensive data sets, which are inconsistent in time and collected from totally different resources/systems. This paper presents the development of a Ship Operation Information Model (SOIM) which considers comprehensive data at low/high-frequency of: noon reports, AIS, weather, loading conditions and numerous onboard sensors measuring operating and motion parameters. The configuration of SOIM in a database management system, which makes synchronized and high-quality data available, provides the basis for improved analyses of various ship performance parameters. The usage of the model is demonstrated by sample performance evaluations.

1. Introduction

Due to the increasing availability of sensor technology on board ships and the ever more advanced penetration of all systems with computer-aided control and data management components, extensive data is available both on board and in the shore-based specialist departments of the ship operators (and possibly also system suppliers). This data can be used to better assess ship operations. Analysis of the data offers significant potential for more efficient, safe, and environmentally friendly operations, e.g. Zhang *et al.* (2021) presented a ship-to-ship collision risk assessment approach based on analysis of vessel operational data and hydro-meteorological conditions. Ship operation data can also play an important role in determining design parameters of future ships, propulsion systems and different on-board facilities. This was also concluded by Patey (2019), who discussed ways to use the collected data to improve new-building designs and retrofit projects. Oh *et al.* (2021) outlined how the most economical operation can be determined by analyzing the operating patterns of ships.

Experience with ship operation data shows that although they can be extensively measured (and thus recorded), fundamental questions about the quality and significance of the data has not yet been adequately answered, which is concluded by many authors who have studied or analyzed operational data, Dalheim and Steen (2020), Oliveira *et al.* (2018), Baumfalk (2017)). This is true in particular for the evaluation of data changes over relatively short periods of time (minutes), where impossible states of the ship (unrealistically large accelerations or decelerations) were documented, Dos Santos Ferreira (2018). Thus, Wagner (2017) discussed filtering methods that should be applied to evaluate operational data of several container ships over a period of more than one year in order to be able to develop a realistic basis for scenario techniques based on these data.

The research presented in this paper has been conducted within the framework of the research project DigitShip, which addresses issues for efficient ship performance and its highly relevant functions: Behaviour in sea-states and under course keeping, status of hull and propeller as well as the response of the engine plant (fuel consumption) to the respective actual performance requirements.

The structured processing and provision of ship operation data including the correlated location- and time-dependent environmental conditions requires the synchronization and identification of the

relationships between various operation data collected from different resources at different frequencies. This will provide a sound basis for the evaluation of ship performance parameters with regard to the optimization of ship operation. However, a comprehensive added value of the operational data can only be developed, if it is possible to establish the context of the data in a meaningful way by means of a physically based overall context. For this purpose, a database with a robust information model for ship operation data was developed and made available for further evaluations via a cloud-based approach. The developed information model as well as the database will be discussed in the following, and the paper will be completed by exemplary performance evaluations.

2. Data sources

The research project is based upon operational data from a 14,000 TEU container ship in the Europe-Asia liner service, using two different sources: a) data from onboard measurements, commonly referred to as "onboard data," and b) data from external sources collected by third parties independent of, but related to, the vessel itself, which primarily include navigational data by means of the Automatic Identification System (AIS) and the prevailing environmental conditions. The term "onboard data" covers all measured variables and information obtained on board the vessel. This includes the status reports ("noon reports") to be kept manually by the crew and the data on loading conditions as well as automatically collected data on all relevant ship systems and on the current motion behaviour of the ship by means of an Inertial Measurement Unit (IMU).

In terms of the frequency with which the data are provided, a distinction is made between "low frequency" for reports and loading condition data and "high frequency" for sensor and motion data. The overall concept can be seen in Fig.1.

2.1. Low frequency data

The low-frequency data comprises the noon reports that are manually issued by the crew on board and the loading condition data that are updated when leaving a port.

2.1.1. Noon report data

The reports are kept manually by authorized crew members on board and, in the case of more highly equipped ships, are available to the shipping company's technical monitoring service via an online connection. For the research project, the cooperating shipping company has set up online access for the research project so that this data from the test container ship is fully available for ship operational analyses. The reports include data for more than 200 parameters of the ship's current condition, onboard systems, weather, and administrative information. The traditional term "noon report" has lost its validity here, as these reports are summarized on an event-basis rather than regularly at 12 o'clock noon.

Events for which the report is updated are differentiated into:

DEPA: Departure from Port, ARRI: Arrival in Port, BOSP: Begin of Sea Passage, EOSP: End of Sea Passage, NOON (Sea): Noon at Sea, NOON (Man): Noon while Manoeuvring, NOON (Anc): Noon at Anchor, NOON (Drf): Noon while Drifting, NOON (Prt): Noon in Port, BANCH: Begin of Anchorage, EANCH: End of Anchorage, BDRIFT: Begin of Drifting, EDRIFT: End of Drifting.

From these events, the following operational states can be derived, which are thus defined for ship operation, and in which a ship should be in exactly one state at any time: 'at sea', 'drifting', 'at anchor', 'manoeuvring' and 'in port'.

The manually maintained data (reported) is supplemented by measurement results provided by the sensors on board, which can be aggregated or averaged over the relevant period using the appropriate

software. These values do not differ significantly from the manually recorded ones, but are used to check the plausibility of the data supplied by the crew. The sensor data itself is recorded separately at higher frequencies and presented in the following.

- Ship: general information, higher-level information about the voyage.
- Navigation: navigational information.
- Loading Condition: basic information about the loading condition of the ship.
- Machinery: information on main engine, auxiliary engines, exhaust aftertreatment systems, fuel including consumption and tank filling levels, propulsion, performance indicators (KPIs).
- Environment: summary of environmental conditions on the route section.

The loading condition data is downloaded from the ship's loading calculator via a web interface of the installed system. Updates are always made at the time of departure from a port (event: DEPA).

- **Hydrostatics:** ship's floating position data with drafts and centers of gravity for the entire vessel.
- **Stability:** Parameter values of the checked stability requirements.
- **Tanks:** Data on filling levels for all tanks with mass and center of gravity.
- **Container Cargo:** detailed information for each container on board.
- **Loading Condition Summary:** masses and centers of gravity for the ship with all mass groups.

Fig.1: Data sources

2.2. High frequency data

The ship's system provides large number of internally collected data. These data comprise original sensor data but also processed values in terms of averaging or other calculation. In addition, an Inertial Measurement Unit (IMU) and a Global Navigation Satellite System (GNSS) are installed to measure the ship's motions in six Degrees of Freedom (DoF). Data from both sources, internal ship systems and additional sensors, are acquired at different sampling rates using a logging system additionally installed on board. The following sections describe the collection of the ship's internal data, the data from additional sensors and the data logging system.

2.2.1 Ship-internal data

The ship is equipped with internal measurement systems which collect more than 400 values in total. Not all values are primarily measured by dedicated sensors but are calculated from combinations of other values, are averaged or summed up. Summarizing, available data are:

- Filling level data for the large number of fuel, ballast and other liquids tanks
- Main and auxiliary engines parameters like temperature, pressure, power, rpm, running hours, fuel data, power and torque
- Navigational data e.g. speed over ground (SoG), speed through water (StW), course, rudder angle, wind speed and direction, position and turning rate
- Cargo related data like the reefer power systems' status

For the project, all data possibly having an influence on the ship's performance is important. Firstly, this concerns some primary power indicators like the engine power, the propeller rpm, the fuel flow rate, fuel temperature, ship speed (over ground and through water), wind speed and direction. At the second glance, some further values which indicate changes in the power demand, e.g. rudder angle, rate of turn and ship motions (see section 2.2.2) are relevant as well. Thirdly, we need to consider values affecting trim and heel, hence the tank filling levels, as well as they affect the ship's resistance curve and other hydrodynamic characteristics.

For the data validation process, the largest possible number of quantities forming a physical relation between each other was selected to be acquired. This allows error checking and validation by only using measured quantities. E.g. it is possible to calculate the engine power from different values like propeller rpm, torque and efficiency but also from fuel density, fuel flow rate and the lower heating value. Considering also external information, the propeller's open water diagram, wake and thrust deduction number, propeller rpm, ship speed, propeller diameter and efficiency values provide the power as well. Thus, there are three different approaches to calculate the same value and check it for errors. Finally, a total of 113 quantities were selected for acquisition.

2.2.2 Additional sensor data

For the analysis of added resistance in waves, the propulsion power can be calculated using selected measurement quantities acquired in section 2.2.1 but time-resolved seaway information is not available. Thus, an indirect approach was employed by measuring the ship's motions in six DoF using an IMU. The propulsion power can then be related to the 6-DoF motions which are further correlated to low frequency seaway spectra data provided by a weather service. In addition, the IMU is used to validate the course as well as to analyse the change in power demand during manoeuvring.

An IMU of type *Octans V Surface* was installed in the engine control room of the ship. It contains three fiber-optic gyros for the rotations (roll, pitch and heading) and three MEMS-based accelerometers for the translations (surge, sway, heave). The system is certified for marine applications and provides a heading accuracy of 0.05° and roll/pitch accuracies of 0.01°. Its accuracy for translations is 5cm or 5%. To reach the heading accuracy level, GNSS latitude and velocity are required. For this, a

dedicated GNSS receiver was installed on the bridge, connected to the IMU via Ethernet. The GNSS receiver was configured to send the ship's position, speed and a time signal to the IMU every second, allowing the IMU to perform the according corrections to reach the highest nominal accuracy.

The IMU delivers the following data to the acquisition system:

- The measurement time (UTC)
- Heading, Roll and pitch angle
- Surge, sway and heave translations
- Surge, sway and heave speed
- Heading rate

In addition, the checksum of the data string as well as status information (valid, invalid or initialising) about individual quantities are provided.

2.2.3 Data logging

A ruggedized computer is used to acquire and store all data. It contains two separate logging instances. One for the ship internal data described in section 2.2.1 and one for the additional sensor data (see section 2.2.2). All data is provided via Ethernet using NMEA strings. Four different data acquisition rates are used. They were defined based on the importance of a quantity for the primary project task and its variability during navigation. Important values changing rapidly are acquired at a rate of 5 Hz. For values changing less quickly like fuel tank filling levels, one value is recorded every minute. Ballast filling levels are recorded every 15 Min, which allows a reasonable detection of hydrostatic changes. Since ship motions change rapidly in waves and a sufficient rate is required to apply filters to the data, IMU data is recorded at the highest rate of 50 Hz.

Data is stored in SQLite databases. SQLite is a file-based database which does not require a server installation but provides an SQL-oriented data access. The database files are located on two SSD drives, arranged in a RAID 1 configuration and thus providing full hard drive redundancy. Further on, the RAID array is required for data exchange to the shore. During selected port calls, one of the drives is checked out and replaced. After the rebuild, which takes less than an hour, the full redundancy is available again. The removed SSD is then taken to shore and data is integrated into the final databases.

2.3. External resources

In addition to the data recorded on board the test vessel, further data from external sources (external provider) are used. These include, on the one hand, the prevailing AIS information and, on the other hand, data describing the environment at the respective locations at the respective times. The latter are often referred to as “weather data” in short. For the research project, the external provider has set up online access for the research project so that these data are fully available for the operational analyses.

2.3.1. AIS data

The AIS data are recorded redundantly for the test vessel. The frequency of recording and thus updating the information and its transmission is 15 minutes. The AIS provided data can be divided into three categories:

- Static: general information for ship identification
- Dynamic: ship navigational information
- in addition to the Voyage related information

2.3.2. Weather data

The evaluation of the properties of a ship in operation is only possible in a meaningful way if the environmental conditions prevailing at the respective locations at the points in time under consideration are comprehensively known. These environmental conditions are also often referred to as weather conditions.

The geographical positions at which the environment-related information is recorded result from the route of the ship under consideration.

The weather data provided is calculated from a network of weather stations and then transferred using mathematical methods to a grid point density (spatial resolution) of 0.5° lat/long at 120-minute intervals. They consist of data for main characteristic parameters for the following categories: Water, Wind, Sea State, Current and Air.

3. Ship Operation Information Model (SOIM)

In principle, well-founded information modeling and the information processing based on it are carried out in clearly defined process steps, Fig.2. For this purpose, standardized software concepts are used in the project. These concepts include, on the one hand, modeling by means of an extended entity-relationship model developed by *Chen (1976)* with the tool pgModeler, <https://pgmodeler.io>, and, on the other hand, the use of an object-relational database, in this case the database management system PostgreSQL. A detailed description of the system architecture can be found in the next section and is visualized in Fig.5.

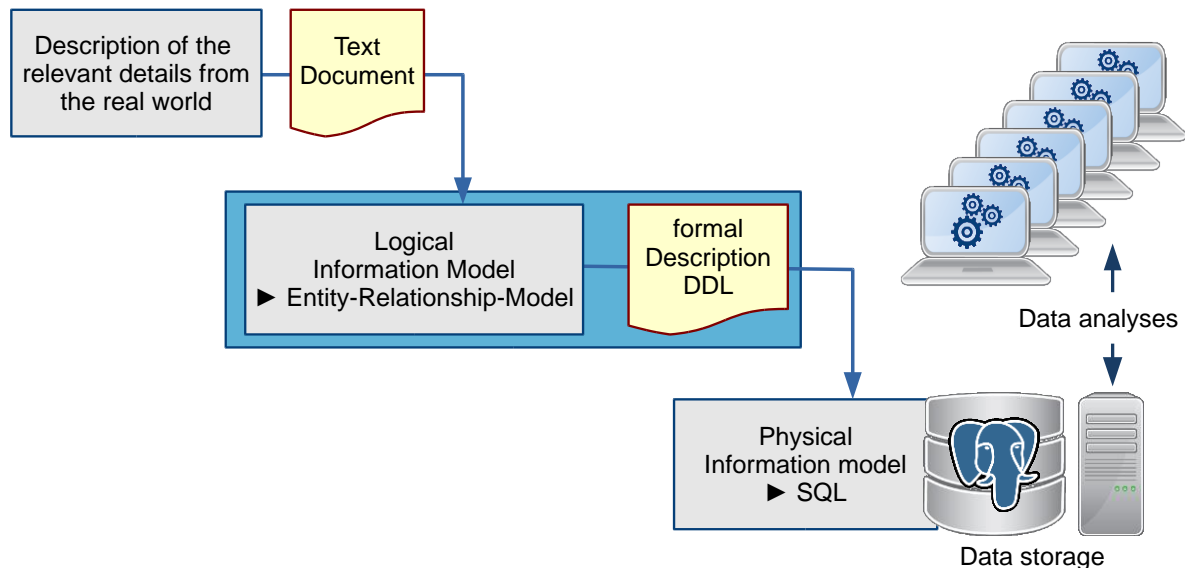


Fig.2: Steps of information modeling and utilization

In the following, the logical ship operation information model is introduced, which is derived from the present textual description of the ship operation data mentioned previously. The information is assigned to different sub-models (schemes) reflecting different data categories from which the structure of the top-level logical information model can be derived. Organizing the ship operation model into many schemes as listed below, Fig.3, in which the ship operation core model plays a central role, has many advantages at the process level of managing the different types of data.

1. ship operation core model: data for ship voyage logistics with information about the associated voyage legs, their assigned operation periods with states and special events, as well as data on position and time definitions.

2. board_data_low_frequency: data of the reports controlled by special events as well as the data of the loading conditions.
3. board_data_high_frequency: data from measurement results of a large number of sensors on board, in addition to the ship motion data recorded by the IMU.
4. external_resources: data from external resources: AIS and environmental data.
5. general_resources: General information which can be used more than once, such as concepts for administrative data.
6. reference_data: Ship reference data containing all information about the ship and its systems, in particular engine data, model test and sea trial results.

Since the reference and general data can be considered as static data that do not change during the ship's voyage, only the first four schemes are described in detail in this paper.

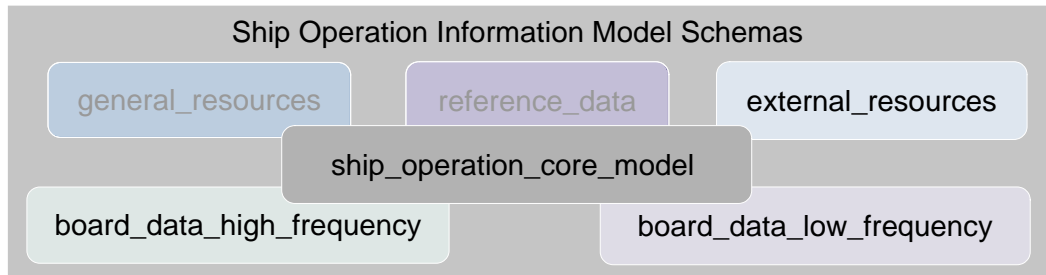


Fig.3: Ship operation information model schemes

3.1. Ship_operation_core_model

In the context of the research project, voyage logistics refer to all information that depicts ship operations and its associated positions over time. This represents the basis for all further information. A 'fleet' is used to group a number of ships according to an arbitrary ordering principle specified by the user. If required, several fleets can be managed simultaneously. A 'ship' is the central information object to which all valid information are assigned. Besides some administrative data, this includes on the one hand the static reference data mentioned previously and on the other hand data of the list of voyages the ship has made. While the reference data are assumed to be time-independent, the data of voyage, which is the period of time from departure from the start port to arrival at the port of destination, is time-dependent.

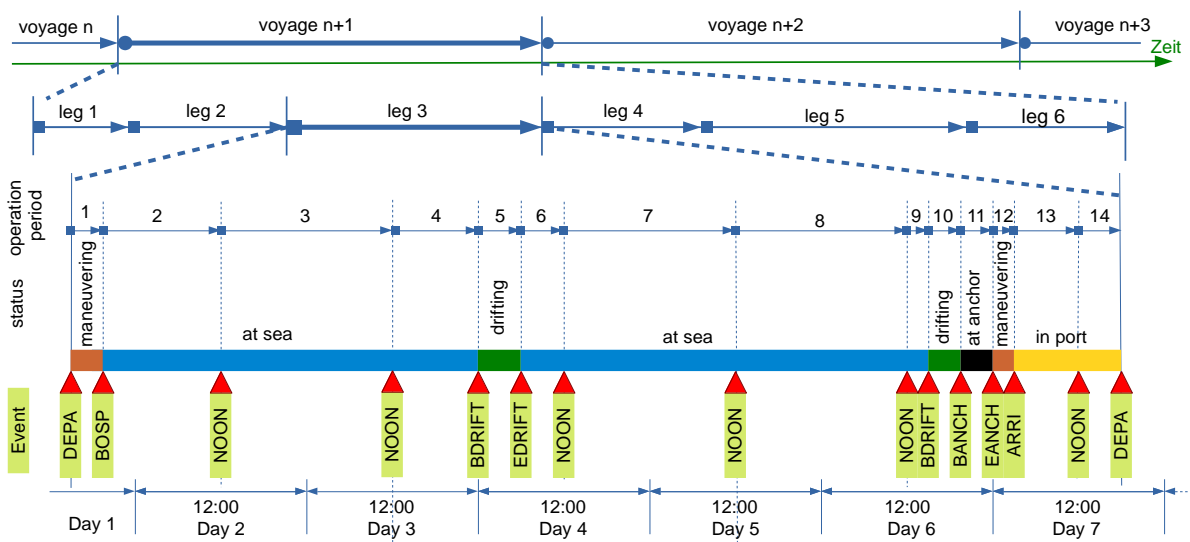


Fig.4: Voyage logistic terms

3.2. board_data_low_frequency

The low-frequency data described in the previous section were modelled in a separate scheme, Fig.6. This data includes the reports generated manually on-board by the crew (reported) and the data obtained automatically from aggregated sensor data (measured), as well as the loading condition data that are typically updated when the ship departs from a port.

Since reports are issued for specific events on board, they refer to the period from the previous (start) event to the event that triggers the report (end event). Therefore, reports are assigned to exactly one reporting period (operation period) via the associated end event. Exactly one manually (reported) and, additionally one automatically (measured) generated report can be assigned to a reporting period. Fig.4 shows the example of a voyage segment already mentioned above the consecutive operating states (in this case 14) for each of which a report is generated. To give an example, the fourth report is generated on the third day of the voyage at the time the ship starts to drift, so the reporting period is from the last noon report to that time. This also results in reporting periods of varying lengths, but not exceeding 24 hours (noon - noon). The loading condition data, on the other hand, is always assigned to exactly one leg of the voyage because of its association to the event: DEPA, as mentioned before. As can be seen in Fig.6, several loading conditions (0..N) can be assigned to each leg (1).

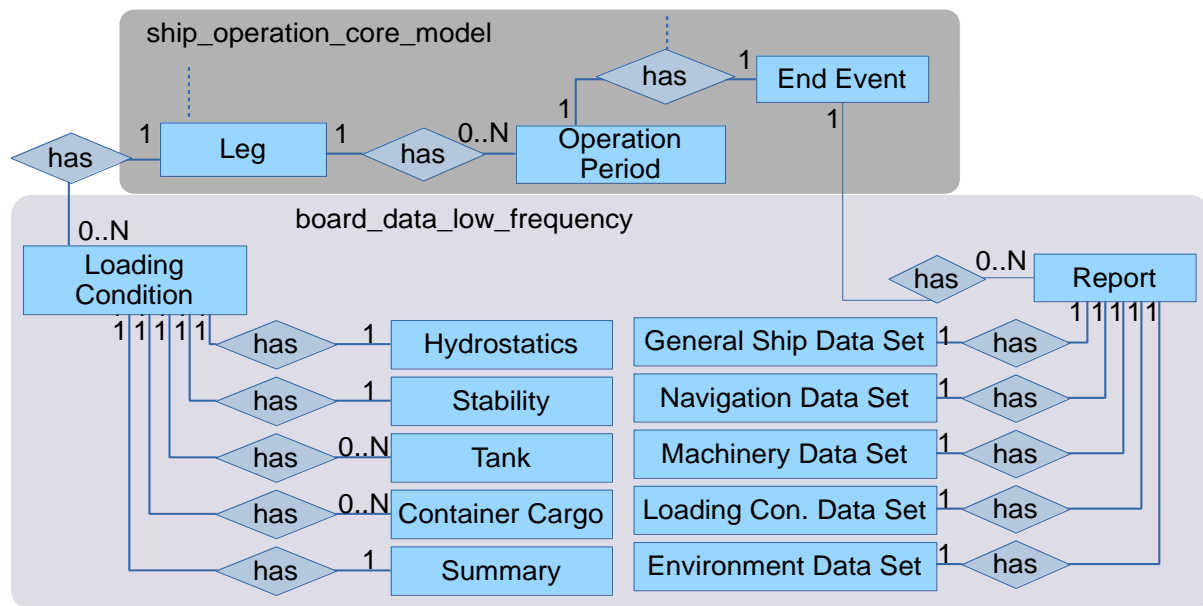


Fig.6: Scheme: board_data_low_frequency; symbols according to Chen (1976)

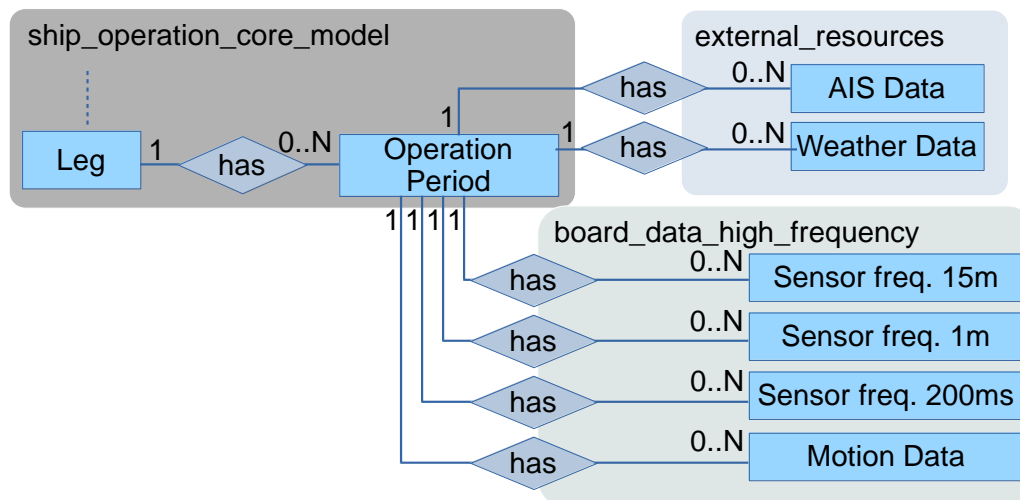


Fig.7: Scheme: board_data_high_frequency/external_resources, symbols according to Chen (1976)

Here, it is necessary to mention that all data are provided with a (UTC: Universal Time Coordinated) time stamp as well as the respective local time. This enables the synchronization of a wide variety of data to one ship in the database, which in turn has many advantages in terms of ship operation data evaluations.

3.2. board_data_high_frequency and external_resources

Fig.7 shows scheme models of the two data sources described previously and their assignment to the operation period:

- External data including AIS as well as environment data.
- The high-frequency data including, on the one hand, the data measured by the sensors on board and relevant for the project and, on the other hand, the motion data of the ship recorded by an Inertial Measurement Unit (IMU) installed especially for the research project. The former were modeled to be stored according to their recording frequencies (15 min, 1 min, and 200 milliseconds).

4. Ship operation data management

The implementation of the ship operation information model with continuous import of ship operation data based on it as well as their evaluation with the goal of ship operation optimization is realized. The system architecture is achieved with four clearly defined components shown in Fig.8 with their interconnections at a higher level of abstraction, in which the simpler representation in Fig.2 is taken up and expanded.

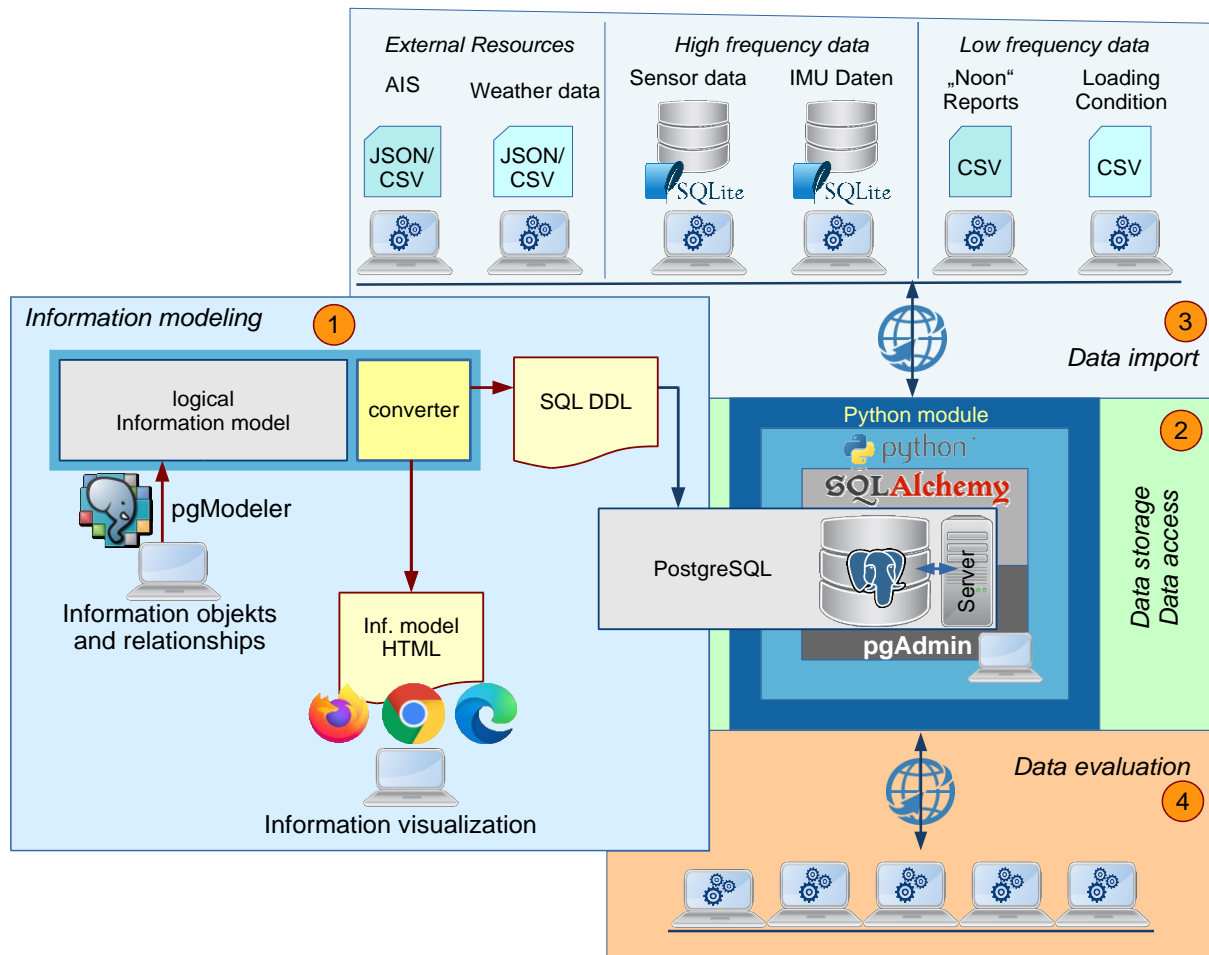


Fig.8: System architecture

These include:

1. The information modeling with the structure of the data management on the basis of a database management system,
2. The database management system in the form of cloud-based data management with specific data manipulation methods for application programming
3. The parsers for data from various sources for pre-filtering and importing into the integrated data management
4. The various application programs for data analyses, each with specific objectives.

4.1. Information modeling

Information modeling is the first process step in which the configuration of the data management for application-specific development environment takes place. For this purpose, the pgModeler software developed by *Silva (2021)* is used in the project. It allows the formulation of the logical information model that formally describes all objects and their relationships to each other, and the conversion of the formulated logical model into various output formats for further use. This includes the output in “SQL DDL” in order to conjugate the database management system in a further step and thus defines the physical model.

Another export format is HTML, which can be used to visualize the model with web browsers and to navigated within it. This is particularly useful for communicating about the model in development as well as in application programming, since no additional software is required for this purpose.

The most important result of the information modeling is therefore the data definition “DigitShip SQL DDL”, which is used to configure the data management.

4.2. Database management system

PostgreSQL, <https://www.postgresql.org>, is used as the database management system. The interactive SQL queries of the database are done by the use of the software pgAdmin, <https://www.pgadmin.org>. Due to the extensive change functions, special rights are implemented for this, which are controlled via the role system of the database management system.

The physical model of the database is a relational model with additions in the direction of an object-oriented model. All information is stored in the form of tables, hence also called object-relational.

The “translation” of the ER model into a table representation takes place automatically by the software pgModeler, whereby also the formulated consistency conditions to the dataset in the form of the appropriate SQL program sequences are considered and transferred to the database.

4.3. Data import

The import of the ship operation data as well as the reference data of the ship and other static data is done via specially developed programs. Access to the database is realized via the DigitShip Python module layer shown in Fig.8.

Data from the following sources are imported and integrated into the comprehensive information model:

- reference data in different formats
- sensor data via SQLite databases, <https://sqlite.org/about.html>
- ship motion data via SQLite databases
- report data via csv formatted files

- loading condition data via csv-formatted files
- AIS data via csv formatted files
- environmental data via csv formatted files

4.4. Data evaluation

The evaluation of the data stored in the database is also performed using the DigitShip Python module layer, which offers the possibility of object-oriented processing of the stored data without having to master the SQL language commands. Selected evaluation examples are discussed in the following section.

5. Examples of ship operation performance evaluation

5.1. Example-1

Based on the first monitored sea voyage of the vessel it is briefly shown, how the developed system can be used to analyse the ship performance based on the method described by *Greitsch et al. (2016)*. The implemented information model can be – due to the modular structure – easily extended by functionalities for filtering, statistical analyses, visualization, or comparison with given design data, e.g. model test or CFD powering performance results. For the shown example, filtering is implemented, according to the given operational status of the ship. This ensures, that only conditions with the ship in sea-passage are further analysed. In the data evaluation of *Greitsch et al. (2016)* the validity of operating conditions of the propeller is checked by plotting the measured torque on the propeller shaft into the propeller open water characteristics in order to see, if it is inline. The measured torque and its corresponding advance number is therefore derived by using the relative rotation efficiency and wake fraction of the design data. Of course this approach is defective, as these data is also dependent on the operational condition of the ship itself. However it gives a fast overall picture of the quality of the operational data. Fig.9 shows the propeller open-water characteristics and the N2N operating conditions of the first journey. As the IM has all relevant measured and reported entity of the dataset available, it is easy to plot additional information into the plot, e.g. measured draught. The evaluation of Fig.9 indicates, that derived torque coefficients of the N2N-data mostly reported within a range of 5% to the CFD results, which usually indicates that the dominance of the data points can be used for more detailed analysis. Furthermore, it is shown the N2N condition in the engine diagram. The N2N data points also follow the power curve for the service prediction. Only single points exceed the nominal power curve, which indicates heavy running.

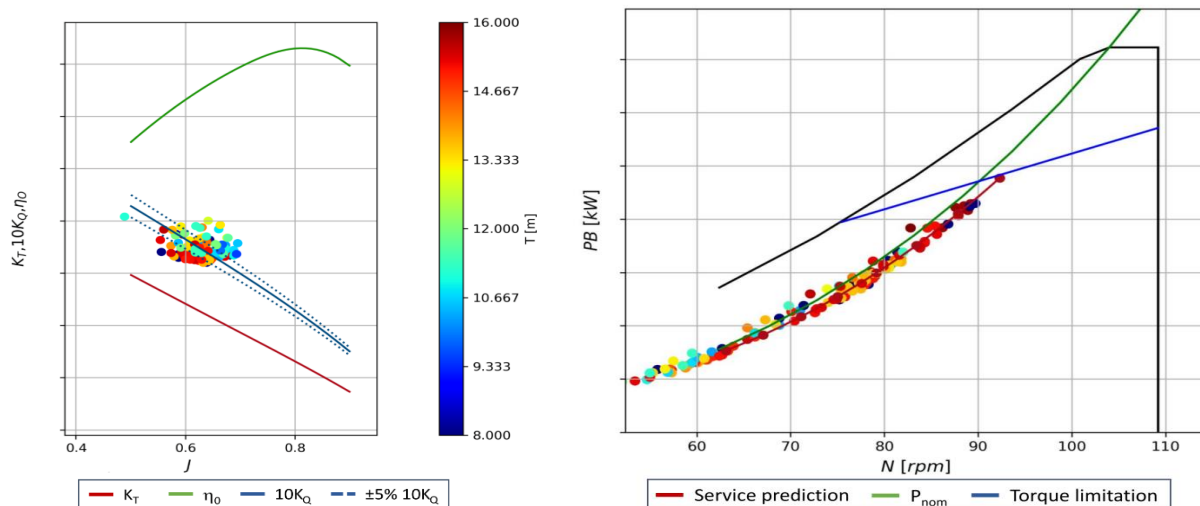


Fig.9: N2N data in comparison with propeller characteristic and engine diagram: scattered points are reported N2N-condition.

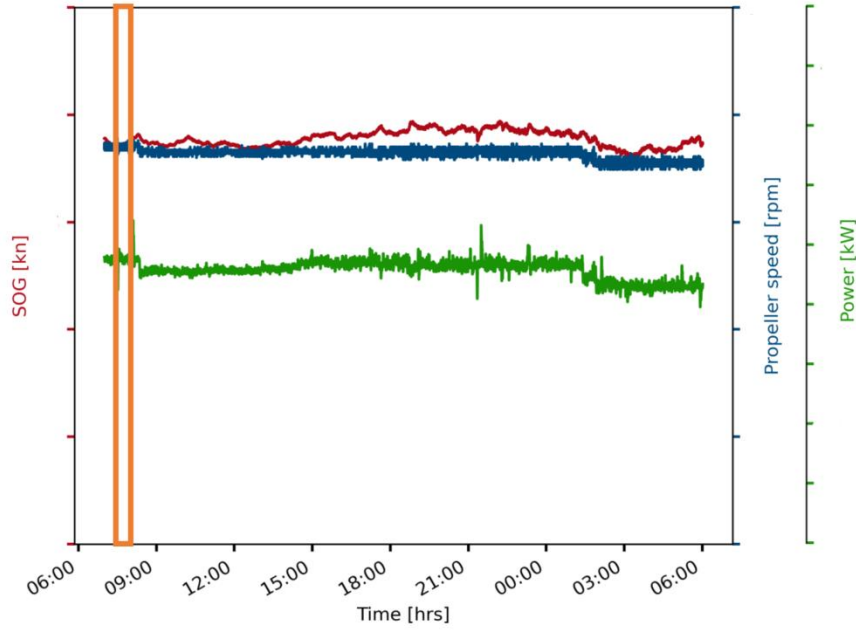


Fig.10: Measured high frequency data for evaluation of ship performance

In the derived ship operation core model, the measured high frequency data is directly linked to the operation periods. Therefore, these data are easily accessible for more detailed analysis. Fig.10 shows the high frequency data of one day at sea. In the Figure the relevant data of speed over ground, propeller speed and power are plotted over the time. During the day at sea the wind condition has changed and also the propeller speed has been adopted over time. Hence the assigned N2N condition is not good for the performance evaluation. With the derived ship core model and its implementation as a python module it is easy to classify the data according to other criteria, e.g. changing weather conditions, constant propeller speed. From the high frequency plot in Fig.10 a smaller averaged time window can be derived, which give a clearer view, than the N2N data.

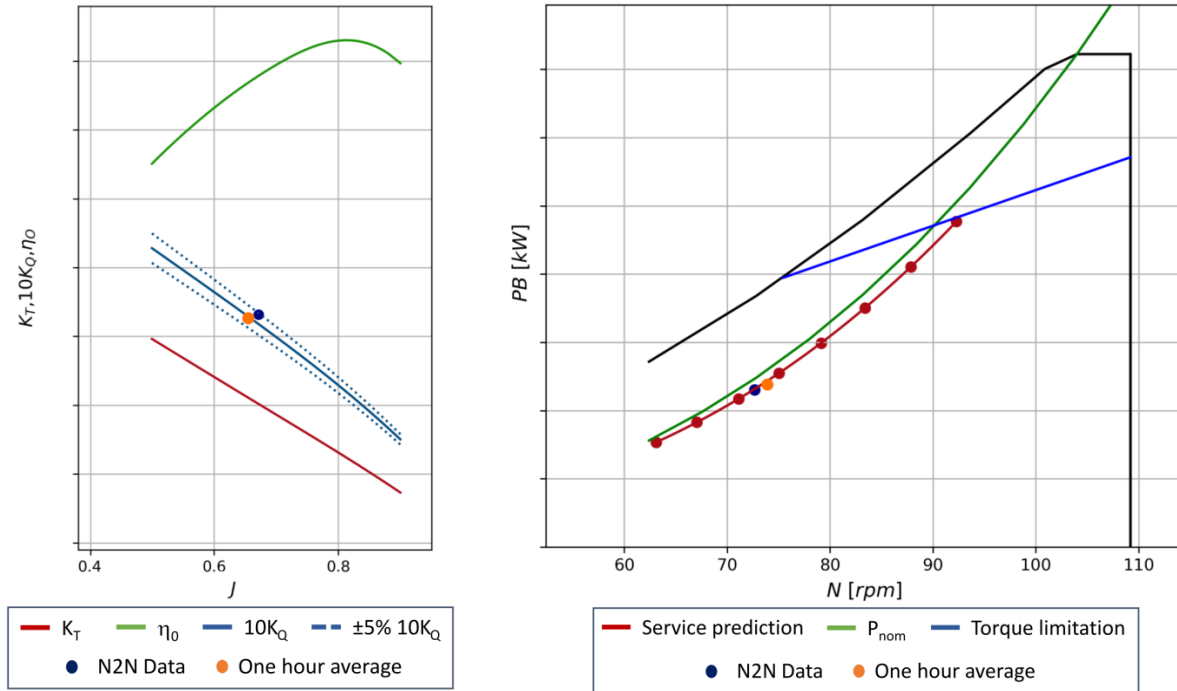


Fig.11: Compared N2N-data with one hour time span for a day at sea in propeller open-water characteristics and engine diagram

Fig.11 shows the result of performance average of one hour taken at the highlighted orange frame of Fig.10. Due to the average over more constant condition the data is more valid when compared with the design data. Additional valid operating conditions can be found even in invalid N2N-data, thanks to the combination with high frequent data. The system can also give detailed view, why the N2N-data of single points is invalid, when compared to design information of the ships propulsion system. Furthermore filtering, comparison and cross correlation with additional onboard measurements are possible as well as with AIS data and external weather information.

The derived system opens the possibility to easily implement multiple functions on the performance evaluation over time of the ship. Hence the system will be enhanced to analyze operational data based on methods described by *Dalheim and Steen (2020)*, *Oliveira et al. (2018)* and *Baumfalk (2017)* or even more in order to give the industry a more valid view on the real performance of the ship over time.

5.2. Example-2

The second example deals with correlated data of the engine. The data is taken from the high frequency measurements of the first voyage stored in the data base. Fig.12 presents the sensor data of velocity (over ground and through water), the shaft speed and the main engine's break power. Based on the main engine's torque measurements, the figure illustrates results for a calculated engine power. Furthermore, the power is normalised by the ship speed, water density and cross section of the ship to obtain the power coefficient. Each of these quantities is shown for the same time frame of 6 h. The calculated and measured engine break power fit very well to each other. However, there are small differences at peaks (visible only using a zoom on the data). These small differences are expected as the calculated power relies on two different sensors for shaft speed and engine torque.

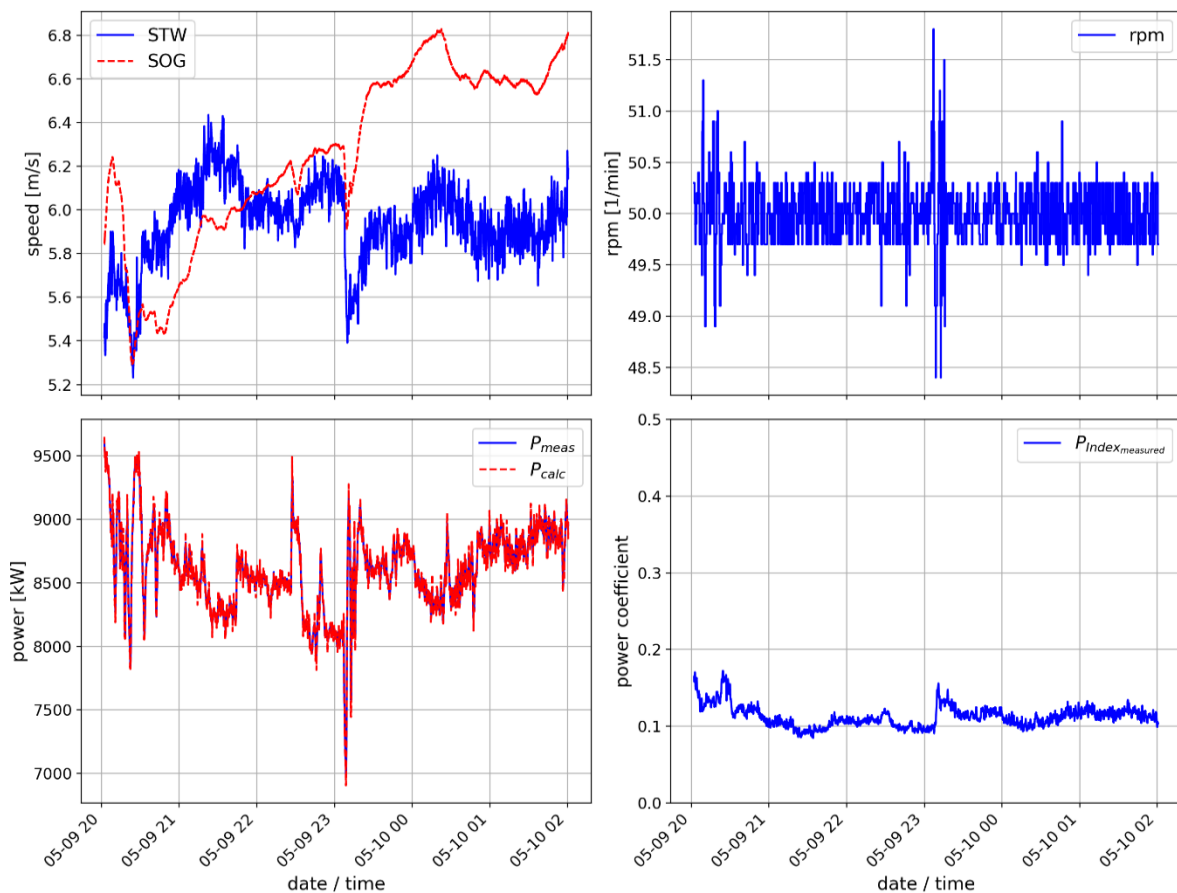


Fig.12: High frequency sensor data from ship speed (STW- through water, SOG – over ground), shaft speed (rpm) and engine break power plotted together with calculated power and power

coefficient for a time frame of 6 h.

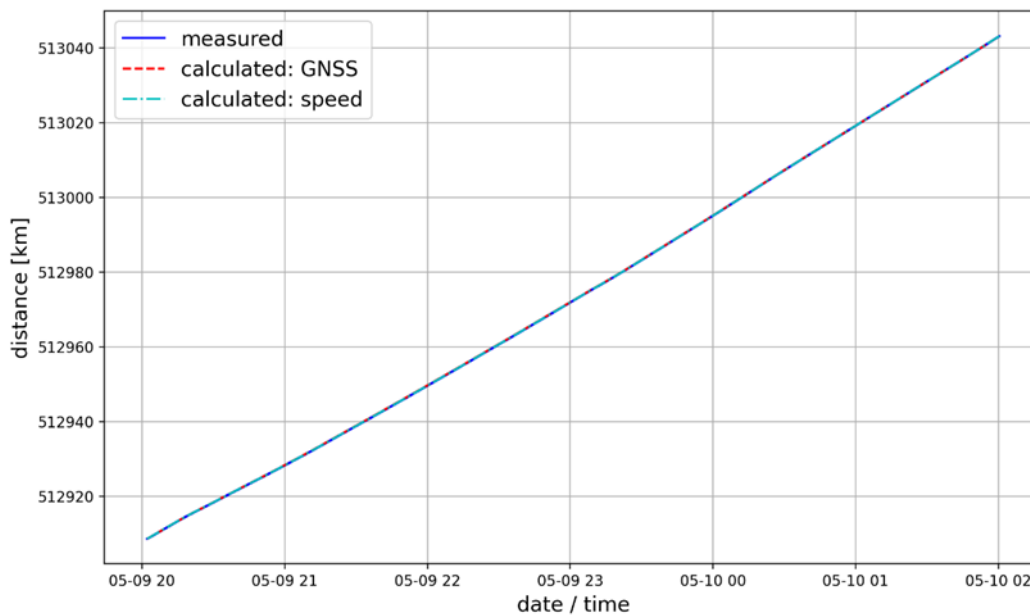


Fig.13: High-frequency sensor data of distance over ground compared to calculations of distance over ground based on ship speed and GNSS coordinates

Three further data sources were correlated to extend this example for the same time frame. Fig.13 presents the relation between the distance over ground sensor (measured), the speed over ground (calculated: speed) and the GNSS coordinates (calculated: GNSS). The speed over ground and the GNSS coordinates were used to calculate the distance of travel of the ship.

The distance between two coordinates was calculated based on Vincenty's formulae. The ship speed was simply integrated over time to obtain the distance. The three results overlap each other.

The two examples demonstrate ways for fast and good correlation procedures. These procedures support the establishment of a data base with reliable data.

6. Conclusions and Future Work

The development of a unified data model for the integrated modeling and management of comprehensive ship operational data at low/high-frequency, including correlated location- and time-dependent environmental conditions, is presented in this paper. Providing synchronized and high quality ship operational data and identifying correlations between these different data collected from different sources with different frequencies is one of the main contributions of this paper. Exemplary evaluations of ship performance parameters using the structured processing approach of the developed model are introduced.

Future work of the research project will include sensor checks. These checks are based on trustworthy limits for extreme values and data changes as well as direct comparison between similar sources, i.e. navigation, machinery, IMU, tank gauging, etc. This enables the evaluation of several mathematical formulations to forecast operational performance of the ship. The formulations include estimation methods for ship resistance in calm water, in waves and wind as well as in manoeuvring and shallow water conditions. The engine power and fuel consumption may be predicted subsequently due to reference data of the propulsion system. Post-processing of the data is required to obtain a smart data base with reliable sensor information. In order to validate this approach, the predicted results will be compared against the data base. Data will be clustered into different operational conditions. Investigations of the influence of physical factors on the ship resistance and accordingly the fuel oil consumption are possible using the mathematical formulations and the clustered data. These factors

could be e.g. fouling of the ship hull, maintenance periods or hull optimisation.

Acknowledgements

The authors wish to express their gratitude to the German Federal Ministry for Economic Affairs and Climate Action (BMWK) and Project Management Jülich (PtJ) for funding the joint research project "DigitShip - Acquisition, analysis and utilisation of operational data for efficient and safe ships" (FKZ 03SX514)

References

BAUMFALK, H. (2017), *Assessment of ISO 19030 based on operational data of a container vessel*, Master thesis, Univ. Rostock

CHEN, P. (1976), *The entity-relationship model toward a unified view of data*, ACM Transactions on Database Systems

DALHEIM O.; STEEN S. (2020), *Preparation of in-service measurement data for ship operation and performance analysis*, Ocean Engineering J. 212

DOS SANTOS FERREIRA, R. (2018), *Sensitivity Analysis of Added Power of Ships in Seaway*, Master thesis, Univ. Rostock

GREITSCH, L., GOEDICKE, T., PFANNENSCHMIDT, R. (2016), *Numerical Towing Tank versus Noon Data – Powering predictions using RANSE CFD*, 1st HullPIC Conf., Castello di Pavone

OH, M.J.; ROH, M.I.; PARK, S.W.; CHUN, D.H.; SON, M.J.; LEE, J.Y. (2021), *Operational Analysis of Container Ships by Using Maritime Big Data*, J. Marine Science and Engineering

OLIVEIRA, D.; GRANHAG, L.; LARSSON, L. (2018), *Performance Values vs. Speed – A Declaration of Independence?*, HullPIC Conf., Redworth

PATEY, M. (2019), *Performance Monitoring Information Feedback to Design*, HullPIC Conf., Gubbio

WAGNER, J. (2017), *Scenario-based Optimization of Merchant Vessels*, Dissertation, Univ. Rostock

ZHANG, M.Y.; MONTEWKA, J.; MANDERBACKA, T.; KUJALA, P.; HIRDARIS S. (2021), *A big data analytics method for the evaluation of ship – ship collision risk reflecting hydro-meteorological conditions*, Ocean Engineering J. 213

Comparing Hydrodynamics of Original and Remodeled Hull Forms and Appendages for Digital Twins

Stefan Harries, FRIENDSHIP SYSTEMS, Potsdam/Germany, harries@friendship-systems.com

Fabian Thies, FRIENDSHIP SYSTEMS, Gothenburg/Sweden, thies@friendship-systems.com

Simon Hauschulz, FRIENDSHIP SYSTEMS, Potsdam/Germany, hauschulz@friendship-systems.com

Jochen Marzi, HSVA, Hamburg/Germany, Marzi@hsva.de

Scott Gatchell, HSVA, Hamburg, Gatchell@hsva.de

Abstract

The paper presents a study on how and at what level a ship hull, its propulsion system and key appendages need to be remodeled if no digital representation is readily available when setting up a digital twin for hydrodynamic assessment for the evaluation of the performance of a vessel. The reengineering of an existing ship with standard CAD modelling techniques does not pose a major challenge in itself but still requires a lot of input data and many hours of interactive work. Two major bottlenecks can be identified: Firstly, gathering sufficient and reliable input data is difficult if not impossible, especially in a pre-contract stage. Secondly, labor intensive, long and costly process will not allow for making decisions under time pressure. Consequently, it is important to understand which level of modelling accuracy is required for what type of assessment. Looking into different application scenarios, the necessary quality for remodeling and consecutive analysis is identified in the present study. This will lead the way towards an efficient assessment process, vital in the overall quest to optimize ship and shipping performance also at fleet level.

1. Introduction

In the maritime industry, as in other industries, too, digital twins are introduced and utilized both increasingly often and more widely so as to improve the performance of a physical asset by means of measurements (e.g. from onboard sensors) and models (i.e., computer representations). The common aims are to (i) better understand the performance of the asset, say a ship as a whole or several of its systems, (ii) study possible ways of improving it and (iii) predict and optimize operational behavior (e.g. with regard to scheduling maintenance, avoiding failure and improving energy efficiency).

Typically, ships integrate numerous systems onboard and many different aspects are of interest, from safety and structural integrity to energy efficiency and economics. Therefore, it can be readily appreciated that presently there are no unified, all-encompassing digital twins at hand. However, specific digital twins are already employed, at least at (sub-)system level. One common bottleneck for a ship's operator is that many important pieces of information that would be required to develop a more complete picture of an asset are not available or not made available.

Very importantly, many shipyards do not provide a mathematically closed definition of the ship's hull form, its appendages and the propulsion system. This is understandable since a lot of intellectual property rights (IPR) and competitive advantage are associated with these shapes. Nevertheless, for the operator this means that those entities which are most decisive for typically 80% or more of the energy consumption – and, hence, for green-house gas emissions and operating costs – are not captured accurately. As a typical fallback position only a few global parameters, primarily the main dimensions, are used to describe the hull form as a basis for hydrodynamics and performance predictions using simplified regression analysis or series data.

A complete reengineering of the ship hull and all other important functional surfaces can be undertaken if sufficient input data are available by developing a closely approximating CAD representation, see *Hansen and Hochkirch (2013)*. Two important questions, however, arise: Firstly, what level of accuracy would actually be needed and, secondly, how could the right level of accuracy be achieved quickly and economically.

This paper is intended to shed light on this by way of an example taken from the German R&D project MariData, <https://maridata.org>. A tanker operated by one of the project's partners, Carl Büttner Shipmanagement, is reengineered at different levels of accuracy on the basis of suitable parametric models within CAESES®, *Harries et al. (2015)*. Different hull form approximations are hydrodynamically analyzed by means of HSVA's database of model tests for similar vessels and, very importantly, high-fidelity CFD simulations. The results of the different analyses are systematically compared and, in addition, benchmarked against full scale predictions based on model tests for the actual geometry as designed. The levels of remodeling and their input requirements will be discussed.

2. Remodeling of geometry for digital twins

2.1. Specific task

Within the MariData project a tanker of 183 m length over all, 32 m maximum beam, 16 m depth, a design draft of 9.50 m (scantling draft of 10.5 m) and a cargo capacity of about 45 000 m³, Fig.1, is studied with regard to its energy consumption. The ship is an oil-chemical tanker, the CB Adriatic (called CBT for brevity), was built in 2019 after having been jointly optimized for its operational profile, i.e., for multiple speeds and drafts. The hull features an asymmetric stern, the propulsion system a tip rake propeller and the rudder a Costa bulb. Results from model tests showed a performance in the top of its class.



Fig.1: CB Adriatic (oil-chemical tanker, IMO 9851696), operated by Carl Büttner Shipmanagement

The project's aim is to set up a digital twin in order to compare consumptions as computed by means of simulations and as measured onboard and to suggest how to further improve energy efficiency. To this end the ship's hydrodynamic performance needs to be simulated for many different operational scenarios, e.g. in calm water, in sea states representative of its operational profile, in both deep and shallow waters, when maneuvering and when under the influence of heavy winds and current. As can be readily appreciated, this calls for suitable geometric representations of the ship hull, the propulsion system, appendages and the superstructure.

2.2. General situation

In an ideal world, the actual geometry of the ship as-built would be digitally available. Unfortunately, for the owner or operator of a ship that is rarely the case. There are methods to scan large structures, see e.g. *Blom and Czapla (2021)*. However, they require post-processing in order to provide useful input for further analysis, e.g. numerical ship hydrodynamics (CFD). Data reduction and repair work in a CAD system such as meaningfully filling up blind spots, bridging holes and removing overlaps are

necessary. In general, recreating geometry is either time consuming, see *Bertram and Harries (2022)*, or subject to unknown inaccuracies. A meaningful industrial approach needs to find the right compromise between necessary effort and required accuracy for a given task.

In general, for digital twins a wide range of representations can be considered, starting with low level geometric models that just need the ship type and some main dimensions as input, hereafter called level 0, and going up to higher level representations that closely capture the vessel as it performs in real life. Fig.2 illustrates that three levels may be distinguished by the level of certainty (inversely, the uncertainty) of the predictions rather than by the comprehensiveness of the input data available. Importantly, it is neither readily obvious what level of geometric accuracy is actually needed for which type of analysis – e.g. comparison between simulations and measurements – nor by which level of geometric representation the performance analysis lies within an acceptable level of certainty. Therefore, it is to be elucidated, at least by means of an elaborated example, what can be considered “suitable” in remodeling. (N.B. A single example clearly will not suffice to draw general conclusions. Nevertheless, it is a starting point.)

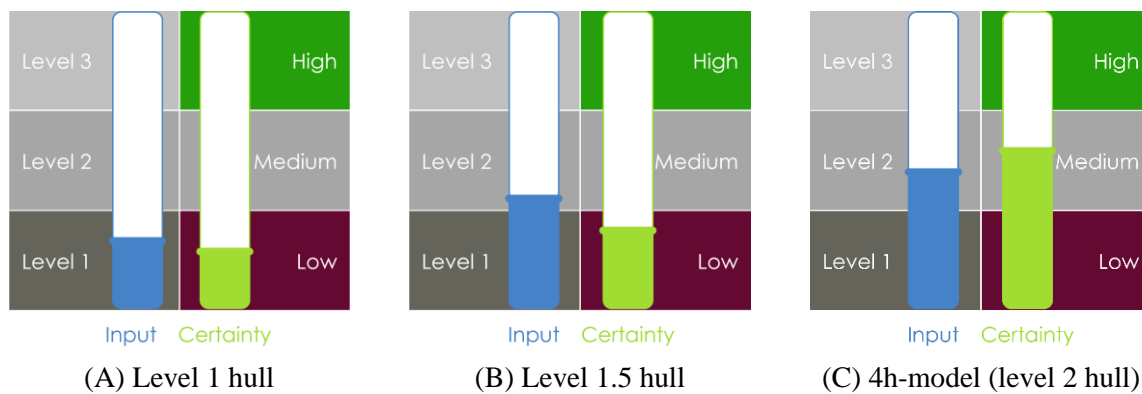


Fig.2: Ambiguity of various levels of input leading to different approximation levels of geometry and achieved certainty with regard to the accuracy of hydrodynamic predictions

As can be appreciated from Fig.2 the amount of geometric input and the resulting (un)certainty of achieving a specific level of hydrodynamic accuracy are not defined precisely. They depend on the ship type and to some extent on the operational profile and conditions. Nevertheless, for the sake of easier communication only three levels shall be considered. For a proposal of definitions see Table I. They follow design considerations as introduced by *Tillig et al. (2017, 2018)* and take into account the analyses of prediction of resistance and power by *Kristensen and Lützen (2013)*.

3. Representations of the ship hull

Various parametric models and approaches of remodeling were created. In the present study, four ship geometries are presented and evaluated:

- The ship hull as model-tested (called original and/or benchmark)
- A ship hull as remodeled parametrically in an automatic procedure within seconds, with data publicly and easily available (called level 1)
- A ship hull as remodeled parametrically in an automatic procedure within seconds, with more detailed data typically available to the owners and/or operator, for instance, data from the loading manual, requiring at most half an hour of work to compile the input (called level 1.5)
- A ship as remodeled interactively by a specialized naval architect within four hours, using an alternative parametric model and data from a digital general arrangement plan, selected inputs from the loading manual and about ten sections provided from 2D-drawings along with flat-of-side and flat-of-bottom curves as well as the center plane curve (called the 4h-model for the sake of easy understanding, corresponding to level 2)

An illustration of these levels is given in Fig.2. Note that level 0 as defined in Table I does not require any actual shape and, hence, no remodeling needs to take place. Furthermore, no level 3 has been studied so far as this would call for operational data to be considered. Finally, it should not be forgotten that there possibly are non-negligible differences between the hull as model-tested and the ship hull as built at full scale.

Table I: Proposed definition of approximation levels for ships typical of the fleet of similar ships (assuming the ship in question does not show uncommon design features)

Appr. Levels	Description	Accuracy of geometry (for hull forms)	(Un)certainity of hydrodynamics
Level 0	<ul style="list-style-type: none"> Main dimensions used in statistical approach 	<ul style="list-style-type: none"> No actual shape produced 	<ul style="list-style-type: none"> Series data and/or historical tank data
Level 1	<ul style="list-style-type: none"> Only the main dimensions are known (similar to concept phase) In addition, DWT and brake power of the main machine are given Design speed must be given 	<ul style="list-style-type: none"> The maximum section and the parallel midship section, if present, can be captured accurately if the bilge radius and the deadrise are known Displacement may be wrong by 5% 	<ul style="list-style-type: none"> Accuracy (standard deviation) is greater than 12% of the expected absolute value of fuel consumption Relative accuracy, e.g. with respect to trim, should be half of the absolute accuracy
Level 2	<ul style="list-style-type: none"> Level 1 plus data from general arrangement Selected geometries (e.g. bow and stern contours, maximum section and sections in fore- and aftbody) Quantities from loading manual (e.g. XCB) 	<ul style="list-style-type: none"> Maximum deviation between designed and modeled geometry should be $\pm 0.05\%$ to $0.1\% L_{PP}$ for most parts of the hull Overall displacement can still be wrong by 1%, except for those drafts for which it serves as input 	<ul style="list-style-type: none"> Accuracy of the expected absolute value should be between 4% and 12% Range of relative accuracies should be half of absolute accuracy
Level 3	<ul style="list-style-type: none"> Level 2 plus additional data, such as <ul style="list-style-type: none"> data from model tests data from sea trials measurements during operation Laser scans of the hull, rudder, propeller, etc. 	<ul style="list-style-type: none"> Difference of the remodeled ship behaves like the difference of the originally modeled ship to the ship as-built 	<ul style="list-style-type: none"> Accuracy of actual fuel consumption below 4% Relative accuracy below 2%

3.1. Ship as model-tested

The benchmark for geometry and hydrodynamics is the model as originally tested at Hamburgische Schiffbau-Versuchsanstalt (HSVA) on behalf of the design office. Here, a very close fit between the digital representation and the fairly large model is attained. According to ITTC Recommended Procedures and Guidelines 7.5-01-01-01 model tolerances should be within ± 1 mm for beam and draft and max. $0.05\% L_{PP}$ for the length of a model. Having installed a thorough inspection procedure for the manufacturing of scale models, HSVA can typically ensure an accuracy of less than 1 mm for its models in all three dimensions. Based on the CBT's model scale of 26.6 this yields a rather low value of ± 0.026 m for the maximum deviation at full scale.

Fig.3 shows the CBT at HSVA during a calm water test at design draft while Fig.4 gives a perspective view of the original hull.

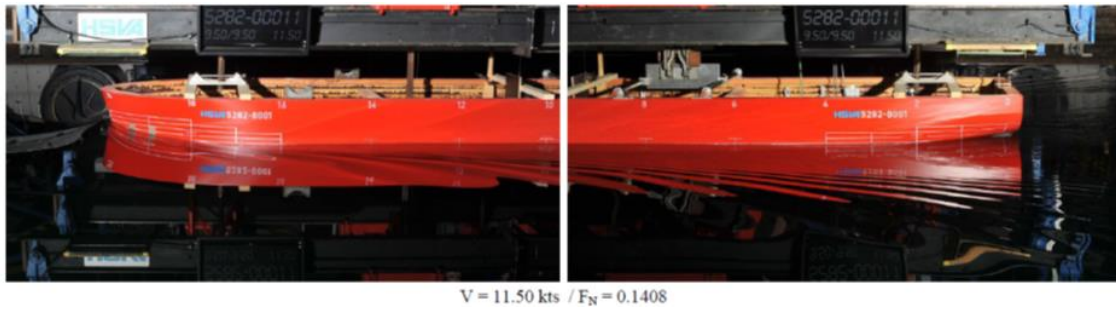


Fig.3: Model test of CBT at HSVA

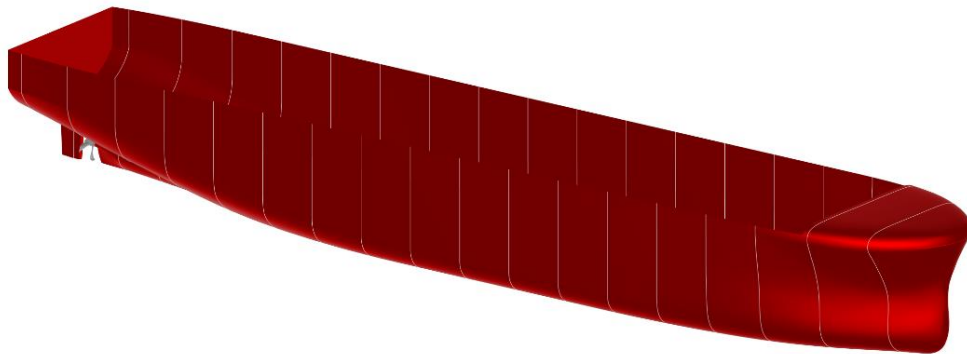


Fig.4: Original hull form as model-tested

3.2. Ship as remodeled within seconds from level 1

The level 1 hull is based on information publicly available, i.e., the length over all (LoA), maximum beam (B), draft (T), deadweight (DWT), ship speed (preferably design speed, if available) and some general information about the ship such as whether or not the hull features a bulbous bow. With the above-mentioned information available, a CAD model of a suitable hull form can be created within seconds, using a sophisticated parametric model.

Such a flexible parametric model, including numerous estimation formulas to calculate any missing dimensions (e.g. the displacement from deadweight), was developed in CAESES® and is used to generate what could be seen as a standard series hull matching the given input parameters. The parametric model itself was developed by evaluating several representative hull forms. Within the model, the forebody, the length of the parallel midbody, the waterline fullness, bilge radius, longitudinal center of buoyancy and longitudinal center of flotation are estimated to represent a common ship of such size and to ensure a good quality hull, i.e., a hull with a hydrodynamic performance which will be among a representative average of recently designed ships. Some parameters, for example, the sectional fullness below the waterline in the fore- and aftbody, are free for adjustment using automated optimizations to match the models hydrostatics to the desired values.

Infrequent (but desirable) design features such as an asymmetric stern are not modeled at this level. Fig.5 presents a rendering of the level 1 hull using the input data of CBT (see also Table I). It should be noted that the remodeling at level 1 took place without utilizing any non-public data.

3.3. Ship as remodeled within half an hour with higher level of information (level 1.5)

The level 1.5 hull is based on the same parametric model as the level 1 hull with the difference that the displacement volume V and the longitudinal center of buoyancy XCB at design draft are prescribed as additional input. Half an hour of work is assumed to be (more than) sufficient to study the loading manual, if available, and to identify V and XCB at, say, design draft. This ensures that the hull, at least at one suitable draft, has similar hydrostatics as the original hull, Table II.

Since within the parametric model the center of flotation (XCF) is determined via an offset from the center of buoyancy it slightly changes compared to the level 1 hull, too. However, the parallel midbody and the length of the forebody are not be affected as those are based on hydrodynamic considerations built into the parametric model already, i.e., the model, even though still at low level, assumes certain parameters according to good design practice.

Naturally, the waterline and sectional fullness of the two hulls will be different. However, in the present case, the differences between level 1 and the level 1.5 are small, since the estimated displacement and center of buoyancy were already pretty close to the original values, Table II. Fig.6 shows a rendering of the level 1.5 hull. The resemblance to the level 1 hull shown in Fig.5 is apparent.

In order to get an appreciation between the differences in geometry Fig.8 presents an overlay of the original and the level 1.5 hull. The overall approximation is pretty fair while there are differences in the fore- and aftbody. The midbody is closely approximated even though the bilge radius was not used as an input.

3.4. Ship as remodeled interactively within four hours

For ship owners and operators more detailed information about the ship in service is often available, for instance, a general arrangement plan (GA), a loading manual (stability book), a model-test report etc. In most of these documents some drawings and valuable information about the geometry can be found, often as planar curves which can be used to remodel (parts of) the ship hull.

For that purpose a second flexible parametric model was created in CAESES® that can be adjusted to a handful of sections and important planar curves such as the center plane curve (CPC), the flat-of-side (FoS) and the flat-of-bottom (FoB). The model is deliberately kept simple and utilizes only

- a flat-of-side surface,
- a flat-of-bottom surface,
- two surfaces for the fore- and aftbody, respectively, and
- a surface for the parallel midbody.

For the CBT the information was extracted from both the GA and the loading manual which were provided in digital form. The following geometric curves were defined using the available 2D-data: FoS and FoB, the CPC of stern and stem, the maximum section plus five sections for the fore- and aftbody, respectively. In order to simplify the remodeling work and keep it within the four hours assigned to it, the CBT's asymmetric aftbody was deliberately neglected and a standard stern, corresponding to the level 1 hull, was utilized.

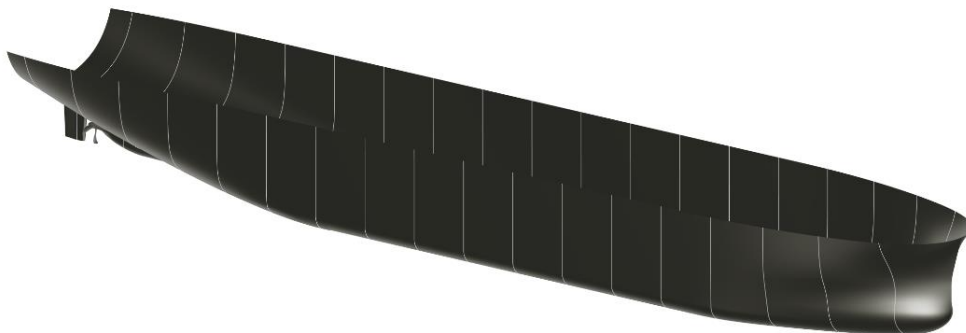


Fig.5: Level 1 hull

Fig.7 shows a rendering of the resulting hull. The geometry is significantly different from the level 1 and level 1.5 hulls and follows the original hull very closely, despite the still rather limited geometrical input. This ensures a hull that features similar hydrostatics and hydrodynamics. However, even such a

4h-model would still require more interactive work and the incorporation of more pieces of information along with additional fairing to fully match the original hull, tangibly increasing the overall time needed.

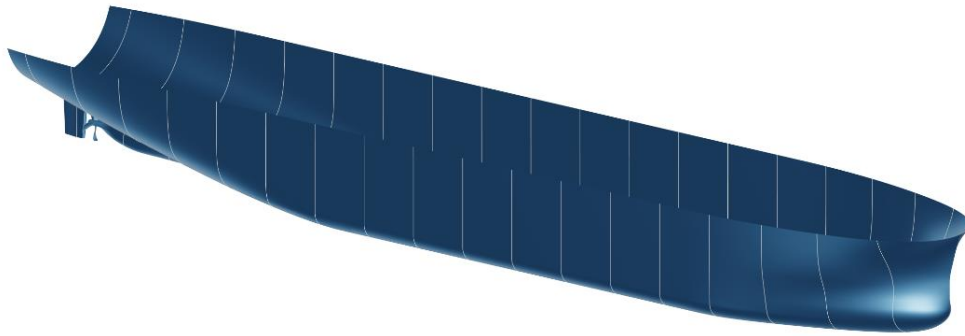


Fig.6: Level 1.5 hull

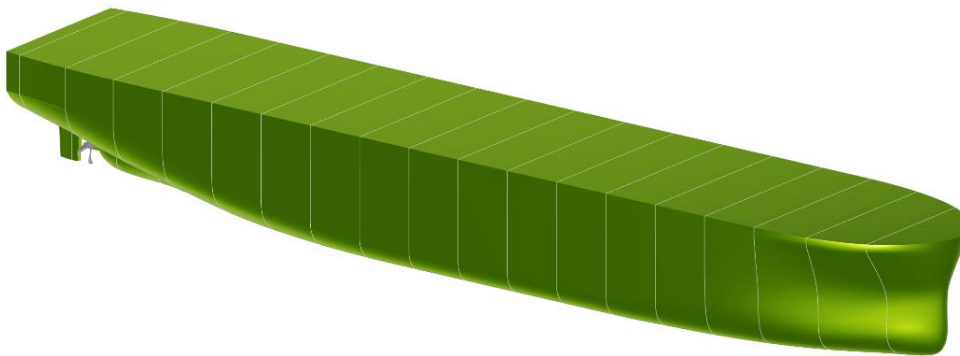


Fig.7: 4h-model (level 2 hull)

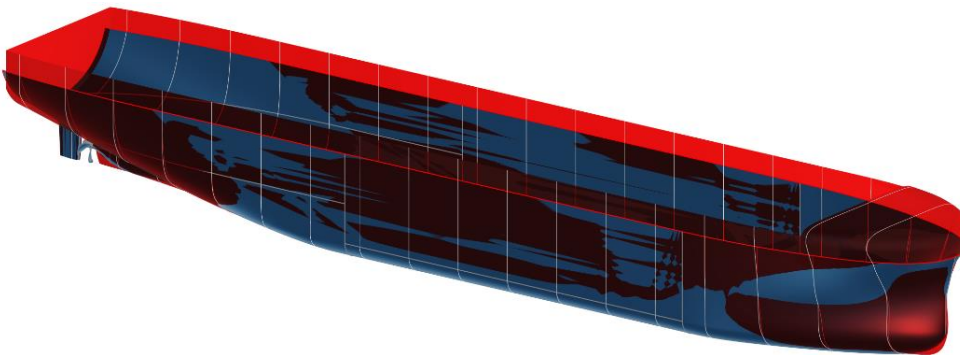


Fig.8: Original (transparent and red) vs. level 1.5 hull (blue)

3.5. Comparison of hydrostatics

In order to understand the differences between the original and the approximated hull shapes a bit better the relative displacement volume as well as the relative longitudinal center of buoyancy vs. relative draft are shown, Figs.9 and 10, respectively. The data are normalized by the original hull's values at the design draft of 9.5 m. (Neither absolute values nor sections can be given for reasons of protecting the design office's intellectual property rights.)

Both the displacement distribution and the position of the longitudinal center of buoyancy differ over draft. The average deviation between the displacement of the level 1 hull and the original hull form is +2.7%, i.e., the educated guess of displacement derived from deadweight turned out to be a little too high. The average deviation of the level 1.5 hull is lower with 0.7%. This is not a surprise since the displacement at design draft as taken from the loading manual was utilized as an input. The difference between the original hull and the 4h-model with respect to displacement are negligible as would be expected since offset data for several sections in both the fore- and aftbody were closely approximated.

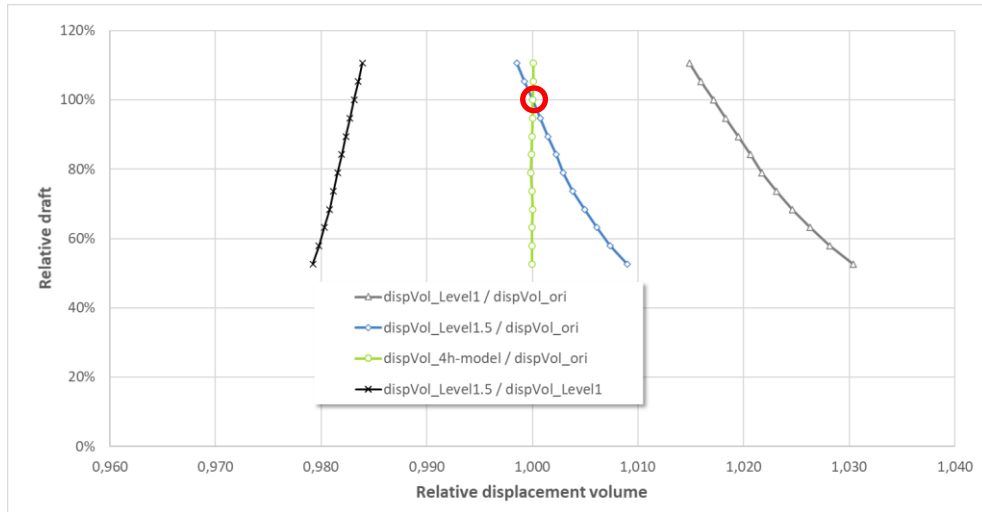


Fig.9: Relative displacement volume (abscissa) vs. relative draft (ordinate), i.e., draft over design draft, between approximating models of different levels and original hull form

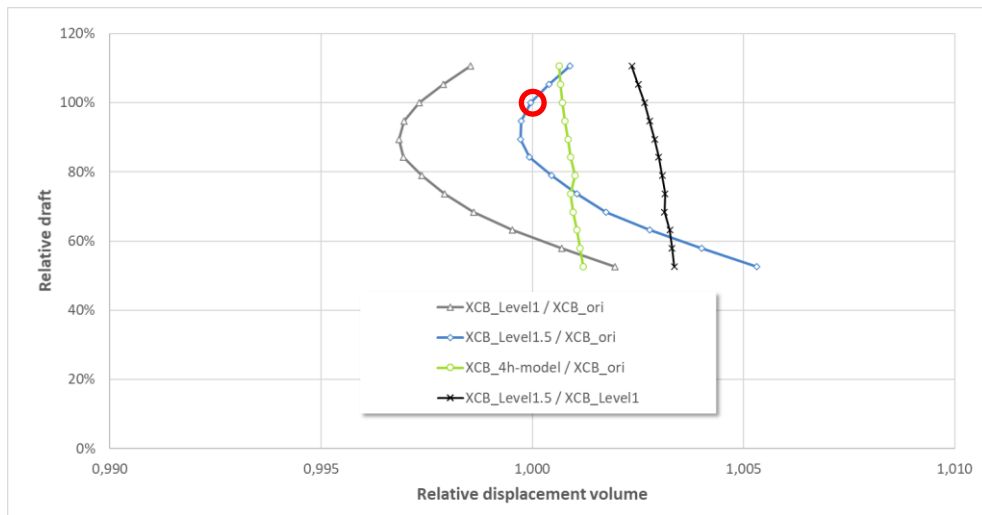


Fig.10: Relative longitudinal center of buoyancy (abscissa) vs. relative draft (ordinate), i.e., draft over design draft, between approximating models of different levels and original hull form

Besides, integral values are usually less sensitive than positional data as many small errors tend to cancel out. It should be noted, that at level 1.5 the displacement and XCB are only defined at design draft (highlighted in green in Table II) and the hydrostatics at all other drafts necessarily differ, see Figs.9 and 10 as well as Table II.

Tab. II: Hydrostatics data of approximating hulls in comparison to original hull for design draft (9.5 m on even keel) and ballast draft (5.5 m at AP and 7.5 m at FP)

Hydrostatics	Original hull (reference)	Level 1 hull	Level 1.5 hull	4h-model
Displacement V at ballast draft	100%	102.68%	100.65%	99.98%
Displacement V at design draft	100%	101.72%	100.00%	100.01%
Center of buoy. XCB at ballast draft	100%	99.88%	100.28%	100.12%
Center of buoy. XCB at design draft	100%	99.73%	100.00%	100.07%
Metacentric height GM at design draft	100% [5.05m]	95.84% [4.84m]	95.84% [4.84m]	100.99% [5.10m]
Wetted surface area S at ballast draft	100%	102.86%	101.37%	99.79%
Wetted surface area S at design draft	100%	101.74%	100.52%	99.84%

Three more data items are given in Table II, namely, the initial stability at design draft expressed as the metacentric height GM at design draft and the wetted surface area S at both ballast and design draft. With regard to the wetted surface area Fig.11 illustrates what levels of approximation could be rightfully

expected if no geometry was available, corresponding to level 0 in Table I. At level 0 only main dimensions are used, *Kristensen and Lützen (2013)*, but even some of these inputs, like the block coefficient, would commonly have to be estimated, too. For the CBT of about 180 m the uncertainty for S at level 0 would amount to approximately -1.5% to $+6\%$. This would naturally result in similar error levels when approximating frictional resistance. (Also see Fig.22 for error levels when using a standard series.)

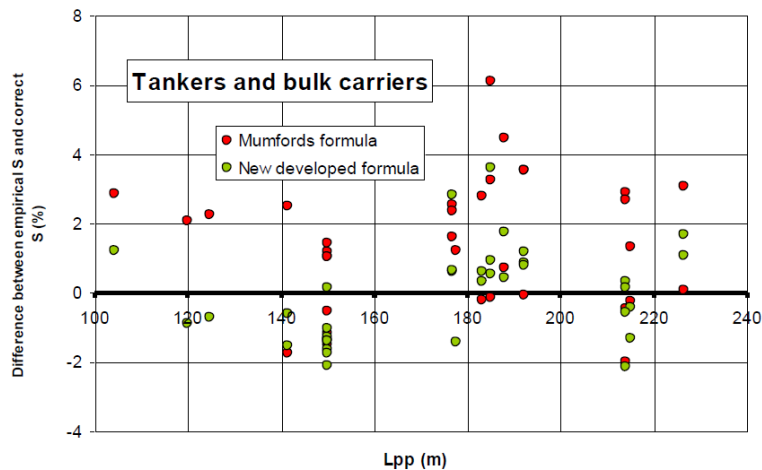


Fig.11: Difference of wetted surface area from empirical formula to correct values, reproduced from Fig. B11, *Kristensen and Lützen (2013)*

4. Representations of the propeller and rudder

4.1. Propeller as remodeled within half-an-hour (level 1)

A fast remodeling of an equivalent propeller, corresponding to a level 1 approximation for hulls, Table I, can be undertaken with the webApp <https://www.wageningen-b-series-propeller.com/>, as introduced by *Harries et al. (2018)*. Only very limited data, publicly available or estimated via a naval architect's educated guesses, serve as input: Propeller diameter, number of blades, expanded area ratio, material, engine output per shaft, rpm, gear ratio, design speed and wake number. Fig.12 shows the propeller generated from FRIENDSHIP SYSTEMS' openly accessible Wageningen webApp. The aftship is that of the level 1 hull.

Note that for level 1 and level 1.5 as well as for the 4h-model a symmetric aftbody was assumed. The propellers direction of rotation for the level 1 approximation is clockwise (seen from the stern). The real propeller for the CBT's asymmetric aftbody, however, rotates counterclockwise. Furthermore, it should be kept in mind that the skeg and bossing differ quite a bit from the original geometry.

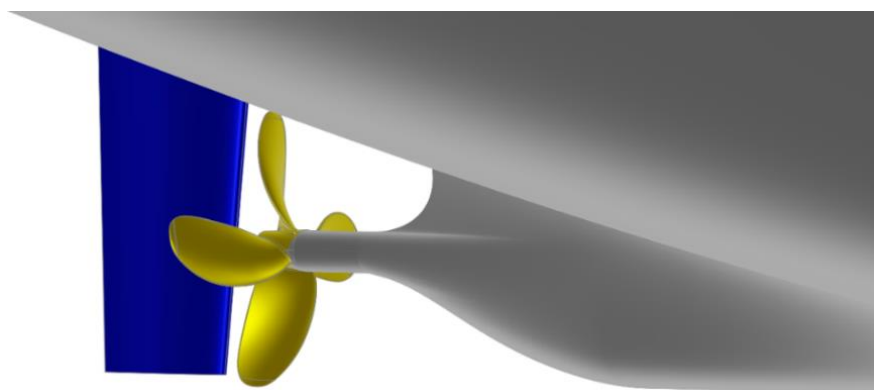


Fig.12: Level 1 remodeling for aftship, propeller (Wageningen) and rudder (as needed for CFD) (higher levels of remodeling cannot be shown here due to confidentiality constraints)

4.2. Propeller as model-tested and used at full scale (level 3)

The CBT's propeller was developed by experts from a large engine manufacturer and thoroughly studied within a model-test campaign. It is a high-efficiency tip-rake propeller adapted to the tanker's wake field. Due to reasons of confidentiality and protection of intellectual property rights it cannot be shown here.

The propeller blade was closely fitted within CAESES on the basis of an independently developed fully-parametric model dedicated to these specialized propeller types. It can be regarded as a level 3 approximation, Table I. The actual remodeling process, using a digital representation of the propeller as built, took a few days of interactive work to ensure a close match. This can be viewed as a representative example in which modeling skills and very advanced CAD functionality need to be brought together for a thorough representation, not necessarily targeting a process of high efficacy but rather of high quality.

The level 3 propeller will be used in various detailed simulations for the MariData project. However, for the present power predictions a simplified approach of an actuator disc was chosen.

4.3. Rudder as remodeled within half-an-hour

A fully-parametric rudder model is used within CAESES to represent the CBT's semi-balanced rudder. The model allows switching between a semi-balanced rudder with skeg, Fig.13 (left) and a spade rudder, Fig.13 (right), by changing a single topology parameter while maintaining all other dimensions and the rudder profiles. In addition, the rudder can feature a Costa bulb, Fig.13, or can be generated without any further energy-saving devices, Fig.12.

The input required again is limited, namely, the rudder's height, chord length at both top and bottom, thickness at both top and the bottom, sweep angle plus profile type (NACA, HSVA, custom profile). A headbox that relates to the rudder's top can be projected onto the stern region of a hull's aftbody to ensure direct connectivity. For purposes of numerical flow simulations gaps can be readily closed, Fig.12.



Fig.13: Rudders generated parametrically within CAESES

5. Hydrodynamic analyses and comparison between model tests and simulations

A comprehensive hydrodynamic analysis was performed using HSVA's in-house CFD code FreSCo+, run for the appended hulls at full scale. The computational model has been generated using HEXPRESS. Mesh sizes for the different simulations vary between 6.2 and 10.1 million cells. The process followed HSVA's best practice guidelines for resistance and propulsion computations. The free surface is considered, and the ship is free to dynamically sink and trim.

5.1. HSVA database, full scale predictions and validation of FreSco+

Fig.14 gives a comparison of power delivered P_D from full scale predictions based on model tests and RANS simulations of self-propulsion including the free surface run with FreSco+ at scantling draft. It also shows the minimum, mean and maximum P_D from HSVA's comprehensive database of similar vessels model-tested over many years. The CFD simulations lie very close to the full-scale predictions. Therefore, the validity of FreSco+ can be rightfully assumed so that the comparisons for the different hull forms can be based on the CFD analyses alone.

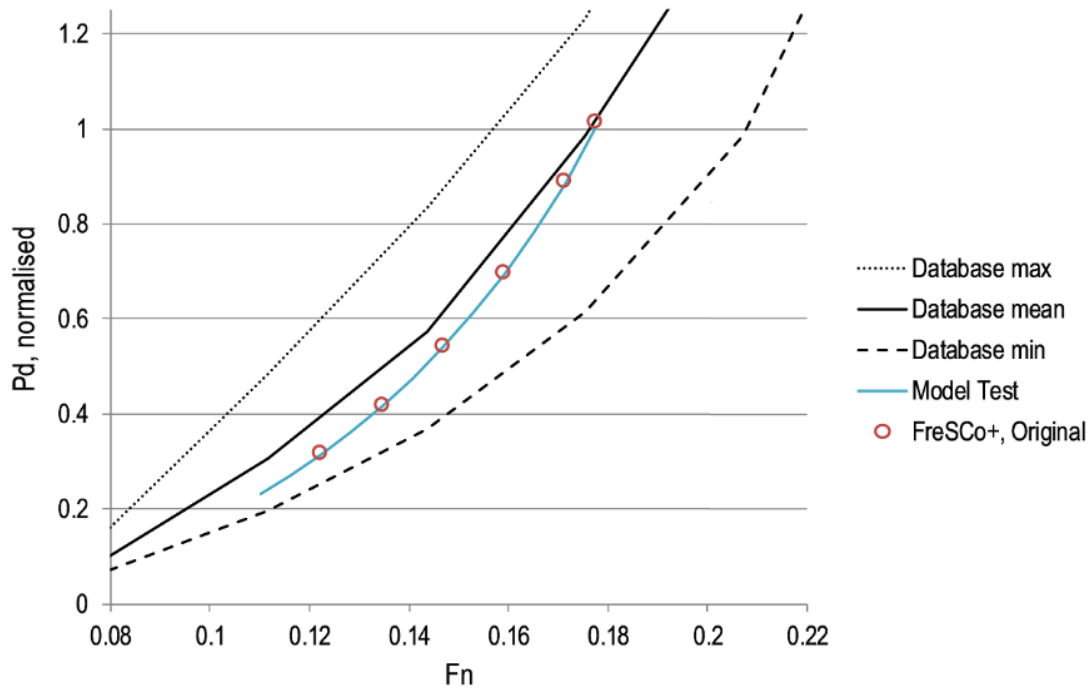


Fig.14: Power delivered P_D from full scale predictions based on model tests, CFD simulations along with range from HSVA's comprehensive database

For reasons of protecting IPR a normalization is chosen for Fig.14, based on power delivered at scantling draft and $Fn = 0.175$ as determined from the model tests. The range between minimum and maximum values is pretty large, meaning that there is quite a lot of uncertainty involved by using level 0 estimates. The mean value from HSVA's database is a bit higher over most of the Froude number range than the CBT's performance, underlining that the tanker is performing really well while at the same time taking into account that a tanker needs to be optimized also for its ballast condition.

5.2. Propulsion performance at full scale

Figs.15 and 16 present pressure distributions from the CFD simulations at different drafts for the original hull, the level 1 hull and the 4h-model. Several differences in the pressure distributions and in the wave contours along the hulls can be seen for both the scantling draft and the ballast draft in Figs.15 and 16. Furthermore, it can be appreciated that the geometric differences are more pronounced in the stern regions, leading to differences in pressures and wave patterns for the design draft while for the ballast condition major differences appear also in forebody.

The wave patterns are displayed in Fig.17 for the hulls at scantling draft and design speed and in Fig.18 for a lower speed, the latter zoomed in for the forebodies. The wave patterns of the original hull and the level 1 hull obviously do not match very closely. Most importantly, the bow wave of the original hull is smaller while the shoulder system shows a different structure, leading towards dissimilar wave interferences.

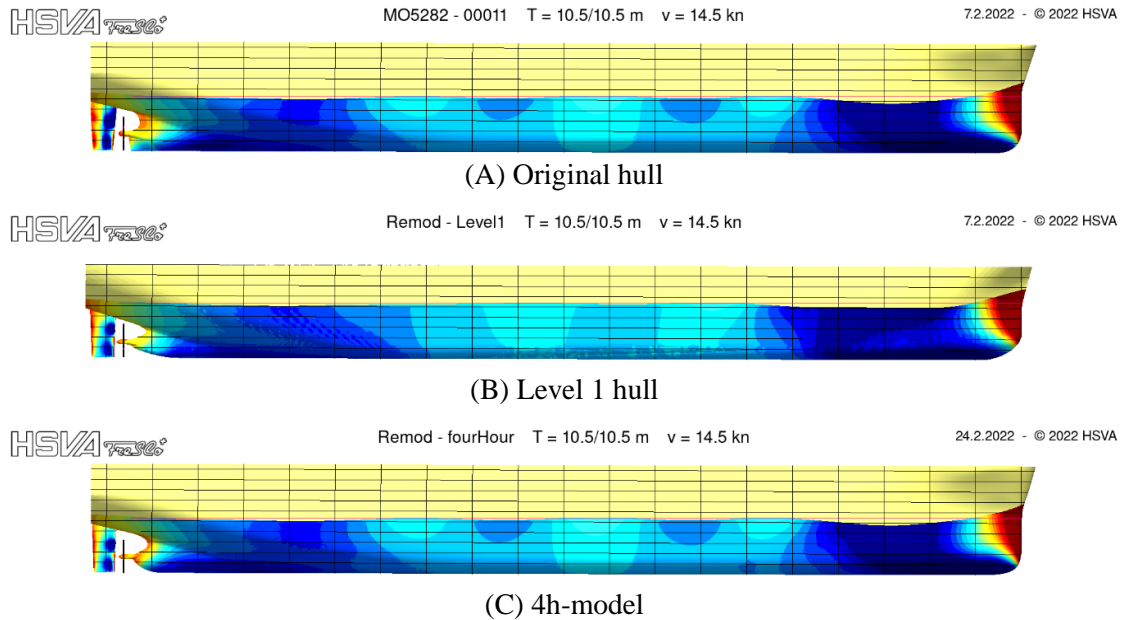


Fig.15: Pressure distributions on different hulls at scantling draft and design speed

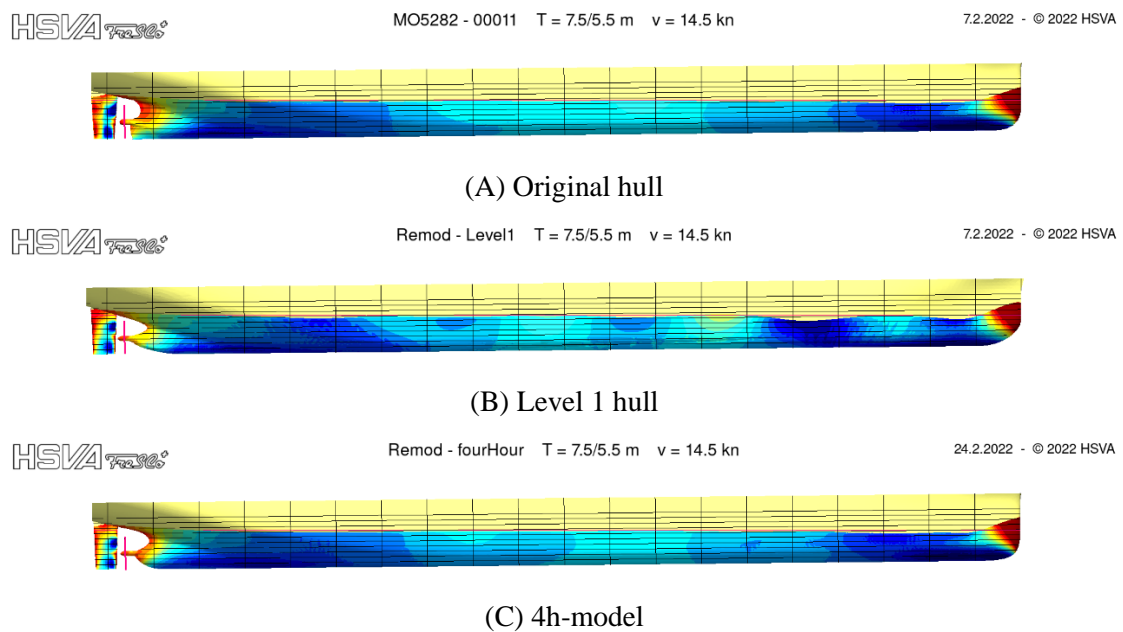
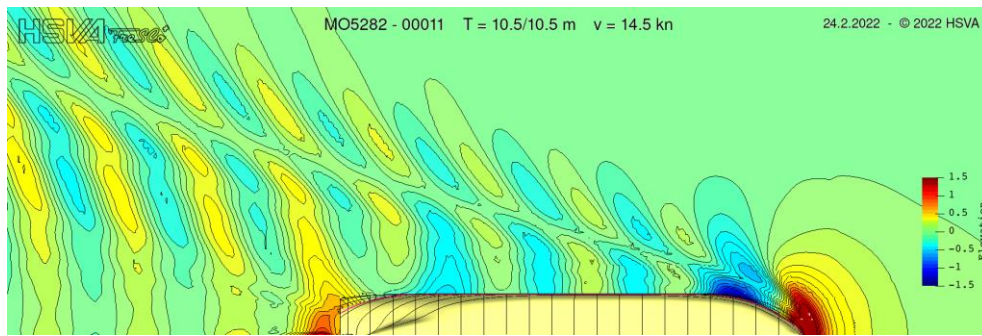


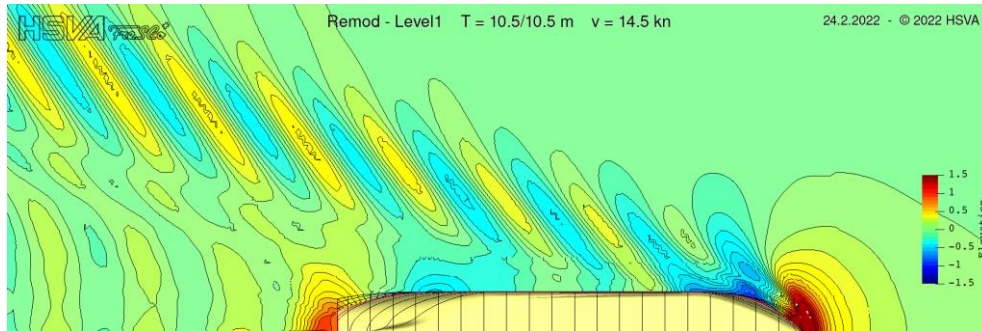
Fig.16: Pressure distributions on different hulls at ballast draft and design speed

The pressure distribution for the forebodies at ballast draft and a lower speed are given in Fig.18. Again, level 1 hull, as would be expected, looks different as indicated in the bow profile, the wave contours and the pressure distribution.

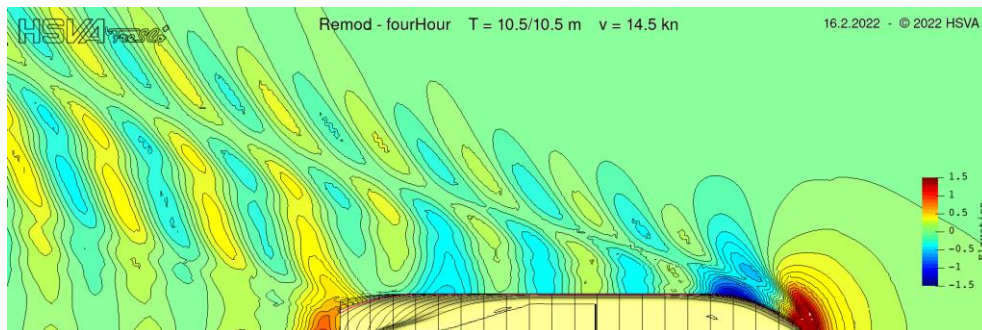
Since the pressure distribution and the wave system generated for the level 1.5 hull is rather close to those of the level 1 hull, they are not displayed here.



(A) Original hull

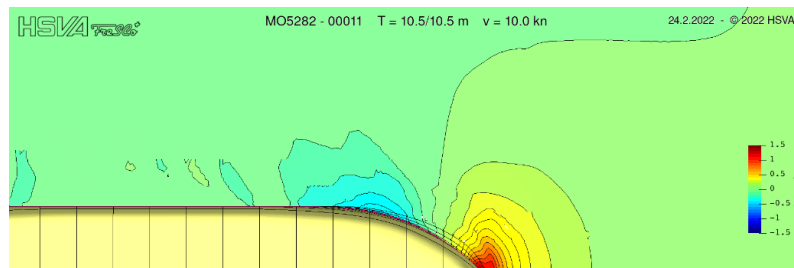


(B) Level 1 hull

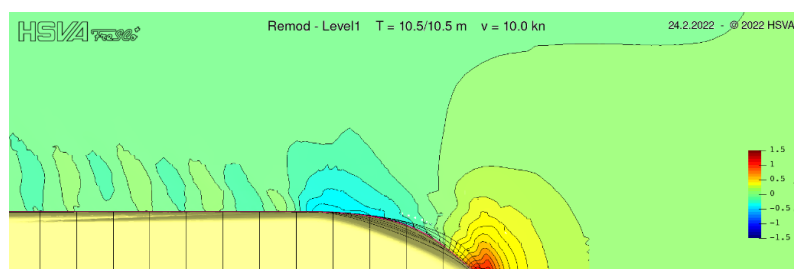


(C) 4h-model

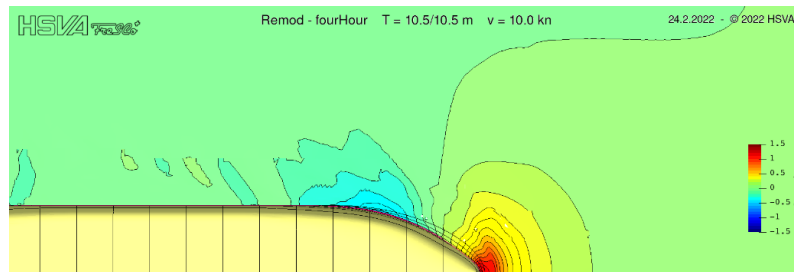
Fig.17: Wave pattern on different hulls at scantling draft and design speed



(A) Original hull

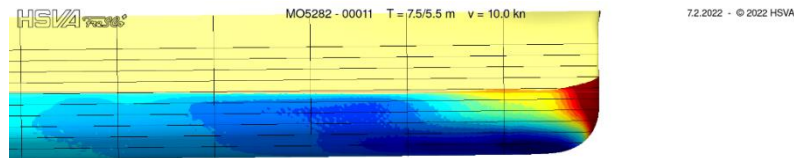


(B) Level 1 hull

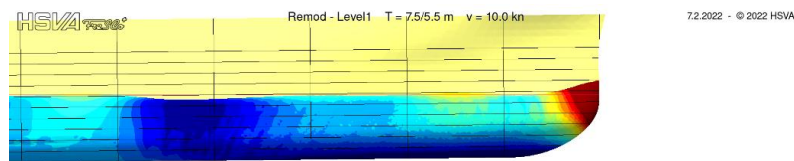


(C) 4h-model

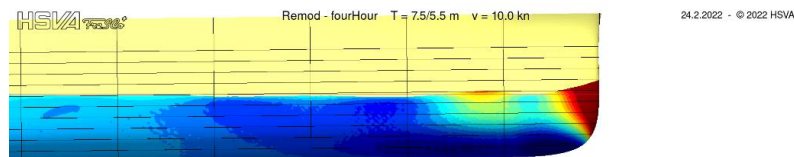
Fig.18: Wave pattern around forebody on different hulls at scantling draft and lower speed



(A) Original hull



(B) Level 1 hull



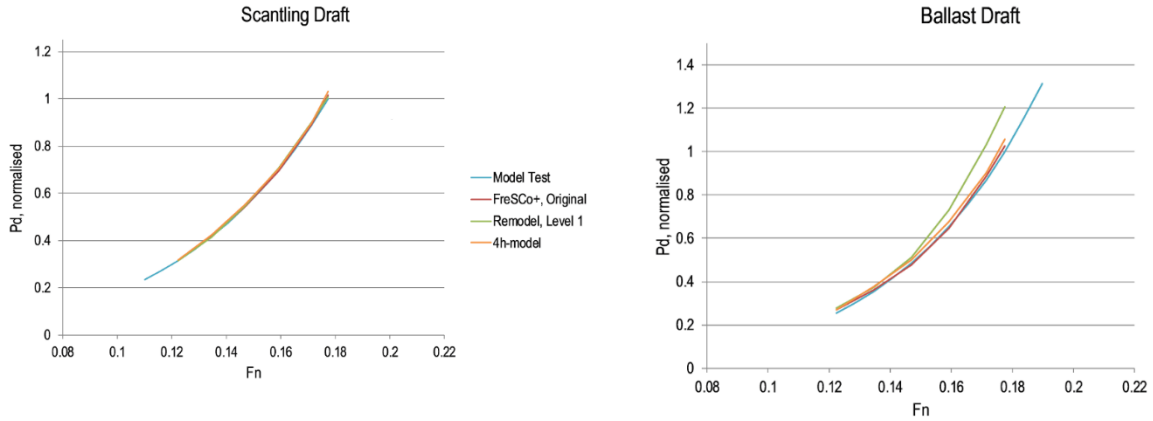
(C) 4h-model

Fig.19: Pressure distributions on different hulls at ballast draft and lower speed

5.3. Further discussion of selected results

Not surprisingly, the various hull geometries yield different hydrodynamic performances at different speeds and at different drafts, even at calm water. There are situations, in which the performance curves for P_D vs. F_n match very closely. However, that needs to be understood as “lucky shots” since for other operating conditions the performance curves often vary quite considerably. Figs.21 and 22 depict a comparison for power delivered P_D vs. Froude number F_n for the original hull, for the level 1 hull and for the 4h-model. For the scantling draft the differences are astonishingly small, see Figs.21(A) and 22(A). However, at ballast draft – which makes up a considerable amount of operating time for tankers – the differences are rather large for the level 1 hull, rising above 15% at higher speeds, while for the 4h-model they are kept at bay reasonably with a maximum deviation of 5% when compared to the CFD data for the original hull, see Figs.21(B) and 22(B).

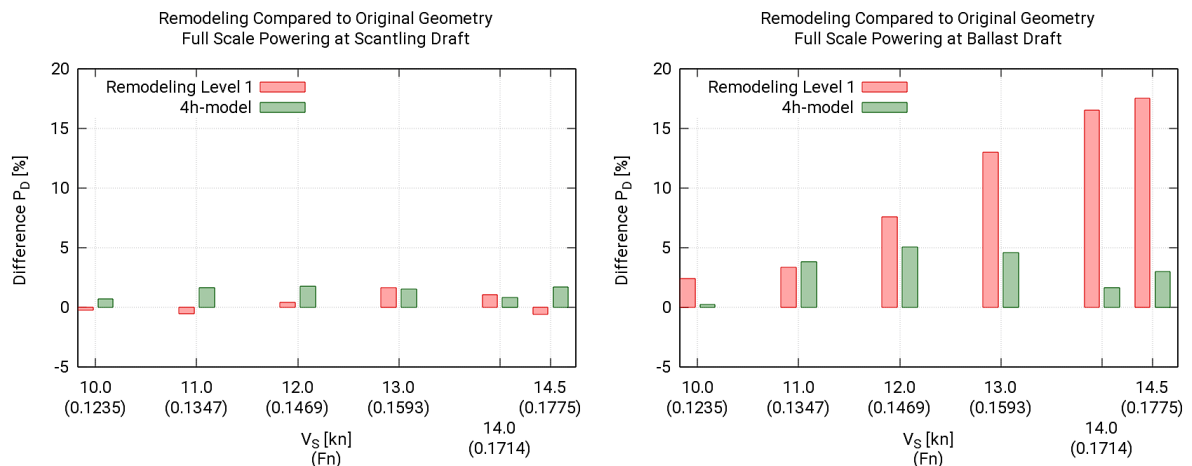
In order to understand typical deviations that a level 0 estimate would entail Fig.22, taken from *Kristensen and Lützen (2013)*, gives an appreciation for a typical series, here *Harvald (1983)*. In the speed range relevant for the CBT, 0.14 to 0.18, the series data lies well above model test data (about 17%), indicating that modern ships are indeed better on average than their predecessors, with differences up to +30% caused by the spread of performance within the fleet.



(A) Speed-power curves at scantling draft

(B) Speed-power curves at ballast draft

Fig.20: Speed-power curves



(A) Differences at scantling draft

(B) Differences at ballast draft

Fig.21: Differences of power delivered P_D between level 1 hull and 4h-model compared to simulations for the original hull at scantling draft

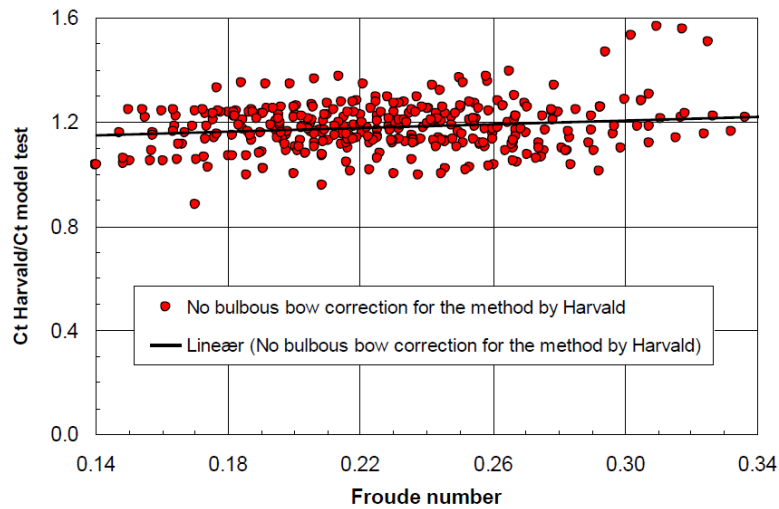


Fig.22: Difference of the total resistance coefficient from an empirical formula, here *Harvald (1983)*, to values from model tests, reproduced from Fig. E3, *Kristensen and Lützen (2013)*

The level 1 hull shows a better agreement with the original hull than what could be expected according to Fig.22 if the Harvald method would have been used instead. This indicates that the mean value of the power consumption predicted with CFD utilizing a level 1 hull is closer to the mean value of the fleet, i.e., the average performance to be expected without yet knowing too many details. Still, the

uncertainty caused by the spread in the fleet remains comparable between series data and the CFD prediction for any level 1 hull. This is because the input values for both the Harvald estimate on one side and the level 1 hull on the other side are very similar. It needs to be kept in mind that the uncertainty is caused by the differences in performance that stem from varying design considerations and from design features that are not captured via the limited input, for instance, the shape of the bulbous bow, waterline shapes, the shape of the skeg, special constraints etc.

Nevertheless, the use of CFD utilizing a level 1 hull can reduce the uncertainty since, contrary to the Harvald method, the parametric model for a level 1 hull may display either a bulbous bow or a straight stem, depending on the ship to be considered. The impact of this, however, has not been evaluated yet.

5.4. Preliminary uncertainty analysis for the level 1.5 hull

When predicting the performance of a hull, either using empirical methods, Fig.22, or simulations with an approximating hull form, Figs.20 and 21, say a level 1 hull, it is crucial to also estimate the expected accuracy. The aim of such an investigation is to predict both the performance itself, more specifically the mean value, and its standard deviation. The standard deviation can be regarded as a measure to quantify how much the performance of the actual ship may vary from the mean performance.

In Tillig *et al.* (2018) a statistical analysis of the accuracy of an empirical power prediction model was presented. It was shown how the total uncertainty can be subdivided into method and design uncertainties. The present study focuses on the comparison of different (re)modeling approaches using exactly the same prediction method. Thus, the method uncertainty reduces to uncertainties due to different mesh qualities for the different hulls investigated. With fine meshes and HSVA's quality assurance that is assumed to be small. Therefore, the primary source of uncertainty is the design uncertainty, i.e., the uncertainty associated with the fact that any approximating hull will necessarily be different from the original.

So as to estimate this design uncertainty one could either put to use a database of model-tested or CFD analyzed ships or, alternatively, perform a comprehensive parametric variation of the hull. While the first option provides quick and reliable results which only include feasible designs, it has the major bottleneck that, often, only a rather limited number of ships have been tested within an acceptably small range of appropriate main dimensions. One could broaden the limits of main dimensions and even mix ships of slightly different topology, for instance, hulls with and without bulbous bows, and possibly include ships with special constraints or requirements, for instance, ice class ships. Nevertheless, that again introduces new types of uncertainties. Meanwhile, the second option, i.e., a parametric variation of hulls that maintain all primary inputs, most importantly the main dimensions, but randomly changes secondary characteristics, opens the door for statistical analyses.

The drawbacks here are high computational efforts and the potential inclusion of infeasible designs. A parametric variation, unless strict constraints are imposed, tends to produce more low performing than high performing variants, which will change the shape of the probability function of the expected performance. Naturally, a certain percentage of low performing designs can always be excluded.

This numerical approach was applied to the level 1.5 hull, i.e., the hull produced parametrically within seconds, knowing the main dimensions and both the displacement and the center of buoyancy at design draft. Ten variables, among others the waterline entrance angle, the longitudinal center of flotation, the transom immersion, the form parameters for the skeg, the position of the forward shoulder and the length of the parallel midbody were varied within a Design-of-Experiment featuring 100 hull variants. The general shape of the hull, e.g. the stem contour, was kept. Technically, all variants can thus be considered valid instances of a level 1.5 hull while the level 1.5 hull discussed so far, Fig.6, constitutes the baseline for normalization and comparison.

The CFD code used for this statistical analysis was the viscous module of SHIPFLOW. For the sake of saving computational resources, only the total resistance was taken into account at design draft and

design speed. Naturally, the better performance measure for such a comparison would have been power delivered. The results of the analysis by means of the total resistance of the variant over the resistance of the baseline level 1.5 hull are presented in the histogram in Fig.23. The baseline level 1.5 hull yields an abscissa value of 1.0 while better hulls have lower and lesser hulls higher values.

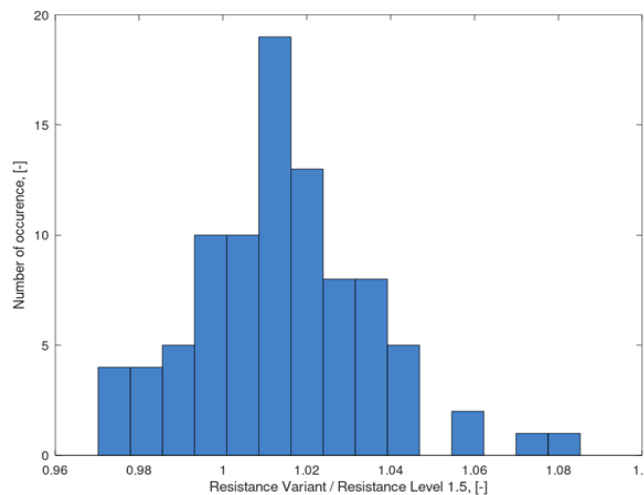


Fig.23: Statistical analysis of resistance for variations of the level 1.5 hull

More hulls are produced with higher resistance than hulls that feature lower resistance, Fig.23, as expected from a randomized variation. The mean value of the resistance of all hulls is at about 2% above the baseline level 1.5 hull. The resistance of the best hull turns out to be about 3% lower than the resistance of the baseline level 1.5 hull.

When disregarding the worst hulls, i.e., hulls that feature a total resistance of 4% above the baseline's value, the standard deviation would be a little below 2%. Note that these results neglect the differences in propulsive efficiency and should be regarded as preliminary results. A full uncertainty analysis would have to comprise a small variation for main dimensions, probably involving even more hull design parameters, and performing high-end self-propulsion simulations. The uncertainty, i.e., the standard deviation of the results, would then most likely further increase.

6. Conclusions and outlook

Many people and the maritime community at large are committed to working towards tangible reductions of energy consumption and green-house gas emissions for ships in operation. Operators not only foot the fuel bill but are also striving to make a difference in reducing their environmental impact. Being able to take decisions what to change, both for the ship as an asset itself, possibly by means of a retrofit, and what to improve in everyday operations requires deeper insight and more accurate knowledge of hydrodynamics. This is because for all cargo ships resistance and propulsion in calm water and in sea states determine the overwhelming portion of total energy demand. Unfortunately, often owners and operators face the predicament of not having a well-defined mathematical model of the geometry of the hull form, the propulsion unit and the appendages at hand or disposing of thorough hydrodynamic analyses as would be needed for their decisions.

This paper discussed techniques of remodeling geometry at different levels in order to provide geometric twins of the ship in operation. The current difficulty is not that an educated naval architect would not be able to remodel all systems in a comprehensive reengineering effort. Rather, the question is what level of remodeling is required and how to achieve it economically.

To this end, a thorough study is presented for a oil-chemical tanker. For this ship a level 0 approximation of hydrodynamics, i.e., an approximation on the basis of series data using main dimensions only, shows too low quality on which to base any reliable operational decision. A level 1 approximation, i.e., an

approximation using main dimensions, a high-level parametric model which is intelligently built on best design practices already, yields surprisingly good results for power delivered at scantling draft and somewhat soberingly large errors for power delivered at ballast draft. A level 2 approximation, realized within four hours of CAD work by a modeling expert, utilizing a high-level parametric model, meanwhile, yields results close to those of the original hull.

In a next step the separate parametric models currently used for level 1 and level 2 shall be unified in order to allow gradually inserting more pieces of information as they become available.

So far, the simulations were done in calm water only. Influences of sea states, wind and current as well as maneuvering still need to be taken into account. Furthermore, it needs to be born in mind, naturally, that the results presented are based on the analysis of one specific tanker and need further extension to make them more general.

Acknowledgements

The authors kindly wish to thank Carsten Leheld, Carl Büttner Shipmanagement, for sharing his valuable insight in ship operations as well as for the provision of data.

Parts of the work presented here were realized within the research and development project MariData, <http://maridata.org/>, funded by the Federal Ministry for Economic Affairs and Climate Action (BMWK) on the orders of the German Bundestag and PtJ as the conducting agency (FKZ 03SX528).

References

BERTRAM, V.; HARRIES, S. (2022), *Re-Creating 3D Ship Geometries as Maps for Inspection and Reporting*, PortPIC 2022, Hamburg

BLOM, M.; CZAPLA, M. (2021), *Direct Integration of 3D Laser Scanning in CAD*, COMPIT Conf., Mülheim, pp.24-29, http://data.hiper-conf.info/compit2021_muelheim.pdf

HANSEN, H.; HOCHKIRCH, K. (2013), *Lean ECO-Assistant Production for Trim Optimisation*, 12th COMPIT Conf., Cortona, pp.76-84, http://data.hiper-conf.info/compit2013_cortona.pdf

HARRIES, S.; ABT, C.; BRENNER, M. (2015), *Upfront CAD – Parametric modelling techniques for shape optimization*, Int. Conf. Evolutionary and Deterministic Methods for Design, Optimization and Control with Applications to Industrial and Societal Problems (EUROGEN), Glasgow

HARRIES, S.; LORENTZ, K.; PALLUCH, J.; PRAEFKE, E. (2018), *Appification of Propeller Modeling and Design via CAESES*, COMPIT Conf., Pavone, http://data.hiper-conf.info/compit2018_pavone.pdf

HARVALD, S.A. (1983), *Resistance and Propulsion of Ships*, Wiley

KRISTENSEN, H.O.; LÜTZEN, M. (2013), *Prediction of Resistance and Propulsion Power of Ships*, Project no. 2010-56, Emissionsbeslutningsstøttesystem Work Package 2, Report no.04, University of Southern Denmark / Technical University of Denmark

TILLIG, F.; RINGSBERG, J.W.; MAO, W.; RAMNE, B. (2017), *Analysis of the Reduction of Uncertainties in the Prediction of Ships' Fuel Consumption – from Early Design to Operation Conditions*, Int. Conf. on Ships and Offshore Structures (ICSOS 2017), Shenzhen, China

TILLIG, F.; RINGSBERG, J.W.; MAO, W.; RAMNE, B. (2018), *Analysis of uncertainties in the prediction of ships' fuel consumption - from early design to operation conditions*, Ships and Offshore Structures

A Digital Twin for the Formulation of Ice Accretion on Vessels

Thomas DeNucci, U.S. Coast Guard, New London/USA, thomas.w.denucci@uscga.edu.de
Daniel Brahan, U.S. Coast Guard, New London/USA, daniel.j.brahan@uscga.edu

Abstract

This paper presents a methodology for predicting ice accretion on vessels operating in high latitudes. The approach combines Newton's Second Law for spray droplet trajectories with streamline velocity to predict mass accumulation of precipitation on the vessel. Inputs to the droplet trajectory model include wind velocity, injection angle, droplet size and droplet velocity. Streamline velocities are generated using Computational Fluid Dynamics (CFD) with crab pots modelled as porous surfaces. The model simulates wave-impact in the Bearing Sea, during recorded and observed weather condition the night of the sinking. Preliminary results, including the nature and location of ice accumulation are presented.

1. Introduction

The fishing vessel 'Scandies Rose', Fig.1, Table I, capsized in extreme spray-icing conditions on December 31, 2019, with the loss of five of seven fishermen onboard. The U.S. Coast Guard and National Transportation Safety Board (NTSB) convened a Marine Board of Investigation to identify causal factors to the vessel's sinking. Testimony identified current vessel regulations under 46 Code of Federal Regulations (CFR) 28.550 may not accurately account for vessel icing on crab pots – a porous surface consisting of webbing and open space where ice can accumulate in a non-uniform pattern. The lack of understanding of icing phenomenon on porous crab pots may put mariners and the marine environment at undue risk.



Fig.1: Fishing vessel 'Scandies Rose' loaded with crab pots, NTSB (2021)

Table I: 'Scandies Rose' principal dimensions and crab pot loading NTSB (2021).

Variable	Value
Length	39.62 m (130 ft)
Beam	10.36 m (34 ft)
Draft	3.44 m (11.3 ft)
Full Load Displacement	1,113 MT (1,095 LT)
Gross Regulatory Tonnage	195 GRT
Propulsion	Detroit Diesel 12V2000 (2)
Number of Crab Pots on Final Voyage	198

1.1 Marine Icing Events

Marine icing events are becoming more and more common. *Huhtanen (2018)* and *Shellard (1974)* provide a comprehensive list of vessels lost at sea as a result or suspected result of ice accretion. The ‘Scandies Rose’ is the second sinking of an Alaskan fishing vessel during heavy icing conditions in recent years. The first was the ‘Destination’ in February of 2017. *NTSB (2018)* concluded that ‘Destination’ capsized with the loss of life of all crewmembers aboard due to prolonged icing and excessive crab-pot loading, which provided both interior and exterior surface area for ice to accumulate in the freezing spray. The analysis by the U.S. Coast Guard Marine Safety Center revealed that added weight high on the vessel from icing left it with a lower freeboard and decreased righting arm (lower stability) and ultimately vulnerable in the severe conditions. Fig.2 shows the result of such extreme spray icing events.



Fig.2: ‘F/V Sandra Five’ following a sea icing event in 2018, *NTSB (2018)*

‘Scandies Rose’ is unique because the survivors could attest to the weather conditions on the day of the incident. The may-day call and report from the rescue helicopter all corroborated the reported weather shown in Table II.

Table II: On-scene weather, *USCG (2021)*

Weather Element	Value
Wind Velocity	18 – 25 m/s (35 – 50 kts)
Wind Direction (Relative to the Vessel)	045°
Significant Wave Height	6 – 10 m (20 – 30 ft)
Wave Interval	9 – 10 sec
Water Temperature	3° C (39° F)
Air Temperature	-12° C (10° F)
Cloud Cover	Low
Precipitation	Snow and freezing spray

1.2. Current Ice Modelling and Forecasting

Overland (1990) and *Fett et al. (1993)* describe the specific hazards associated with marine sea spray icing. To estimate the amount of sea spray ice accretion, *Overland (1990)* developed a model that

estimates the rate of ice accretion based on wind speed, air temperature, sea temperature and the freezing point of seawater (-1.7°C for the North Pacific). The model is valid for vessels that are between 20 and 70 m in length and for sea surface water temperatures between 1.0°C and 7.0°C . Fig.3 shows the prediction for a vessel heading into or abeam of the wind for water temperature of 3.0°C .

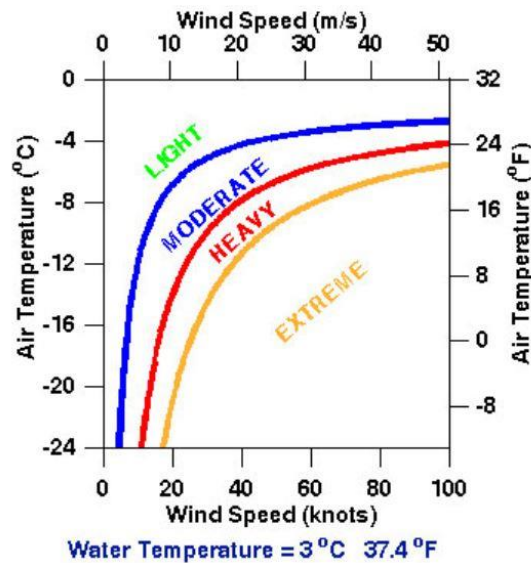


Fig.3: Icing conditions for water temperatures of 3.0°C , *Overland (1990)*.

The Overland Method predicts the sea spray icing as “light”, “moderate”, “heavy”, and “extreme” based on the rate of predicted ice accumulation or ice class. Typical rates associated with each ice class are shown in Table III.

Table III: Icing rate prediction, *Overland (1996)*

Ice Class	Light	Moderate	Heavy	Extreme
Icing Rate (cm/h)	< 0.7	0.7 – 2.0	2.0 – 4.0	> 4.0

In the case of the ‘Scandies Rose’, the vessel would have been experiencing extreme sea spray icing as a result of air temperature, water temperature and wind speed, corresponding to an ice accumulation rate greater than 4.0 cm/h (1.6 in/h). Wave characteristics and swell, including the significant wave height, wave period, wave length and relative direction also play an important role in the rate at which ice accumulates. Although this method is a reliable predictor of meteorological icing, it fails to account for localized weather conditions, sea spray, and specific vessel geometry; also it has not been harmonized with (U.S.) stability and icing regulations.

2. Fishing Vessel Stability and Icing Regulations

‘Scandies Rose’ was subject to the stability standards identified in 46 CFR Part 28 Subpart E, *NTSB (2021)*. The ‘Scandies Rose’ did not operate on an international voyage and therefore was not subject to the international regulations and survey requirements of Safety of Life at Sea (SOLAS) set forth by the IMO. Additionally, ‘Scandies Rose’ was not subject to the fishing vessel stability rules set forth in the International Code on Intact Stability, or IS Code, to include icing on fishing vessels.

If ‘Scandies Rose’ was subject to meeting the requirements of IS Code, the vessel was operating outside the region required to undergo stability analysis with ice accumulation, *IMO (2008)*. IS Code 6.3.2 only requires icing analysis if the vessel operates within specific regions of the world; for the Pacific Northwest, IS Code requires icing analysis when vessels operate within the Bering Sea. ‘Scandies Rose’ sank south of the Aleutian Islands or outside the Bering Sea meaning that while icing criteria should be considered in a stability report, the vessel would not be required by international regulation to undergo a stability analysis with icing.

Despite the differences in the location of ice accumulation in the Bering Sea, the maximum assumed icing quantities on fishing vessels are identical between 46 CFR 28.550 and IS Code; 6.3 – 30 kg/m² ice on horizontal surfaces and 15 kg/m² ice on vertical surfaces. The ice accumulation equates to a thickness of 3.3 and 1.65 cm, respectively. The ice loading prescribed in both sets of regulations causes a twofold decrease in vessel stability:

1. Weight addition largely on surfaces that are predominantly higher than the vessel's center of gravity (kg) decreases stability.
2. Parallel sinkage caused by an increase in weight or displacement and subsequent reduction in vessel freeboard or reserve buoyancy.

There are additional limitations to the regulatory schemes which further jeopardize mariners. First, the regulations assume a uniform ice loading and do not consider the effects of listing due to off-center weight additions. The assumption is questionable because vessels rarely have wind and seas directly off the vessels' bow; in fact, many recent icing surveys document asymmetrical icing, *NTSB (2018)*. Second, the rulesets assume that icing is applied over the top and sides of the fishing pots, commonly referred to as the "shoebox method." This is an important assumption to note as crab pots are not constructed of a closed exterior but are built of a frame with webbing surrounding the frame. The effects of these phenomena cause a third, and perhaps most important, limitation of the ruleset: a loss of stability by induced list from added icing weight.

The weather, when applied to the different rulesets, can result in vastly different estimates of topside ice. The weight of the assumed ice, determined by the operational area of the vessel, is shown in Table IV.

Table IV: Comparison of icing required by ruleset and estimations using on scene weather

Source of Icing Estimate	Horizontal Weight (kg)	Vertical Weight (kg)	Total (kg)	Total (MT)
46 CFR 28.550 South of 66°30' North	5,621	4,308	9,929	9.93
46 CFR 28.550 North of 66°30' North / IS Code in Bering Sea	11,242	8,616	19,858	19.89
Overland Method On Scene Weather (from Table II)	48,397	37,129	85,526	85.53

3. Approach

Because fishing vessel ice accretion first begins as water droplets, it is imperative to know where the water droplets land on the vessel. This was the first problem that was attempted to be solved. The flight path of any sea spray is also subject to the air flow surrounding the vessel. So once, an accurate model of sea spray trajectory was produced, it could then be combined with airflow analysis conducted with Computational Fluid Dynamics (CFD) software to gain an understanding of where droplets begin to accumulate on the vessel. This approach accurately modelled the velocity flow field that affects the droplet trajectories and ultimately where water droplets accumulate on the vessel. Following this analysis, mass flux from the free surface, or wind generated sea spray, and mass flux from wave induced sea spray may be analysed to yield the quantity of water emanating from the free surface. Once the mass is known, a thermodynamic model may be implemented to quantify the mass of sea spray which freezes on the vessel, *Dehgahni-Sanij (2017)*. It will be assumed the remainder of the sea spray will flow off the deck to the sea.

The problem is a non-linear, iterative problem, particularly, any ice which accretes on the vessel, in particular the crab pots, affects the air flow, which affects the droplet trajectory and subsequent icing locations on the vessel. Ideally, this will be solved in an iterative fashion. This paper lays the

groundwork for this follow-on research into icing accretion on a vessel and lays the foundation for the complete model by modelling sea spray trajectory and CFD analysis of the vessel with crab pots. Only then can a vessel's stability characteristics begin to be analysed.

4. Modelling Sea Spray Trajectory

To understand where ice will build up on a crabbing vessel, it is necessary to first build a sea spray trajectory model. This was accomplished using a numerical method of modelling sea spray described by *Dehghani et al. (2016a)*. This method implements Newton's second law for droplet motion and substitutes body, drag, and added mass forces. The governing equation for the particle motion is:

$$m_d \frac{dV_d}{dt} = \rho_d \forall_d g - C_{dr} \frac{\pi D^2}{8} \rho_a |V_d - V_a| (V_d - V_a) + \rho_a \forall_d C_{ad} \frac{D(V_d - V_a)}{Dt} + \rho_a \forall_d \left(\frac{DV_a}{Dt} - g \right) \quad (1)$$

where m_d is the mass of the droplet, t is time, V_d is droplet velocity, V_a is air velocity, ρ_d is water density, \forall_d is droplet volume, g is gravity, C_{dr} is drag coefficient, D is droplet diameter, ρ_a is air density, and C_{ad} is the added mass force coefficient.

4.1. Two-Dimensional Sea Spray Analysis with Constant Flow Field

Eqs.(2) and (3) are the x-direction (longitudinal or bow-stern direction) and z-direction (height) velocity and acceleration for particles solved from Eq.(1).

$$\dot{x} = \frac{dx}{dt} \quad \ddot{x} = -\frac{3C_{dr}}{4D(\gamma+C_{ad})} (\dot{x} - U) \sqrt{(\dot{x} - U)^2 + \dot{z}^2} \quad (2)$$

$$\dot{z} = \frac{dz}{dt} \quad \ddot{z} = \left(\frac{1-\gamma}{\gamma+C_{ad}} \right) g - \frac{3C_{dr}}{4D(\gamma+C_{ad})} (\dot{z}) \sqrt{(\dot{x} - U)^2 + \dot{z}^2} \quad (3)$$

where C_{dr} depends on the droplet Reynolds number, γ is the liquid density to air density ratio and U is the relative velocity of the wind to the vessel. These equations assume that the relative velocity of the flow field only acts in the x-direction at a constant velocity. While this assumption simplifies the solution, it does not account for the actual streamlines that are encountered as well as the variance of velocity above the free surface.

Table V: Initial conditions as specified by *Dehghani et al. (2016a)*

Variable	Value
Initial Velocity of Droplets	0-40 m/s
Droplet Diameter	0-7000 μm
Injection Angle from X axis in X-Z plane	70°

The droplet trajectory equation was solved with initial conditions which varied droplet size with the initial velocity; droplets with larger diameters were initiated at slower speeds than droplets with smaller diameters. Droplets are assumed to initiate in a direction parallel to the vessel's stem at the waterline. A constant wind velocity in the opposite direction of the vessel, or the wind coming off the bow was implemented with a constant vessel forward speed. In addition, the droplet sizes and initial velocities were varied – that is the largest droplets had the slowest initial velocity – yet were initiated in a direction parallel to the vessel's stem. Trajectory equations were solved with a Forward Euler numerical solver and the same initial conditions as described by *Dehghani et al. (2016b)*, shown in Table V. Our results replicated the work, confirming the validity of the solver.

4.2. Analysis of Two-Dimensional Sea Spray Trajectory with Two-Axis CFD Velocity Flow Field

A simulation of the droplet trajectories with two-dimensional CFD velocity flow fields are shown in Fig.4 with a silhouette of the 'Scandies Rose' overlayed. Droplet diameter and initial velocity were

varied with the same initial conditions described in Table V with all droplets initiated at the stem. CFD simulations with a two-dimensional flow field indicated that the smallest droplets were most susceptible to the velocity flow field. However, with higher injection velocities, these droplets typically were injected into the air flow at a height well above the vessel causing the droplets to bypass the vessel entirely, identified by the droplet passing over the superstructure of the ‘Scandies Rose’ in Fig.4. Due to their small size, low mass and subsequently lower potential icing contribution, these smaller droplets were ignored in future simulations.

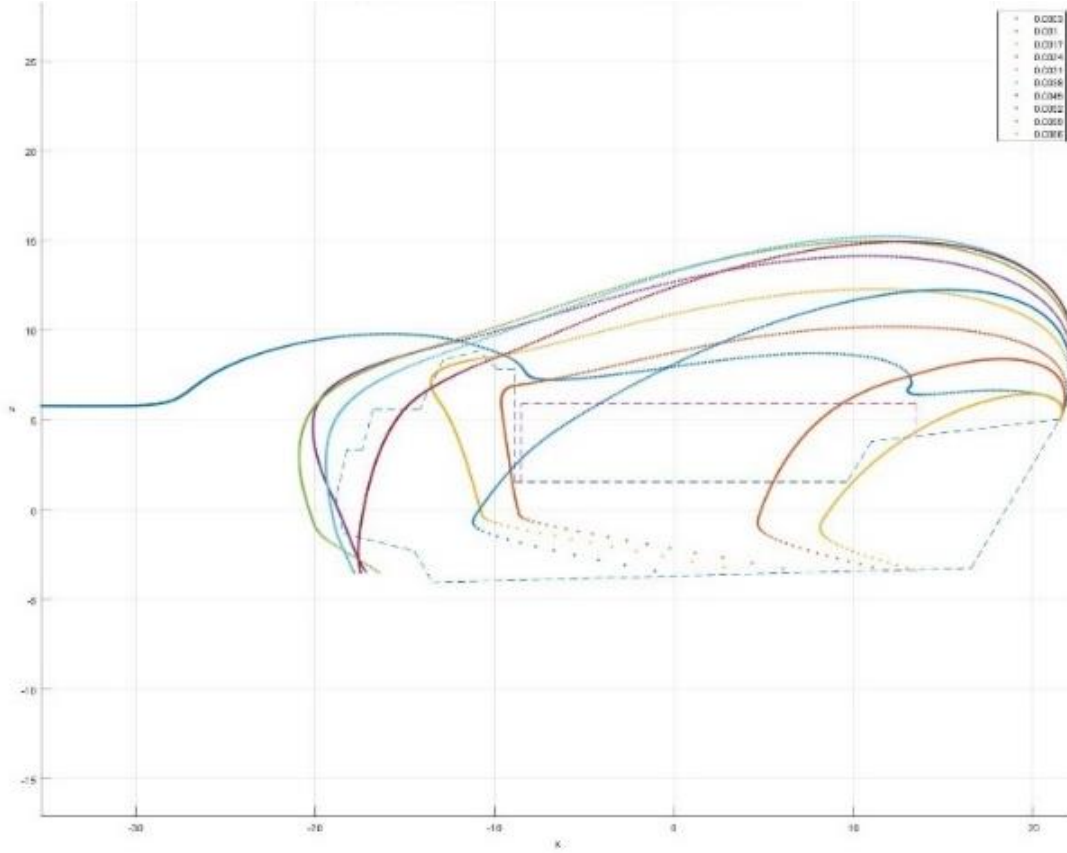


Fig.4: Droplet trajectories in two-dimensions with a two-dimensional flow field from CFD incorporated. Vessel speed is -10 kts (transiting forward) with flow field at 40 kts. Droplet sizes and initial velocities were varied.

4.3. Governing Equations in Three-Dimensions with a Three-Axis Flow Field

After verifying that the two-dimension constant velocity flow field worked, the equations were modified to model droplet trajectory and accept a flow field in three dimensions. Eqs.(4)-(6) are the result of adding in the three-dimensional flow field and trajectory.

$$\dot{x} = \frac{dx}{dt} \quad \ddot{x} = -\frac{3C_{dr}}{4D(\gamma+C_{ad})}(\dot{x} - U_x)\sqrt{(\dot{x} - U_x)^2 + (\dot{y} - U_y)^2 + (\dot{z} - U_z)^2} \quad (4)$$

$$\dot{y} = \frac{dy}{dt} \quad \ddot{y} = -\frac{3C_{dr}}{4D(\gamma+C_{ad})}(\dot{y} - U_y)\sqrt{(\dot{x} - U_x)^2 + (\dot{y} - U_y)^2 + (\dot{z} - U_z)^2} \quad (5)$$

$$\dot{z} = \frac{dz}{dt} \quad \ddot{z} = \left(\frac{1-\gamma}{\gamma+C_{ad}}\right)g - \frac{3C_{dr}}{4D(\gamma+C_{ad})}(\dot{z} - U_z)\sqrt{(\dot{x} - U_x)^2 + (\dot{y} - U_y)^2 + (\dot{z} - U_z)^2} \quad (6)$$

In Eqs.(4)-(6), the velocity flow field of the relative wind, U , is broken down into three components: U_x , U_y , and U_z . y describes the droplet's motion in the y -direction with starboard being positive.

4.4 Simulating Three-Dimensional Droplet Trajectory with Constant Flow Field

With the initial analysis of the two-dimensional case complete, a three-dimensional case in a constant flow field was analysed. Instead of varying the droplet diameters and velocities, as done in Fig.4, the droplet's mass and momentum were randomized. While droplet diameter and initial velocity could be randomized themselves, using mass and momentum instead ensured that a larger diameter droplet would not be initiated at an unrealistic velocity. Table 6 shows the initial conditions for the three-dimensional case. Droplet mass corresponds to a droplet diameter ranging from $2,400 \mu m$ to $6,600 \mu m$ which are within the bounds outlined in Table 5. While the initial momentum sometimes creates situations where the initial velocity is outside the bounds of Table 5, these situations are rare and are shown in the situations where the droplets exceed a height of approximately 10 meters in the z-direction.

Table 6. Initial conditions for a three-dimensional droplet trajectory analysis.

Variable	Value
<i>x-position</i>	0 – 5 m
<i>y-position</i>	-2 – 2 m
<i>z-position</i>	2 – 5 m
Droplet Mass	$(7.4 - 154) 10^{-6} \text{ kg}$
Droplet Momentum	$(3 - 15) 10^{-4} \text{ kg-m/s}$
θ	50 – 80 degrees
φ	-45 – 45 degrees

θ is the initiation angle in the X-Z plane, and φ describes the initiation angle in the X-Y plane. The initial conditions in Table 6 describe a box where droplets may initiate, with angles varied in the three-axis coordinate system.

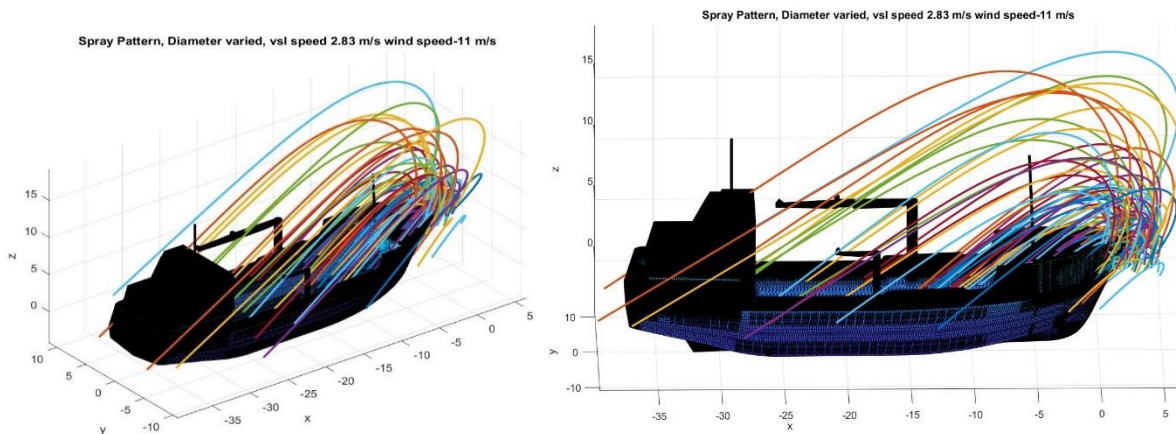


Fig.5: Initial conditions varied with vessel velocity of -5.5 knots and a constant wind profile of 22 knots off the bow. A CAD model (without crab pots) of ‘Scandies Rose’ is superimposed.

Increasing the magnitudes of either the vessel's velocity or wind velocity would a situation where the droplets begin to fall in vicinity of the vessel's fishing deck. Fig.6 shows the vessel with a velocity of -7.78 knots and the same constant wind profile.

To accurately predict the location and quantity of ice buildup on the vessel, the droplet trajectory model needed to include the local effects of heavy weather, most notably the impact of wind velocity on the particle trajectories. Further complicating this problem were the crab pots on the deck of the vessel. Therefore, CFD analysis was conducted on the vessel model with wind velocities imported to the droplet trajectory model. This will identify the likely locations of sea spray and ultimately ice accretion.

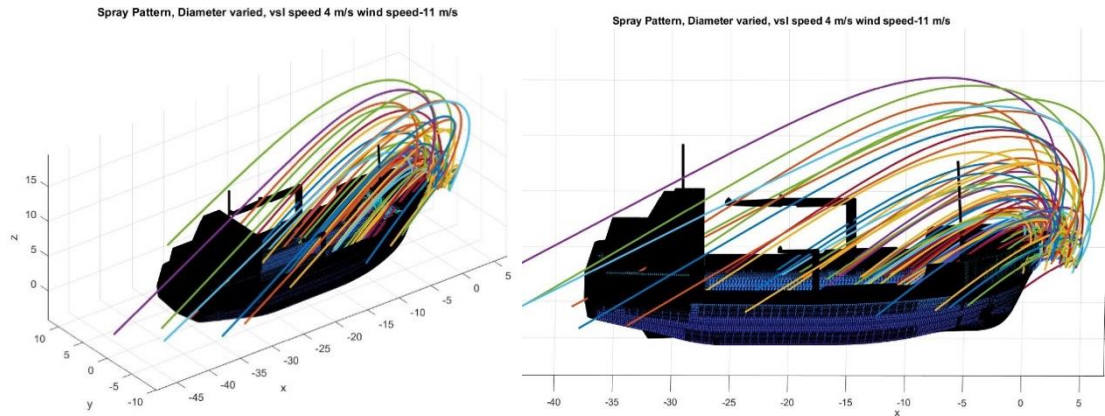


Fig.6: Effect of increasing vessel velocity in the constant flow field case

5. CFD Model of Airflow Across the Vessel

As mentioned previously, the methodologies presented in *Overland (1990)* do not effectively take into account vessel geometry *Dehghani-Sanij (2017)*. It is critical to consider geometry, as ice accretion may occur higher rate due to the concentration and travel of the streamlines over the vessel. Recent tests show that the weight of the ice accreted in the pots, due to the webbing, equaled or exceeded a pot's original weight, *Lewandowski et al. (2022)*. Also, *Overland (1990)* did not take into account the spray generated by the vessel itself. To analyze the streamlines over the vessel and through the crab pots, Orca3D Marine CFD, a combination of the Orca3D marine design plug-in for Rhino and the Simerics-MP (Multi-Purpose) CFD software was used.

5.1. Gunwale and Crab Pots

The unique geometry aboard commercial fishing vessels typically includes a high gunwale, used to protect the crew while setting and retrieving crab pots, and the pots themselves. On the 'Scandies Rose', the gunwale has a minimum height of 1.2 m with the area of setting and retrieving pots being approximately 1.6 m high. The crab pots typically measure 2.45 m by 2.45 m by 0.9 m and weigh a total of ~380 kg. Witness testimony indicated that 198 crab pots were loaded onto the 'Scandies Rose' on her final voyage; the pots were arranged in six tiers with the entire first tier placed on end to often accommodate crew movement fore and aft along the vessel, *NTSB (2021)*. Fig.7 shows an actual crab pot and the Rhinoceros 3D model which includes the exterior structure (solid steel tube), webbing and crab access.



Figure 7. Crab pot and 3D model

Modelling the entire ship and its crab pot load to determine the flow velocity is impractical. The CFD model would require a huge number of cells and an enormous amount of time and computing power. Investigative meshing at the cell size of 0.01m did not even resolve the webbing around the crab pot

structure. If the mesh size was decreased to resolve the flow through the webbing, in 3D space the cell count around the pots would have to increase by at least a factor of 10^3 . For illustration purposes, if 1M cells were dedicated to the pots, at least one billion cells would be needed to adequately resolve the flow.

Three options were considered to reduce the size of the problem. First, the creation of mesh refinement zones around the six faces of each pot were considered. This solution, in addition to being labour intensive (model set-up), would still result in a model with over 400M cells – which is still a huge model. Next, the authors considered eliminating the grid dedicated to capturing the motions of the vessel and the free surface. Although this would reduce the model size, the end goal was to analyse the vessel at her operating speed in waves, where the presence of sea spray would contribute directly to icing. Finally, a small collection of pots was analysed using refinement zones – one around each face – to visualize the flow. The pots were then be modelled as porous surfaces using the Darcy-Forchheimer Law to recreate the flow behaviour. This approach would replicate the flow without computationally intensive meshes and grids necessary to resolve the flow through the pot webbing.

5.2 Darcy-Forchheimer Law

According to the Darcy Law, the pressure loss in a porous medium is directly proportional to the flow velocity at very low flow velocities (Reynolds Numbers less than 10). In this flow regime, viscous losses govern the pressure loss. After this proportionality with the flow rate, pressure losses increase rapidly and become a quadratic function of velocity commonly referred to as the Forchheimer flow regime. The general form of the Darcy-Forchheimer equation is:

$$\frac{\Delta P}{L} = \frac{\mu}{K} V + \frac{\rho F}{\sqrt{K}} V^2 \quad (7)$$

where the left side of the equation is referred to as the pressure gradient or pressure loss per unit length in the direction of flow. The first term on the right side of the equation is the Darcy expression where μ represents the dynamic viscosity (source of fluid friction at low Reynolds numbers) and K is the permeability, which is a representation of the available flow paths in the fluid. Permeability is a function of the porosity which captures the percentage of voids in the porous surface. The second term on the right side of the equation is the Forchheimer term, which includes ρ a density term and F the Forchheimer coefficient, which represent friction due to geometry.

The porosity is calculated by measuring the void volume in the porous medium; the permeability and Forchheimer coefficient are obtained using a curve fit second order polynomial on experimental data.

The specific form of the equation used in the CFD solver is shown as Eq.(8):

$$\frac{\Delta P}{\Delta x} = -\left(\frac{\beta}{\alpha} \mu V + \frac{\beta^2}{\sqrt{\alpha}} \rho C_d |V| V\right) \quad (8)$$

Where C_d = quadratic drag coefficient

α = permeability

β = porosity

μ = dynamic viscosity

The input to the CFD solver is thickness, permeability and quadratic drag coefficient. The experimental approach to solving this using Orca3D Marine CFD follows.

5.3. Experimental CFD Data

To determine the permeability and quadratic drag coefficient of the crab pots, the starboard bow of the ‘Scandies Rose’ was modelled using Orca3dMarine CFD. This model included the ship hull, deck,

gunwale, three pots positioned vertically and one pot positioned horizontally atop the three pots. The wind direction was 45° off the starboard bow and nine different measuring points for both velocity and pressure were added to the model. The pressure drop across the crab pot webbing was recorded for a range of wind speed. Fig.8 shows the model and data for a wind speed of 15.5 m/s (30 knots).

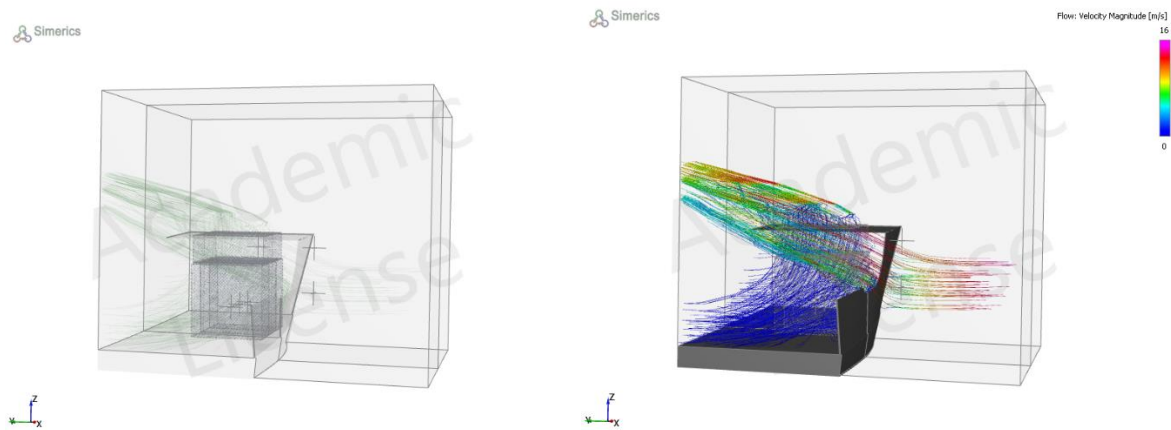


Fig.8: Model and velocity results (streamlines) for a wind speed for 15.5 m/s (30 knots).

One interesting result, shown in Fig.8, due to the combined effect of the gunwale and crab pot geometry is the velocity stall, i.e., velocity is zero, inside the pot itself. This effect manifested itself in the higher wind speeds and may be a contributing factor to the ice build on the starboard of the vessel.

After the simulation converged for each set of velocity and pressure drop data, a second-order polynomial was fit through the results. The data is illustrated in Fig.9.

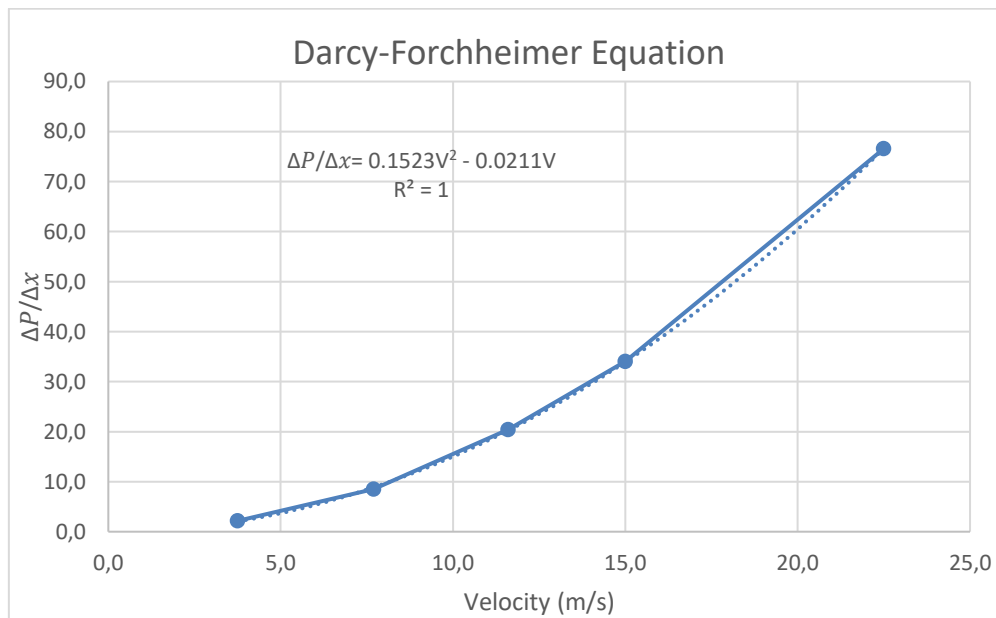


Fig.9: Darcy-Forchheimer Equation for *Scandies Rose* Crab Pots

Using the coefficients of the polynomial and crab pot web geometry, the derived values for the porous surface is shown in Table VII. The simulation setup and results are illustrated in Fig.10.

Table VII: Porous surface parameters used in the CFD simulation

Porosity	0.905
Permeability (m ²)	7.09 x 10 ⁻²
Quadratic Drag Coefficient (1/m)	3.96 x 10 ⁻⁴

5.4. Validating the Porous Surface

The porous surface, as a substitute for the complex crab pot geometry, was validated by comparing surface pressure drop and velocity across the porous surface with those measured across the crab pots. To do this, pressure and velocity fields were generated at unique locations for each case as output from the CFD simulation. The scattered data was interpolated throughout the control volume and random point by point comparison were made for 10,000 points at five different wind velocities, yielding an average error of less than 3.6%.

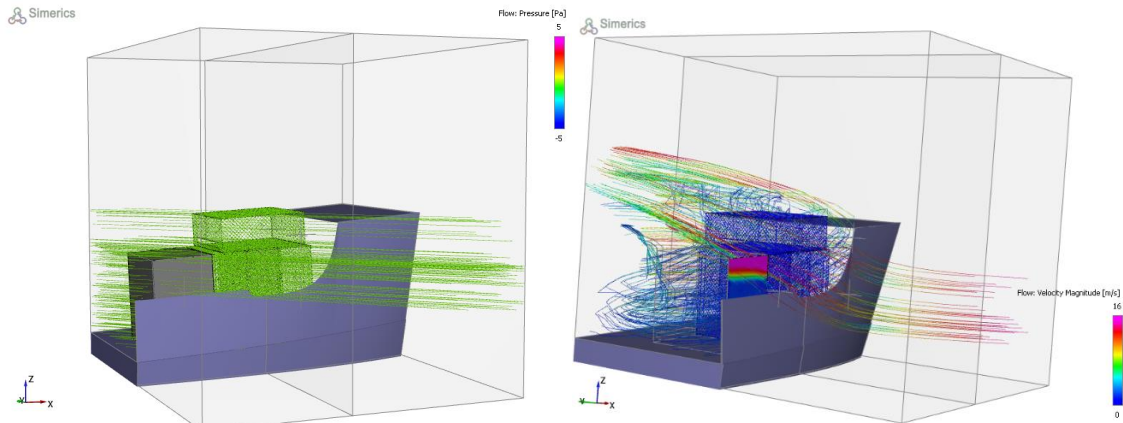


Fig.10: The porous surface model of a crab pot validated in the CFD simulation

6. ‘Scandies Rose’ Porous Surface Model

The porous surface model was now analysed in 30 knot (15.5 m/s) winds 45° off the starboard bow. The vessel speed was set to six knots and the 198 crab pots were modelled as porous surfaces with the parameters described in Table VII. Two nested box refinement zones were placed around the crab pots to ensure that the flow would be resolved inside the crab pots. The resulting model, shown in Fig.11, contained over 124M cells.

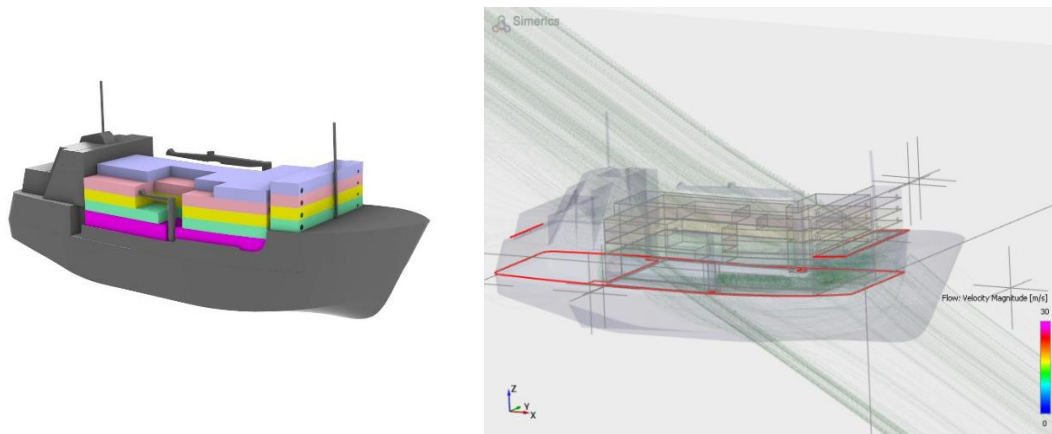


Fig.11: ‘Scandies Rose’ CFD model with crab pots modeled as porous surfaces

At the preliminary stages of the simulation, high speed vortices along starboard waist and gunwale of the vessel within the outermost row of vertical crab pots were evident, Fig.12.

As the simulation continued, the velocity stall was once again observed along the starboard side of the vessel in the first two rows of the first tier of crab pots. The stall was also observed in the forward section of the pots across the breadth of the vessel and within the lower tiers of bow pots. These results are illustrated in Fig.13.

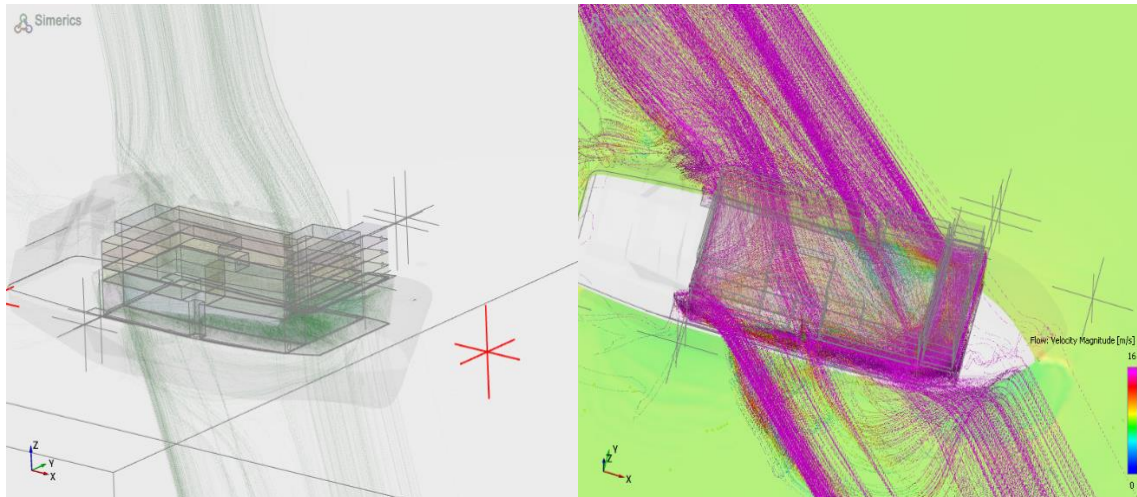


Fig.12: Initial vortices along starboard waist of the 'Scandies Rose'

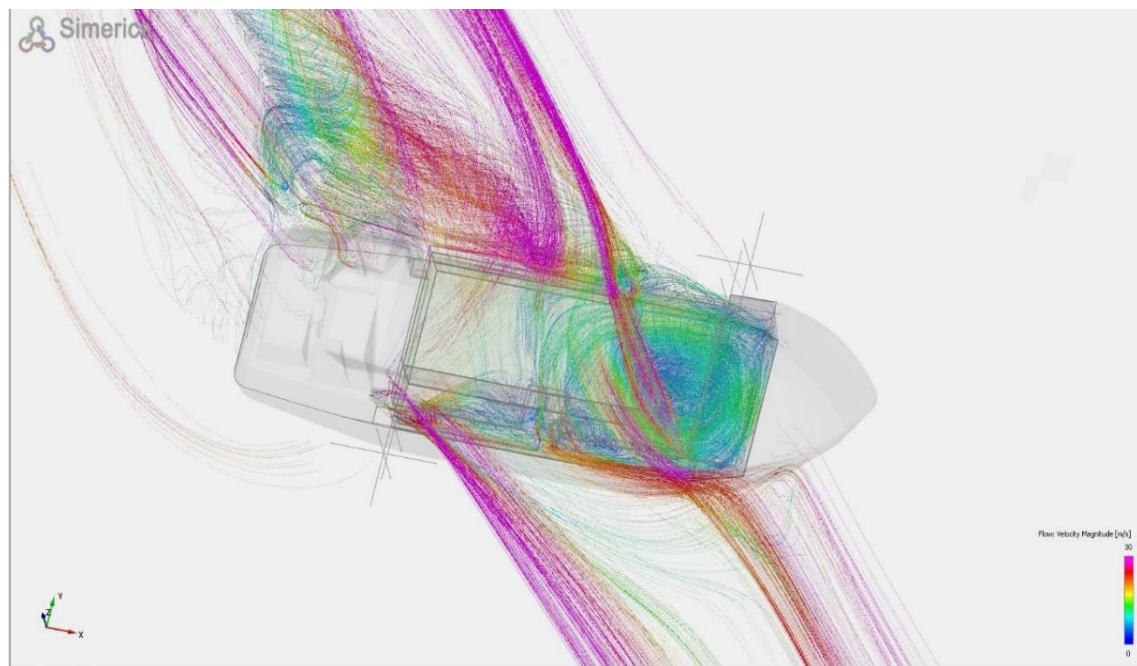


Fig.13: Velocity stall within the crab pots

As the simulation runs, the velocity distribution for the entire fluid domain is generated at user defined frequency intervals. The velocities are then combined with the particle trajectory model to understand where spray falls on the vessel.

7. Combining CFD Output with Droplet Trajectory Model

Wind velocities were now combined with the three-dimensional droplet trajectory model to analyse the spray droplets. Table VIII describes the initial conditions used in this simulation; droplet mass and momentum initial conditions remain the same as listed in Table VI. These conditions describe the location off the starboard bow of the vessel, beginning just forward of where the working deck begins. Fig.14 displays the result of the case of the vessel traveling at a speed of six knots with a wind speed of 15.5 m/s off the bow.

Table VIII: Initial conditions for a three-dimensional droplet trajectory analysis.

Note: origin has been shifted to amidships for this simulation.

Variable	Value
x-position (forward of amidships)	6 – 12 m
y-position (negative is starboard)	-8 – -5 m
z-position (above the free surface)	0 – 2 m
θ	50 – 100°
φ	-45 – -105°

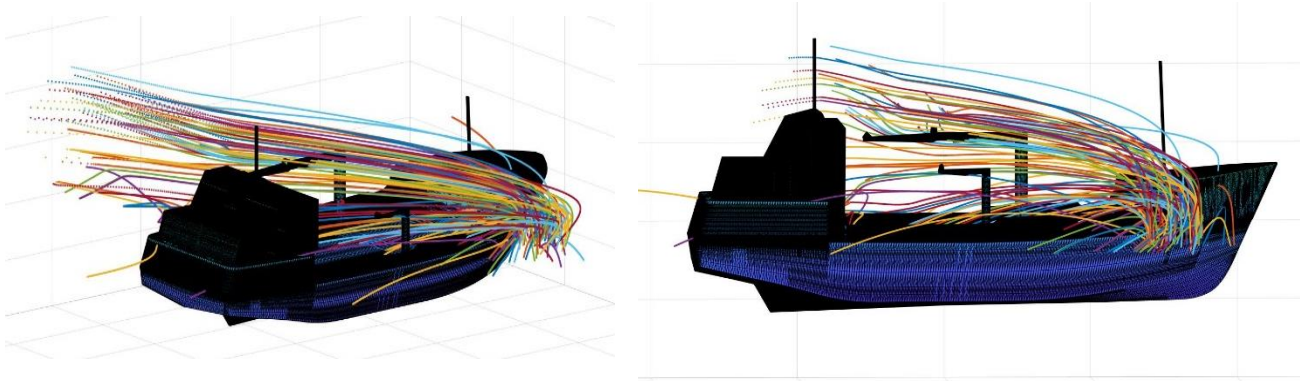


Fig.14: Results of the droplet trajectories with the initial conditions described in Table VIII with the flow velocities from the CFD simulation.

The differences between the analysis completed with a constant wind velocity and the output from CFD are stark. Although the crab pot stack is not shown in Fig.14, it has been properly modelled in the CFD simulation. Comparing the particle trajectories in Fig.14 with the velocity flow in Fig.10, almost the entirety of the spray droplets travel on a trajectory toward the forward, starboard portion of the crab pot stack. While a mass flux and thermodynamic analyses have not been completed, the authors postulate that ice will rapidly accumulate in this region of the vessel. These results are consistent with events experienced by mariners, Fig.2.

The surviving crew members of ‘Scandies Rose’ described the icing on the vessel as a “glaze,” *Free State Reporting* (2021). It can be assumed that crew members were describing the top of the crab pot stack, as this was the only location of the stack visible from the pilothouse or after regions of the vessel. The location of the area of the heaviest spray as identified by these simulations is an area that would not have been visible to any of the crew onboard; pathways to the bow were non-existent and visibility was limited due to the arrangement of the crab pot stack. Therefore, the crew would not have a clear understanding of the quantity of ice onboard the vessel at the time of sinking.

8. Way Forward

With the foundation of the sea spray analysis laid, the effect of true wind on the entire vessel with the crab pots, modelled as a porous surface, has been analysed with CFD software. The resulting velocity distribution has been incorporated with a three-dimensional droplet trajectory model to predict where ice will accumulate. This approach surmounts the limitations of previous approaches by considering the sea spray, localized weather conditions and unique geometry.

Next, a mass-flux analysis of both surface and vessel generated waves may then be conducted effectively quantifying the mass of sea water on deck. This will then be incorporated with thermo-dynamic models to determine the quantity of that water that freezes versus the quantity the returns to the sea. As these events unfold, it is important to conduct a time-step, iterative analysis where the CFD model is reanalysed with ice as the water begins to freeze. This phenomenon can be analysed through the CFD software by changing the porosity constants of the mesh. After a given number of iterations or

cycles, the quantity, and location of ice in the longitudinal, transverse and vertical directions, can then be quantified for subsequent stability analysis.

Computationally, the simulation is still too large, and the model needs to be further refined. In the next simulation, the refinement boxes will be adjusted to reduce the overall size of the model. To do this, the cell size of the outer refinement zone will be increased while the geometry of the inner refinement zone will be adjusted to capture the starboard and forward pots only. The target size of the model is 80-90M cells.

Acknowledgements

The authors appreciate the gracious assistance of Larry Liebman and Bruce Hays at Orca3d Marine, Chenjie Wang at Simerics and Miad Yazdani for their advice and support with this research.

References

- DEHGHANI, S.; MUZYCHA, Y.; NATERER, G. (2016a), *Droplet Trajectories of Wave Impact Sea Spray on a Marine Vessel*, Cold Regions Science and Technologies, Elsevier, pp.1-9
- DEHGHANI, S.; NATERER, G.; MUZYCHA, Y. (2016b), *Droplet Size and Velocity Distributions of Wave-Impact Sea Spray Over a Marine Vessel*, Cold Regions Science and Technologies, Elsevier, pp. 60-67
- DEHGHANI-SANIJ, A.; DEHGHANI, S.; NATERER, G.; MUZYCHA, Y. (2017), *Sea Spray Icing Phenomena on Marine Vessels and Offshore Structures: Review and Formulation*, Ocean Eng., Elsevier, pp. 25-39
- FETT, R.; ENGLEBRESTON, R.; PERRYMAN, D. (1993), *Forecasters Handbook for the Bearing Sea, Aleutian Islands and Gulf of Alaska*, Naval Research Laboratory
- FREE STATE REPORTING (2021), *Scandies Rose Marine Board of Investigation Hearing Transcript*, Court Reporting Transcription, Free State Reporting Inc.
- HUUHTANEN, J. (2018), *Collection and analysis of Arctic Maritime Accident Data*, Master's Thesis, Aalto University
- IMO (2008), *International Code on Intact Stability (IS Code)*, Int. Maritime Org., London
- LEWANDOWSKI, M.; WURL, M.; REGAN, S.; ELLIOTT, T.; TRUBAC, K.; BURCH, W. (2022), *Ice Accretion on Crab Pots*, Rapid Evaluation and Analysis of Current Technologies Report
- NTSB (2018), *Capsizing and Sinking of Fishing Vessel Destination*, Final Report, National Transportation Safety Board
- NTSB (2021), *Marine Accident Report: Capsizing and Sinking of Commercial Fishing Vessel Scandies Rose*, Final Report, National Transportation Safety Board
- OVERLAND, J. (1990), *Prediction of Vessel Icing for Near-Freezing Sea Temperatures*, J. Weather and Forecasting, pp. 62-77
- SHELLARD, H. (1974), *The Meteorological Aspects of Ice Accretion on Ships*, World Met. Org.
- USCG (2021), *Scandies Rose Search and Rescue Overview*, Marine Board of Investigation Exhibit 076, United States Coast Guard

Model Predictive Approach for Realistic Operational Decisions in Sea Passage Simulation

Jon S. Dæhlen, SINTEF Ocean AS, Trondheim/Norway, jon.daehlen@sintef.no
Endre Sandvik, SINTEF Ocean AS, Trondheim/Norway, endre.sandvik@sintef.no
Ulrik Jørgensen, SINTEF Ocean AS, Trondheim/Norway, ulrik.jorgensen@sintef.no

Abstract

The ability to predict the performance of novel subsystems and ship concepts is more important than ever now that the industry faces application of new systems of which little or no operational experience exist. Long-term simulation, with time horizons of months or even years, is a tool used in research and industry to predict the potentials and benchmark performance of novel concepts. Sea passage operation in the simulations, e.g., choice of speed and route, affect predictions of performance directly and can ultimately influence decisions for new-build and retrofit solutions. This paper suggests and tests a method for dynamically altering the speed of the simulated ship depending on the ship's performance, present weather, and weather forecast. Knowledge of how the ship will behave in various conditions are represented by a hydrodynamic ship simulation model, and an optimization algorithm is used as the inference engine.

1. Introduction

In accordance with the United Nations Sustainable Development Goal 13, the International Maritime Organization (IMO) has set goals to reduce greenhouse gas emissions (GHG) from the international shipping industry with 50% by 2050. As the global amount of shipping has grown by 250% in the last four decades, *Eskeland et al. (2016)*, IMO has also set supporting goals for emissions per transport work, aiming at 40% reduction by 2030, and 70% by 2050, *IMO (2018)*. Transition into low-, and zero-carbon fuels such as hydrogen, ammonia and methanol appear to be probable solutions to mitigate the carbon footprint of international shipping. However, these fuels require large amount of energy in production, and as the global demand for green energy will rise rapidly during the coming decades, it is a general opinion that the fuel price will increase significantly in the future, *Lindstad et al. (2021)*. Although energy-saving measures such as economy of scale and speed reduction still may have potential, there are practical limitations, and ways to improve existing, - and introduction of new technology is under continuous development, *Lindstad et al. (2018)*.

Alternative hull shapes, *Lindstad et al. (2019)*, friction reduction such as air-lubrication of the hull, exploiting wave energy using under-water wings, *Bøckmann and Steen (2016)*, and assisting ship propulsion with sails, are a few promising examples on technological innovations to make ships more energy efficient (often referred to as energy-saving devices). Several studies have done simulations to evaluate the effect of such measures on a particular ship on a given route, comparing ships with and without energy-saving devices. However, when considering realistic weather which varies both along the temporal and geospatial dimensions, the simulation result becomes highly sensitive to the route and speed decisions even with a conventional ship, *Sandvik et al. (2020)*. Common for all energy-saving measures are that they will alter the environmental conditions (i.e. wind and waves) impact on the ship's response, and studies has shown that for e.g. wind-assisted ship the saving potential is significantly larger than a conventional ship, *Bentin et al. (2016)*.

Traditionally, ship design is a highly experience-based discipline, using existing designs and operational profiles as basis for new developments. The increased complexity of how novel energy-saving measures will impact the operational routing and thereby the operational profile, poses a challenge as existing data cannot be used to the same extent as today when evaluating a prospective design at an early stage. Design decision to achieve low-emission or zero-emission ship concepts, through novel energy carriers and/or energy saving devices, affects the capital expenditures (CAPEX) and operational expenditures (OPEX) may pose challenges for operational performance and requirements (e.g. fuel availability, attainable speeds). Hence, due to their far-reaching consequences,

these decisions are made in the early and concept design phases. Our aim with the development of the present model is to provide necessary analysis functionalities that enhances ship owner's and designer's knowledge of realistic performance of concept ships in the early design stages.

1.1. The operational profile of a future ship

If simulation is used actively in the ship design, the scenario where the ship is evaluated in will have a direct impact on the ship design and choice of fuel and technology. In that sense, the scenario should reflect how the ship will be used in the future, which may not be how a ship of the same segment is operated today. As the world fleet becomes increasingly more energy efficient and environmentally friendly, the benefits, possibilities, drawbacks and limitations of the fuel and technology used to achieve this will be reflected in how the ships are operated on a day-to-day basis, and how the owner of the commodities to be transported sets requirements to the shipment service to lower transport costs. When opening this pandoras box, questions at all levels of the ship operation organization (and to the value chain itself) appear:

- Logistics: How will the world trade pattern look like in the future? Will the centralization of production in Asia continue, or will it shift to other parts of the world, *Cariou (2002)*, *Cariou and Lindstad (2021)*?
- Fleet: How will the future fleet size and mix look like, *Pantuso et al. (2014)*? More autonomy may motivate smaller, more flexible ships, but economy of scale has been a contributor to energy efficiency so far, *Akbar et al. (2021)*, *Lindstad et al. (2012)*.
- Scheduling: Will the constraints as of today such as hard limits for port calls be more flexible to allow for more energy-efficient ship operation? How will shipping contracts be in the future, *Montserrat (2021)*?
- Operational: As the fuels of the future is likely to be more expensive and possibly have more range limitations than conventional fuels, and to get maximum effect of energy-saving devices, will the variations in speed and route choices have larger variance than today? How will the operational profile for the life span of a ship built today look like?

Maritime stakeholders, e.g., ship owners, operators, regulators, and vendors, must manoeuvre towards a sustainable future exposed to the uncertainty of the boundary conditions these questions represent. Mitigating this uncertainty during design of new ships and retrofits involves awareness that ships may end up serving another trade route with other operational factors and constraints than originally planned for. Schedule optimization given a logistic demand and a fleet has been extensively researched, *Christiansen et al. (2013)*; however, to investigate how the schedule will change in the future, a guiding input should be how a low-emission and zero-carbon ship is best operated. For wind-assisted propulsion a lot of research has been done on how to simulate such a vessel, *Tillig and Ringsberg (2019)*, and the impact of sails has been evaluated for ships with and without sail assistance, sailing the same route at the same speed, *Tillig and Ringsberg (2020)*, *Van der Kolk et al. (2019)*, concluding that operational decisions such as speed have a high impact on the performance of the sailing ship, *Lu and Ringsberg (2020)*. Further, research has been done for weather routing of wind-assisted ships, however the hydrodynamics of the ship models used to evaluate solutions is generally simplified. Speed optimization has been investigated, *Tillig et al. (2020)*. However the speed was kept static for each sea passage. Thus it seems timely to explore a simulation method incorporating dynamic speed adjustments demonstrated in the tool GYMIR, *Dæhlen et al. (2021)*, replicating the processes of making operational decisions during simulations based on knowledge of the relevant ship model, as is the basic concept of Model Predictive Control, *Moradi (2003)*. The GYMIR simulator uses an agent-based discrete-event simulation strategy to combine hydrodynamic ship models developed in the ship design tool suite ShipX, *Fathi (2018)*, *Fathi and Hoff (2017)*, with hind- or forecast sea and weather data. Further, to mimic the decisions taken on the bridge during a voyage, the proposed method will assume that the weather forecast has a limited range in time, and that new forecasts arrive at regular intervals. In this paper the operational decisions are limited to the speed for the sea passage, however, the simulation architecture may incorporate path alterations as well.

2. Active scenario generation in discrete-event simulation

The presented sea-passage decision logic exploits the agent-based architecture of GYMIR. The simulation framework is designed so that the only requirement set to an agent is that it must return a time in the future where the simulator must be re-evaluated (i.e., next time step). Among the returned value from all agents, the discrete-event logic will find the one closest in the (simulated) future and select this as the next step where all agents will be re-evaluated. Originally the simulator consists of two agents, namely:

- The ship model with a set of waypoints and associated speed policies, calculating the power consumption, speed and ship response for a given waypoint. It returns the time required to reach the next waypoint on the route. This represents the ship that is object to the decisions taken.
- Weather data, giving the weather at the current time and position for use in the ship model. It returns the time when new data is available on the time dimension of the data set. This represents the weather that the ship is sailing through, i.e. slightly different from the forecast in a non-ideal world.

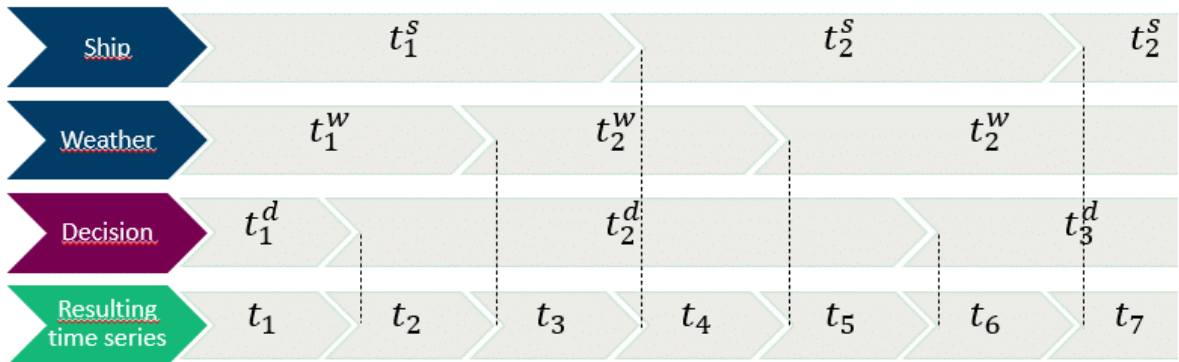


Fig.1: Decision stage integrated (red color) as an agent in discrete-event simulation strategy. Agents from basis simulation in blue.

These two forms the "basis" simulation stage, i.e. the simulation to be optimized. To this list the decision-making algorithm is added as shown in Fig.2.

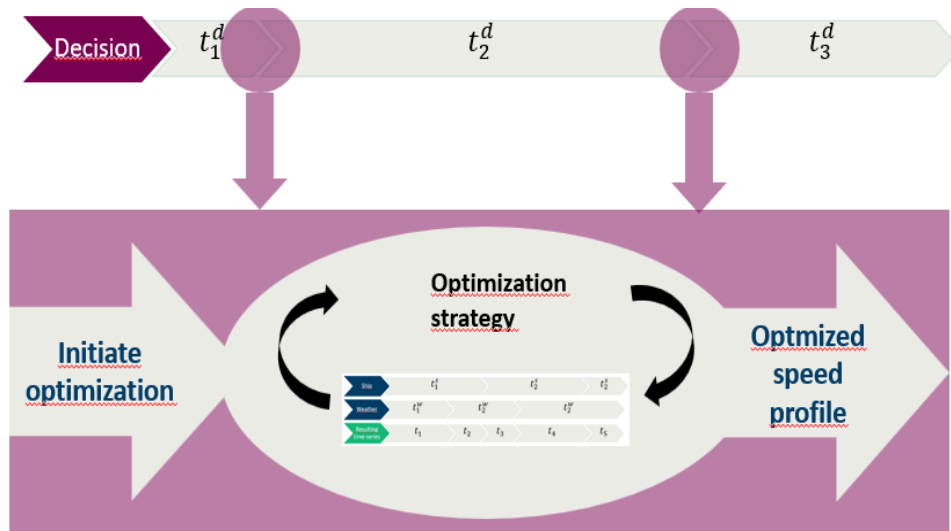


Fig.2: Decision stage detailed. Each time a new weather forecast is available, an optimization strategy using simulations to evaluate solutions is initiated with the current time and position of the basis simulation. The optimized speed profile is implemented in the basis simulation until a new forecast is available.

We assume that the sea passage plan is up-dated every time a new forecast is available, this will be the required return value from the decision-making agent. Each time a new forecast is available, the algorithm applies an optimization strategy using the GYMIR simulator itself with the newly arrived forecast data, forming the "decision" simulation stage. The ship model in this stage may be the same as in the basis simulation (i.e. the captain has perfect knowledge on how the ship behaves), or some erroneous or simplified (i.e. the captain has flaws) model. In any case, the optimized speed profile is transferred to the basis stage, and the simulation progresses while the decision algorithm is inactive until new forecast data is available.

2.1. Optimization strategy

The objective of the decision stage is to find the speed profile for the remainder of the sea passage that minimizes energy consumption, given the latest weather forecast data and a hard constraint on the time of the port call at the end of the sea passage simulation. This time is denoted t_{end} , and together with the time for the start of the sea passage t_{start} its maximum duration in hours can be expressed as $t_{max \text{ duration}}$. Set in an initial procedure before the basis simulation is executed is also the number of speed changes the decision stage should allow from the current position to origin, n_{change} , as well as the set $V_{alternatives} \in R_1$ of size $n_{alternatives}$ speed options that can be selected at each speed change. The decision stage is executed with the current time and position of the ship in the basis simulation, as well as the waypoints for the remainder of the simulation as input. Based on this, the decision stage will divide the remainder of the sea passage into n_{change} legs of equal length. Speed profiles are generated by varying the legs with speeds from $V_{alternatives}$, resulting in $n_{speed}^{n_{change}}$ simulations to be evaluated. Figure 2 illustrates how the optimization strategy is evaluated within the decision stage agent to update the speed profile of the basis simulation.

3. Results

For continuity, the ship model of a medium-range tanker is used as benchmark both in the basis and the decision stage, as well as the same transatlantic route from U.S (origin) to Europe (destination) from, *Dahlen et al. (2021)*, was selected for demonstrating the decision strategy. The length of the sea passage is 4607 nm, and the maximum allowed time consumption for the sea passage was set based on an average obtained speed of 11.6 kn. This makes the "slow-steaming" solution of 11 kn continuous invalid, which would have been an obvious solution as constant elements of OPEX such as crew cost and auxiliary energy consumption is not included. Table I summarizes some key parameters used in the simulation.

Table I: Static optimization parameters

Parameter	Value	Description
T_{start}	January 1 st 2018 00:00 GMT	Absolute time for start of sea passage from origin
t_{end}	January 17 th 2018 14:35 GMT	Absolute latest allowed time for port call at destination
$t_{max \text{ duration}}$	397	Maximum allowed time for sea passage (hours)
$n_{intervals}$	3	Speed intervals for remainder of sea passage (size of V)
$n_{alternatives}$	3	Number of (discrete) speed alternatives in each interval, i.e. size of $V_{alternatives}$
$t_{forecast}$	10	Length of forecast in days
$V_{alternatives}$	{11.0, 12.0, 13.0}	Speed alternatives in each interval in knots
V_i	$\{v_{1,i}, v_{2,i}, \dots, v_{n_{intervals},i}\}$	Optimal speed profile for remainder of sea passage (output from decision stage, implemented in basis simulation) at day i .

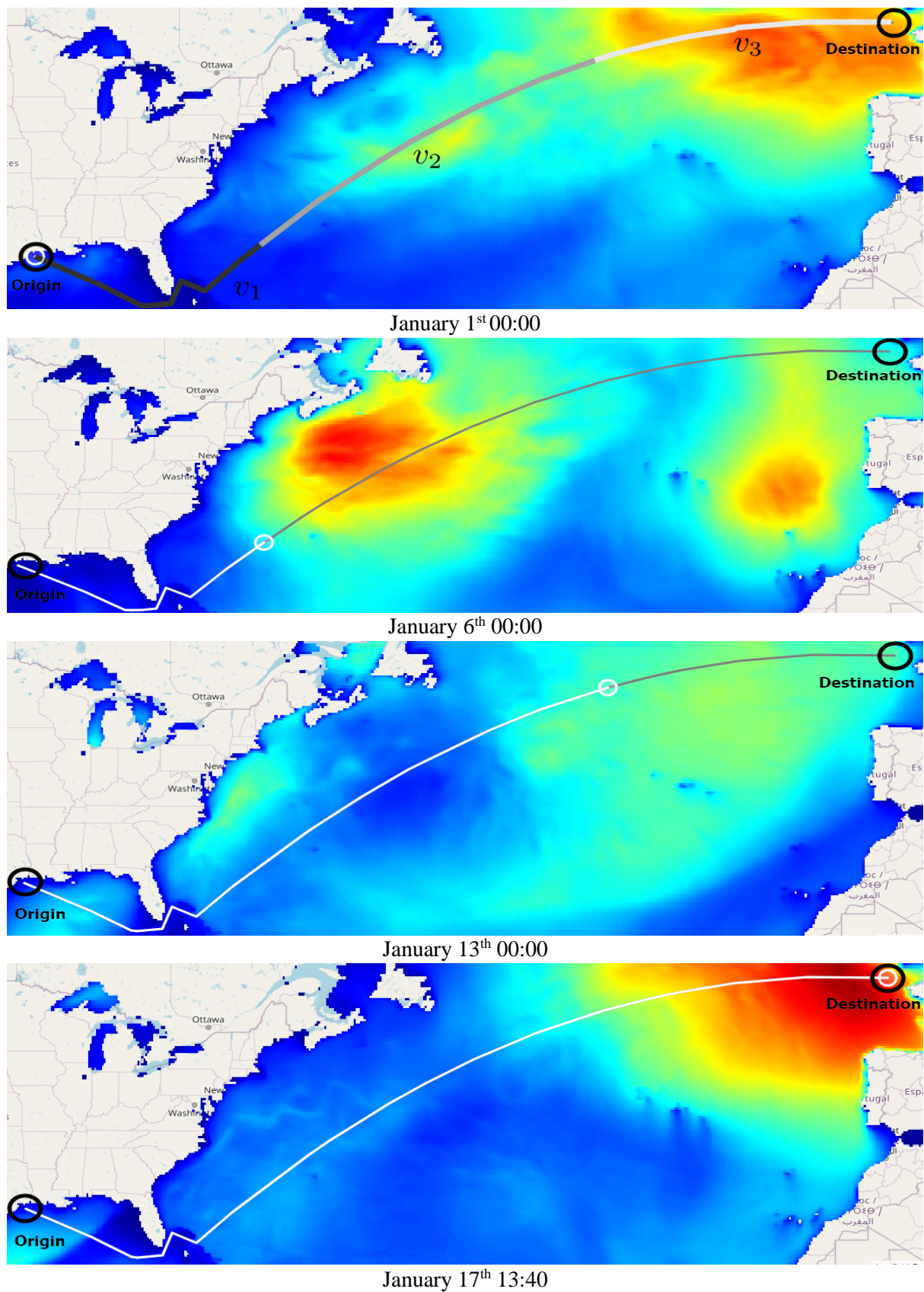


Fig.3: Illustration of the sea passage in the "perfect forecast" scenario from origin (Gulf of Mexico) to the destination (English Channel) and the significant wave height encountered in background colour. From above, the first figure illustrates the planning stage when leaving origin. Second and third figure illustrates the weather at the time of the first and second speed change, while the last illustrates how the ship encounters a storm when arriving at destination.

All weather and sea state data is retrieved from the ECMWF using the CDS service, *Hersbach et al. (2018)*. For the "perfect forecast scenario" and for the basis simulation in the "realistic forecast scenario", the "Reanalysis" dataset is used. As historic forecast data proved difficult to retrieve, the "ensemble mean" dataset was used as a substitute for forecast. This deviates slightly from the reanalysis, however the uncertainty does not increase with the time horizon into the future. The forecast horizon was reduced to only cover 10 days to replicate a realistic length of the forecast, and outside the range of the forecast calm sea is assumed in the decision stage. The update interval of the forecasts is set to each day at midnight, i.e. the decision stage is re-evaluated once a day.

3.1. Perfect forecast scenario

Using the same weather data source in the basis simulation as in the decision stage, this will represent a case in which the captain has perfect information of the weather on the route before leaving origin. As this "forecast" will cover the total duration of the passage, no new forecasts will arrive, and the passage will be divided into $n_{intervals}$. This speed profile will be implemented and never re-evaluated because no new information would be present. Fig.3 illustrates the sea passage with the wave height encountered at each speed change. As only one speed profile is calculated at day 1, thus only one set of optimal speed profiles are calculated (V_1), the subscript indicating the day of the decision is neglected in the figure.

Of the 27 speed profile candidates in the decision stage, four has an average speed of less than 11.6 knots and thus can be rejected without performing a simulation. Further, 12 more is rejected after simulation due to involuntary speed loss leading to too low average speed and following constraint violation. 11 candidates left, the three with the lowest energy consumption are shown in Fig.4.

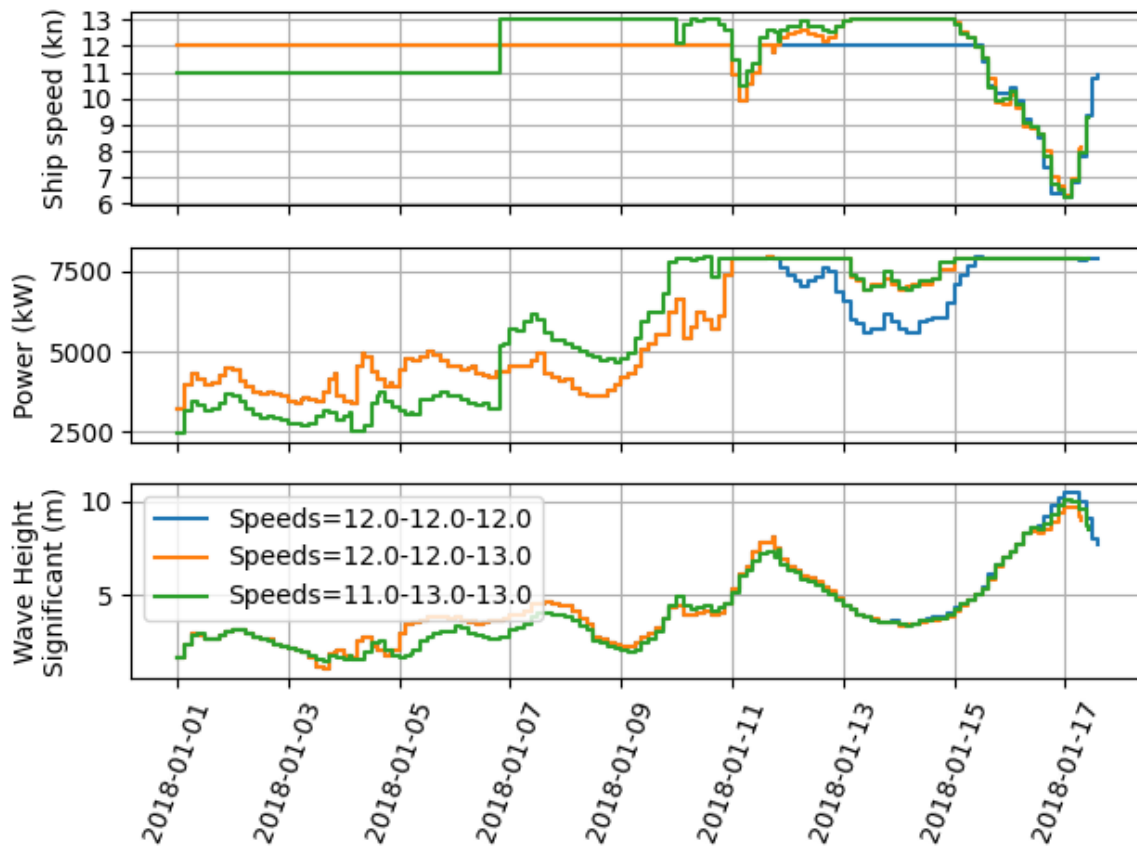


Fig.4: Optimized speed profiles using forecast with perfect accuracy and temporal coverage. Figure shows the three evaluated profiles with lowest energy consumption, within the time constraint. Legend describes the speed in each interval of the profiles.

The significant wave height time series show that the ship encounters both calm and harsh conditions during its voyage. Relatively calm weather is encountered in all scenarios from departure until January 5th. From this point, the ship experiences several periods of harsh wave conditions with significant wave height exceeding 5 metres. Finally, nearing the destination at the entrance to the English Channel, the ship encounters a storm with significant wave height exceeding 10 metres in several scenarios.

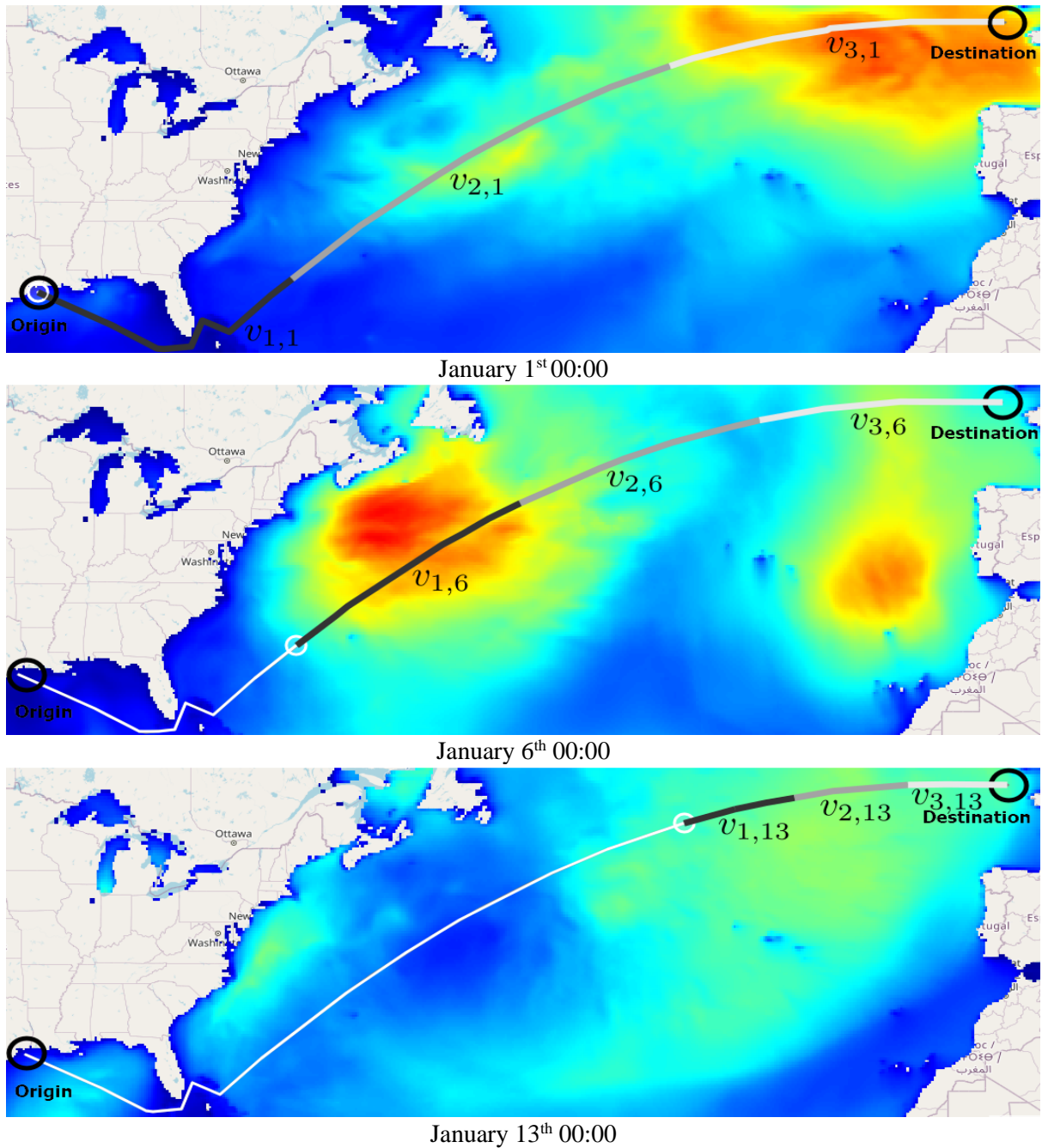


Fig.5: Illustration of the sea passage in the "regular forecast" scenario from origin (Gulf of Mexico) to the destination (English Channel) and the significant wave height encountered in background colour. From above, the first figure illustrates the planning stage when leaving origin at day 1. Note that the last part of the plan will not be based on forecast data due to limited temporal range on this. The second figure illustrates the 6th time the decision stage is evaluated, the forecast now covering the remainder of the sea passage. The third figure shows the 13th evaluation of the decision stage, the speed intervals being truncated as the basis simulation progresses.

These wave and wind conditions causes involuntary speed loss as the required propulsion power to maintain speed exceeds the installed power system capacity. This information is present to the optimization routine before the ship enters the storm, and thus the speed profiles holding a high speed before encountering the storm is preferred to minimize energy consumption while meeting the arrival time criterion. Summarized, the speed profile aiming at 12 kn in all intervals has the lowest energy consumption (2197 MWh) and would be the one implemented to the basis simulation stage.

3.2. Regular forecast scenario

In the regular forecast scenario, a 10-day forecast is assumed to become available every day at midnight, triggering a re-evaluation of the decision stage. Since the planned sea passage duration is approximately 16.5 days for the base-case, weather and sea states for the remaining period are assumed not known in the first part of the simulation. As the basis simulation progresses and the remaining distance of the sea passage shrinks, the size of the speed intervals will be reduced as n_{change} is kept constant. This will in essence make the resolution of the speed profile increase as the simulation progresses, as illustrated in Fig.5. It may, however, be argued that at early stages in the sea passage rougher plans are laid due to uncertainty in weather, berth availability etc., while the details and fidelity is increased as voyage uncertainties are reduced and amount of viable options decrease during later stages.

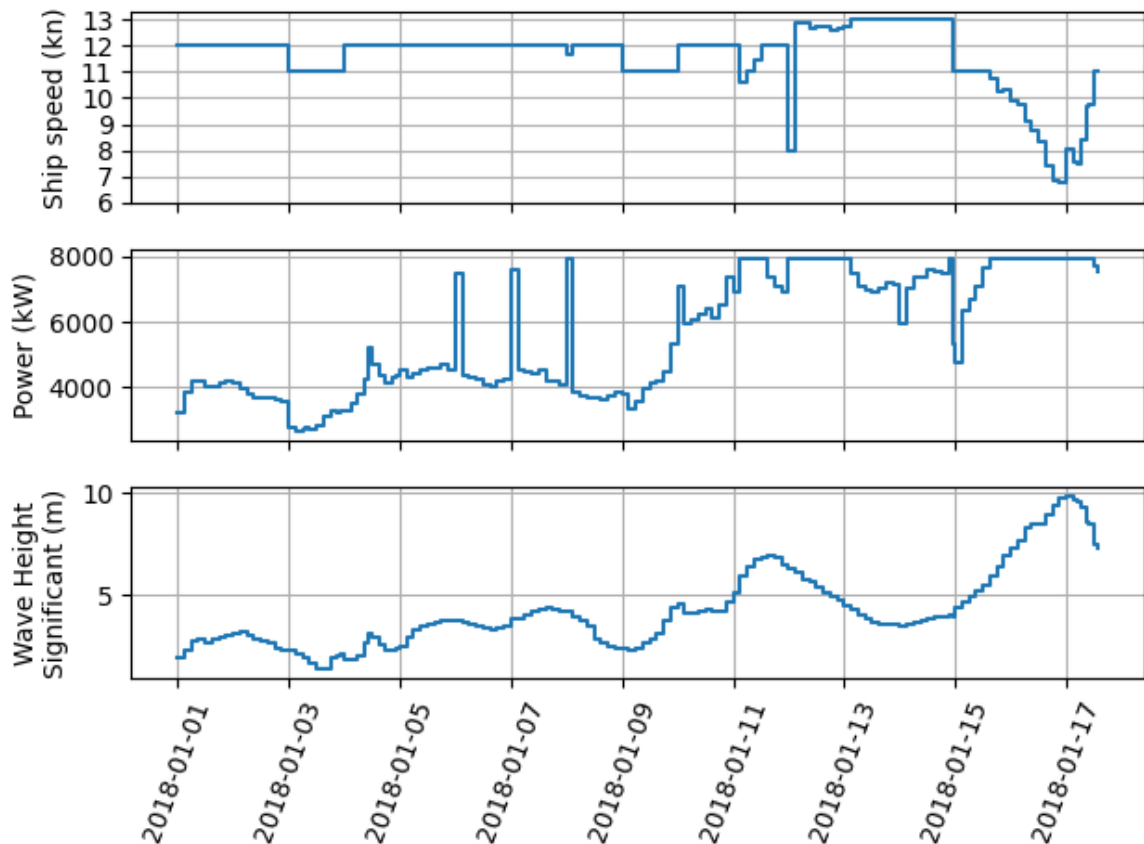


Fig.6: Optimized speed profiles using imperfect forecasts with temporal coverage of 10 days. Figure shows the resulting basis stage simulation.

Fig.6 shows the resulting basis stage simulation. Due to the limited forecast horizon, the future presence of the storm is not known until approximately January 5th. The response of the optimization routine until this point is to vary the speed between 11 and 12 kn to save energy (which would be optimal neglecting involuntary speed loss). When the full extent of the storm is revealed in the

forecast, the decision stage increases the speed to 13 kn in the period of more calm sea between January 13th and 15th to cope with the involuntary speed loss encountered between January 15th and 17th. In contrast, optimal speed profile in the scenario with perfect forecast did not need to increase the speed at the later phases of the sea passage. This scenario claimed 2197 MWh of energy. The similar figures can be explained by the former scenario keeping a slightly higher speed of 12 kn during the first half of the journey while the weather was calm, while the latter altered to 11 knots on some occasions. Further, as the regular forecast scenario achieves increased fidelity for its speed input intervals as the basis simulation progresses, better speed profiles can be taken later in the simulation with frequent speed changes, while the perfect forecast scenario is forced to keep the speed constant for the second and third fraction of the sea passage.

4. Discussions

This paper presents a model for simulating realistic operational profiles for virtual testing of future ship concepts and subsystems. The case study conducted shows how the behaviour and performance of a case ship is altered by varying its speed profile resulting in different weather conditions faced along the route. Ultimately, our aim is replicate realistic sea passages in which the ship's speed is adjusted according to both present and forecast weather conditions as well as other operational factors and constraints.

The current version of the model does require further development to achieve this goal. First, limiting the decision variables to only speed represents a major abstraction of reality, where also path is an essential part of planning of safe and efficient passage. Second, as observed in the present case study, other factors than energy efficiency and arrival time must be included to achieve realistic sea passages. In the presence of winter storms, with significant wave height exceeding 10 m, safety of crew, vessel and cargo is paramount. Third, more knowledge of the weather and sea state beyond the range of the forecast should be available in the decision stage, as at least some statistical assumptions based on season and region will be available to an experienced captain.

Further work will include modelling of actions prior to and during extreme weather events and factors and response variables providing sufficient description of risks and costs associated with harsh weather navigation. We must emphasize that it is not our aim that the model avoids all challenging conditions. The model should produce a long-term variation of wave and wind conditions which is as realistic as possible. Achieving this requires further improvement of the representation of weather forecasts, either in the form of historical forecasts for marine applications or through a stochastic model capable of replicating the uncertainty of forecasts for varying lead times.

5. Conclusion

It was argued for an improved strategy for creating realistic scenarios for sea-passage simulations to evaluate the performance of novel fuels and energy-saving technology. An extension of an existing simulation package was presented, which mimics operational decisions before and during a sea passage, considering a knowledge base of the characteristics and performance of the ship, as well as uncertainty in how the weather will evolve. Simulation results proved that the strategy is able to optimize the speed profile of a ship on a trans-Atlantic voyage and alter plans as forecasts unveil information during the sea passage.

Acknowledgements

This study has been financially supported by and is a part of the dissemination activities for the Norwegian Research Council (Norges Forskningsråd) project 237917 - The SFI Smart Maritime, and project 313863 ZeroCoaster.

References

- AKBAR, A.; AASEN, A.K.; MSAKNI, M.K.; FAGERHOLT, K.; LINDSTAD, E.; MEISEL, F. (2021), *An economic analysis of introducing autonomous ships in a short-sea liner shipping network*, Int. Trans. Operational Research 28(4), pp.1740-1764
- BENTIN, M.; ZASTRAU, D.; SCHLAAK, M.; FREYE, D.; ELSNER, R.; KOTZUR, S. (2016), *A New Routing Optimization Tool-influence of Wind and Waves on Fuel Consumption of Ships with and without Wind Assisted Ship Propulsion Systems*, Transportation Research Procedia 14, pp.153-162, <https://doi.org/10.1016/j.trpro.2016.05.051>
- BØCKMANN, E.; STEEN, S. (2016), *Model test and simulation of a ship with wavefoils*, Applied Ocean Research 57, pp.8-18
- CARIOU, P. (2020), *Changing demand for maritime trade*, OECD, https://www.itf-oecd.org/sites/default/files/docs/changing-demand-maritime-trade_0.pdf
- CARIOU, P.; LINDSTAD, E. (2021), *Container Shipping Decarbonization Pathways*, New Maritime Business, Springer, pp.75-93
- CHRISTIANSEN, M.; FAGERHOLT, K.; NYGREEN, B.; RONEN, D. (2013), *Ship routing and scheduling in the new millennium*, European J. Operational Research 228(3), pp.467-483, <https://doi.org/10.1016/j.ejor.2012.12.002>
- DÄHLEN, J.S.; SANDVIK, E.; RIALLAND, A.I.; LAGEMANN, B. (2021), *A Method for Evaluating Ship Concepts in Realistic Operational Scenarios using Agent-based Discrete-Event Simulation*, COMPIT, Mülheim, pp.141-150, http://data.hiper-conf.info/compit2021_muelheim.pdf
- ESKELAND, G.S.; LINDSTAD, H.E.; SANDAAS, I.; STEEN, S. (2016), *Revitalization of Short Sea Shipping Through Slender, Simplified and Standardized Designs*, SNAME Maritime Convention
- FATHI, D.E. (2018), *ShipX Vessel Responses (VERES)*, User's Manual, SINTEF Ocean
- FATHI, D.E.; HOFF, J.R. (2017), *ShipX Vessel Responses (VERES) Theory Manual*, SINTEF Ocean
- HERSBACH, H.; BELL, B.; BERRISFORD, P.; BIAVATI, G.; HORÁNYI, A.; MUÑOZ SABATER, J.; NICOLAS, J.; PEUBEY, C.; RADU, R.; ROZUM, I.; SCHEPERS, D.; SIMMONS, A.; SOCI, C.; DEE, D.; & THÉPAUT, J.N. (2018), *ERA5 hourly data on pressure levels from 1979 to present*, Copernicus Climate Change Service (C3S) Climate Data Store (CDS), <https://doi.org/10.24381/cds.bd0915c6>
- IMO (2018), *Strategy on Reduction of GHG Emissions from Ships*, Resolution MEPC.304(72)
- LINDSTAD, E.; BØ, T.I.; ESKELAND, G. (2018), *Reducing GHG emissions in Shipping-measures and options*, SINTEF Ocean
- LINDSTAD, E.; BORGES, H.; SANDAAS, I. (2019), *Length and hull shape importance to reach IMO's GHG target*, SNAME Maritime Convention
- LINDSTAD, E.; GAMLEM, G.; RIALLAND, A.; VALLAND, A. (2021), *Assessment of Alternative Fuels and Engine Technologies to Reduce GHG*, SNAME SMC, <https://doi.org/10.5957/SMC-2021-099>
- LINDSTAD, H.; ASBJØRNSLETT, B.E.; STRØMMAN, A.H. (2012), *The Importance of economies*

of scale for reductions in greenhouse gas emissions from shipping, Energy Policy 46, pp.386-398

LU, R.; RINGSBERG, J.W. (2020), *Ship energy performance study of three wind-assisted ship propulsion technologies including a parametric study of the Flettner rotor technology*, Ships and Offshore Structures 15(3), pp.249-258

MONTSERRAT, O.A. (2021), *An Analysis of Liner Shipping Network Efficiency through the Network of Contracts and Operational Processes*, MSc, Erasmus University Rotterdam

MORADI, M.H. (2003), *Predictive control with constraints*, JM Maciejowski, Pearson Education Ltd

PANTUSO, G.; FAGERHOLT, K.; HVATTUM, L.M. (2014), *A survey on maritime fleet size and mix problems*, European J. Operational Research 235(2), pp.341-349

SANDVIK, E.; NIELSEN, J.B.; ASBJØRNSLETT, B. E., PEDERSEN, E., & FAGERHOLT, K. (2020), *Operational sea passage scenario generation for virtual testing of ships using an optimization for simulation approach*, J. Marine Science and Technology, pp.1-21

TILLIG, F.; RINGSBERG, J.W. (2019), *A 4 DOF simulation model developed for fuel consumption prediction of ships at sea*, Ships and Offshore Structures 14(sup1), pp.112-120

TILLIG, F.; RINGSBERG, J.W. (2020), *Design, operation and analysis of wind-assisted cargo ships*, Ocean Engineering 211, 107603

TILLIG, F.; RINGSBERG, J.W.; PSARAFTIS, H.N.; ZIS, T. (2020), *Reduced environmental impact of marine transport through speed reduction and wind assisted propulsion*, Transportation Research Part D: Transport and Environment 83, 102380

VAN DER KOLK, N.; BORDOGNA, G.; MASON, J.C.; DESPRAIRIES, P.; VRIJDAG, A. (2019), *Case study: Wind-assisted ship propulsion performance prediction, routing, and economic modelling*, Int. Conf. Power & Propulsion Alternatives for Ships

Another Step towards Remote Inspections of Maritime Vessels using Tailored Inspection Drones Instrumented with Computer Vision

Erik Stensrud, DNV, Oslo/Norway, erik.stensrud@dnv.com

Kristian Klausen, ScoutDI, Trondheim/Norway, kristian.klausen@scoutdi.com

Abstract

This paper provides an updated progress status since COMPIT 2020 on new capabilities of the inspection drone system and computer vision for inspections in enclosed spaces.

1. Introduction

The paper provides an update on R&D results since COMPIT20. The motivation and background of this R&D project is provided in COMPIT19, *Stensrud et al. (2019)*, and previous results were reported in COMPIT20, *Stensrud et al. (2020)*.

2. Field trial onboard a stainless steel, chemical tanker

A field trial onboard an FPSO was reported in COMPIT20, *Stensrud et al. (2020)*. Another field trial was later conducted onboard the chemical tanker MS Latana , <https://utkilen.no/fleet/core-trade>, in a stainless steel tank. At first, it was tested operating the drone by wifi/bluetooth, i.e. without the tether. The mirror-like reflecting surface of stainless steel posed however some challenges for wireless signal transmission, so it was decided to use the tethered solution, Fig.1.

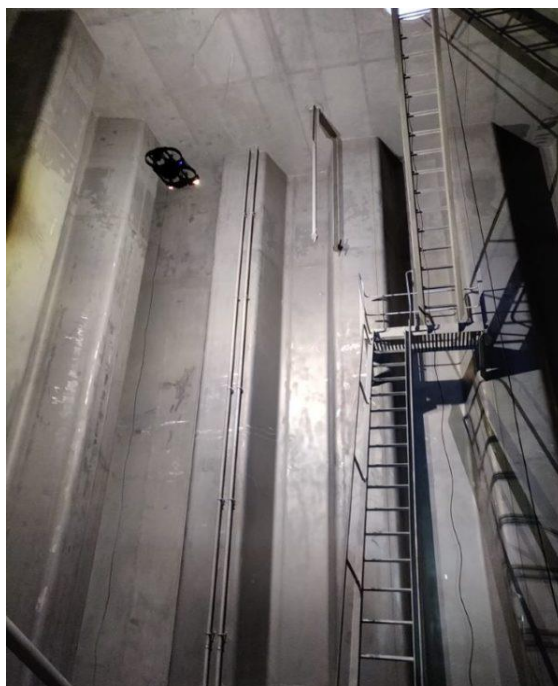


Fig.1: The Scout 137 Drone System inspecting the Latana Chemical Tanker

Two major milestones were reached in this trial. First, the drone pilot operated the drone from outside the tank, i.e. beyond line of sight (BLOS). BLOS drone operation has since been demonstrated at several occasions, see for example <https://www.scoutdi.com/casestudies/non-entry-tank-inspection/>.

The second milestone was that the attending surveyor acknowledged that the survey was “class equivalent”. That is, the drone inspection complied with DNV’s survey requirements, notably the requirements for visual close-up inspection quality.

In addition to the compliance with visual close-up quality, the drone enabled visual close-up inspection of the upmost parts of the compartment, a new capability, as the owner claimed that they “haven’t been this high in the tank before”. The tether system allowed for continuous inspection, saving time, and eliminated the risk of signal loss during flight. The anti-collision system prevented contact with the structure.

Several technology advances contributed to this milestone. The surveyor reported that:

- Live video stream was submitted to a tablet of sufficient size and video quality. The tablet made it possible to zoom directly in the livestream while flying.
- The high video quality made it possible to see both cracks and pittings.
- Hovering stability and maneuverability of the drone were very good.
- Collision prevention can be set to specific distances, an offset. The drone pilot can use this offset to maneuver the drone along e.g. a weld from start to stop with the same distance all the way.
- The drone generated a point cloud while flying. This is enabled by a positioning system combined with a lidar. The point cloud could in the future be used to create a 3D model of the compartment. (This technology is referred to as SLAM – Simultaneous Localization and Mapping.)
- The positioning system enables marking specific locations if something suspicious is detected, and then review the corresponding video sequences at a later time.

Other observations by the surveyor:

- Compared to erecting scaffolding or do a rafting inspection of tanks, this is a time-saving way of doing inspections. The preparations are few, and flying time to do close-up examination of the tank is probably 3-4 hours. (Tank dimensions were: height 11.5 m, width 9.5 m, and length 13.75m.)
- The drone is equipped with light producing approx. 10000 lumen. (For comparison, the surveyors torch is 650 lumen). This allows the drone to do the overall visual examination at a distance of 3 meters, probably even more, without additional light sources.
- For close-up visual examination, the drone can be maneuvered at high precision, and the operator can also move the camera up and down. This allows inspection of pipe openings within the tank and close-up of details like nozzles.
- Tank damages caused by the drone are not likely to happen. The drone is lightweight and made of softer materials than the tank. The drone might cause minor indents in the tank if falling from the top, which is an unlikely event.

3. Automated damage detection

At COMPIT 2020, crack detection in single images was reported, *Stensrud et al. (2020)*. In this section, we motivate for, and summarize results of, detecting and tracking cracks in videos. A corrosion detector has also been developed and compared to human performance on image level. In addition, we report preliminary learnings in extending the scope from cracks and corrosion to other damage types: grooving corrosion, pitting corrosion, and deformations.

3.1. Automated crack detection in videos

In remote visual inspection, the surveyors inspect the videos instead of being physically present on the site. Remote visual inspection is applicable when inspecting confined spaces, such as cargo or ballast water tanks, with drones. The robots capture many hours of video, often hundreds of hours, and it is therefore tedious to review the whole video. It would be useful if the surveyor could review only video frames containing an anomaly, and video inspection time would be further reduced if an anomaly is detected as the same anomaly across video frames rather than being detected as a new

anomaly in every video frame that it appears in. It is therefore important both to detect anomalies in the first place and to recognize the same anomaly, i.e. the same object, across video frames by tracking it from frame to frame.

A computer vision-based anomaly detection and object tracking system has therefore been developed. Currently, it detects and tracks only cracks. The system consists of two main modules, an object detection module and an object tracking module which tracks the detected object over the consecutive frames and maintains a unique index for the object.

The system performs object detection based on a bounding-box approach. The different classification techniques in images, object detection, image classification, and semantic segmentation, are explained in our COMPIT2020 paper, *Stensrud et al. (2020)*. General data collection and preparation was reported in our COMPIT19 paper, *Stensrud et al. (2019)*. The details of the object detection and tracking study (data, data augmentation, methods, algorithms, and detailed quantitative results) is reported in our paper by *Xie et al. (2021)*. Here, we report some extracts, only.

The training data were divided into training and validation datasets to train and find the best model. The model is fitted to the training dataset. The validation set is used to find the best fit. Table I shows descriptive statistics, and Fig.2 shows example images of the training and validation datasets.

Table I: Training and validation datasets - descriptive statistics

Description	Training data	Validation data
No. of images	2090	178
No. of ground truth bounding-boxes	3177	245

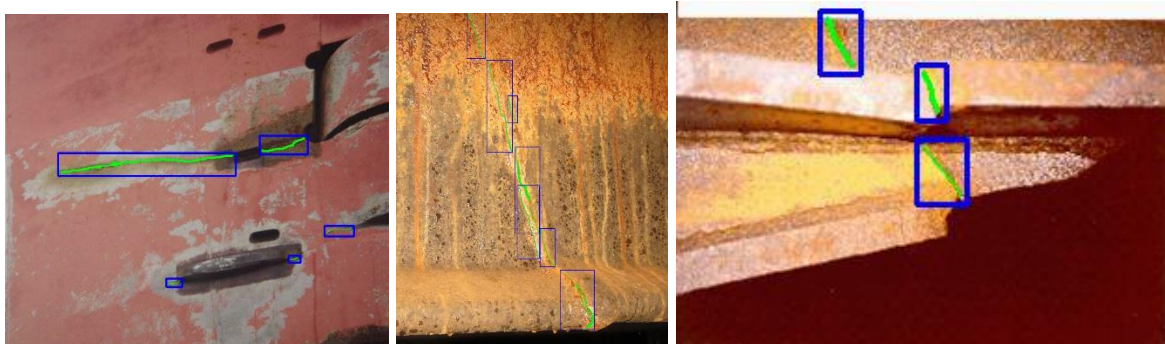


Fig.1: Labelled training and validation data – example images

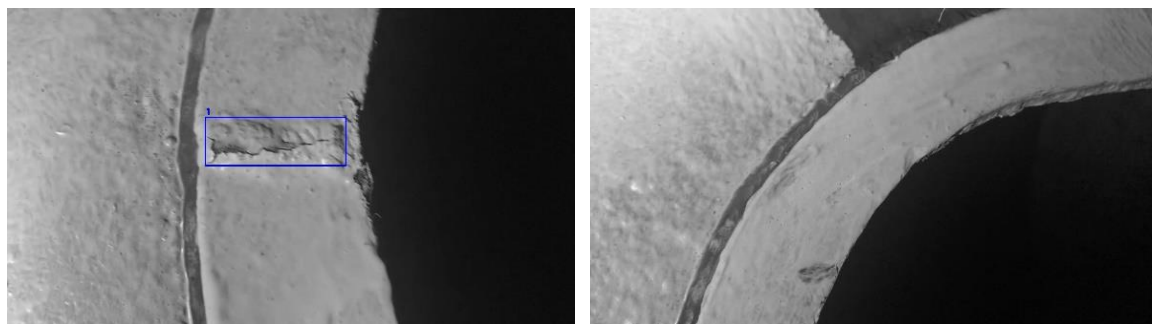


Fig.3: Test dataset – example of video frames (in grayscale): frame with crack (left); frame without crack (right)

The test data was a single video containing a single crack. The video was recorded with a handheld device. Fig.3 shows two video frames examples. Descriptive statistics for the video are reported in Table II. The object detection and object tracker modules were both tested on this video. Comparing the images in Figs.2 and 3, it should be observed that the crack in the video data frames may be

considered as quite different from the single images used to train and validate the model. In technical terms, the crack in the video probably is “out-of-distribution” to some extent. A low detection and tracking performance might therefore be expected.

Table II: Test dataset – descriptive statistics of the video

Description	N	Comment
Total no. frames	595	
No. of frames with the crack	450	Frames no. 42-491

Results: The basic evaluation metrics are True Positives (TP) and False Positives (FP). The decision of whether a detection is a TP or FP depends on the degree of overlap of the ground truth bounding box and the predicted bounding box. The degree of overlap is measured with Intersection over Union (IoU). Different IoU thresholds were evaluated in the study. A lower IoU threshold means that we require a smaller overlap between the ground truth bounding box and the predicted bounding box to count it as a hit. IoU threshold of 0.3 is reported in this study. For further examples and explanations of IoU thresholds, we refer to *Stensrud et al. (2020)*.

The results are of two kinds, object detection and object tracking, respectively. The object detection results are presented in Table III. 412 of the 450 actual video frames with cracks were detected, i.e. 92% (TP). There were also 47 false detections (FP). The detections were made in frames no. 45 - 595.

Table III: Object detection test results on video frames; IoU=0.3

Description	N
TP	412
FP	47

The goals of adding object tracking to the object detection is partly to increase the number of TPs and reduce the number of FPs, but primarily to recognize the crack across video frames by assigning it an identity, and ID. Comparing the results in Table IV and Table III, it is observed that the object tracker contributed to an increase in TPs from 412 to 439, i.e. 98% detection rate, and a decrease in FPs from 47 to 24. More importantly, the tracker was able to identify the cracks as only two different cracks. Without the tracker, there would have been identified 459 separate cracks (412+47), and the surveyor would have had to review all these video frames. Table V shows that the actual crack was correctly tracked through most of the video frames in which it appears. However, a false track was identified in video frame no. 562 and then tracked through 23 frames.

Table IV: Object detection test results enhanced by the object tracker on video frames; IoU=0.3

Description	N
TP	439
FP	24

Table V: Object tracking test results on video frames; IoU=0.3

Object ID	Frames
1	45-483
2	562-585

Discussion of the results. The results suggest that the object tracking module adds some value in reducing the number of FPs and FNs, but most importantly, it aids the surveyor by having to review a much smaller part of the video. For practical matters, this implies that the surveyor will still need to perform a risk-based review of parts of the video where no findings were reported. It also implies that the surveyor will spend extra time reviewing parts of the video where findings were reported, to discover they were just false alarms. However, the total survey time of the video could be significantly reduced with the aid of this object detection and tracking system.

3.2. Automated detection of other damage types

Automated corrosion detection and assessment of the corrosion extent: A corrosion detector has been developed that assesses the percentage corrosion of a given area. The extent of the corrosion is the basis for rating the coating condition according to *IACS Rec. 87 (2015)*, Table VI. The performance has been compared to human level performance. The current results suggests that it performs on par with humans. It should be noted that in the study also the human surveyors evaluated the images, only, and not the physical structure. This study is fully reported in *Hamre and Chen (2022)*.

Table VI: Coating condition rating

	GOOD (3)	FAIR	POOR
Breakdown of coating or area rusted (1)	< 3%	3 – 20 %	> 20 %
Area of hard rust scale (1)	-	< 10 %	≥ 10 %
Local breakdown of coating or rust on edges or weld lines (2)	< 20 %	20 – 50 %	> 50 %
Notes			
(1) % is the percentage of the area under consideration or of the "critical structural area"			
(2) % is the percentage of edges or weld lines in the area under consideration or of the "critical structural area"			
(3) spot rusting i.e. rusting in spot without visible failure of coating			

Automated corrosion detection and assessment of other damage types: Other damage types include groove, pits, and deformations. The general learning so far is that it is challenging, and maybe even impossible, to translate guidelines by IMO and IACS (2015) intended for human experts into precise formulas and algorithms. Therefore, the requirements themselves might need to be changed to fit what an algorithm can do and not do.

4. Drone system capabilities

The inspection drone must be able to be used in GPS-denied environments, be able to avoid collisions, and to be able to geo-tag any recorded data in the tank. This section presents some of the results from the manufacturer of the inspection drone used in the project, ScoutDI, <https://scoutdi.com>. They are divided in the following categories: Navigation and Control; Flying a pre-planned inspection route; Cloud-based laser data processing; and Close-up imaging.

4.1. Navigation and Control

When the drone is being operated by a pilot, it is important that it is easy to maneuver the drone to the desired position. The drone is now equipped with improved control algorithms, which makes it easier to slide along walls and other objects while inspecting. Furthermore, a new "close inspection mode" is introduced, which reduces the distance from the object to the camera down to 40 cm. Both of these features are now available in the commercially available inspection drone Scout 137. This drone is depicted in Fig.4.

The manual operation of the drone should be so easy that minimal pilot training is required, and that the surveyor can both operate the drone and inspect at the same time, without the need for a dedicated drone pilot.

4.2. Flying a pre-planned inspection route

In this research project, we have demonstrated integration between external inspection planning tools and the inspection drone. This will allow inspectors to plan an inspection route in a 3D model, and later have the drone execute this flight plan. Experimental testing to be conducted this year.

4.3. Cloud-based laser data processing

In this research project, we are evaluating using cloud-based computing resources to process sets of laser data that is larger than what the drone can handle on-board. This will allow for more accurate map generation using more complex and compute-intensive algorithms. In the end, the user will be able to run the processing on a web-portal.



Fig.2: Scout 137, an inspection drone specialized to tank inspections, <http://scoutdi.com>

4.4. Close-up imaging

The close-up imaging capabilities enables the operator to download a full resolution 4K image of a video frame in order to inspect it more closely. The real video stream on the operator's tablet shows only a limited resolution.

5. A new survey process – preliminary design

The survey process depicted in Fig.5 is based on some assumptions about technology maturity in the short term, i.e. the next couple of years. The process described below is early thinking on how the survey processes may be changed and adapted to benefit from emerging technologies such as automated drones and computer vision. They are as follows.

3D models might not contain all geometric details of the compartment, and therefore, an initial mapping flight is required to obtain the “as-built” 3D geometry before the flight can be planned, (Fig.5, step 0). It is still an open question whether the flight can be automatically planned immediately following the 3D mapping, or the mapping flight has to be a separate flight before planning close-up inspection points and the flight path. However, the initial 3D mapping will be conducted only once in the vessel's lifetime.

The drone can fly a pre-planned path but is not “intelligent” enough at present to spot suspects and change its flight plan to have a closer look (Fig.5, step 4). Therefore, the use of the term “autonomous” might be disputed.

As for the computer vision (Fig.5, step 6), false positives and negatives are expected. Therefore, a human expert must perform an independent verification (IV) the findings reported and do spot checks in areas where no findings were reported (Fig.5, step 7) and correct the automatically reported findings.

The remaining steps are “business as usual”, assessing the condition of the compartment, reporting, and submitting the quality-assured data to the repository, the product model (Pmod).

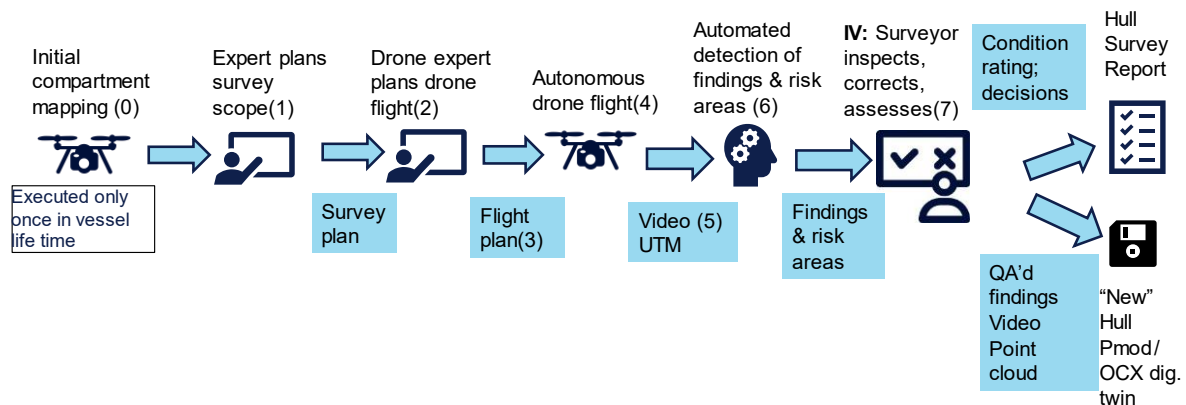


Fig.5: A new survey process

5.1. Tool support

The tool support, Fig.6, includes a survey planner and a flight planner that automate as much as possible of the planning process. The flight IV tool enables verification and pre-approval of the flight plan. It could be a simulator enabling spot checks of what the camera will see at the close-up locations, distances and camera angles. The digital inspector is the data collection system onboard the drone, capturing video, lidar point clouds, UTMs, tagged with their locations, and the actual flight plan. The findings detector is the automatic damage detector. In a first step, it is expected to be run on the video offline because of the required processing power. The drone's onboard computer is not expected to provide sufficient processing power. The findings IV tool will be the video inspection tool (elaborated in section 5.2), at present. In the future, video footage with marked findings may be stitched to form a 3D image of the compartment, for easier verification. The captured data and findings are automatically submitted to the product model, Pmod.

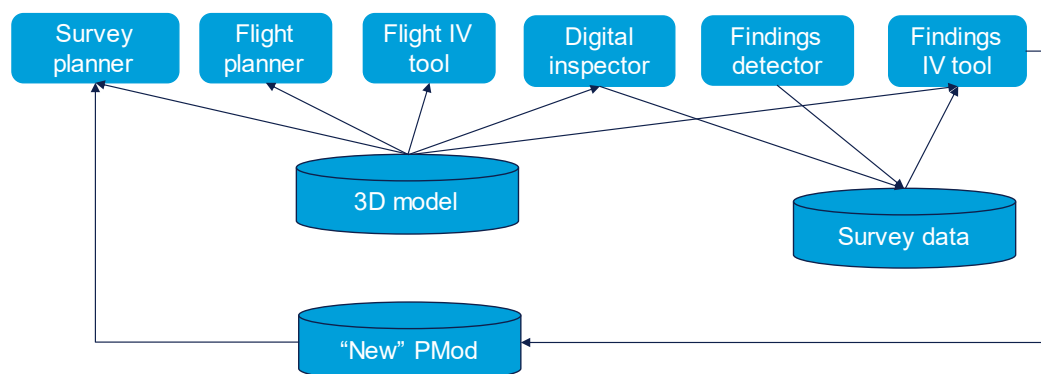


Fig.3: Software infrastructure – main components

Currently, a web application prototype is being developed that contains functionality of several of the components in Fig.6, as indicated in the menu on the left in **Error! Reference source not found..**

5.2. Video inspection tool

A video inspection tool has been developed to improve the effectiveness of video-based inspection, Fig.7. We have many hundreds of hours of videos of mooring chains, for example. The video inspection tool highlights the video frames where anomalies were detected and brings the attention to this subset of video frames. Furthermore, the object tracking system groups video frames that show the same defect. The surveyor can inspect a video frame where an anomaly is detected and either

confirm the finding or reject it as false positive. If it is rejected, it is removed from all the video frames that detected this anomaly. It is also planned to include functionality for adding anomalies in video frames where the automated system did not detect an anomaly, i.e. false negatives.

Together, this functionality enables independent verification of findings. Furthermore, the functionality enables retraining and improvement of the ML-algorithm since the surveyor corrects the automated system as part of the survey process.

Fig.7 shows the current user interface of the video inspection tool. The video is shown to the left and the 3D model to the right. The small blue rectangle in the video frame (left image) indicates a detected crack. The number “6” above the rectangle indicates that this is the sixth potential crack found in this video. The pink irregular patch indicate corrosion. The blue buttons beneath the video frame with text inside are buttons to play and stop the video, and the bar below it shows which frames contain a finding (blue color) and which frames do not (white color). A finding can be confirmed or rejected. The drone position and orientation matching the video frame is shown in the 3D model with a drone symbol and a red arrow, respectively. The blue buttons at the bottom of the 3D model provide various functionalities. For example, the 3D model can be shown from the drone’s perspective; the lidar point cloud can be overlaid; and so on.

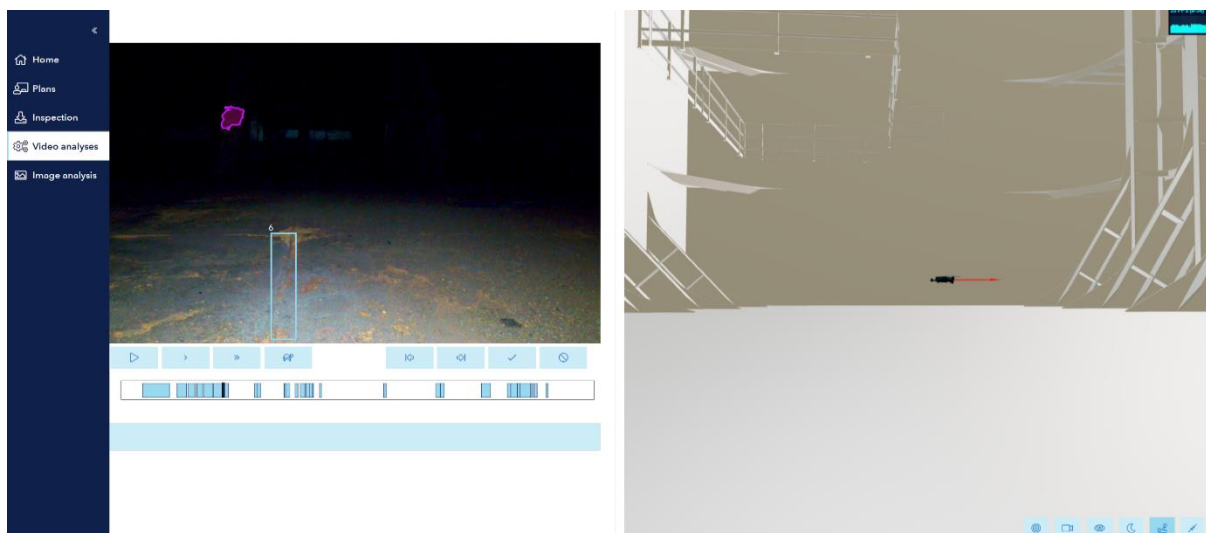


Fig.7: Web application with video inspection tool – user interface

The tool provides the surveyor/structural specialist with a good overview, and as the location of the video-view is visible as one scroll through the video-frames, it is easy to move to the areas of structural interest.

The feedback from surveyors is that the algorithms highlight the same issues as a human and trained surveyor would focus on, when looking at the same area. The majority of the false positives are also easy to rule out, with minimal effort.

In case one sees e.g. cracks in the coating being highlighted, whether this must be regarded as a finding or not, will depend on the structural location. Crack in coating in a given location, could be a finding which would require further inspection (removal of coating, cleaning) in order to check out the highlighted issue.

The tagging of findings in a 3D model will avoid the rediscovery of old and already reported and assessed findings accepted without repairs. Typically, this involves past dents and buckling findings, which are already found to be within established acceptance criteria several years back. This is a particular challenging issue on older vessel with much accumulated minor deficiencies, as both owner, inspection companies and Class Society changes personnel as time passes. Very few hull inspection

programs are able to track 100% of past findings, and in case they do, they are not easily available to e.g. the rope access personnel at the time of the “new” discovery. Hence valuable time is wasted by the 3rd party inspectors on describing, measuring and reporting defects, before the surveyor also spends time on comparing past PDF or Excel reports, only to rule out the finding. With inaccuracy, or lack of proper location description in some of the past reporting (wrong location, frame no, etc.), this often leads to new NDT’s being taken as part of the assessment. With a system where the findings are located and stored directly in the drone generated/existing 3D model, one can avoid these situations. Older vessels might not have 3D models, so the plan is to be able to generate them from 3D lidar point clouds, automating as much as possible of the conversion from a point cloud to a 3D model.

6. Conclusions and further work

The tracking of defects through individual video frames contributes to reduced manual effort in the video review. The performance of the computer vision (still some false negatives and false positives) requires a human expert in the loop to review and correct the false alarms and perform a risk-based review of parts of the video where no findings were reported. Despite these limitations, our surveyors still express that it adds value in reducing their effort to inspect the video. The performance is expected to increase as more data are collected and the algorithms are better tuned. However, it is an open question whether false positives and negatives will approach zero in the future.

The BLOS capability of the drone reduces the number of man entries. The drone itself can in some circumstances closely inspect upper areas in compartments that are inaccessible to humans, or at least so costly to inspect that it is not done.

The drone-based inspection is still purely visual, unlike the surveyor who can touch, remove scale and coating to inspect below the visible surface. Therefore, other compensating measures are being investigated.

There is still a number of investigations needed, for example to experiment with drone speeds, cameras, and light, to comply with the requirements for close-up photo quality; and experiments with lidar on the drone to assess 3D accuracy.

Acknowledgements

This research is partly funded by the Research Council of Norway through the ADRASSO and REDHUS projects, grant numbers 282287 and 317773, respectively.

References

- IACS (2015), *Guidelines for coating maintenance & repairs for ballast tanks and combined cargo/ballast tanks on oil tankers*, Recommendation 87, https://www.iacs.org.uk/media/2675/rec_087_pdf1213.pdf
- HAMRE, G.; CHEN, Y. (2022), *Computer vision for remote inspection*, DNV working paper
- STENSRUD, E.; SKRAMSTAD, T.; CABOS, C.; HAMRE, G.; KLAUSEN, K.; RAEISSI, B. (2019), *Automating inspections of cargo and ballast tanks using drones*, 18th COMPIT Conf., Tullamore
- STENSRUD, E.; SKRAMSTAD, T.; BASHIR, M.; GARETT, J.; HAMRE, G.; KLAUSEN, K.; RAEISSI, B.; ROSSVOLL, P.; XIE, J.; ØDEGÅRDSTUEN, A. (2020), *Towards Remote Inspections of Maritime Vessels Using Drones Instrumented with Computer Vision and Hyperspectral Imaging*, 19th COMPIT Conf., Pontignano
- XIE, J.; STENSRUD, E.; SKRAMSTAD, T. (2021) *Detection-Based Object Tracking Applied to Remote Ship Inspection*. Sensors 21(3), 761, <https://doi.org/10.3390/s21030761>

Super-Parametrizing CAD Models for Efficient Shape Optimization via Parametric Model Embedding

Andrea Serani, CNR-INM, Rome/Italy andrea.serani@cnr.it

Matteo Diez, CNR-INM, Rome/Italy, matteo.diez@cnr.it

Abstract

Methodologies for reducing the design-space dimensionality in simulation-driven design optimization have been recently developed based on unsupervised machine learning methods. These methods provide reduced dimensionality representations capable of maintaining a certain degree of design variability. Nevertheless, they usually do not allow to use the original CAD parameterization, representing a limitation to their widespread use in the industrial field, where the design parameters often pertain to well-established parametric CAD models. This work presents how to embed the parametric-model original parameters in a reduced-dimensionality representation. The method, which takes advantage from the definition of a newly-introduced generalized feature space, is demonstrated to the reparameterization of a free-form deformation design space.

1. Introduction

The need for increasingly performing functional-surface designs is constantly growing in many engineering fields, requiring increasingly accurate analysis and innovative solutions. The latter can be achieved via the simulation-driven design optimization (SDDO), *Harries and Abt (2019)*, paradigm, which integrates shape parameterization models, numerical solvers, and optimization algorithms. The demand for highly innovative designs often requires global optimization on ever-larger design spaces, with an ever-increasing number of design variables, leading unavoidably to the so-called curse of dimensionality (CoD), *Bellman (1957)*, for which the performance of an optimization algorithm degrades as the dimensionality of the problem increases. This strongly motivates the need of reducing the dimensionality of the design space before the optimization, especially in industrial design, where time resources are generally limited, *Serani et al. (2021)*. The remedy can be found in those dimensionality reduction techniques classified as unsupervised learning, feature learning, or also representation learning, *Bengio et al. (2013)*.

High-dimensional SDDO problems may be reduced in dimensionality using off-line design-space dimensionality reduction methods. Off-line or upfront methods have been developed focusing on the assessment of design-space variability and the subsequent dimensionality reduction before the optimization is performed. A method based on the Karhunen-Loève expansion (KLE, equivalent to the proper orthogonal decomposition, POD) has been formulated in *Diez et al. (2015)* for the assessment of the shape modification variability and the definition of a reduced-dimensionality global model of the shape modification vector. No objective function evaluation nor gradient is required by the method. The KLE is applied to the continuous shape modification vector, requiring the solution of a Fredholm integral equation of the second kind, *D'Agostino et al. (2020)*. Once the equation is discretized, the problem reduces to the principal component analysis (PCA) of discrete geometrical data. Off-line methods improve the shape optimization efficiency by reparameterization and dimensionality reduction, providing the assessment of the design space and the shape parametrization before optimization and/or performance analysis are carried out. The assessment is based on the geometric variability associated to the design space, making the method computationally very efficient and attractive (no simulations are required). Recently, *Khan et al. (2021)* have sequentially hybridized the design-space dimensionality reduction via KLE with the active subspace method, *Lukaczyk et al. (2013)*; *Tezzele et al. (2018)*, extracting the so-called functional features of designs in term of the geometric feature learned with KLE.

Although such methodologies have demonstrated their capability to alleviate the CoD, providing a reduced dimensionality representations capable of maintaining a certain degree of the original design

variability, they usually do not allow to use directly the original design-space parameterization, going back to the original space from the latent space. This aspect represents a limit to their widespread use in the industrial field, where the design parameters often pertain to well-established parametric models (e.g., CAD models).

The objective of this work is to discuss and demonstrate how to embed the parametric-model original parameters in a reduced-dimensionality representation. The proposed method, here introduced and called parametric model embedding (PME), represents a direct way to go back to the original parameterization from the reduced-dimensionality latent space, allowing therefore for the super-parametrization of the original parametric model.

The proposed method uses a generalized feature space that includes shape modification and design variables vectors together with a generalized inner product, aiming at resolving a prescribed design variability by properly selecting the latent dimensionality. A demonstration of the PME method is provided for the design-space reparameterization of a 22 design variables space based on free-form deformation (FFD), *Sederberg and Parry (1986)*.

2. Design-space dimensionality reduction

Consider a manifold \mathcal{G} , which identifies the original/parent shape, whose coordinates in the 3D-space are represented by $\mathbf{g}(\boldsymbol{\xi}) \in \mathbb{R}^3$; $\boldsymbol{\xi} \in \mathcal{G}$ are curvilinear coordinates defined on \mathcal{G} . Assume that \mathbf{g} can be transformed to a deformed shape/geometry $\mathbf{g}'(\boldsymbol{\xi}, \mathbf{u})$ by

$$\mathbf{g}'(\boldsymbol{\xi}, \mathbf{u}) = \mathbf{g}(\boldsymbol{\xi}) + \boldsymbol{\delta}(\boldsymbol{\xi}, \mathbf{u}) \quad \forall \boldsymbol{\xi} \in \mathcal{G} \quad (1)$$

where $\boldsymbol{\delta}(\boldsymbol{\xi}, \mathbf{u}) \in \mathbb{R}^3$ the resulting shape modification vector, defined by arbitrary shape parameterization or modification methods (e.g., CAD parameterization, Bezier surfaces, FFD, NURBS, etc.), and $\mathbf{u} \in \mathcal{U} \subset \mathbb{R}^M$ is the design variable vector. Fig.1 shows an example of the current notation.

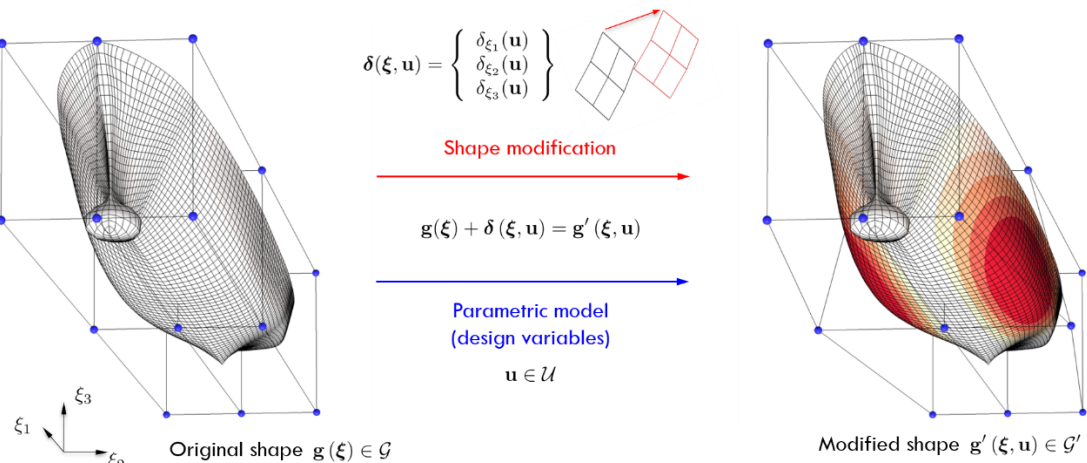


Fig.1: Shape modification example and notation

Consider the definition of the optimal design, through a SDDO optimization problem

$$\min_{\mathbf{u} \in \mathcal{U}} f(\mathbf{u}) \quad (2)$$

as a problem affected by epistemic uncertainty, where \mathbf{u} can be assumed as an uncertain/random parameter. The idea is that the optimal design, within the design space, exists but, before going through the optimization procedure, is unknown. Accordingly, the design variable vector \mathbf{u} is assigned with a probability distribution function $p(\mathbf{u})$, representing the degree of belief in finding the optimal solution in certain region of the design space. Consequently, the shape modification vector $\boldsymbol{\delta}$ goes stochastic and can be studied as random fields, e.g., by using the KLE, equivalent to POD.

2.1 Karhunen-Loève expansion: dimensionality reduction in the continuum geometric space

Consider $\delta(\xi, \mathbf{u})$ as belonging to a Hilbert space $L^2_\rho(\mathcal{G})$, defined by the generalized inner product

$$(\mathbf{a}, \mathbf{b})_\rho = \int_{\mathcal{G}} \rho(\xi) \mathbf{a}(\xi) \cdot \mathbf{b}(\xi) d\xi \quad (3)$$

with associated norm $\|\mathbf{a}\| = (\mathbf{a}, \mathbf{a})_\rho^{1/2}$, where $\rho(\xi) \in \mathbb{R}$ is an arbitrary weight function. Consider all possible realization of \mathbf{u} , the associated mean vector of δ is

$$\langle \delta \rangle = \int_{\mathcal{U}} \delta(\xi, \mathbf{u}) p(\mathbf{u}) d\mathbf{u} \quad (4)$$

and the associated geometrical variance equals to

$$\sigma^2 = \langle \|\widehat{\delta}\|^2 \rangle = \iint_{\mathcal{U}, \mathcal{G}} \rho(\xi) \widehat{\delta}(\xi, \mathbf{u}) \cdot \widehat{\delta}(\xi, \mathbf{u}) p(\mathbf{u}) d\xi d\mathbf{u} \quad (5)$$

where $\widehat{\delta} = \delta - \langle \delta \rangle$, with $\langle \cdot \rangle$ the ensemble average over \mathbf{u} .

The aim of KLE is to find an optimal basis of orthonormal functions for the linear representation of $\widehat{\delta}$:

$$\widehat{\delta}(\xi, \mathbf{u}) \approx \sum_{k=1}^N x_k(\mathbf{u}) \phi_k(\xi) \quad (6)$$

where

$$x_k(\mathbf{u}) = (\widehat{\delta}, \phi_k)_\rho = \int_{\mathcal{G}} \rho(\xi) \widehat{\delta}(\xi, \mathbf{u}) \cdot \phi_k(\xi) d\xi \quad (7)$$

are the basis-function components usable as new (reduced) design variables. The optimality condition associated to the KLE refers to the geometric variance retained by the basis functions through Eq.(6). Combining Eqs.(5)-(7) yields

$$\sigma^2 = \sum_{k=1}^{\infty} \langle (\widehat{\delta}, \phi_k)_\rho^2 \rangle \quad (8)$$

The basis retaining the maximum variance is formed by those ϕ , solutions of the variational problem

$$\begin{aligned} \max_{\phi \in L^2_\rho(\mathcal{G})} \quad & \mathcal{J}(\phi) = \langle (\widehat{\delta}, \phi)_\rho^2 \rangle \\ \text{subject to} \quad & (\phi, \phi)_\rho = 1 \end{aligned} \quad (9)$$

which yields (Diez *et al.*, 2015)

$$\mathcal{L}\phi(\xi) = \int_{\mathcal{G}} \rho(\xi') \langle \widehat{\delta}(\xi, \mathbf{u}) \otimes \widehat{\delta}(\xi', \mathbf{u}) \rangle \phi(\xi') d\xi' = \lambda \phi(\xi) \quad (10)$$

where \mathcal{L} is the self-adjoint integral operator whose eigensolutions define the optimal basis functions for the linear representation of Eq.(6). Therefore, its eigenfunctions (KL-modes) $\{\phi_k\}_{k=1}^{\infty}$ are orthonormal and form a complete basis for $L^2_\rho(\mathcal{G})$. Additionally, it may be proven that

$$\sigma^2 = \sum_{k=1}^{\infty} \lambda_k \quad \text{with} \quad \lambda_k = \langle x_k^2 \rangle \quad (11)$$

where the eigenvalues λ_k represent the variance retained by the associated basis function ϕ_k , through its component x_k . Finally, the solution $\{\phi_k\}_{k=1}^{\infty}$ of Eq.(10) are used to build a reduced dimensionality representation of the original design space; defining the desired confidence level l , with $0 < l \leq 1$, the number of reduced design variables N in Eq.(6) is selected such as

$$\sum_{k=1}^N \lambda_k \geq l \sum_{k=1}^{\infty} \lambda_k = l\sigma^2 \quad \text{with} \quad \lambda_k \geq \lambda_{k+1} \quad (12)$$

2.2 Principal component analysis: dimensionality reduction in the discretized geometric space

Discretizing \mathcal{G} by L elements of equal measure $\Delta\mathcal{G} = 1$, sampling \mathcal{U} by a statistically convergent number of Monte Carlo (MC) realizations S , so that $\{\mathbf{u}_k\}_{k=1}^S \sim p(\mathbf{u})$, and organizing the discretization $\mathbf{d}(\xi, \mathbf{u}_k)$ of $\hat{\delta}(\xi, \mathbf{u}_k)$ in a data matrix \mathbf{D} of dimensionality $[3L \times S]$

$$\mathbf{D} = \begin{bmatrix} d_{1,\xi_1}(\mathbf{u}_1) & d_{1,\xi_1}(\mathbf{u}_S) \\ \vdots & \vdots \\ d_{1,\xi_1}(\mathbf{u}_1) & d_{1,\xi_1}(\mathbf{u}_S) \\ d_{1,\xi_2}(\mathbf{u}_1) & d_{1,\xi_2}(\mathbf{u}_S) \\ \vdots & \vdots \\ d_{L,\xi_2}(\mathbf{u}_1) & d_{L,\xi_2}(\mathbf{u}_S) \\ d_{1,\xi_1}(\mathbf{u}_1) & d_{1,\xi_1}(\mathbf{u}_S) \\ \vdots & \vdots \\ d_{L,\xi_3}(\mathbf{u}_1) & d_{L,\xi_3}(\mathbf{u}_S) \end{bmatrix} \quad (13)$$

the integral problem of Eq.(10) reduces to the PCA of the autocovariance matrix \mathbf{A} of \mathbf{D} , such that

$$\mathbf{A}\mathbf{W}\mathbf{Z} = \mathbf{Z}\mathbf{\Lambda} \quad \text{with} \quad \mathbf{A} = \frac{1}{S} \mathbf{D}\mathbf{D}^T \quad (14)$$

where \mathbf{Z} and $\mathbf{\Lambda}$ are the eigenvectors and eigenvalues matrices of $\mathbf{A}\mathbf{W}$, with \mathbf{W} the diagonal matrix of the weight with dimensionality $[3L \times 3L]$ that is defined as

$$\mathbf{W} = \begin{bmatrix} \frac{\rho_1}{\sigma^2} & & & & \\ & \ddots & & & \\ & & \frac{\rho_L}{\sigma^2} & & \\ & & & \frac{\rho_1}{\sigma^2} & \\ & & & & \ddots \\ & & & & & \frac{\rho_L}{\sigma^2} \\ & & & & & & \frac{\rho_1}{\sigma^2} \\ & & & & & & & \ddots \\ & & & & & & & & \frac{\rho_L}{\sigma^2} \end{bmatrix} \quad (15)$$

with ρ_i (with $i = 1, \dots, L$) the weight coefficient for each element of \mathcal{G} and all zeros out of the diagonal. Note that \mathbf{Z} contains the discrete representation of the desired eigenfunctions ϕ_k .

2.3 Parametric model embedding

The design-space dimensionality reduction via KLE/PCA as already shown its capability in reducing the design-space dimensionality before the optimization loop, alleviating the well-known optimization problems associated with the CoD, e.g., *Diez et al. (2016a)*. Nevertheless, if the dimensionality reduction procedure is fed only with information on the shape modification vector, the method does not directly provide a way to return to the original design variables from the so-called latent space (the reduced dimensionality representation of the original shape parameterization). Two significant

criticalities ensue: (1) shape modification-based KLE obliges the user to change the shape modification methods and implement a new one using the eigenfunctions ϕ_k ; (2) moreover, depending on the bounds applied to the reduced design variables \mathbf{x} , there is not guarantee that the shape produced using KLE eigenvectors actually belongs to the original design space, thus potentially resulting in design infeasibilities.

In order to overcome these limitations, the idea is to augment the data matrix used for the dimensionality reduction procedure with the values of design parameters from the original parameterization. This allows to identify a reduced dimensionality representation using directly the original design variables (in addition to the reduced dimensionality representation of the shape modification vector), as conceptually shown in Fig.2.

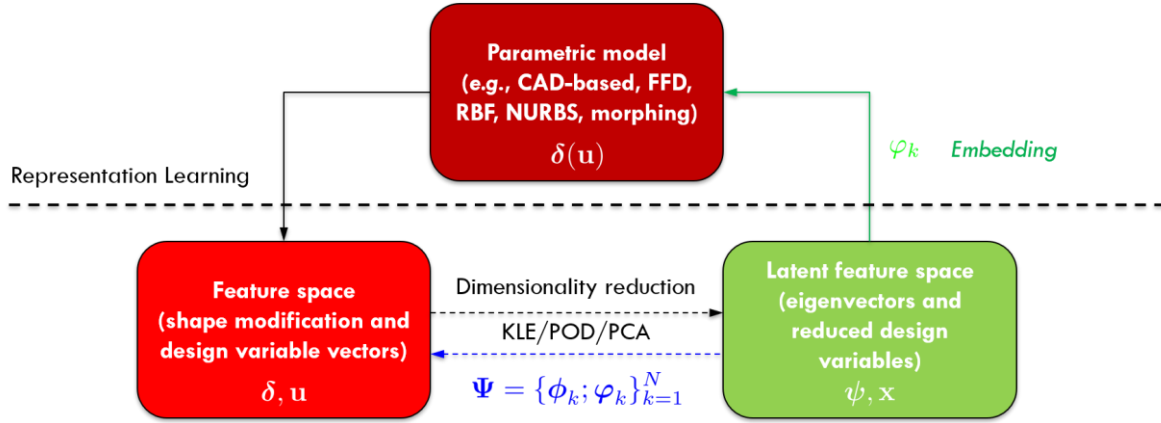


Fig.2: Parametric model embedding concept

Practically, the embedding is achieved defining a new matrix \mathbf{P} of dimensionality $[(3L + M) \times S]$, where the matrix $\mathbf{U} = [\mathbf{u}_1 - \bar{\mathbf{u}}, \dots, \mathbf{u}_S - \bar{\mathbf{u}}]$ of the original design variables (with $\bar{\mathbf{u}} = \langle \mathbf{u} \rangle$) is added to the data matrix \mathbf{D} and giving to \mathbf{U} a null weight such that

$$\mathbf{P} = \begin{bmatrix} \mathbf{D} \\ \mathbf{U} \end{bmatrix} \quad \text{and} \quad \mathbf{C} = \begin{bmatrix} \mathbf{W} & \mathbf{0} \\ \mathbf{0} & \mathbf{0} \end{bmatrix} \quad (16)$$

and so recasting Eq.(14) to

$$\tilde{\mathbf{A}}\mathbf{C}\Psi = \Psi\tilde{\Lambda} \quad \text{with} \quad \tilde{\mathbf{A}} = \frac{1}{S}\mathbf{P}\mathbf{P}^T \quad (17)$$

It can be proven that, having given a null weight to the component of \mathbf{P} corresponding to \mathbf{U} , Eqs.(14) and (17) provides the same eigenvalues and eigenvectors (considering the geometrical component ϕ_k of Ψ). In addition, the solution of Eq.(17) provides the eigenvector components ϕ_k that embeds the original design variables \mathbf{u} .

In order to reconstruct at least all the samples in \mathbf{D} the reduced design variables \mathbf{x} (or super-parameters) are bounded such as $\inf\{\alpha_k\} \leq \mathbf{x} \leq \sup\{\alpha_k\}$, with

$$\alpha_k = \mathbf{d}^T \mathbf{C} \Psi' \quad \text{for } k = 1, \dots, S \quad (18)$$

where Ψ' contains only the first N eigenvectors of Ψ , retaining the desired level of variance of the original design space. The PME is finally achieved reconstructing the original design variables by

$$\hat{\mathbf{u}} = \bar{\mathbf{u}} + \sum_{k=1}^N x_k \phi_k \quad (19)$$

3. Example application

The PME method is demonstrated for the shape reparameterization of the DTMB 5415 model, an open-to-public naval combatant hull widely used as benchmark in the ship hydrodynamic community,

Grigoropoulos et al. (2017). The design space has been defined within the activities of the NATO Science and Technology Organization, Applied Vehicle Technology (AVT), Research Task Group (RTG) 331 on “Goal-Driven, Multi-Fidelity Approaches for Military Vehicle System-Level Design”, Beran et al. (2020). The original design space is formed by $M = 22$ design variables, defined by the FFD method, Sederberg and Parry (1986). Specifically, the demi-hull is put in a lattice of $9 \times 3 \times 3$ nodes in the $\xi_1 \xi_2 \xi_3$ reference system, Fig.3. Note that the FFD lattice perfectly fit the demi-hull maximum dimension. Only 21 nodes are active (see blue sphere in Fig.3) and their degrees of freedom (DoF), associated to the design variables, are summarized in Table I (only one active node has two DoF, all the others have one DoF). Note that the lower and upper bound for \mathbf{u} are provided normalizing the lattice in a unit cube.

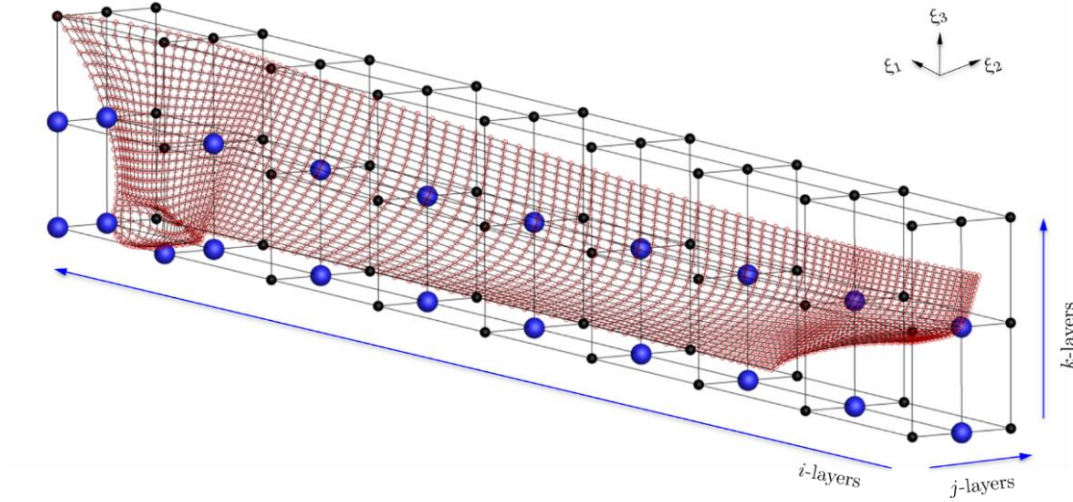


Fig.3: FFD design space definition and grid nodes used for the dimensionality reduction

Table I: FFD design variables definition

Design variable	i -layer	j -layer	k -layer	DoF	Lower bound	Upper bound
u_1	1	2	1	ξ_2	-0.500	0.500
u_2	2	2	1	ξ_2	-0.500	0.500
u_3	3	2	1	ξ_2	-0.500	0.500
u_4	4	2	1	ξ_2	-0.500	0.500
u_5	5	2	1	ξ_2	-0.500	0.500
u_6	6	2	1	ξ_2	-0.500	0.500
u_7	7	2	1	ξ_2	-0.500	0.500
u_8	8	2	1	ξ_2	-0.500	0.500
u_9	9	2	1	ξ_2	-0.500	0.500
u_{10}	1	2	2	ξ_2	-0.500	0.500
u_{11}	2	2	2	ξ_2	-0.500	0.500
u_{12}	3	2	2	ξ_2	-0.500	0.500
u_{13}	4	2	2	ξ_2	-0.500	0.500
u_{14}	5	2	2	ξ_2	-0.500	0.500
u_{15}	6	2	2	ξ_2	-0.500	0.500
u_{16}	7	2	2	ξ_2	-0.500	0.500
u_{17}	8	2	2	ξ_2	-0.500	0.500
u_{18}	9	2	2	ξ_2	-0.500	0.500
u_{19}	9	1	2	ξ_3	-0.250	0.250
u_{20}	9	1	1	ξ_1	-0.025	0.025
u_{21}	9	1	1	ξ_3	-0.100	0.100
u_{22}	8	1	1	ξ_1	-0.025	0.025

The PCA is trained by a set of $S = 1000$ MC samples, following *Diez and Serani (2020)*, where a parametric and statistical analysis conditional to the number of MC samples has been conducted. For the sake of simplicity, in the following, KLE refers to the dimensionality reduction based on the shape modification vector only, whereas PME refers to the dimensionality reduction using both the shape modification and the design variables vectors. The geometry is discretized by 90×25 grid nodes (shown with red circle in Fig.3), providing a data matrix \mathbf{D} of dimension $[6750 \times 1000]$. A weight coefficient $\rho_i = 1$ (see Eq.(15)) is imposed for all the grid nodes below the water line, while a null weight ($\rho_i = 0$) is used for the nodes above.

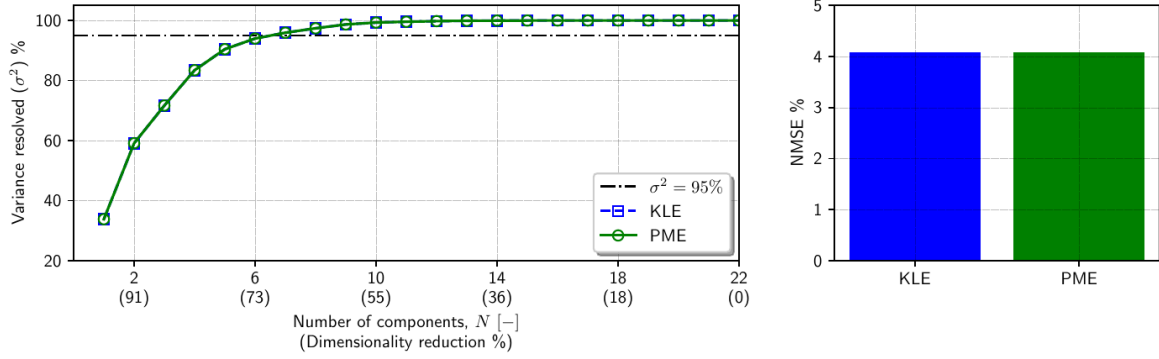


Fig.4: Variance resolved as a function of the number of reduced design variables (left) and NMSE (right) obtained with KLE and PME

Fig.4 shows the variance resolved by KLE and PME and the corresponding normalized mean squared error (NMSE) in reconstructing the matrix \mathbf{D} , where the desired level of variance to be retained was set to 95%. Specifically, Fig.4 (left) shows how KLE and PME cumulative sums of the eigenvalues (as percentage of the total variance) perfectly coincide. The number of reduced design variables to retain at least the 95% of the original geometric variance is equal to $N = 7$, achieving a dimensionality reduction close to 70%. Fig.4 (right) provides the corresponding $\text{NMSE} = 4\%$, showing again the consistency of the PME approach with KLE. The corresponding eigenfunctions ϕ_k , that can be used as shape modification basis by KLE, are shown in Fig.5 (top). Note that the PME method provides exactly the same eigenvector components for the shape representation, but in addition provides also the basis φ_k that embeds the original design variables (see Fig.5, bottom), allowing to use original shape modification method/parameterization without the need of using the geometrical eigenfunctions ϕ_k .

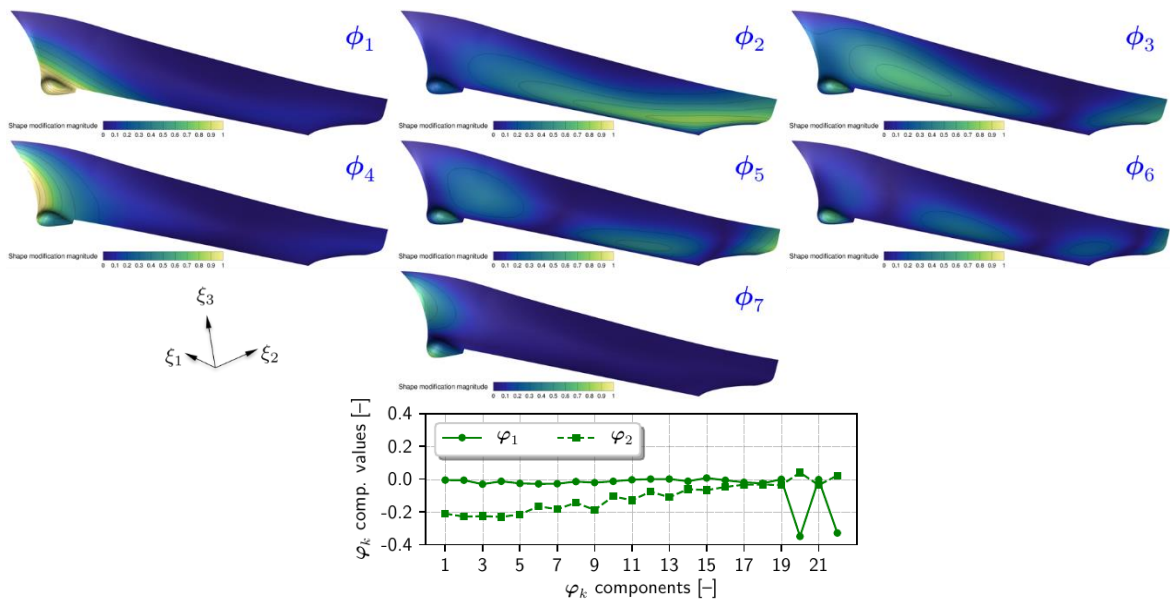


Fig.5: Design-space dimensionality reduction modes: (top) the shape modification vector modes ϕ_k and (bottom) first two modes φ_k that embeds the original design variables.

Once more, to show the consistency of PME with KLE, Fig.6 shows the correlation of the reconstruction error (normalized squared error, NSE) for each MC sample in \mathbf{D} , along with its probability density function (PDF). It is evident how the two approaches perfectly match. Furthermore, it may be noted how the mode of the NSE is lower than the mean value (NMSE), meaning that there are a large number of reconstructions below the NMSE threshold (complement of the variance retained). An example of geometry reconstruction is shown in Fig.7. Specifically, Fig.7 (top) shows one of the 1000 MC samples in \mathbf{D} obtained with FFD, KLE, and PME, from left to right, respectively and they are superposed in Fig.7 (bottom left). Minor differences can be seen comparing the FFD (black) with KLE (blue) and PME (green) and a detail of sonar dome is provided in Fig.7 (bottom centre and right). KLE in blue and PME in green show the same reconstruction error due to the truncation of the eigenvector expansion up to N (see Eqs.(6) and (19), respectively).

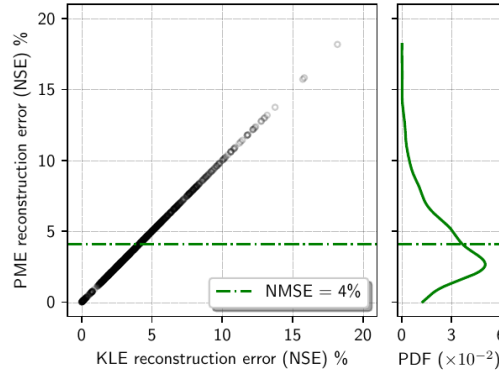


Fig.6: Correlation of KLE and PME reconstruction errors for geometry data set \mathbf{D} , along with PDF

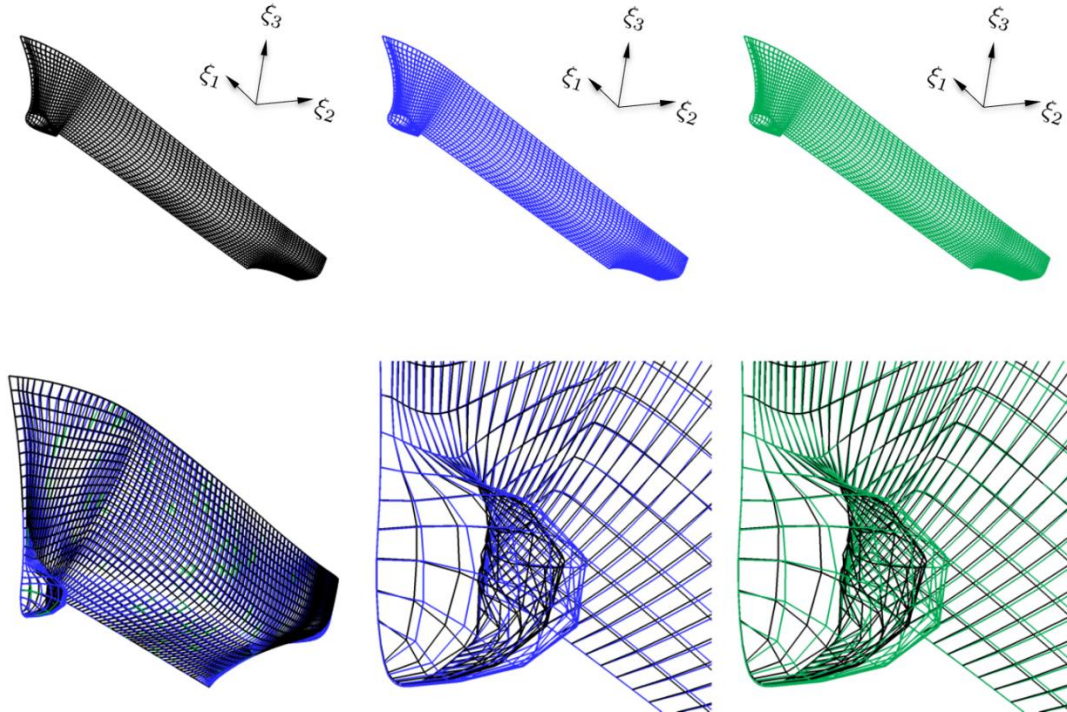


Fig.7: Example of reconstruction of a geometry of the data set \mathbf{D} : (top) design variant (left), reconstruction via KLE modes (centre), and reconstruction via PME (right); (bottom) shapes superposition and a detail of the sonar-dome differences.

Finally, selecting 1000 random samples of the reduced design variable vector \mathbf{x} , Fig.8 shows the corresponding reconstruction of the original design variables $\hat{\mathbf{u}}$: on bottom, each j -th sample is shown with a blue dot, for each component of $\hat{\mathbf{u}}$ (columns); on top, the corresponding PDF. It can be noted, that embedding the design variables allows to fill the whole original design space, but (at the same time)

provides many design variable vectors out of the domain bounds, thus producing possible infeasibilities. Nevertheless, this last point can be easily addressed, for consequent SDDO procedure, by penalizing those design the fall out of the original design space.

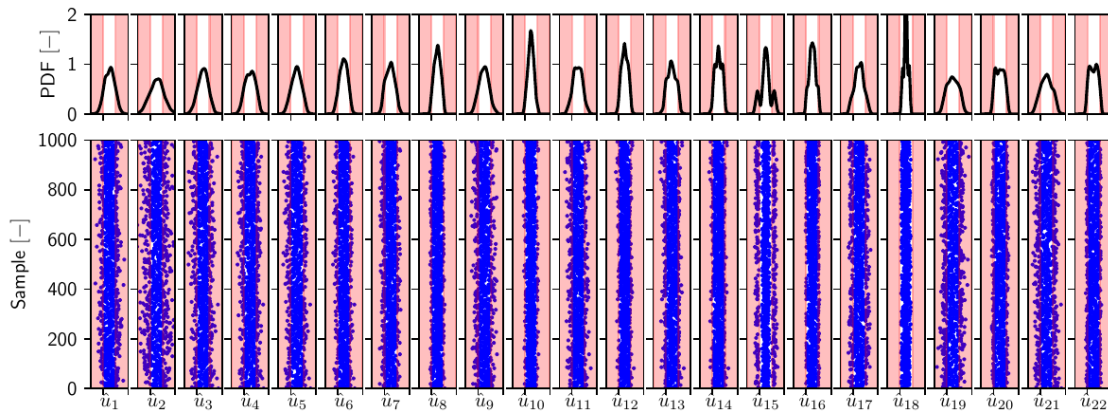


Fig.8: Reconstruction of the original design variable via PME for 1000 random samples

4. Conclusions and future work

A methodology to address the curse of dimensionality in shape optimization has been presented. The parametric model embedding method has demonstrated to be capable of providing a reduced dimensionality representation of the original design parameterization, using the original design parameters. The method extends the original design-space dimensionality reduction procedure based on the KLE of the shape modification vector, presented in *Diez et al. (2015)*. The autocovariance matrix of the shape modification vectors is augmented with the associated design variable vector. To the latter is imposed a null weight. This provides to PME the capability of achieving the same results of KLE in terms of design-space assessment and dimensionality reduction. In addition, PME provides a basis to embed directly the original design variables. This last point has a notable industrial implication, because overcome one of the previous limitations associated to the KLE, *i.e.*, the impossibility to return easily to the original parameterization. PME is demonstrated for an FFD-based design space of 22 design variables, providing the pathway for a possible direct integration in CAD software and shape optimization toolchain, releasing them from the necessity to implement a new shape modification based on the geometric component of the KLE eigenvectors.

Despite the evident benefits that PME provides to shape optimization, it is still relying on the linearity approximation of KLE and could not be as much efficient when strong nonlinearities are present in the shape parameterization or when the design-space dimensionality reduction procedure is extended to its physics-informed versions, *Diez et al. (2016b)*, where nonlinearities can arise from the physical quantities. For these reasons, future work will investigate the possible extension of PME to nonlinear dimensionality reduction methods, *D'Agostino et al. (2017)*.

Acknowledgements

The work is conducted in collaboration with the NATO task group AVT-331 on “Goal-driven, multi-fidelity approaches for military vehicle system-level design”.

References

- BELLMAN, R.E. (1957), *Dynamic programming*, Princeton University Press
- BENGIO, Y.; COURVILLE, A.; VINCENT, P. (2013), *Representation learning: A review and new perspectives*, IEEE Trans. Pattern Analysis and Machine Intelligence 35(8), pp.1798-1828

BERAN, P. S.; BRYSON, D.; THELEN, A. S.; DIEZ, M.; SERANI, A. (2020), *Comparison of multi-fidelity approaches for military vehicle design*, AIAA Aviation 2020 Forum (p.3158)

D'AGOSTINO, D.; SERANI, A.; CAMPANA, E. F.; DIEZ, M. (2017), *Nonlinear methods for design-space dimensionality reduction in shape optimization*, Int. Workshop Machine Learning, Optimization, and Big Data, pp.121-132

D'AGOSTINO, D.; SERANI, A.; DIEZ, M. (2020), *Design-space assessment and dimensionality reduction: An off-line method for shape reparameterization in simulation-based optimization*, Ocean Eng. 197: 106852

DIEZ, M.; CAMPANA, E. F.; STERN, F. (2015), *Design-space dimensionality reduction in shape optimization by Karhunen–Loève expansion*, Computer Methods in Applied Mechanics and Eng. 283, pp.1525-1544

DIEZ, M.; SERANI, A.; CAMPANA, E. F.; VOLPI, S.; STERN, F. (2016a), *Design space dimensionality reduction for single-and multi-disciplinary shape optimization*, 17th AIAA/ISSMO Multidisciplinary Analysis and Optimization Conf., (p. 4295)

DIEZ, M.; SERANI, A.; STERN, F.; CAMPANA, E.F. (2016b), *Combined geometry and physics-based method for design-space dimensionality reduction in hydrodynamic shape optimization*, 31st Symp. Naval Hydrodynamics, Monterey

DIEZ, M.; SERANI, A. (2020), *From Uncertainty Quantification to Shape Optimization: Cross-Fertilization of Methods for Dimensionality Reduction*, In International Conference on Uncertainty Quantification & Optimisation, pp.3-19, Springer, Cham

GRIGOROPOULOS, G.; CAMPANA, E. F.; DIEZ, M.; SERANI, A.; GOREN, O.; SARIÖZ, K.; DANISMAN, D.; VISONNEAU, M.; QUEUTEY, P.; ABDEL-MAKSoud, M.; STERN, F. (2017), *Mission-based hull-form and propeller optimization of a transom stern destroyer for best performance in the sea environment*, VII Int. Conf. Computational Methods in Marine Engineering (MARINE 2017)

HARRIES, S.; ABT, C. (2019), *Faster turn-around times for the design and optimization of functional surfaces*, Ocean Eng. 193, 106470

KHAN, S.; SERANI, A.; DIEZ, M.; KAKLIS, P. (2021), *Physics-informed feature-to-feature learning for design-space dimensionality reduction in shape optimisation*, AIAA Scitech 2021 Forum (p.1235)

LUKACZYK, T.; PALACIOS, F.; ALONSO, J.J.; CONSTANTINE, P. (2014), *Active subspaces for shape optimization*, 10th AIAA Multidisciplinary Design Optimization Specialist Conf., National Harbor

RAGHAVAN, B.; BREITKOPF, P.; TOURBIER, Y.; VILLON, P. (2013), *Towards a space reduction approach for efficient structural shape optimization*, Struct Multidiscip. Optim, 48, pp.987-1000

SEDERBERG, T.W.; PARRY, S.R. (1986), *Free-form deformation of solid geometric models*, 13th Annual Conf. Computer Graphics and Interactive Techniques, pp.151-160

SERANI, A.; STERN, F.; CAMPANA, E.F.; DIEZ, M. (2021), *Hull-form stochastic optimization via computational-cost reduction methods*, Engineering with Computers, pp.1-25

TEZZELE, M.; SALMOIRAGHI, F.; MOLA, A.; ROZZA, G. (2018), *Dimension reduction in heterogeneous parametric spaces with application to naval engineering shape design problems*, Adv Model Simul Eng Sci, 5(1), 25

Development of an Early-Stage Design Tool for Rapid of Distributed Ship Service Systems Modelling in Paramarine – A Submarine Case Study

Muhammad Mukti, UCL, London/UK, hary.mukti@ucl.ac.uk

Rachel Pawling, UCL, London/UK, r.pawling@ucl.ac.uk

David Andrews, UCL, London/UK, d.andrews@ucl.ac.uk

Abstract

The sophisticated 3D based synthesis that is enabled by the UCL Design Building Block (DBB) approach means the designer can model distributed ship service system(s) (DS3) physical entities to whatever level of detail deemed necessary well beyond the DS3 concept design level. The high flexibility of the Paramarine ship design toolset, particularly the descriptive ability provided by the DBB objects through storing data at different levels of design granularity, enables design exploration to different levels of design hierarchy. However, several drawbacks have been found in implementing such a sophisticated (fully 3-D) modelling tool in Early Stage Ship Design (ESSD). These include the effort to model or create each of the numerous features and placing them individually in the vessel's configuration. The paper presents the development of an ESSD tool that can rapidly generate a submarine early stage design with significant DS3 definition. That definition is sufficiently descriptive but still general enough to allow the level of flexibility in design exploration required at early design stages. The tool aimed to make the 3D based synthesis execution process as simple as possible so that the designer is able to manipulate the 3D architecture of the vessel and focus on important architecturally driven decision making in ESSD. An ocean going conventionally powered submarine case study was undertaken and demonstrated the capability and the flexibility of the tool.

1. Introduction

As a Physically Large and Complex System (PL&C), Andrews (2012), the submarine design process encompasses various design phases and is conducted by different organisations. The design process consists of several concept, assessment or feasibility, followed by contract or project definition to fix price and check out the selected design remains balanced (especially the buoyancy and stability balance which is more demanding in submarine design than surface ship design) before proceeding to detailed design, Andrews (1994). However, in the initial sizing of complex vessels, where recourse to type ship design can be overly restrictive, one crucial set of design features has traditionally been poorly addressed. This is the estimation of the weight and space demands of the various Distributed Ship Services System(s) (DS3), which is “a collection of connected components that provide a service from one or multiple sources to multiple users, via connections throughout the ship, directed towards defined functions, supporting specific operations of the vessel”, Mukti *et al.* (2021). Such an approach inhibits the ability of the concept designer to consider the impact of different DS3 options, Andrews (2018).

Given the advancement of computer graphics, not utilising such technology to better synthesise DS3 in ESSD was seen to be not taking advantage of Computer-Aided Design (CAD) developments. Thus, this paper begins by outlining a proven design method utilising a sophisticated fully three-dimensional (3D) Computer-Aided Ship Design (CASD) software that could potentially accommodate both the synthesis of the whole submarine as well as that for the DS3. This is followed by investigating the modelling issues in using such a CASD tool for DS3 synthesis. Sections 4, 5, and 6 describe a new tool to mitigate the identified issues. After that, a case study demonstrates the applicability of the new tool, followed by conclusions and recommendations.

2. Computer-Aided Ship Design

In this section, a short review of a CASD approach that could potentially accommodate DS3 synthesis is provided and then the potential emergent issues using such CASD are discussed.

2.1. The UCL Design Building Block Approach

The UCL Design Building Block (DBB) approach, *Andrews and Dicks (1997)*, is a proven design method and was implemented as the SURFACE CONcept (SURFCON) module (for both surface ships and submarines as shown in Fig.1) in the sophisticated fully three-dimensional (3D), commercial naval architectural CAD software Paramarine™, <https://paramarine.qinetiq.com/products/paramarine/index.aspx>, *Andrews and Pawling (2003)*.

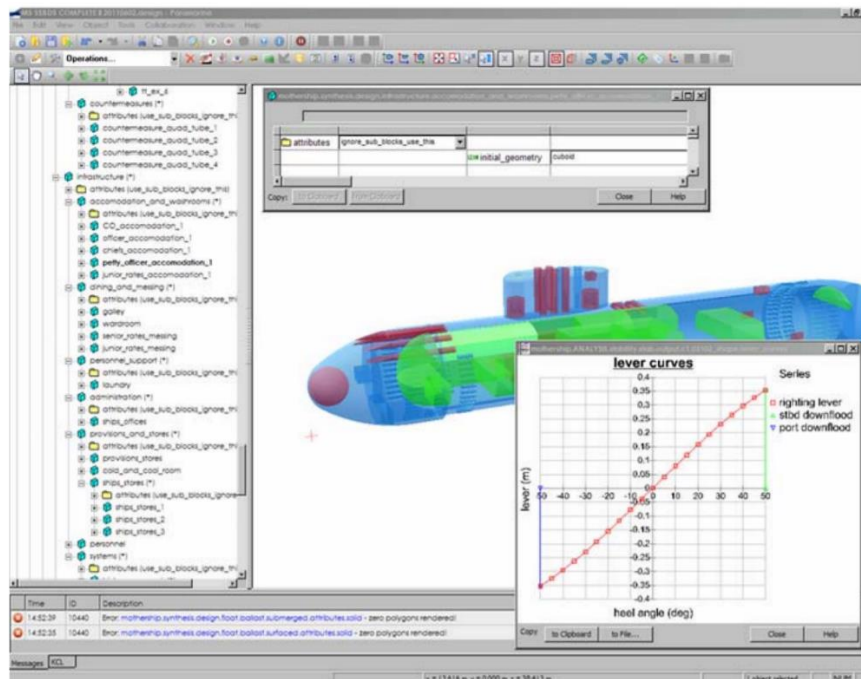


Fig.1: Screenshot of Paramarine showing interactive numerical, tabular, and graphical information in the Design Building Block objects, *Pawling and Andrews (2011)*

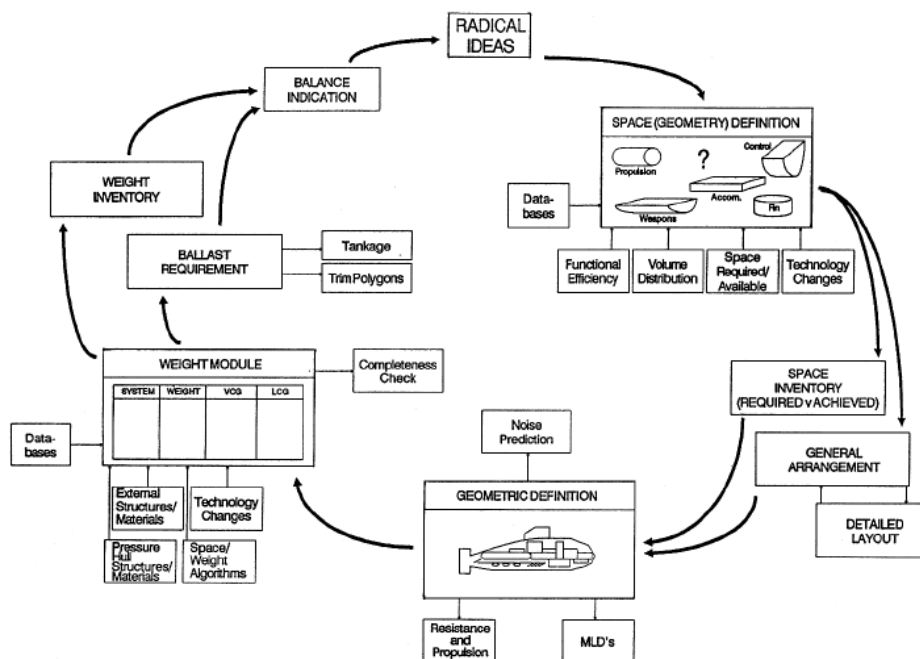


Fig.2: Logic of Design Building Block implementation to submarine design in SUBCON, *Andrews et al. (1996)*

The Implementation of the DBB approach in Paramarine™ provides an object-oriented and top-down approach that allows discrete objects to be modelled and manipulated in different levels of granularity. These objects can attach information in a form of string and numerical data, such as weight and geometry and even can be assigned different sizing algorithms, *Pawling (2007)*. It can start by developing a small number of coarse models as indicated by ‘Space (Geometry) Definition’ in Fig.2. These models can be based on equipment databases, including new equipment that is under development, reflecting the technology and configurational innovations implicit in commencing the process through fostering ‘Radical Ideas’ (top of Fig.2). As the design progresses, the coarse model of a few Super Building Blocks (SBB), may not fully populate the enclosed volume. This is then broken down into more detailed blocks as necessary as reflected in the building block design phases for surface ship design (e.g. topside and major feature design phase and super building block -based design phase), *Andrews and Pawling (2008)*. From these assembled blocks the ship design can be manipulated and assessed under a block object called a Master Building Block (MBB) defining the whole vessel characteristics, *Andrews and Pawling (2003)*, until the design is balanced, i.e., reach an acceptable performance, *Andrews (2018)*.

2.2 Automated Approaches

Since the DBB implementation has been designer-led, decisions are made by the designer, as opposed to highly automated approaches. In previous submarine design research at UCL, *Purton et al. (2015)* created an automated design tool that he called Submarine Preliminary Exploration of Requirements by Blocks (SUPERB). This uses high-level input and sizing algorithms provided by the UCL design procedure to arrive at crude numerical syntheses. The numerically balanced Pareto Front solutions are then assessed and the front ‘lowered’ from more detailed consideration, *Purton (2016)*. Before this UCL work, the US submarine builder, Electric Boat and US Navy’s Naval Sea Systems Command (NAVSEA) also developed Submarine Concept Design (SUBCODE) using one hundred Microsoft® Excel® workbooks to automate the early stages of submarine design, *Mahonen et al. (2007)*. More recent work is the application of the packing approach model (pioneered by *van Oers (2011)* and, subsequently, *Duchateau (2016)*) for the conceptual design of submarines, *Cieraad et al. (2017)*.

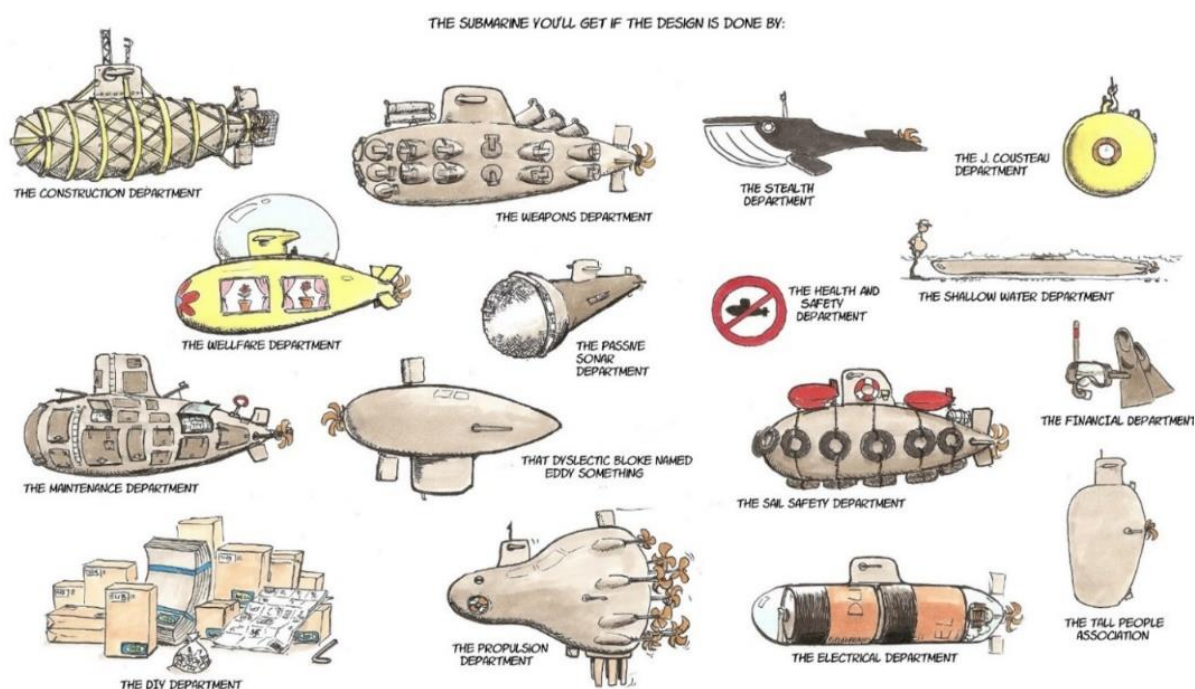


Fig.3: Submarine design for different “objectives” due to CDR Boomstra RNLN, *Duchateau (2016)*

Automated approaches hardcode design steps, many design algorithms, and their assumptions for sizing often implying, but not limited to, how the spaces are arranged within the vessel. This, in turn, makes

the software program follow several design decisions automatically every time an unbalanced condition occurs in the design. This can then allow hundreds of concept designs to be generated quickly but all based on ‘hidden’ configurational assumptions. Such an automated approach is consequently difficult to be assessed, i.e., is not revealed easily (if at all) to the designer and thus is a ‘black-box’ synthesis. The danger of such black-box approaches is that not only do they inhibit creativity and the introduction of innovations, but also could constrain the overall ship design size early in the design process. Whereas *Andrews (2011)* has strongly argued, any design solution should emerge from a proper Requirement Elucidation dialogue with requirement owners or stakeholders. Such a dialogue aims to balance different visions or objectives across multiple design stakeholders in the eventual complex vessel design (see Fig.3). This requires an approach like the UCL DBB approach that is human-centred (glass-box) rather than computer-centred (black-box) and thus architecturally driven.

2.3 Gulfs of Execution and Evaluation

Although the synthesis of the whole submarine design could have been developed using the sophisticated 3D based synthesis UCL DBB approach, there were several drawbacks in implementing such a sophisticated (fully 3D), high-fidelity, high-capability Computer-Aided Design (CAD) modelling tool in ESSD. These included the difficulties due to modelling or creating each of the numerous features and placing them individually. The latter can be considered laborious and demanding, especially if detailed modelling must be carried out after each design change and iteration, *Andrews et al. (2009)*. Such modelling effort can be referred as to the Gulfs of Execution and Evaluation, see Fig.4), which qualifies the overall level of effort required in making a system perform the desired task correctly, *Norman (2013)*. Therefore, the 3D based synthesis was then reduced to what can be called ‘2.5D’ to allow a simpler architecturally oriented design tool to be developed in-house for specifically surface ship research and education referred as to the UCL JavaScript layout exploration tool, *Pawling et al. (2015)*, *Kouriampalis et al. (2021)*. In the current paper, an alternative solution was developed without creating a further separate or standalone design tool like the UCL Javascript tool. That tool sacrificed many advantages of using 3D based synthesis and 3D informed dialogue, which Paramarine facilitated and was seen to be necessary for exploring the submarine DS3 in ESSD.

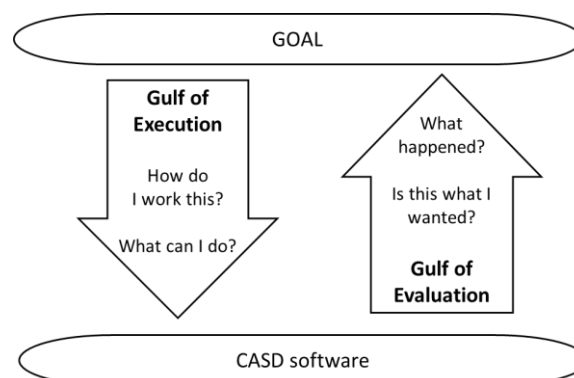


Fig.4: Gulfs of Execution and Evaluation, *Norman (2013)*

2.4 Initial Investigation

The advantages of using the sophisticated 3D based synthesis UCL DBB approach in SURFCON Paramarine for DS3 were investigated, *Mukti et al. (2019)*, using an SSK example, which was selected based on a previous study, *Mukti and Randall (2017)*. *Mukti et al. (2021)* presented an early version of DS3 synthesis retaining design flexibility and avoiding bottom out the preferred design. It utilised “Submarine Flow Optimisation” SUBFLOW for DS3 together combined with the UCL Design Building Block approach, *Andrews et al. (1996)*, Fig.5. That implementation revealed the technical issues in integrating the network-based sizing approach with the submarine design process using SURFCON Paramarine (i.e., a significant amount of Gulfs of Execution and Evaluation was required when using both approaches), which could inhibit exploring DS3 options in ESSD. This is discussed further in the following section.

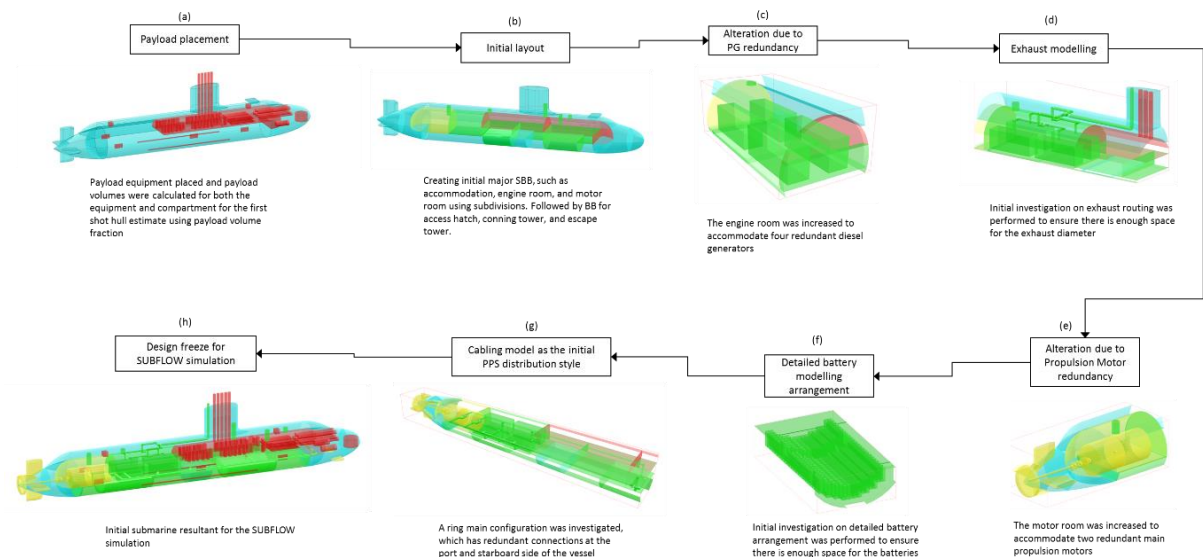


Fig.5: Summary of Power and Propulsion System (PPS) Case Study, *Mukti (2022)*

3. Development of the Approach

Normally, to create an object in Paramarine, the designer requires five steps as illustrated in Fig.6 (left), click object, click insert, click the type of the placeholders, click the rename column, and then click OK. Other possible approaches exist e.g., copy, and paste from a pre-defined template. Still, it required at least three steps (e.g., to rename each of the relevant objects). This process was considered to inhibit the important benefit of the UCL DBB approach, since many clicks would be required if one design consisted of hundreds of objects where design exploration aims to explore multiple designs.

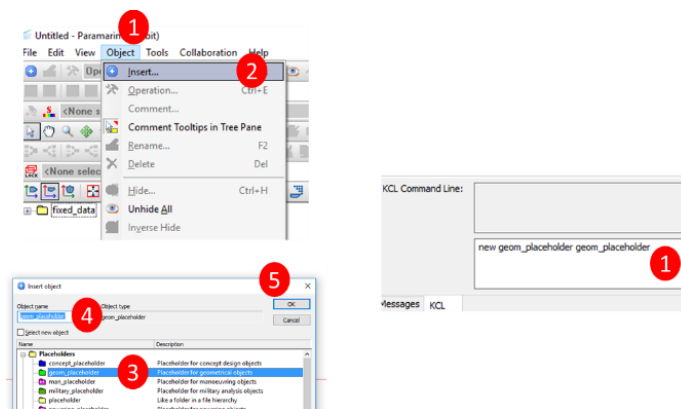


Fig.6: Illustrative modelling effort in Paramarine showing the manual process (left) and the use of a single line of KCL codes (right)

Fortunately, Paramarine has an alternative modelling approach using a KCL line as shown in Fig.6 (right). Only one step, one line of KCL command is required to create an object in Paramarine. This greatly reduced the effort of modelling in Paramarine. Now the question would be how to utilise this feature without constraining the design and retaining the benefits from the UCL DBB approach. Therefore, several programs in Excel were created to automate the modelling effort using KCL lines.

This was first tested to automate the modelling effort of a refined physical model of a submarine case study, *Mukti et al. (2021)*. The comparison is illustrated in Fig.7. Fig.7 (left) shows the theoretical modelling required to model 277 building blocks for DS3 components of that submarine case study. Since each DS3 component would require an equipment object (5 clicks), a geometric object (5 clicks), inserted as a SURFCON building block object and modelled DS3 routings (100 clicks) this suggests if there are 277 DS3 components building blocks the theoretical effort required would be some 30,000

clicks for a single design. Meanwhile, following the steps number in Fig.7 (right), all numerical input data defined in spreadsheet programs could be converted to 12,780 KCL lines within 40-50 s.

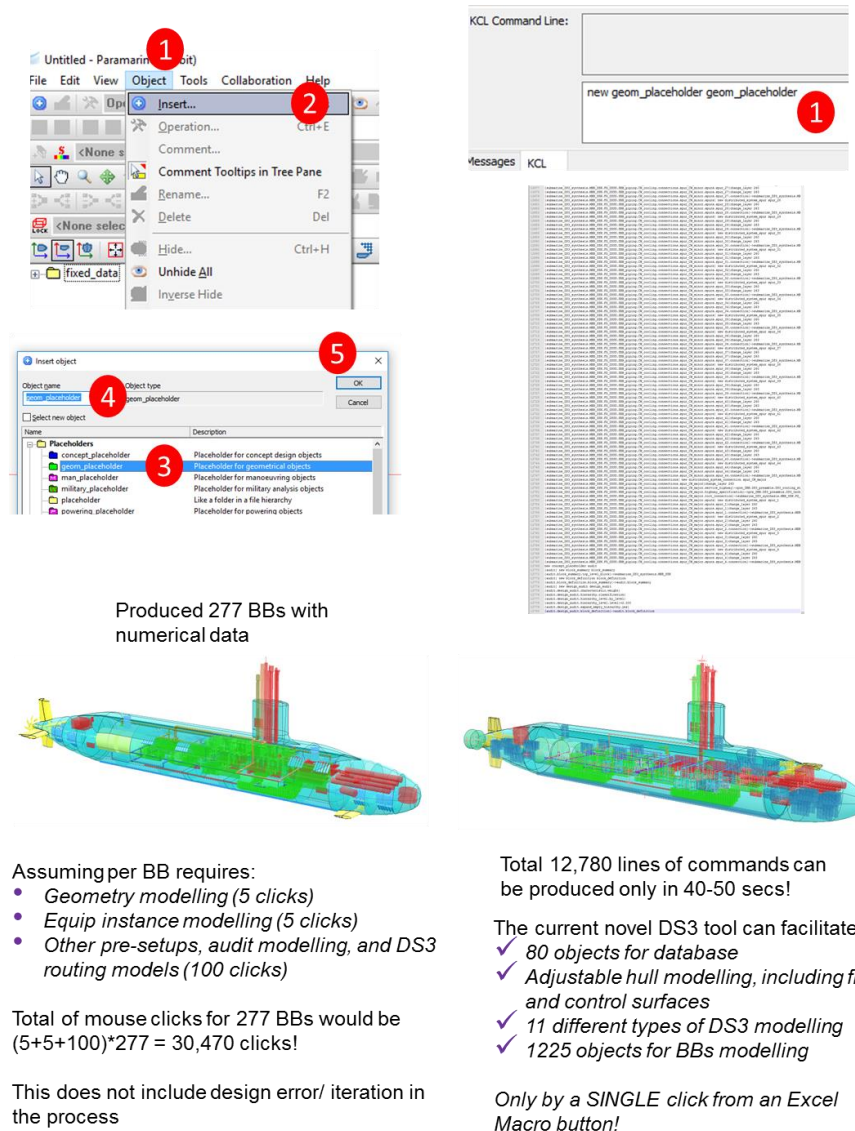


Fig.7: Theoretical modelling effort of a submarine case study, *Mukti et al. (2021)* in Paramarine showing the manual process (left) and the use of KCL macro line (right)

Given the use of Excel and KCL can potentially alter the Gulf of Execution in modelling DS3 in Paramarine, the next section outlined a new approach utilising such tools.

4. The Network Block Approach

As described in the previous section, the procedure to model a DS3 component as a Design Building Block object, including connecting it to another Design Building Block, required at least 40 clicks. This meant, if a design consists of 50 pairs of connected building block objects, the modelling process would require at least 2000 clicks. This would not include any design changes or alterations to the modelling. Such a laborious process is depicted as the “bottleneck” process in red in Fig.8 and considered as the ‘repetitive/routine task’ for the Gulfs of Execution and Evaluation, Fig.4, in modelling DS3 in ESSD. This could then distract the designer from the benefit of the UCL Design Building Block implementation for DS3 synthesis in Paramarine.

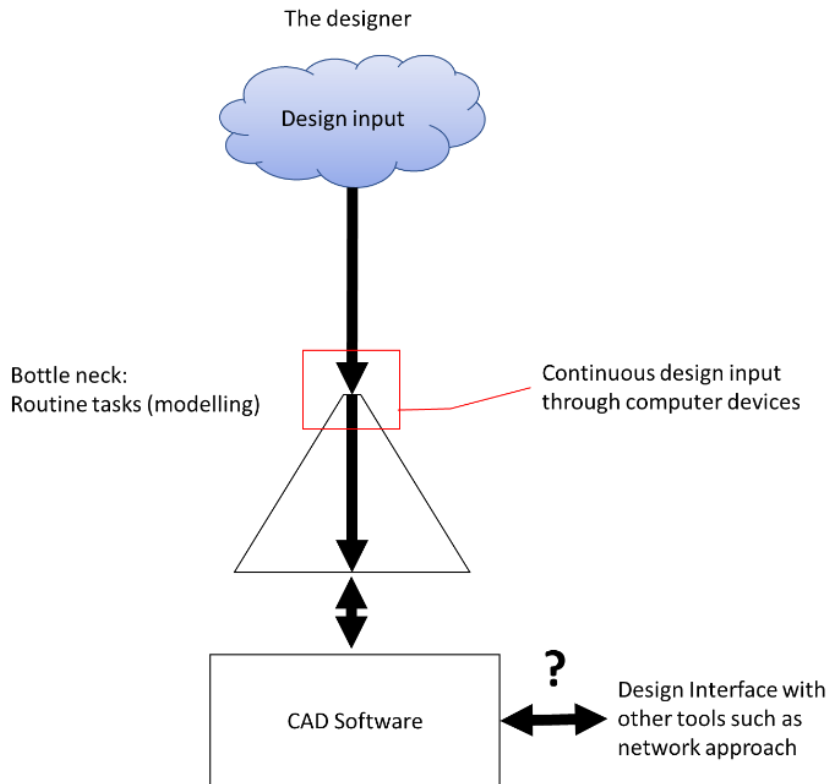


Fig.8: Data flow problem, showing the input and the bottleneck problem in blue and red, respectively

It was found in the design undertaken in this research, the reliance on the software was increased once the design had been developed into a sufficient level of details for DS3 synthesis. This is indicated by the question mark in Fig.8. For example, the need to extract specific design data to other tools, as demonstrated Mukti *et al.* (2021), Fig.5, was found to be time-consuming. Multiple clicks were required including tracing the location of the relevant DBB objects in a specific DBB hierarchy within hundreds of DBB objects and putting the data manually into MATLAB. This reliance may not be an issue if, for example, the analysis is not directly part of the design synthesis process and thus the process is not iterative, i.e., it would not be necessary to feed the data back to the Paramarine ship synthesis process simultaneously. However, in the proposed approach, the SUBFLOW network activity was significant in the DS3 synthesis process, meaning frequent data transfer and so the speed of data flow between design tools mattered. Such rapidity of transfer was seen to be essential to ensure the designer could perform the many iterations required to design DS3 physically and logically (see DS3 framework, Brefort *et al.* (2018)). Thus, the manual process, as demonstrated in Fig.5, was considered prohibitively long and thus not readily plausible for the design to incorporate sufficient key DS3 components in ESSD without a new approach.

The new approach, termed Network Block Approach (NBA), consisted of frameworks, methods and design tools that employed a strategy to ‘intercept’ data flow before being inputted to Paramarine and use of Excel spreadsheet input (as shown in green in Fig.9). Although Paramarine already has an interface with Excel as an object, using this Excel object in Paramarine makes the Excel file embedded in the Paramarine file, which complicates the MATLAB to read such an embedded file for network analysis. Using Excel with Paramarine is also not novel, Fiedel (2011), Thurkins (2012), Jurkiewicz *et al.* (2013), but using Excel to combine the UCL DBB approach with the SUBFLOW simulation for DS3 synthesis has not been done before. The NBA was not just an Excel tool, it comes with extensive frameworks and methods, Mukti *et al.* (2022), that leverage and sit in the gap between the benefits of the Paramarine 3D based synthesis tool and the SUBFLOW network-based DS3 synthesis.

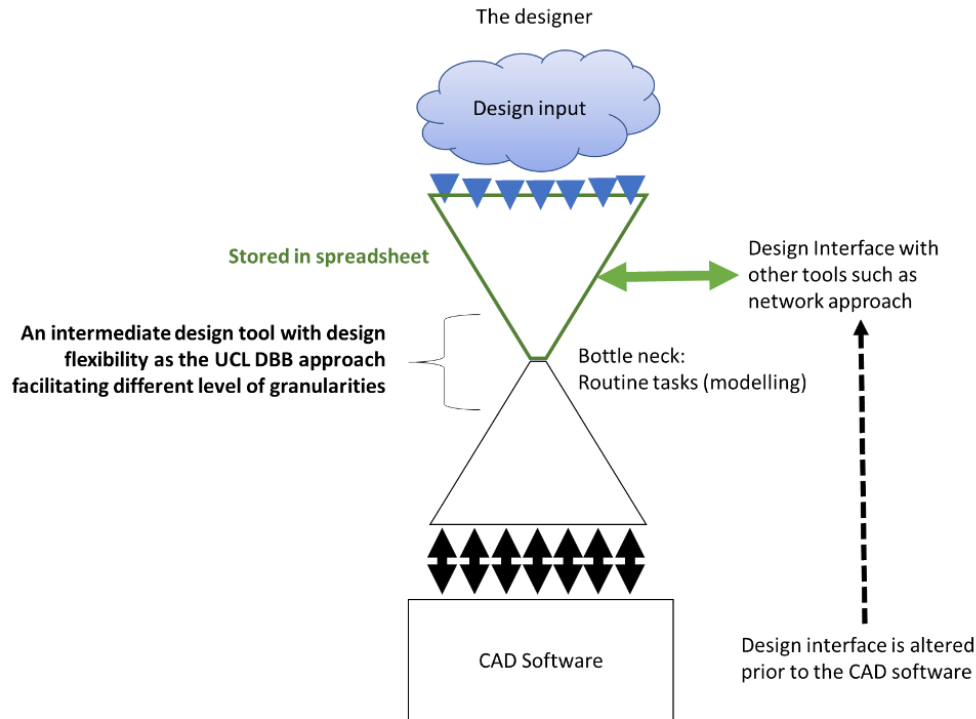


Fig.9: A proposed strategy for data flow adopted by the Network Block Approach, showing the bottleneck issue in Fig.8 can be mitigated by the spreadsheet tool in green

With the proposed approach, the designer can define design data in the spreadsheet program instead of inserting manually into Paramarine. Thus, the necessary data has been converted to thousands of lines of code, which can be more than 20,000 lines of ‘Kernel Command Language’ (KCL) lines. Paramarine can then automatically produce objects necessary for any DS3 synthesis, based on such KCL lines. This has been shown to save days of laborious modelling in Paramarine and unlocked the possibility for employing a new approach, such as the network-based DS3 synthesis using MATLAB. This was achieved without losing the benefits of a 3D architecturally centred submarine and DS3 synthesis and the 3D informed dialogue that SURFCON Paramarine provides. Since the design data was readily available in the spreadsheet environment, this was transferred to MATLAB with ease, unlike the manual procedure in the first pre-NBA implementation, *Mukti et al. (2021)*.

Table I: Summary of programs in the Network Block Approach

Program	Description	Function
MMP	Main Menu Program	Execution menu to compile all programs
DPP	Design Preamble Program	Hardcoded design setup
DAP	Design Analysis Program	Hardcoded analysis setup
HGP	Hull Granularity Program	Input for hull size
VGP	Volume Granularity Program	Input for spaces
WGP	Weight Granularity Program	Input for weight
EDP	Equipment Database Program	Input for equipment data
CGP	Component Granularity Program	Input for DS3 components for arrangement and SUBFLOW
SPP	System Preamble Program	Input for DS3 connections
SCP	System Connection Program	Input for DS3 connection and SUBFLOW

The programs in the NBA are listed in Table I. The Main Menu Program (MMP) is a menu to execute all the programs in the NBA with a single ‘click’. The MMP was also connected to the Design Preamble Program (DPP) and the Design Analysis Program (DAP). The DPP and DAP were hardcoded KCL

scripts for automatically setting up the analytical capability available in the Paramarine system, including the audit function. The application and description of the programs in Table I within the NBA are discussed in next the section.

5. Submarine Case Study

To test whether the new tool could rapidly capture the style choices of DS3 at component granularity level and could be validated with available data, a case study was developed with the payload and style choices akin to the ocean-going 2500 tonne generic submarine extracted from the database used in the annual UCL submarine design exercise, *UCL-NAME (2014)*. This case study is described in more detail in *Mukti et al. (2022)*. The output of the programs is summarised in Fig.10, which shows how the output of each program is integrated into the whole submarine design. The inputs required for each program in the case study is now described in the following subsections.

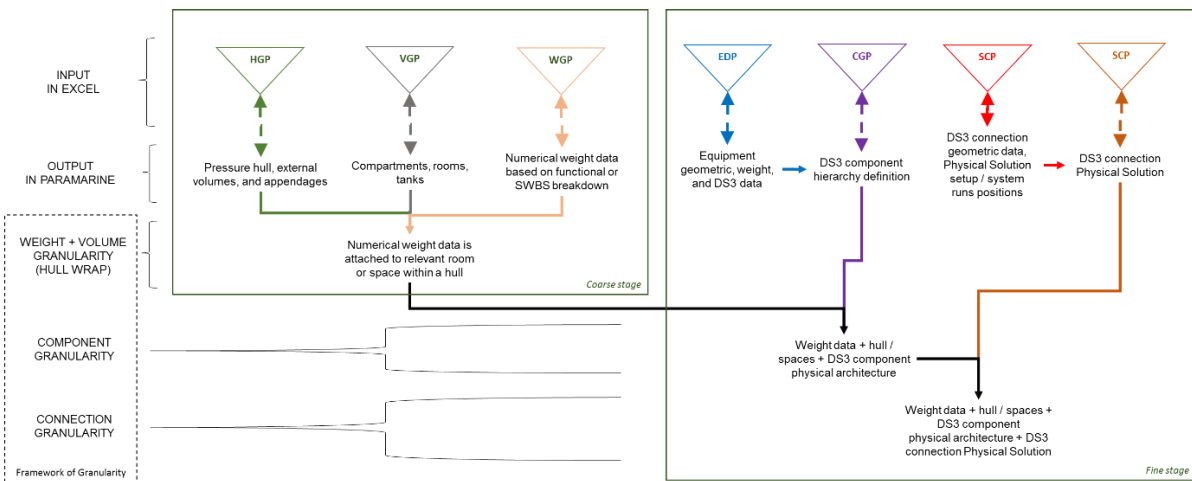


Fig.10: Output summary of the programs in the Network Block Approach; see Table I for acronyms

5.1 Main Menu Program

The Main Menu Program (MMP) was developed based on the macro interface that Paramarine provided. It contains several macro buttons: to open software; to open a Paramarine file; to build a KCL script; and to generate the KCL script from all programs (see Fig.11 for compilation sequence).

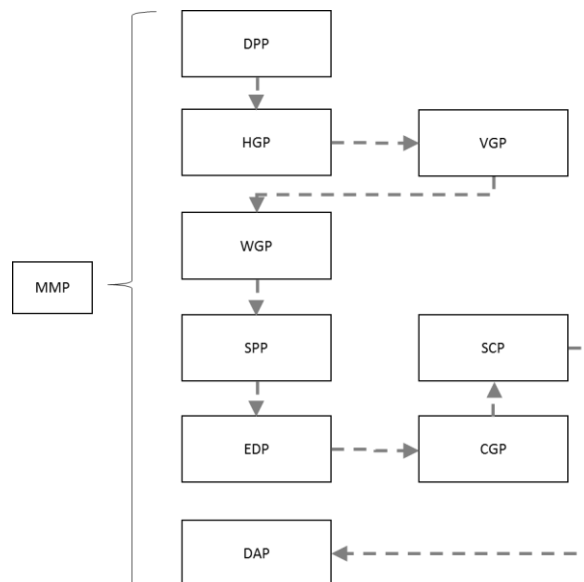


Fig.11: Compilation sequence of all programs in Table I

The MMP works closely with the Design Analysis Program (DAP) and the Design Preamble Program (DPP), which hardcoded the Gulf of Execution for performing necessary naval architectural analyses in Paramarine. The output of DPP is called DPPO (output) consisting of:

- weight group classifications (UCL SUB Weight Groups), *UCL-NAME (2014)*
- consumables (seawater, freshwater/ diesel oil, lube oil, LOX)
- ship conditions (surfaced or submerged)
- crew types (not used)
- other characteristics, e.g., costs

4.2 Hull Granularity Program

The Hull Granularity Program (HGP) provides a scalable submarine hull configuration with a specific chosen style, *Andrews (2021)*, which is a single hull with a casing configuration, Fig.12. Any different major style will require a new HGP. To develop a new HGP, one can first manually model the submarine in Paramarine and then create the macro script based on such models.

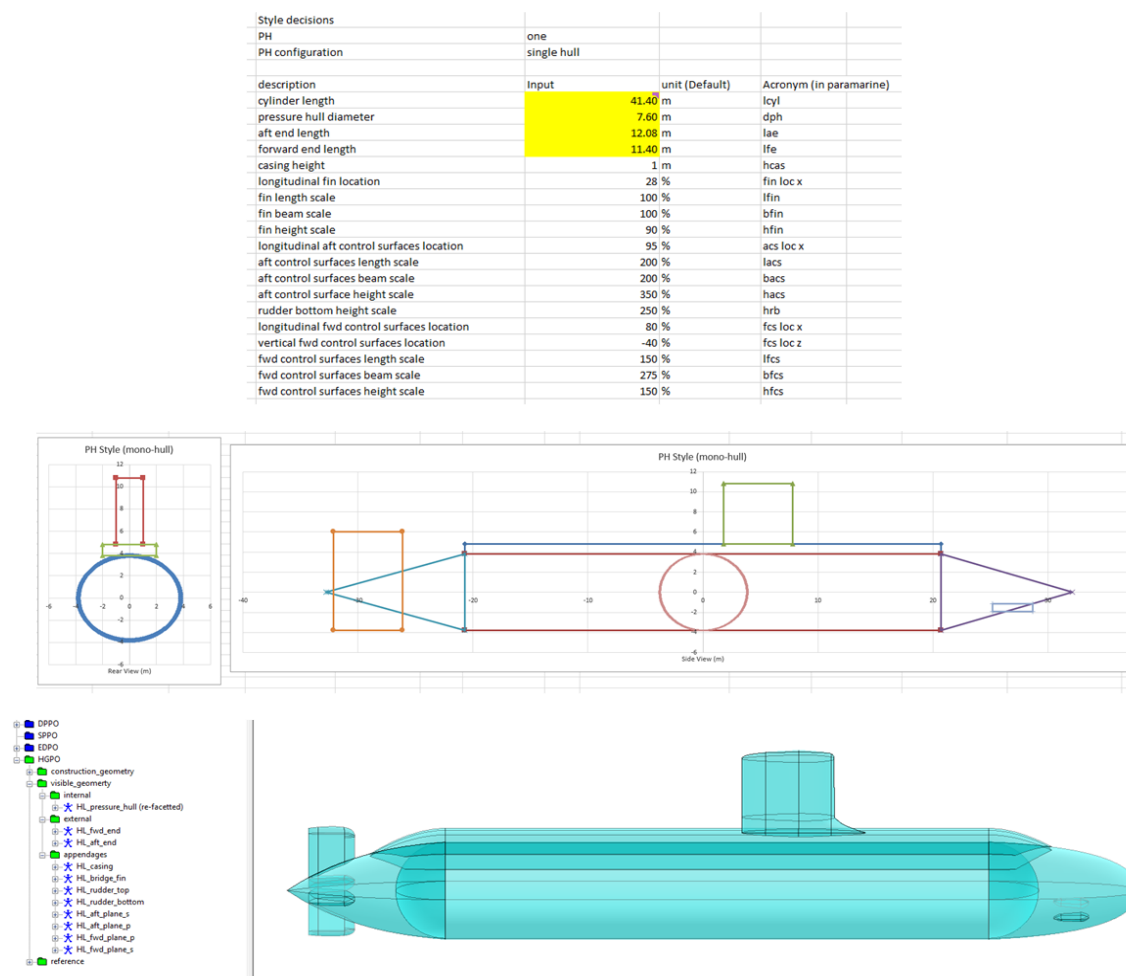


Fig.12: Layout of the HGP showing the input in Excel (top) and the output in Paramarine (bottom)

4.3 Volume Granularity Program

The Volume Granularity Program (VGP) consists of inputs to define spaces on the vessel as given in Fig.13. The building blocks for spaces are defined based on names, BB hierarchy (to level 4), two points (A and B) defining the boundary of the blocks, location of the space relative to the hull model defined in VGP, tank definition. This spreadsheet layout reveals the input of the case study reached up to 800 inputs (35 by 23), which included “string” data input as well as numerical data input.

(INFO ONLY)		FUNCTIONAL FOR SPATIAL PHYSICAL ARCHITECTURE (BB management based on functionality>> location)																		permeability		surfaced		submerged		FLU		FA	
		Notes/Tag		1		2		3		4 Point A		Point B		intersect		intersect													
Call ID	Name	Description	SA/Comp	Functional	MBB	FG	SBB	BB1	X	Y	Z	X	Y	Z	Y/N	Type	solid	permeability	light	deep	light	deep	consumable	compensating					
1	BB_VL_FF_EA	Free flood volume aft occupied by equipment	FF	float	MBB	VGP	AXT	BB_VL_FF_EA	-12.8	-4.0	-3.8	-26.7	4.0	3.8	yes	external	HL_aft_end	90	90										
2	BB_VL_FF_MA	External main ballast tank volume aft	MBB	float	MBB	VGP	AXT	BB_VL_FF_MA	-26.7	-4.0	-3.8	-26.7	4.0	3.8	yes	external	HL_aft_end	90	90					0	0	100	100		
3	BB_VL_FF_MP	External main ballast tank volume forward	MBB	float	MBB	VGP	FXT	BB_VL_FF_MP	-26.7	-4.0	-3.8	-26.7	4.0	3.8	yes	external	HL_fwd_end	90	90					0	0	100	100		
4	BB_VL_FF_FF	Free flood volume forward occupied by equipment	FF	float	MBB	VGP	FXT	BB_VL_FF_FF	-26.7	-4.0	-3.8	-26.7	4.0	3.8	yes	external	HL_fwd_end	90	90					0	0	100	100		
5	BB_VL_FF_BR	Bridge for volume	FF	float	MBB	VGP	APP	BB_VL_FF_BR	-3.8	-2.7	3.8	-12.8	2.7	12.8	yes	pendage	HL_bridge_fin	90	90										
6	BB_VL_FF_CA	Casing volume	FF	float	MBB	VGP	APP	BB_VL_FF_CA	-3.8	-2.7	3.8	-12.8	2.7	12.8	yes	pendage	HL_casing	90	90										
7	BB_VL_FF_RT		FF	move	MBB	VGP	APP	BB_VL_FF_RT	-32.1	-2.0	0.0	-26.1	2.0	6.8	yes	pendage	HL_rudder_top	90	90										
8	BB_VL_FF_RB		FF	move	MBB	VGP	APP	BB_VL_FF_RB	-32.1	-2.0	3.8	-26.1	2.0	0.8	yes	pendage	HL_rudder_bottom	90	90										
9	BB_VL_FF_AP		FF	move	MBB	VGP	APP	BB_VL_FF_AP	-32.1	-5.0	-2.0	-26.1	5.0	2.0	yes	pendage	HL_aft_plane_p	90	90										
10	BB_VL_FF_AS		FF	move	MBB	VGP	APP	BB_VL_FF_AS	-32.1	-5.0	-2.0	-26.1	5.0	2.0	yes	pendage	HL_aft_plane_s	90	90										
11	BB_VL_FF_FP		FF	move	MBB	VGP	APP	BB_VL_FF_FP	-20.7	-5.0	-3.8	-22.1	5.0	3.8	yes	pendage	HL_fwd_plane_p	90	90										
12	BB_VL_FF_FS		FF	move	MBB	VGP	APP	BB_VL_FF_FS	-20.7	-5.0	-3.8	-22.1	5.0	3.8	yes	pendage	HL_fwd_plane_s	90	90										
13	BB_VL_FF_MR	Motor room	RM	move	MBB	VGP	PHA	BB_VL_FF_MR	-24.5	-3.8	-1.1	-14.4	3.8	1.1	yes	internal	HL_pressure_hull	90	90										
14	BB_VL_FF_RM	Engine room	RM	infrastructure	MBB	VGP	PHA	BB_VL_FF_RM	-24.5	-3.8	-1.1	-14.4	3.8	1.1	yes	internal	HL_pressure_hull	90	90										
15	BB_VL_FF_TA	Trim tank aft	TA	float	MBB	VGP	PHA	BB_VL_FF_TA	-24.5	-3.8	-1.1	-14.4	3.8	1.1	yes	internal	HL_pressure_hull	90	90		0	30	0	30		seawater			
16	BB_VL_FF_BI	Bi-ge tank	RM	float	MBB	VGP	PHA	BB_VL_FF_BI	-21.2	-3.8	-1.1	-20.8	3.8	1.1	yes	internal	HL_pressure_hull	90	90										
17	BB_VL_FF_LO	Lubricant oil tank	DV	infrastructure	MBB	VGP	PHA	BB_VL_FF_LO	-20.8	-3.8	-1.1	-20.8	3.8	1.1	yes	internal	HL_pressure_hull	90	90					0	0	0	0	100	100
18	BB_VL_FF_OA	Fuel tank aft	DV	infrastructure	MBB	VGP	PHA	BB_VL_FF_OA	-20.8	-3.8	-1.1	-20.8	3.8	1.1	yes	internal	HL_pressure_hull	90	90					0	0	0	0	100	100
19	BB_VL_FF_SA	Storage aft	RM	infrastructure	MBB	VGP	PHA	BB_VL_FF_SA	-20.8	-3.8	-1.1	-20.8	3.8	1.1	yes	internal	HL_pressure_hull	90	90									seawater	
20	BB_VL_FF_CO	Control room	RM	fight	MBB	VGP	PHA	BB_VL_FF_CO	-6.4	-3.8	-1.1	-6.4	3.8	1.1	yes	internal	HL_pressure_hull	90	90										
21	BB_VL_FF_AMS	Auxiliary Machinery Space (AMS)	RM	infrastructure	MBB	VGP	PHA	BB_VL_FF_AMS	-6.4	-3.8	-1.1	-6.4	3.8	1.1	yes	internal	HL_pressure_hull	90	90										
22	BB_VL_FF_MS	Messico etc	RM	infrastructure	MBB	VGP	PHA	BB_VL_FF_MS	-6.4	-3.8	-1.1	-6.4	3.8	1.1	yes	internal	HL_pressure_hull	90	90										
23	BB_VL_FF_CM	Fuel tank mid	DV	infrastructure	MBB	VGP	PHA	BB_VL_FF_CM	-6.4	-3.8	-1.1	-6.4	3.8	1.1	yes	internal	HL_pressure_hull	90	90					0	100	0	100	100	100
24	BB_VL_FF_BA	Battery aft	RM	infrastructure	MBB	VGP	PHA	BB_VL_FF_BA	-6.4	-3.8	-1.1	-6.4	3.8	1.1	yes	internal	HL_pressure_hull	90	90									seawater	
25	BB_VL_FF_TM	Trim and Compensating tank	TA	float	MBB	VGP	PHA	BB_VL_FF_TM	-6.4	-3.8	-1.1	-6.4	3.8	1.1	yes	internal	HL_pressure_hull	90	90					0	30	0	30		seawater
26	BB_VL_FF_SF	Storage forward	RM	infrastructure	MBB	VGP	PHA	BB_VL_FF_SF	-6.4	-3.8	-1.1	-6.4	3.8	1.1	yes	internal	HL_pressure_hull	90	90										
27	BB_VL_FF_FW	Fresh water tank	RM	infrastructure	MBB	VGP	PHA	BB_VL_FF_FW	-7.2	-3.8	-1.1	-7.2	3.8	1.1	yes	internal	HL_pressure_hull	90	90										
28	BB_VL_FF_WS	Weapon storage compartment	RM	fight	MBB	VGP	PHA	BB_VL_FF_WS	-8.8	-3.8	-1.1	-8.8	3.8	1.1	yes	internal	HL_pressure_hull	90	90										
29	BB_VL_FF_AD	Accommodation	RM	infrastructure	MBB	VGP	PHA	BB_VL_FF_AD	-8.8	-3.8	-1.1	-8.8	3.8	1.1	yes	internal	HL_pressure_hull	90	90										
30	BB_VL_FF_TB	Space for ATP and WRT	RM	fight	MBB	VGP	PHA	BB_VL_FF_TB	-20.7	-3.8	-1.1	-20.7	3.8	1.1	yes	internal	HL_pressure_hull	90	90										
31	BB_VL_FF_BF	Battery forward	RM	infrastructure	MBB	VGP	PHA	BB_VL_FF_BF	-8.8	-3.8	-1.1	-8.8	3.8	1.1	yes	internal	HL_pressure_hull	90	90										
32	BB_VL_FF_OF	Fuel tank forward	DV	infrastructure	MBB	VGP	PHA	BB_VL_FF_OF	-16.7	-3.8	-1.1	-16.7	3.8	1.1	yes	internal	HL_pressure_hull	90	90					0	100	0	100	100	100
33	BB_VL_FF_SC	Sewage tank	RM	infrastructure	MBB	VGP	PHA	BB_VL_FF_SC	-16.7	-3.8	-1.1	-16.7	3.8	1.1	yes	internal	HL_pressure_hull	90	90									seawater	
34	BB_VL_FF_TO	TOT	RM	fight	MBB	VGP	PHA	BB_VL_FF_TO	-20.1	-3.8	-1.1	-20.1	3.8	1.1	yes	internal	HL_pressure_hull	90	90										
35	BB_VL_FF_TB	Trim tank forward	TA	float	MBB	VGP	PHA	BB_VL_FF_TB	-20.7	-3.8	-1.1	-20.7	3.8	1.1	yes	internal	HL_pressure_hull	90	90					0	30	0	30		seawater

Fig.13: Layout of the VGP showing major inputs required in defining spaces on the vessel

4.4 Weight Granularity Program

The Weight Granularity Program (WGP) defines numerical weight on the vessel, Fig.14. This consists of naming convention to reflect the Weight Group (WG) number, weight location (“manual” if it is defined in x, y, z coordinates), building block hierarchy (to level 5), volume location defined in the Volume Granularity Program (VGP), and the numerical weight data. The number of inputs in the WGP for the submarine case study was about 1800 inputs, assuming there are 10 inputs for each weight.

(INFO ONLY)		FUNCTIONAL FOR SPATIAL PHYSICAL ARCHITECTURE (BB management based on functionality>> location)										Location			Permanent	
Call N	Name	Weight Type	Weight Location	1	2	3	4	5	X	Y	Z	Initial	WG	Weight		
1	NL_2_MCC	permanent		MBB	FG	SBB	BB1	BB2	0	0	1.47	BB_VL_MV_RM_MR	2	3.3		
2	NL_4_SCC	permanent		MBB	WGP	FG	fight	SBB	control_data	BB_NL_4_SCC	0	0	2.65	BB_VL_FH_RM_CO	4	0.8
3	NL_4_miscellaneous_control_instrumentation	permanent		MBB	WGP	FG	fight	SBB	control_data	BB_NL_4_miscellaneous_control_instrumentation	0	0	1.82	BB_VL_FH_RM_CO	4	2
4	NL_4_data_handling_computer_display	permanent		MBB	WGP	FG	fight	SBB	control_data	BB_NL_4_data_handling_computer_display	0	0	1.93	BB_VL_FH_RM_CO	4	3.5
5	NL_4_navigation_equipment	permanent		MBB	WGP	FG	fight	SBB	control_data	BB_NL_4_navigation_equipment	0	0	0.68	BB_VL_FH_RM_CO	4	2.1
6	NL_4_internal_comms	permanent		MBB	WGP	FG	fight	SBB	control_data	BB_NL_4_internal_comms	0	0	2.88	BB_VL_FH_RM_CO	4	0.9
7	NL_4_main_passive_sonar_array	permanent	manual	MBB	WGP	FG	fight	SBB	sonar	BB_NL_4_main_passive_sonar_array	0	0	-0.8		4	5.5
8	NL_4_main_passive_sonar_dome	permanent		MBB	WGP	FG	fight	SBB	sonar	BB_NL_4_main_passive_sonar_dome	0	0	-0.3	BB_VL_FF_FF	4	3.6
9	NL_4_other_sonar_arrays	permanent	manual	MBB	WGP	FG	fight	SBB	sonar	BB_NL_4_other_sonar_arrays	0	0	5.2		4	2.5
10	NL_4_other_sonar_windows	permanent		MBB	WGP	FG	fight	SBB	sonar	BB_NL_4_other_sonar_windows	0	0	4.7		4	2.6
11	NL_4_sonar_processing_display	permanent		MBB	WGP	FG	fight	SBB	sonar	BB_NL_4_sonar_processing_display	0	0	2.65	BB_VL_FH_RM_CO	4	7.5
12	NL_1_periscope_supports_wells	permanent		MBB	WGP	FG	fight	SBB	periscope	BB_NL_1_periscope_supports_wells	0	0	-0.03	BB_VL_JA_RM_SF	1	2
13	NL_4_periscopes	permanent	manual	MBB	WGP	FG	fight	SBB	periscope	BB_NL_4_periscopes	0	0	9.27	BB_VL_FF_FF	4	4
14	NL_4_periscopes_hoists_buffers	permanent		MBB	WGP	FG	fight	SBB	periscope	BB_NL_4_periscopes_hoists_buffers	0	0	5		4	1.3
15	NL_4_periscope_bearings_hull_glands	permanent		MBB	WGP	FG	fight	SBB	periscope	BB_NL_4_periscope_bearings_hull_glands	0	0	6.79	BB_VL_FF_FF	4	1.2
16	NL_4_wireless_mast_hoist	permanent		MBB	WGP	FG	fight	SBB	mast	BB_NL_4_wireless_mast_hoist	0	0	11.35	BB_VL_FF_FF	4	1.5
17	NL_4_wireless_RX_TX	permanent		MBB	WGP	FG	fight	SBB	mast	BB_NL_4_wireless_RX_TX	0	2.97	BB_VL_FH_RM_CO	4	2.3	
18	NL_4_radar_mast_hoist	permanent		MBB	WGP	FG	fight	SBB	mast	BB_NL_4_radar_mast_hoist	0	0	8.95	BB_VL_FF_FF	4	2.5
19	NL_4_radar_set	permanent		MBB	WGP	FG	fight	SBB	mast	BB_NL_4_radar_set	0	0	3.08	BB_VL_FH_RM_CO	4	0.4
20	NL_4_EW_mast_hoist	permanent		MBB	WGP	FG	fight	SBB	mast	BB_NL_4_EW_mast_hoist	0	0	8.2	BB_VL_FF_FF	4	2.7
21	NL_4_EW equip	permanent		MBB	WGP	FG	fight	SBB	mast	BB_NL_4_EW equip	0	0	2.5	BB_VL_FH_RM_CO	4	1.4
22	NL_1_torpedo_loading_hatch	permanent		MBB	WGP	FG	fight	SBB	torpedo	BB_NL_1_torpedo_loading_hatch	0	0	4.15	BB_VL_FH_RM_WS	1	0.7
23	NL_7_torpedo_tubes	permanent		MBB	WGP	FG	fight	SBB	torpedo	BB_NL_7_torpedo_tubes	0	0	2.55	BB_VL_FH_RM_WS	7	36
24	NL_7_torpedo_CP	permanent		MBB	WGP	FG	fight	SBB	torpedo	BB_NL_7_torpedo_CP	0	0	1.37	BB_VL_FH_RM_WS	7	1
25	NL_7_torpedo_stowage_handling_gr	permanent		MBB	WGP	FG	fight	SBB	torpedo	BB_NL_7_torpedo_stowage_handling_gr	0	0	2.88	BB_VL_FH_RM_WS	7	22.3

4.5 Equipment Database Program

The Equipment Database Program (EDP) defines the input necessary to create a physical model of a DS3 component. The input consists of name, shape, dimensions, orientation, BB hierarchy, WG classifications, weight, connection points, Fig.15. For the submarine case study, there were 365 equipment objects, which means 5100 input data, assuming each component requires 14 inputs.

4.6 Component Granularity Program

The Component Granularity Program (CGP) provides input for integrating DS3 components into the whole submarine design. As shown in Fig.16, the inputs for the DS3 components: the type of components, which could be equipment (DB) or numerical (NL), *Mukti et al. (2022)*; equipment data defined in EDP; BB hierarchy (up to level 4), relative position in X-, Y-, Z- axes relative to the space block, space block defined in VGP. Unlike database (DB) components, numerical (NL) components could be used to handle DS3 components that lacked sufficient detail in ESSD.

	(INFO ONLY)		troubleshooting	OPTIONAL FOR SPATIAL PHYSICAL ARCHITECTURE (BB management based str from stbd(-) to port(+))				4 BB Level (Initial Location axis reinitial				
Call N	Name	Object Type (nu	Equipment from Database	MBB	FG	SBB	BB1	X%	Y%	Z%	X/Y/Z compartment	
1	BB_DB_FO_VV_TK_a	equipment	DB_FO_VV_TK_a	MBB	CGP	FO	BB_DB_FO_VV_TK_a	4	0.0	0.0	0.0	BB_VL_IA_DV_OA
2	BB_DB_FO_VV_TK_m	equipment	DB_FO_VV_TK_m	MBB	CGP	FO	BB_DB_FO_VV_TK_m	4	0.0	0.0	0.0	BB_VL_IA_DV_OM
3	BB_DB_FO_VV_TK_f	equipment	DB_FO_VV_TK_f	MBB	CGP	FO	BB_DB_FO_VV_TK_f	4	0.0	0.0	0.0	BB_VL_IA_DV_OF
4	BB_DB_DT_CO_AC_a	equipment	DB_DT_CO_AC_a	MBB	CGP	DT	BB_DB_DT_CO_AC_a	4	0.8	0.0	0.0	BB_VL_FH_RM_CO
5	BB_DB_DT_CO_AC_f	equipment	DB_DT_CO_AC_f	MBB	CGP	DT	BB_DB_DT_CO_AC_f	4	-0.4	0.0	0.3	BB_VL_FH_RM_WS
6	BB_DB_DT_PU_AC	equipment	DB_DT_PU_AC	MBB	CGP	DT	BB_DB_DT_PU_AC	4	0.5	0.0	0.0	BB_VL_FH_RM_CO
7	BB_DB_DT_SA_DC	equipment	DB_DT_SA_DC	MBB	CGP	DT	BB_DB_DT_SA_DC	4	0.1	0.0	0.3	BB_VL_FL_FF_BR
8	BB_DB_DT_AK_DC	equipment	DB_DT_AK_DC	MBB	CGP	DT	BB_DB_DT_AK_DC	4	-0.5	0.0	0.3	BB_VL_FL_FF_BR
9	BB_DB_DT_CN_DC	equipment	DB_DT_CN_DC	MBB	CGP	DT	BB_DB_DT_CN_DC	4	-0.3	0.0	0.3	BB_VL_FL_FF_BR
10	BB_DB_DT_EW_DC	equipment	DB_DT_EW_DC	MBB	CGP	DT	BB_DB_DT_EW_DC	4	-0.2	0.0	0.3	BB_VL_FL_FF_BR
11	BB_DB_DT_RA_DC	equipment	DB_DT_RA_DC	MBB	CGP	DT	BB_DB_DT_RA_DC	4	-0.1	0.0	0.3	BB_VL_FL_FF_BR
12	BB_DB_DT_SO_DC	equipment	DB_DT_SO_DC	MBB	CGP	DT	BB_DB_DT_SO_DC	4	-0.2	0.0	0.0	BB_VL_FL_FF_FF
13	BB_DB_DT_SC_DC	equipment	DB_DT_SC_DC	MBB	CGP	DT	BB_DB_DT_SC_DC	4	0.2	0.0	0.0	BB_VL_FH_RM_CO
14	BB_DB_DT_MC_DC	equipment	DB_DT_MC_DC	MBB	CGP	DT	BB_DB_DT_MC_DC	4	0.7	0.0	0.0	BB_VL_MV_RM_MR
15	BB_DB_DT_DD_IC_a	equipment	DB_DT_DD_IC_a	MBB	CGP	DT	BB_DB_DT_DD_IC_a	4	0.1	0.0	0.5	BB_VL_MV_RM_MR
16	BB_DB_DT_DD_IC_m	equipment	DB_DT_DD_IC_m	MBB	CGP	DT	BB_DB_DT_DD_IC_m	4	-0.8	0.0	-0.3	BB_VL_FH_RM_CO
17	BB_DB_DT_DD_IC_f	equipment	DB_DT_DD_IC_f	MBB	CGP	DT	BB_DB_DT_DD_IC_f	4	-0.1	0.0	0.5	BB_VL_FH_RM_WS
18	BB_DB_DT_DD_AN_p	equipment	DB_DT_DD_AN_p	MBB	CGP	DT	BB_DB_DT_DD_AN_p	4	-0.6	0.4	-0.6	BB_VL_MV_RM_MR
19	BB_DB_DT_DD_AN_s	equipment	DB_DT_DD_AN_s	MBB	CGP	DT	BB_DB_DT_DD_AN_s	4	-0.6	-0.4	-0.6	BB_VL_MV_RM_MR
20	BB_DB_DT_DD_MN_p	equipment	DB_DT_DD_MN_p	MBB	CGP	DT	BB_DB_DT_DD_MN_p	4	-0.5	0.2	-0.4	BB_VL_FH_RM_CO

Fig.16: Layout of the CGP showing major inputs required in defining DS3 components on the vessel

4.7 System Preamble Program

The System Preamble Program (SPP) provides an input menu to physically define DS3 connections. As shown in Fig.17, it consists of the name of the connection, DS3 technology (e.g., cabling, piping, trunking), mitred bend assumption, the shape of the connection (circle or rectangle), cross-sectional dimensions, and UCL submarine weight classification. For the submarine case study, there were more than 400 connections and thus 3600 inputs if each connection requires 9 inputs.

able size from industry that can be used for multiple services)				must larger than Width				(select from column B	
Call Ni	Name	DS3 Technology	Mitred Bends (yes/no)	Section Shape (Circle/Rectangle)	Width (mm)	Height (mm) (only for rectangle)	nd Radius (m)	Weight Classification (1 to 9 UCL)	Valid Service 1 Va
1	DT_1	cabling	yes	circle	89	89	98	3	DT
2	DT_2	cabling	yes	circle	89	89	98	3	DT
3	DT_3	cabling	yes	circle	89	89	98	3	DT
4	DT_4	cabling	yes	circle	89	89	98	3	DT
5	DT_5	cabling	yes	circle	89	89	98	3	DT
6	DT_6	cabling	yes	circle	89	89	98	3	DT
7	DT_7	cabling	yes	circle	89	89	98	3	DT
8	DT_8	cabling	yes	circle	89	89	98	3	DT
9	DT_9	cabling	yes	circle	89	89	98	3	DT
10	DT_10	cabling	yes	circle	89	89	98	3	DT
11	DT_11	cabling	yes	circle	89	89	98	3	DT
12	DT_12	cabling	yes	circle	89	89	98	3	DT
13	DT_13	cabling	yes	circle	89	89	98	3	DT
14	DT_14	cabling	yes	circle	89	89	98	3	DT
15	DT_15	cabling	yes	circle	89	89	98	3	DT
16	DT_16	cabling	yes	circle	89	89	98	3	DT
17	DT_17	cabling	yes	circle	89	89	98	3	DT
18	DT_18	cabling	yes	circle	89	89	98	3	DT
19	DT_19	cabling	yes	circle	89	89	98	3	DT
20	DT_20	cabling	yes	circle	89	89	98	3	DT

Fig.17: Layout of the SPP showing major inputs required in defining physical DS3 connections

In the SPP, the location of system highways can also be adjusted as is shown in Fig.18. This provides identifications to be used in the System Connection Program (SCP). System highways consisted of some pre-defined longitudinal lines from forward to aft of the vessel and could be modelled as a highway object in Paramarine.

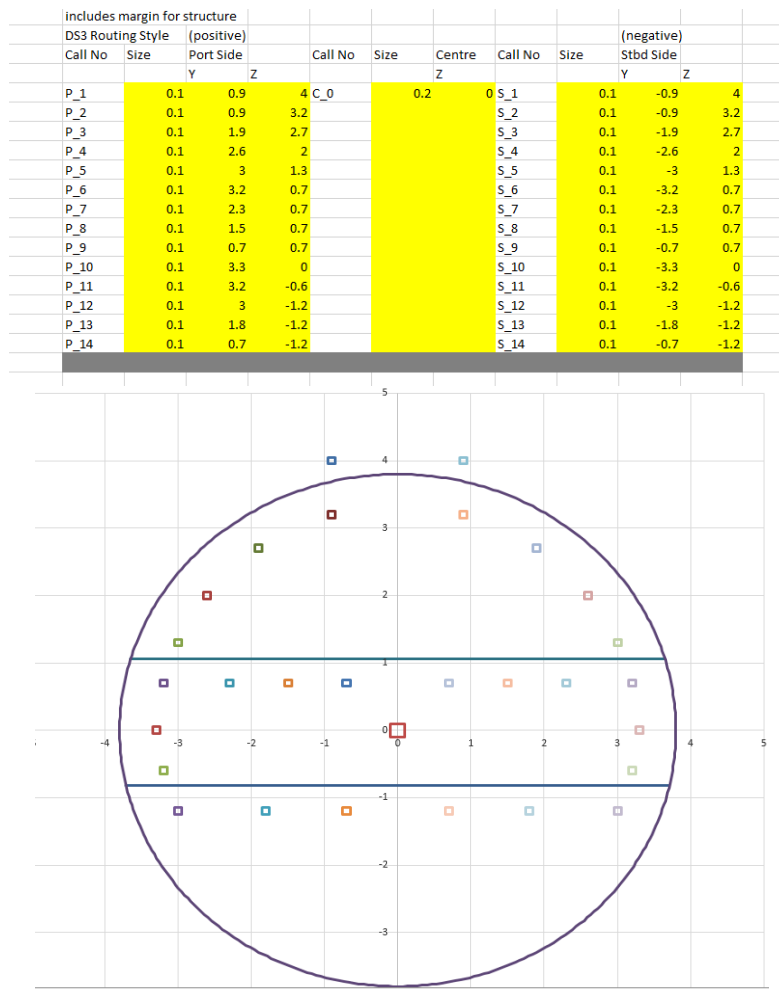


Fig.18: System highways setup in the SPP showing an initial highways visualisation (bottom) and major inputs required in defining system highways on the vessel (top)

4.8 System Connection Program

Like CGP, the SCP also provides necessary inputs for integrating DS3 connections into the whole submarine design. The inputs consist of connection name, physical connection, type of connections, highway defined in SPP, BB hierarchy (up to level 4), the connected DS3 components (source and sink), Fig.19.

				spur must use				FUNCTIONAL FOR SPATIAL PHYSICAL ARCHITECTURE				LOGICAL ARCHITECTURE (II	
ID	Medium (m)	Notes	PL ID	Object Type	Type of Connections	Use Set Highway	Use Set Highway	1	2	3	4	SELECT FROM ARRANGEMENT	TO
				Physical	(system_connection/dis	(yes/no)		MBB	FG	SBB	BB1	Object Source (from)	Dependency 1
1 DT_1			PL0	yes	system_connection	yes	P_9	MBB	SCP	DT	BB_DT_1	BB_DB_DT_CO_AC_a	BB_DB_DT_DD_LC_m
2 DT_2			PL0	yes	system_connection	yes	P_9	MBB	SCP	DT	BB_DT_2	BB_DB_DT_CO_AC_f	BB_DB_DT_DD_LC_f
3 DT_3			PL0	yes	system_connection	yes	P_9	MBB	SCP	DT	BB_DT_3	BB_DB_DT_PU_AC	BB_DB_DT_DD_LC_m
4 DT_4			PL0	yes	system_connection	yes	P_9	MBB	SCP	DT	BB_DT_4	BB_DB_DT_SC_DC	BB_DB_DT_DD_LC_m
5 DT_5			PL0	yes	system_connection	yes	P_9	MBB	SCP	DT	BB_DT_5	BB_DB_DT_MC_DC	BB_DB_DT_DD_LC_a
6 DT_6			PL0	yes	system_connection	yes	P_9	MBB	SCP	DT	BB_DT_6	BB_DB_DT_DD_LC_a	BB_DB_DT_DD_AN_p
7 DT_7			PL0	yes	system_connection	yes	P_9	MBB	SCP	DT	BB_DT_7	BB_DB_DT_DD_LC_a	BB_DB_DT_DD_AN_s
8 DT_8			PL0	yes	system_connection	yes	P_9	MBB	SCP	DT	BB_DT_8	BB_DB_DT_DD_LC_m	BB_DB_DT_DD_MN_p
9 DT_9			PL0	yes	system_connection	yes	S_9	MBB	SCP	DT	BB_DT_9	BB_DB_DT_DD_LC_m	BB_DB_DT_DD_MN_s
10 DT_10			PL0	yes	system_connection	yes	P_9	MBB	SCP	DT	BB_DT_10	BB_DB_DT_DD_LC_f	BB_DB_DT_DD_FN_p
11 DT_11			PL0	yes	system_connection	yes	S_9	MBB	SCP	DT	BB_DT_11	BB_DB_DT_DD_LC_f	BB_DB_DT_DD_FN_s
12 DT_12			PL0	yes	system_connection	yes	P_9	MBB	SCP	DT	BB_DT_12	BB_DB_DT_DD_MN_p	BB_DB_DT_DD_AN_p

Fig.19: Layout of SCP showing major inputs required in defining DS3 connections on the vessel

The number of inputs of the SCP for the submarine case study was 4700 as each connection required 10 inputs and there were 470 connections.

4.9. Summary of the Programs

Although the lines of codes are not necessarily a metric of goodness, the summary of codes of each program is shown in Table II and the output summary in Paramarine is shown in Fig.20. Improvements were made to the proposed programs for performing the modelling task in Paramarine. The proposed programs could convert within a minute on a standard PC machine the input data provided in the submarine case study, which consisted of some volume objects, more than 150 numerical weight objects, 200 component objects, and 400 connection objects, to 20,000 lines of KCLs. Therefore, the execution time of the programs, for sending macros to Paramarine, was driven by the quality of the code and there remains scope for this to be further improved. The actual code is over 8000 lines long.

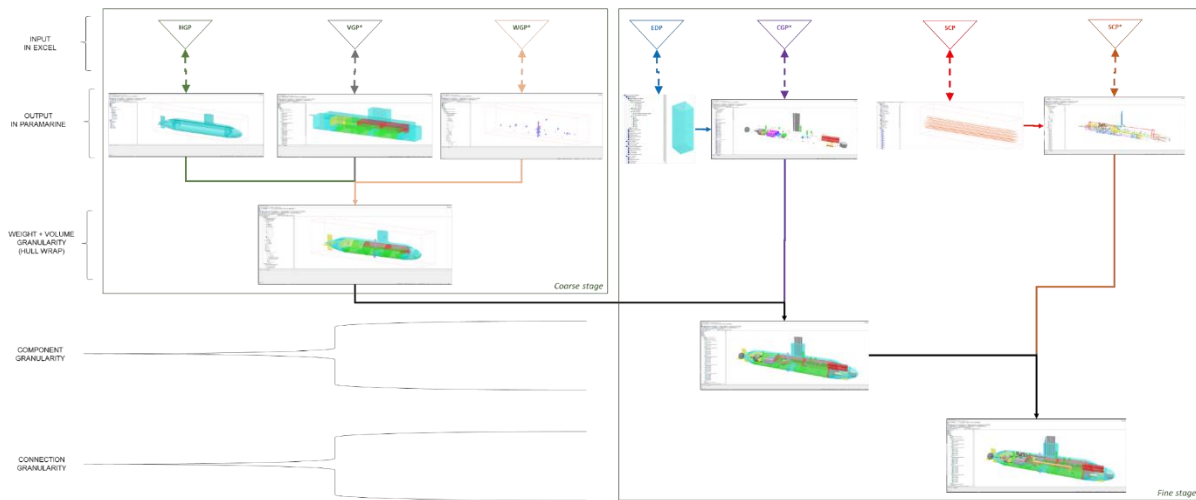


Fig.20: Output summary of NBA programs in SURFCON Paramarine (see Fig.10, Mukti *et al.* (2022))

Table II: Summary of codes in the Input Data Centre

Program	Description	Script Identifier	Size (Lines)
MMP	Main Menu Program	A_A_MMP	42
DPP	Design Preamble Program	A_B_DPP	238
DAP	Design Analysis Program	A_C_DAP	537
HGP	Hull Granularity Program	C_A_HGP	1460
VGP	Volume Granularity Program	C_B_VGP	910
		C_C_VGP	254
		C_D_VGP	148
WGP	Weight Granularity Program	B_A_WGP	710
		B_B_WGP	191
EDP	Equipment Database Program	D_A_EDP	556
		D_B_EDP	1200
CGP	Component Granularity Program	D_C_CGP	555
		D_D_CGP	684
		D_E_CGP	81
SPP	System Preamble Program	E_A_SPP	369
SCP	System Connection Program	E_B_SCP	300
		E_C_SCP	756
KCL Output			>25000

6. Critique of the New Design Tool Applied to a Submarine Study

As discussed in Section 2, most automated approaches hardcode design steps, many design algorithms and their assumptions for sizing often implying, but are not limited to, how the spaces are arranged within the vessel. This, in turn, makes the software program follow several design decisions automatically every time an unbalanced condition occurs in the design. This can then allow hundreds of concept designs to be generated quickly by the computer(s) but all based on ‘hidden’ configurational assumptions. Such an automated approach is consequently difficult to be assessed, i.e., is not revealed easily (if at all) to the designer and thus is a ‘black-box’ synthesis. The implementation of the UCL DBB approach in Paramarine for DS3 was intended to commence a new ship design from a blank sheet. It must be emphasised that although the Paramarine has some hardcoded sizing algorithms as objects (e.g., “generator_sizing” object), the designer still can choose whether to use such objects without the need to modify the main codes of the software, which is the opposite of the black-box system. What makes modern automation have black-box characteristics is not just their inaccessible algorithms or data but also the difficulty in determining the causal link between input databases or design rules and the resulting options generated.

Assuming the development of the tool is before commencing a given design study there would seem to be a trade-off between the level of design automation and the transparency of the tool. Fig.21 shows the more choices, decisions, or design algorithms hardcoded into the tool means the less design effort to generate more design concepts. However, this then reduces the flexibility of the design tool and makes the tool highly opaque as those hardcoded inputs are not revealed easily to the designer using the system, i.e., a black-box tool. Conversely, the glass-box, SURFCON Paramarine design tool with the intent to be able to explore radical solutions, starts the design ab initio, to be highly flexible, without any step-by-step menu (or any dialogue box) for commencing a new submarine design study, which means require more designer inputs, i.e., more design effort than the black-box tool. Therefore, the solution space produced by a glass-box approach will be less populated than the myriad design solutions produced by a black-box approach, however as *Purton (2016)* showed each solution may not be practical and the solution space is likely to be much more restricted, *Andrews (2018)*.

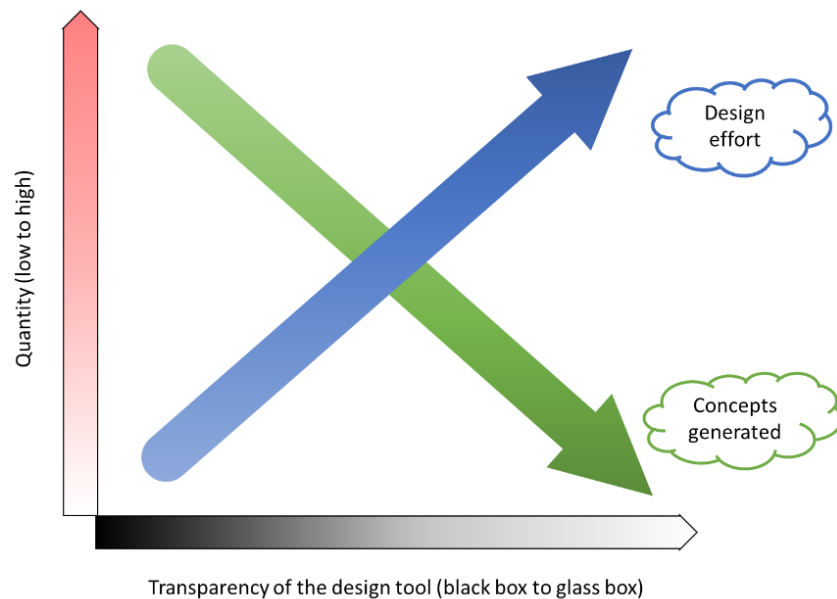


Fig.21: A simplified nature of the Computer-Aided Ship Design tool, with the X-axis as the indicator of design transparency, i.e., it is getting darker on the left-hand side (for black-box approach) and getting brighter on the right-hand side (for glass-box approach) while the Y-axis indicates the level of quantities from low (white) to high (red), which corresponds to the design effort in blue and the number of design solution(s) produced by the tool in green

This then raises questions as to what should be automated in the design tool and what should not. Fig.22 summarises important decision making, such as choice of design algorithms, which should be kept as the input and not hardcoded into design tools. This will not constrain the overall ship design solution space size early in the design process and so retain design flexibility. This is because in ESSD any design study should rapidly evolve as part of the Requirement Elucidation dialogue, *Andrews (2018)*. Thus, in the initial case study (see Section 2.4), the engine room was quickly resized due to the need to fit additional diesel generators for necessary redundancy. Therefore, the proposed Network Block approach allowed design flexibility and only automated routine tasks - Gulf of Execution. Thus, only the routine could be simplified while acting within the design tool should not resort to hardcoding design steps or choices and for the selection of such design algorithms the choice must be with the designer.

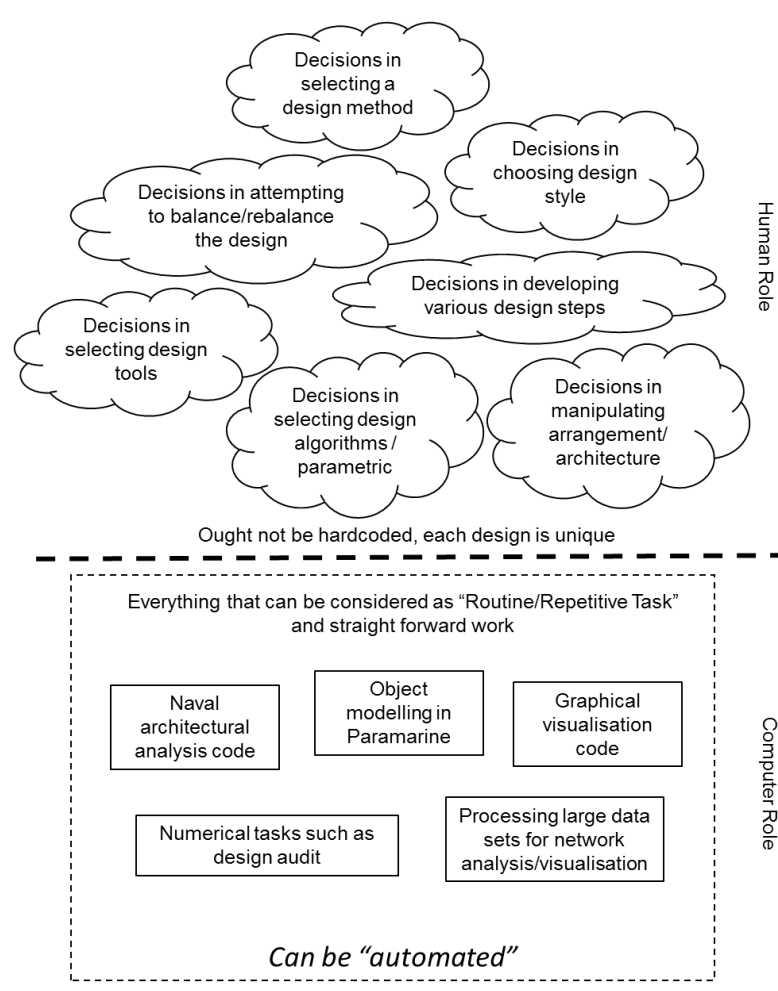


Fig.22: Decision making CAD processes vs human designer showing what ought to be automated and what ought not

7. Conclusions on the New Tool

This paper has outlined a new tool to mitigate modelling issues for DS3 in ESSD using a sophisticated 3D CASD system. A more plausible submarine design than 2.5D definition could now be produced more quickly, enabling a 3D informed dialogue and more realistic space reservation for DS3 routing. Highly automated 3D modelling of DS3, the transparent approach is now possible, which mitigates the demanding modelling task in implementing the UCL DBB approach in SURFCON Paramarine. However, as part of the justification of the ability of the Network Block Approach (NBA) to assist in the DS3 synthesis of submarines, it was necessary to test its sensitivity to different design decisions. This next step is to be addressed in future papers.

Acknowledgements

This research was supported by the Indonesia Presidential Scholarship (managed by Indonesia Endowment Fund for Education – LPDP) and the UCL Joint Scholarship awarded to the first author.

References

- ANDREWS, D.J. (1994), *Preliminary Warship Design*, Trans. RINA 136
- ANDREWS, D.J. (2011), *Marine Requirements Elucidation and the Nature of Preliminary Ship Design*, IJME 153
- ANDREWS, D.J. (2012), *Art and science in the design of physically large and complex systems*, Proc. Royal Society A: Mathematical, Physical and Eng. Sciences 468 (2139), pp.891-912
- ANDREWS, D.J. (2018), *The Sophistication of Early Stage Design for Complex Vessels*, IJME Special Edition, 472 Part A
- ANDREWS, D.J. (2021), *Who Says There Are No Real Choices in Submarine Design?* WARSHIP 2021, RINA
- ANDREWS, D.J.; CASAROSA, L.; PAWLING, R. (2009), *Integrating Simulation and Computer Aided Ship Design Software and Processes*, RINA Int. Conf. Computer Applications in Shipbuilding (ICCAS)
- ANDREWS, D.J.; CUDMORE, A.C.; HUMBLE, P. ; WILSON, D. (1996), *SUBCON - A New Approach to Submarine Concept Design*, RINA Warships Proc. Symp. Naval Submarines 5: The Total Weapons System, London
- ANDREWS, D.J.; DICKS, C.A. (1997), *The Building Block Design Methodology Applied to Advanced Naval Ship Design*, Proc. Int. Marine Design Conf. (IMDC)
- ANDREWS, D.J.; PAWLING, R.J. (2003), *SURFCON A 21st Century Ship Design Tool*, 8th Int. Marine Design Conf. (IMDC), Athens
- ANDREWS, D.J.; PAWLING, R.J. (2008), *A Case Study in Preliminary Ship Design*, RINA IJME 139
- BREFORT, D.; SHIELDS, C.; HABBEN JANSEN, A., DUCHATEAU, E.; PAWLING, R.; DROSTE, K.; JASPER, T.; SYPNIEWSKI, M.; GOODRUM, C.; PARSONS, M.A.; KARA, M.Y.; ROTH, M.; SINGER, D.J.; ANDREWS, D.; HOPMAN, H.; BROWN, A.; KANA, A.A. (2018), *An architectural framework for distributed naval ship systems*, Ocean Eng. 147, pp.375-385
- CIERAAD, S.; DUCHATEAU, E.; ZANDSTRA, R.; DE BROEK-DE BRUIN, W.H. van (2017), *A Packing Approach Model in Support of the Conceptual Design of Naval Submarines*, 16th COMPIT Conf., Cardiff
- DUCHATEAU, E.A.E. (2016), *Interactive evolutionary concept exploration in preliminary ship design*, Ph.D. thesis, TU Delft, <https://doi.org/10.4233/uuid:27ff1635-2626-4958-bcdb-8aee282865c8>
- FIEDEL, E.R. (2011), *Cooling System Early-Stage Design Tool for Naval Applications*, Master's thesis, MIT
- JURKIEWICZ, D.J.; CHALFANT, J.; CHRYSSOSTOMIDIS, C. (2013), *Modular IPS machinery arrangement in early-stage naval ship design*, 2013 IEEE Electric Ship Technologies Symp., Arlington

KOURIAMPALIS, N., PAWLING, R.J.; ANDREWS, D.J. (2021), *Modelling the operational effects of deploying and retrieving a fleet of uninhabited vehicles on the design of dedicated naval surface ships*, Ocean Eng. 219: 108274

MAHONEN, C.; SPRADLEY, W.; GERDON, M. (2007), *Automating Early Stage Submarine Design: Development of the Submarine Concept Design (SUBCODE) Program*, ASNE Day, Arlington

MUKTI, M.H. (2022), *A Network-Based Design Synthesis of Distributed Ship Services Systems for a Non Nuclear Powered Submarine in Early Stage Design*, Ph.D. thesis, University College London

MUKTI, M.H.; PAWLING, R.J.; ANDREWS, D.J. (2021), *Distributed Ship Service Systems Architecture in The Early Stages of Designing Physically Large and Complex Vessels: The Submarine Case*, IJME 163

MUKTI, M.H.; PAWLING, R.J.; ANDREWS, D.J. (2022), *The Network Block Approach Applied to the Initial Design of Submarine Distributed Ship Service Systems*, 14th Annual Int. Marine Design Conf., Vancouver

MUKTI, M.H.; PAWLING, R.J.; SAVAGE, C.; ANDREWS, D.J. (2019), *Distributed Ship Service Systems Architecture in the Early Stages of Physically Large and Complex Products*, ICCAS Int. Conf. Computer Applications in Shipbuilding, Rotterdam

MUKTI, M.H.; RANDALL, R.E. (2017), *Graphic Method for Improved Indonesian Navy Submarine Design Acquisition; the Investigation of Small (Midget) Naval Submarine Development*, RINA Warship: Naval Submarines & UUVs, Bath

NORMAN, D. (2013), *The design of everyday things*, MIT Press

OERS, B.J. van (2011), *A packing approach for the early stage design of service vessels*, Ph.D. thesis, TU Delft

PAWLING, R.J. (2007), *The Application of the Design Building Block Approach to Innovative Ship Design*, Ph.D. thesis, University College London

PAWLING, R.J.; ANDREWS, D.J. (2011), *A Submarine Concept Design - The Submarine as an UXV Motherhip*, Warship 2011: Naval Submarines and UUVs, Bath

PAWLING, R.J.; PIPERAKIS, A.; ANDREWS, D. (2015), *Developing Architecturally Oriented Concept Ship Design Tools for Research and Education*, 12th Int. Marine Design Conf. (IMDC), Tokyo

PURTON, I.M. (2016), *Concept Exploration for a Novel Submarine Concept Using Innovative Computer-Based Research Approaches and Tools*, Ph.D. thesis, University College London

PURTON, I.M.; PAWLING, R.J.; ANDREWS, D.J. (2015), *The Use of Computer Tools in Early Stage Design Concept Exploration to Explore a Novel Submarine Concept*, 12th Int. Marine Design Conf. (IMDC), Tokyo

THURKINS, E.J. (2012), *Development of an early stage ship design tool for rapid modeling in Paramarine*, Master's thesis, MIT, <http://dspace.mit.edu/handle/1721.1/74992>

UCL-NAME (2014), *Submarine Data Book*, University College London

Developments toward a Common Maritime ICT architecture

Ørnulf Jan Rødseth, SINTEF Ocean, Trondheim, Norway, OrnulfJan.Rodseth@sintef.no
Marianne Hagaseth, SINTEF Ocean, Trondheim, Norway, Marianne.Hagaseth@sintef.no

Abstract

This paper proposes a common ICT reference architecture to overcome current application or geographic "silos" in digital maritime communication. The architecture is called reference architecture since it only specifies the generic case. If desired, it can be developed into a more concrete architecture, e.g. on national or port level. The different protocols can be developed based on this generic specification. As the generic definitions are already agreed on, it should be easier to achieve the necessary interoperability between the different domains. Some reference processes are being developed in IMO. In Norway, the new collaborative research project "Intelligent Ship Transport System" will investigate these issues, closely aligned with developments in IMO and in selected international standards organizations, mainly IEC and ISO.

1. Introduction

Digital communication in the maritime sector has been available since the 1980s when Inmarsat and a few other satellite communication providers made it possible to exchange digital information between ships and shore. In 2020 it was estimated that almost 70000 vessels were equipped with satellite terminals, NSR (2021). Together with increasing digitalization onboard the ship, in ports, and by maritime authorities, a complex digital system is now emerging in the maritime domain. Section 2 will discuss the difference between digitization and digitalization and point out the need for standards to reap the potentially great benefits that digitalization can give.

There are several maritime digitization standards available as well as in development. In addition to mandatory standards such as for automatic identification systems (AIS), existing industry standards include bridge networks, automation interfaces, ship-shore communication, and electronic port clearance. Section 3 will give a brief overview of the most important of these standards and how they fit into a physical maritime ICT architecture.

Unfortunately, many of these standards are developed in application or geographic "silos" and are only marginally harmonized, if at all. However, the silo approach is often necessary to keep complexity under control: It is not possible to develop one universal standard for everything and by that ensure global interoperability. This would create too many interdependencies between different elements in the standard as well as between each element and the many different application areas for the standard. This makes development very complicated and maintenance impossible.

It is possible to overcome the silo-problem by establishing a common ICT reference architecture. ICT architectures can be of many forms and functions, Aerts *et al.* (2004), but here we will use a relatively simplistic variant based on an earlier paper, Rødseth (2011). The proposed reference architecture will be described in section 4. This section will also explain how the reference architecture can be used to make independently developed standards more harmonized.

Parts of the proposed reference architecture is already in development by the Facilitation committee in the International Maritime Organization (IMO) and section 5 will give some background for this work, its status, and further plans.

Section 6 will conclude the paper with a short conclusion and some of the plans for a new Norwegian R&D project called "Intelligent Ship Transport Systems" (ISTS).

2. Digitization, digitalization, and the digital transformation

Digitalization is sometimes illustrated as a three-layered pyramid, as shown in Fig.1. The left-hand diagram shows the digitalization pyramid, and the right-hand rectangles show the corresponding role of standards.

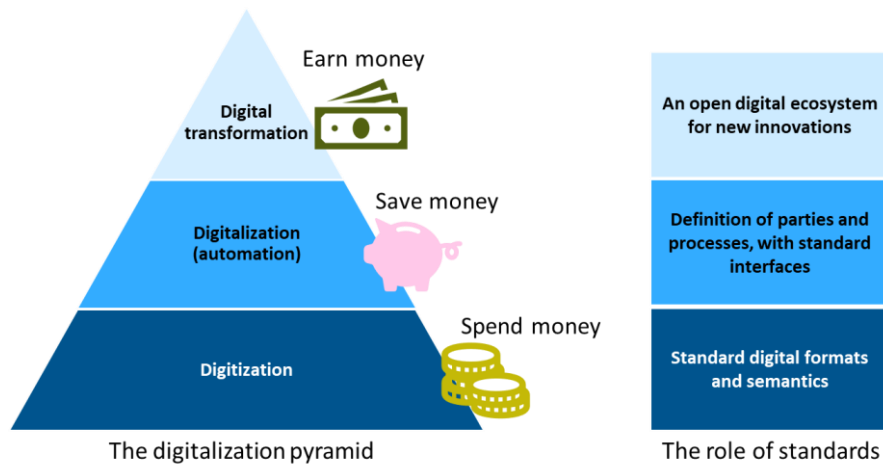


Fig.1: Digitalization pyramid

The lowest layer is digitization, which transfers information that was previously in analogue form, e.g. voice or paper into the corresponding digital representation, *Gartner (2022)*. There are different interpretations of this term, e.g. that an electronically scanned document is a digitized version of the original, but in this paper, it is assumed that digitization converts the material into a machine readable and understandable format. Digitization is a time consuming and expensive activity that does not necessarily return much on investments. The main benefits of digitization are generally related to the possibility of storing information electronically, e.g. physical space and monetary savings. One should note that digitization also requires digital connectivity, i.e. the ability to collect information electronically and transfer it to storage.

Digitization will not necessarily reduce the workload in the processes affected. Digitization may actually increase workload if, e.g. web forms have to be filled in instead of just writing the information directly on paper forms. To reduce work related to data entry and verification, digitalization is necessary to automate the work processes and allow direct machine to machine communication. However, digitalization cannot be done without digitization. Digitalization is changing the business processes to use digital information, *Gartner (2022)*. This also normally include a high degree of automation of more trivial tasks such as data entry or verification. This enables, e.g. the use of fully automated reporting to various authorities through a maritime single window. This can mean significant savings, although the digitalization process also can be resource demanding and expensive.

Standards play an important role in both digitization and digitalization. They will reduce complexity by providing a framework and templates for the work and can also provide interoperability between different parties when their work processes are digitalized. Having generally accepted standards for digitalization can also contribute to the creation of a "digital ecosystem" where many parties use the same information models and data exchanges. This makes it much easier to create new and innovative applications to further increase automation and efficiency, or to develop completely new processes and business models. This is what often is called the digital transformation. This is where the renewal of the maritime industry can take place and where new business methods and tools can be developed.

In the maritime sector, standards will be a prerequisite to reach the digital transformation stage. As illustrated in Fig.2, the smartphone market consists of more than 7.5 billion smartphones where there are essentially only two different software platforms, Android and iOS, <https://www.statista.com/statistics/330695/number-of-smartphone-users-worldwide/>, https://en.wikipedia.org/wiki/Comparison_of_mobile_operating_systems. In comparison, there are about 96000 ships in international trade,

larger than 100 GT, *UNCTAD (2020)*. In addition, virtually all of these ships have different ICT infrastructures. On the land side, *Lloyd's (2019)* lists around 8000 ports around the world. Again, most of these ports are different and use different software for their management functions.

The mobile phone market is more than large enough to support an organic evolution of the platform technology. This cannot be expected in the maritime sector where international cooperation must be established to develop the necessary standards to ensure a more homogenous maritime ICT architecture, and by that a suitable platform for more extensive innovations in digitalization and automation.

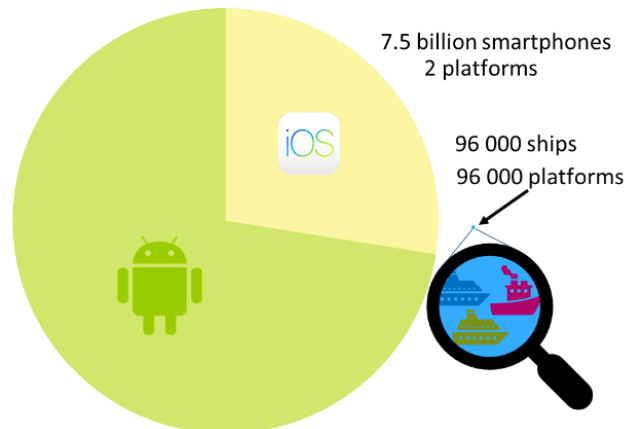


Fig.2: Relative sizes of markets for smartphones and ships

Thus, standards are critical for efficient digitalization of the maritime sector. However, as was pointed out above, the shipping sector is small and cannot rely on organic evolution of the necessary ICT standards. This means that the sector needs a more structured and cooperation-oriented approach to development of standards.

Digital business ecosystems are often quoted as directly connected to the digital transformation, *Hanelt et al. (2021)*, and may be characterized, among other things, by a more extensive and novel types of cooperation between parties. One may argue that this also favours active participation in standardization activities. It is a relatively small business community and wishing to take an active position in the digital transformation will require cooperation in standards development and building new alliances to other parties.

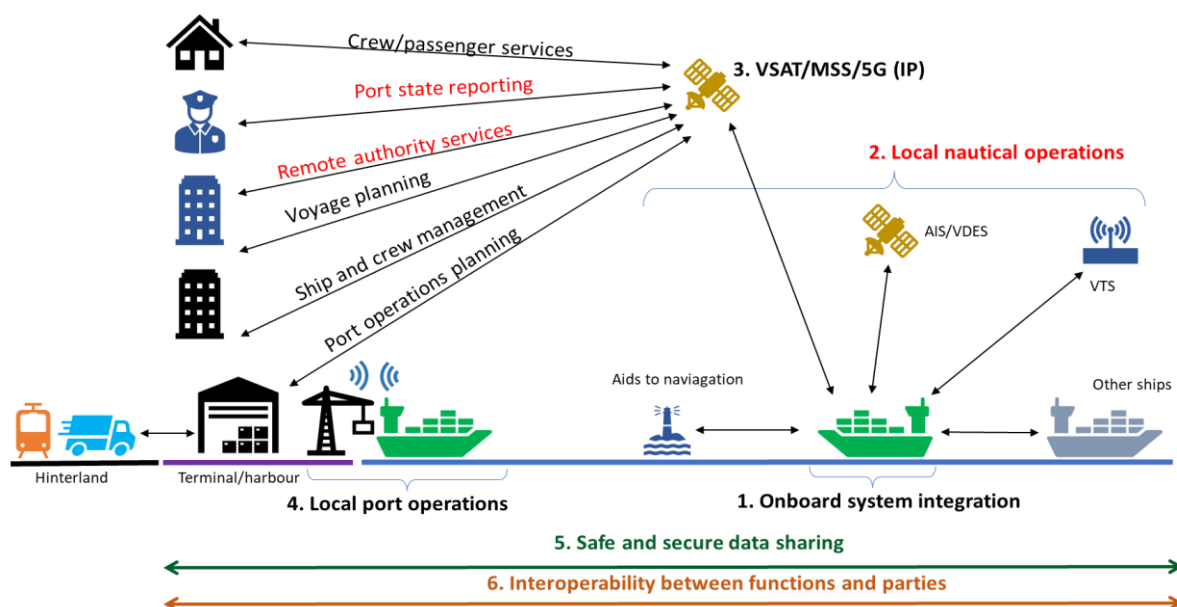


Fig.3. The ship's digital context

3. An overview of some existing and emerging maritime ICT standards

Even when we concentrate on information exchanges related to ships, the digital interactions in the shipping community are quite complex as illustrated in Fig.3

A wide range of different parties need to communicate with the ship in addition to ship internal integration. The figure numbers four main classes of communication as follows:

1. Onboard system integration represents onboard data networks, protocols and infrastructure that makes data from the ship system available.
2. Local nautical operations are communication implemented on mandatory channels such as AIS and VHF radio (red label) and which is used to communicate with other ships or entities in the fairways.
3. VSAT/MSS/5G (IP) is communication that is done via satellite (VSAT or Mobile Satellite Systems – MSS) or land digital infrastructure, e.g. 5G mobile data. This includes business to authority (red lines) as well as business to business (black). This type of communication is normally via various Internet Protocols (IP) and can be both mandatory exchanges with authorities (red) or more commercial and operational exchanges (black).
4. Local port and terminal operations are communication related to infrastructure in port, such as mooring systems, cold ironing or cargo handling. Currently this is mostly voice over VHF, but it is expected that many of these systems may be automated in the future, e.g. with the development of the new VHF Data Exchange System (VDES).

In addition to the actual communication facilities, there are also two other dimensions of electronic communication that needs to be considered:

5. Safe and secure data sharing to ensure that communication is not tampered with or overheard when it is of a confidential nature.
6. Interoperability between functions and parties to make it easier to share information between parties, independently of in what context the information was acquired.

Fig.3. can be seen as an illustration of the physical maritime ICT architecture. It defines the different communication links as well as the more general interoperability and safety/security perspectives. The focus is more on a case-by-case physical inter-connection between stakeholders than on a systematic principle for construction of the relevant protocols.

There are several specifications available or under development. Table I lists some of the most relevant. The Committee/Group column specifies what organization is responsible for the standard and what technical committee (TC), sub-committee (SC) and/or work group (WG) that does the actual work. The status field gives the status of the specification:

- Ed. N: Published as edition N
- Rev: Currently under revision by committee
- CD: Currently as Committee Draft
- CDV: CD for Voting
- WD: Currently as working draft
- Online: Continuously updated, available online.
- Drafts: Not necessarily an official release or preliminary specifications

The table rows are grouped into the same categories as in Fig.3., where each category is separated by a double line. The security standards are not included in the overview (group 5). The last group represents data models or more general interoperability standards. Most of the standards are produced by IEC (International Electrotechnical Commission) or by ISO (International Organization for Standardization). VDES is a collective term for ITU (International Telecommunication Union) and IALA (International Association of Marine Aid to Navigation)

tional Association of Aids to Navigation and Lighthouse Authorities) specifications for the VHF Data Exchange System. This is an extension of the current AIS services in the VHF band. IMO is also active in specifications of high-level guidelines (not technical standards), the IMO Reference Data Model, and the Common Maritime Data Structure (CMDs). This is done by the Facilitation Committee (FAL) and the Navigation, Search and Rescue sub-committee (NCSR) respectively. Finally, the Digital Container Shipping Alliance is also producing some specifications.

Table I: An overview of some relevant maritime ICT standards

Standard	Name	Committee/Group	Status
IEC 61162-450	Maritime navigation and radiocommunication equipment and systems – Digital interfaces - Part 450: Multiple talkers and multiple listeners - Ethernet interconnection	IEC TC80/WG6	Ed. 2 Rev.
IEC 61162-460	Maritime navigation and radiocommunication equipment and systems – Digital interfaces - Part 460: Multiple talkers and multiple listeners - Ethernet interconnection – Safety and security	IEC TC80/WG6	Ed. 2 Rev.
ISO 19847	Ships and marine technology — Shipboard data servers to share field data at sea	ISO TC8/SC6/WG16	Ed. 1 Rev.
ISO 4891	Ships and marine technology — Navigation and ship operations — Smart logbooks for shipping	ISO TC8/WG10	CD
ISO 16425	Ships and marine technology — Guidelines for the installation of ship communication networks for shipboard equipment and systems	ISO TC8/SC6/WG16	Ed. 1 Rev
ISO 23816	Ships and marine technology — Secured ship network based on IPv6 Ethernet network	ISO TC8/WG10	WD
VDES	VHF Data Exchange System, various specifications	IALA, ITU	Drafts
ISO 28005-1	Ships and marine technology — Electronic port clearance (EPC) — Part 1: Message structures	ISO TC8/SC11/WG2	Ed. 1 Rev
IEC 63173-2	Maritime navigation and radiocommunication equipment and systems - Data interface - Part 2: Secure communication between ship and shore (SECOM)	IEC TC80/WG7	CDV
ISO 23807	Ships and marine technology — General requirements for the asynchronous time-insensitive ship-shore data transmission	ISO TC8/WG10	WD
IMO CG	Guidelines for authentication and integrity	IMO FAL	WD
IMO FAL	IMO Reference Data Model	IMO FAL	Online
IMO NCSR	Common Maritime Data Structure (S-100)	IALA/IHO S-100	Online
ISO 28005-2	Ships and marine technology — Electronic port clearance (EPC) — Part 2: Core data elements	ISO TC8/SC6/WG2	Ed. 2
ISO 28005-3	Ships and marine technology -- Electronic port clearance (EPC) -- Part 3: Part 3: Technical standard for administrative and operational data exchanges	ISO TC8/SC6/WG2	WD
IEC 61162-1	Maritime navigation and radiocommunication equipment and systems – Digital interfaces - Part 1: Single talker and multiple listeners	IEC TC80/WG6	Ed. 6 Rev
ISO 19848	Ships and marine technology — Standard data for shipboard machinery and equipment	ISO TC8/SC6/WG16	Ed. 1 Rev
IALA S-211	IALA Port Call Message Product Specification	IALA eNav Committee.	Drafts
DCSA JIT	Just in time port call	DCSA	Ed. 1.1

Table I omits standards and specifications that are not so relevant for use on the ships, including commonly used UN/EDIFACT standards used in international trade, and particularly container shipment operations. As can be seen from the table, there are several standards available and mostly they are complementary. However, there are some important gaps in alignment between standards that should be addressed:

- There is a significant lack of coordination on specifications for ship to shore communication. This results in several similar specifications.
- More importantly, there is too little harmonization on data models which causes problems with the detailed semantics of similar data objects from different specifications.
- In general, one should also aim to align complementary standards to a common architectural framework so that the scope and interfaces between different specifications become clearer.

These issues will be returned to in the next section.

4. A maritime ICT reference architecture

As can be seen from Fig.3, the maritime ICT context is complex with a high number of different information exchange and network standards. As concluded at the end of the previous section, these are still being developed in their own "silos" with little coordination with other standards for adjacent applications or areas.

To address this problem, one might want to develop one holistic, all-integrating standard, but this is for several reasons not possible. One problem is the different communication channels utilized in the area and very different physical properties for each, that makes it impossible to use, e.g. general IP type protocols on all. A more central problem is that the complexity of such a universal specification would be prohibitive for effective development and maintenance. Also, the different business and organizational domains are overlapping with other domains even further from the ship-land interface that would also need to be taken into consideration, and further increasing the complexity.

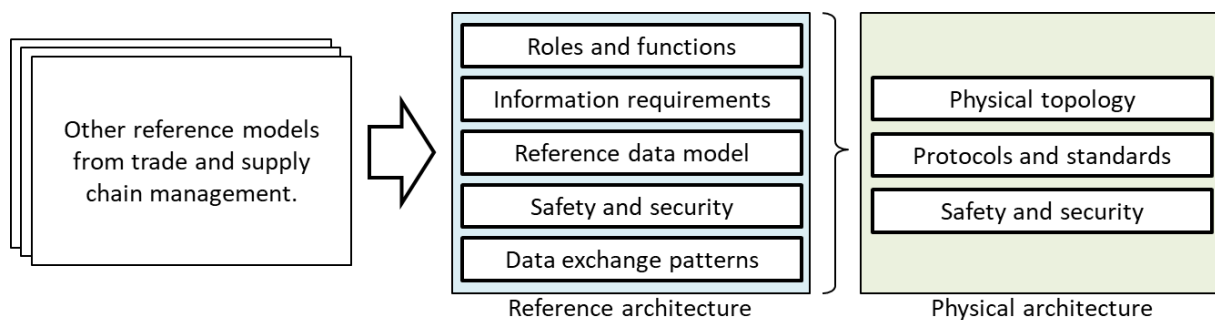


Fig.4: Outline of an ICT reference architecture

A more viable solution is to develop a reference architecture that can act as a pattern for the development of the individual standards. A reference standard can be seen as a requirements specification that the physical architecture can be based on. Specific protocols and standards will be part of the physical architecture as well as the specification of the actual topology and any necessary infrastructure services. The reference architecture may also use building blocks from other reference architectures. In Norway, the ARKTRANS model, *Natvig et al. (2009)*, has been proposed, but with limited uptake. However, some components may still be useful. The ITS community has also proposed some architectures that may be considered, e.g. the US National ITS Architecture, <https://highways.dot.gov/public-roads/septoct-1998/national-its-architecture>, or the EU FRAME Architecture, <https://frame-online.eu/first-view/what-is-an-its-architecture>.

For the purposes of the maritime domain, we propose a relatively simplified reference architecture with the following main components:

1. Roles and function: A general description of the most common parties to the different information exchanges and for what purpose they communicate. As the physical organization vary between ports, ships and authorities, this type of description should focus on higher level "roles" and "functions" rather than the physical institutions and the specific local work processes. This could be called the logical architecture. It is also important to focus on the interactions between roles to perform a given function rather than the internal process that each role uses to implement the function. The main purpose is to describe interfaces.
2. Information requirements: The general information requirements for each role to perform its side of a specific function. This defines the information that must be available and possibly transmitted between the roles.
3. A reference data model giving semantically unambiguous definitions of information elements that are common to different functions. This would allow the implementation of different protocol standards for the different functions but ensure that the same meaning and representation is given to each common information element. This is already being developed within the IMO framework for some of the information requirements (IMO 2022).
4. Safety and security mechanisms need to be defined to ensure that critical data cannot be tampered with, and that confidential data cannot be listened into. This may also include information backup procedures, fall-back solutions in case of critical component failures etc.
5. Data exchange patterns: Where relevant, a definition of a common approach to how information is exchanged. This should include the typical message exchange patterns as well as the transport protocols used. This should also provide safety and security mechanisms that are used during exchanges of information.

By defining these general elements in the ICT reference architecture, one should be able to define the individual components of the physical architecture independently, but still retain a good level of interoperability in the system.

The physical architecture will probably consist of three main components:

1. Physical topology: A description of how parties are interconnected. This is most likely an evolving specification with some differences between different geographic regions.
2. Protocols and standards: These are the actual protocols used in communication between parties, implementing the physical topology. If linked to a reference architecture, these elements will be a realization of the information requirements, reference data model, and data exchange patterns from the reference architecture.
3. Safety and security: This is the same element as in the reference architecture, but with specific implementations related to the physical topology and the real protocols.

Thus, the physical architecture will be one possible realization of the reference architecture.

5. The IMO reference data model

The reference data model described in the previous section is already being developed in the IMO Facilitation committee by the Expert Group on Data Harmonization (EGDH), *IMO (2022)*. This is called the IMO reference Data Model (IRDM). The IRDM was initially developed to harmonize standards from World Customs Organization (WCO), UNECE and ISO with respect to reporting formalities defined in the IMO Facilitation Convention. Later it has been extended to cover parts of other IMO instruments such as SOLAS and MARPOL, as well as more operational concepts like just in time arrival for ships to port.

Part of the reference processes is also being developed in IMO. At time of writing a correspondence group is tasked to deliver guidelines on harmonized communication and electronic exchange of operational data for port calls to the IMO FAL Committee meeting number 46 in April 2022. This will be a good starting point for further work on the reference architecture. Also, the parties and connectivity

will most likely have to be addressed by the correspondence group, but this remains to see.

The e-navigation activity in the IMO Maritime Safety Committee (MSC) and its Navigation, Communication, Search, and Rescue sub-committee (NCSR) has also defined an e-navigation architecture that can be used as input to a more general specification. Other inputs can also be taken from the intelligent transport systems (ITS) research area. The Common Maritime Data Structure (CMDS) is also a part of the e-navigation framework. It is based on the International Hydrographic Office (IHO) S-100 Universal Hydrographic Data Model. Discussions are ongoing on how this framework can be aligned with the IRDM.

One important aspect of the development of the IMO Reference Data Model is that it has created a focal point for digital standardization in the maritime domain. More and more stakeholder groups are now recognizing the need for standardization and the need for harmonization between standards. As an example, a new work item was approved by ISO Technical Committee 8 (Ships and marine technology) in December 2021 to develop a harmonized just in time arrival interface based on input from among others, International Association of Ports and Harbours (IAPH), DCSA, and IALA. This will become the new ISO 28005-3 standard.

6. Conclusions and way ahead

This paper has given an overview of the increasing interest in maritime digitalization, the need for standards, and the importance of linking the standards to a reference architecture to enable better harmonization between the standards. It is our belief that the activities in IMO on the development of the IMO Reference Data model may be a game changer in this as it has helped to bring the importance of harmonized standards to the attention of the maritime community. There is also work ongoing in IMO to extend the reference data model to also include roles and message exchange patterns. This may be a start of a new reference architecture for the maritime ICT community.

Norway has just started a new cooperative research and development project called "Intelligent Ship Transport System" (ISTS). This project will investigate these issues through a bottom-up process where reference architecture elements will be developed based on developing industry standards. This will be combined with a top-down activity where existing architectures, e.g. e-navigation and ITS, will be used to define the overall structure of the new maritime reference architecture. The work will be closely aligned with developments in IMO and in selected international standards organizations, mainly IEC and ISO. The project started in the autumn of 2021 and will run for 36 months.

Acknowledgements

This work has been supported by the Research Council of Norway through grants 309255 (Maritime digital ecosystem) and 326679 (Intelligent ship transport systems). It has also received funding from the European Union's Horizon 2020 research and innovation programme under grant agreement No 859992 (AEGIS).

References

- AERTS, A.T.M.; GOOSSENAERTS, J.B.; HAMMER, D.K.; WORTMANN, J.C. (2004), *Architectures in context: on the evolution of business, application software, and ICT platform architectures*, Information & Management 41(6)
- GARTNER (2022), *Gartner Glossary*, Gartner Group, <https://www.gartner.com/en/glossary>
- HANELT, A.; BOHNSACK, R.; MARZ, D.; ANTUNES MARANTE, C. (2021), *A systematic review of the literature on digital transformation: Insights and implications for strategy and organizational change*, J. Management Studies 58(5), pp.1159-1197

IMO (2022), *The IMO Compendium on Facilitation and Electronic Business*, The IMO Reference Data Model, <https://imo.org/en/OurWork/Facilitation/Pages/IMOCompendium.aspx>

LLOYDS (2019), *Lloyd's Maritime Atlas of World Ports and Shipping Places 2020-2021*, ISBN 9780367427108

NATVIG, M.K.; WESTERHEIM, H.; MOSENG T.K.; VENNESLAND, A. (2009), *ARKTRANS The multimodal ITS framework architecture Version 6*, SINTEF Report A12001

NSR (2021), *Maritime SatCom Markets*, Northern Sky Research

RØDSETH, Ø.J. (2011), *A maritime ITS architecture for e-navigation and e-maritime: Supporting environment friendly ship transport*, 14th Int. IEEE Conf. Intelligent Transportation Systems (ITSC)

UNCTAD (2020), *UNCTAD 2020 Handbook of Statistics*, United Nations, Geneva

Utilization of OCX as Part of 3D Model Based Approval in Ship Design Process

Myeong-Jo Son, NAPA Ltd., Helsinki/Finland, myeong-jo.son@napa.fi

Tapio Seppälä, NAPA Ltd., Helsinki/Finland, tapio.seppala@napa.fi

Jani Merikanto, NAPA Ltd., Helsinki/Finland, jani.merikanto@napa.fi

Ove Aae, DNV, Oslo/Norway, ove.aae@dnv.com

Ole Christian Astrup, DNV, Oslo/Norway, ole.christian.astrup@dnv.com

Abstract

As various CAD vendors support to export ship models in Open Class 3D Exchange (OCX) format, NAPA has developed OCX interface not only exporting own model in OCX format, but also importing OCX format to be re-created as NAPA model and further to be utilized in various ways, such as rule scantling, direct strength analysis, 3D model review, drafting, and 3D model translator. This paper demonstrates how a modern structure design tool can improve the ship design process with the help of the OCX format and demonstrates the workflow with several practical examples.

1. Introduction

Open Class 3D Exchange (OCX) format has been developed within APPROVED project, Astrup (2020) and the main purpose of this format is to include most of the necessary structural information along with 3D geometries for 3D Model Based Approval (3D MBA) of a ship, Moser and Astrup (2018), Astrup (2019). As there are OCX consortium established, <http://www.3docx.org>, not only CAD vendors, but also the most of major classification societies, and ship design companies have joined to discuss OCX use cases, to develop further the OCX format, and to extend its coverage to other domains, such as Finite Element Analysis (FEA), or naval architectural assessment of load line, tonnage, and fire safety.

As a CAD vendor, NAPA sees OCX has good potential, since this concept opens new possibilities to utilize best-of-breed tools, which will boost the digital transformation of the shipbuilding and ship design industries from classical drawing-based design towards seamless information exchange using a 3D model. In addition, there is lots of efforts savings in the development itself, instead of having individual interfaces between different software packages, but keeping the OCX interface in live and at the up-to-date status all the time as a main interface of 3D model.

As various CAD vendors in OCX consortium support to export ship models in OCX format already, e.g. AVEVA, HEXAGON, SIEMENS, and CADMATIC, <http://www.3docx.org>, NAPA has developed OCX import feature to re-create the model description in OCX into NAPA model in NAPA Designer, which is 3D CAD for the early design of a ship targeting a whole ship modeling for both of structure and compartment, and being widely used in the real projects in worldwide shipbuilding industries, including major shipyard such as HHI, DSME, *Hulkkonen et al. (2017)*. This imported 3D model is further to be utilized in various ways which are essential design works for 3D model-based approval or are useful to interoperate other design/engineer tools which are not yet supported with OCX, but with interoperable with the neutral CAD/CAE formats. The key areas of the utilization in ship design process are as follows:

- Rule scantling: interface to various classifications' rule check software packages
- Direct strength analysis: FE model creation/modification, interface to FEA software (MSC Nastran, Ansys, and DNV GeniE)
- 3D model review: sharing of 3D model in web environment for the review and commenting
- Drafting: generation of 2D drawings
- 3D model translator: export OCX model back to other CAD formats (IGES, JT, STEP, HTML, 3D PDF, etc), to other downstream CAD systems (AVEVA Marine, CADMATIC, or CATIA)

In addition, the design iteration during rule scantling, which has been performed in the rule calculation software of the classification society, can be done in CAD system through this OCX interface, which enables 3D model to be always up to date, to be ready for the following design/engineer works, such as FEA, 2D drawing generation, the further detailed structural design or even other functional design like outfitting. In this paper, we introduce these functionalities in NAPA Designer with DNV rule check software; Nauticus Hull.

2. Model generation using OCX

In OCX file format (.3docx), data can be classified into three different parts; structures, compartments, and ship's data that is useful or necessary for 3D MBA. NAPA imports all these three parts as their own categories. Structures (all sub xml elements under ocx:Panel) are to be made into Steel 3D model, compartments (ocx:Arrangement) are to be converted to Arrangement 3D model, and other data (ocx:Header, ocx:ClassificationData, ocx:BuilderInformation, ocx:CoordinateSystem) is to be input in Reference system in the ship project.

2.1. Structure model

NAPA Steel model consists of a set of MainObjects. A basis of MainObject is either of surface geometries that are a surface or a surface object (surface limited with the boundary in the utilization of plane, surface, or combined surface, or the modified surface using geometric operation). In addition to this geometry representation, it needs to be defined with StructureType which is a similar type with the function type in OCX schema, that is functional zone/area/division of a ship. And another key aspect of MainObject is that it needs to be included in Steel Arrangement, which is a hierarchical model tree for the structure model of a ship. In OCX schema, ocx:Panel is comparable to this MainObject. In other words, MainObject has its own plates, stiffeners, brackets, openings, and seams. Thus, ocx:Panel would be directly converted to be a MainObject in NAPA. Fig.1 demonstrates an example of OCX import of a structure model in NAPA Designer. In the upper side of the figure shows the concept of MainObject and its StructureType with the color code. In the lower side of the figure shows the display with plates and stiffeners from the same model. And when we take a look into the longitudinal bulkhead as an example, that the concept of a MainObject converted from ocx:Panel can be seen easily and clearly that it has multiple plates and stiffeners.

It is essential to create a surface out of ocx:UnboundedGeometry in ocx:Panel to define MainObject correctly. There are two ways to create the surface with boundary from OCX schema. One is to use ocx:LimitedBy which is either geometries in the form of a curve, or any other OCX items as a reference that are defined in the file. From this approach, 3D model can be relation-based model, that is dependent to one to another, to enable the model modification in a convenient way, that once one structure part is moved to another location, then all relevant structures would be modified accordingly. The other possible way to define the boundary is more straight-forward way to use ocx:OuterContour which is the geometric representation of the boundary of ocx:Panel. In NAPA, the latter approach is adopted, since it is safer, and more robust to get an as good import result as possible. Even if there was an error or a failure in the import of some ocx:Panels all other ocx:Panels can be imported without issues. In other words, if there is a failing or missing ocx:Panel exists while importing, and this ocx:Panel is being referred by other ocx:Panel as one of their boundaries, then all these ocx:Panels cannot be imported consequently. As an auxiliary backup, if there is missing definition or problem in ocx:OuterContour, then NAPA take the boundary data from ocx:LimitedBy, but mainly with ocx:FreeEdgeCurve3D, for the same reason that described above. In conclusion, the structure model in 3D which is being created by ocx:OuterContour without any relational definitions, can be processed within NAPA to have a topological relation with the series of automatic geometry operations to be capable to use in the further utilization areas for 3D MBA, such as FEM modeling and 2D drawing generation, etc., that are explained in Chap 3.

In order to set StructureType correctly from ocx:functionType, a tool for mapping is provided. After the initial check on OCX file to be imported, all ocx:functionTypes in the file are sorted out to prepare

the initial mapping based on NAPA's own rule. Then, the end user can check and modify the mapped StructureType when it needs to do. In addition, the model can be adaptively imported with the filter of ocx:functionType, in other words, only the selected ocx:functionTypes can be imported or not imported. For example, when the function type of SHELL is excluded from the structure type mapping that can be seen in Fig.2, then even though the ship model in OCX file contains the shell plates, 3D structural model without shell plates can be imported accordingly.

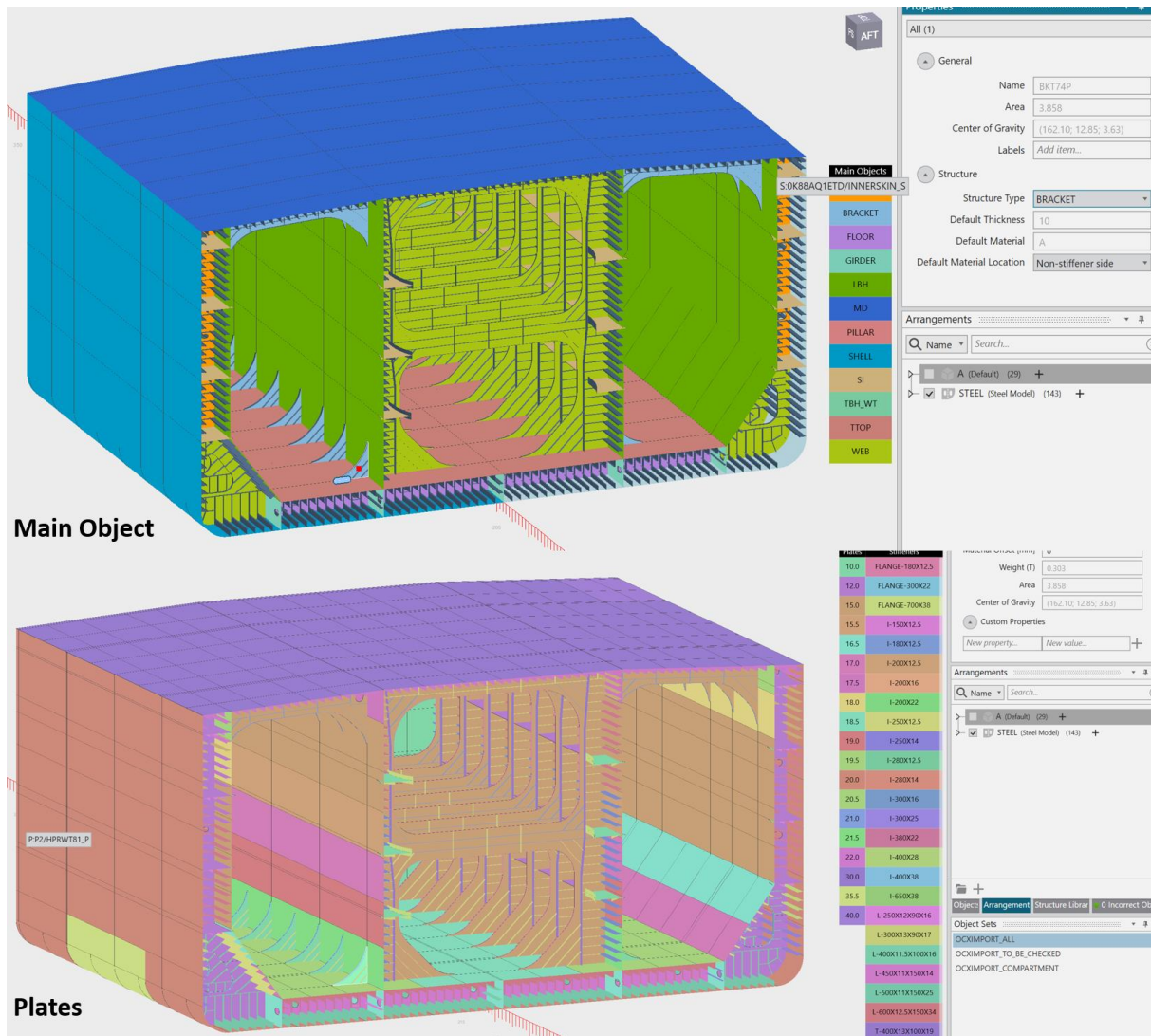


Fig.1: Structure model creation with OCX file in NAPA Designer

A name in ocx:Panel is to be used as the unique name or ID of MainObject, so that the additional check of the uniqueness and the naming rule compliance is done before the creation of MainObject. But this name element in OCX schema is an optional data, since in some CAD systems, a name for the object is not mandatory or supported. In this case, ID in ocx:Panel is to be used instead when there is no name in ocx:Panel.

As StructureType in NAPA is essential for its own characters of MainObject, when there is ocx:Panel without ocx:functionType, in spite of its necessity to be defined according to OCX schema, this panel cannot be created as MainObject. So, when this happens, default value of StructureType is to be applied and the corresponding error logs are written in the import log file for the further check. In similar, if the thickness of plates or the material are missing in the file, then the pre-set values for each StructureType in NAPA are to be used instead to establish 3D model even there exists the defects in OCX file itself.

For various use cases, NAPA offers the adaptive import for each OCX structural object types, i.e., panel, plate, opening/hole, stiffener, bracket, and pillar, and by the name of panels if the panels with the specified names are indicated separately. For better understanding before the import of OCX file, when the OCX file is loaded, then NAPA quickly checks the file and shows which structural object types of OCX exist in the file, and how many objects per each structural object types exist as shown in Fig.3.

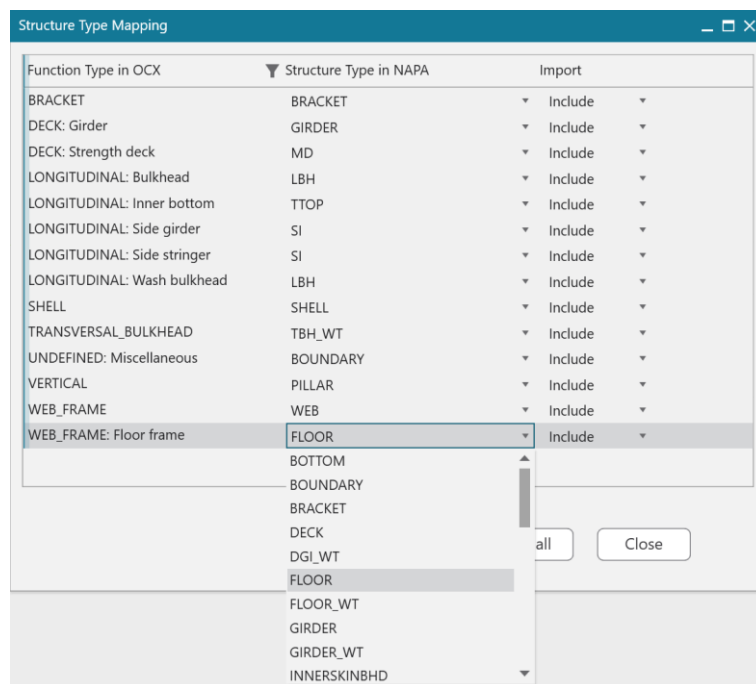


Fig.2: Structure type mapping to *ocx:functionType*

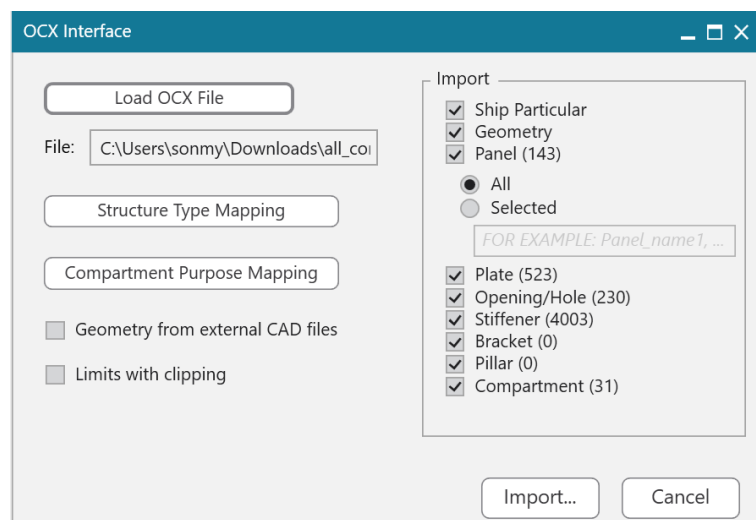


Fig.3: OCX file pre-check before the import

The structural objects as parts of *ocx:Panel* are plates, openings or holes, stiffeners, brackets, and pillars. In order to create these structural objects correctly, it needs to create the mapping tables of *ocx:ClassCatalogue*, in advance. There are three catalogues available from *ocx:ClassCatalogue*, that are *ocx:MaterialCatalogue*, *ocx:XSectionCatalogue*, and *ocx:HoleShapeCatalogue*. In general, OCX deals with a ship, and the most ships being built nowadays are made with steel material, so that most of *ocx:MaterialCatalogue* can be thought to be the steels with the different grades. Thus, it is efficient to check the material name and its grade to match with the default available materials in NAPA steel library first. If there are no matches, then it tries to find the existing material based on the material

properties such as Young's modulus, and Poisson ratio, and yield stress. If there is no material found from NAPA material library with this additional check, then it creates the new material and adds it to the material library of the project of NAPA, to be utilized on plates, stiffeners, brackets, and pillars while importing.

From `ocx:XSectionCatalogue`, a set of stiffener profiles can be created. There are various types of stiffener profiles available in the OCX schema, and NAPA makes the initial mapping based on each type of stiffener profile and adds them to the NAPA Stiffener library. And this library is used while importing stiffeners, pillars, and the stiffeners on brackets.

For the last of catalogues, there is `ocx:HoleShapeCatalogue`. Since in a ship structure, there are lots of standardized opening/hole which are used for the purpose of an access or piping, so that these similar types of openings/holes are defined by types and its parameters. NAPA has the same concept to support this parameters-based opening/holes modeling as Opening library. Thus, these type-parameters openings are converted to the profile in Opening library, and 3D contour openings are being utilized as the curve with the name, and it is applied to the surface by a deduction operation.

After the creation of `MainObject`, when there exist plates on it, then the seams are imported using `ocx:SplitBy` first. After the completion of the seam arrangement, there would be the plates generated by NAPA which form physically separated elements. So, it is efficient to utilize `ocx:CenterOfGravity` which is mandatory element in `ocx:Plate` to find the corresponding plate element to assign plate thickness and material. Thus, in OCX import stage of the plate, any other geometrical definitions are not used (`ocx:OuterContour`, `ocx:LimitedBy`), unless if there is no `ocx:CenterOfGravity` in `ocx:Plate`, even though this means OCX file has a defect against OCX schema. In this case, from the closed contour curve of `ocx:OuterContour`, the center of gravity is calculated.

2.2. Compartment model

NAPA Arrangement model consists of a set of Compartments. A basis of Compartment is Room which is a set of limits or surfaces that can form a closed volume. In addition to this geometry representation, it needs to be defined with Purpose which is a similar type with `ocx:compartment Purpose` in OCX schema. And another key aspect of Compartment is that it needs to be included in Compartment Arrangement, which is a hierarchical model tree for the compartment model of a ship. Fig.4 demonstrates the result of the compartment model created using OCX import.

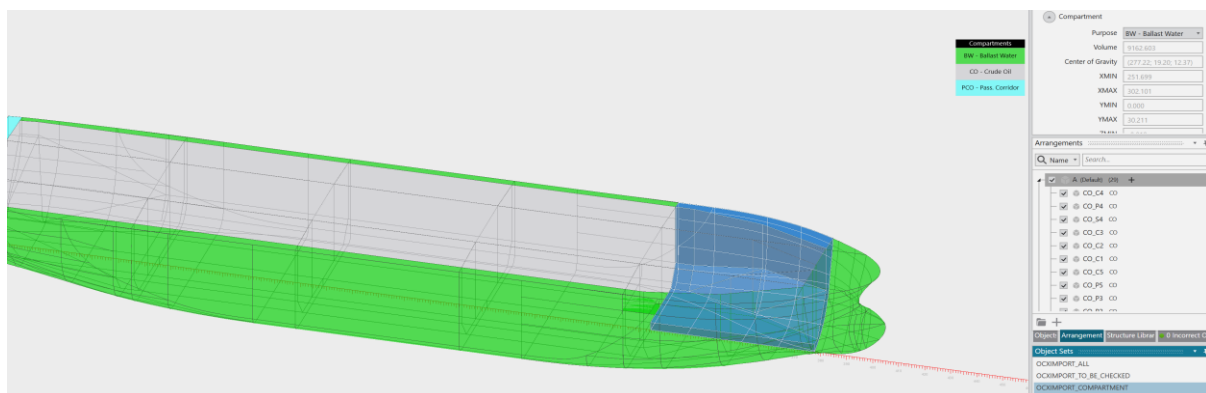


Fig.4: Compartment model creation with OCX file in NAPA Designer

In OCX schema, `ocx:Compartment` consists of a set of `ocx:CompartmentFaces`, which contain the geometric definition of a surface and its boundary curve. Thus, to create a Room, the geometric tool to define a volume from a set of surfaces is required. And compared to a surface creation, this volume creation would be more sensitive or fragile, highly dependent on the accuracies in each boundary of surfaces to fit each other without gaps. In the example of the highlighted Compartment in Fig.4, it is being converted from `ocx:Compartment` with 52 `ocx:CompartmentFaces`.

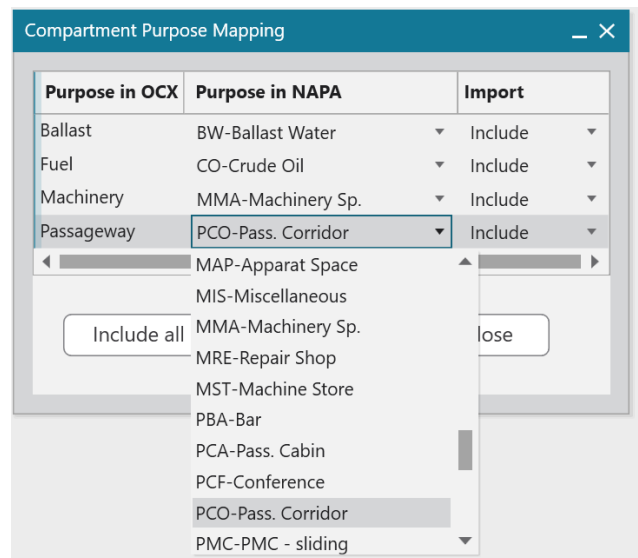


Fig.5: Compartment purpose mapping with ocx:compartmentPurpose

Similar to the structure model, once a Room is created successfully, then ocx:compartmentPurpose is to be converted to Purpose in NAPA in order to be Compartment. The purpose mapping tool is provided with initial mapping based on NAPA's own rule, and also it is possible to import or not import adaptively by ocx:compartmentPurpose as shown in Fig.5.

2.3. Reference system and general information

From OCX file, there exist also useful data apart from 3D model definition itself, that are the frame systems, the principal dimensions. First, the frame system can be found in ocx:CoordinateSystem. There are ocx:FrameTables with ocx:XRefPlanes, ocx:YRefPlanes, and ocx:ZRefPlanes but these are used as reference plane for ocx:UnboundedGeometry or ocx:LimitedBy instead of a frame system itself in some CAD systems, so that it is inaccurate to use this ocx:XRefPlanes to define the frame system. In other words, if every frames are to be set in ocx:XRefPlanes, then there are over hundreds of ocx:XRefPlanes, and these are quite inefficient way to define the frame system. Thus, from OCX schema v2.8.6, there exists ocx:VesselGrid which consists of ocx:XGrid, ocx:YGrid, and ocx:ZGrid. And each grid has the spacing group which define grid number and its position and the spacing. So, from this ocx:VesselGrid, Frame Systems can be imported in NAPA from OCX.

The other useful data in general information is ocx:ClassificationData. There are ocx:PrincialParticulars which contains the main dimensions of a ship, the service speed of a ship, and the block coefficient. As this xml file is ocx:ClassificationData, so that there also exists the basic classification information including the newbuilding classification society and identification data of the ship. These values are transferred to the corresponding items in Reference System in NAPA.

In addition, if there are available data in ocx:BuilderInformation regarding the yard, designer, owner, and the year of build, or in ocx:Header regarding to the name of vessel, author and the organization of the project, and the originating system of the model, and its version, and the file creation time, then these data also can be inputs for Background and Identification, or Various in Reference System in NAPA. Because there are no differences between user-created project model or OCX-imported project model, the end user can refer to Reference System to understand that the model has been built by OCX import or by manually modeling.

2.4. Model validation

As the import of OCX file means re-creation of the 3D model from data and definitions, the result of the imported geometries needs to be validated with the key values from the OCX file. In a global

level, upon the load of OCX file, NAPA Designer checks if OCX schema version of the file is met with the supported versions (which is v2.8.5 or above), checks if there are any critical errors on the files before the import.

While importing to create the NAPA structure model, any errors on geometries are to be checked with a higher priority, and to be logged along with any possible reasons for that issue. Then, any missing structure metadata such as a function type, a material, a plate thickness, or stiffener profile is checked as well.

In addition to this basic-level check while OCX importing, there are key values that could be utilized to validate the result of the imported model. For the structural objects, the center of gravity, the weight from OCX file can be used to compare with those computed from the imported model in NAPA. In addition, the number of plates, the number of stiffeners, and the length of stiffeners also can be checked as criteria that the model is created correctly according to OCX file. For the compartment, the center of gravity and the volume are to be checked as the model validation. In this tool, 1% of tolerance is allowable for the length, the weight, and the volume, while the distance tolerance between the center of gravity is 5 cm. As the main target of 3D model is initial design phase, so that plates and stiffener tend to be not designed precisely, but roughly so that their sizes are relatively long compared to the actual plates/stiffeners that are being designed in the detail/production phase. From this background and assumption, the validation tolerances have been determined.

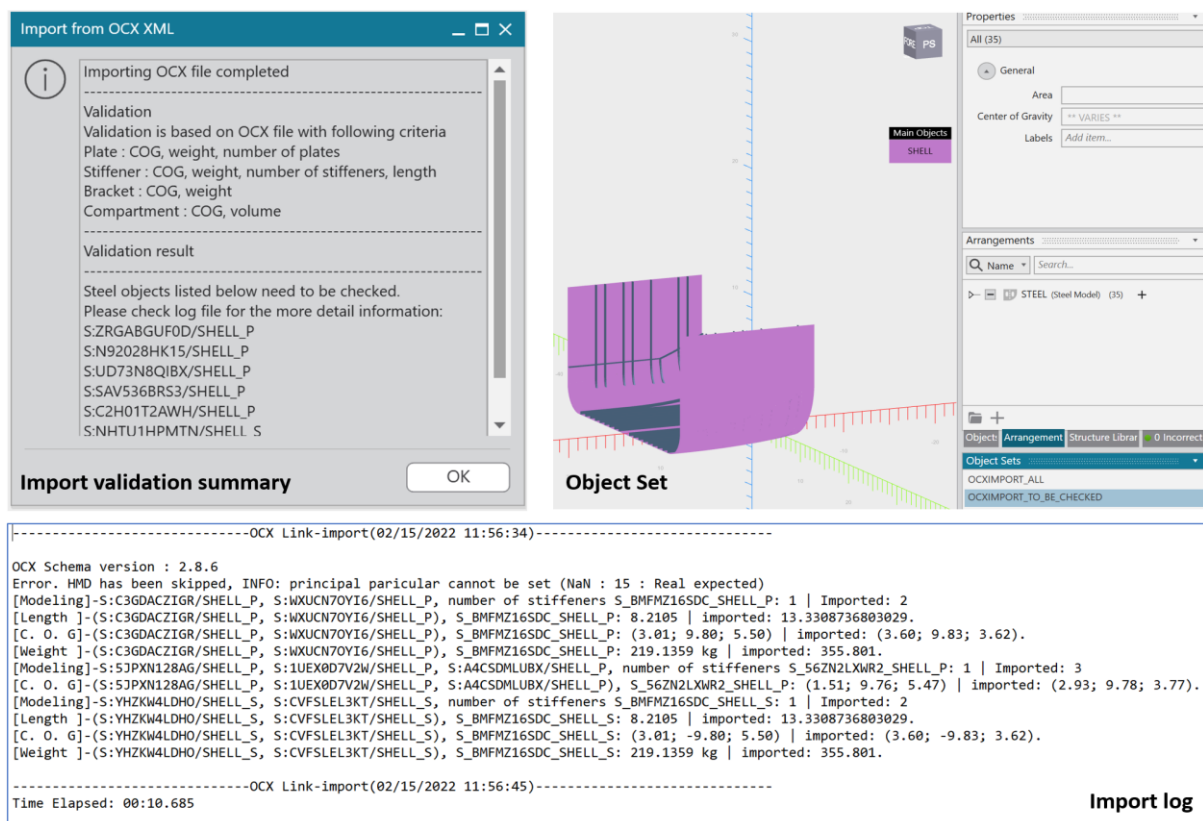


Fig.6: Model validation after OCX import

If there are the structural objects that are filtered out by above mentioned validation criteria, then these objects are grouped as Object Sets to be displayed only without any other successful objects together, which gives the instant and clear view to identify the issue, and the names or IDs of the objects are shown in the pop-up dialog. In addition to this, the detailed information why those objects are filtered out, and by which criteria, and how big the difference between OCX file and the imported are written in the log file. These are shown in Fig.6.

3. Utilization of OCX-based 3D model

3.1. Rule scantling

NAPA supports the interfaces to the most of major classification societies' rule calculation software, such as ABS Eagle UDM, BV Mars, ClassNK PrimeShip-Hull, DNV Nauticus Hull, DNV Poseidon (GL), KR SeaTrust-HullScan, and LR DIME & RulesCalc, *HULKKONEN et al. (2017)*, as shown in Fig.7. Those interfaces are the file-based approach that NAPA creates 2D cross-section model or 3D model in a file as an input for those software packages. All these interfaces to the rule check software packages can be applied to 3D model created by OCX file in NAPA as well.

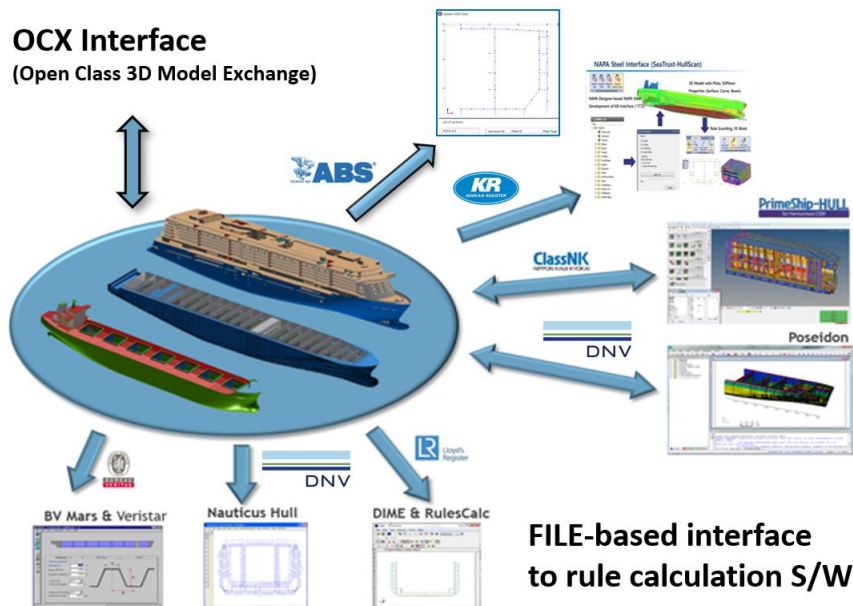


Fig.7: Interfaces to rule check software packages from NAPA

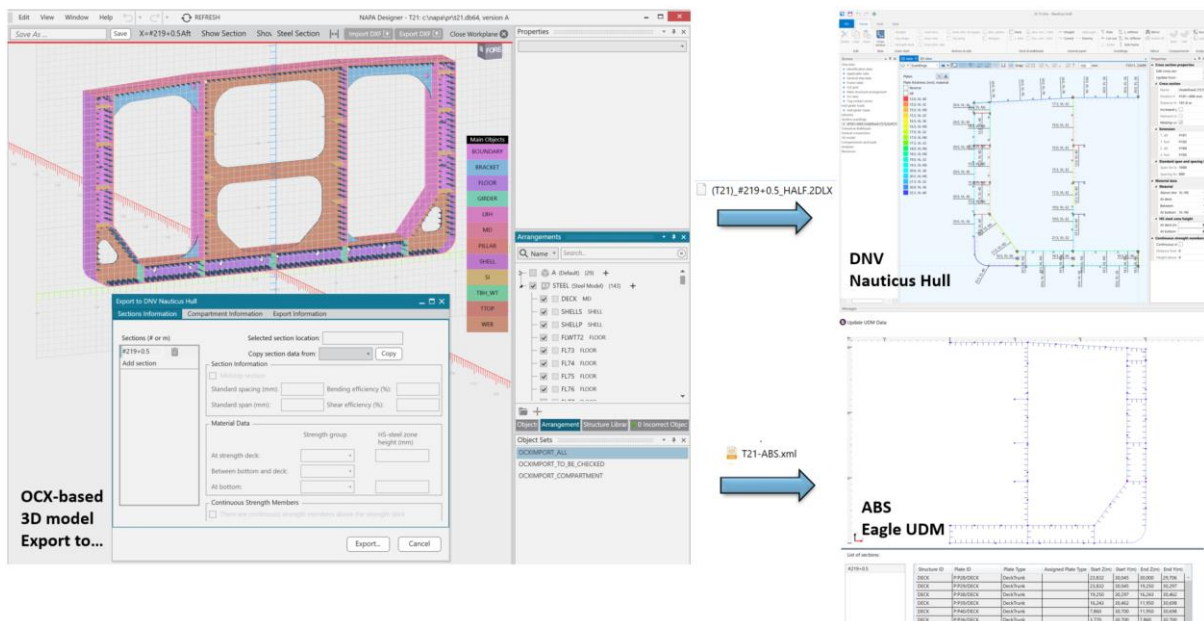


Fig.8: Automatic generation of the cross-sections in rule check packages from OCX-based 3D model

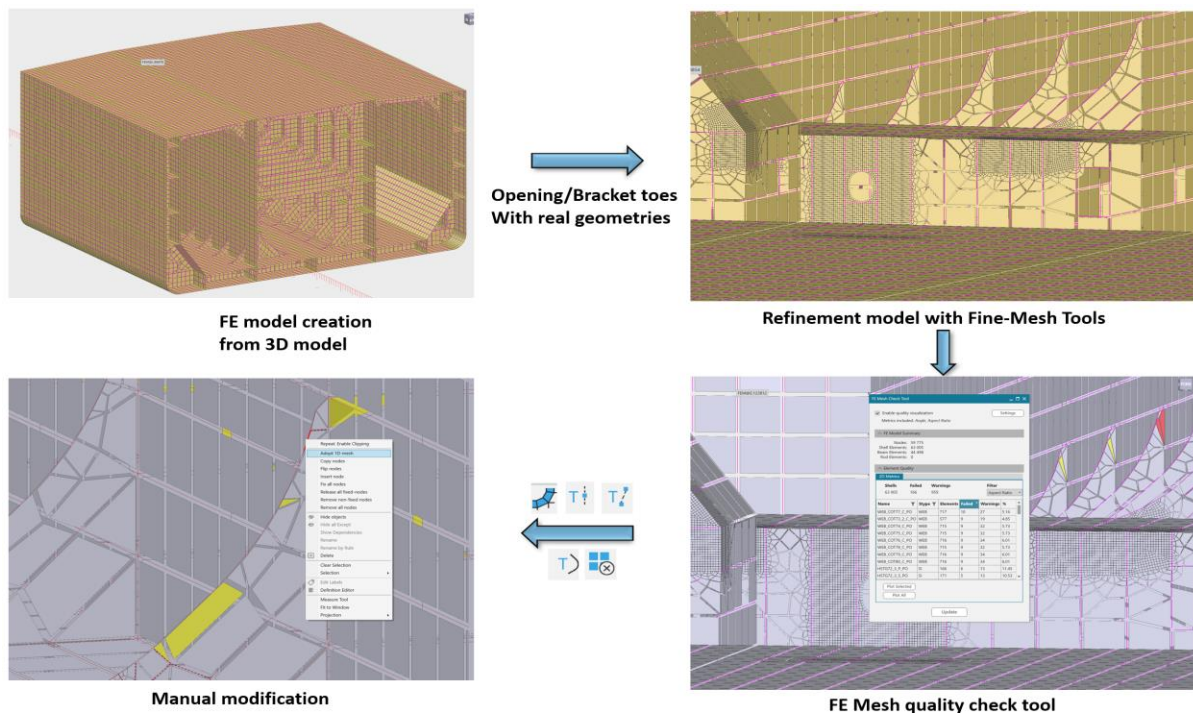
For example, Fig.8 shows how the interfaces to the different classification societies' rule calculation software work with the same 3D model which has been created by OCX file. In this example, 2dlx file for DNV Nauticus Hull is created and imported in Section Scantlings of the project, and from the

color code, plate thickness and materials are seen clearly to be transferred. Likewise, xml file for ABS Eagle UDM is created within the same project, and this file is imported to ABS UDM software to check 2D cross-section model. In real world, there would be the case while the structural design of a ship remains still, but only the newbuilding classification society can be changed, which means the applicable rule is changed so that new model should be prepared to run the calculation with the corresponding rule calculation software. In this scenario, a single OCX file can be translated to the various rule calculation input files through NAPA Designer.

In recent years, lots of efforts have been made by the classification societies such as ClassNK and KR to improve on the interfaces between NAPA Designer and the rule scantling software by accessing NAPA model directly with NAPA application programming interface (API), which eliminates the intermediate file creation. As the OCX-based 3D model in NAPA works in the same way as the 3D model directly created by modeling process in NAPA it can be utilized by these advanced direct interfaces as well. Thus it can enhance the accuracy, reduce the loss between data transfer by exporting/importing the intermediate file, and save time on additional manual input of missing data which are not covered within the interface file scope, and enable to update/modify the model after rule calculation also through API (result back).

3.2. Direct strength analysis

Finite element (FE) model preparation with plates as shell elements, and stiffeners as either line elements (beam/rod) or shell elements is one of common engineering work during the design stage of a ship. Using this FE model, finite element analysis is performed as direction strength analysis of a ship hull structure for the global and the local assessment. 3D model created using OCX file as described in Section 2, can be directly used to be converted to FE model instantly with various idealization options. The upper left-hand side of Fig.9 shows the coarse mesh model created by default meshing option with the mesh size of 800 mm, with a *MainObect* as a shell element, and a stiffener as s beam element, and the omit of an opening if the size of it is over 30% of the given mesh size.



by changing mesh size on the local area, adding guidance line to get grid-like meshes, copying existing mesh arrangement to other area, and re-arrangement of the free-edge nodes by adopting nodes arrange from longitudinal nodes. These series of mesh modifications are followed by mesh quality check tool as shown in Fig.9.

Not only coarse mesh model, but also refinement model for the local assessment can be prepared by fine-mesh tools in NAPA Designer as shown in the upper right-hand side of Fig.9. When FE model with the coarse mesh is created with idealization option for example, an opening to be omitted, can be updated to use the real geometries on the target area of the local assessment. Then fine mesh, for example, with mesh size of 50 mm can be generated instantly on the area on top of the existing coarse mesh model inheriting all elements properties of plates/stiffeners. The utilization of the real geometries in the details of the hot spot area for the local analysis by adaptive changes on the selected structural objects is one of strength in efficient FE model creation by NAPA Designer.

Fig.10: Automatic FE model grouping based on OCX-based compartment model

written in Patran session file, or as a part of Ansys CDB and DNV SESAM GeniE file. Fig.10 demonstrates the different grouping results of FE model by a compartment, which are generated in Stanford polygon file (PLY) format separately per each compartment group to visualize how this grouping works.

3.3. 3D model review and information sharing

The 3D model in NAPA generated from the OCX file can be reviewed in NAPA Viewer web application. It offers easy access to the model through a web browser without need for installing any separate application on the end user's device. The 3D model with its attribute data as present in the OCX file is available for simultaneous review by multiple users, which may represent any stakeholder the host administrator has granted access for. The application accurately displays the model while restricting access to sensitive information, such as geometry, as the file itself is not shared with the end users. A commenting interface enables assigning user specific comments to the model which can reference to objects in the model and be indicated in graphics by 3D markers. In addition to the 3D view of the model NAPA Viewer offers a possibility to generate 2D sections of the model. In the 2D sections the model is represented as in 2D drawings for efficient and accurate review of a particular section. In Fig.11, a VLCC (Very Large Crude-oil Carrier) cargo hold model generated from the OCX file is shown in NAPA Viewer.

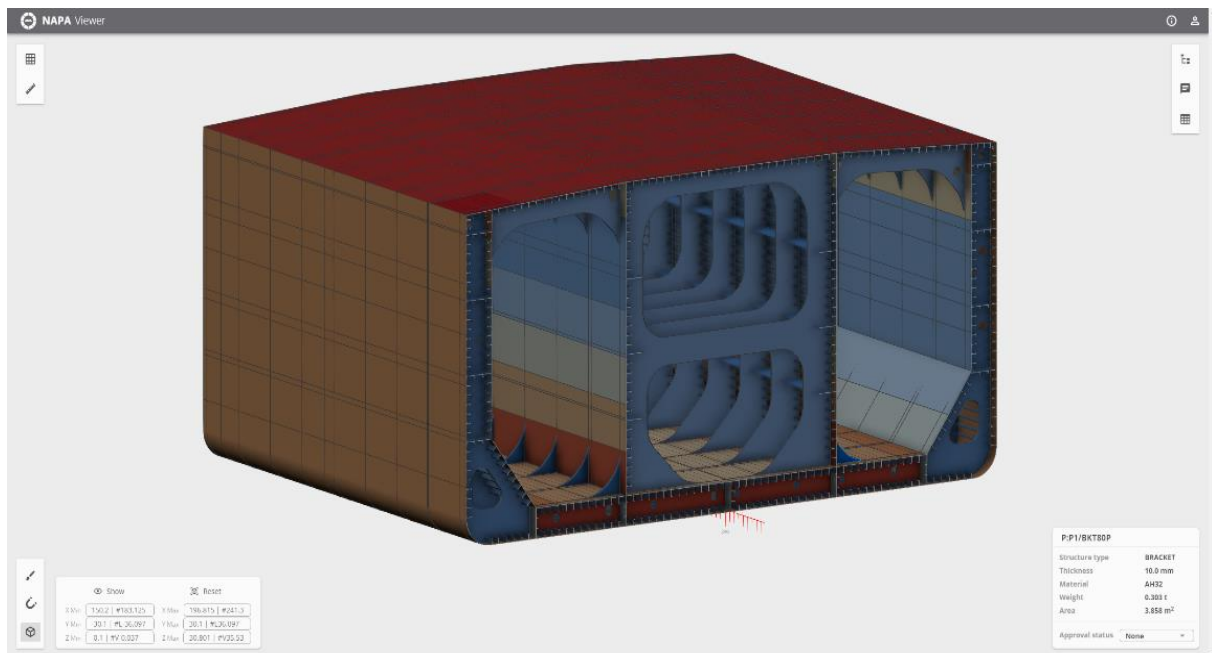


Fig.11: 3D Model generated from OCX available for model review in NAPA Viewer

3.4. 2D Drawing generation

Even if one of the primary targets in 3D MBA is to reduce the need for classic 2D drawings they will have a key role in the ship design process at least in near future. To make the transition to 3D MBA easier classification drawings from the 3D model originating from OCX model can be created when needed with NAPA Drafting application. It has tools for maintaining and updating the drawings when the design evolves staying all the time connected to the 3D model. It is based on Autodesk's AutoCAD technology covering all the needs of 2D Drafting and NAPA technology covering the information extracted and updated from the 3D model. Annotation tools which automatically fetch attribute data from the model are available for completing the drawing. A section drawing in NAPA Drafting from a 3D model generated from the imported OCX file is shown in Fig.12.

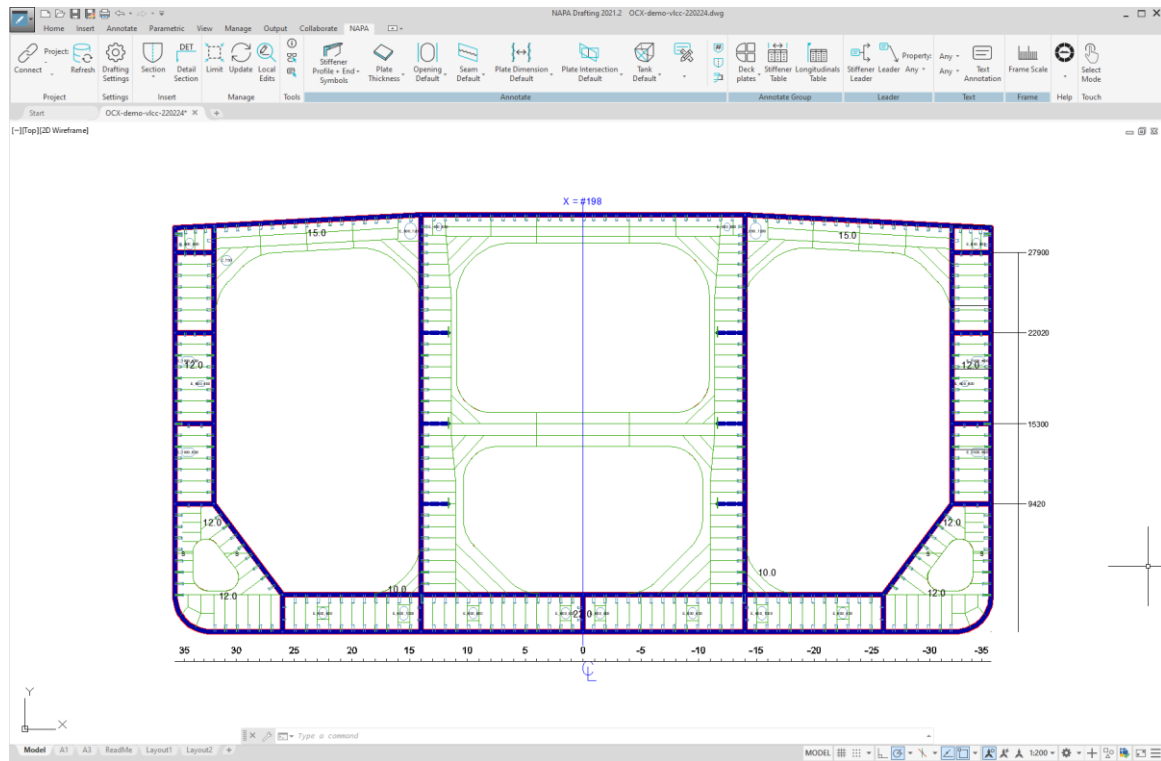


Fig.12: 2D Drawing generated from the OCX based model in NAPA Drafting

3.5. 3D model translator

3D model created by OCX file in NAPA can be translated to the other CAD formats such as IGES, JT, STEP, and so on, and in publish formats such as 3D PDF, and HTML. Fig.13 demonstrates two examples of the model export in IGES and HTML from the OCX-based 3D model. In IGES file, NAPA exports not only geometries but also hierarchical model tree with structure objects' names, with the colors as same as they are visualized in NAPA Designer at the time of CAD export. On the other hand, HTML, which is one of publish format that can be visualized in the modern internet web browser such as Internet Explorer, Chrome, etc., has much more meta data than CAD formats. As shown in the right-hand side of Fig.13, the stiffener profile, the stiffener name, the stiffener ID, the structural object type, and the stiffener material can be found from the property window. NAPA viewer offers an excellent tool for 3D MBA without any installation of CAD software, but HTML or 3D PDF can be good alternative to share the model with the essential metadata and hierarchical tree with the stakeholders around a ship not only during the ship design phase, but also during the operation and the maintenance period.

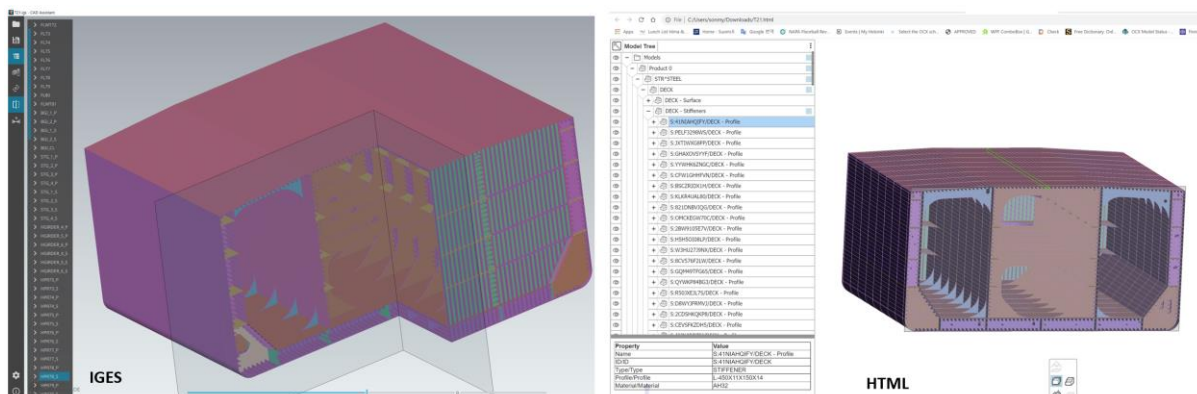


Fig.13: 3D model translated to other CAD formats from OCX

Another possible use case for the CAD translation would be the extraction of geometries from 3D model into the well-known CAD formats that would be supported by other design/engineer software packages which do not support OCX interface yet, or do not have even any plan to support OCX format.

In addition to these CAD formats, NAPA supports the interface to some of the ship production design CAD solutions such as AVEVA Marine (AM), CADMATIC to use the 3D model in NAPA to be utilized in the downstream design process. An existing OCX model from a downstream production system for example of a sister vessel could be imported in OCX format to speed up the early 3D modelling work in alternative. Afterwards, the updated model can be ready in OCX format from NAPA for the exchange with other systems. Also, NAPA structural model can be exported in the form of a solid representation to have a plate with thickness to any mechanical CAD systems capable of importing STEP file, and this enables to support the outfitting design in the early stage.

3.6. Advanced application developed by users' customization

NAPA Designer supports C# scripting and NOM (Napa Object Model) API to the end users to support the customization. Using this modern development environment, users can develop the series of script to run automated modeling or additional operations which are not yet supported by NAPA Designer or can create the plugin application which launches together when NAPA Designer starts. As an example, there is the *FEMCtrl* plugin that can import FE model of BDF format to define the loads and boundary conditions in NAPA, to run FEA solver and to post the results in NAPA modeling workspace. As another example, there is the script that can import back the result of the rule scantling from DNV Nauticus Hull to update the scantling results to 3D model. To achieve the design optimization, there have been joint research between NAPA, shipyards, and classification societies, *Shimakawa et al. (2019)*, *Hulkkonen et al. (2019)*. All these customized scripts or plugin applications can also be applied to the model created from an OCX file.

4. Utilization of OCX for direct interface to rule check software

DNV has developed the automated batch execution using the script file and OCX file to run the rule calculation for local assessment for the cross-section of a ship by Nauticus Hull, and to write the corresponding results in the xml file. By adopting this method, the design iteration during the scantling is possible without leaving NAPA Designer, by executing Nauticus Hull in background to get the calculation result until it satisfies the rule requirement. Fig.14 shows the difference between the process of the rule scantling iteration using file-based interface which has been explained in Sub-chapter 3.2, and the design iteration that is possible from the direct interface using OCX.

When OCX file is prepared along with 3D model itself, the position of the cross-section and the relevant data are input by the end user. This section definitions and data are made into Javascript file with commands using Nauticus Hull API. By executing Nauticus Hull from NAPA Designer with argument to execute the Javascript file upon the start of the program, a series of the automated processes such as importing OCX file to create 3D model inside of Nauticus Hull, and creating the cross-section model by the definition in the Javascript and writing the local assessment results after rule calculations, terminating Nauticus Hull upon the successful execution, and parsing the result xml file to make the results visualized in form of a table in NAPA Designer, are performed. With this Mid-cargo hold model of VLCC, it takes around 1.5 minutes for all above-mentioned processes.

The local rule calculation results can be shown in the grid view for plates and stiffeners as shown in the lower left-handed side of Fig.14. This grid consists of the same column names and values as shown in DNV Nauticus Hull result tables. The table support filtering from each column headers, and there are two columns (Material, Thickness) of the plate results, and another two columns (Material, Profile) of the stiffener results that can be changeable by the end user. By checking the structural objects that fails to meet the rule requirement, the design parameters such as plate thickness, material, stiffener profile can be re-designed. Whenever the model is updated then by re-running calculation

command, the series of processes is repeated to update the result tables. This rule scantling iteration can be done until all structural objects satisfy the rule requirement, then 3D model can be updated immediately with the updated properties of plates and stiffeners.

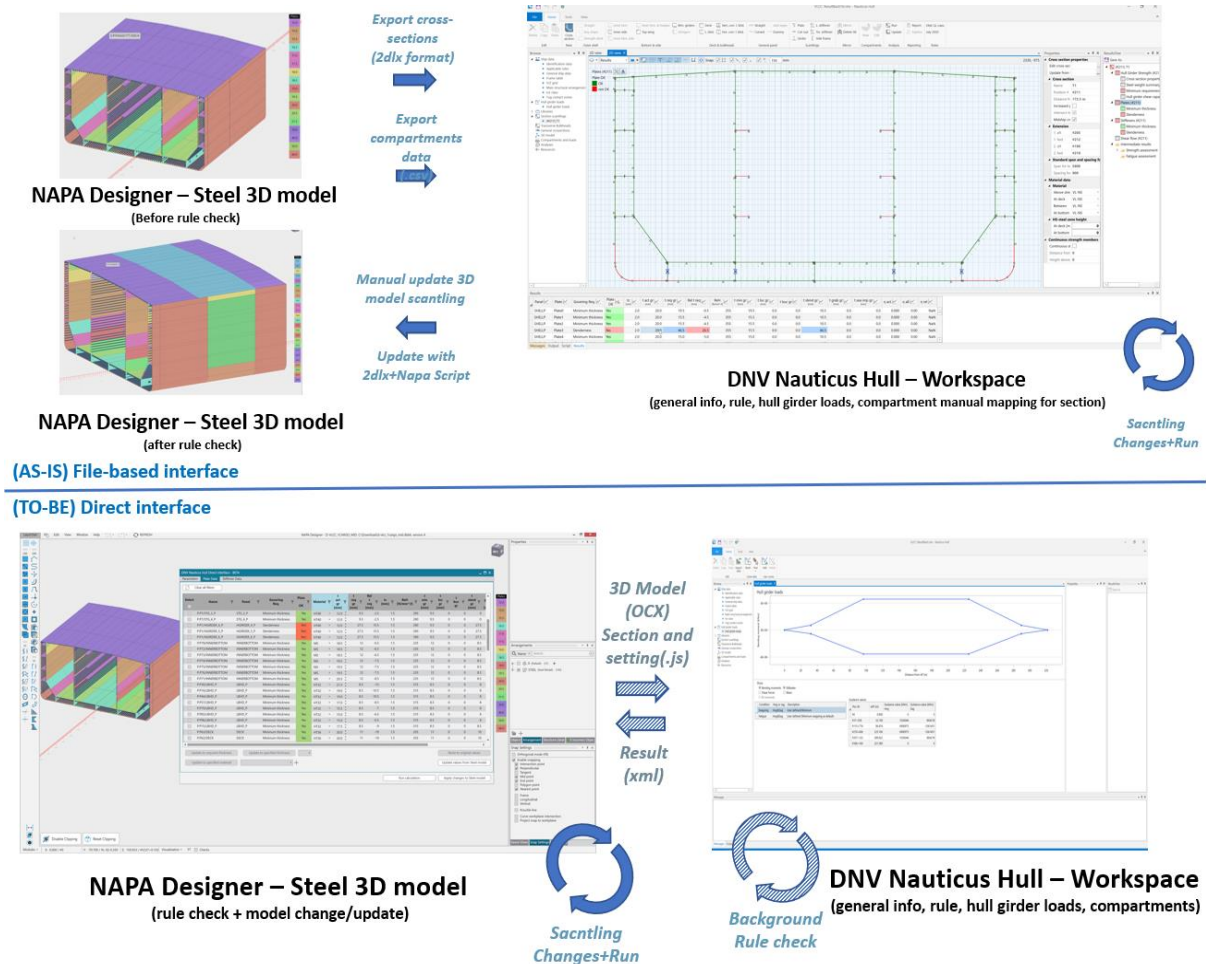


Fig.14: Direct interface between NAPA Designer and DNV Nauticus Hull using OCX

During this direct interface between two systems, OCX takes a part of transferring 3D model. Rather than exporting OCX file after the model change, but by modifying the only changed properties on the structural objects in OCX file directly, the time to export and import OCX file can be shortened to make the design process more feasible and leaner. However, when there are the physical changes of the model such as changing the geometries, inserting new seams, or making new plates arrangement, or changing the spacing of the longitudinal stiffeners, then OCX file should be prepared again by OCX interface to get the corresponding result appropriately.

5. Conclusion and future works

OCX format has been researched, introduced and modified for more than five years. Now more and more CAD vendors, classification societies, shipyards, and design companies have interest in OCX and take actions to benefit from it, and thus take a step forward for 3D MBA. NAPA has been closely cooperating with shipyards, and classification societies over 3D MBA using OCX and has both conducted and is still participating in several joint develop projects to make OCX interface more feasible and to be utilized on a variety of applicable areas over the design of a ship. The interface of OCX is still in development and test phase, so more OCX files from the real project generated from various CAD vendors need to be tested to secure the quality of 3D model while eliminating possible incompatibilities on OCX interface.

The changes from the conventional paper/drawing-based approval to 3D MBA is still challenging even by using OCX interface, since it requires not only CAD system, and the ship model from 2D to 3D, but also to change the design process in shipyards or design companies, also to change the approval process in the classification societies at the same time. Thus, NAPA will closely discuss the newly found issues on the way to apply 3D MBA using OCX and keep the development efforts continuously for more accurate transferring of 3D model, widening the use cases and applicable areas from the single 3D model source to improve the productivity in the design work, especially in the early design phases.

As future tasks, the commenting interface will be developed jointly with NAPA and DNV, to exchange formal commenting of the model review during 3D MBA between NAPA Viewer/NAPA Designer and DNV SESAM Insight, which is main 3D model viewer for OCX based models on the web-based technology. In addition, the research result of APPROVE+ would be followed to be introduced as extension of OCX interface in NAPA, including FE loading and boundary condition definition with 3D model, and a load line, tonnage and fire safety assessment with OCX.

References

ASTRUP, O.C. (2019), *APPROVED redraws requirements for class verification*, The Naval Architect, May

ASTRUP, O.C. (2020), *OCX-Open Class 3D Exchange. A digital specification of the hull structure for the Classification of Ships*, The Norwegian Research Council, Report No.: 2019-1093

HULKKONEN, T.; SHIN, H.C.; YI, N.H.; JANG, D.H., JANG, T.K. (2017), *Enabling a paradigm shift in ship structural design with a 3D approach*, Int. Conf. Computer Applications in Shipbuilding (ICCAS), Singapore

HULKKONEN, T.; MANDERBACKA, T.; SUGIMOTO, K. (2019), *Digital twin for monitoring remaining fatigue life of critical hull structures*, 18th COMPIT, Tullamore, pp.415-427

MOSER, U.; ASTRUP, O.C. (2018), *Approaching Design Review by Classification Society based on Digital Information Derived from the Customer's Design Models*, 17th COMPIT Conf., Pavone, pp.116-131

SHIMAKAWA, Y.; MIURA, Y.; MASUI, T.; HAYASHI T.; SAKAGAMI M. (2019), *Process integration of structural design promoted by 3d model based approval*, Int. Conf. Computer Applications in Shipbuilding (ICCAS), Netherlands

Enhancing Offshore Service Vessel Concept Design by Involving Seakeeping - Developing a Framework to Efficiently Design High-Performance Offshore Service Vessel Concepts

Philip Bronkhorst, BW Offshore, Oslo/Norway, philip.bronkhorst@bwoffshore.com
Roy de Winter, C-Job Naval Architects, Hoofddorp/The Netherlands, r.dewinter@c-job.com
Thijs Velner, C-Job Naval Architects, Rotterdam/The Netherlands, t.velner@c-job.com
Austin A. Kana, Delft University of Technology, Delft, The Netherlands, a.a.kana@tudelft.nl

Abstract

This paper describes a design framework to efficiently design high-performing Offshore Service Vessel (OSV) concept designs incorporating seakeeping. The proposed framework optimizes the main particulars and length of different hull sections to maximize performance for key performance indicators (KPIs), including ship resistance, lightship weight, and seakeeping. For this work, seakeeping performance is measured by the Operability Robustness Index (ORI), which considers the area of operation, motion limits, and motion characteristics. An initial stability constraint ensures feasibility. The framework generates a Pareto-frontier showing the trade-offs between KPIs and the corresponding variable combinations. A case study is performed to validate the framework. Comparing the Pareto-optimal solutions with the existing baseline concept design, the ORI can be increased up to 3.6%, the lightship weight decreased by 21.1% and the ship resistance decreased by 13.0%.

1. Introduction

The growth in the offshore wind industry has increased demand for offshore service vessels (OSVs), *Loos et al. (2020)*. These vessels often operate in harsh conditions, and many feature motion-compensated equipment. Consequently, their performance is heavily dependent on their seakeeping characteristics. Conventional ship design processes fail to effectively consider seakeeping early in the design process. This leads to the potential of suboptimal vessel designs. To design high-performing OSVs efficiently, there is a need for ship design methods that consider seakeeping effectively early in the design process. In recent years, C-Job has been developing the Accelerated Concept Design methodology (ACD) *De Winter et al. (2020)*. In the ACD framework, efficient global optimization algorithms are linked to a parametric modeling environment. The ACD framework is implemented in the NAPA software (Naval Architectural Package). Utilizing the NAPA environment and the ACD optimization philosophy, a framework is developed to effectively consider the seakeeping behavior as an optimization objective amongst other relevant, mostly conflicting design objectives such as costs, weights, and resistance. This design methodology is also considered a ‘holistic’ design method.

2. Gap Analysis

2.1. The conventional ship design process

Ship design is a complex multifaceted problem, requiring the integration of many engineering disciplines. The end goal is to design a ship that can carry out its designated task, doing so in a cost-efficient way. Many design trade-offs exist, and compromises are made throughout the design process. ‘A successful ship design is the result of good and close cooperation between the designer, the customer, the yard, and the equipment suppliers’, *Vossen et al. (2013)*. In the last 70 years, many new developments have been introduced by academia and industry. These range from developing certain ship design processes, such as the design spiral, to more advanced design and calculation methods with the onset of computer-aided design (CAD). The former, known as the ‘ship design spiral’, is an iterative process whereby the ship design progresses towards a converged solution. In theory, following the design spiral allows for an ideal converged design solution. In practice, a ship design process tends to differ, which the spiral fails to capture, *Pawling et al. (2017)*. Shortcomings of the ship design spiral, noted by numerous research, are:

- The design spiral assumes various aspects of the ship design occur sequentially. In practice, during the design process, the time pressure forces simultaneous engineering of various aspects of the ship design. Some ship aspects, such as seakeeping and ship resistance, need to be considered simultaneously as they are principally intertwined.
- The design spiral assumes the iterative process leads to an ideal solution. Each step provides input to the consecutive step. As such, the initial design direction governs each consecutive step. Hence, the spiral constrains the design space rapidly. Rather than converging to an optimal design solution, the design spiral attempts to make the initial design direction 'work'.
- The design spiral was developed during a time when computers were in an infantile phase, *Nowacki (2010)*. This is reflected by the design spiral, as it only addresses design aspects that could be deducted at the time. Since the 2000s, computers can extensively assist naval architects in the design of ships. As such, contrary to making a certain design 'work', naval architects are more than ever enabled to find optimal design solutions.

To conclude these findings, the design spiral was created to enable naval architects to develop ships effectively without the use of computers. In the 21st century, computers can assess lots of ship variables simultaneously. This can enable naval architects to create high-performing vessel designs. To do so, holistic ship design methods have been developed.

2.2. Holistic design methods

Making the correct design decisions early in the design of a vessel is highly important yet challenging. To mitigate this challenge and facilitate the design of high-performing vessels the concept design phase should consider all relevant aspects to the vessel *Papanikolaou (2010)*, *Andrews (2017)*. The development of computing technology has enabled naval architects to approach ship design in such a manner regardless of the complexity, *Nowacki (2010)*. In the last decade, much effort has been made by academia to develop such design methods in the form of ship synthesis models, *Andrews (2017)*, *Nowacki (2010)*. These methods have started to gain traction by the industry and are typically called 'holistic' design approaches. Broadly speaking, these methods optimize a set of design variables to a set of design objectives by the means of various evaluation methods by an optimization\ algorithm in an iterative process. Additionally, the subsequent design must satisfy certain constraints. This (simplified) working principle is depicted in Fig.1.

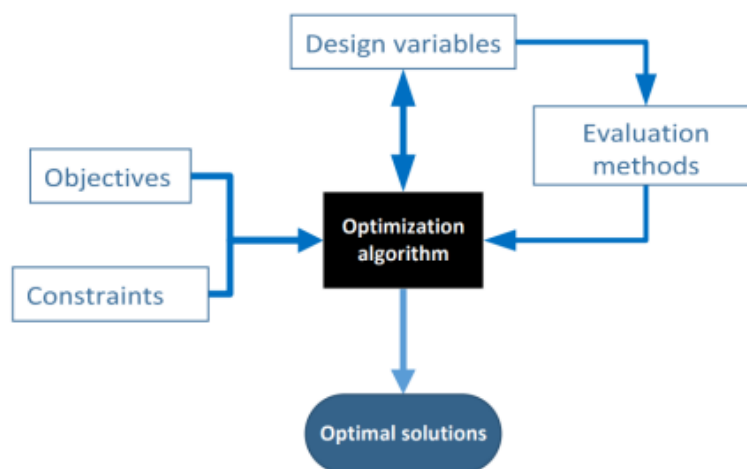


Fig.1: Holistic design method working principle

The outcome of the depicted procedure is a set of 'Pareto -optimal' solutions. These are design solutions on a Pareto- frontier, indicating the trade--offs between two or more design objectives. Naval architects can identify the exact trade--offs and determine optimal design solutions. These efforts have been extended to incorporate the estimation of various vessel aspects during the concept design phase, which

was previously only done in later design phases. C--Job's ACD method also concerns such an approach, as it can deal with conflicting objectives while dealing with physical and regulating authorities-imposed constraints, *De Winter et al. (2020)*. Thereby, the risk of having to do sub-optimal design 'work' is mitigated during contract and detail design. Ultimately, naval architects are given the freedom to choose a configuration that best suits the client's demands.

Applying the ACD method requires determining the design drivers and corresponding objectives, constraints, and parameters relevant to OSV design. Specific focus is given to parameters determined during concept design.

2.3. Design drivers

The design drivers are based on requirements for OSV types: Platform Supply Vessels (PSVs), Anchor Handling Tug Suppliers (AHTSs), Offshore Subsea Construction Vessels (OSCVs), and walk-to-work (W2W)-vessels. The design drivers and their corresponding objectives (key performance indicators), constraints parameters, and required design input are:

- Seakeeping capability - Ability to operate in harsh environments. Reflected by a measure of operability, the Operability Robustness Index (ORI), a robust indicator of seakeeping performance, *Gutch et al. (2017)*.
- Ship resistance - The ship resistance translates to power requirement and fuel costs. Hence, this objective forms a relative indication of OPEX to differentiate between different configurations, which forms an important design driver during concept design.
- Lightship weight - The lightship weight indicates the required materials and fabrication for a vessel. Thereby, the objective allows for weighing the CAPEX between different configurations.
- Vessel stability - The initial metacentric height of vessels is a measure of feasibility for vessels, as it is required to satisfy a minimum criterion.
- Vessel size - The size of the vessel may be bound by requirements to ensure suitable space for machinery, equipment, accommodation, and so forth. During concept design, the naval architect can indicate certain boundaries to the minimum or maximum values.

A framework has been developed taking into consideration the OSV design drivers. This will be discussed in the next section.

3. Method

In this section, it is described how the ACD framework has been extended such that all the OSV design drivers can be considered.

3.1. Used software

The framework has been developed using C-Job's optimization algorithm and a parametric modeling environment in the form of NAPA. NAPA provides an integrated development environment (IDE) as well as multiple software packages relevant to the design of vessels using the code 'NAPA Basic'. The framework has been developed within NAPA's IDE. Thereby, all input, output, and intermediate data are managed within the IDE. The Naval Architect is provided with a user interface (UI) for the management of all parameters and results.

3.2. Optimization algorithm

Section 2 indicated a parametric ship model linked to various evaluation methods can improve the efficiency of ship design. Critically, the parameters will need to be steered by an optimization algorithm to maximize the evaluated performance. In complex design problems, such as a ship design problem,

there is often no one ‘optimal’ design solution. Rather, the naval architect has to decide the best compromise between conflicting design requirements. For example, decreasing the beam of a ship might decrease ship resistance but increase the maximum roll motion. Thereby, the ship resistance is improved at the cost of seakeeping performance. To best decide the trade-off, the extremities of the design space must be fully explored. To do so, C-Job developed several efficient global optimization algorithms which are specifically designed to limit the number of expensive simulations while considering the entire objective and constraint space by making use of cheap surrogate functions.

The OSV design is optimized with the SAMO-COBRA algorithm, which is short for Self-Adaptive Multi-Objective Constrained Optimization by using Radial Basis Function Approximations, *De Winter et al. (2021)*. SAMO-COBRA starts with a small number of initial designs which are well spread among the parameter space. The initial designs are evaluated on the real objective and constraint functions in the NAPA software resulting in a set of parameters with their corresponding objective and constraint scores. These scores are used to train Radial Basis Functions (RBFs) which form an approximation of the true objective and constraint functions. Then in each iteration of the algorithm, SAMO-COBRA considers the entire design space by using the computationally cheap RBF approximations to search for new feasible Pareto-efficient solutions. The solution which scores the best in both objectives simultaneously while being feasible is selected for evaluation. A multi-objective performance measure that indicates if a solution is close to the Pareto front and encourages diversity among the Pareto frontier is the Hypervolume Indicator, *Riquelme (2015)*. The solution that leads to the highest predicted hypervolume is selected for evaluation on the computationally expensive functions in the NAPA software. The results from these functions are added to the set of parameter, objective, and constraint scores after which the RBFs are automatically updated. The search for new feasible Pareto-efficient solutions is continuous until the user is happy with the results or until a predefined limit like passed time or the total number of real function evaluations has been reached.

The result of the optimization algorithm is a set of incomparable evaluated solutions on the Pareto frontier which form the trade-off between the objectives. Each solution on the Pareto frontier is an optimal solution until the preferences of all stakeholders are known and a decision can be made on which vessel to take to the next design phase. An example of a classical trade-off that can often be found on the Pareto frontier of a ship design problem is Light Ship Weight versus Resistance at the design speed. A long and slender ship will have less resistance compared and a higher steel weight compared to a shorter and wider variant.

3.3. Framework

The general framework, Fig.2, can be divided into five parts, these are elaborated in the following:

1. Input parameters

This part of the framework defines the minimum input required to the optimization to assess the identified design drivers. A base hull shape that is to be transformed is defined. The base hull can be created in Rhinoceros3D or other similar software and is imported as an IGS file. Additionally, parameters defining the initial bilge keel dimensions, motion-sensitive equipment, area of operation, and loading conditions are defined:

- Bilge keel (BK) dimensions - The influence of a bilge keel is calculated according to Ikeda’s method. To do so, a base bilge keel height, moment arm, and bilge keel length, *Ikeda (2004)*. The dimensions are scaled according to the dimensions of each iteration.
- Motion sensitive systems specification - This item defines the motion limits and location of motion-sensitive equipment. The location forms the input to the calculation of motion response on the location of the equipment (local RAOs). The motion limits in the form of motions, velocities, and accelerations form input to the ORI calculation.
- Area of operation - The area of operation directly influences seakeeping performance. Parameters reflecting the area of operation and environment are defined. To calculate the ORI, ocean data such as the wave spectrum and scatter diagram are required. Both are calculated

following guidelines from *DNV (2010)*. Specifically, a Pierson-Moskowitz (PM) spectrum model and a two-parameter Weibull distribution for the scatter diagram are used. The framework automatically calculates the wave spectrums and scatter diagram based on the input parameters. Both the wave spectrums and scatter diagram provide input to the calculation of the seakeeping objective.

- **Loading condition** - To assess the vessel stability and total displacement, the operational loading condition is established. Specifically, the weight and VcG w.r.t. deck of the deck load and accommodation and the VcG of the hull and ballast w.r.t. the ship depth is defined. These parameters form input to the deadweight in the initial stability calculation and the draft for ship resistance and seakeeping performance.

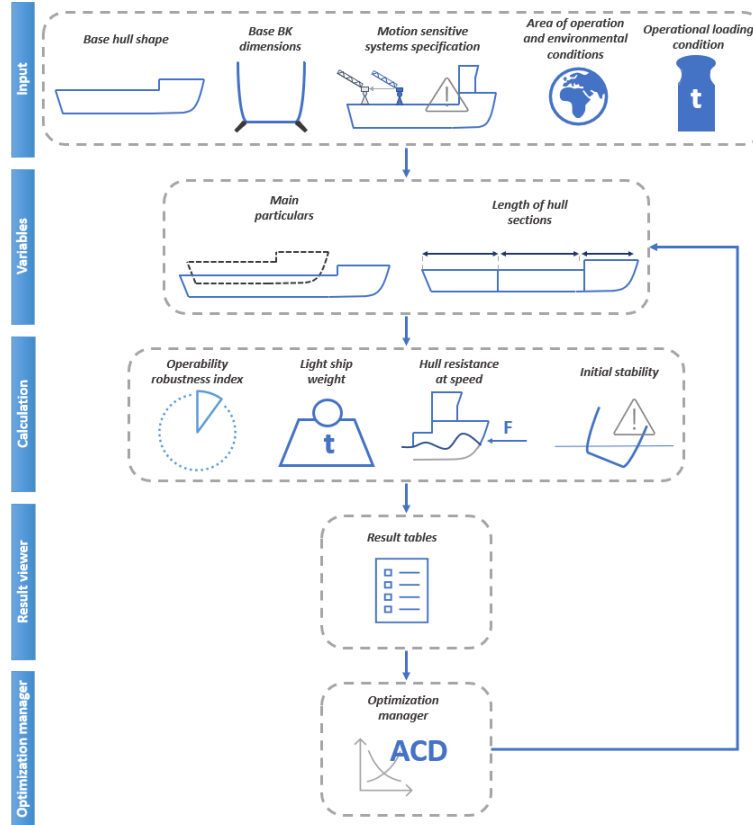


Fig.2: Framework

2. Design variables

In this section, the framework variables are defined. During an optimization run, these values are changed by the algorithm per iteration. If needed, a user can also input variables manually. Thereby, the global dimensions and front, aft, and global prismatic coefficients are varied. A description of each specific variable item is given below:

- **Main particulars** - The beam and draught are changed individually. The total length of the vessel is changed by varying the length of specific sections of the hull. Thereby, the length is defined as,

$$L_{tot} = L_{afts} + L_{mids} + L_{fws}$$

L_{afts} , L_{mids} , and L_{fws} are the aft-, mid-, and forward- section lengths of the hull. By changing these parameters, the aft-, mid-, and forward prismatic coefficients, L/B ratio, and L/D are adjusted. Alternative bow shapes, V/U-based sections, and finer hull shaping are not captured by this method.

- **Length of hull sections** - In this item, the aft-, mid-, and forward -section lengths of the hull are varied, which are summed to determine the total length of the ship. The variable length and beam form input to the hull form transformation method. The variable main particulars

form input to vessel reference dimensions, which are called upon for the ship resistance calculation and motion analysis. Based on the variables, the bilge keel moment arm and length are calculated, whereby,

$$RBILGE = \sqrt{VcB^2 + (0,5B)^2}$$

and,

$$LBILGE = L_{mids} \cdot \eta_{LBILGE}$$

$RBILGE$ is the moment arm, $LBILGE$ the length of the bilge keel. On some vessels, the bilge keel length may be slightly longer than the midship length to further increase roll damping. To account for this, a lengthening factor, $\eta_{L-bilge}$, can be defined. The variables further form input to the calculation, which is discussed in the next subsection.

3. Calculation

This part of the framework performs all necessary calculations, following the predefined objectives and constraint functions. The variables form input to a freeform deformation (FFD) method. The FFD method transforms the base hull shape to an iteration-specific hull shape. Following the hull shape transformation, the ORI, lightship weight, initial stability, and ship resistance are calculated:

- **Operability robustness index** - The operability robustness index (ORI) forms a robust criterion to measure seakeeping performance developed by *Gutch et al. (2020)*. The ORI is based on the vessel RAOs, area of operation, and motion limits. RAOs are first calculated by NAPA's seakeeping application, which contains a strip theory formulation. As an input, area of operation, iteration specific hull shape, vessel loading condition draught and GMT is used. Additionally, the radius of gyration is calculated as a factor of the length and width of the iteration. This factor is defined by the user and can be based on reference vessels. The roll damping factor is determined following Ikeda's method, which requires the length, height, and moment arm of the bilge keel. These dimensions are automatically scaled based on the iteration-specific ship dimensions. The full derivation of the ORI is given in the paper by *Gutch et al. (2020)*. To calculate the ORI requires **Error! Reference source not found.**the following calculation procedure: Based on the area of operation, as well as iteration specific hull shape, vessel loading condition draught and GMT ,

$$H_j(\omega; \beta) = \frac{s_j(\omega; \beta)}{\zeta(\omega)}$$

$H_j(\omega; \beta)$ is the RAO per DoF j , $s_j(\omega; \beta)$ the vessel response output signal which is partially dependent on wave frequency ω and wave angle β , and $\zeta(\omega)$ the wave excitation input signal. Once the RAOs have been calculated, the vessel response spectrum is calculated,

$$S_j(\omega; \beta; T_p) = |H_j(\omega; \beta)|^2 S_\zeta(\omega; T_p)$$

$S_\zeta(\omega; T_z; H_s)$ is the wave spectrum. The area enclosed by the spectrum forms a measure of variance (spread of vessel response), also known as the spectral moment m_n ,

$$m_n(n; \beta; T_z) = \int_0^\infty \omega^n \cdot S_j(\omega) \cdot d\omega$$

Depending on the value of n , the zeroth, first or second spectral moment is calculated. These represent the variance of response for motion, velocity, and acceleration, respectively. The root of this variance gives the standard deviation, σ_j ,

$$\sigma_j(n; \beta; T_z) = \sqrt{m_n(n; \beta; T_z)}$$

which forms input to the tolerable significant wave height, $H_{s, tol}(n; \beta; T_z; \sigma_{j, tol})$ for a specific peak period, together with a particular motion limit $\sigma_{j, tol}$,

$$H_{s, tol}(n; \beta; T_z; \sigma_{j, tol}) = \sigma_{j, tol} \frac{H_s}{\sigma_j(n; \beta; T_z)}$$

The percentage operability is then calculated by comparing the evaluation of the scatter diagram. Specifically, evaluated is the percentage of the occurring waves that do not exceed the tolerable significant wave height. Hence, the total percentage operability is:

$$\text{PercOp} (n; \beta; \sigma_{j,tol}) = \frac{\sum f_{T_Z|H_s} (T_Z | H_s \leq H_{s,tol}(n; \beta; T_Z; \sigma_{j,tol}))}{\sum f_{T_Z|H_s} (T_Z | H_s)}$$

As the percentage operability is determined for a range of motion limits up until the maximum motion limit (where the limit is $\sigma_{j,tol,max}$). The resultant data provides a curve showing percentage operability as a function of the motion limit. *Gutch et al. (2017)* only considered the ORI for a single motion, with constants n and β .

Considering $\text{PercOp} (\sigma_{j,tol})$, the ORI is calculated by integrating and normalizing the area under the curve,

$$\text{ORI} = \frac{\int_0^{\max(\text{PercOp})} \text{PercOp} (\sigma_{j,tol}) d(\text{PercOp})}{\max(\text{PercOp}) \cdot 100}$$

The procedure above describes the calculation of tolerable significant wave height for an individual motion limit. *Gutch et al. (2017)* only considered a single limit in their research. However, to efficiently consider seakeeping, all limits should be considered. To do so, a modification is made to the calculation of the tolerable wave height, $H_{s,tol}$. This equation is evaluated for a range of motion limits of a specific DoF and type of motion. For example, for a maximum heave acceleration limit of \ddot{z}_{limit} of $1[m/s^2]$, percentage operability is evaluated for limits \ddot{z}_{limit} of 0.1, 0.2, 0.3, ..., $1.0[m/s^2]$. The number of steps in which the limit is varied is constant for each motion limit. For each 'step,' or percentage of the motion limits ($\%limit$) the most stringent motion limit is critical and limiting to the operability of the ship. The critical motion limit results in the lowest tolerable wave height. Hence the calculation of ORI is expanded by evaluating for each step,

$$H_{s,tol}(\%limit, \beta; T_Z) = \min (n; H_{s,tol}(\beta; T_Z; \sigma_{j,tol}))$$

Thereby considering each motion limit. Once the tolerable wave height per limit step is known, the corresponding $\text{PercOp} (\beta; \%limit)$ is calculated. Finally, the ORI is evaluated:

$$\text{ORI}(\beta) = \int_0^{100\%} \text{PercOp} (\beta; \%limit) d(\text{PercOp})$$

- **Lightship weight** - This item estimates the lightship weight of the iteration. To calculate the lightship weight, the hull shape is estimated by the quadricubic number, *Aasen and Bjørhovde (2014)*.,

$$m_{ls} = \eta_{ls-contingency} \cdot k \cdot N_{qc}$$

m_{ls} is the lightship weight, k is a parameter determined based on a regression analysis of similar vessels from C-Job's reference vessel 'RefWeb.' $\eta_{ls-contingency}$ is a contingency factor, as there is still uncertainty involved (especially during concept design). N_{qc} is the quadricubic number which is calculated by,

$$N_{qc} = L^{4/3} \cdot B \cdot D^{1/2} \cdot \left(1 + \frac{3}{4}Cb\right)^{1/2}$$

This equation shows the differing influences of length, beam, draught, and block coefficient, for instance, length exponentially increases lightship weight due to a required increased bending stiffness and so forth, *Aasen and Bjørhovde (2014)*. This formulation was shown to provide good accuracy by multiple studies, *Ho et al. (2012)*.

- **Initial stability** - The initial stability in the form of transverse metacentric height (GM_T) is calculated. To begin, an estimate for KG is made by the following equation,

$$KG = \frac{KG_{ss}m_{ss} + KG_{dl}m_{dl} + KG_h m_h + KG_b m_b}{\sum m_i}$$

ss denotes the superstructure, dl the deck load, h the hull and b the ballast. The values for the superstructure and deck load form input to the calculation. The mass of the hull and the weight of the ballast is calculated by,

$$m_h = m_{ls} - m_{ss} - m_{dl}$$

and,

$$m_b = m_{disp} - m_{ls} - m_{dl}$$

The displacement weight, m_{disp} , is calculated by NAPA's hydrostatic calculation package for the iteration draught. The vertical center of gravity of both the hull and ballast are estimated based on a factor defined by the user. By subtracting KG from KMT , an initial estimate for GMT is obtained,

$$GMT = KMT - KG$$

KMT is calculated by NAPA's hydrostatic calculation package.

- Ship resistance - To calculate the ship resistance, use is made of the NAPA Resistance and Propulsion manager application. This application provides a multitude of widely used empirical methods. Of these methods, Holtrop & Mennen is found to obtain accurate results for a wide range of vessels (*Holtrop et al. (1982)*), and a calculation package is available in NAPA. It should be noted that during the optimization, accuracy boundaries such as the L/B and B/T ratio ranges may be exceeded. At these extremities, Holtrop & Mennen is still able to calculate the ship resistance with limited accuracy. In these regions, the ship resistance calculation provides more of relative comparison between different variable combinations.

4. Result viewer

This section provides the output of the calculation. These results are either used by the optimization to determine the variables for a new iteration or presented to the naval architect. The multi-dimensional Pareto frontier is presented, showing the trade-offs between objective scores. The actual optimum solution can further be deliberated by the naval architect when the relative importance of various design drivers is known.

5. Optimization manager

This section manages the optimization. A user can select certain experiment settings and execute the optimization. Thereby, the user defines the variables with maximum and minimum values, objectives, constraints, and constraint values, constant values, and what components of the optimization to include.

4. Case study

4.1. Vessel introduction

The 'US Wind Feeder' is a vessel designed to support the construction and logistics of offshore wind farms in the United States. Specifically, the vessel allows non-American wind turbine installation vessels (WTIV) to construct wind farms in compliance with the Jones Act. To maximize operability, the vessel features a motion-compensated platform design by Ampelmann. Thereby, operability is a critical design driver, to enable a continuous supply of turbine components to the WTIV. The second design driver is costs- both CAPEX and OPEX. The vessel is part of a new business case proposing that maximizing WTIV's installation capability minimizes the building costs of a wind farm. Subsequently, the vessel's CAPEX -linked with the lightship weight is a critical component. Additionally, the CAPEX is interlinked with seakeeping performance. The Ampelmann platform forms a significant portion of the CAPEX - around 20% in the current concept - to realize high operability. Better seakeeping capabilities, lead to lesser requirements for the Ampelmann, improving its CAPEX. The ship's resistance is of lesser concern, as the wind farm site is close to shore. Based on the vessel's design philosophy, input to the optimization has been determined, which is given in the next section.

4.2. Optimization input

The optimization input has been determined together with C-Job naval architects. Three motion limit cases have been defined, following the locations shown in Fig.3. Motion limit case 1 concerns the motion-compensated Ampelmann platform. Motion limit case 2 concerns the risk of a turbine blade tip touching the water, which imposes a heave limit. Motion limit case 3 concerns a maximum amount of

blade accelerations, which the turbine blade can sustain. The corresponding exact limits and locations are given in Table I. Two loading conditions have been optimized. The heaviest operational loading condition, when the ship is fully loaded with turbine components, forms loading condition 1 (LC1). The lightest loading condition under which accelerations are important, which is when lifting the last item, forms loading condition 2 (LC2).

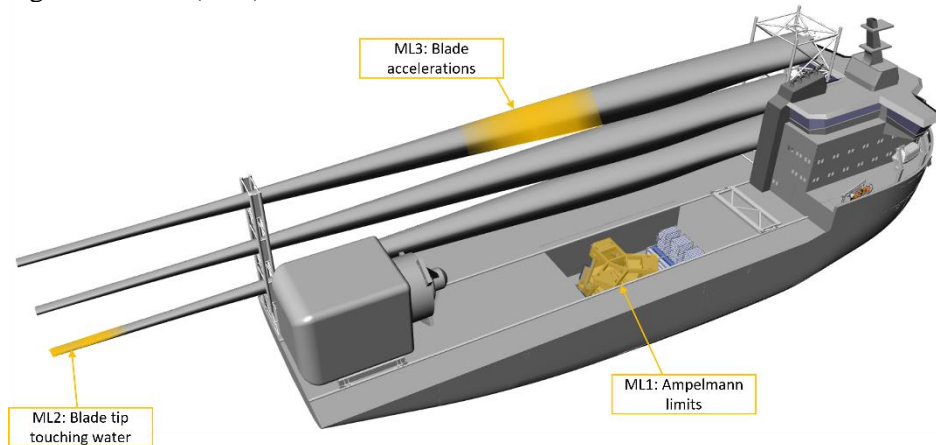


Fig.3: Motion limits case study

Table I: Optimization settings

Input				
<i>Input</i>	<i>Symbol</i>	<i>Setting/specification/value</i>		<i>Unit</i>
Area	-	23, North Atlantic Ocean, East Coast USA		-
Hull shape	-	US Wind Feeder concept		-
Angle incoming waves	α_{RAO}	30.0		°
Motion sensitive equipment	-	Case 1: Ampelmann platform, near CoB Case 2: Lifting operation Case 3: End of blade tip		-
Loading condition	-	Condition 1: Maximum loading condition Condition 2: Lifting last item		-

Variables				
<i>Variables</i>	<i>Symbol</i>	<i>Lower limit</i>	<i>Upper limit</i>	<i>Unit</i>
Aftship length	L_{afts}	30.0	50.0	m
Midship length	L_{mids}	10.0	40.0	m
Forwardship length	L_{fws}	30.0	50.0	m
Beam	B	17.0	28.0	m
Draught	T	4.5	7.5	m

Constraints				
<i>Constraints</i>	<i>Symbol</i>	<i>Lower limit</i>	<i>Upper limit</i>	<i>Unit</i>
Metacentric height	GM_T	2.0	-	m
Total length	L_{tot}	90.0	-	%

Objectives		
<i>Objectives</i>	<i>Symbol</i>	<i>Unit</i>
ORI	ORI	-
lightship weight	LSW	t
Ship resistance	SR	kN

Algorithm settings		
<i>Item</i>	<i>Setting</i>	<i>Unit</i>
Algorithm	SAMOCOBRA	-
Maximum iterations	300	#

5. Results

5.1. General results

Six optimization runs have been completed, each varying in either motion limit case or loading condition. The Pareto frontier has been found for all optimization runs as seen by the progression in hypervolumes in Fig.5, which all converge to an asymptote. Fig.4 shows each optimization's asymptote converging at a different value. As described in section 3.2 a higher hypervolume implies better objective scores.

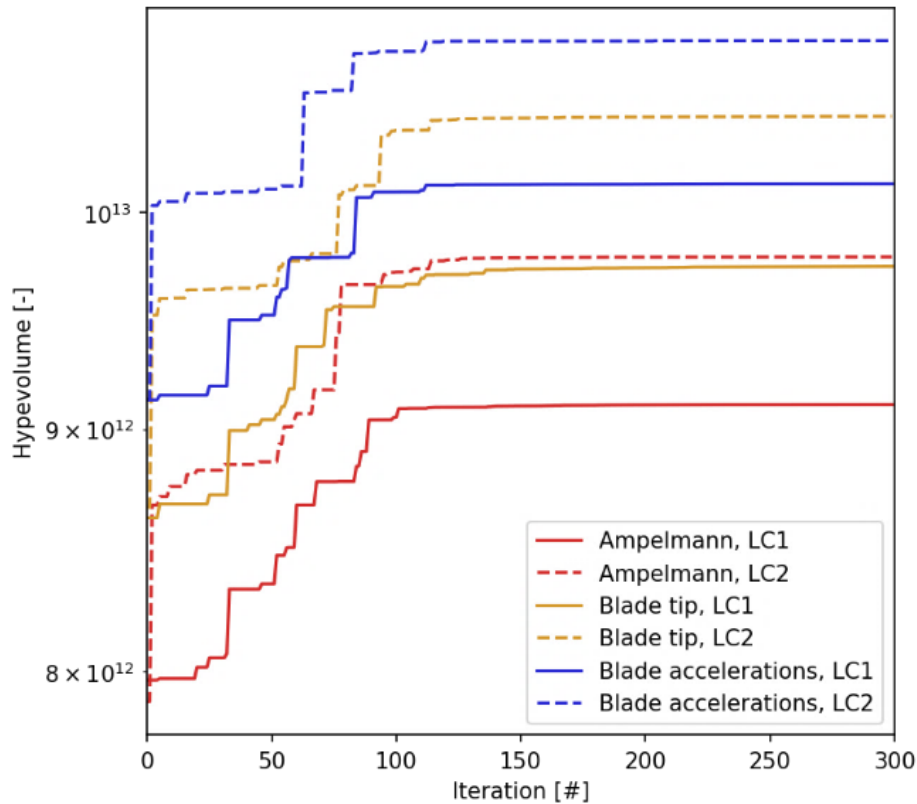


Fig.4: Hypervolume progression for six case study optimization runs

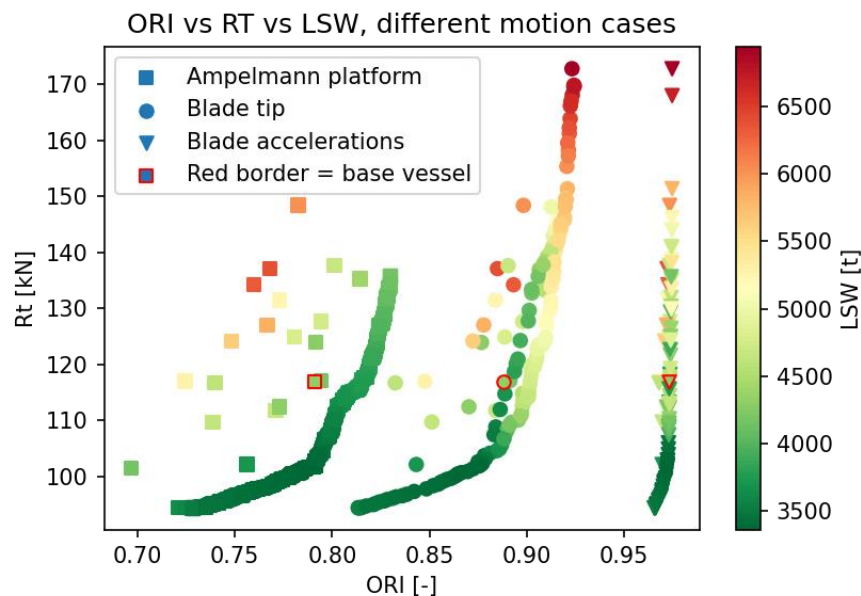


Fig.5: Optimization results for different motion limit cases

Fig.5 shows the Pareto frontiers of three different motion cases for one loading condition. All three Pareto frontier show better performance scores compared to the original solution. The highest combined objective scores are found when optimizing for the blade accelerations, followed by blade tip motions and the Ampelmann platform. Thereby, the Ampelmann platform forms the constraining motion limit case and will be further optimized upon in the study.

The effect of the two loading conditions (LC1 and LC2) becomes apparent when comparing the corresponding Pareto-frontiers in Fig.6.

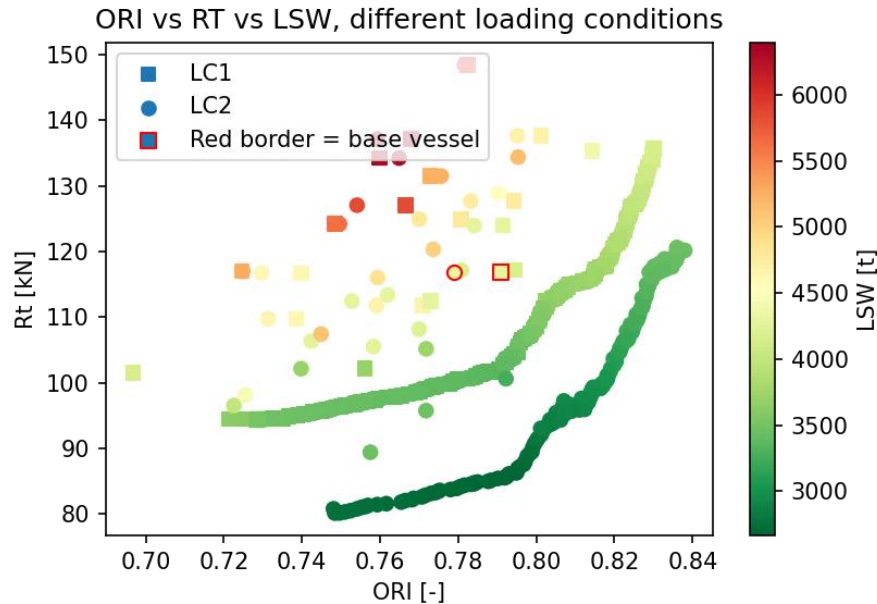


Fig.6: Optimization results for different loading conditions, with Ampelmann motion limits

Fig.6 shows LC2 allows for lower ship resistance and slightly lower lightship weight, whilst maintaining the same ORI value compared to that of LC1. LC2 allows for a slenderer vessel to satisfy the *GMT* constraint of 2 m, specifically vessels of around 19 m wide. The *GMT* constraint is satisfied for vessels at least 23 m wide for LC1. These slender vessels will not be feasible for LC1. Hence, LC1 is the critical loading condition. Together with the motion limits of the Ampelmann platform, which govern the maximum attainable seakeeping performance, this forms the critical vessel condition. In the next section, the results for this vessel condition will be further deliberated.

5.2. Analysis on critical vessel condition

The correlations between variables, feasible solutions, and high objective scores, can be illustrated by a parallel coordinate. Fig.7 shows the parallel coordinate plot of the results of the US Wind Feeder in critical condition for limiting motion cases 1 and LC1. In this plot, variable combinations have been scaled according to the ORI value. Per objective, the following correlations can be observed:

- Correlations between ORI value and variables - The resulting ORI value spans between 0.75[-] and 0.85[-]. All associated percentage operability values are quite high. A long aft ship and short forwardship, together with a high draught show to result in an ORI value. The parallel coordinate plot shows a trend of ships with short mid- and forwardship, and long aft ship attaining a high ORI value. The overall length is shown to be between 90 and 105 m, showing shorter vessels can attain a high ORI. The beam is adjusted to result in an initial *GMT* of 2 m, which reduced roll accelerations and allows for a high ORI value. This indicates that the Ampelmann platform's acceleration limits govern the seakeeping performance. Additionally, a higher block coefficient (*CB*) corresponds to a high ORI value.

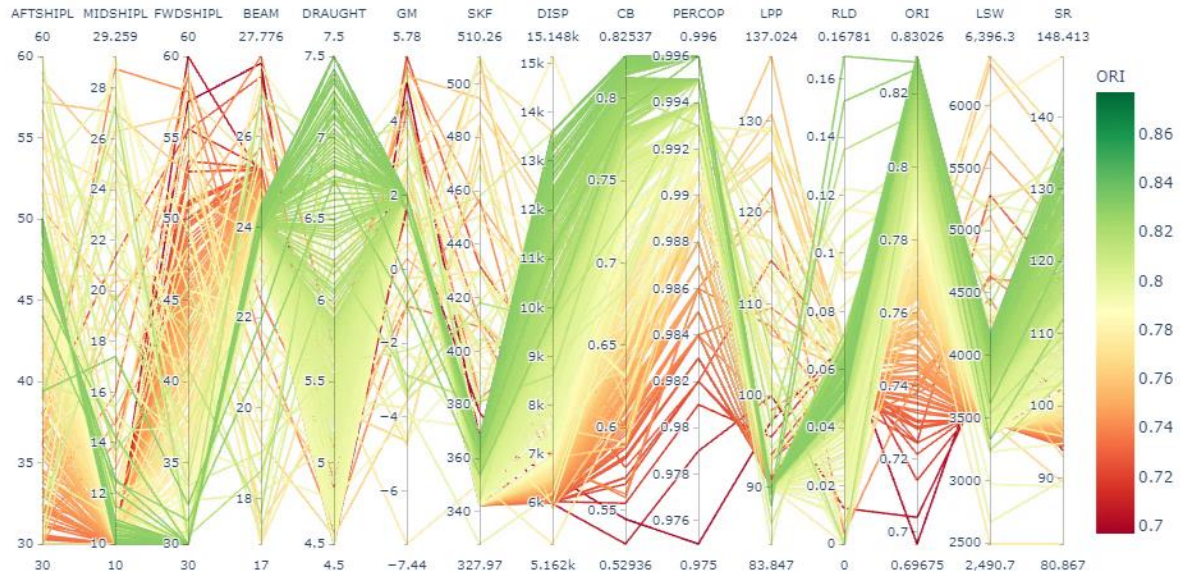


Fig.7: Parallel coordinate plot for US Wind Feeder case, LC1 and Ampelmann motion limits

- Correlations between initial stability and variables – Fig.7 shows how the optimization steers variable combinations towards a *GMT* of 2 m, as this allows a high ORI score. Consequently, this results in an inverse relationship between the draught and the beam. A slenderer beam requires the draught to be higher to satisfy the *GMT* constraint, and vice versa.
- Correlations between lightship weight and variables - A direct and positive correlation exists between length, beam, draught, and block coefficient. This is seen in the parallel coordinate plot. Additionally, most of the results have an LSW between 3500-4300 t, due to the relative shortness of Pareto-optimal vessels. The vessels with a higher ORI are seen to have a higher lightship weight, due to having a higher draught and block coefficient, hence a trade-off exists between ship resistance and draught.
- Correlations between ship resistance and variables - The ship resistance is seen to vary between 95-130 kN for most results. Shorter aft ship and longer forward ship lead to a lower ship resistance. The draught is seen to have an inverse relationship with ship resistance. Vessels with a deeper draught may be slenderer whilst satisfying the *GMT*, though it is not seen to result in a lower ship resistance. The adverse effects of a higher draught supersede the positive effects of a lower beam on ship resistance. The vessels with a higher ORI are seen to have a higher ship resistance, due to having a higher draught and block coefficient, hence a trade-off exists between ship resistance and ORI.

The framework does not provide one singular optimal solution. Rather, it provides insight into the combination of variables resulting in 'optimal solutions', solutions that maximize performance into one objective for a certain value for another objective. These results are shown in a Pareto-front in the next subsection. Additionally, these attainable values are compared to the current US Wind Feeder concept of C-Job.

5.3. Comparison with base vessel

Fig.8 shows the detailed optimization results with the Pareto-frontier. When compared with the current concept design, annotated as 'base design', all Pareto-optimal solutions show an improvement over the base design in lightship weight. Additionally, some Pareto-solutions show improvements in both ORI, ship resistance, and lightship weight. The solution with the same ORI but improving the ship resistance and lightship weight has been highlighted, as well as the solution with a similar ship resistance but improved ORI and lightship weight. The extremes of the Pareto-frontier are also annotated. Table II shows corresponding variables, KPI scores, and other parameters of these design solutions.

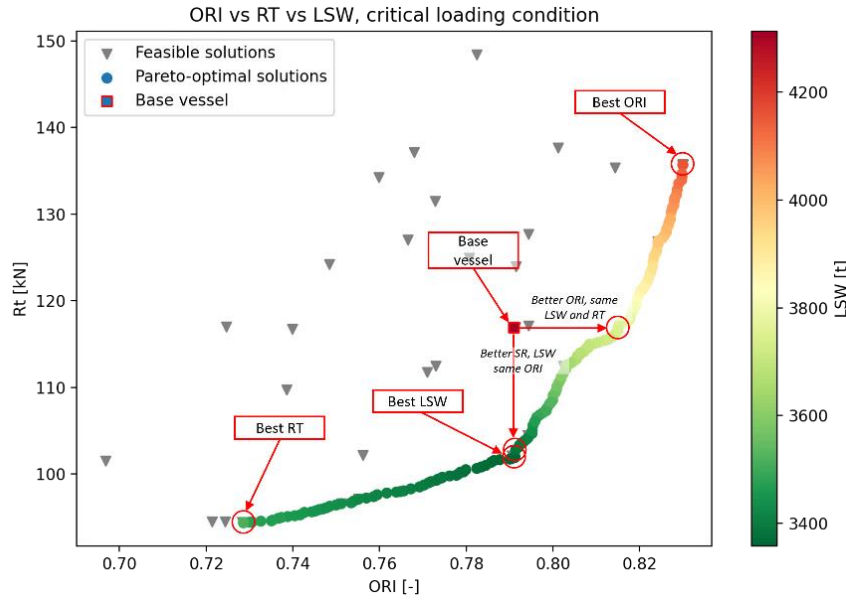


Fig.8: Detailed Pareto-frontier of case study, LC1, and Ampelmann motion limits

Table II: Overview of specific results of optimization for US Wind Feeder case study

Results of optimization for US Wind Feeder concept - critical condition								
Variables	Symbol	Value	Value	Value	Value	Value	Value	Unit
Solution	—	Base vessel	Same RT, better ORI and LSW	Same ORI, better RT and LSW	Best ORI	Best LSW	Best RT	—
Aftship length	L_{afts}	46.00	50.00	49.25	49.80	50.00	30.00	m
Midship length	L_{mids}	23.00	10.00	10.4	10.20	10.00	10.00	m
Forwardship length	L_{fws}	34.50	30.00	30.35	30.00	30.00	50.835	m
Beam	B	23.80	23.99	23.6	24.22	23.48	25.26	m
Draught	T	5.50	5.98	4.5	7.50	4.50	4.50	m
Block coefficient	C_B	0.72	0.78	0.72	0.83	0.73	0.58	—
Metacentric height	GM_T	2.18	2.00	2.00	2.00	2.00	2.00	m
Stationkeeping force	SKF	398.78	354.70	342.38	367.44	342.38	342.36	kN
Operability robustness index	ORI	0.791	0.815	0.791	0.830	0.791	0.729	—
Difference ORI w.r.t. base vessel	-	-	3.03	0.00	3.55	0.00	-7.84	%
Percentage Operability	$PercOp$	99.2	99.4	99.2	99.6	99.2	98.3	%
Lightship weight	LSW	4310	3760	3450	3880	3360	3510	t
Difference LSW w.r.t. base vessel	-	-	-12.76	-21.14	-9.98	-22.04	-18.56	%
Ship resistance	R_T	116.93	116.90	101.79	135.69	101.91	96.36	kN
Difference R_T w.r.t. base vessel	-	-	-0.03	-12.95	16.04	-12.85	-17.49	%

Below, improvements in objectives are further elaborated:

- **Improvements in ORI** - The ORI shows to be improved up to 3.6%, depending on the combination of variables. The ORI is improved over the base vessel by increasing the aft ship length, draught, and subsequently the block coefficient, thereby keeping GMT at 2.0 m. The design solution with the highest ORI also shows a minor improvement in operability, namely 99.6% over 99.2%. This does show that the base vessel should already allow for good year-round operability. The solutions offering the lowest lightship weight and ship resistance do so by minimizing draught. The vessel with the best ORI has an estimated lightship weight of 16.0% than that of the base vessel. The vessel with the lowest ship resistance shows a decrease of -7.8% in ORI. Hence, a trade-off exists between lightship weight and ship resistance. Though the ORI is only marginally improved, the framework can show that other performance criteria could significantly be optimized whilst maintaining seakeeping performance. Thereby, the naval architect might pursue extreme design solutions, which it would normally not dare to do so.
- **Improvements in lightship weight** - Design solutions close to the Pareto frontier allow for a reduction in lightship weight between 12.8% and 22.0%. The framework results showed that

shorter vessels (length = 90 m) can attain good seakeeping performance. Due to the shorter length, the lightship weight is also substantially decreased. Furthermore, the lightest solutions are characterized by a minimal draught and low block coefficient, further reducing the different terms in equation 7.6. Thereby, the lightship weight depends on variables similar to the ship resistance, yet a trade-off exists between lightship weight and ORI.

- Improvements in ship resistance - The Pareto-optimal design solutions allow for a reduction in ship resistance of up to 17.49%. These solutions achieve a lower ship resistance due to a shorter length, and subsequently lower frictional ship resistance. Additionally, it is that a reduction in block coefficient and draught, a typical indication of a finer hull shape, further reduces ship resistance. The opposite holds for the ORI, as the vessel with the highest ORI value shows a reduction in ship resistance compared to the base vessel. Hence, on the Pareto-front, a trade-off occurs between ship resistance and seakeeping.

The results above clearly show how the framework can efficiently explore the design space to find optimal design solutions and provide design trade-offs of conflicting requirements. In doing so, and thereby providing the Pareto frontier, the naval architect is provided with tons of useful design information. The base design, created with much deliberation by expert Naval Architects, shows the difficulty of designing a concept that maximizes performance in either one objective at once. This led to an over-dimensioned vessel design to guarantee seakeeping performance.

6. Discussion

This paper shows the advantages of using a holistic design approach for OSV design. The discussed framework can efficiently explore the concept design of OSVs, thereby effectively involving seakeeping. Specifically, it showed to be able to find substantial improvements over the base concept initially developed by C-Job. The seakeeping objective, ORI, can be increased up to 3.6%, the lightship weight decreased by 21.1% and the ship resistance decreased by 13.0%. These improvements can be achieved whilst satisfying the initial stability constraint. By being able to explore the design space early in the design process, the correct design direction can be decided. Thereby, the framework proves to be a powerful tool for the 21st-century naval architect. It should be noted that the possible design directions are still constraint by the user set boundaries, as well as possible limiting input factors such as the hull shape and loading condition. It is recommended that any naval architect carries out a sensitivity study on input parameters when applying the framework. In particular, the hull shape can significantly influence framework results. As a future development, further refining the hull shape parameters will further expand the possibilities of the framework. Caution should be applied when further developing the lightship weight and ship resistance into measures of CAPEX and OPEX. These objective values are partially determined by using reference databases. Thereby, there are inaccuracies present which may be reduced with direct analytical methods. Regardless, the framework provides a powerful tool in the arsenal of a naval architect. More precise ship design evaluation methods could be implemented as well as more parameters, constraints and objectives could be explored to further enhance the ACD framework. Thereby, C-Job's Accelerated Concept Design philosophy is further developed by applying a holistic approach accelerating the concept design process as well as generating better concepts.

Acknowledgments

This work was performed as part of the MSc thesis for the lead author, in Marine Technology at the Delft University of Technology in the assignment of C-Job Naval Architects. We would like to acknowledge both Delft University of Technology and C-Job for the support of this research.

References

- AASEN, R.; BJØRHOVDE, S. (2014), *Estimating weight and CG in the early design phase*, 51, pp.13-17
- ANDREWS, D. (2018), *The sophistication of early stage design for complex vessels*, Special Edition

DNV (2010), *Recommended practice: Environmental Conditions and Environmental Loads*, DNV-RP-C205, Det Norske Veritas

DE WINTER, R.; VAN STEIN, B.; DIJKMAN, M.; BÄCK, T.H.W. (2019), *Designing ships using constrained multi-objective efficient global optimization*, Machine Learning, Optimization, and Data Science

DE WINTER, R.; FURUSTAM, J.; BÄCK, T.H.W.; MULLER, T. (2020), *Optimizing Ships Using the Holistic Accelerated Concept Design Methodology*, Practical Design of Ships and Other Floating Structures (PRADS)

DE WINTER, R.; VAN STEIN, B.; BÄCK, T.H.W. (2021), *SAMO-COBRA: A Fast Surrogate Assisted Constrained Multi-objective Optimization Algorithm*, Evolutionary Multi-Criterion Optimization

GUTCH, M.; STEEN, S.; SPRENGER, F. (2020), *Operability robustness index as seakeeping performance criterion for offshore vessels*, Ocean Eng. 217

HO, C.; OKAFOR, D.; DEGREGORY, J.; TONTARSKI, N.; STOREY, T.; LIN, Z. (2012), *8520 TEU dual fuel container ship for the far east - mediterranean trade route*, 2011 - 2012 Dr. James A. Linsnyk student ship design competition

IKEDA, Y. (2014), *Prediction methods of roll damping of ships and their application to determine optimum stabilization devices*, Marine technology and SNAME news 41(02), pp.89-93

NOWACKI, H. (2010), *Five decades of computer-aided ship design*, Computer-Aided Design 42(11), pp.956-969

PAPANIKOLAOU, A. (2010), *Holistic ship design optimization*, Computer-Aided Design 42(11), pp.1028-1044

PAPANIKOLAOU, A. (2019), *A Holistic Approach to Ship Design*, Springer

PAWLING, R.; PERCIVAL, V.; ANDREWS, D. (2017), *A study into the validity of the ship design spiral in early stage ship design*, J. Ship Production and Design 33(2), pp.81-100

RIQUELME, N.; VON LÜCKEN, C.; BARAN, B. (2015), *Performance metrics in multi-objective optimization*, Latin American computing conference IEEE.

VAN DER LOOS, A.; NORMANN, H.; HANSON, J.; HEKKERT, M. (2020), *The co-evolution of innovation systems and context: Offshore wind in Norway and the Netherlands*, Renewable and Sustainable Energy Reviews

VOSSSEN, C.; KLEPPE, R.; RANDI, S. (2013), *Ship design and system integration*, DMK Conf.

Human Machine Interface for Ships with Wind-Assisted Propulsion

Stephan Procee, NHL, Stenden/The Netherlands, stephan.procee@nhlstenden.com

Abstract

This paper outlines a framework for a user interface that combines the performance model of a wind assisted propulsion system. It will show the variables that can be chosen like, the amount of diesel propulsion and the course relative to the wind subject to ambient conditions. The associated predicted speed is shown in relation to the mission which is defined by a destination and a desired time of arrival. The paper will describe a basic performance prediction of a wind assisted ship, and the framework for a user interface that has an ecological component to it and aims at utilizing the on-board user's longstanding expertise in weather prediction and the safe and effective ship's progress.

1. Introduction

As we see the shipping world actually taking a first step in the transition to a smaller ecological footprint, manufacturers of wind assisted propulsion appear to provide a solution, at least partially, to reduce carbon dioxide emission. Among the variety of these systems, the two major working principles are wind foils and wind rotors. Both working principles are currently employed in varying products and configurations, but in all cases, they work as auxiliary propulsion to the conventional propulsion, which are, almost exclusively, diesel engine driven propellers. In such ships the conventional propulsion provides for a basic speed of the vessel, and the auxiliary wind appendage is to add some propulsion to that, hopefully leading to more speed, in which case there's the option to reduce the main engine's thrust and reduce emission as a consequence or, alternatively, enjoy the higher speed and reduce effective sailing time which has a positive consequence for exhaust emission as well, (i.e., less time to burn fuel).

Now that we see more and more shipping companies start introducing this hybrid type of propulsion, it becomes interesting from the routing perspective how these prototypes are going to be deployed. As said, most providers see the auxiliary as a sort of potential saving during the execution of their sailing plan. However this 'hoping for the best' might not fully utilize the potential of the combined wind and motor propulsion. The importance of this seems to be overlooked. Not many studies can be found on the operational aspects, that is choosing the amount of diesel power and the vessel's course in the light of the day-to-day strategy of the operator on board. When we aim at operating ships using least fuel or emitting least gas or with the least ecological impact, in a broad sense these are all synonymous, then we need to bring the operators on board into the equation. Their daily maintenance and operational decisions will have a key role in the success or failure of this innovation. Shore based support is expected to be limited in this respect because there will not be much expertise on this field of wind assistance for the foreseeable future. Knowledge of plain sailing, i.e. exclusively propelled by sail, is not a part of Nautical Colleges' curricula neither is it part of the STCW, for example. Creating a knowledge and training base for seamen to operate safely and efficiently wind assisted seagoing vessels might take a decade, at least.

This paper outlines a framework for a user interface that combines the performance model of a hybrid propulsion system. It will show the variables that can be chosen like the amount of diesel propulsion and the course relative to the wind. The associated predicted speed is shown in relation to the mission which is defined by a destination and a desired time of arrival. As can be expected, the shortest geographical connection between departure and destination will not per definition comprise of the optimal route for a vessel that depends on conventional and wind propulsion. Sea state and ocean circulation are also major factors that influence the ship's speed and progress. Propulsion and course are choices made by the operator on the bases of wind, current sea state and the target (goal). The quality of the prediction of wind speed and wind direction is analyzed in order to demonstrate its potential magnitude, i.e. the uncertainty. The effect of this quality of wind prediction on the performance of a wind assisted vessel can be visualized in the HMI. The quality of the prediction of sea state and surface

current is not analyzed in this paper. However, both are to be incorporated in the HMI as they are an integral part of voyage planning and execution.

2. Speed Prediction Model

In order to demonstrate the elementary relation between force and speed acting on a wind assisted motor ship the following, highly simplified, approximation can be used. Considering a wind assisted ship's model with dimensions tentatively chosen so to meet the following characteristics, Fig.1:

1. The main propulsion M_{prop} is expressed in tonnes force generated by the propeller, relates to the vessel's speed through the water S_w with relation $S_w = (2.88 \cdot M_{prop})^{0.5}$, hence 50 tonnes of propulsion force relates to ~12 kn on a calm-water surface. (This is a highly simplified approximation aiming at an elementary relation between force and speed, i.e. $F=C \cdot V^2$).
2. The wind propulsion W_{prop} is the longitudinal decomposed force of the wind lift W_{lift} generated by either the rotor, the foil or the sail.
3. The direction of W_{lift} is perpendicular to the direction of the apparent wind θ_r .
4. The force of W_{lift} is a function of the apparent wind speed W_r and relates $W_{lift} = 0.036 (W_r)^2$; hence 20 kn relative wind speed, i.e. 5 Bft, relates to ~14 tonnes of force.
5. The vector of the relative wind is the sum of the vector of the true wind W_t and the induced wind, i.e. the opposite of the vessel's speed.
6. The resulting speed from main propulsion and assisted wind propulsion can be estimated with the relation $S_w = (2.88 \cdot (M_{prop} + W_{prop}))^{0.5}$.
7. Current, i.e. the horizontal progress of the water constituting either tidal stream or meteorological circulation or both, has an effect on the induced wind. The ship's velocity vector, relative to water, is to be added by the current vector resulting in a so-called ground speed, i.e. the speed relative to ground. The induced wind vector is the opposite of the ground speed vector.

Fig.1 shows a ship's true course, i.e. relative to geographic north, and speed in the black colored 'true course' vector. The medium in which the ship sails, moves in the direction and with speed depicted as the blue colored 'current' vector. The composition of these two vectors is the speed and direction relative to the earth, in the Figure depicted as 'Course over Ground' (in black). The wind direction is relative to true north, therefore called 'true wind' in the picture it is depicted by the green vector. The wind's angle of attack to the ship, i.e. to its center line, is shown as the angle θ_t . The opposite of the ground course is the 'induced wind', which is the wind that is felt when true wind would be absent. The composition of induced wind and true wind is called the 'apparent wind', depicted by the purple vector. The ship's sail or foil or rotor generates a 'lift force' perpendicular to the direction of the apparent wind, this is shown by the red vector. The lift force can be decomposed in an along-ship component, which contributes to the ship's propulsion, and an athwart ship component, this is not shown in Fig.1 in order to improve clarity. The athwart ship component does not contribute to the propulsion. On the contrary, it produces a leeway of the vessel and subsequent induced drag due to the asymmetrical flow of water around the hull.

In a situation with wind speed of e.g. 20 kn and a propulsion envelope of e.g. 20 to 50 tonnes, the relation between the angle of attack of the true wind θ_t and the ship's speed can be calculated on the basis of the decomposition shown in Fig.1. The influence of surface current and sea state is kept out of this example for the sake of simplicity. Fig.2 shows the polar diagram of predicted hull speed (through water).

As already explained, the amount of conventional speed is a choice as well as the wind's angle of attack is a choice, that is the chosen course of the ship relative to the wind. The mission of merchant shipping usually is to reach a destination, i.e. a certain place on earth at a certain time of arrival. The way to fulfill the mission is generally called routing, and it depends on many factors, of which fuel economy might have priority. In order to visualize the mission, a target direction and target speed can be determined based on the position of the vessel and its predicted progress. The latter depending on the vessel's speed potential in relation to external factors like weather, sea state and current.

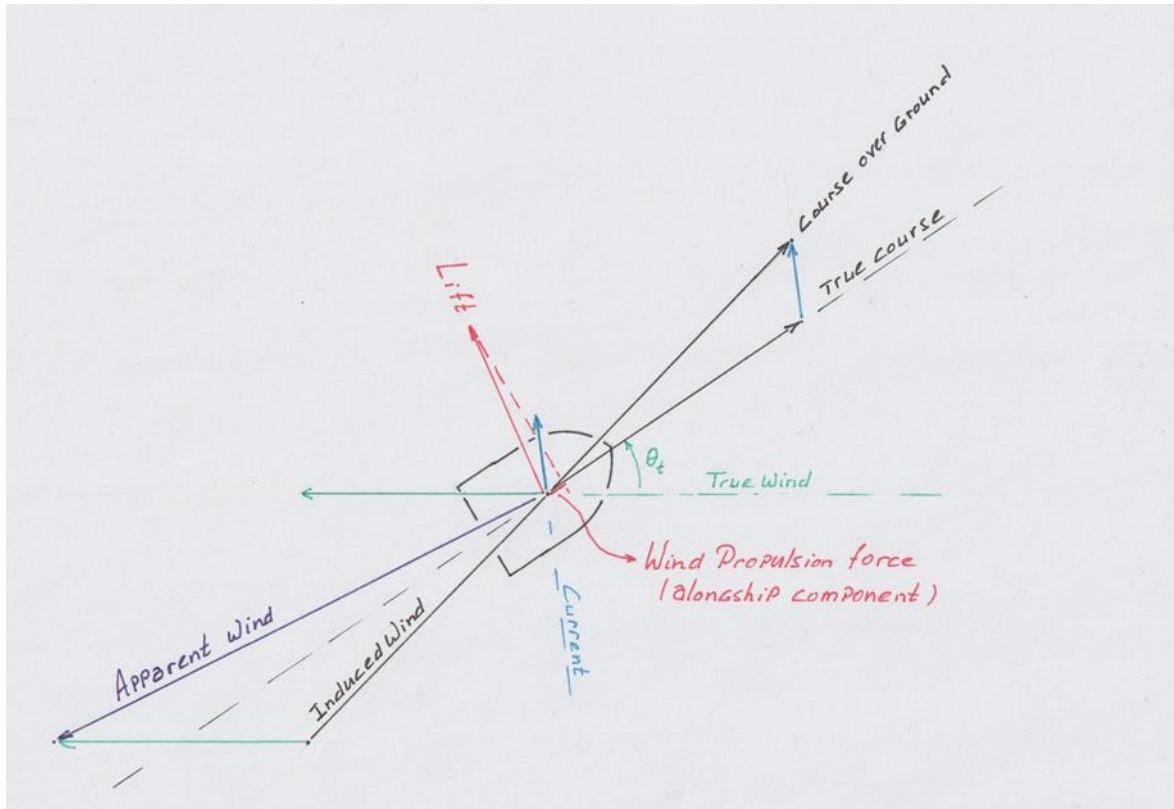


Fig.1: Decomposition of speed and force

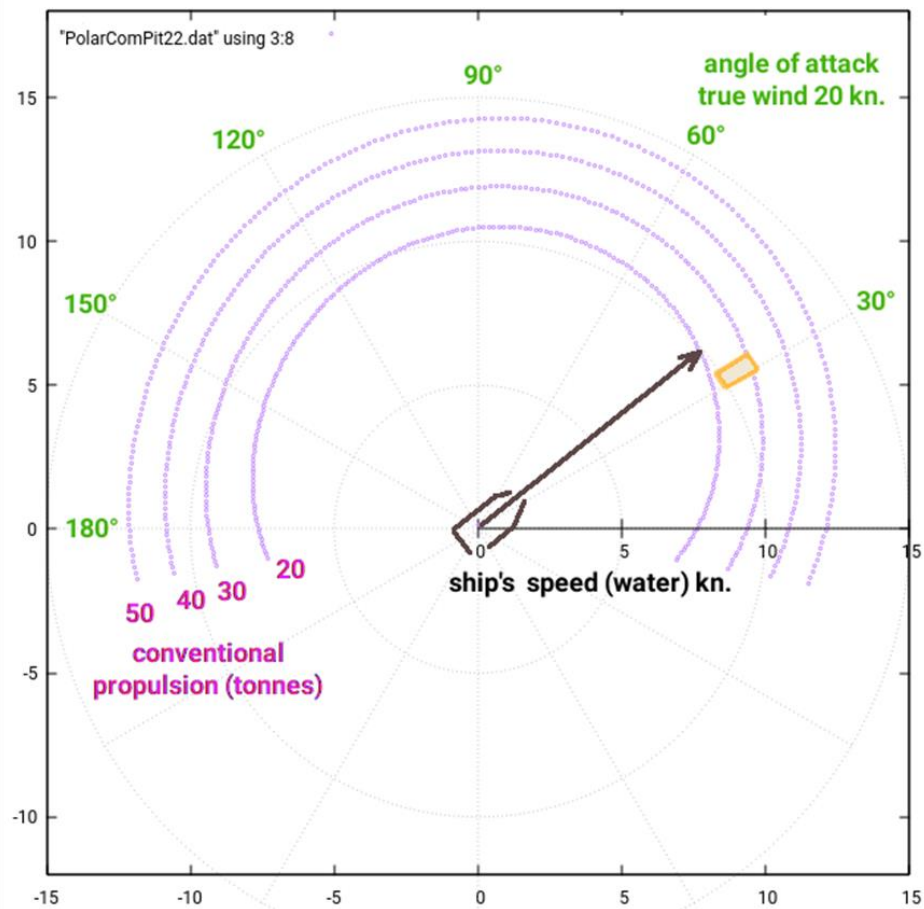


Fig.2: Speed Prediction as function of conventional propulsive power and the wind's angle of attack.

This is shown as the orange shaded box in Fig.2. Because of the limited or unpredictable character of weather the target speed and target direction are expected to be rather vague at the start of a mission and become stricter, i.e. with a smaller margin for speed and course, as the destination gets nearer. Routing can be regarded as the choice to adjust the course of the vessel with regard to wind and weather and the amount of conventional propulsion in order to stay within the margins of the mission's target. This choice, however, becomes complex when the progress of the vessel must balance e.g. between least fuel consumption and complying with a defined ETA and dealing with the limited reliability of weather forecasts several days ahead in time. The principle working, is that the ship's heading and speed, can be chosen so as to fulfill the prediction for the set goal, in which case the vector's arrow head locates inside the orange box, or, when circumstances favor an alternative, like in this example, the course can be chosen some 10° to port where 10 kn ship's speed can be reached with less conventional thrust. This is shown in Fig.2. Many alternatives are possible. The choice is to be made by the navigator on a day-to-day basis.

3. Forecast Verification and the Inferred Confidence Interval

Verification of weather forecasts is a relatively young field. *Joliffe and Stephenson* (2020) state that the World Meteorological Organization published a comprehensive survey of forecast validation methods in use in the late 1980s.

Although it is common that predictions are provided for a period of four to five days ahead, providing a confidence interval associated with the prediction is not customary. Hence limited research into the reliability of weather prediction has been carried out in order to derive an objective indication of a possible magnitude of the confidence interval.

Because wind prediction, i.e. speed and direction, greatly affects the secondary propulsion of the hybrid propelled vessel and data on the subject is relatively easy to retrieve the analysis is focused on validating predicted wind direction and wind speed. For that purpose the observed and predicted data is retrieved from a weather station on one of the Shetland Islands. Choosing a station on that location has the advantage that a supposed effect of nearby land is minimal; a station on such location resembles most to a situation on the open sea. Besides that, the sensors of this particular station are located almost at sea level, i.e. elevated at 15 ft relative to sea level, which presumably relates to mean sea level.

During the period December 08 2020 to May 21 2021, every three hours a broadcast weather observation is logged together with four predictions each a day further ahead in time. In order to limit the data set, predictions and the observation at 12 hours UTC is selected for every day during the period. This provides 124 valid daily combinations of observed and predicted wind speed and direction. The analysis comprises of comparing the forecast wind speed and direction with the observed speed and direction. It is hypothesized that the quality of the forecast is lower when it is predicted further away in the future. That means that the discrepancy between predicted and observed wind will likely be smaller when the forecast is only one or two days ahead as compared to e.g. a forecast that is four days in advance.

If this discrepancy and its relation to the days ahead can be determined for the recorded 124 data points in time, we can infer a 95% confidence interval for both predicted wind speed and wind direction. This confidence interval has an effect on the confidence interval of the ship's performance prediction in such a way that the prognosis for the ship's progress as function of location and time comes with a 95% confidence margin. This margin constitutes of the minimum likely progress on the basis of ship's course, speed and predicted weather and a maximum likely prognosis. It is of course the Master's decision to weigh the prognosticated progress against the risk of deviating from the geographical shortest route, which is usually the great circle on ocean crossings.

For every day in the period, the associated predicted wind is retrieved, that is four days prior to this day there was a 4d prognosis of the wind for the given day. Also three days prior to this day there's a 3d prognosis, and so forth. The quality of the forecast is inferred from the magnitude of the residuals, i.e. predicted minus observed.

In order to develop a practical instrument for the routing of wind assisted propelled vessels a measure is required to express the confidence envelope within which the combination of wind speed and direction is likely to fall. A further analysis on the frequency of combinations shows that for the one day forecast, i.e. P1, 116 cases out of 124 were within the speed margin of 8mph and 106 cases were within the direction margin of 23° and 103 cases were within their respective margin of speed and direction. This means that an atmospheric development, that is not covered by the meteorological model, will likely have an effect on both direction and wind speed, hence the 103 cases, i.e. 83% of the time during the analyzed period.

Table I: Percentage of Residuals in Wind Speed and Direction

days	Speed		Direction		both	cases
prior	margin	percentage	margin	percentage		
1	± 8mph	93%	± 23°	85%	83%	124
2	± 10mph	96%	± 45°	94%	93%	123
3	± 11mph	97%	± 45°	95%	93%	122
4	± 12mph	98%	± 68°	98%	97%	121

From Table I it might be concluded that the prediction intervals of both speed and direction forecast must be regarded as increasing in dimension as the predicted period is further ahead in time. And also it appears that in the majority of cases the meteorological anomaly, i.e. a disturbance not predicted by the weather forecast model, has an effect on both wind speed and wind direction prediction. From this the consequence for the speed prediction model can be inferred.

Based on the daily forecasts and observations of Station 3002 (Baltasound) over the period December 2020 till May 2021 the one day ahead predicted wind speed and wind direction will be within a margin of 8 mph. and 23° of the predictor with 83% confidence. As the period of forecast reaches the maximum of 4 the confidence rises to 97% although at much bigger margins of 12 mph and 68° in direction.

4. Effect on speed potential

The margin in forecast speed and direction, mentioned in the previous paragraph, can be incorporated in a speed prediction calculation. This prediction can be visualized in a polar diagram, Fig., showing the predicted speed as function of the angle of attack θ_i , i.e the course of the vessel relative to true wind. The relation between conventional propulsion, wind propulsion and θ_i is explained in the following paragraph.

The green circle represents the speed potential without the wind assistance. Based on the simplified model and a tentatively chosen thrust of 30 tonnes this equates to 9.4 kn relative to the water.

With the assistance of wind propulsion the potential speed is calculated as function of the angle of attack. The true wind speed of 20 kn is tentatively chosen; This relates to approximately Bft 5. (Note that the Beaufort scale originally relates to the sea state and therefore expresses the effect of wind force. While wind speed is objectively quantifiable, the wind force expressed in the Beaufort scale is a subjective quantity. Experienced observers, however, show a remarkable consistence in their estimate of wind force.) The speed potential is calculated for every one degree of θ_i with six variants. These variants express the forecast margins in speed and direction. For example, at $\theta_i = 30^\circ$, the speed potential is calculated for 13 kn, 20 kn and 27 kn (8 mph \approx 7 nm/h = 7 kn) and 7°, 30° and 53°, resulting in nine combinations of predicted speed within 83% confidence. This equates to a potential speed ranging from 9.6 kn to 13.1 kn. The nine variants within this range are shown in the plot for the given $\theta_i = 30^\circ$. In this case, it can be concluded that within the speed and direction margins associated with the one day forecast the potential speed will be higher than that without wind assistance in 83% of the time. Hence, considering a routing measure, i.e. change course to reach $\theta_i = 30^\circ$, in order to increase the ship's speed will have a positive effect in 83% of the time.

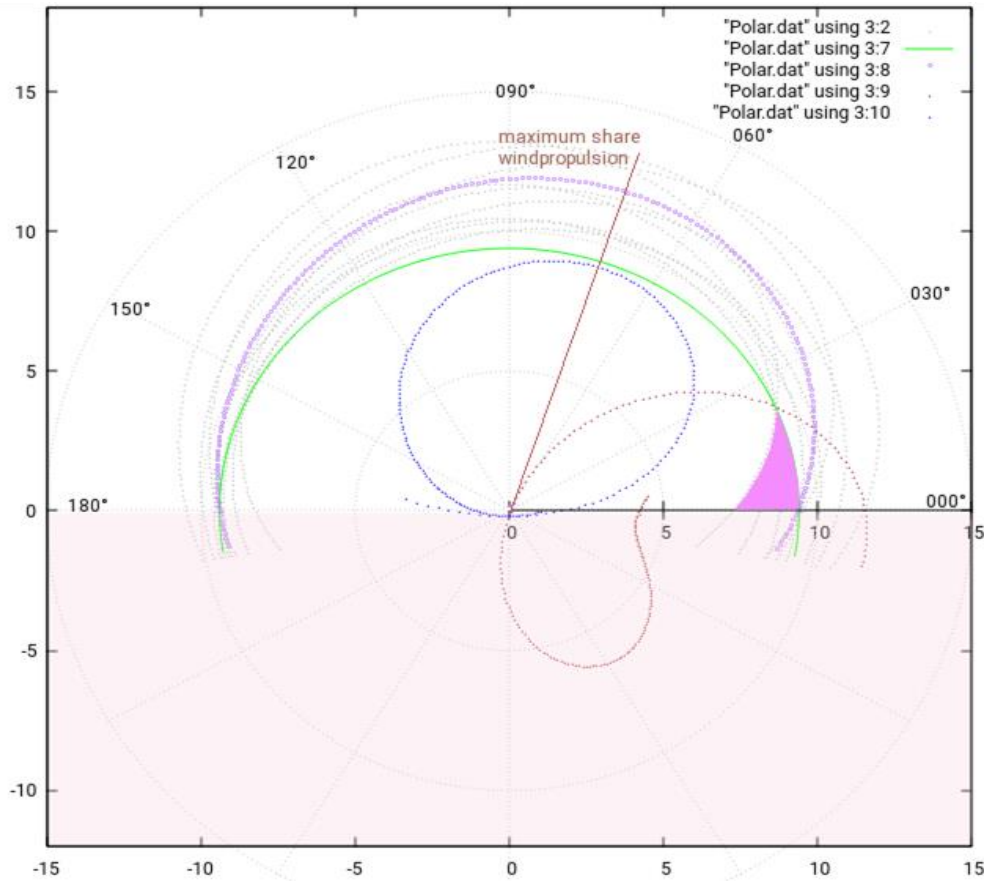


Fig.3: Predicted Speed with 30 tonnes conventional propulsion and 20 kn true wind; weather forecast one day (P1)

For angles of attack between zero (000° or dead ahead) and 180° (tailwind) the wind propulsion is positive, that is, it has the same direction as conventional propulsion. The opposite, the red shaded area in Fig.3 is the case for wind attacking the other bow of the vessel. In the latter case, either the rotor sail is to change the direction of rotation, or the foil's flap is to change side in order to gain speed from the wind. Assuming that a symmetric configuration of hull and superstructure has no influence on the wind propulsion potential when wind is attacking from either port or starboard side, the effective use of the polar speed prediction diagram can be limited to the one un-shaded side shown in Fig.3, be it mirrored over the longitudinal axis of the vessel (000°-180°)

From Fig.3 it becomes clear that the effect of the margin in wind direction, i.e. $\pm 23^\circ$, is large in a head wind situation. When the wind is predicted to be dead ahead the expected wind propulsion is zero, or even negative when the induced wind drag of the foil or rotor is taken into account. However, in cases that the observed wind direction deviates from the predicted direction, a positive effect can be met. This is shown by the outer limit of the predicted speed plot. In the case that a negative effect is met, shown by the magenta shading in Fig.3, the observed wind is attacking from the opposite bow, and by reverting either the rotor direction or the foil's flap, the effect will become positive. This means that the magenta area in Fig.3 is a non operational area in practice. The blue curve in Fig.3 shows the share of wind thrust in the total propulsion, the brown curve the differentiated wind thrust. The maximum wind thrust can be derived from the zero crossing of the differentiate at $\theta_i \approx 70^\circ$.

5. Routing considerations

When, for simplicity's sake, current and sea state are not taken into consideration the routing task can be restricted to determining isochrones, a.k.a time fronts or distance potentials. These are made on the basis of the predicted wind, the amount of conventional propulsion and the ship's predicted speed. Many

authors, e.g. *Hofmann-Wellenhof et al. (2003)*, have excellently covered routing and guidance for air and land based navigation. However, this is routing associated with a topological network, where nodes and legs are defined in position and impedance among others. Marine navigation, on the other hand, does not use a defined network of routes in general. Although few cases of defined routes exist, e.g. safe water tracks or, to a limited extent, Traffic Separation Schemes, these are not topologically structured. An initiative to design a network model, based on observed density of AIS broadcasts, i.e. *Oltman (2015)*, did not mature enough beyond the ACCSEAS project duration to find common ground in the maritime community. This, however, might be the first applicable model suitable for the previously mentioned network-based routing.

Aimed at ocean navigation, *van der Ham et al. (1983)* provide a method for determining the least time track from a number of consecutive isochrones which are each based on the speed vs. wave height performance of the ship and the expected sea state for the moment associated with the isochrone. The same approach can be used for determining the least time track for a wind assisted vessel. In the following example, Fig.5, the working principle for the determination of the least time track of a wind assisted vessel is demonstrated.

Suppose the geographical shortest connection between the point of departure **A** and the point of destination **B** is given by a Loxodrome, also known as Rhumbline. (Although a Great Circle is the shortest surface connection between two points on a sphere, for distances shorter than 400 nm, the difference between rhumbline and great circle is negligible, hence a rhumbline is used for simplicity.) Further, that in the given situation the transit time, **A** to **B**, is expected to last two days for the wind assisted vessel used in this example. And also, that for day one, i.e. P1, the weather forecast predicts a wind speed 20 knots and wind direction from **B** to **A**, so literally, head wind for the vessel on a direct course. From the polar diagram, Fig.3, the speed potential can be found for this direct course, i.e. head wind, 9.39 kn., meaning there's no wind assistance at all. Alternatively, a course might be steered e.g. 30° off the direct course. This would result in a predicted speed of 10.95 kn, hence gaining 1.5 kn from the wind assistance. Suppose the prediction for day two, i.e. P2, is equal to day one. In order to reach the destination, after day one the vessel's course is changed 60°, thus again heading 30° relative to wind, albeit from the other bow. Therefore the predicted speed is 10.95 kn. The standardized investment in the longer track can be estimated as $\sec 30^\circ = 1.15$ which is slightly less than the standardized increase in speed, which is 1.17. Hence, the increase in speed at a deviation of 30° does compensate for the extra miles. However, when the speed made good (SMG) is taken into consideration, Fig.4. (SMG is defined as the projected speed towards the destination.) It can be inferred from the polar plot that SMG has a maximum at an angle of attack, i.e. course, 15° relative to the true wind direction.

In the case of wind from **B** to **A**, i.e. headwind, deviating 15° resulting in 10.23 kn predicted speed, which is an increase by 1.08 which outweighs the extra distance factor of 1.015. Hence, maximizing SMG by deviating from the direct course is advantageous and reduces the transit time by a factor of 0.94 (i.e. $1.015/1.08 = 0.94$).

The construction of a Least Time Track on the basis of two or more time fronts, also referred to as isochrones, is as follows, Fig.5. From the point of departure **A** the distance potential is plotted based on the wind forecast and the associated speed prediction. Table II contains the speed prediction S_w as function of the angle of attack θ , and the expected progress for the duration of the forecast, i.e. 24 h in the example. This results in the blue curve, i.e. the 24 h isochrone. From each of the plotted points, the plotting is repeated, thus each point of the 24 h isochrone is the basis for multiple, usually three or four, distance potentials based on the speed prediction diagram (P2) for the second day of forecast. The outer limit of the resulting cloud of distance potentials is regarded the 48 h isochrone, also shown in blue. The least time track may now be constructed as the shortest connection between destination **B** and the 48 h isochrone, resulting in way point two (WP2), followed by finding the shortest connection between WP2 and the 24 h isochrone, thus defining WP1. The least time track, shown in black, is now defined as the direct connection between **A** - **WP1** - **WP2** and **B**.

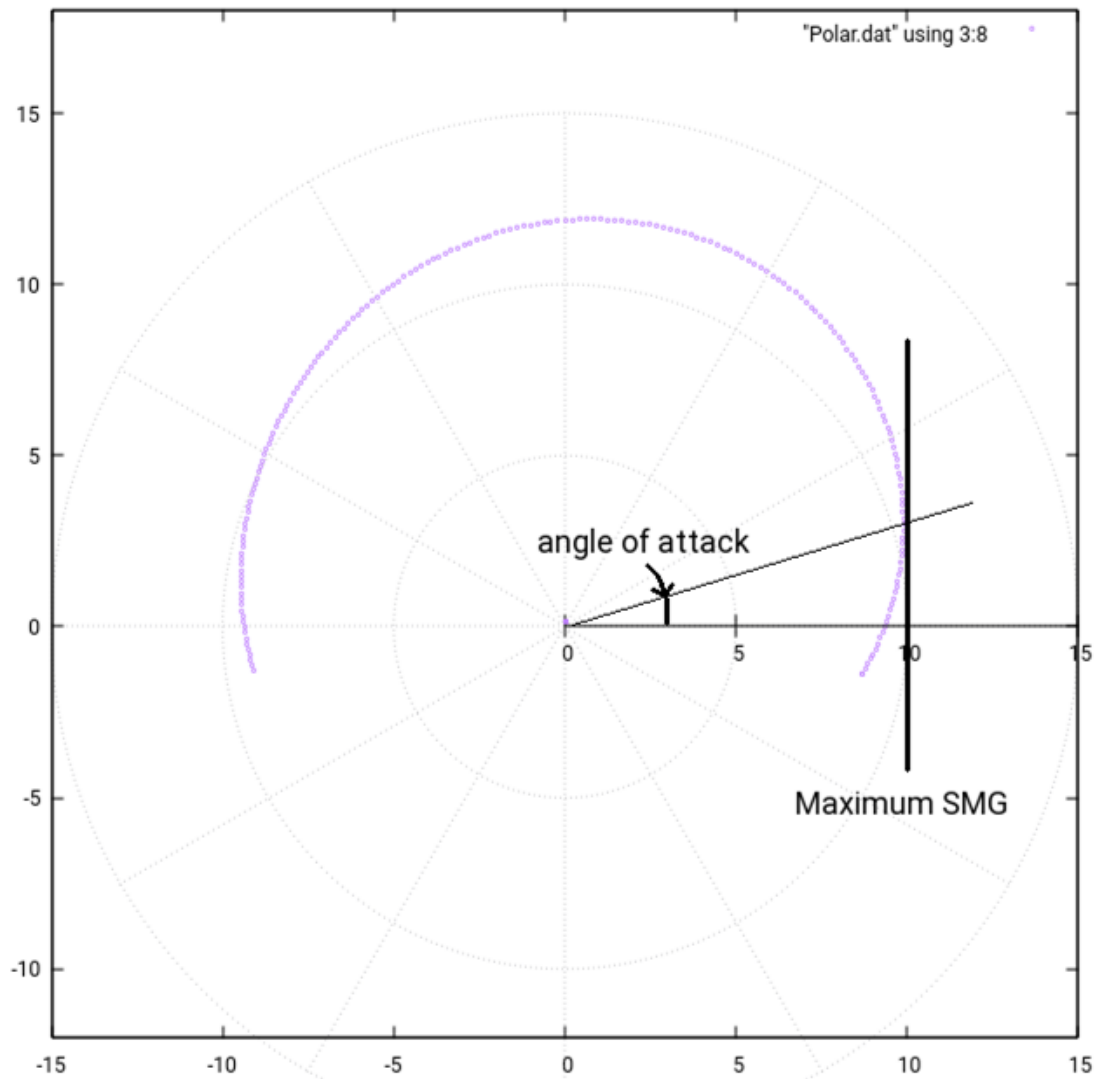


Fig.4: Maximizing SMG on Polar Prediction Plot

In the given example the forecast wind direction is assumed to have veered 30° for day two (P2). The effect of this forecast wind direction is incorporated in the constructed 48h isochrone of Fig.5.

Table II: S_w as function of θ_t at windspeed 20 kn. P1 83% confidence boundaries minimum and maximum distance per day

θ_t	S_w kn	24h progress nm predictor	minimum 24h	maximum 24h
0°	9.39	225	171	274
15°	10.23	246	206	298
30°	10.95	268	230	314
45°	11.49	276	n.a.	n.a.
60°	11.80	284	n.a.	n.a.

The constructed isochrones are based on the predicted wind direction and speed. From the forecast verification it has become clear that the forecast values must be regarded predictors and have an associated confidence interval. The magnitude of that interval, is expressed in Table I. For the second day of the forecast (P2) a speed prediction diagram is calculated in which the gray dots express the speed potential for the outer limits of the interval that is associated with the predictor. The magnitude of the interval for the one day (P1) forecast are plotted in the example route between **A** and **B**. Table II expresses the predicted speed through the water as function of the angle of attack, and its effect of the

estimated progress in 24 h. The confidence interval for P1 provides a lower boundary for the 24 h progress and an upper boundary.

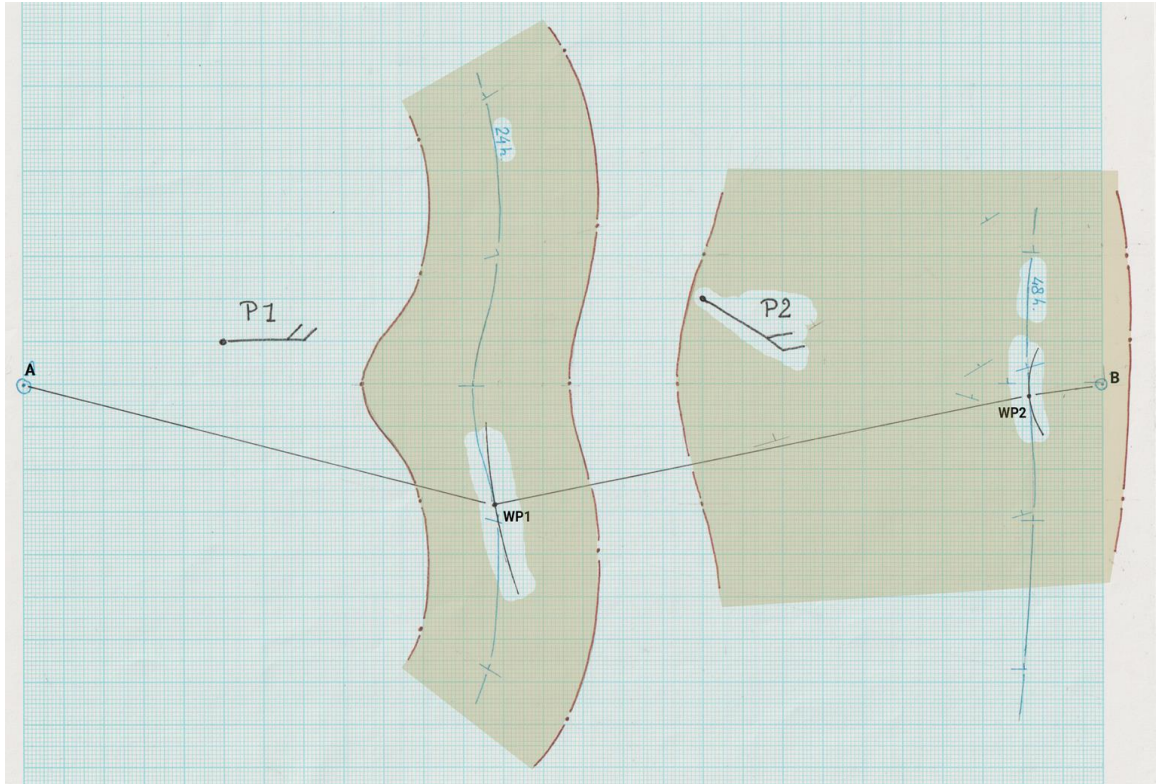


Fig.5: Construction of Least Time Track based on Isochrones and their Confidence Intervals

In Fig.5 this interval is expressed as the greenish shaded band around the 24h isochrone. The meaning of this band is that on the basis of the forecast accuracy for one day, i.e. P1, and dependent on the chosen angle of attack (the predicted progress will be within that band in 83% of the time.

The values for minimum and maximum progress at 45° and 60° angle of attack are left out (n.a.) because the deviation from the path to the relatively nearby destination is large and for this example with headwind towards the destination these courses are not deemed effective.

The forecast accuracy for two days (P2) is worse compared to that of P1, the interval for speed and direction, Table I, therefore is bigger. The effect of that lesser accuracy on the speed prediction is expressed in the diagram, Fig.6. The projected upper and lower boundaries of the 24 h progress are shown in Table III. As is expected the margin in progress is wider although the confidence level is slightly higher, i.e. 93%. This margin is visualized in Fig.6 as the greenish shaded band around the 48h isochrone.

Table III: S_w as function of θ_t at windspeed 20 kn. P2 93% confidence boundaries minimum and maximum distance per day

θ_t	S_w	24h progress nm. predictor	minimum 24h	maximum 24h
0°	9.39 kn	225	103	316
15°	10.23 kn	246	144	329
30°	10.95 kn	268	184	334
45°	11.49 kn	276	n.a.	n.a.
60°	11.80 kn	284	n.a.	n.a.

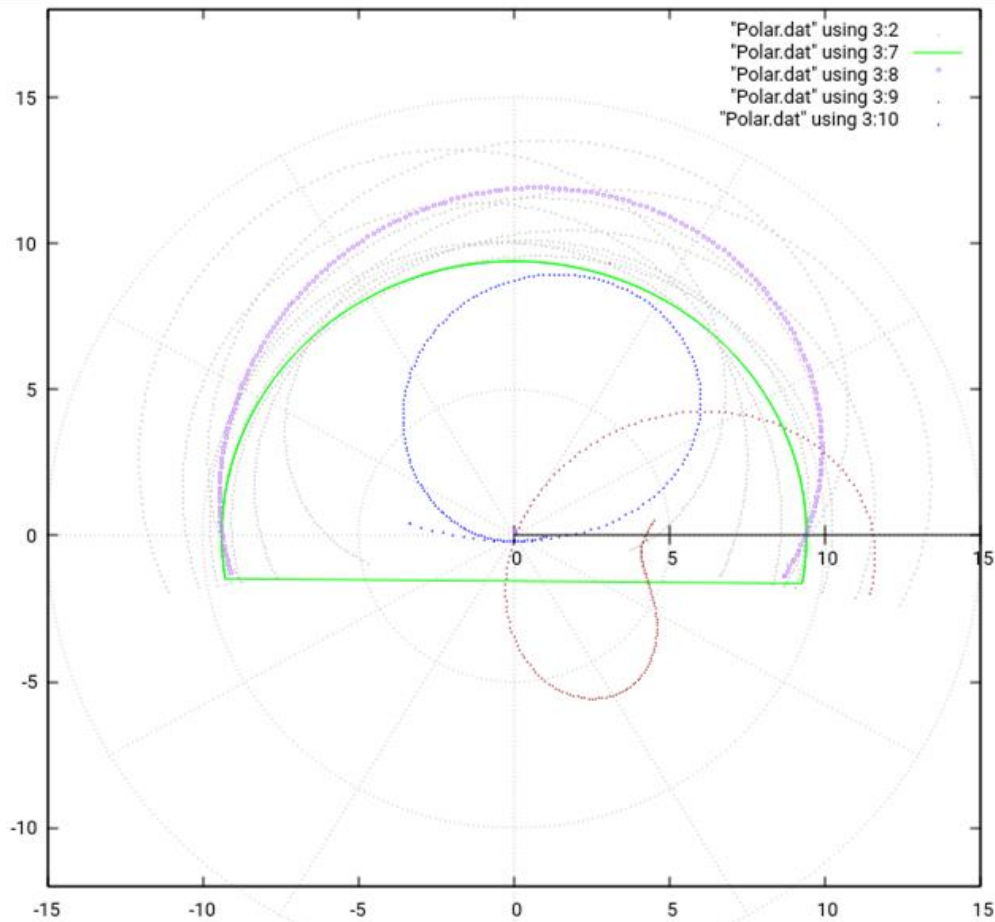


Fig.6: Speed prediction diagram Two day forecast, 30 tonnes conventional propulsion, 20 kn wind

From the example it might be concluded that multiple day weather forecasting is not accurate enough to calculate a least time route for a wind assisted propelled Motor Vessel. As is shown in the example plot for a relatively small, two day voyage, the width of the confidence interval is almost as wide as one day sailing which renders long term planning, i.e. allowing a deviation from the direct route in order to maximize the SMG, hardly usable.

In the analysis given here, only the effect of the confidence interval for wind speed and direction is used. Another major factor that affects speed hugely is sea state. Sea state, i.e. wave height, wave length or period and wave direction, can be expressed in a standardized effect on the speed through the water S_w . Although sea state can be regarded as a physical quality of the sea surface and can therefore be predicted on the basis of sustained wind speed and wind direction and its fetch, it will, however, be limited in accuracy too because wind speed and direction are limited in their forecast accuracy. Moreover, the interaction between wind and sea, i.e. current and tidal stream, and the effect of the depth of the water on wave speed are complicating factors that make an accurate prediction of the sea state at a particular location and point in time an even bigger challenge. Swell, i.e. past sea state that progresses without the underlying cause, may cross the present sea state resulting in a complicated pattern of two or more wave fields.

6. Conclusion

Given a wind assisted motor vessel and a sufficiently accurate prediction of the wind direction and wind speed, the predicted vessel's speed can be expressed as function of the amount of conventional propulsion and the chosen course, i.e. the wind's angle of attack. This speed prediction can be used in relation to the vessel's mission, i.e. destination and ETA. From the predicted weather and the associated predicted speed, isochrones can be constructed to define a least-time track from departure to destination.

The limited accuracy of meteorological models, however, lead to an increasingly bigger margin in speed prediction when a multiple day forecast is to be used. The analysis referred to in this paper was limited to wind speed and wind direction only. It may be expected that the limited forecast accuracy of sea state, ocean current and tidal stream will contribute to the grand total of uncertainties in the predicted speed. Notwithstanding these inaccuracies, the navigators on board of the pre - industrial ocean sailing vessels managed to derive seasonal optimum routes which are still published in *Admiralty (1973)*. Hence, the apparent necessity to employ competent professionals that have learned to utilize the wind assisted vessel safely, effectively and efficiently in the daily chaotic wind and weather with which they are confronted in the wild. Machine prediction, like the meteorological model validated in this analysis, i.e. Station Baltasound at the Shetland Islands, seems to lack sufficient quality to provide for long term prognosis to base a least time track on.

References

- ADMIRALTY (1973), *Ocean passages for the world*, The Hydrographer of the Navy
- HOFMANN-WELLENHOF, B.; LEGAT, K.; WIESER, M. (2003), *Navigation*, Springer, pp.299-335
- JOLIFFE, I.T.; STEPHENSON, D.B. (2020), *Forecast verification*, Wiley & Sons
- OLTMAN, J.-H. (2015), *Accseas North Sea region route topology model (nsr-rtm)*, Tech. Rep., IALA
- VAN DER HAM, C.J.; KOREVAAR, C.G.; MOENS, W. D.; STIJNMAN, P.C. (1983), *Meteorologie voor de zeevaart*, Unieboek bv, pp.304-312

Autonomous Shipping in Real Conditions: The Practical Experience

Alexander Pinskiy, Russian University of Transport, Moscow/Russia, al@marinet.org

Abstract

This paper describes the importance and the latest developments in the field of autonomous navigation (use of automatic and remote control of maritime vessels), focusing on practical experience gained during the Autonomous and Remote Navigation Project. It includes explanation of the methodology approaches and technical solutions, progress and outputs of the autonomous navigation trials in real commercial operation conditions.

1. Introduction

Implementation of autonomous, i.e. automatically and remotely controlled vessels in the spotlight of the leading maritime powers and the International Maritime Organization (IMO). Maritime Autonomous Surface Ships (MASS) shall make navigation much safer, while directly reducing ship operation costs for shipping companies. In general, this will be a new technological revolution in maritime transport, which can change the industry model itself.

The key economic effect from the introduction of MASS is undoubtedly formed by increasing the safety of navigation. The human factor, despite the widespread use of navigation automation technologies, remains the main cause of incidents at sea. According to one of the largest financial and insurance concerns, Allianz Global Corporate & Specialty AG, the cost of losses in shipping due to human errors in 2017 amounted to US\$1.6 billion, *Allianz (2018)*. According to various researchers, at least 80% of incidents in maritime transport occur due to human factors, and it is practically the only factor in collisions, grounding and incidents on board, *Hanzu-Pasara et al. (2008)*, *Grech et al. (2008)*.

Reduction of the human factor influence, in accordance with current IMO policy, is achieved through constantly improving requirements for crew training and organization of watchkeeping on board, which in practice means increase in the costs of training, certification and control of crew actions – what inevitably leads to increase in crew costs. At the same time, all over the world there is a steady decline of interest to marine professions, decrease in the number of those who go to work in this industry – and this additionally exert pressure on shipping companies in terms of availability of qualified personnel.

At the same time, according to the analysis of the Singapore Registry of Ships, *SRS (2014)*, the main elements of the human factor remain subjective reasons, such as loss of attention or violation of conventional requirements known to the crew, problems in work coordination, feeling unwell – while insufficient training and control are directly the reason for the very low number of incidents.

Today, the direct costs of shipping companies for the crew on board, including ensuring its life and safety, needs on board, are estimated as average 30-40% of ship operation costs or about 10% of the total trip rate, *Gardiner (2011)*. And, considering the current structure of ship operation costs, this is almost the only source of economic efficiency available to shipping companies.

Moreover, the reduction of the crew on board will allow to optimize other costs: from the fuel consumption due to slow steaming to the implementation of more efficient ship design with a smaller number of rooms with life support systems. The impact of slow steaming on the economics of shipping is available even right now: for example, a decrease in ship speed from 16 to 11 knots leads to fuel savings of about 50% per distance traveled, *Rødseth and Burmeister (2012)*. At the same time, slow steaming leads to an increase in the duration of the voyage, as a result of which the manning costs increase, what at some point neutralizes the savings due to lower fuel consumption. Reduction of manning costs would allow to extend the practice of slow steaming which have both economic and environment effect.

Therefore, the expectations of shipowners from the new technology are very high: this is probably the only case in many years when shipowners will not have to pay an increase in costs for safety improvements, but, on the contrary, will be able to reduce their operating costs. According to a study by the Norwegian Association of Shipowners, 5% of shipowners expect autonomous ships to appear in their fleet by 2025, and 50% expect this to happen by 2050, *NSA (2019)*. The Japanese Nippon Foundation plans that 10% of Japanese ships will become autonomous by 2030 and up to 50% by 2040, <https://fathom.world/japan-plans-to-make-50-of-domestic-fleet-unmanned-by-2040>.

2. The latest developments

In the early 2010s, the successes associated with the introduction of artificial intelligence and machine learning for unmanned technologies in other modes of transport, *IAPT (2012)*, and the rapid growth of maritime satellite telecommunications, as well as the shortage of personnel that European countries and Japan, served as prerequisites for the start of active practical developments in the field of autonomous navigation.

In 2012, with the support of the EU, the first large-scale research project on autonomous navigation, MUNIN (Maritime Unmanned Navigation through Intelligence in Networks), was initiated, the participants of which were organizations from Germany, Norway, Sweden, Iceland and Ireland, *Rødseth and Burmeister (2012)*. Within MUNIN, a theoretical concept of an autonomous ship, controlled by on-board automatics under the control of an ashore center, was developed. The project was completed in 2016 and became the first milestone in the modern development of autonomous navigation, having formed the main architectural, functional and technological approaches, <http://www.unmanned-ship.org/munin/news-information/downloads-information-material/munin-deliverables/>.

In 2016 in Norway, the Kongsberg with the support of the Norwegian government, created the world's first test area for autonomous ships in Trondheim and another one in 2017 in Horten, *NN (2017c)*.

In 2017, Rolls-Royce, together with the Finnish Technical Research Center VTT, opened a test area and a research center for autonomous ships in Turku, where the Falco remote-controlled ferry was tested already in 2018, *Gibson (2018)*. This became part of the international project AAWA (Advanced Autonomous Waterborne Applications) funded by the Finnish Technology and Innovation Funding Agency (TEKES) and implemented by a consortium including Rolls-Royce, Deltamarin, Inmarsat, DNV-GL, Intel and VTT, *NN (2018)*. In the same 2017, Rolls-Royce, together with Svitzer, with the support of the Danish Maritime Administration, tested the remote-controlled tug Svitzer Hermod in the port of Copenhagen, *NN (2017a)*. And Wartsila tested the remote control of the 80 m Highland Chieftain via satellite - for the first time outside the line of sight.

In 2018, ABB also tested the remote control in real conditions on the 34 m ferry Suomenlinna II in Finland. In October 2019, ABB signed a contract with Keppel Offshore & Marine for the trial operation of an autonomous tug at the Port of Singapore with the support of the Government of Singapore and the American Bureau of Shipping ABS. And in March 2020, Wartsila launched a joint project with the Port and Maritime Administration of Singapore to equip an autonomous tug, which is funded by the Maritime Administration and the government fund MINT.

These experiments clearly proved the viability of remote control of ships - which, however, does not solve the key problem of the human factor, but reduces it by transferring the decision maker from the ship to more comfortable conditions.

In December 2017, Kongsberg announced its flagship autonomous navigation project, the Yara Birkeland, an 80 m electric container ship that was to be the first self-guided vessel, *NN (2017b)*. At the first stage of operation of Yara Birkeland, the control systems must be tested under the control of the crew, then undergo trial operation in remote mode with the crew on board, then in autonomous mode, followed by reduction of the crew on board. The announced start of testing was shifted from 2018 and is now planned for 2022.

In Japan, in June 2018, the Ministry of Land, Infrastructure, Transportation and Tourism set a goal to ensure the introduction of autonomous courts in the country starting from 2025. In October 2018, the Centers for the Promotion of the Marine Innovation Strategy were established, where Oshima Shipbuilding, MHI Marine Engineering, NYK, MTI, MOL, Mitsui E&S Shipbuilding and others were involved, *NN (2019)*. In the same year, ClassNK announced the development of a Conceptual Design Guide for Automated/Autonomous Vessels.

In 2019, under the auspices of the Nippon Foundation and with the support of the Japanese government, the DFFAS (Designing the Future of Full Autonomous Ship) project was launched to ensure the introduction of autonomous ships in Japan from 2025. The project participants were 22 Japanese companies (by 2021 their number increased to 30), including NYK and NYK Group, NTT Communication, Furuno, JRC, Tokio Keiki, Japan Marine United Corporation, Nabtesco Corporation, Nippon Shipping Co., Mitsubishi Heavy Industries Co., Mitsubishi Research Institute Inc., Kinkai Yusen Kaisha and others. Subsequently, the project became part of the MEGURI 2040 program, which should ensure the transition to autonomous ships by 2040 for at least 50% of the Japanese merchant fleet, which now numbers about 4 thousand ships, *Bloomberg (2021)*.

As part of these projects, in September 2019, NYK completed the world's first transition of a large-capacity vessel supported by autonomous navigation tools: the Iris Leader vessel made a voyage from the port of Dongguan (China) to the port of Nagoya (Japan). The ship was controlled by the crew using the navigation system Sherpa System for Real Ship (SSR) as a decision support system, *MSC (2020a)*.

In China, autonomous ships are considered today as part of the national Smart Ship program being implemented in the country. In 2003, an Innovation Center for Intelligent Control and Applied Technology for Marine Equipment was established in China, with the support of which the construction of the first "smart ships" began in 2016. In 2018, the China State Shipbuilding Corporation, together with the China Classification Society, announced plans to build autonomous ships, which were supported by the Chinese government. The main focus of development lies in the field of control of technical facilities, which is based on the rapidly growing backlog of China in the field of engine building and the production of marine equipment.

In 2019, the corporation reported on an experimental voyage of a dry cargo ship, the technical means of which were remotely controlled, and in December 2019, China's first test of an autonomous vessel, the 13-meter JinDouYun-0, took place, *MSC (2021a)*. In the autumn of 2021, the electric container ship Zhi Fei (117 m, 300 TEU), *Cox (2021)*, was launched, which should be equipped with autonomous navigation systems and, in fact, repeat and surpass the Yara Birkeland project - but it is possible that the tests of the Chinese vessel will precede the start Norwegian tests.

In 2019 a group of Russian companies has started the Autonomous and Remote Navigation Trial Project as a world's largest trials in real commercial operations. The approach and the outputs of this project are presented below with detail of the practical experience obtained.

It is also worth noting the South Korean Autonomous Ship Development Project, initiated by the Ministry of Industry, Trade and Energy and the Ministry of Maritime Transport and Fisheries, which should achieve the 3rd level of autonomy by 2025. Government investments in the project amount to more than 130 million US dollars, the project participants are Hyundai Heavy Industries, Daewoo Shipbuilding and Samsung Heavy Industries and others, *Shin (2021)*.

Since 2017, the question of autonomous navigation is being considered by IMO: on the 98th-100th sessions of the Maritime Safety Committee (MSC). The 101st session approved the structure of a guideline for MASS trial projects, *MSC (2019a)*, which defines the requirements for MASS testing and trial operation. At the 100th session, four levels of autonomy of ships were determined, *MSC (2019b)* - so far only for the purpose of regulatory scoping exercise, but, probably, they will also be used in the future as an international classification. All leading classification societies in the world have also issued MASS guidelines, which reflects the existing high level of technological readiness for their

implementation: *DNV-GL (2018)*, *CCS (2018)*, *RS (2020)*, *BV (2017)*, *Class NK (2018)*, and others. The availability of separate technologies for autonomous navigation is also demonstrated by a number of trial projects carried out in recent years in various countries.

3. Autonomous and Remote Navigation Trial Project

Since the experiments in various countries have proved the feasibility of autonomous navigation technologies, the next step to be its implementation to the widespread practical operation. It is obvious, that new technologies are developing and maturing not in scientific centers or in R&D departments of technology companies, but in consumers utilizing them in their every-day practice. Like the aerial drones, where the existing design was developed more than 20 years ago, but real breakthrough came only after these drones became available for any company, even for any household. As soon as thousand people and organizations started to use aerial drones, we saw hundreds new ways of their usage – from TV cameras to pizza delivery – and we saw the real technical boom in this industry. The same should be done in the maritime industry as well.

The aim Autonomous and Remote Navigation Trial Project (ARNTP) was to open opportunities for every shipping company to try and to implement autonomous navigation solutions – facilitate the technology development in this area. As from 2019 the ARNTP is being implemented by three Russian major companies together with a number of technology companies and universities under umbrella of Industry Association MARINET, *MSC (2020b)*.

The aim of the project is to develop and to test standard set of technologies for MASS and approach for its implementation on different commercial vessels with different levels of current automation and with different operation conditions. The general purpose of the project is to open opportunities for a wide MASS trial operation by shipping companies under the flag of the Russian Federation since 2021.

The project involves the following commercial vessels by the major Russian shipping companies:

- Rabochaya, motor barge owned by Rosmorport, IMO: 9838371, MMSI: 273436710, home port: Saint Petersburg, project: HB900, currently operating in the Black Sea together with REDUT dredger;
- Pola Anfisa, general cargo ship owned by Pola Rise, IMO: 9851115, MMSI: 273448220, home port: Saint Petersburg, project: RSD-59, currently operating in the Mediterranean and Black seas; and
- Mikhail Ulyanov, shuttle tanker owned by SCF, IMO: 9333670, MMSI: 273328440, home port: Saint Petersburg, project: R-70046, operating in the Barents Sea.

Experimental remote control stations (RCS) are installed in the offices of Pola Rise (connected to m/v Pola Anfisa) and SCF (connected to m/v Mikhail Ulyanov), and on board of dredger Redut (connected to m/v «Rabochaya»).

Experimental hardware on board has been developed and installed in accordance with the project documentation agreed by the Russian Maritime Register of Shipping (RS), surveyed by RS after installation and does not create safety risks or influence other onboard systems of ships. The connection to existing on board systems was agreed with the systems manufacturers and shipowners, whilst the mechanical Mode Switch was installed on the connection line to actuators which provide physical link with ship bridge. In addition, a constant indication is available on board and in RCS regarding the status of mode switch and availability of autonomous navigation (a-Navigation) systems.

In 2019 a risk analysis was performed related to the functioning of new systems and arrangement of trials, which was taken into account as part of systems requirements and trial program. The trials program includes remote operation (via remote control station (RCS), with permanent contact with the supervising crew onboard), automatic navigation (using autonomous navigation system under the

supervision of the crew onboard and additional control by the remote operator), and automatic navigation in heavy traffic areas. While the implemented approach supposes symbiosis of automatic, remote, and manual modes of control during the same voyage, depending on the situation, the trials of remote operation and automatic navigation were split to get more clear results about the implementation of each specific system.

Preliminary tests of the systems were conducted on shore using dedicated simulators (including simulations based on the various field data gathered from the vessels during the first stage of the trials). The trial program provides full and constant control by ship's master during tests of automated and remote operation, immediate switch to normal operation in case of any errors or limitations: critical deterioration of weather conditions, intense shipping traffic, malfunctions on board etc.

On the basis of developed requirements to systems, results of preliminary on-shore tests and analysis of systems operation on board, in December 2020, the Russian Maritime Register of Shipping issued the Approval in Principle for systems of a-Navigation.

The core of the project is the probation of the comprehensive set of a-Navigation systems for high seas (including autonomous navigation system, optical surveillance and analysis system, coordinated motion control system, and remote control station) during real commercial voyages. From September 2020 data on systems performance during actual commercial operation of all ships is being collected and analyzed (without a possibility to influence the work of actuators). In February 2021 the trials continued with the phase of immediate control by a-Navigation systems of actuators on board under the crew's supervision and additional control by the shipping company, *MSC (2021b)*. During 2021 the trials were conducted during 28 commercial voyages, *MSC (2021c)*.

The architecture of the technical solutions consists both of traditional (incl. mandatory) systems and new solutions: Autonomous Navigation System, Optical Surveillance and Analysis System, Remote Control Station and Bridge Advisor, Fig.1.

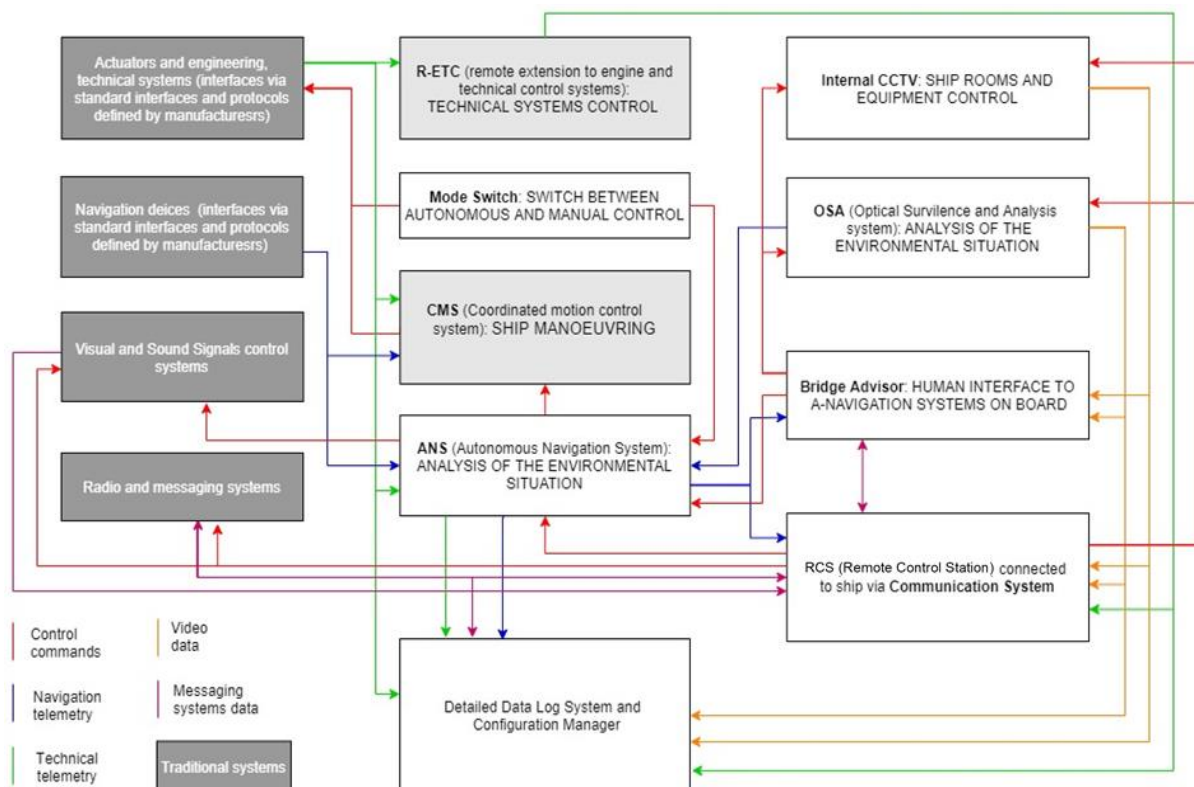


Fig.1: Architecture of the technical solutions within the ARNTP

This architecture is similar to the architecture developed during the MUNIN projects as well as the approach to the symbiosis and combination of various ship control modes on the same MASS and during the same voyage.

The methodology of ARNTP is the principle of Complete Functional Equivalence presupposes the full performance of all these functions, regardless of control methods, including through the use of automatic and remote control. On the one hand, it guarantees that MASS, when interacting with other actors, are guided by and perform well-known and mandatory functions, and on the other hand, it allows to operate MASS within the framework of the current international regulation as is, without requiring to change it. Requirements to every a-Navigation system were formulated in accordance with this principle: for example, the minimum parameters of visual detection of objects should not be lower than the accuracy of human vision, the set of analyzed data should correspond to the one that an officer should receive and interpret, etc.

To ensure this principle, a-Navigation systems are projected onto the current functions fulfilled by the crew (as it is provided in International Convention on Standards of Training, Certification and Watchkeeping for Seafarers (STCW Convention) and other regulation): gaps serve as functional requirements for these systems or an explicit restriction on their use at the current moment (if it is impossible to implement the necessary requirements now). At the same time, this makes it possible to ensure a gradual process of introducing a-Navigation technologies by a shipping company, when, depending on the level of automation of ship processes, certain functions can be excluded from the set of functions performed by the crew members, with a corresponding reduction of the ship's crew.

Following the Complete Functional Equivalence principle, the autonomous navigation system (ANS) performs the functions of automatic analysis of the environment, the passage along a given route (in automatic mode and remote control mode), offering automatic decision-making on maneuvering while taking into account the parameters of the vessel and COLREGs-72 provisions. ANS includes Sensor Fusion Module (SFM), Automatic Collision Avoidance Module (ACAM) and ANS Client (representing extended functionality of ECDIS).

The Sensor Fusion Module (SFM) integrates, synchronises and validates navigational data from different sources such as the radar, AIS, positioning, compass, weather station, etc, and the optical system OSA. This is similar to an officer onboard who has to gather data from all of these navigational devices, his eyes and integrate it into a single picture in his mind.

The Automatic Collision Avoidance Module (ACAM) keeps to the route and calculates the maneuvers of the vessel to avoid collisions with other vessels and navigational hazards in accordance with rules determined by COLREGs-72. These detailed rules are provided as per clear official recommendations from the Russian Federal Agency for Marine Transport for automatic collision avoidance systems. Strictly determined algorithms of this nature make MASS 100% predictable, even when placed in comparison with a traditionally crewed ship.

The ANS Client integrates all the data from mandatory and additional electronic charts (such as ICE or SAT images) and any other available information, and presents it via human interfaces that are similar to ECDIS.

The Optical Surveillance and Analysis System (OSA) is an optical system that detects and recognises surrounding objects. It transmits this data in a machine-readable form to the ANS while also sending the processed video image to human interfaces (such as the Remote Control Station and Bridge Advisor).

The OSA resolves the challenging task of fulfilling conventional requirements of providing visual observation in a completely autonomous mode while sitting in parallel to human-operated remote mode. Although we are only beginning the process of training the OSA neural network to reliably recognize any objects in different conditions at this current time, we believe that this automated approach that

does not rely on human-operated remote controls will pay off in the future. This therefore goes a step further than simply moving human operation and oversight from onboard to shore.

At the same time, the OSA allows us to improve the quality of situational awareness for humans, both on board and in the RCS. Augmented reality (an image with additional indicative information) and even completely virtual models (in case of poor visibility or problems with the communication channel between the remote control and the vessel) may well become common everyday tools of navigators in the near future.

Internal CCTV provides various tasks like indoor video recording, automatic control over the condition of rooms (movement, change of geometric parameters, etc.), equipment (change of indication, switch states, etc.), cargo (displacement, crumbling, tilt and other parameters), and the transmission of this video information to the Bridge Advisor and Remote Control Station (RCS).

The Remote Control Station (RCS) is a workstation for a remote control operator and is designed to solve the entire range of remote monitoring and control tasks. It is located outside the controlled vessel and is the equivalent of a highly ergonomic ship's bridge and a central control station, Fig.2.



Fig.2: Remote Control Station (Rosmorport)

RCS is designed to simultaneously display to operator various data, those equivalent to the information on the ship's navigation bridge:

- Navigation systems interface including ECDIS equivalent, autonomous navigation system and control interfaces of ship onboard radars;
- Video information display interfaces on the ambient surroundings and control of the optical surveillance and analysis system;
- Interfaces of the remote engine and technical monitoring system allowing surveillance and control of the unattended engine room;
- Interfaces of video information display and internal ship's CCTV control;
- Interfaces of the ship motion control (joystick system);
- Radio interaction terminals for an RCS operator to interact with the onboard radio equipment (VHF and MF-HF radio stations, MF-HF radiotelex, Inmarsat station, Navtex receiver and public address system) connected to the corresponding devices on board;
- Microphones and speakers for interaction with the public address system and receiving audio signals and video communication with the crew on board;
- Indicators and interfaces of the a-navigation settings and diagnostics system.

The Coordinated Motion Control system (CMS) transmits ANS commands to the ship actuators. It thus performs the same functions as the helmsman who converts the officer's orders to actions regarding steering and engine control. By CMS we consider ship heading or a trajectory control system which is already understood and used on a small but growing segment of highly automated vessels. Currently CMS allows support through human control or follows a given trajectory with high accuracy while taking into account existing weather conditions and the ship model. By connecting CMS to ANS we allow for the control of propulsion and steering systems both automatically and remotely.

The trials program includes remote operation (via remote control station (RCS), with permanent contact with the supervising crew onboard), automatic navigation (using autonomous navigation system under the supervision of the crew onboard and additional control by the remote operator), and automatic navigation in heavy traffic areas. While the implemented approach supposes symbiosis of automatic, remote, and manual modes of control during the same voyage, depending on the situation, the trials of remote operation and automatic navigation were split to get more clear results about the implementation of each specific system.

As of December 2021, the trial program is wholly fulfilled on Rabochaya, and currently, Rosmorport is continuing experimental use of a-Navigation systems onboard Rabochaya in its regular operation. The trial program on Pola Anfisa is near completion and is planned to be fulfilled in March 2022. The trial program on Mikhail Ulyanov is postponed due to requirements for a planned upgrade of the existing systems connected to the a-Navigation systems and to be continued in 2022.

In parallel, the national regulation of MASS use is developed. The following three levels of legislation have been developed to ensure widespread operation of the MASS under of the current international regulation, *MSC (2020c)*:

- Federal Law "On Amendments to the Merchant Shipping Code of the Russian Federation and certain legislative acts of the Russian Federation in terms of legal relations arising from the use of autonomous ships". It introduces the conceptual apparatus and fundamental provisions into national legislation at the level of the Merchant Shipping Code and individual federal laws taking into account recent results for Regulatory Scoping Exercise on MASS use conducted by International Maritime Organization (IMO);
- Government Decree "On conducting an experiment for the trial operation of autonomous vessels under the State flag of the Russian Federation in the period from 2021 to 2025". It regulates the operation of MASS under the Russian flag for a "transitional" period until 2025 and defines the requirements by the Russian flag administration to the organization of such operation, taking into account the IMO Interim Guidelines for Mass Trials;
- Technical regulation of a-Navigation means: Guidelines on the classification of MASS by Russian Maritime Register of Shipping and Rules for the COLREG-72 application in automatic control systems (the latter are algorithmized in univocal and determined way the provisions of COLREG-72).

4. Outputs of the practical operation

The practical experience of MASS trials during ARNTP shows of a very wide range of issues that appear when using autonomous navigation means in real conditions and vary depending on the specifics of the vessel, shipping company, region, etc. Without the widespread use of MAAS in the real practice of shipping companies, it is impossible to assess the real features of the application of a-Navigation, and, therefore, to formulate further specific regulation of MASS.

The results of the MASS trials can indicate that from seafarer, shipowner, and administration views, a MASS can be considered as a traditional ship, but with more capabilities of supervision and control options. Shipowner and master, at that, continue to play their roles as responsible persons while the options available allow them to use autonomous and remote control means to add or replace the

traditional ones in the cases when safety and efficiency of shipping can be increased. Also, triple supervision onboard (automatic systems, remote operator, and crew onboard) can substantially increase safety at the most dangerous ships like large passenger ships and ships carrying dangerous goods.

Implementation of the complete functional equivalence principle, in complying with the current COLREGs requirements as well, provides that other navigation participants do not need to pay any special attention to MASS. From the point of view of other navigators, such MASS do not differ from the traditional ships at interactions that ensure their coexistence within the current safety regulation as well.

In order to comply with the principle of full functional equivalence, we see the need for a symbiosis of the three control methods on MASS - automatic, remote and manual, the choice of each should be determined by the shipping company depending on the prevailing conditions, the type of vessel and the nature of its operation. For example, the a-Nav systems currently being tested in Russia make it possible to automatically control a ship on the high seas under normal conditions in accordance with COLREG-72, radio communication with other ships is carried out using the remote control, and traditional control is used in extremely difficult conditions, including the situations where the officer in charge of the watch is nowadays required to immediately notify the master of the ship in accordance with the STCW Code (Part A, Chapter VIII - Watchkeeping). But in any case, at each moment of time, MASS as a whole shall comply with the principle of complete functional equivalence - i.e. the full range of functions currently provided for the crew on board.

The trials of remote operation were made in February – April 2021 and indicated that a remote operator can provide watchkeeping and control MASS in normal conditions in high seas at the same level of safety as a navigator onboard. The major issues limiting a broad commercial use of the remote control concern telecommunication reliability and night vision:

- Reliable telecommunication between the RCS and the controlled MASS is vital for remote operation: even a several-second break during manual maneuvering by a remote operator may cause danger for safe navigation. While there are WiMAX and LTE technologies available for a short distance (up to 25 miles) that can provide a sufficient level of reliability, it is obvious that the only option for long distances is satellite communication. The standard level of sea mobile satellite services hardly maintains the required reliability, so it is necessary to agree with telecommunication providers on specific services for MASS remote operations with significantly higher costs.
- Currently, the only way to provide a sufficient level of visual observation by a remote operator during nighttime is to use thermal cameras. This will substantially increase the equipment price for autonomous ships and require the remote operator to have dedicated skills in environment assessment relying on infrared images.

It should be additionally mentioned that currently, there are no remotely operated marine radars, while the only data transmission from onboard radar to RCS is not enough to ensure functional equivalence to the navigator on the bridge. While most engineering systems installed at the ships with unattended machinery spaces can be controlled via RCS, the currently used marine radars do not have such functionality

The trials of automatic operation have been conducted since February 2021 in combination with remote control and since May 2021 with the only use of automatic control. The overall duration of automatic navigation during the trials in 2021 is more than 100 hours during different voyages. The general results of the trials, with some reservations, indicate that in normal conditions an automatic navigation can provide the same level of efficiency as human control, and the autonomous navigation system mostly can recognize on its own the situations when the automatic control is restricted (as it is prescribed by the Recommendations on COLREGs applications for MASS use by the Federal Agency of Maritime and River Transport of the Russian Federation). At the same time, currently it is inferior in quality of control by a highly qualified navigator. The major issues concern non-standard situations:

- Collision avoidance algorithms based on direct COLREGs provisions are properly working in standard situations, while in non-standard cases (with various possible interpretations of the COLREGs provisions, especially in heavy traffic areas) either human control or algorithm based on “ordinary practice of seafarers” is required. Since currently there are no common formal explanations of the “ordinary practice of seafarers”, this opens a way for different approaches for collision avoidance in non-standard situations by various manufacturers, which may lead to risks for safe navigation.
- Since automatic control is limited in some circumstances, it is necessary to plan in advance when during the voyage a human control (either by the crew onboard or a remote operator) might be required. Such planning is one of the new competencies for seafarers operating MASS.
- Understanding of signs and triggers of non-standard situations, when automatic control is restricted, or its efficiency is limited, as well as failures of a-Navigation systems, is another important new competence for seafarers operating MASS. Also, this shall be reflected in the Safety Management System of the shipping company operating a MASS.
- Integration of a-Navigation systems with the existing control systems onboard retrofit (traditional) vessels could be challenging since the last ones are not designed for control by external computer systems. That requires to implement integration on case-by-case scenario with potentially required changes in the existing systems, which increase complexity and cost of implementation of a-Navigation on retrofit vessels.

Also, for effective a-Navigation development, it would be reasonable to facilitate safety regulation enhancement for all vessels by formalizing “ordinary practice of seafarers”, which will allow avoiding risks identified above and improve seafarers’ training, and also by expanding mandatory AIS use to all ships and offshore platforms/constructions. Such an approach will substantially improve the situation awareness not only for the MASS but for traditional ships and monitoring services. Also, the sharing of real-time information on MASS maneuvers via AIS (VDES) with other autonomous and traditional ships could be a promising opportunity for safer and more transparent MASS operations.

5. Conclusion

The autonomous navigation is one of the most important new technologies for the maritime industry and it requires strong practical experience for the further development.

To ensure the widespread use of MASS in real conditions, they must fully enforce the implementation of all existing management functions provided for by the current international regulation for the ship's crew. This will ensure, on the one hand, the uniformity of regulation in relation to the global fleet, and on the other hand, it will reduce the risks and fears regarding the new technology. The Complete Functional Equivalence principle is a proper ground for this.

The latest developments and ARNTP, in particular, prove the availability of the a-Navigation technologies and establishing common approach to the system architecture and requirements.

The outputs of the a-Navigation trials in real operation conditions provided in the paper show that we are very close to the new era of autonomous shipping. Some technical and regulatory obstacles are being identified and would be solved in the nearest future.

References

ALLIANZ (2018), *Safety and shipping review*, Allianz Global Corporate & Specialty

BLOOMBERG (2021), *First Autonomous Cargo Ship Faces Test With 236-Mile Voyage*, Bloomberg

BV (2017), *Guidelines for Autonomous Shipping*, Bureau Veritas

- CCS (2018), *Guidelines for autonomous cargo ships*, China Classification Society
- Class NK (2018), *Guidelines for Concept Design of Automated Operation / Autonomous Operation of ships (Provisional Version)*, Class NK
- COX, A. (2021), *China's first autonomous boxship readies to enter service*, Splash247, <https://splash247.com/chinas-first-autonomous-boxship-readies-to-enter-service/>
- DNV-GL (2018), *Autonomous and remotely operated ships*, DNVGL-CG-0264
- GRECH, M.; HORBERRY, T.; KOESTER, T. (2008), *Human Factors in the Maritime Domain*, CRC Press
- GARDINER, N. (2011), *Ship Operating Costs 2011-2012: Annual Review and Forecast*, Drewry Maritime Research
- GIBSON, R. (2018), *Rolls-Royce and Finferries demo world's first fully autonomous ferry*, Cruise and Ferry
- HANZU-PAZARA, R.; BARSAN., E.; ARSENIE, P.; CHIOTORIOU, L.; RAICU, G. (2008), *Reducing of maritime accidents caused by human factors using simulators in training process*, J. Maritime Research V/1
- IAPT (2012), *A global bid for automation: UITP Observatory of Automated Metros confirms sustained growth rates for the coming years*, Int. Association of Public Transport
- MSC (2019a), *Interim Guidelines For Mass Trials*, MSC.1/Circ.1604
- MSC (2019b), *Report of the Maritime Safety Committee in its 100th session*, MSC 100/20
- MSC (2020a), *Report on MASS trials conducted in accordance with the Interim guidelines for MASS trials*, MSC 102/INF.8 submitted by Japan
- MSC (2020b), *Ongoing MASS trials in the Russian Federation*, MSC 102/5/29.
- MSC (2020c), *Development of interim regulatory measures for operation of MASS in the Russian Federation*, MSC 102/5/14
- MSC (2021a), *Report on MASS trials*, MSC 104/INF.14 submitted by China
- MSC (2021b), *Comments on document MSC 102/5/29*, MSC 103/5/9
- MSC (2021c), *Results of Maritime Autonomous Surface Ships (MASS) trials conducted in the Russian Federation in 2021*, MSC 105/INF.12
- NN (2017a), *Test of Remote Controlled PSV Successful*, The Maritime Executive
- NN (2017b), *Norway Provides Grant for Construction of Yara Birkeland*, World Maritime News
- NN (2017c), *New Norwegian Autonomous Shipping Test-Bed Opens*, The Maritime Executive
- NN (2018), *Commercial remote controlled ships by 2020, says AAWA*, Digital Ship
- NN (2019), *Maritime autonomous surface ships: development trends and prospects*, Mitsui & Co. Global Strategic Studies Institute Monthly Report

NSA (2019), *Think Ocean - Maritime Outlook Report 2018*, Norwegian Shipowners Association

RØDSETH, Ø.J.; BURMEISTER, H.C. (2012), *Developments towards the unmanned ship*, Int. Symp. Information on Ships (ISIS), Hamburg

RS (2020), *Guidelines on the classification of maritime autonomous surface ships (MASS)*, ND No. 2-030101-037, Russian Maritime Register of Shipping

SHIN, J.H. (2021), *South Korea embarks on ambitious autonomous ship project*, The Korea Herald

SRS (2014), *Profile of Maritime Incidents*, SRS e-Bulletin Q1, Singapore Registry of Ships

Evaluation of Ship Energy Models and Route Optimization

Pauline R. Bellingmo, SINTEF Ocean AS, Trondheim/Norway, pauline.bellingmo@sintef.no

Brian Murray, SINTEF Ocean, Trondheim/Norway, brian.murray@sintef.no

Ulrik Jørgensen, SINTEF Ocean AS, Trondheim/Norway, ulrik.jorgensen@sintef.no

Armin Pobitzer, SINTEF Ålesund AS, Ålesund/Norway, armin.pobitzer@sintef.no

Svein P. Berge, SINTEF Ocean AS, Trondheim/Norway, svein.berge@sintef.no

Ole G. Rørhus, Norwegian Electric Systems AS, Ålesund/Norway,
ole.rorhus@norwegianelectric.com

Abstract

A weather routing system for a ferry in Norway has been developed. In this paper three different models for estimating the energy consumption have been evaluated. The three energy models include two data-driven models, i.e., a linear regression model and a hybrid model, and a simulation-based energy model. The hybrid energy model performed best with the highest accuracy and at the lowest run time. Moreover, using the hybrid energy model, the weather routing system has been tested and evaluated. The results show typical energy savings up to 1.5% are achieved.

1. Introduction

Today, more than 80% of the volume of international trade in goods is carried by sea (UNCTAD, 2021). By 2050 the total transport activity is expected to more than double from 2015 (ITF, 2021). According to the International Maritime Organization's initial greenhouse gas strategy, international shipping should reduce CO₂ emissions by 50% by 2050 compared to 2008 (IMO, 2019). This urges for radical change and innovation in the maritime sector. There exist different measures to reduce the emissions from shipping, some are related to the ship design, others to the operation of the ship. One such measure that applies to operational ships is weather routing, where you try to determine the optimal route that gives the lowest energy consumption given the weather conditions. By reducing the energy consumption of a vessel, the operating company will save money and reduce the environmental footprint.

Existing literature and services mainly focus on weather routing for deep-sea shipping where a large amount of energy can be saved by avoiding the roughest weather, e.g. StormGeo's S-Suite, <https://www.stormgeo.com/products/s-suite/s-planner/>, or NavStation, <https://www.navtor.com/weather-solutions>. For deep-sea shipping, route optimization is estimated to reduce emissions by 7% (Lindstad, 2013). However, there is also great potential for energy savings using weather routing on short-sea shipping. A weather routing system for short-sea shipping estimated the ratio of cost saving between 3% and 18% depending on the weather conditions (Grifoll et al., 2018). In the EU, short-sea shipping made up half of the total sea transport of goods at sea to and from the main port in 2020 (Eurostat, 2022). This means that emission reductions in short-sea shipping will have a considerable effect on the overall CO₂ emissions.

A prerequisite for utilizing weather routing is to have a model that predicts the energy consumption of the vessel accurately and quickly. Given a numerical vessel model and sea and weather conditions, the energy consumption can be estimated using a simulation tool. A vessel model consists of differential equations that describe the ship. The parameters in these equations, such as added resistance from the environment, can be estimated using towing tanks. The accuracy of a vessel model depends on the number of differential equations used and the accuracy of the vessel parameters. Typically, using a larger number of differential equations will give a more accurate vessel model. However, a large set of differential equations may be computationally demanding to solve and thus time consuming. Hence, when applying simulation for energy estimation in weather routing, simpler models are usually implemented, as shown in (Kobayashi et al., 2015), where a simulation-based method is presented for weather optimization for deep sea voyages.

With large amounts of operational ship data and environmental data available, there has been an increased interest in using machine learning (ML) methods for estimating the energy consumption. Often, regression models are used to predict the energy consumption using engine RPM, ship velocity and weather data as inputs. Various machine learning models are applied in regression settings, with linear regression among the least complex. Artificial neural networks (ANNs) have in recent years gained popularity due to their state-of-the-art performance in many fields e.g. computer vision (Voulodimos et al., 2018). Using ANNs trained on vessel and environmental data, the shaft power can be estimated with a mean absolute percentage error (MAPE) between 2-8% (Bui-Duy and Vu-Thi-Minh, 2021; Parkes et al., 2018, 2022; Petersen et al., 2012). However, ANNs are most effective in the presence of large amounts of data. With limited data, deeper networks are more likely to overfit to the dataset. The multi-layer perceptron (MLP), also known as a fully connected network, is often utilized in regression tasks. If one views a single layer of such a network without activation functions, it will function as a linear regressor. As such, linear regression is a shallow variant of an ANN. A comparative study of different ML models for predicting fuel consumption for ships showed that a simple linear regression model attained comparable results with the deeper and more advanced ML methods, i.e. ANN (Gkerekos et al., 2019).

A challenge when using ML models is that they are often used as black boxes, meaning that the underlying causality is unknown. Facilitating trust in such methods is a challenge, as the interpretability of ML models is limited. Pure ML methods fit a model to the data without knowledge of the underlying relationships. To increase the trust of ML models, they are combined with physical knowledge of the data. This is called hybrid physics-guided ML. Hybrid physics-guided ML have been applied within the fields of air-foil aerodynamics (Pawar et al., 2021) and energy fusion (Piccione et al., 2020) with promising results. To the authors knowledge, hybrid models have still not been used to estimate the energy consumption of vessels.

This study presents results from a research project named Smartshiprouting (THE RESEARCH COUNCIL OF NORWAY, 2019). The work in this paper is a continuation of the weather routing system described in (Bellingmo et al., 2021) and (Jørgensen et al., 2022). The previous papers have described the development of three different models used to predict the energy consumption of a ferry in the transit phase. This includes a linear regression model, a hybrid physics-guided machine learning model, and a simulation-based model. In this paper, these energy models will be evaluated thoroughly based on select Key Performance Indicators (KPIs). Moreover, the weather routing system will be tested and evaluated.

2. Use Case

To develop a weather routing system, data was gathered from an electrical car ferry in Norway, see Fig.1. The ferry operates between two ports. There are several ferries operating on the same route, forcing the ferry have an arc shaped route, i.e. not the shortest possible route, in order to keep a safe distance to the other ferries. This can be seen in the position track of the ferry from one day illustrated in Fig.2.



Fig.1: Use case ferry, source: Fjord1

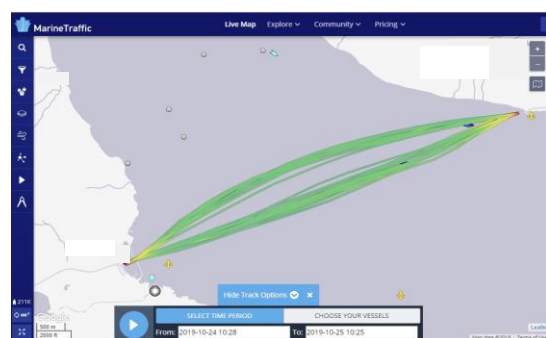


Fig.2: Operational track pattern, source: Marinetrtraffic

For this study, we have set up a logging system to continuously send operational data. Data from more than 2200 trips have been gathered and used for establishing the energy model, training, and testing. The weather routing system is developed for the transit phase, as it is the longest and most energy consuming phase with the most intricate interplay between vessel and environmental forces (Bellingmo et al., 2021). This weather routing system has been developed for research purposes and it is not currently used in operation.

2.1 MetOcean Conditions

Fig.3 shows the MetOcean conditions in the area where the ferry operates for a period of approximately four months. In this area, the ferry experiences wind from all directions with speeds from 0 to 20 m/s, with moderate wind from the southwest representing the most common condition. The current mainly comes from the northwest or southeast, following the shape of the fjord the ferry operates in, Fig.2. The data includes current speeds up to 0.7 m/s. Regarding the waves, the majority comes from the northwest, where the fjord is open towards to open sea, with significant waves heights below 1.5 m.

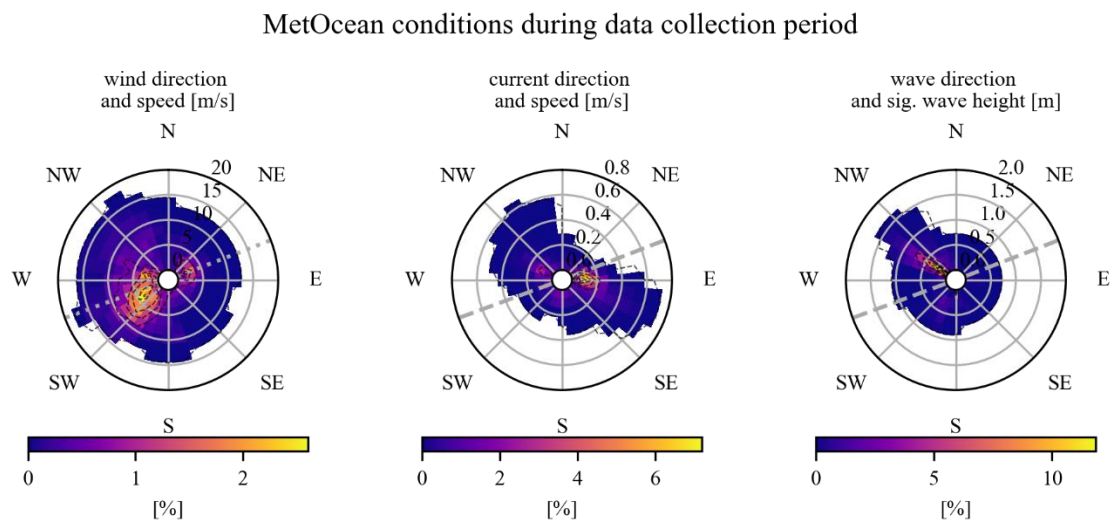


Fig.3: MetOcean conditions in area of ferry's operation. Directions given follow meteorological conventions, i.e. indicate the direction wind, currents, and waves are coming from. Color indicates share of collected data with a specific combination of direction and strength of the individual variables. Dotted lines represent average course over ground for the two legs of the ferry route.

3. Energy Models

Three energy models used to predict the energy consumption of a ferry have been developed (Bellingmo et al., 2021; Jørgensen et al., 2022). This includes a linear regression model, a hybrid model, and a simulation model. All the energy models estimate the energy consumed by the ferry in the transit phase. When referring to the energy consumption, we focus on the propulsion energy alone.

3.1 Linear Regression Model

The first energy model is a data-driven machine learning (ML) model, more specifically a linear regression model. The ML model uses MetOcean data and operational data from the ferry to estimate the energy, Fig.4. An initial version of the linear regression model is described in (Bellingmo et al., 2021). The model was improved in (Jørgensen et al., 2022) by including vessel draft and trim measurements and expressing the model parameters such that the correlation between them is minimized. The model estimates the energy based on average speed over ground (SOG), longitudinal and transverse current and wind speed, wave encounter frequency, significant wave height (H_s), trim, and draft.

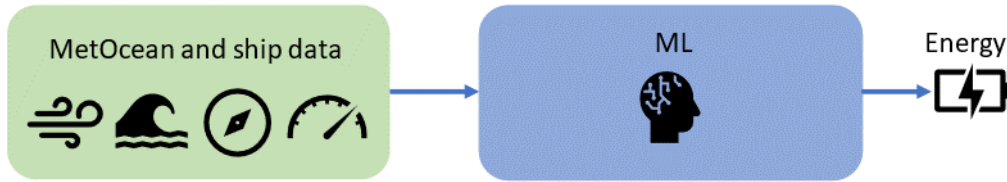


Fig.4: Linear regression model

In this study, linear regression is utilized to predict the energy consumption. Linear approaches are typically more interpretable than more complex approaches, such as deep neural networks. Furthermore, with limited data, deeper networks are more likely to overfit to the dataset, reducing the generalizability of the model. It was, therefore, deemed appropriate to investigate the use of linear regression, both due to the existence of limited data, i.e. 2200 trips, as well the enhanced interpretability of such models.

3.2 Hybrid Model

In (Jørgensen et al., 2022) a hybrid physics-guided model (hereafter referred to as hybrid model) was developed. This model is an extension of the linear model, combining physical models with a linear regression model, Fig.5. The model utilizes known physical relations between the input parameters and the energy consumption, e.g. how wind and current affect the lift and drag forces on the vessel. Such relationships are non-linear, and their inclusion in the model thereby provides a layer of non-linearity. Speed over ground squared was also added as an input parameter, such as to add further non-linearity to the model. In addition to the original input parameters used in the linear model, a set of enhanced physics-based parameters is used as input to the regression model. This contributes to discover further unknown relationships in the data. Hence, the hybrid aspect of the model can be considered an initial transformation of the data to attain more meaningful features. Machine learning is then applied to these features to learn a second transformation of the data that maps to the energy consumption of the vessel.

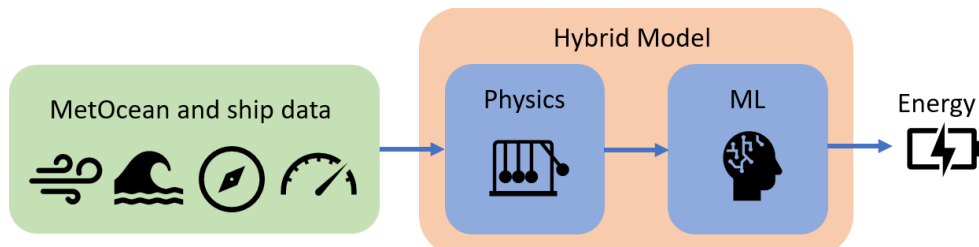


Fig.5: Hybrid energy model

3.3 Simulation

The third energy model is a simulation-based model as illustrated in Fig.6. More specifically, it is a discrete event simulator named Gymir developed by SINTEF Ocean. Gymir is presented in (Dæhlen et al., 2021) and can be used to evaluate ship concepts in realistic conditions given a vessel model. The simulator is mainly used in the vessel's design phase where no or little data is available. As presented in (Bellingmo et al., 2021), the simulation-based energy model utilizes a vessel model prepared by the ShipX numerical software package (Fathi, 2018; Fathi and Hoff, 2017). For a fixed draft and trim, ShipX uses a 3D-model of the hull and potential flow strip theory to compute the residual resistance. Note, however, that the current vessel model shape does not apply very well with strip theory. Moreover, the vessel has gone through physical changes after creation of the model and the vessel model used in the simulation is only valid for a certain loading condition and trim angle. To have a more accurate energy estimation for different loads and trim angles, multiple vessel models must be provided, and values need to be interpolated between them. However, for this study, only one vessel model is available. This vessel model is developed for medium load and with a levelled trim angle. Due to all the inaccuracies, we cannot expect accurate results from the simulation, but it will nevertheless provide important insights into the model comparison.

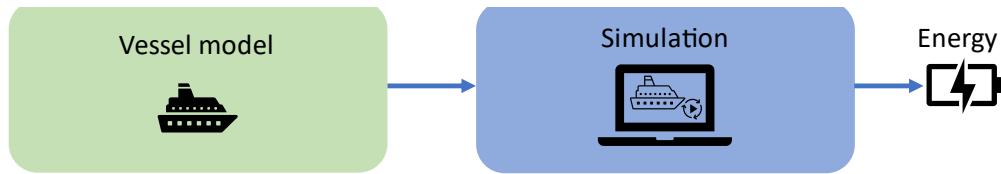


Fig.6: Simulation model

4. Optimization

A route optimizer has been developed to find the route with the lowest energy consumption for the ferry. The methodology for developing the route optimization is described in (Bellingmo et al., 2021). As this study focuses on the transit phase, the optimization only optimizes the route in transit. The route optimization is illustrated in Fig.7. The inputs to the optimization are the ferry schedule, trim and draft measurements from the vessel before departing, weather forecast, and an initial route. The route optimization modifies the geography and speed profile of the initial route and estimates the energy consumption using the energy model. The optimization is limited by the required time of arrival given by the ferry schedule and a safety zone where the vessel can safely operate. Comfort is not included as an optimization criterion. Once the optimization process converges, it outputs an optimal route.

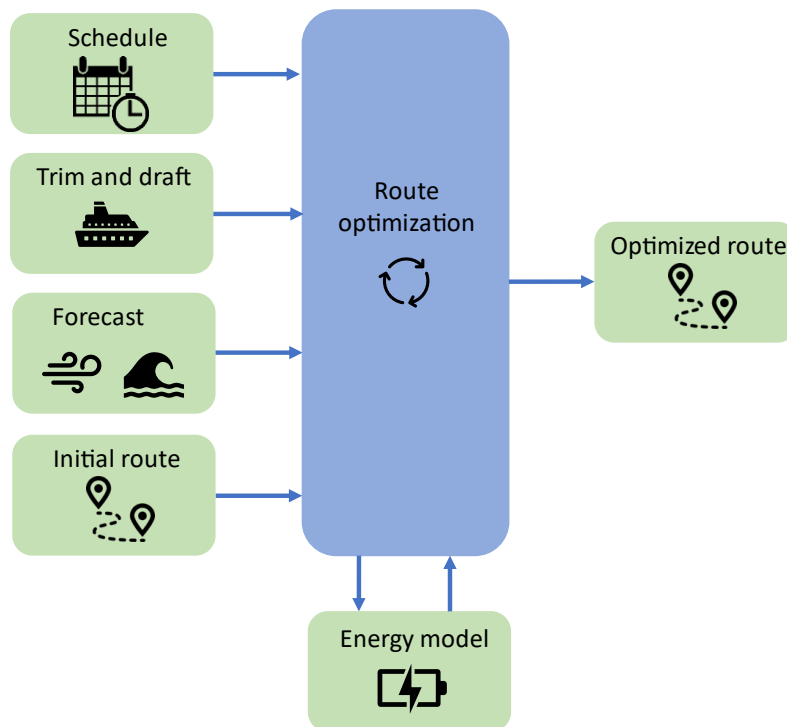


Fig.7: Route optimization

5. Results

Data from 2200 trips have been gathered with operational data from the ferry and weather data from open-source meteorological services, provided by the Norwegian Meteorological Institute. The data has randomly been divided in two data sets, one training set (70%) and one test set (30%), Table . The test data set has been used to evaluate the energy models and the optimization. The test data set is unknown for the data-driven model but will have representative weather conditions for the area since it is randomly divided.

Table I: Data divided in training and test sets

Data set	Trips
Training	1530
Test	670

5.1 Evaluation of Energy Models

The two data-driven models, i.e. the linear regression model and the hybrid model, have been trained on the training data set, **Table I**. All three energy models have been tested using the test data set. The accuracy of the energy models is measured using the mean absolute percentage error (MAPE),

$$MAPE = \frac{100\%}{n} \sum_{i=1}^n \left| \frac{M_i - E_i}{M_i} \right|,$$

where n is the number of trips, M_i is the measured energy, and E_i is the estimated energy. The average run time of each model is also calculated as the mean run time of all the trips in the test set. Table illustrates the results of the investigated energy models.

Table II: Evaluation of energy models

Energy model	MAPE test set [%]	Avg. run time [s]	MAPE heavy weather [%]	MAPE light weather [%]
Linear regression model	5.22	< 1	6.95	4.66
Hybrid model	4.53	< 1	5.18	4.64
Simulation	12.58	17	19.12	10.15

To evaluate the effect of weather on the performance of the models, the test set is further separated into three subsets. The first represents heavy weather, the second light weather, and the third the remainder of the data. In this study, we consider the wave height, current speed and wind speed when defining the weather severity. Categorizing the severity across such a parameter set is, however, more complex than setting a univariate threshold. As such, Principle Component Analysis (PCA) (Jolliffe, 2002) is applied to compress the weather data to a single dimension. Hence, a threshold with respect to light and heavy weather can be applied in a univariate manner in this subspace. This is illustrated in Fig.8, where the thresholds for heavy weather, T_H , and light weather, T_L , are defined based on the mean weather, μ_w , and standard deviation, σ_w , as:

$$T_H = \mu_w + \sigma_w$$

$$T_L = \mu_w - \sigma_w$$

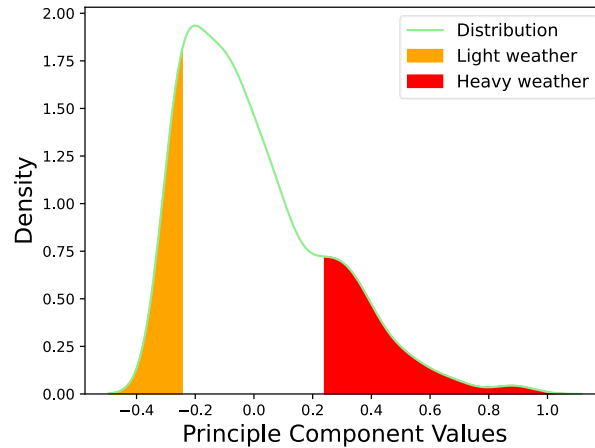


Fig.8: Distribution of weather conditions using PCA

As such, all trips where the weather was below T_L are categorized as light weather, and all those above T_H categorized as heavy weather. Of the 680 trips in the test set, 119 are categorized as heavy weather, and 110 as light weather. Fig.9 illustrates the distribution of percentage error results for light and heavy weather conditions for each model investigated.

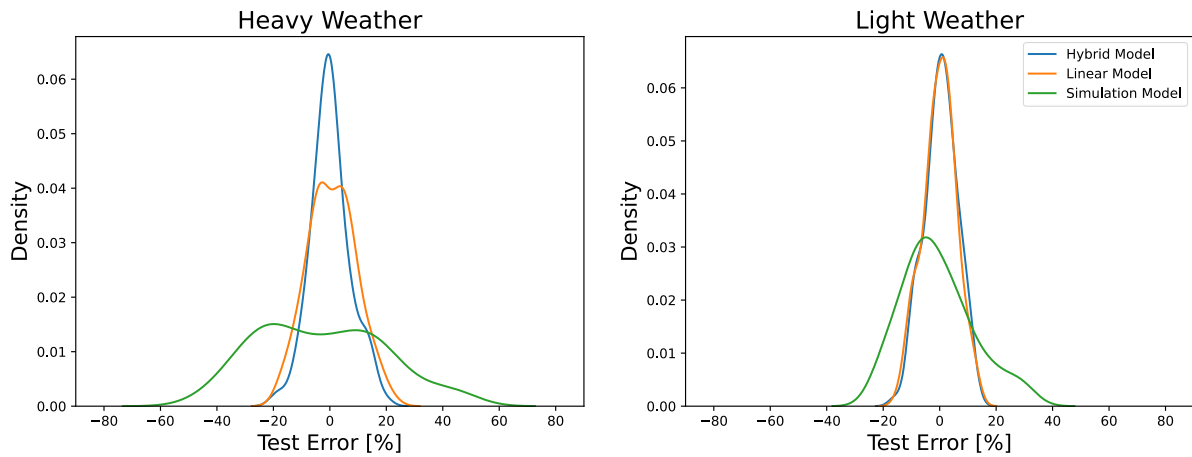


Fig.9: Distribution of percentage error for the hybrid model (blue line), linear model (orange line), and the simulation model (green line). The percentage error distribution in heavy weather is shown on the left and light weather on the right.

5.2 Discussion

Table II shows that the hybrid model is the most accurate model with 4.53% MAPE for the test set. The linear regression model is slightly less accurate than the hybrid model with a 5.22% MAPE for the test set. The results show that by including non-linear physical relations to the ML energy model, i.e. the hybrid model, the accuracy has increased compared to the purely ML-based linear regression model.

By applying the models to the data sets corresponding to heavy and light weather, the effect of increased weather severity can be evaluated. Fig.9 illustrates the distribution of the absolute percentage error for the trips in the heavy and light weather data sets. It is evident from the figure that the hybrid model has the best performance in heavy weather, with a tightly bounded distribution centered about zero error. The linear model, however, has a broader distribution resulting in a larger error. This is confirmed by the MAPEs given in Table II, where the hybrid model has 5.18% MAPE, while the linear model has a MAPE of 6.95%, which is almost 2% higher. The increased accuracy of the hybrid model in heavy weather may be due to the inclusion of physical relations of the wind and current in this model.

For light weather, the error distributions of both the ML-based models are almost identical, where both are tightly bounded about zero. This indicates that the models are highly accurate in light weather. This is confirmed by the MAPE, where both lie about 4.6%. This means that the models are more accurate in light weather than heavy weather. Looking at the distribution of weather conditions in Fig.8, one can see that the light weather is closer to the main portion of the data than the heavy weather. Since the light weather is more typical for this dataset, this may explain why the accuracy is higher for light weather than the heavy weather. From the MAPEs in Table II, one can see that the hybrid model performs slightly worse in light weather than overall. The hybrid model, being more robust to variations in weather conditions, has likely fit more to the data overall, and, therefore, performs slightly worse when further from the mean of the data.

The simulation is not able to match the level of accuracy of the ML-based models with an MAPE of 12.58% on the test set. In light weather, the accuracy of the simulation is higher than overall, with a MAPE of 10.15%, while in heavy weather the accuracy is significantly reduced, with a 19.12% MAPE. Still, the simulation had significantly lower performance than the ML-based models. Fig.9 also shows that the distribution of the absolute percentage error is much broader in heavy conditions than in light

conditions, indicating a high sensitivity to weather. Furthermore, the distributions indicate that the simulation model slightly underestimates the energy consumption in general. Since the accuracy of the simulation depends on the accuracy of the vessel model, this indicates that the vessel model is not very accurate. This is as expected since this specific vessel is not very well estimated by strip theory. Also, the simulation does not account for trim, draft or current, which are all included in the ML models. Moreover, the simulation does not account for implicit effects e.g., wear and tear on the hull and propulsion system. To account for these parameters, the simulation would require a specific model for each condition, which presumably would enhance performance accuracy. However, acquiring new models is expensive.

Regarding the run time, the linear regression model and the hybrid model are quite fast and both use less than 1 s, see Table II. The simulation on the other hand is more time consuming with an average run time of 17 s. During this time, about 70-80% is spent on setting up the simulation including starting a Java Virtual Machine (JVM) and unzipping vessel model files. These steps are only necessary once but is done for each trip with the given setup. Consequently, simulation time can easily be reduced significantly if desired.

Compared to purely physics-based models, data-driven models are able to discover more specific behaviour within the datasets they are trained on. Implicit effects such as wear and tear on the hull and propulsion system will also be accounted for. Hence, they are capable of being more accurate than simulation models in certain cases but are less generalizable as they are constrained to the domain of the data they are trained on. However, since the hybrid model includes physical knowledge, this model should be slightly better at generalization than the linear regression model. The linear regression model's ability to generalize depends on the quantity and variation of the training data. In this study, the data-driven models have been trained on data from one ferry operating on one short route. As described in Section 2.1, the waves and current in the gathered data have little variation regarding the direction and magnitudes. The results showed that the data-driven models were highly accurate for the test data from the same route. However, when using the data-driven models for a different route with other conditions, e.g. different waves and current, the models will likely have a lower accuracy. In theory, the simulation-based energy model is the most generalizable of the three models investigated since it is purely physics-based. However, due to the low accuracy vessel model used in the simulation, this may not be the case for this simulation model.

Since the hybrid model has the highest accuracy and lowest run time, it is deemed the most suitable for use in the route optimization algorithm.

5.3 Evaluation of Route Optimization

Using the hybrid energy model to estimate the energy consumption, the route optimization is tested on the test data set. The optimized route is compared with the original route, that is the actual route sailed. The energy saved in the optimization is defined as,

$$\text{Energy saving} = \frac{E_{opt} - \hat{E}_{org}}{\hat{E}_{org}} \cdot 100\%,$$

where E_{opt} is the energy of the optimized route in transit and \hat{E}_{org} is the energy consumption of the original route in transit estimated using the energy model. The energy of the optimal route is compared with the estimated energy of the original route instead of the measured energy to minimize the influence of the uncertainty of the energy model. An overview of the performance of the optimization is given in Table III.

Table III: Energy savings and run time for entire test data and energy savings in different weather

	Energy savings test set	Energy savings heavy weather	Energy savings light weather	Run time
Mean	-0.68%	-0.77%	-0.57%	111 s
Std	0.75%	0.76%	0.59%	90 s

The energy savings given in Table III shows that the weather routing system is able to reduce the energy consumption by 0.68% on average for the test set. With a standard deviation of the energy saving of 0.75%, it is almost as large as the average savings, indicating that most of the energy savings lie between 0-1.43%. The energy savings for heavy weather is higher than the average, indicating that the algorithm is able to utilize the weather to its benefit. For light weather, the energy savings are less than the average. On average, the optimization uses less than two minutes to optimize a trip. However, the variation is large with a standard deviation of 90 s.

A heat map of the routes sailed for the original routes and optimized routes in different weather conditions is shown in Fig.10.

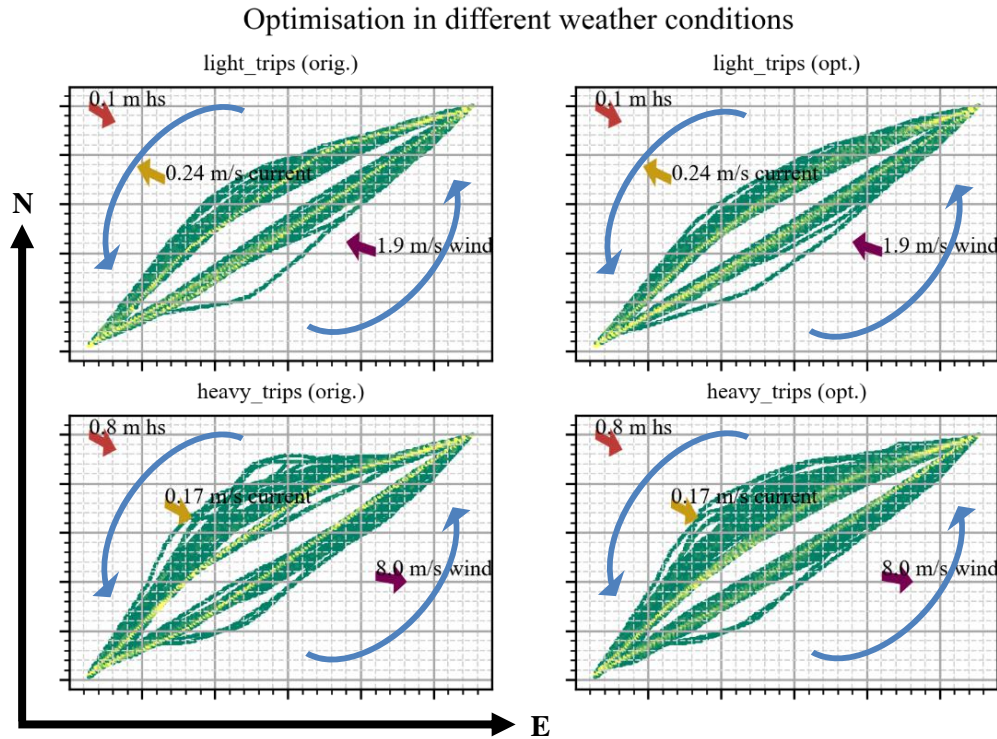


Fig.10: Heat map of routes in different weather conditions. The brighter the color, the more frequent the route is. The figures on the left show the original routes, on the right the optimized routes. The first row shows the routes in light weather, the second row in heavy weather. Red arrows indicate average wave direction and wave height, yellow arrows the average current direction and speed, purple arrows average wind direction and wind speed, and curved blue arrows the travelling direction.

The heat map of routes shown in Fig.10 illustrates that in light weather, both the original and optimal routes generally follow the shortest paths within the safety zones. In heavy weather, all the weather forces come from the west/northwest, where both wind and waves have increased significantly compared to the light weather. Having the weather from the west/northwest, the ferry experiences weather from behind when travelling the northbound route, while the weather is against for the southbound route. One can see that this has an impact on the route choices in the southbound route, where the routes tend to have a longer distance, i.e. not the shortest path. This trend is observed for both the original route, when steered by a captain, and the optimized route. This indicates that these route choices are performed with intention to minimize the added resistance from the weather forces. Since both the captain and the route optimization tend to choose a longer route in heavy weather, the difference in energy consumption between the original route and optimized route is relatively small. However, if an inexperienced captain was to sail this route, he/she may have chosen the shortest path with possible added resistance. Thus, if the optimized route was compared with the route of an inexperienced captain, the energy saving would likely have been larger. Furthermore, a standard route

will be input to the optimization when utilized on board a vessel, as opposed to the actual route. The relative energy savings of an optimized route compared to a standard route should be much larger than for the route followed by an experienced operator. The use of such optimized routes will, furthermore, provide a form of standardization across operators, irrespective of their level of experience.

By inspecting the northbound route, it is observed that the route optimization sometime does not choose the shortest path even with low weather resistance. This is also observed for the original route. The route optimization seems to be influenced by the initial route, since the optimization uses the original route as the initial route.

6. Conclusions and Further Work

A weather routing system has been tested and evaluated. This included testing different models for estimating the energy consumption of a ferry. The results showed that the hybrid model was the best model with the highest accuracy and low run time. The linear regression model had comparable results with the hybrid model but was slightly less accurate and less robust to more severe weather conditions. Both the linear regression model and the hybrid model significantly outperformed the simulation-based energy model. The results showed that the route optimization was able to typically save up to 1.5% energy following the optimal route compared to the originally sailed route. Additionally, the optimization had higher savings in heavy weather than light weather. The weather in the investigated region, however, was generally limited. Furthermore, the sailing route of the ferry is low in complexity, with quite uniform exposure to the weather. The potential energy savings for vessels operating in more severe weather on sailing routes with more variability are expected to be larger than those found in this study.

The weather routing system developed can be utilized for any type of vessel, not just ferries, regardless of the energy source, as long as operation data from the vessel is available. This weather routing system will be tested and validated on the vessels for Havila Kystruten (project number 331765 at the Research Council of Norway). Havila Kystruten will be exposed to more severe weather than the ferry investigated in study. As such, it is expected that the potential energy savings are much larger.

Acknowledgements

This work is partially funded by the Research Council of Norway through the project SMARTSHIPROUTING (THE RESEARCH COUNCIL OF NORWAY, 2019). The authors would like to thank the project owner Norwegian Electric Systems and the project partners HAV Design and Havila Kystruten. Furthermore, we would like to thank Fjord1 for allowing us to collect operational data from one of their ferries.

References

- BELLINGMO, P.R.; POBITZER, A.; JØRGENSEN, U.; BERGE, S.P. (2021), *Energy Efficient and Safe Ship Routing using Machine Learning Techniques on Operational and Weather Data*, 20th COMPIT Conf., Mülheim
- BUI-DUY, L.; VU-THI-MINH, N. (2021), *Utilization of a deep learning-based fuel consumption model in choosing a liner shipping route for container ships in Asia*, Asian J. Shipping and Logistics, 37(1), pp.1-11, <https://doi.org/10.1016/j.ajsl.2020.04.003>
- DÆHLEN, J.S.; SANDVIK, E.; RIALLAND, A.I.; LAGEMANN, B. (2021), *A Method for Evaluating Ship Concepts in Realistic Operational Scenarios using Agent-based Discrete-Event Simulation*, 20th COMPIT Conf., Mülheim
- EUROSTAT (2022), *Short Sea Shipping - Country Level - Gross Weight of Goods Transported to/from Main Ports*, https://ec.europa.eu/eurostat/databrowser/view/mar_sg_am_cw/default/table?lang=en

FATHI, D.E. (2018), *ShipX Vessel Responses (VERES), User's Manual*, <https://usermanual.wiki/Document/VeresManual.1512625556/view>

FATHI, D.E.; HOFF, J.R. (2017), *ShipX Vessel Responses (VERES), Theory Manual*, <https://usermanual.wiki/Document/VeresTheoryManual.1635197901.pdf>

GKEREKOS, C.; LAZAKIS, I.; THEOTOKATOS, G. (2019), *Machine learning models for predicting ship main engine Fuel Oil Consumption: A comparative study*, Ocean Eng. 188, <https://doi.org/10.1016/j.oceaneng.2019.106282>

GRIFOLL, M.; MARTÍNEZ DE OSÉS, F.X.; CASTELLS, M. (2018), *Potential economic benefits of using a weather ship routing system at Short Sea Shipping*, WMU J. Maritime Affairs, 17(2), pp.195-211, <https://doi.org/10.1007/s13437-018-0143-6>

IMO (2019), *Initial IMO GHG Strategy*, Int. Maritime Organization, London, <https://www.imo.org/en/MediaCentre/HotTopics/Pages/Reducing-greenhouse-gas-emissions-from-ships.aspx>

ITF (2021), *ITF Transport Outlook 2021*, Int. Transport Forum, <https://doi.org/10.1787/16826a30-en>

JOLLIFFE, I.T. (2002), *Principal Component Analysis*, Springer (Vol.2)

JØRGENSEN, U.; BELLINGMO, P.R.; POBITZER, A.; BERGE, S.P.; MURRAY, B. (2022), *Ship Route Optimization Using Hybrid Physics-Guided Machine Learning*, (Under review)

KOBAYASHI, E.; HASHIMOTO, H.; TANIGUCHI, Y.; YONEDA, S. (2015), *Advanced optimized weather routing for an ocean-going vessel*, 2015 Int. Assoc. Institutes of Navigation World Congress

LINDSTAD, H. (2013), *Strategies and measures for reducing maritime CO2 emissions*. <https://core.ac.uk/download/pdf/52099779.pdf>

PARKES, A.I.; SAVASTA, T.D.; SOBEY, A.J.; HUDSON, D.A. (2022), *Power prediction for a vessel without recorded data using data fusion from a fleet of vessels*, Expert Systems with Applications 187

PARKES, A.I.; SOBEY, A.J.; HUDSON, D.A. (2018), *Physics-based shaft power prediction for large merchant ships using neural networks*, Ocean Eng. 166, pp.92-104

PAWAR, S.; SAN, O.; AKSOYLU, B.; RASHEED, A.; KVAMSDAL, T. (2021), *Physics guided machine learning using simplified theories*, Physics of Fluids 33(1), <https://doi.org/10.1063/5.0038929>

PETERSEN, J.P.; JACOBSEN, D.J.; WINTHER, O. (2012), *Statistical modelling for ship propulsion efficiency*, J. Marine Science and Technology 17(1), pp.30-39

PICCIONE, A.; BERKERY, J.W.; SABBAGH, S.A.; ANDREOPOULOS, Y. (2020), *Physics-guided machine learning approaches to predict the ideal stability properties of fusion plasmas*, Nuclear Fusion 60(4)

RESEARCH COUNCIL OF NORWAY (2019), *Selvlærende ruteoptimalisering for skip – Prosjektbanken*, <https://prosjektbanken.forskningsradet.no/en/project/FORISS/295763?Kilde=FORISS&distribution=Ar&chart=bar&calcType=funding&Sprak=no&sortBy=date&sortOrder=desc&resultCount=30&offset=0&Prosjektleder=Svein+Peder+Berge>

UNCTAD (2021), *Review of Maritime Transport 2021*, United Nations, New York

VOULODIMOS, A.; DOULAMIS, N.; DOULAMIS, A.; PROTOPAPADAKIS, E. (2018), *Deep*

Learning for Computer Vision: A Brief Review, Computational Intelligence and Neuroscience,
<https://doi.org/10.1155/2018/7068349>

Digitalization of Maritime Commissioning: A System for Automatic Content Creation and Augmented Reality-based Commissioning Execution

Ahmed Elzalabany, Hamburg University of Technology, ahmed.elzalabany@tuhh.de

Vincent Settler, Hamburg University of Technology, vincent.settler@tuhh.de

Robert Rost, Hamburg University of Technology, robert.rost@tuhh.de

Hermann Lödding, Hamburg University of Technology, loedding@tuhh.de

Abstract

Ship commissioning is an essential process in the maritime industry where all components in the ship are tested to ensure that client requirements and specifications are fulfilled. Commissioning consists of three main phases: preparation, execution, and documentation. Commissioning test preparation and execution require a long time, high effort, and experience to perform. To enhance the process of commissioning, by supporting commissioning planners and engineers, a comprehensive digital commissioning system was developed. The system presented in this paper employs an automation approach for more efficient preparation of commissioning content, and uses Augmented Reality for commissioning execution.

1. Introduction

To guarantee that a newly-produced ship conforms to all requirements agreed upon in the contract between the client and the shipbuilder, as well as the standards and norms set by the classification society, the ship goes through a process called “ship commissioning”, *Weber (2019)*. Throughout the process, “commissioning tests” represent the primary work packages. Commissioning tests contain all necessary details for verifying that every component in the bill of materials (BOM) conforms to the specifications. Furthermore, commissioning tests define the final acceptance protocols which are signed by the main stakeholders marking a successful handover.

Similar to the process of commissioning in the field of civil engineering, a ship requires longer than twelve months to be successfully commissioned, *Ebertshäuser et al. (2020)*. Due to the long time, and consequently the high cost invested in the whole process, commissioning has a great impact on the business, and is considered an essential process in the lifecycle of shipbuilding. Commissioning preparation, execution, and documentation are the three primary phases of the process. During the phase of preparation, various commissioning tests, including other content, are authored by commissioning planners, and when preparation is finished, the content is handed over to the engineers to perform the commissioning throughout the execution phase. At the end of commissioning, documentation takes place where commissioning protocols are produced, signed, and achieved to be viewed later whenever needed, e.g., during maintenance.

This paper places focus on the phases of preparation (authoring) and execution by introducing a digital solution that solves the deficits associated with both phases. The deficits arise mainly due to the large number of interdependent commissioning tests that exist in the process. Commissioning a big ship may require ten thousands of tests to be authored and executed, and maintaining an overview of the complex mesh of interdependencies between all commissioning tests is therefore difficult. Moreover, authoring such a number of tests using traditional methods and tools requires high effort and is subject to mistakes. Finally, commissioning tests take a static form, e.g., paper documents and PDF files, which introduces problems during the phase of execution. For example, component localization, navigation in ship, and maintaining a dynamic overview of other activities that may negatively influence the process of commissioning are tasks that are not easily achievable when relying solely on static paper documents.

Nowadays, the process of shipbuilding is evolving toward digitalization to overcome the deficits of paper-based work. *Friedewald et al. (2016)* describe how productivity in manual processes can be increased by the integration of digital assistance systems. Moreover, a system introduced by *Friedewald*

et al. (2021) sets basis for authoring and scheduling digital commissioning information. As a continuation to the work introduced by *Friedewald et al.* (2021), this paper discusses the current process of commissioning, and its deficits in more depth, and presents an authoring system for an automatic generation of commissioning information, as well as an Augmented-Reality-based digital assistant, which is connected to the authoring system through a digital twin.

2. Process of Ship Commissioning

A One-of-a-Kind product, such as a ship, contains complex components arranged in unique configurations according to the client specifications. Due to the unique structure of the ship, and unlike mass production, there are no standard work plans that can entirely apply for every produced ship to ensure quality and requirement fulfillment. Therefore, a shipbuilder begins the commissioning process by creating a new work plan for each newly produced ship, hence the phase of commissioning preparation. During the phase of preparation, the bill of materials is viewed for extracting commissioning-relevant technical specification data, and accordingly commissioning tests are created. Commissioning tests are then assigned the necessary resources, and finally a time plan for executing the tests is created. At this point, the phase of execution may begin.

The commissioning execution phase is concerned with performing all tests authored within the preparation phase. Highly trained engineers, with different expertise, are assigned for ensuring that all components exist as planned and are fully functional. When a test is completed, the commissioning engineer produces a protocol to document the result of the test. In the case of an irregularity, the issue is raised to the responsible personnel so that it can be resolved, and the test is eventually repeated. This process also takes place in the presence of the client and the classification society.

Due to the high workload, and to achieve the highest possible throughput, the commissioning process usually takes place parallel to the final assembly processes, *Weber* (2019). In many cases, parallel construction may interfere with commissioning. For example, noise or mechanical vibration caused by assembly work can make it difficult to test devices that are sensitive to such disturbances. Therefore, conflicts arise between commissioning and construction. Such conflicts show that the commissioning process is “interdependent” in nature, meaning that specific requirements have to be fulfilled before executing a commissioning test. Therefore, interdependencies must be taken into consideration when authoring and executing commissioning tests. The next sections describe the preparation and execution phases of commissioning tests in more detail.

2.1. Commissioning Preparation Phase

Commissioning is characterized by a sequential workflow, e.g., a task B may not be performed before task A is completed. In such case, both commissioning tests are considered interdependent. Interdependencies can be categorized as either organizational or technical depending on the constraint imposed on the tasks to be executed, *König et al.* (2007). For example, when the use of a power grid is required for testing the operational capability of electrical devices, a technical interdependency arises. Meaning that the operational test is dependent on the power grid, and therefore, a task for testing the power grid has to be performed first. On the other hand, testing the proper running of highly sensible sensors requires a surrounding area that is free from disturbances, e.g., mechanical vibrations or noise. That means while executing that task, no other task can be operated on in the vicinity that causes such disturbances, which is an example for organizational interdependencies.

Interdependencies show that the commissioning preparation phase requires active collaboration between different departments in the shipyard to obtain an overview of the assembly process. The following section mentions the involved actors and describes the information exchanged within the preparation phase.

2.1.1. Actors and Information Exchange within the Commissioning Preparation Phase

When considering the sequential nature of commissioning and the dependence to the assembly process, it becomes clear, that preparing the entire commissioning process requires extensive effort from commissioning planners. Due to the variety of components in the ship, different expertise is needed for commissioning preparation: highly experienced electrical engineers are responsible for authoring commissioning content for electrical systems in the ship, while mechanical systems require expertise of mechanical engineers. Therefore, a team of engineers from different backgrounds work together to create the content and documents needed for the entire commissioning process. The documents are handed over to the commissioning engineers for performing the necessary tests. Fig.1 shows the building blocks of commissioning content and the respective consumers of such content.

Commissioning information follows a hierarchical framework, as shown in Fig.1. That means that commissioning planners assign each assembly group in the ship a commissioning program, which includes several commissioning tests. The lowest level in the hierarchy is a commissioning step. The structure of a commissioning program varies from a shipyard to another. But it is common that a program serves as a document for listing all commissioning tests that are performed on the components of an assembly group. Moreover, a program contains information about the resources required for all commissioning tests in the program.

A commissioning test is the most significant information block in the process, and may occupy a single or multiple pages in the corresponding commissioning program. A test contains concrete technical instructions defined in the form of commissioning steps. Each step may describe only a single task, and in most cases such task must be performed on the lowest component in the assembly group of a system. For example, one step in the commissioning of an electrical motor could be the inspection of a power cable. Commissioning steps are organized in a table that represents the sequence of execution. The table of steps also contains columns for step description, as well as placeholders for readings obtained by the commissioning engineer.

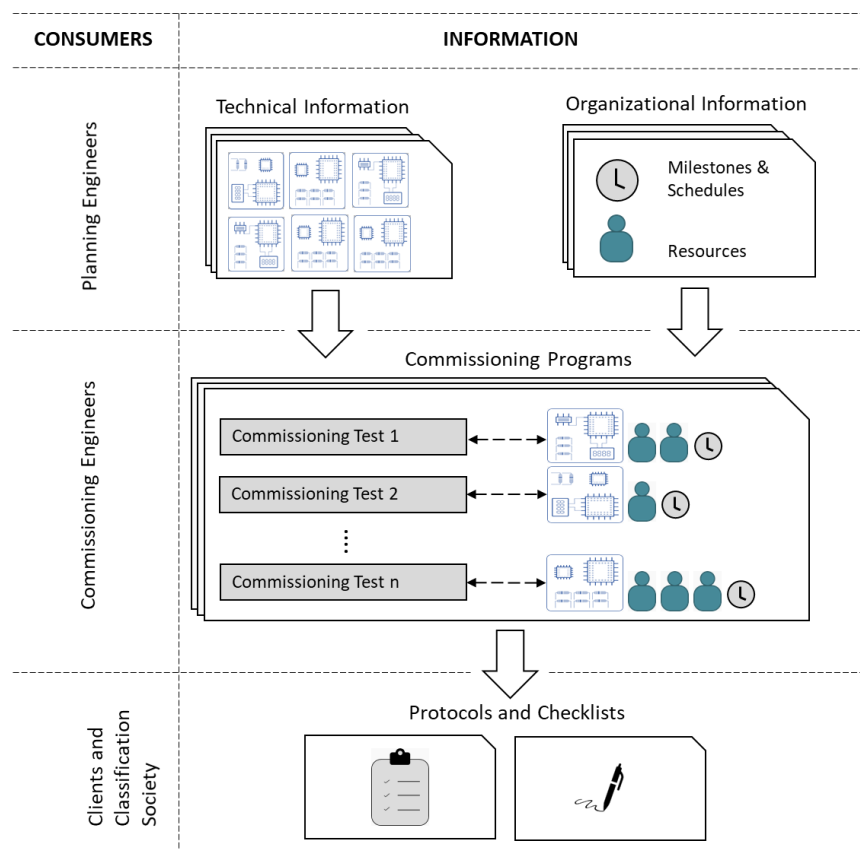


Fig.1: Information Building Blocks of Commissioning

The component to be inspected in a commissioning step (or test depending on the complexity of the component) is identified by an alphanumeric code that corresponds to the bill of materials. In some cases, technical drawings or data sheets are attached to provide further information about the component if needed. Finally, a commissioning test page contains a table for signatures so that commissioning engineers, among other participants, can sign the document to indicate that the test is completed.

2.1.2. Deficits and Motivations for Digitalizing Commissioning Preparation

Commissioning planners need a dynamic overview of the assembly status to avoid planning commissioning tests that may conflict with the assembly. Furthermore, information about existing resources should also be updated constantly to allow commissioning planners to prepare the commissioning schedules accordingly. However, maintaining such an overview is not easy to achieve. One central reason is that both production and commissioning processes rely heavily on paper documents. To solve such a problem, a digital commissioning system was developed by *Friedewald et al.* (2021).

Moreover, since every ship differs from the other, commissioning test specifications also differ, and therefore, the content has to be created individually, mostly from scratch, which takes time and costs. A digital system capable of adapting existing commissioning tests to new equipment configuration has the potential to significantly improve the process

2.2. Commissioning Execution Phase

Analyses from the field show that two types of commissioning tests are performed during the execution phase: installation and behavioral tests. An installation test ensures that the right component is properly installed. For example, making sure that an electrical component has the right connections. Behavioral tests, on the other hands, are performed to verify the correct behavior of the component. For example, an air conditioning unit produces the right minimum and maximum temperatures.

Before performing the tests, commissioning engineers are supplied with all relevant content produced in the preparation phase. It is a standard procedure to perform the commissioning tests twice: once in an internal testing stage, where the engineer performs the test without the presence of the client. And the second time in the official acceptance stage, in which all stakeholders are present. The reason is to detect faults early in the internal testing stage and to act fast in case of a failure before the official acceptance stage. Internal testing also takes part in parallel to the production process. The execution phase is finished when the final acceptance protocols are signed by all participants. Fig.2 shows the stages of commissioning execution including the participants in each stage:

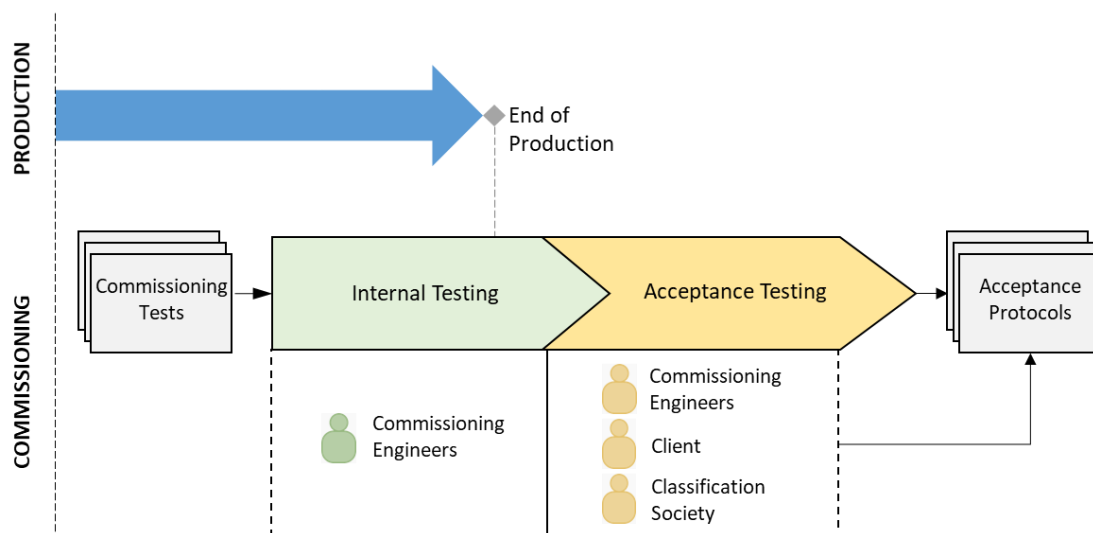


Fig.2: Commissioning Execution Stages

2.2.1. Feedback Handling During the Commissioning Execution Phase

During the commissioning execution, it is mandatory to give feedback on technical circumstances and organizational events. Therefore, feedback can be categorized into two types: technical and organizational feedback.

Technical feedback relates to the machine and its components in a physical way. Most likely an engineer gives technical feedback to a specific component during a commissioning step. This can be measured data, as the minimum and maximum value of sensors measurement range. Often, obtaining a technical feedback is the main task of executing the commissioning step.

Organizational feedback, on the other hand, is concerned with reporting schedule information, as well as unexpected disturbances. When reporting schedule information, time and date of the completion of commissioning steps and tests can be submitted in a way so that the scheduling operators, as well as the engineer, can keep track of the overall progress. Moreover, disturbances and unseen circumstances that cause problems, inaccuracies or can even be so severe that the fulfilling of a task is not possible without further action, are also noted down in the commissioning protocols.

2.2.2. Deficits and Motivations for Digitalizing Commissioning Execution

Due to the interdependencies between commissioning tests, a linear list of tasks is therefore not feasible. Keeping track of interdependencies between tests and steps is a fundamental part of the digital assistance. Interlinking the textual data of commissioning with CAD data of the ship or its components has the potential to organize the large list of commissioning tasks into meaningful packages which provides the engineer with a productive sequence of execution. Together with the current state of such steps and tests, it can be used for planning or scheduling of future tasks, as discussed by *Friedewald et al.* (2021).

Heavy reliance on paper documents also affects the work of commissioning engineers. It is common that an engineer must personally investigate the site on the ship before performing a test to ensure that the site is disturbance-free. This leads to a waste of time. Moreover, during the inspection, some components may be difficult to locate, and searching a paper document for the location is time consuming. Finally, at the end of the acceptance testing phase, signed protocols and checklist are archived in paper form, which causes difficulties in later information retrieval. A digital assistant would be beneficial to overcome such problems.

While *Meluzov et al.* (2020) provide a comprehensive digital solution for maintenance tasks in maritime industry, a similar approach still is not available for the field of commissioning. Using mobile end devices such as tablets or smartphones, supported with modern technology like augmented reality and backend-communication, is a promising approach to overcome many of the problems. There are prerequisites that are particular to the field of commissioning that need to be addressed.

3. Digital Commissioning System

Friedewald et al. (2021) present a web-based system for authoring and scheduling commissioning tests, as well as visualizing interdependencies between the tests. The system shows that interdependencies follow a hierarchical pattern and can be generated from the assembly tree of a 3D CAD model. The system also offers visualization of commissioning test locations and disturbance factors, a feature implemented to detect nearby disturbance factors when scheduling commissioning tests. As an extension to the system by *Friedewald et al.* (2021), this chapter presents further functionalities for optimized authoring, as well as execution of commissioning tests supported by an Augmented-Reality-based digital assistant. As a general overview, Fig.3 shows how the authoring system and the AR digital assistant interact with each other:

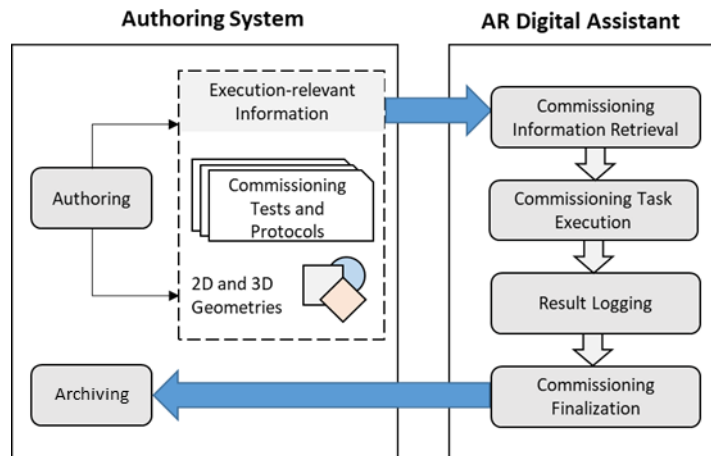


Fig.3: Information Flow between Authoring and Digital Assistant Systems

3.1. Template-based Authoring for Commissioning Preparation

To overcome the high effort of manually creating numerous commissioning tests, this section presents an authoring system which employs commissioning templates for automatic generation of commissioning tests. To create a digital solution for generating commissioning tests, a data model had to be first developed, therefore, commissioning test documents, previously mentioned in section 2.1.1, were analyzed and the following data model was derived accordingly:

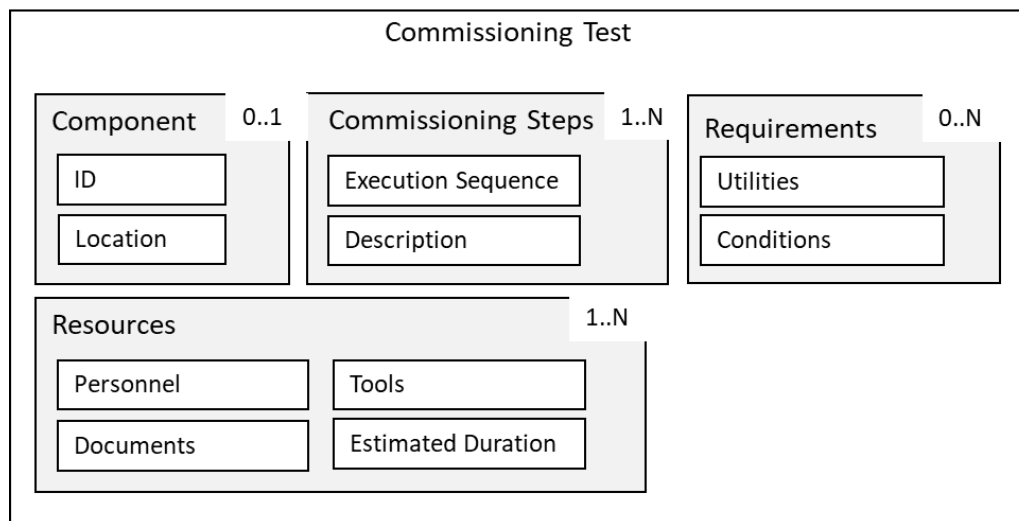


Fig.4: Commissioning Test Information Model

The following sections show how the data model is utilized for creating reusable commissioning test templates.

3.1.1. Reusability of Technical Specification Data

As discussed in chapter 2, creating test specification data from scratch is a time-consuming task. Therefore, it is useful to examine the possibility of reusing specification data for more efficient authoring. Nonetheless, such data needs to be adapted to the individual component inspected. For example, chiller systems used in ships vary in capacity and size, and accordingly, different types of compressors are used. To inspect chiller compressors, it is expected that specification data for compressors may vary as each compressor has a different operating mechanism. Within the context of commissioning, chiller compressors share the same test specification parameters as follows:

- Proper installation
- Preparatory measurements
- Fulfillment of safety requirements
- Correct minimum and maximum value limits

For this example, and many other components, it is possible to develop a generic specification model, within the context of commissioning. This model can be reused across different components in the ship. However, due to the variety of components, a single model might not be feasible for all of them. It is required to develop individual models for different component classes; for example, one model for compressors (including all compressor types), and a different model for condensers. Although it might seem that developing multiple models requires a high effort, the benefit should outweigh the effort. On the one hand, generic models can be reused for future commissioning processes on different ships, and on the other hand it requires less effort to create one generic model than multiple specific ones for similar components. Fig.5 shows a technical specification model for compressors in the context of commissioning:

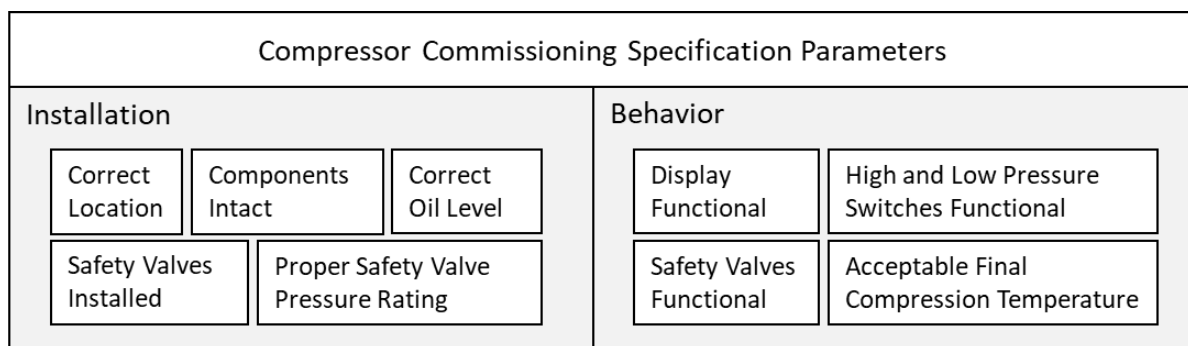


Fig.5: Technical Specification Parameters for Compressors in the Context of Commissioning

When examining the model shown in Fig.5, it is obvious that commissioning engineers would inspect compressors in the ship by performing two types of checks: Installation checks and behavior checks (refer to section 2.2). An installation check is performed to confirm the compressor is properly mounted inside the chiller system, and ready to operate. A behavior check is performed to verify proper functionality of the compressor under regular and extreme circumstances.

3.1.2. Templating of Commissioning Test Specifications

Each parameter in the specification model shown in Fig.5 defines an independent check to be performed during the inspection of a chiller compressor. Systematically, a single check can be considered a commissioning step in the model of commissioning tests (see Fig.4). As shown in Fig.5, the parameters of the compressor model are general enough to be used across different types of compressors in the ship, and since each parameter defines a single commissioning step, it is possible to use the parameters for creating a generic commissioning test template for inspecting all compressors of the same class in the ship.

Furthermore, to achieve full reusability of commissioning test specification data, information about the resources and requirements for inspecting a component need to be organized in templates as well. Therefore a list of equipment and tools relevant for inspecting each class of components needs to be implemented. The idea is to categorize ship components in classes and identify each class with a unique text identifier. For each class, a commissioning template containing sub templates for technical specification parameters, resources, and requirements can be created. This template gets stored in a central database to be later retrieved when concrete commissioning tests need to be generated. To generate commissioning tests for specific components, the components are grouped according to their classes, and suitable templates are then matched with each component according to the unique text identifier.

Using the approach of templating requires specific indication of commissioning relevant parameters, such as low and high acceptable pressure values for compressors. This way, when a component is matched with the correct commissioning template, these concrete values stored in the component sheet would be automatically assigned to the respective template parameters. Hence, a concrete commissioning test would be generated.

3.1.3. Implementation of the Templating Approach

To test the feasibility of templating, a web application was developed. At first, the template name and its scope are defined by general details and unique identifiers (see ① in Fig.6). Work steps can be dynamically created and enhanced by a sequence number and a description ②. The description shown provides instructions to verify the diameter of the pipe to be inspected. Concrete diameter values are not given, but instead implicitly written as tagged parameters: #DIAMETER_MIN and #DIAMETER_MAX. These parameters will be replaced with concrete values when a commissioning test is generated from the template by matching it with a concrete component fitting the identifiers. Technical requirements are chosen from a predefined list ③ and necessary resources from a predefined hierarchical lists ④&⑤.

Fig.6: Web Application for Commissioning Template Creation

To prepare the components of the ship to be matched by the templates, the same identifiers as well as concrete technical parameters need to be added to each component, Fig.7. The left-hand side of the figure shows a section of a bill of material where an assembly with the title “Pipes1” is selected, and the right-hand side shows a list of attributes assigned to the assembly.

The template identifier parameter shows that the component belongs to the (identifier) class of pipes. Moreover, two parameters DIAMETER_MIN and DIAMETER_MAX have the values 20 and 21 cm respectively. These parameters will be automatically detected when creating commissioning tests from a matching predefined template. And consequently, a concrete description for the commissioning step can be automatically generated.

Such a functionality saves the commissioning planner the effort of manually typing every technical parameter in the commissioning test description. Moreover, multiple commissioning steps can be generated at once, which saves time and effort.

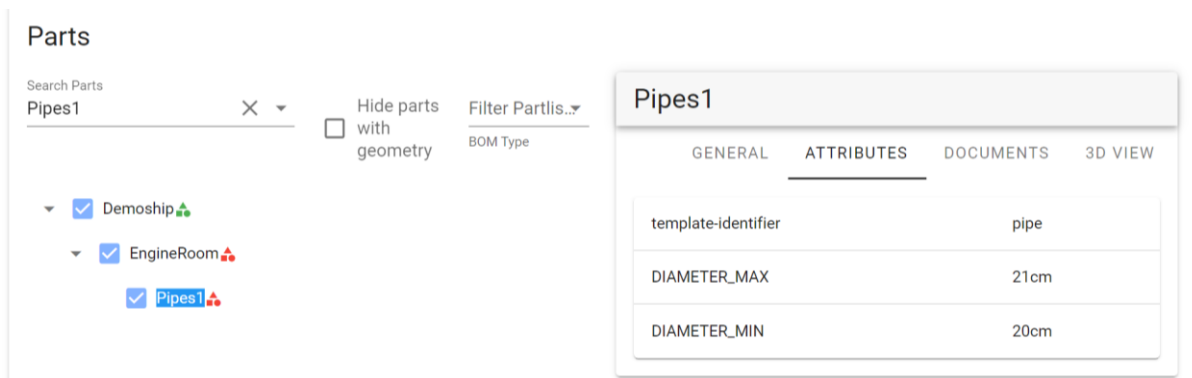


Fig.7: Component Technical Parameters

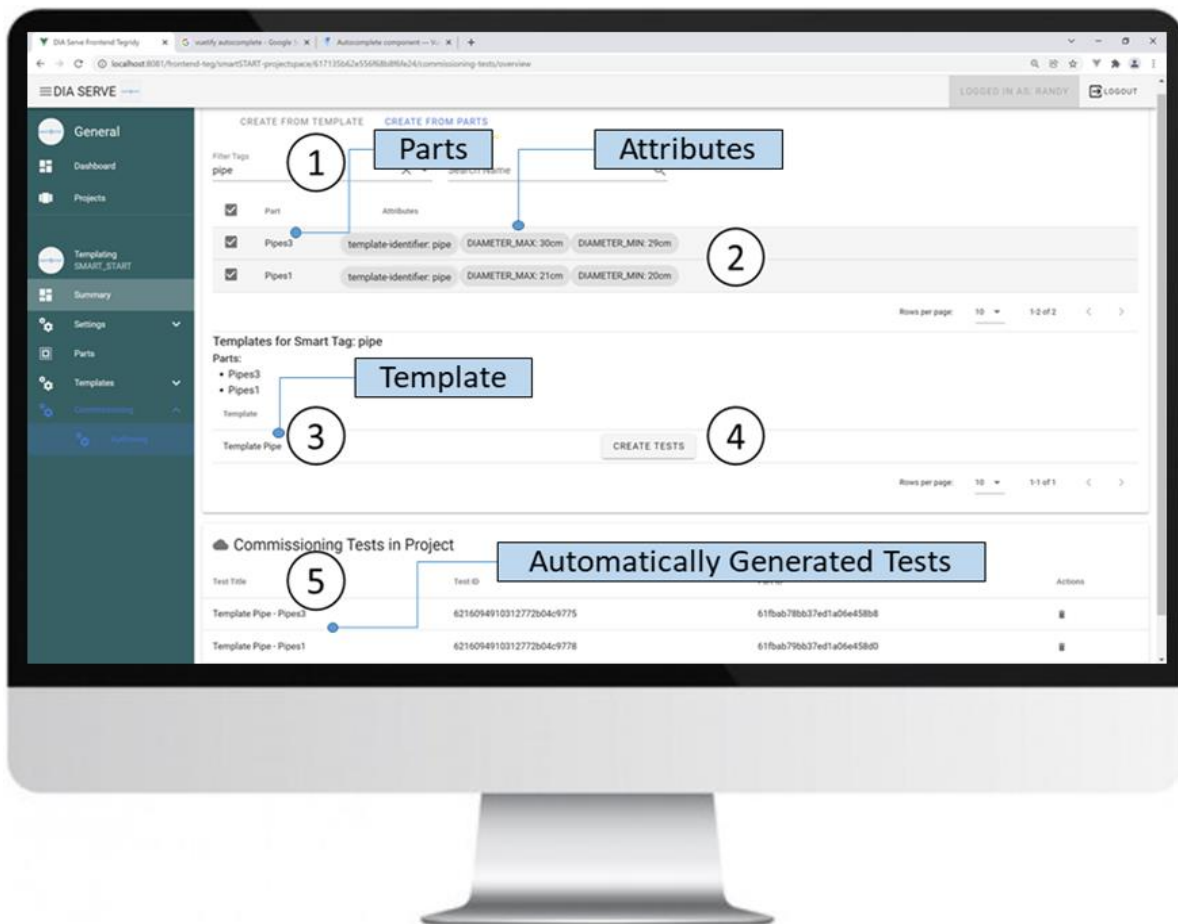


Fig.8: Automatic Generation of Commissioning Tests from Predefined Templates

Fig.8 shows that a list of parts, tagged as commissioning-relevant by the engineers, appears when a concrete commissioning plan is created for a particular ship ②. The system automatically detects

matching templates based on the identifier keyword, e. g. “pipe” ①, and recommends to apply the template ③. When a matching template is applied to the specific component④, the descriptions of commissioning steps are parsed to identify the tagged parameters (e. g. #DIAMETER_MIN) and to replace them with the concrete values of the components. Finally, the corresponding commissioning test is automatically created⑤.

Since parameters, like the ones described above, are traditionally maintained in separate systems (ERP, PDM or PLM) or separate lists, the commissioning authoring system provides interfaces to import, and use the parameters in the template procedure.

3.2. Augmented Reality-based Commissioning Execution

To overcome the deficits of using paper-based commissioning test documents, such as localization of hidden components on the ship, and maintaining an overview of interdependencies and disturbances, a mobile digital assistant system was developed. The digital assistant is handed to the engineers in the field. Running on a tablet pc, the digital assistant can provide visualization of general and specific information in 2D and 3D, and is capable of using Augmented Reality to guide the commissioning engineer throughout the commissioning process from beginning to end. It also brings the ability to give feedback on errors and progress in the different stages of an engineer’s assignment on commissioning.

3.2.1. Commissioning Visualization

The digital assistant provides the benefit of visualization of commissioning information. In adaptation, it proved beneficial to use both, 2D and 3D visualization. Information can be allocated in 2D on a map of the commissioning engineer’s operational area, e.g., a room, zone, or a whole deck. The users will get a quick overview of current states, e.g., current disturbances in their working area. The position of related equipment can be shown on the map by transposing the 3D coordinates from the CAD model to the 2D plan (see component / location in Fig.9). Since the necessary information is provided, the 2D view gives an intuitive way to illustrate and find the route, while non accessible areas will be considered and visualized by the digital assistant without additional effort.

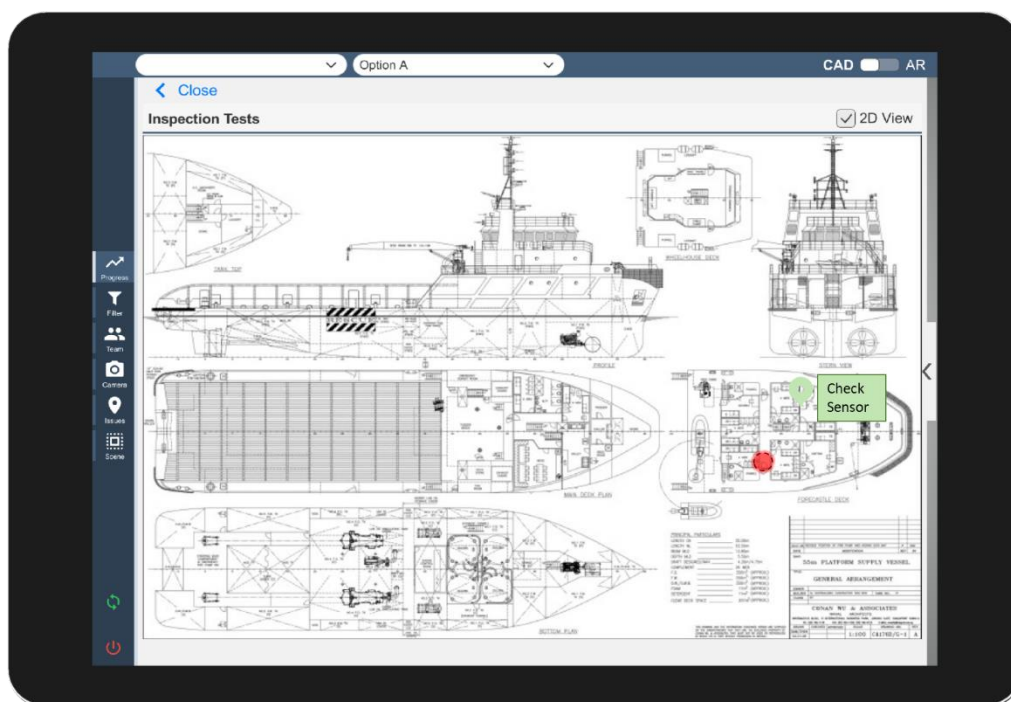


Fig.9: 2D-overview (map based on *Conan Wu & Associates Pte Ltd* (2010))

Fig.9 shows the map of a ship, the workspace of an engineer where a sensor has to be checked, and a disturbance in that area.

While the 2D view uses a classical approach to visualize general information, a corresponding 3D approach can provide more focused information. Once the engineers reach their working area, they can switch to the 3D view, Fig.11. Using Augmented Reality, Fig.10, the digital assistant displays the information the engineers need to fulfill their current commissioning steps as an overlay to the camera image.

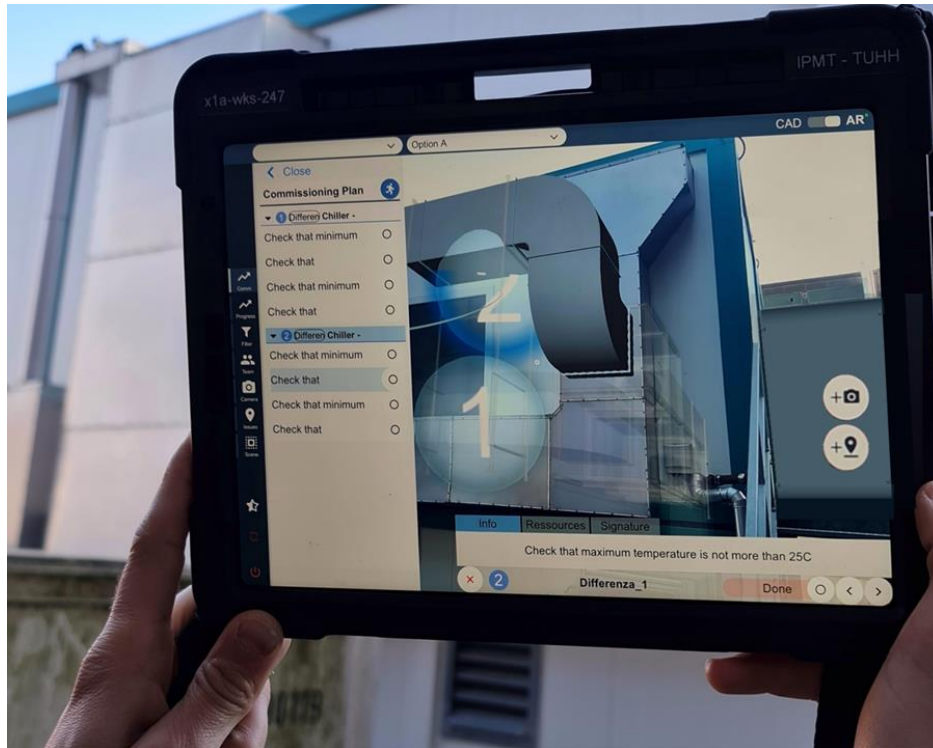


Fig. 10: AR view of the digital assistant

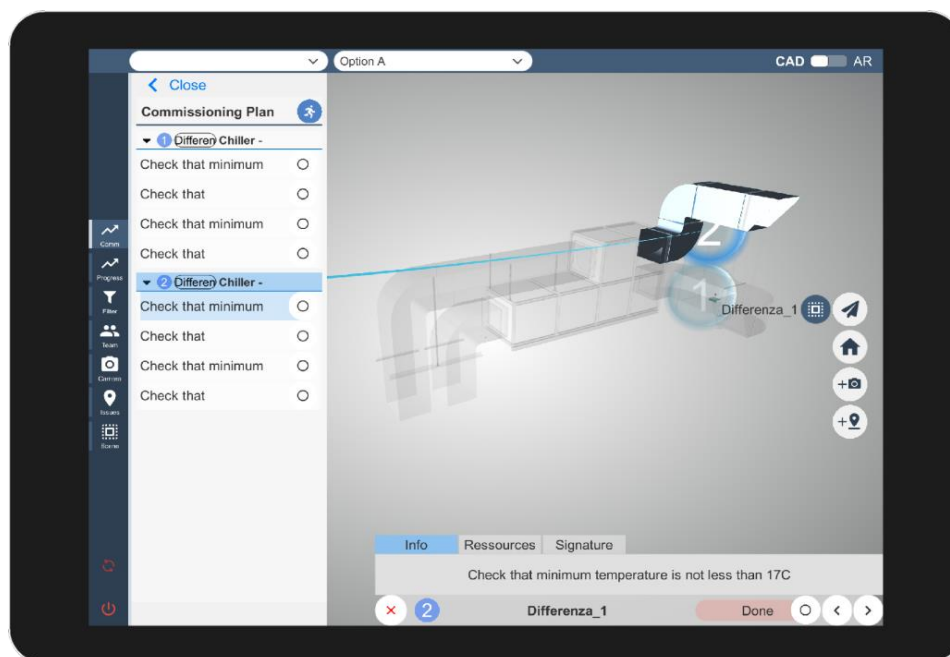


Fig. 11: 3D view of the digital assistant

Only relevant information should be shown by the digital assistant. In the 2D view, using transparency for information less relevant like disturbances that are not on the engineer's current route is such an approach. Also, if the entire operational area is large, it is advantageous to sort the view of the currently workable steps by their distance towards the engineer. Therefore an algorithm was implemented in the digital assistance which combines commissioning tests belonging to the same assembly group and sorts these groups based on the distance to the user. The result is indicated by assigned numbers which are present in 3D-space on the right side but as well in the 2D-list on the left side, Fig.11.

3.2.2. Technical and Organizational Feedback Handling

The traditional way of submitting commissioning feedback is mainly through the use of paper documents. Such an approach is slow since those issues cannot be resolved instantly due to the use of paper documents. Therefore, the developed digital assistant provides a functionality for capturing and submitting feedback data. The user interface contains input fields for the values the engineer could submit. These are tied to the different steps within the commissioning tests. The reported values can be either numbers (often tied to physical properties and units) or text. Moreover, a feedback can be supplemented by photos. Which means that the digital assistant provides the ability to create pictures, either by using the physical camera of the mobile device, or by capturing screenshots of the current display view. The pictures can be attached to specific steps, or a whole test, and sent along with the feedback to be reviewed by the responsible personnel.

4. Conclusion and Future Work

To enhance the process of commissioning, a digital system was developed for automating the authoring of commissioning content, as well as for assisting commissioning engineers with their tasks during the phase of commissioning execution. The automatic authoring employs an approach of "templating" commissioning test specification data, which significantly reduces the high effort of creating commissioning tests from scratch. Moreover, a digital assistant, taking the form of a tablet application, was developed to assist the commissioning engineer by maintaining an overview of all commissioning tasks in a user-friendly interface, and providing the engineer with localization capabilities via the technology of Augmented Reality.

The developed system still has the capability to improve by further reducing the effort of creating commissioning templates. This can be done by employing 3D mesh analysis for automatic assignment of attributes to the components in the bill of materials to be tested. Moreover, the developed Augmented Reality-based digital assistant system can be equipped with more capabilities for automatic capturing of technical measurements to speed up the process.

Acknowledgements

The presented work is funded by the German Federal Ministry of Economics and Energy (Bundesministerium für Wirtschaft und Energie – BMWi) due to a decision of the German Bundestag.

References

- CONAN WU & ASSOCIATES PTE LTD (2010), *55M Platform Supply Vessel*, Technical Drawing
- EBERTSHÄUSER, S.; JOUINI, S.; BOTH, P.; GRAF, K.; REXROTH, K.; TRAUNSPURGER, R. (2020), *BIM-basierte Integrale Planung: Gemeinsamer Schlussbericht*
- FRIEDEWALD, A.; HALATA, P.S.; MELUZOV, N.; LÖDDING, H. (2016), *Die Produktivitätswirkung von Augmented Reality in der Unikatfertigung*, Megatrend Digitalisierung - Potenziale der Arbeits- und Betriebsorganisation, GITO, Berlin, pp.141-162
- FRIEDEWALD, A.; KÖSTER, N.; ELZALABANY, A. (2021), *Scheduling and Visualization of*

Acceptance Tests and their Dependencies for an Augmented Reality-based Commissioning Assistance System, 20th COMPIT. Conf., Mülheim, pp.162-175

KÖNIG, M.; BEISSERT, U.; STEINHAUER, D.; BARGSTÄDT, H.-J. (2007), *Constraint-based simulation of outfitting processes in shipbuilding and civil engineering*, 6th EUROSIM Congress on Modeling and Simulation

MELUZOV, N.; ROST, R.; FRIEDEWALD, A. (2020), *Holistic Maintenance Support with a Digital Assistance System*, 19th Int. COMPIT Conf., Pontignano, pp.48-62

WEBER, K.H. (2019), *Inbetriebnahme Verfahrenstechnischer Anlagen*, Springer

Concept to Reality: Implementing a Digital Twin for Ship Production

Carsten Zerbst, PROSTEP, Hamburg/Germany, Carsten.Zerbst@PROSTEP.com

Ulrike Lutz, PROSTEP, Hamburg/Germany, Ulrike.Lutz@PROSTEP.com

Alexander Danetzky, PROSTEP, Hamburg/Germany, Alexander.Danetzky@PROSTEP.com

Abstract

This paper presents the status in the ProProS research project achieved over the last 2½ years. Together with Fr. Lürssen Yard and the university RWTH Aachen we developed the concepts and prototype implementation for a digital twin for ship production. This enables users on the yard to have a near-time view of the status of production processes and create a new planning baseline with reasonable effort. The estimates for the new planning are based on the production structure as well as on historical data collected in the same solution, thus providing a repeatable estimation method.

1. Introduction

Managing the shipbuilding production process is no easy task. There are a lot of factors that make the managing process quite complex. Some of them are shipbuilding specific, e.g. the huge number of parts or design changes even after production starts. Other problems are also seen elsewhere, like delays in the delivery chain, illness among the personnel, missing or late feedback from delivery or production. The combination of those problems makes the managing process difficult, especially as there is no adequate tool support covering the whole process. As a result, the production process is often planned only once in weekly or even monthly slices. If the original planning is no longer valid, the dates are often simply shifted, but not replanned.

The demonstrator software developed in the research project ProProS aims at helping the shipbuilding industry to perform better planning of the manufacturing process and thus reduce time and effort. The base idea is to enable planners to run a complete Deming, Fig.1, process over and over again with reasonable effort. The 'Plan' phase is based on a detailed bottom-up planning methodology to estimate product times accurately. Track-and-trace data collected in the production is used to perform an automated check if the developed plan is still valid or needs adjusting in the next *Act* phase.

As many of the underlying ideas for ProProS were already presented in Zerbst (2021), this paper gives only a rough overview of the underlying design principles in the second chapter. The third chapter concentrates on solving the constrained planning problem, followed by some additional information we found noteworthy about the developed demonstrator. The fourth chapter contains a summary of the gained knowledge and a preliminary outlook on how to apply this in the shipbuilding industry.

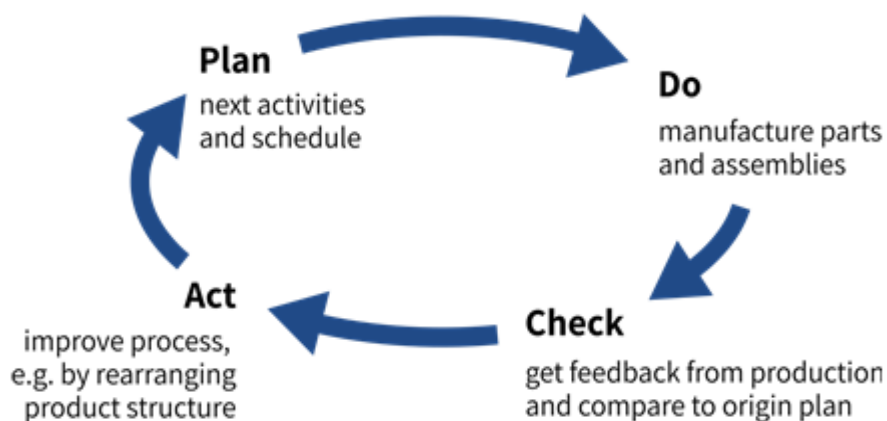


Fig.1: The Deming Cycle, Deming (1986)

2. Production Planning

This chapter lays out the underlying methodology applied in the ProProS research project to perform the ‘Plan’ phase from the Deming circle. As with any project planning, this requires an estimation of the effort and duration of the production activities. This estimation is based on a bottom-up approach, using the preliminary and/or final design data into account. The planning process starts with the assembly structure defined in the CAD tool as well as some yard specific information on the production methodology, Fig.2. The assembly structure contains the order, in which parts are assembled to a complete vessel. It covers both the overall layout, (e.g. the section erection order) and details like a bracket welded only after joining two sections in the drydock. The production methodology contains rules e.g. what production activities are needed e.g. to knuckle a profile or produced an assembly on a panel line. It is applied like a template on the assembly structure to get an activity network as found in Fig.3.

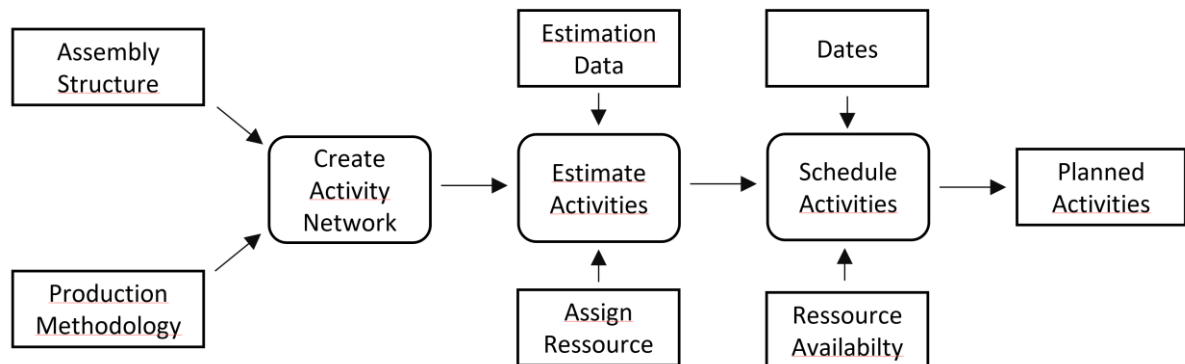


Fig.2: Steps to get planned activities

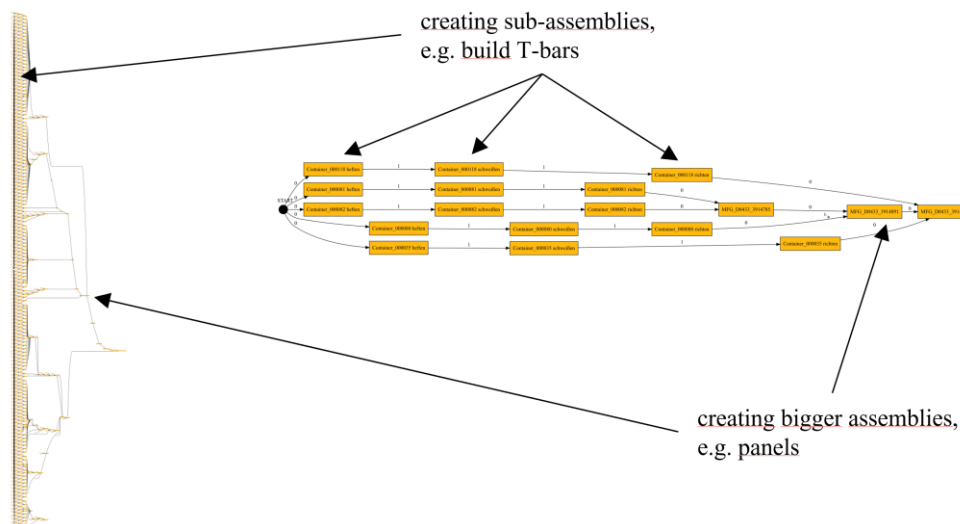


Fig.3: Activity networks showing both the sub-assembly as well as the assembly phase

Each box in the network represents an individual activity applied on a specific set of parts with specific manufacturing technology. Therefore it is possible to estimate the effort needed to perform the activity. The estimation is based on formulas using the information on the assembly as well as constants based on historical information. In this step, we also assign resources like workplaces or the number of persons working to the activities. The resource assignment uses some rules on how many persons to assign to an assembly of a certain type and duration. Knowing the estimated effort and the number of assigned resources it is now possible to calculate the estimated duration for the activities.

As the last step, we need to schedule the activities. The aim is to calculate the start and end times of the activities so that restrictions like the earliest possible start date or amount of available personnel are

not exceeded. As a result, we get the set of planned activities, which is then used in production to perform the ‘Do’ step in the Deming cycle.

Using the feedback from the shop floor it is possible to compare the original schedule with the current production status and thus perform the Deming ‘Check’ step to see if the project is still on track. If it becomes necessary, to create new planning, the ‘Plan’ step is rerun again before starting into the next ‘Do’ step. The feedback from production or delivery is used here as input to reschedule the activities. Possible usage is e.g. to set the finish data of an already activity to tomorrow or reduce the number of available workers.

After giving this short introduction we now concentrate on the scheduling methodology developed in the project. As we found no out-of-the-box solution which runs in a reasonable timeframe on the quantity structure known in shipbuilding with the complex boundary conditions given by e.g. resource availability in shifts, we had to develop this on our own.

3. Scheduling Implementation

The implementation of the scheduling is a core part of the ProProS demonstrator. As seen in Fig.3 our input is an activity network covering the production processes from the initial tack weld up to the complete section. One could clearly distinguish to different phases: the sub-assembly phase creating assemblies like girders or panel and assembly phase, combining those sub-assemblies to bigger and bigger units. Before scheduling, the activity network is prepared and already contains the estimated duration of all activities and predecessor/successor relations. Additionally, all nodes have a set of assigned resources, e.g. number of welders or a building place. Last but not least we know the resource availabilities like shift times, weekends, bank holidays in form of a resource calendar.

The task for the scheduling is to find an activity start sequence with the best fitness while respecting all constraints. From an engineering perspective, there is little if any flexibility on the order in the assembly phase: a girder should be welded on a deck panel before creating a section. But the sequence of the individual sub-assemblies is not dictated by the assembly order, and this contains most activities.

Mathematically speaking this is an optimization problem on the directed graph

$$G=(V, E)$$

where the activities are the vertices V and the successor and predecessor relationships defined by work preparation (Fig.4 Unseq.) as well as an activity start sequence (Fig.4 Solution A, B) as edge E . The possible activity start sequences result in several solutions

$$Y \in \mathbb{R}^n$$

These solutions could be evaluated using a cost function

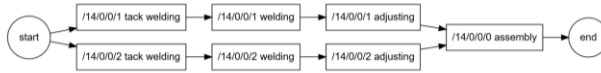
$$\varphi : \mathbb{R}^n \rightarrow \mathbb{R}$$

We now have to find an optimal solution Y which has a minimum in the cost function

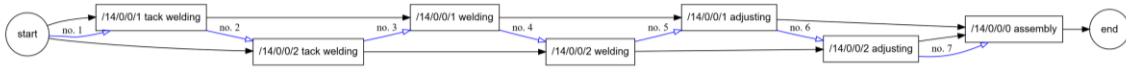
$$\min_{y \in Y} \varphi(y)$$

As we are talking about activity start sequence, this poses a discrete optimization problem. These are considered to be more complex to optimize than those with continuous design variables. In reality, we did not find an out-of-the-box solution that answered our needs. That’s why we implemented our solution aiming for a good balance between finding a good scheduling solution and reasonable runtime. The overall flow of this solution is found in Fig.5. The steps found in the inner grey box are used to create valid solutions for our domain problem, which is then wrapped in an outer optimization loop calculating the costs and whether to continue searching.

Unsequenced



Solution A



Solution B



→ Successor ▷ Temporal Sequence

Fig.4: Add sequence to activity structure

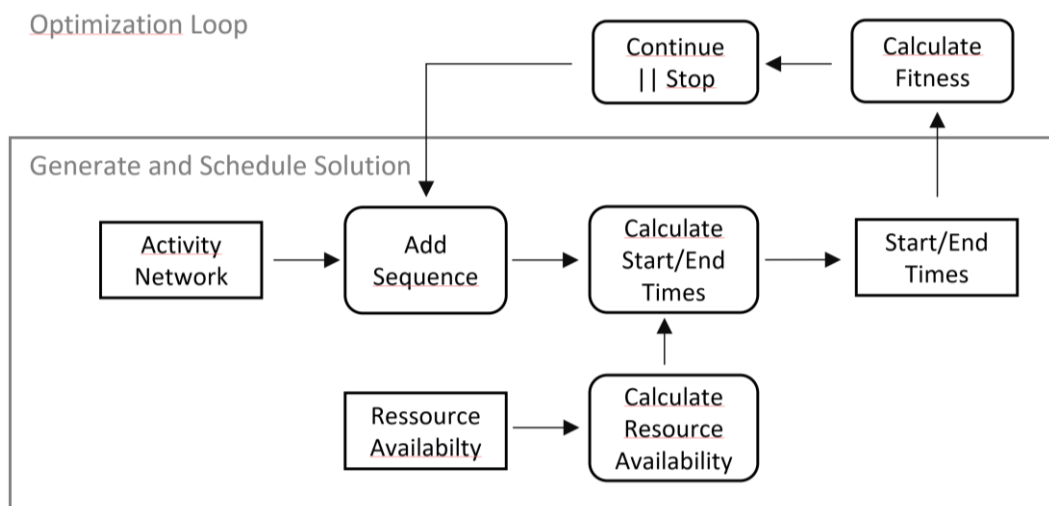


Fig.5: Steps to find a schedule

The first step to creating a valid solution is adding a global sequence to the activities. There are some restrictions given by the successor relationships in the activity network, but we are still free to e.g. first finish all activities on one subassembly and then go to the next one or hop across the activity network. An example is seen in Fig.5, the activity sequence in solution A is staying with the activity type whereas the sequence in solution B stays with the assembly. Currently, we add the activity sequence in random order, taking only the successor relationship into account.

The second step is to calculate all activities' start/end times. Following the activity start sequence, we check if the direct predecessor is already finished. If not, the simulation time is increased until the predecessor is finished. When increasing the simulation time we check for finished activities based on their end times and release their resources for further reuse. Secondly, we check that all needed resources are available. If not, the simulation time is again forward until an ending activity is finished to release them. After both preconditions are met, the end time is calculated using the expected duration and the resource calendar. The resources are blocked until that end time. This method does not require using a fixed time resolution nor has problems using different resource types.

This process to generate and schedule a solution is enclosed into an optimization algorithm, to find a sequence with minimal costs. We consider the total time spent from start to end as the most important factor for the cost calculation. Other cost functions are possible. One idea is to give an extra malus if

tack welding, welding and straightening for the same assembly does not run in a close sequence, or if the amount of work in progress (read: number of parts lying around on the shop floor) becomes too high. *Strobel-Hoffmann (2022)* also investigated calculating the sensitivity against disturbances, but the runtime is a problem.

The prototype uses simulated annealing, described by *Martins (2021)*, as an optimization algorithm. The underlying idea is to pick a solution in the neighborhood of the previous one and compare their cost function. This distance to the neighbor should decrease the closer we come to the simulation end. We choose the number of identical nodes in the sequence as criteria, e.g. solutions A and B from Fig.4 have a distance of 6/7, as they share only one common node in the sequence.

To avoid prematurely narrowing on a suboptimal solution, it is then decided to either continue with the better solution or jump to the worse one and continue from there. This decision is based on a randomly drawn reference value

$$r \in \mathcal{U} [0,1]$$

and calculating the jump probability based on the difference of the cost function and the current annealing temperature T

$$P = \exp\left(\frac{-(f(x_{new}) - f(x_{prev}))}{T}\right)$$

The new solution is taken over if the jump probability exceeds the reference value. The annealing temperature is decreased when running the simulation loop, using an exponential decrease

$$T = T_0 \alpha^k$$

over the iterations k . We decided on a start temperature of 100 decreasing with a cooling rate in the range of 0.9 – 0.95. To allow running the optimization on assembly structures with different sizes, we must norm the result of $f(x)$ to stay in a range of e.g. 0 – 10. As a reference value, we use the runtime of the unconstrained problem (infinite resources) on the critical path. This is then used to calculate the cost based on the found total runtime of a solution like

$$f(x) = \frac{t_{solution} - t_{criticalPath}}{t_{criticalPath}}$$

The results of this optimization are pretty decent for the intended purpose. Scheduling a complete section is done in approximately 5 minutes, respecting all given boundary conditions.

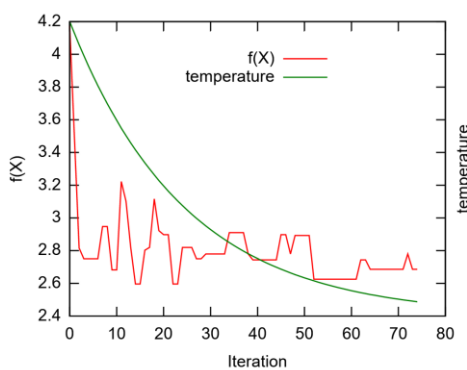


Fig.6: Optimization convergence

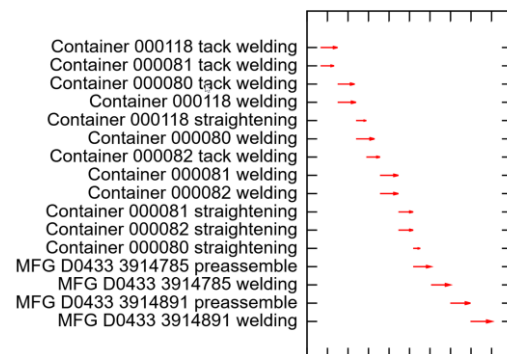


Fig.7: Example calculation

Simulated annealing is known to be a fast optimization algorithm, but it has also its downsides. A typical optimization run is found in Fig.6. The diagram shows both the decreasing temperature as well as the cost function plotted over the iterations. Simulated annealing is famous for often missing the global optimum, so the final result in iteration 75 is most probably neither the global nor a local optimum (e.g. found on iteration 23). On the other side, it converges within an acceptable timeframe and that's why it is a descend choice for an interactive tool like ProProS.

An example result for a small part of the complete activity network is shown in Fig.7. We provided only resources supporting two parallel tack welding, welding, or straightening activities and then get a nice schedule staying within the given boundary conditions.

The described scheduling algorithm is implemented as a separate component in the complete ProProS prototype (see Fig.7). It is implemented in Java and gets the activity structure and boundary conditions like start/end dates, effort, assigned resources etc. as input. The results are written back and then updated on the server. That way the scheduling component could be tested and used independently from the main server. The calculation is currently triggered on demand by a user from the web UI served from the main ProProS Server.

We use a similar setup for information coming from the design office as well as shopfloor information collected by the trace & track system. They are also implemented as separate components to easily adapt to systems already existing in a yard.

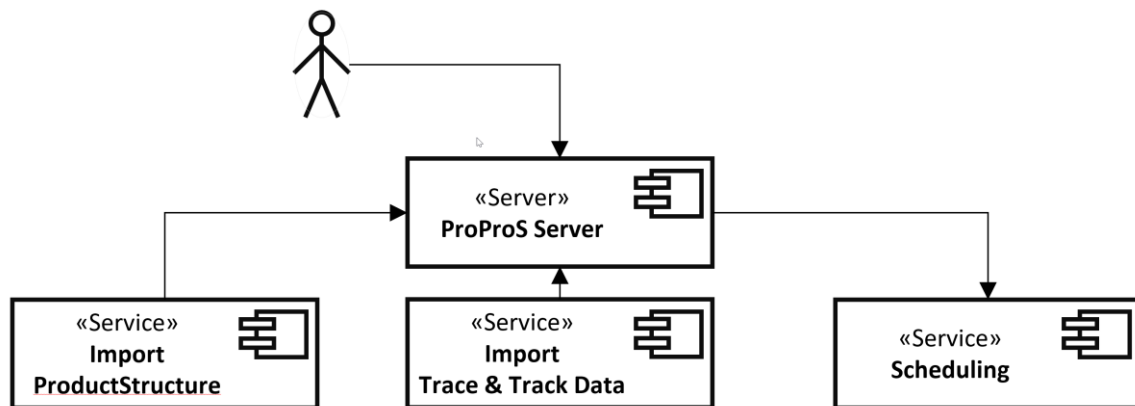


Fig.7: Deployment diagram of ProProS prototype

4. Conclusions

With the scheduling algorithm in place, we have implemented all necessary components to achieve the goal of the ProProS research project. The prototype supports the main use cases defined in the original research proposal:

- Create an estimation on the effort and total duration to build a section using a fine-granular bottom-up mechanism (Deming ‘Plan’)
- Provide insight on the impact caused by changing available resources like workers or building places (Deming ‘Act’)
- Using shopfloor data on e.g. delayed activities to show differences (Deming ‘Check’)
- Rerun Deming cycle with a reasonable effort

Unlike previous solutions, e.g. Koch (2011), the prototype uses a bottom-up approach to estimate the efforts needed in production and then develops a schedule that could be used as input for an MES system. Running the estimation and scheduling on the quantity structure known in shipbuilding is not easy. We tested several generic optimization solutions both from open-source and commercial vendors before we decided that we need to implement a problem-specific solution as outlined in chapter 2.

With this solution in place, we are now able to run the use cases described above on real yard data. As of writing this paper, we still have 9 months before the end of the research project. We already started with enhancing the user interface, *Zerbst (2021)*, based on the feedback from yard professionals working. A second aspect to be finished before the end of the research project is to enlarge the activity network by adding activities for part manufacturing like plate and profile cutting. This allows having an even better forecast on when to start manufacturing processes. Last but not least we will check, whether we could enhance the formulas used for effort estimation based on the trace and track information from the shop floor.

Acknowledgements

We would like to thank our PROSTEP colleagues Jan Bitomsky and Nils Sonnenberg for working on this project. We would also like to thank our master students Christina Strobel-Hoffman and Zarana Patel for their work. We further like to thank all colleagues from Fr. Lürssen and WZL who participate in the R&D project. And last but not least special thanks to Stefan Harries for providing some advice on optimization literature.

References

- DEMING, W.E. (1986), *Out of the crisis*, MIT, Center for Advanced Engineering Study
- KOCH, T. (2011), *Simulating the Production of Future Marine Products*, COMPIT Conf., Berlin
- MARTINS, J.; NING, A. (2021), *Engineering Design Optimization*, Cambridge University Press
- STROBEL-HOFFMANN, C. (2022), *Robuste Optimierung unter begrenzten Ressourcen*, TU Darmstadt
- ZERBST, C. (2021), *Deming Cycle Enabled: A Digital Twin for Ship Production*, COMPIT Conf., Mülheim

Quick Patch Design and Repair Planning using Software Tool for Carbon-Reinforced Epoxy Type of Repairs for Ship Structures

Arijana Milat, Alveus d.o.o., Rijeka/Croatia, arijana.milat@comparepairs.com

Darko Frank, Alveus d.o.o., Rijeka/Croatia, darko.frank@comparepairs.com

Abstract

Various ships experience frequent problems of corrosion and cracks, therefore ship owners seek a quick response from the ship repair companies. One of these quick repair solutions is COMPA Repairs technology, based on the application of carbon and glass fibres reinforced with epoxy resin onto a damaged surface, which enables the repair done during voyage or port operations. This paper presents the software tool for automatic generation of the composite patch design which enables a quick response to a ship-owner request. The software gives the suitable number of carbon and glass layers to be applied for the requested repair using the calculations based on the DNV regulation requirements. Moreover, it automatically generates the service report for the class approval.

1. Introduction

Various ships operate in harsh environments and experience frequent problems of corrosion and cracks affecting different systems and structures: pipes, valves, decks, tanks etc. The examples of damaged structures are presented in Fig.1. In such situations, ship owner or ship operator seeks an effective and fast repair solution to reduce potential risks, assure alignment with the international maritime regulations and minimize the time delays to its ships. Usage of traditional repair service such as steel cutting and welding requires redirection of a ship to a shipyard which results substantial vessel downtime and loss of revenue. The traditional approach requires a replacement of a part of ship structure, even when a problem is present only in a small section. In addition, this method requires the removal of parts, equipment or ship interior details, leading to greater expense and additional downtime to execute the repair. Most importantly, the welding cannot be applied in all areas of a ship since some locations are adjacent to fuel tanks and pose a potential fire risk, causing a cutting and welding procedure to be dismissed if fuel tanks are not emptied and properly cleaned before the repair.

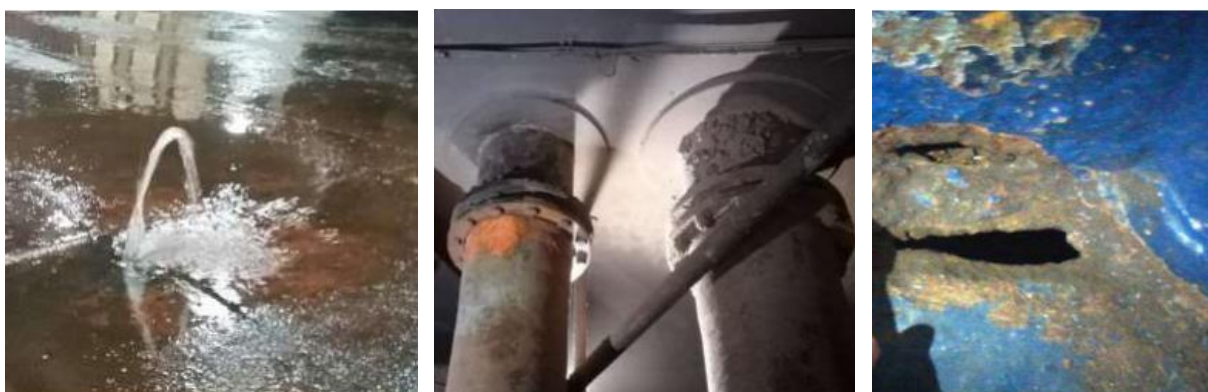


Fig.1: Various damages on ship structures

The potentially cost and time efficient alternative repair solution is a bonded patch repair based on fibre reinforced polymer (FRP), *Echtermeyer et al. (2014)*. This solution utilises fibres mixed with polymer resin. By curing, the resin hardens and bonds the fibres to the damaged surface permanently and the resulting composite material patch reinstates the damaged material's strength and provides water tightness; see the schematic representation of the composite patch on Fig.2.

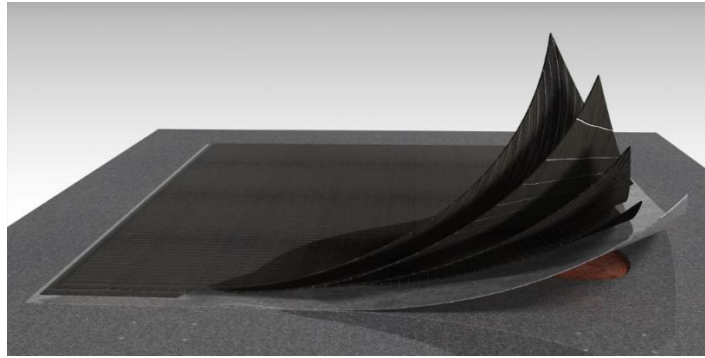


Fig.2: Schematic composite patch layup

This kind of composite repairs entered the service in aviation industry more than 30 years ago and were functionally used for crack repairs, *Baker (1984)* and structural reinforcements, *Baker et al. (1993)*. The recent overview also showed that the composite repairs are very cost effective, *Budche et al. (2018)*. Some years later, the composite repairs were also used to repair cracks and corrosion on ships and marine offshore installations, *Dalzel-Job et al. (2003)*, *Turton et al. (2005)*, *McGeorge et al. (2009)*. The composite patches used on board ships proved to be very durable and were reported to be functional even after more than 10 years in service, *Grabovac (2003)*. The EU funded project “CO-PATCH” made progress with designing patches for typical repairs on board ships and also showed that it is possible to monitor repaired cracks using strain-gauge technology, *Rodriguez et al. (2012)*. In parallel, composite repairs were also used in civil engineering for buildings and bridges, *Lim et al. (2016)*. Regardless of the industry branch, it seems that the most of applications and research efforts were focused on corroded and leaking pipes, *Saeed et al. (2014)*, *Linden et al. (2012)*. Consequently, many commercial products in a form of repair kits for composite repair of pipes emerged over the years and some of them were discussed in *Barkanov and Dumitrescu (2017)*. However, the unanimous opinion of the classification societies that have the authority over approval of the repairs in shipbuilding, is that there is still not enough practical evidence to support the claims that the composite repairs should be recognised as the permanent or in some cases even as temporary repairs in shipping industry.

This paper introduces a software tool that follows the principles of the mentioned repair service using the bonded patches and generates the patch design in a way that gives the suitable combination of bonded layers according to the damaged structure and conditions.

2. Ship repairs using COMPA Repairs technology

The specific composite ship repair described within the paper uses the COMPA Repairs technology, the solution that utilises the combination of carbon-reinforced epoxy and glass-reinforced epoxy layers that bonds onto damaged surface resulting a new layer of watertight and strong material. It is applicable for pipes, valves, plates such as bulkheads and tank plates etc. The main functionalities of the repair are: leakage prevention, prevention of further corrosion development, strength reinforcement (normal or shear stress relaxation), reduction of crack growth when possible.

The repair can be done during ship’s voyage or operations in the port which makes it attractive to the shipowner.

3. COMPA Repairs software

3.1. Usage

COMPA Repairs software is a software tool for automatic generation of the patch design for providing the ship repair service COMPA Repairs. It suggests the number of layers to be applied for requested repair, recommends the necessary patch thickness and adequate specific weight of the fibres

depending on a repair position, and suggests the type of resin to be used based on the application temperature. Also, the repair provider, i.e. the software user, can automatically create a service report in just one click. The calculations for obtaining the COMPA Repairs patch design are based on the DNV regulation requirements. Another functionality of the tool is the capability of calculating costs needed for the COMPA Repairs service and automatically creating an offer in Excel form.

The software is developed in python language using the python module Qt Designer for GUI, specifically PySide2. It is applicable on Windows platform, accompanying with the simple to use installation. Only pre-requisitions are MS Office tools, Word, and Excel.

Software has been tested by the COMPA Repairs team in several stages of its development and has been validated by comparing the software results with the specifications of existing repairs that have been applied on-board a ship and verified. Therefore, the software composite layup can be considered as valid for practical applications.

3.2. Graphical User Interface

The main GUI consists of one tab with basic information, Fig.3, and several tabs describing repair cases depending on the user's specifications, Fig.4.

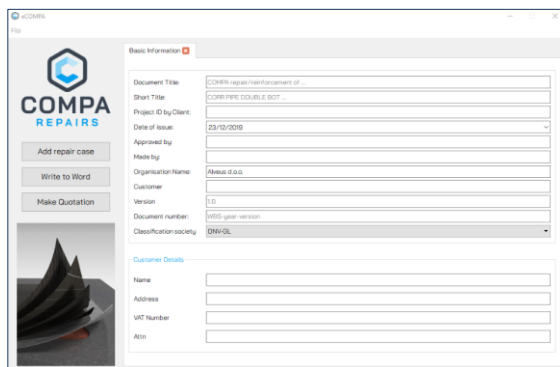


Fig.3: GUI window with basic information

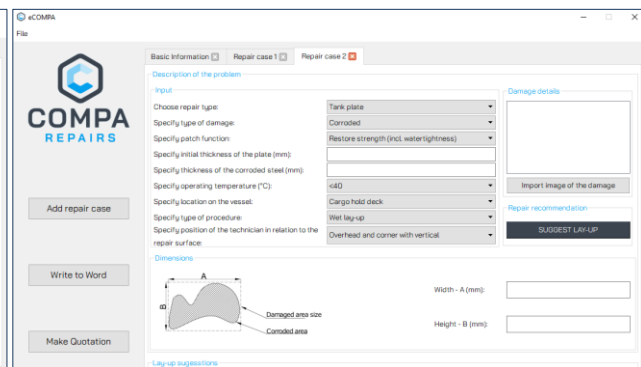


Fig.4: GUI window with selected repair case

The user can choose:

- Type of repair: straight / curved / Y junction / T junction pipe; tank plate / two plate intersection / three plate intersection; complex geometry and other
- Type of damage: corroded or crack
- Type of procedure: wet lay-up or vacuum bagging
- Repair aim (only for plates): restoring watertightness only or restoring watertightness and strength

Also, the user can describe the problem and import an image of the damage.

3.3. Layup suggestion

The software calculates and suggests patch layup i.e. required material and total thickness for different repair cases: corroded pipes, cracked or corroded tank plating and valves in general. Suggested layup is a result of the regression analysis of numerous finite element calculations that cover the whole design space (all thicknesses, diameters, pressures etc.). The procedures to obtain patch designs are described within Chapter 4.

Prior to layup suggestion, the user needs to fill in the required input parameters depending on the type of repair. When pipe repair is involved, patch design depends on the size of the outer diameter, distance between the supports, damage length and nominal design pressure. Regarding the type of procedure, only wet lay-up is applicable for the pipe repair cases. When tank repair is involved, patch

design depends on initial thickness of the plate, thickness of the corroded plate, and height and width of the corroded area. In this case, the purpose of the patch can be to restore strength or to restore watertightness only and two types of procedures are enabled: wet lay-up or vacuum bagging. In addition, it is also important to specify the position of the technician in relation to the repair surface because that depends on the selection of the proper material surface weight. In both repair cases, operating temperature is needed to select the proper type of resin material.

Additional functionality of the software is to compare layup with different material surface weight, where applicable, Fig.5. For example, if the suggested layup uses fibre specific weight of 300 g/m², the user can change different value of glass fibre surface weight or carbon fibre surface weight. This functionality enables user to choose according to the material availability. The change is also dependent on the structural dimensions and every specific weight is not always feasible. The feasibility of the selection is under control of the software.

Form

Lay-up comparison

Layer	Thickness, mm	Orientation, °	Fibre	Surface weight, g/m ²
1	0.206	-	Chopped strand glass fabric	150.0
2	0.206	-	Chopped strand glass fabric	150.0
3	0.206	-	Chopped strand glass fabric	150.0
4	0.268	0	BI-Axial 0/90 carbon fibre fabric	200.0
5	0.268	0	BI-Axial 0/90 carbon fibre fabric	200.0

Glass Surface weight (g/m²): 150.0

Carbon Surface weight (g/m²): 200.0

Total thickness (mm): 1.154

Accept

Fig.5: GUI window to compare different material surface weight

eCOMPA

Basic Information Repair case 1

Description of the problem

Input

Choose repair type: Tank plate

Specify type of damage: Corroded

Specify patch function: Restore strength (incl. watertightness)

Specify initial thickness of the plate (mm): 12

Specify thickness of the corroded steel (mm): 1

Specify operating temperature (°C): <40

Specify location on the vessel: Cargo hold deck

Specify type of procedure: Wet lay-up

Specify position of the technician in relation to the repair surface: Overhead and corner with vertical

Damage details

Import image of the damage

Repair recommendation

SUGGEST LAY-UP

Dimensions

Width - A (mm):

Height - B (mm):

Lay-up suggestions

Layer	Thickness, mm	Orientation, °	Fibre	Surface weight, g/m ²
1	0.274	-	Chopped strand glass fabric	200
2	0.274	-	Chopped strand glass fabric	200
3	0.274	-	Chopped strand glass fabric	200
4	0.268	0	BI-Axial 0/90 carbon fibre fabric	200
5	0.268	0	BI-Axial 0/90 carbon fibre fabric	200
6	0.268	0	BI-Axial 0/90 carbon fibre fabric	200
7	0.268	0	BI-Axial 0/90 carbon fibre fabric	200
8	0.268	0	BI-Axial 0/90 carbon fibre fabric	200
9	0.268	0	BI-Axial 0/90 carbon fibre fabric	200

Compare different surface weight

Check lay-up acceptance

Reset to recommended thickness

Resin to be used: West System 105/205

Recommended thickness (mm): 2.966

Actual thickness (mm): 2.966

Fig.6: Example of a repair case of corroded tank plate and suggested patch layup

If the user is not satisfied with the recommended layup, there is a possibility to manually add or delete one or more layers. Actual thickness is automatically calculated, and it can be compared with the recommended thickness which is visible on the screen. After modification, the user can check the acceptance of layup and calculated patch thickness.

The example of one tank repair can be seen in Fig.6, where besides the layup suggestion, the patch dimensions can be calculated according to the user's input dimensions for the corroded area.

3.4. Output documents

The software has the module for automatic generation of the repair plans for a class approval. Based on the user's specifications, the software writes a report in Word document containing the basic information of service provider and customer, repair details and instructions and risk assessment.

There is also a module used for automatic generation of the quotation for a client based on cost calculations. The offer is created in Excel document. Total cost consists of material cost, repair labour cost, travelling cost and engineering labour cost which are calculated based on the user input prices.

4. Theoretical background and analyses

4.1. Obtaining composite patch layup

The most important process of the repair preparation is obtaining the composite patch layup in terms of appropriate number of carbon-reinforced epoxy layers that will give sufficient strength and watertight when applied on damaged area.

Within the software, the calculation of appropriate number of layers for pipe repairs is based on the numerical results, whereas for the case of tank repairs, the calculation is based on practical experience.

4.1.1. Patch layup for corroded pipes

Patch design for corroded pipes is obtained using the results of a numerical model analysed with finite element method in Ansys 19.2 APDL. The analyses have been conducted for the straight pipe only and because simplification, the patch layups for curved, Y-junction and T-junction curve have been considered as for the straight pipe. Further development of COMPA software will consider the numerical analyses of before mentioned pipe types.

The appropriate number of carbon-reinforced epoxy layers is given from the results of a parametric study where following parameters were analysed: outer pipe diameter in range of 50 mm to 1000 mm; distance between the supports in range of 1 to 6 m; and nominal design pressure in range of 1.5 to 60 bar. Finite element model of pipe structure included only a composite part, see Fig.7. The steel part was neglected because it has been assumed that the pipe is a standard one that can withstand the given pressure.

The goal of each FE analysis was to obtain a minimum required number of layers with, at which the patch design satisfies Tsai-Wu failure criteria, meaning that the material satisfies the strength criteria. The Tsai-Wu failure criteria, *Tsai and Wu (1971)*, is expressed by the Tsai-Wu strength index which indicates that the material will fail if the value of index is greater than 1. The example of the results for one parametric case is presented in Fig.8. Other values were obtained by trilinear interpolation.

The material properties of glass/epoxy and carbon/epoxy are calculated according to DNV recommendations (DNV). The calculations for the elastic properties of a single chopped strand mat were considered for glass/epoxy, and the calculations for the elastic properties of a single unidirectional ply were considered for carbon/epoxy layer.

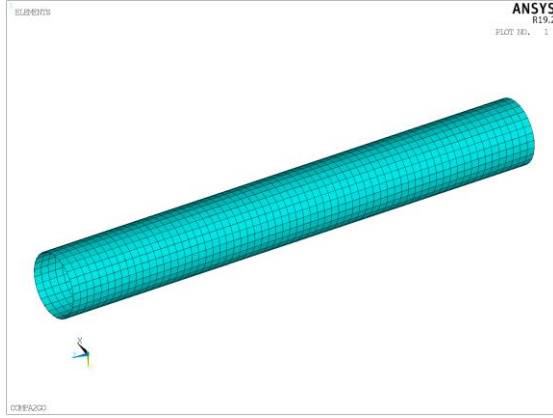


Fig.7: Example of FE pipe model

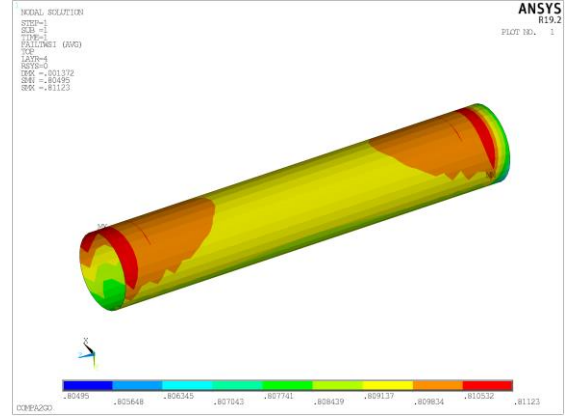


Fig.8: Tsai-Wu failure criteria index in layer where maximum occurs

The thickness of one bi-axial 0/90 carbon-reinforced epoxy layer (t_c) is calculated by:

$$t_c = \frac{\text{surfWeight} * 0.134}{100}, \quad (1)$$

where *surfWeight* denotes material surface weight in g/m^2 . In dependence of the pipe outer diameter size, COMPA Repairs takes into consideration maximum applicable carbon surface weight, presented in Table I.

Table I: Maximum applicable carbon surface weight used by COMPA Repairs

Pipe diameter	Carbon surface weight
< 70 mm	100 g/m^2
< 150 mm	200 g/m^2
< 350 mm	300 g/m^2
> 350 mm	400 g/m^2

The thickness of one glass-reinforced epoxy layer (t_g) is calculated by:

$$t_g = \frac{\text{surfWeight} * 0.137}{100}. \quad (2)$$

It is recommended to use 3 layers of glass fibres, required for the prevention of the galvanic corrosion.

Regarding the epoxy resin, Table II shows the recommended resins in dependence of operating temperature.

Table II: Resin used for patch layup

Operating temperature	Resin material
< 40°C	West System 105
< 55°C	Pro-Set LAM 125(135,145)/224
< 80°C	Pro-Set LAM 125(135,145)/224 with post curing
< 135°C	Pro-Set HTP 182/284 with post curing
< 180°C	Pro-Set M 1020/2016 with post curing

COMPA repair for corroded pipe can be performed using only wet lay-up procedure (hand lamination without vacuuming).

4.1.2. Patch layup for tank plates

The repair cases for tank plates are divided by the type of damage: corroded plates or plates with crack. In both cases, the plates can be straight, corner with two plate intersection and corner with three plate intersection.

When COMPA Repairs is used for corroded tank plates, its purpose can be to restore the full strength of the plating in corroded area, or to restore watertightness only. When used for cracked tank plates, the purpose can be for restoring watertightness only.

Material specific weight depends on the working position of the technician in relation to the repair surface as shown in Table III.

Table III: Recommended material specific weight in relation to the working position of the technician

Material specific weight	Working position of the technician in relation to the repair surface
max 200 g/m ²	Overhead and corner with vertical
max 300 g/m ²	Vertical and corner
max 400 g/m ²	Horizontal

The repair can be performed using wet lay-up procedure or vacuum bagging.

When wet lay-up is used, the thicknesses of one layer are calculated by Eqs.(1) and (2) for carbon/epoxy layer and glass/epoxy layer, respectively.

When vacuum bagging is used, the thicknesses of one carbon/epoxy layer (t_c) and glass/epoxy layer (t_g) are calculated by:

$$t_c = \frac{\text{surfWeight} * 0.107}{100} \quad (3)$$

$$t_g = \frac{\text{surfWeight} * 0.104}{100}. \quad (4)$$

Using the practical experience, the patch layup for tank plates always consists of 3 layers of glass/epoxy fibres. In order to restore the full strength of the damaged plating, total thickness of carbon/epoxy fibre should be 2 times of the thickness of corroded steel. When the repair is needed to restore watertightness only, 3 layers of glass chopped strand fibre and 2 layers of carbon bi-axial 0/90 fibre are used. As in the case of pipe repairs, the resin used for patch layup depends on the operating temperature and recommendations are given in Table II.

4.2. Obtaining patch dimensions

Considering tank repairs only, the dimensions of the patch need to be calculated.

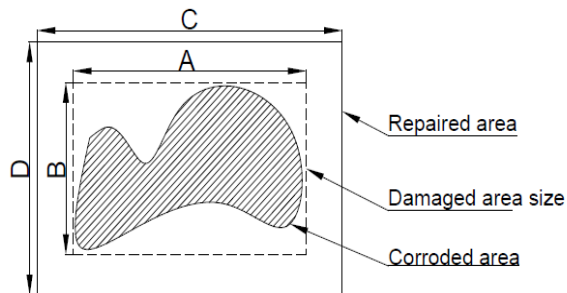


Fig.9: Dimensions for the patch over corroded area

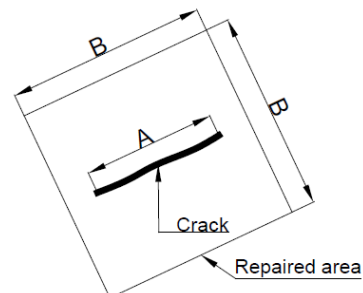


Fig.10: Dimensions for the patch over crack

If the damage is corroded area, Fig.9 shows the sketch of the patch dimensions, where the values A and B are provided by the client and the values of C and D are calculated by Eqs.(5) and (6) for the purpose of watertightness only, and Eqs.(7) and (8) for the purpose of strength and watertightness.

$$C = A + 40 \text{ cm} \quad (5)$$

$$D = B + 40 \text{ cm} \quad (6)$$

$$D = B + 60 \text{ cm} \quad (7)$$

$$D = B + 60 \text{ cm} \quad (8)$$

If the damage is crack, Fig.10 shows the sketch of the patch dimensions, where the value of A is given by the client and the value of B is calculated by:

$$B = A + 40 \text{ cm} \quad (9)$$

5. Conclusion

The software presented in the paper is a tool enhancing the ship repair service that bonds fibre reinforced plastic material onto the damaged structure. The software gives a customized composite patch design and significantly speed up the process of responding to the ship-owner request. The patch design is suggested using the calculations based on the DNV regulation requirements and within the software, the user can automatically generate the service report for a class approval containing all the repair details and instructions and risk assessment.

Further development will include more repair cases and improvement of the numerical calculations. Other development will include the software usage on different platforms for example web-based or mobile application enabling the repair technicians to create patch design on site before the repair process.

Acknowledgement

Development of COMPA Repairs software was part of the COMPA 2GO project that has received funding from the European Union's Horizon 2020 research and innovation programme under grant agreement No 806018.

References

- BAKER, A. (1984), *Repair of cracked or defective metallic aircraft components with advanced fibre composites - an overview of Australian work*, Composite Structures 12, pp.153-181
- BAKER, A.; CHESTE, R.; DAVIS, M.; ROBERTS, J.; RETCHFORD, J. (1993), *Reinforcement of the F-111 wing pivot fitting with a boron/epoxy doubler system-materials engineering aspects*, Composites 24, pp.511-521
- BARKANOV, E.N.; DUMITRESCU, A. (2017), *Non-destructive Testing and Repair of Pipelines*, Springer
- BUDCHE, S.; BANE, M.D.; DE BARROS, S. (2018), *Bonded repair of composite structures in aerospace application: a review on environmental issues*, Applied Adhesion Science 6/3
- DALZEL-JOB, J.; SUMPTER, J.; LIVINGSTONE, F. (2003), *Composite Patch Repair of Steel*, Proc. Advanced Marine Materials, Technology and Applications, London
- DNV (n.d.), *High speed and light craft, Pt.3 Ch.4 Sec.6-2 Elasto-mechanical properties of FRPs*, DNV, Hovik

ECHTERMEYER, A.T.; McGEORGE, D.; GRAVE, J.H.L.; WEITZENBOCK, J. (2014), *Bonded patch repairs for metallic structures – A new recommended practice*, J. Reinforced Plastics and Composites 33(6), pp.579-585

GRABOVAC, I. (2003), *Bonded composite solution to ship reinforcement*, Composites, Part A: Applied Science and Manufacturing 34, pp.847-854

LIM, K.S.; AZRAAI, S.N.A.; NOOR, N.M.; YAHAYA, N. (2016), *An Overview of Corroded Pipe Repair Techniques Using Composite Materials*, J. Chemical, Molecular, Nuclear, Materials and Metallurgical Eng. 10/1

LINDEN, J.M.; KOPPLE, M.; ELDER, D.; GIBSON, A.G. (2012), *Modelling of composite repairs for steel pressure piping*, 15th European Conf. Composite Materials, Venice

McGEORGE, D.; ECHTERMEYER, A.T.; LEONG, K.H.; MELVE, B.; ROBINSON, M.; FISCHER, K.P. (2009), *Repair of floating offshore units using bonded fibre composite materials*, Composites: Part A 40, pp.1364-1380

RODRIGUEZ, E.; DE LA MANO, R.; BLANCO, L. (2012), *Crack repair of steel vessels with bonded composite patches – damage control with FBGS*, 15th European Conf. Composite Materials, Venice, pp. 24-28

SAEED, N.; RONAGH, H.R.; VIRK, A. (2014), *Composite repair of pipelines, considering the effect of live pressure-analytical and numerical models with respect to ISO/TS 24817 and ASME PCC-2*, Composites Part B: Engineering 58, pp.605-610

TSAI, S.W.; WU, E.M. (1971), *A general theory of strength for anisotropic materials*, J. Composite Materials 5, pp.58-80

TURTON, T.J.; DALZEL-JOB, J.; LIVINGSTONE, F. (2005), *Oil platforms, destroyers and frigates - case studies of QinetiQ's marine composite patch repairs*, Composites, Vol. Part A: Applied Science and Manufacturing 36, pp.1066-1072

Methodology for Approval of Autonomous Ship System CONOPS

Marianne Hagaseth, SINTEF Ocean, Trondheim/Norway, mhaga@sintef.no

Ørnulf Jan Rødseth, SINTEF Ocean, Trondheim/Norway, ojr@sintef.no

Per Håkon Meland, SINTEF Digital, Trondheim/Norway, phm@sintef.no

Egil Wille, SINTEF Ålesund, Ålesund/Norway, ew@sintef.no

Brian Murray, SINTEF Ocean, Tromsø/Norway, brian.murray@sintef.no

Pia Meling, MASSTERLY, Oslo/Norway, pia.meling@massterly.com

Abstract

This paper outlines a methodology to describe the concept of operations (CONOPS) of autonomous ship systems. The intention of this methodology is to formalize the activities performed by the various actors in the autonomous ship system, both the ship itself, the remote-control centre, and others. The activities are described in the context of the various voyage phase patterns (cargo operations, berthing, sailing etc) that a voyage consists of and the required ship processes (navigation, cargo handling etc.). The description can be used for approval of the autonomous ship system and for safety and security analysis.

1. Introduction

Autonomous ship systems must be at least as safe and secure as conventional ships. To ensure this, the concept of operation (CONOPS) for an autonomous ship system must be described for each of its areas of operation and for its intended usage. Currently, few formalities exist on how to ensure that all aspects regarding autonomous, supervised, and manual operations are covered.

Currently, autonomous ship systems are approved according to what is described as alternatives and equivalent design as described by IMO, *IMO (2013)*. This can be carried out for ship processes, systems, or components that either directly or indirectly propose alternative ways of compliance with prevailing regulations. For instance, the Norwegian Maritime Authority uses the approach of alternative and equivalent design when approving autonomous ship systems, *IMO (2013)*. This is done in lack of specific regulations for autonomous ship systems; however, IMO has started work on this in their scoping exercise, *IMO (2021)*.

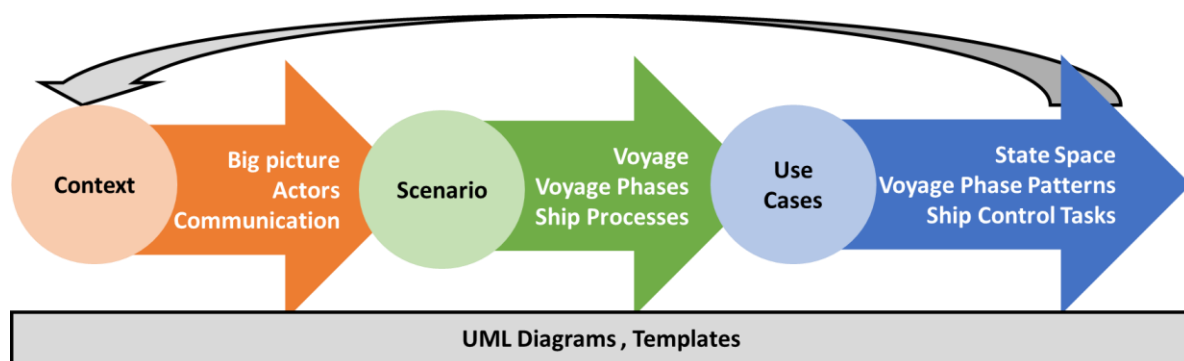


Fig.1: Methodology Overview

An important aspect is that the autonomous ship system must be approved for a certain operation in a given geographical area. This means that a CONOPS is needed, that is, a detailed description of the autonomous ship system's operation. In this paper, we will demonstrate a methodology to formalize these descriptions. The methodology is based on UML (Unified Modeling Language) models describing the use cases and activities, the state transitions and message sequences. Activity diagrams give an overview of the needed operations during a voyage. This means that the autonomous ship system's operation can be described based on formalized templates using UML and then detailing this description to the scenario at hand through several iterations, see Fig.1. This is based on a methodology previously

described in (Rødseth *et al.*, 2021) and (Rødseth, 2021). This paper will give a practical example of application of this methodology for an autonomous cargo ferry crossing the Oslo fjord.

In addition to being used during approval, a formalized description of the operation of the autonomous ship system can be used during testing of the system and the description of the test procedures.

2. Background for the Methodology

2.1 Handover

Constrained autonomy means that the automation systems and human operators must cooperate on more equal terms, and we do not expect the system to be fully autonomous, i.e. a Remote Control Centre (RCC) operator must be available. Further, the RCC operator must trust that the automation is able to notify the operator in time for him or her to get situational awareness and conduct corrective actions in cases where the automation encounters problems. This means that the RCC operator does not need to be available at all times, for instance during the less demanding operations. Also, the automation must ensure that alerts are sent to a human operator in cases when the automation detects that it is not able to handle the situation. If the automation does not get positive response from the RCC operator, the automation must transfer the ship to a pre-defined fallback condition to avoid an unacceptable risk to the ship or environment. The RCC operator can take direct control of the autonomous ship system at any time.

A related concept to the handover between the RCC operator and the automation on board is the accountability of autonomous ship systems as described in Myhre *et al.* (2020). They argue that accountability is an important part of the design of an autonomous ship system, in that a clear description of accountability is needed regarding who is legally accountable for the system, how the hand-over is done, how to ensure that exactly one party is accountable at any given time, and how to handle cases where the accountable party is not able to fulfil its obligations. This can be seen as a formalization of the more equal term cooperation between automation and humans.

2.2 Autonomous Ship System

According to ISO (2021), an Autonomous Ship System is defined as all elements that interact to ensure effective functioning of the autonomous and non-autonomous processes and equipment that are necessary to perform the ship's operation or voyage. This means that the safe and secure operation of the autonomous ship will depend on systems not located on the ship, for instance a Remote Control Centre, its operators and the available communication systems. Further, this means that the description of hand-over between the various parts of the ship system and the accountability of each of the components will be an important design criterium.

2.3 Human-Automation Interaction in Autonomous Ship Systems

The ship system described here is not fully autonomous, meaning that the automation cannot solve all issues without help from a human operator. On the other hand, the ship's automation systems can perform some operations safely on its own, under some well-defined conditions. In addition to this, the RCC operator can take direct control of the ship at any time, while the operator can also trust the ship to notify him in time for getting situational awareness and taking proper action, alternatively going to a fallback state if the operator fails to react in time.

ISO (2021) defines 'automation' as the implementation of processes by automatic means, while a ship system's process or equipment is said to be 'autonomous' if some of its components are designed and verified to be safely controlled by automation with no human intervention. These two definitions lead to the conclusion that automation can be used to provide autonomy, and that autonomy emerges when the system is designed, approved and deployed to be operated without human intervention or supervision for certain periods of time, Rødseth *et al.* (2021).

2.4 Level of Human Control in the Autonomous Ship Systems

ISO (2021) suggests that the level of human control on a process may be divided into three levels:

- C0 is where automation handles the system control task and where a human is not needed at all.
- C1 is where the human has responsibility for some parts of the system control task while the automation handles others, for instance when the automation can handle encountering of one ship at open sea, while sailing in more densely trafficked areas cannot be automatically handled.
- C2 is where the human has the full responsibility for the system control task, and where automation is only assisting or offering advice to the human.

2.5 Level of Automated Control in the Autonomous Ship Systems

The level of automation may also be divided into three levels, *ISO (2021)*:

- A0 is where automation is not able to control the process alone and always requires human attention.
- A1 is the degree where automation can handle some parts of the processes, but not all.
- A2 is where automation can control all aspects of the process and does not need human assistance.

2.6 Degrees of Autonomy

Fig.2 shows the suggested degrees of autonomy when taking into account the level of human control (C0, C1, C2) and the level of automated control (A0, A1, A2).

	C2	C1	C0
A2	OA	AC	FA
A1	OA	AC	
A0	OE		

Fig.2: Degree of Autonomy [from *ISO (2021)*]

ISO (2021) proposes that these levels can be described as follows:

- Fully autonomous (FA): This is when the ship system is approved for operation completely without operators. Operators may still monitor the system, but they will not need to intervene. This means that the accountability is on the automation system.
- Autonomous control (AC): This is when the automation can control the systems under certain conditions and where humans should be available to intervene when required. The conditions are described by a set of state variables and values. The availability of the humans is described by the response time, Fig.3. This means that the accountability is divided between automation and human, and that this transfer of control and the related conditions for this must be clearly defined. The automation can be trusted in that it will either notify a human operator in time for him to be able to get situational awareness, react and solve the situation, or if this is not possible (the operator does not answer or communication is down), the automation will go to a fallback state.
- Operator and automation (OA): Automation can do certain control tasks and will give assistance, but a human is required to be near a control position so that he or she can supervise the process and

intervene when necessary. This means that the human is the accountable party, and that they do not rely on the automation to notify about the operation. However, the operator will possibly receive alarms from the onboard systems than they must handle. An example here is when the operator is in direct control but that the navigation is done by an autopilot.

- Operator exclusive (OE): Automation can only give limited assistance, and the operator needs to be continuously in control of the processes. This means that the human is the accountable party. An example here is when the operator is directly steering the ship.

For this paper, the AC and OA levels are the most relevant, since we do not assume the ferries to be fully autonomous with no operators available, and we also assume that direct control by the RCC operator is only needed in specific cases, and not continuously.

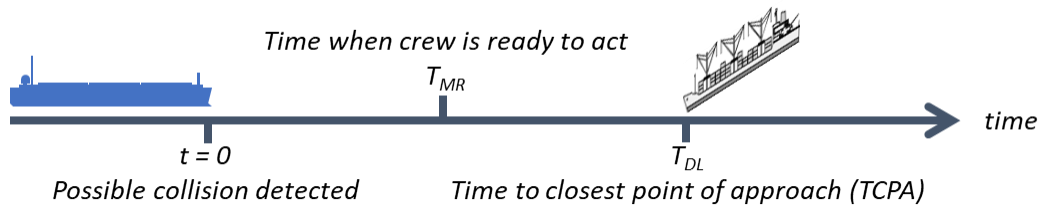


Fig.3 Response time for human operators, (Rødseth, 2021)

2.7 Generalization

When the methodology has been applied for several autonomous ship systems and several operations, this may result in a set of generalized descriptions that can be used as pattern or templates for describing a different concept of operation for a similar autonomous ship system. The lower part of Fig.1 indicates that a set of generalized descriptions as UML diagrams and templates may be used as input for new descriptions of operations. Each voyage phase can be selected from a generalized description, and the specific context, state variables and values and use cases can be fine-tuned to the specific case at hand.

3. Methodology with VesselAI Example

The methodology consists of three main steps to set up the CONOPS, Fig.1, the description of the Context (Section 3.1), the Scenario (Section 3.2) and the Use Cases (Section 3.3). The concept of operation will be specific for each autonomous ship system with its specific context and operational area. However, if descriptions of general voyage phase patterns, processes, use cases and templates are available, they can be used to simplify the specification of a CONOPS for a certain autonomous ship system. The description of the CONOPS can be done through several iterations.

The methodology is exemplified with a scenario from the VesselAI project (<https://vessel-ai.eu/>) covering autonomous cargo ferries sailing between Moss and Horten, crossing the Norwegian Oslo fjord. In this case, a Remote Control Centre will be utilized, with operators having the role of an onshore captain in cases when the autonomous ferries need support, e.g. to recover from a fallback state. The scenario is further described in the following sections.

3.1. Context

The context of the autonomous ship system consists of a high-level description of the system, an overview of the physical characteristics of the ship, a description of the external actors to the system, that is, sensors, automation in port and relevant services, a high-level description of the Remote Control Centre (RCC) being part of the autonomous ship system, and lastly, a description of the communication systems that are used between the various parts in the autonomous ship system, see the left (orange) part of Fig.1. This description is according to what is summarized in the Autoship project report on autonomous ship design standards, Rødseth et al. (2021).

3.1.1 Big Picture

Fig.4 shows a possible route for the autonomous ASKO ferries planned to cross the Oslo fjord between Moss and Horten from 2022. This ship system consists of two ferries crossing the Oslo fjord carrying 16 trucks each on a 50-minute crossing with four trips scheduled each day in each direction. The ferries are unmanned and supervised, as well as monitored and controlled by an operator in a remote control centre in Horten. The ferries are electric, and in each of the two ports, berthing and de-berthing is done by auto-mooring systems, and loading and unloading of the trailers is done with unmanned terminal tractors. The containers are picked up by electric, manned trucks and are delivered to ASKO warehouses on each side. In this description, we will only look into one ferry, meaning that we will not cover the handover between several RCC operators.

These unmanned ferries operate in an area with relatively dense traffic, where manned vessels are sailing both as part of regular short sea operations (up to five car ferries running between Moss and Horten every 20 minutes), traffic in and out of Oslo and Drammen following the traffic separation lane in the middle of the fjord, and also local unpredictable traffic, for instance leisure boats often sailing closer to one of the shore sides. Also note that the ASKO ferries need to cross the track of the car ferries, since the ASKO quay is to the north in Horten, and to the south in Moss, compared to the car ferry quays. Thus, navigating out of port and approaching the port are likely to be the most demanding parts since in this area the ASKO ferries must turn around to leave/approach the port.

Fig.4 shows an example route where the voyage from Horten (west) to Moss (east) is divided into five phases, A for leaving the port of Horten, B when starting the first leg of the crossing, C, when crossing the traffic separation zone, D, when sailing the last leg, and E, when approaching the port of Moss.

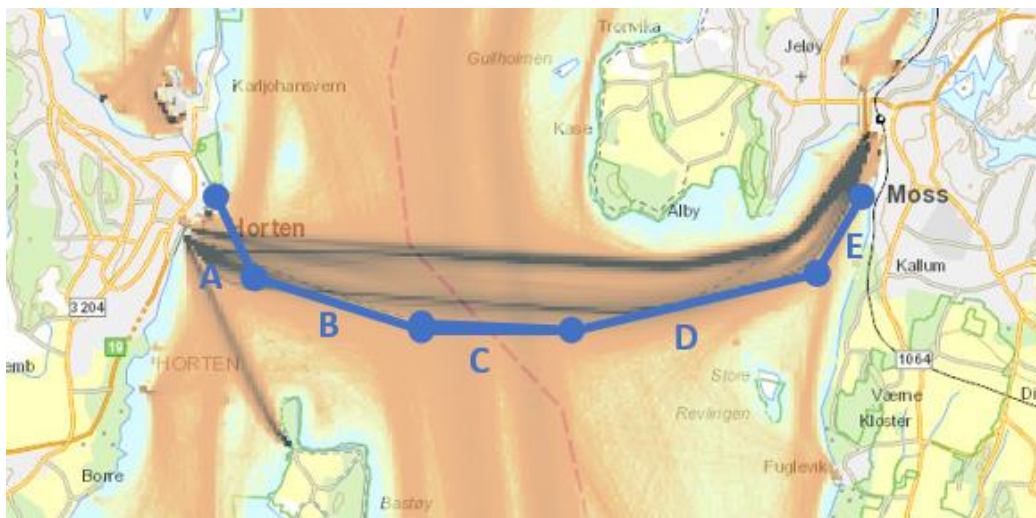


Fig.4: Example route for ASKO ferries crossing the Oslofjord [from <https://kystinfo.no/>]

The autonomous ship system used as an example in this paper is simplified, and will consist of one unmanned ferry, sensors onboard and onshore, and an operator available in the RCC. The RCC operator will have available automatic monitoring equipment similar to that used for Vessel Traffic Services (VTSs), in addition to functionalities especially developed for the operation, supervision and monitoring of unmanned ships. This will be AI algorithms for prediction of the behaviour of the traffic in the area of operation of the ferries, and AI algorithms to predict possible conflicts with other traffic at earlier stages than usual, to be able to reduce the number of evasive manoeuvres for the ferry.

3.1.2 Physical Characteristics of Ship

The ASKO ferries has a capacity of 16 Euro trailers. Length is 67.4 m, beam 15 m and draught 3.7 m. Service speed is 8 kn and max speed is 10 kn, meaning that the crossing between Moss and Horten will

take about 50 minutes. The battery capacity is 1.85 MWh which ensures fully loaded sailing for 4 h at 8 kn. The loading/unloading time is 65 minutes.

3.1.3 Actors

Each of the central actors in the autonomous ship system must be described. This includes the level of automation, level of human control, and degree of automation, according to Section 2.4, 2.5 and 2.6. It can be useful to start with a set of actors described in UML and then select the actors from these. Examples are actors for sensors and various communication means.

The two main actors in the ASKO autonomous ship system are the Remote-Control Centre (RCC) operator and the Autonomous Onboard Controller (AOC), Fig.5.

The RCC will have functionalities such as:

- Remote control, monitoring and operation of the ship
- Handling exceptions
- Follow-up activities during the voyage, e.g. contact with other vessels, ports, government, etc.
- Planning of maintenance, schedules and voyages
- Cargo management such as contact with cargo providers, customers, terminal workers etc.
- Ordering of services, equipment and technologies needed for the maintenance of the ship
- Safety and preparedness activities

The RCC can remotely operate or take control of the ships and perform the connection with other conventional ships, possibly other RCCs, Vessel Traffic Service (VTS) centres or others that require information from the ASKO ferry. This includes information exchange with the ports and requires awareness about the communication availability and integrity between the RCC and the ferry to ensure that the accountability is correctly handled, *Myhre et al. (2020)*.

An important part of the RCC tasks related to the ASKO ferries, is to utilize tools based on AI algorithms to predict the routes for all manned vessels surrounding the unmanned ASKO ferry. The purpose of this is to improve the situational awareness for the RCC Operator during the ASKO ferry voyages and also to reduce the number of evasive manoeuvres needed during the voyage. Better predictions of the behaviour of the nearby traffic should reduce the number and severity of critical situations that the ferries run into. Also, in VesselAI, work is performed to improve the planning of the route that the ASKO ferries will take on their voyage between Moss and Horten, and especially to calculate the optimal starting time for the voyage. When the best possible time slot for the voyage is selected based on the predicted nearby traffic, the number of cases where hand-over by the RCC operator is needed, will be held at a minimum. Likewise, the number of cases where the ferries need to go into fallback states, may also be held at a minimum.

In addition to this comes the possibility for the VesselAI-tools to conduct anomaly detection, meaning that the system can detect that the nearby traffic is diverging from their predicted behaviour.

The AOC will have the following tasks:

- Interact with onboard systems to execute the autonomous operations
- Interact with external sensors and systems, for instance external infrastructure, which may be shore-based or land-based, weather data from sensors and navigational aids from external sources for instance lidars in the port used for positioning during berthing and de-berthing
- Interact with other vessels
- Interact with VTSs, e.g. sending current route plan
- Report real-time information to the RCC
- Calculate own capacities based on internal factors (own capacity, propulsion system, ballast

and trim, technical condition, power production) and external factors (fairway conditions, weather, traffic, geography, digital infrastructure)

- Validate the communication link between the ship and the RCC

In a testing phase, the ASKO ferries will be operated from a RCC in Horten with crew onboard. When the testing and approval is finished, the ASKO ferries will operate unmanned.

Fig.5 shows that both the RCC and the AOC can access the onboard systems and that the RCC and the AOC must communicate directly to be able to handle the accountability of the whole autonomous ship system. Also, both the RCC and the AOC must interact with external actors. The external actors include:

- Autonomous terminal tractors that are used for roll-on and roll-off of the trailers from/to the ferries
- Automated mooring system activated from the ferry when it is being moored or is leaving the berth
- Local Positioning System (LPS) which is a more accurate positioning system used in the port to aid in mooring, berthing and cargo operations
- The operation area for the ASKO ferries is covered by Horten VTS, so the RCC Operators need to interact with this.
- Other ships: The autonomous ship system may also have to interact with other ships in the area. This may be through voice for the RCC Operator or via electronic message exchange for the ferry.

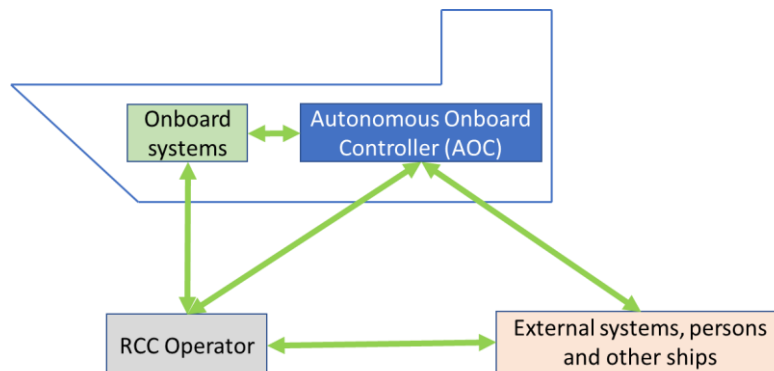


Fig.5: Autonomous Ship System

3.1.4 Communication Systems

The communication between the RCC and the ASKO ferries will need to have relatively high bandwidth for remote control of the ferries, typically via internet protocols over mobile data, for instance MBR (Maritime Broadband Radio, <https://www.kongsberg.com/no/maritime/products/bridge-systems-and-control-centres/broadband-radios/maritime-broadband-radio/>).

For communication between the ferries and the mooring system, dedicated short range and real-time lines for direct control is needed. These may have lower requirements to the bandwidth required but high demands on low latency and jitter.

3.2. Scenario

The operation itself is described as a scenario containing a voyage including its voyage phases and the sequence of each phase, see middle (green) part of Fig.1 and further description in Section 3.2.2. Also, the ship processes that are needed to control the ship in its various operations, need to be described, see Section 3.2.3.

3.2.1 Voyage

The big picture description of the context is formalized in an UML activity diagram as shown in Fig.6. This shows a possible, overall UML activity diagram for an ASKO ferry operating between Moss and Horten. Each of the activities must be further described and detailed with several other UML diagrams.

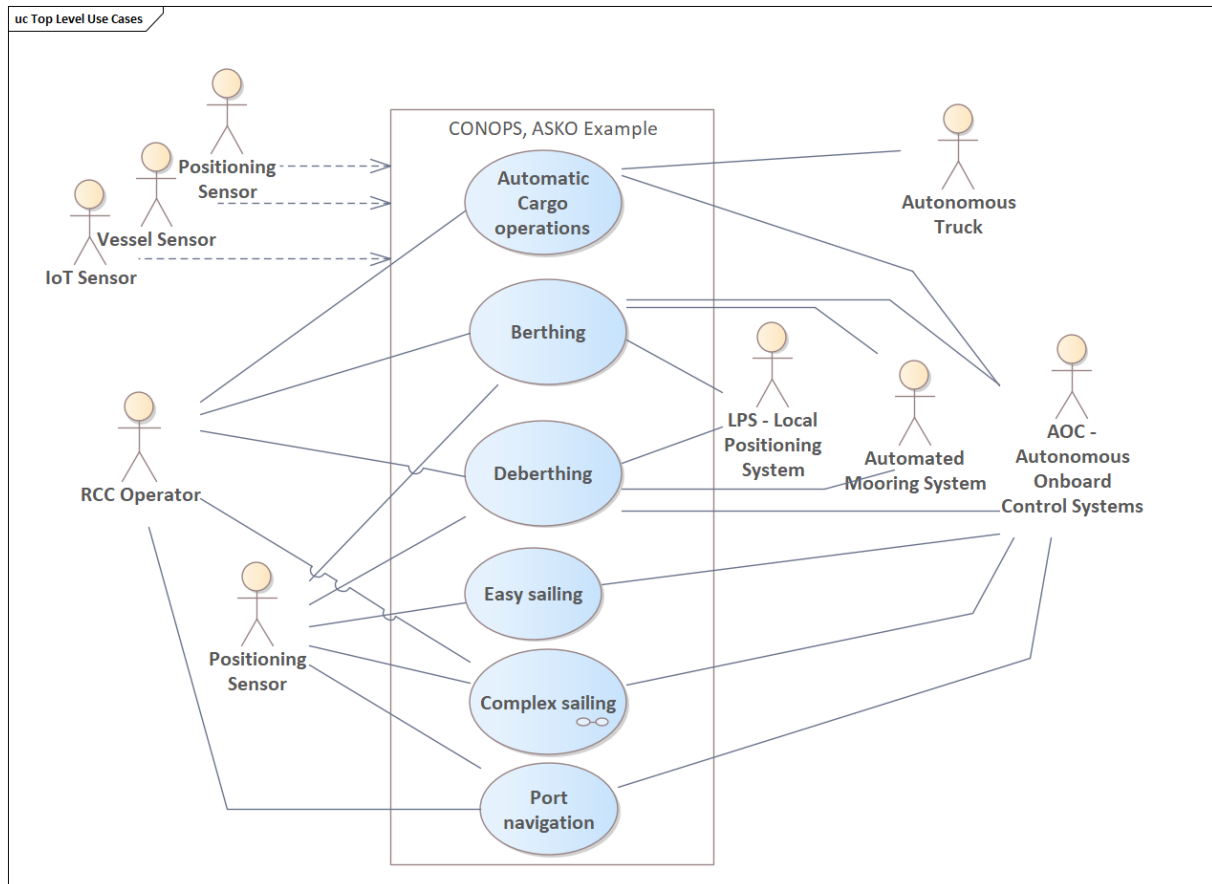


Fig.6: UML Top Level Activity Diagram

3.2.2 Voyage Phases and Sequence

Fig.7Error! Reference source not found. gives an example of how a voyage from Horten to Moss with the ASKO ferries can be described by a sequence of voyage phases.

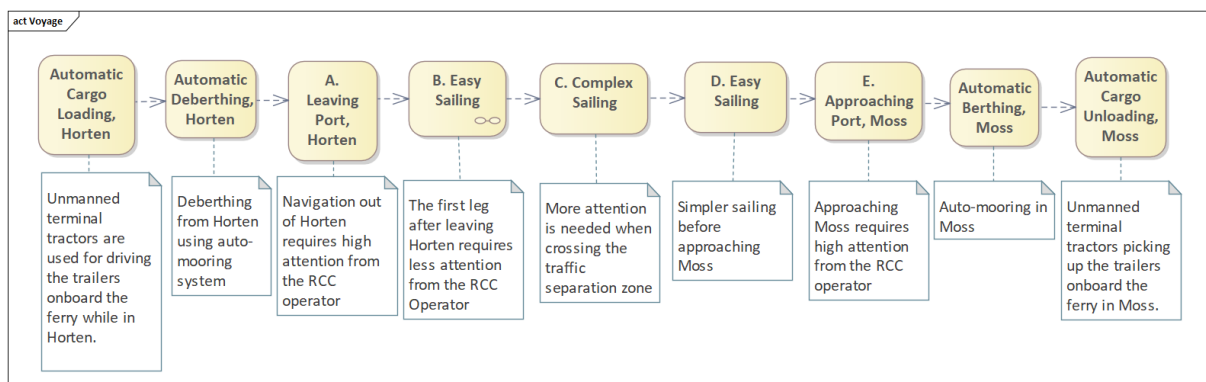


Fig.7: ASKO Ferry voyage phases

The voyage phases shown in Fig.7 can be generalized into voyage phase patterns, Fig.9: Automatic Cargo Loading/Unloading, Deberthing, Berthing, Easy sailing, Complex sailing, and Port Navigation.

The actual voyage phases must be detailed for the specific scenario. In some cases, templates for these descriptions can be used as an initial description, and then updated with the specific requirements.

3.2.3. Ship Processes

Fig.9 shows the two most relevant ship processes for the ASKO scenario, namely Navigation and Cargo Handling. For navigation, the following is important processes for this scenario, *Rødseth et al. (2021)*:

- Situational awareness, that is, to verify the location, observe weather and sea, determine visibility, detect and classify objects and obstacles and assess own ship and the traffic situation.
- Manoeuvring the ship, that is, to do short term planning of safe operations, keep track, speed and course, avoid obstacles and avoid grounding, operate automation systems, for instance acknowledge that an auto-mooring-operation can start, or do manual berthing or unberthing when the operational state makes it impossible to do this automatically, and interaction with other actors during manoeuvring, for instance other ships or the VTS.
- Voyage management, that is, planning and re-planning of the voyage done by the RCC operator based on the prediction algorithms for the traffic during a possible crossing and prediction of the route for the ASKO ferry, do pre-departure and pre-arrival checks, monitor voyage and act on deviations that are not handled by the ASKO ferry by itself.
- Communication during voyage, that is, communication involving other ships, RCC and VTS.

The cargo handling for the ASKO ferries will be done by automatic trucks moving the trailers on and off the ferry. After the trailers have been placed on the quay, they are picked up by manned electric trucks driving the trailers to their destination.

Other ship processes not shown in Fig.9 may include deck operations, cargo, stability, hull integration, machinery and technical systems, security, safety and emergency management, environmental protection and maintenance, ship administration and planning.

3.3. Use Cases

The third part of the methodology is the description of Uses Cases, see right (blue) part of Fig.1. Each use case is described by a State Space, Section 3.3.1, and some Ship Control Tasks, Section 3.3.3. Each ship control task can span several voyage phase patterns and may be automatic (indicated with green colour in Fig.9 or semi-automatic (indicated with orange). Black colour indicates that the combination of ship process and voyage phase is not relevant.

Fig.9 shows how a set of Ship Control Tasks can be defined for a set of ship processes and voyage phases. For each use case, the State Space is described by text, and the Ship Control Tasks is described by various UML diagrams and related textual descriptions. Use case diagrams for each Ship Control Task will cover UML diagrams for:

- Activities, including fallback activation
 - UML Activity diagrams for the overall description of each ship control task, Fig.10.
 - UML State diagrams for detailed activity description, Fig.11.
- Transfer of Control describing the human-automation interface: The "accountable" actors are actors that can make an independent operative decision, i.e. either a human or automation that is qualified as autonomous. Transfer of control describes the transfer of accountability between actors in a specific ship control task.
 - UML Collaboration diagrams: For the ASKO scenario, this is indicated in Fig.12.
- Communication describing the information flow between actors to be able to assess the safety and security for the communication systems.
 - UML Sequence diagrams, Fig.13.

3.3.1 State Space

The state space for each ship control task is described by a set of variables used to describe the condition under which the ship system will operate in this use case. Typical variables may be:

- Level of human control (C0, C1, C2) for the actors in the autonomous ship system, e.g.
 - Availability of the RCC Operator
 - Ability of the RCC Operator to get situational awareness
 - Response time for the RCC Operator
 - Possibility to divide responsibility between human operators and automatic systems.
 - Human control needed during cargo operation
 - Human control needed during mooring operation
- Level of automation (A0, A1, A2) for each actor in the autonomous ship system including the ship, the mooring system, and terminal tractors.
- Operator response time in the cases where an automatic actor in the autonomous ship system is in direct control, but control is needed to be handed over to a human.
- Traffic condition, e.g. density of traffic and type of traffic
- Geographic or fairway conditions, e.g. whether the voyage is in open waters or in a narrow channel.
- Operational status:
 - Own ship condition, e.g.:
 - Condition of the ship and its manoeuvrability
 - Availability of ship sensor data (e.g. position data, radar, cameras)
 - Availability of communication
 - For berthing, condition of mooring system, and ship's ability to communicate with this
 - For cargo operations, condition of the terminal tractors picking up and delivering the trailers and their possibility to support automatic loading and unloading
 - For cargo operation, status (e.g. ready for loading/unloading) of cargo onboard or on shore
 - Availability, range and status for external sensors:
 - Sensors during sailing (radars, cameras)
 - Sensors during berthing and deberthing (eg. local positioning system as lidar, cameras)
 - Terminal status e.g. quay is free to start the unloading operation
- Weather situation (wind, current, waves)

For the ASKO ferries, the state space can be described by the variables as shown in Fig.8. These are some examples, meaning that more variables are needed for a complete description, and also more details regarding the actual values.

Voyage Phases	Degree of autonomy	Operator response time T_{DL}	Traffic condition	Geographic conditions	Operational status	Weather	Voyage Phase Pattern
Automatic Cargo Loading, Horten	Autonomous control (AC)	1 min, operator available, and takes over if notified by automation.	NA	NA	Check if cargo and autonomous trucks are available for loading	NA	Automatic Cargo Handling
Automatic Deberthing, Horten	Autonomous control (AC)	1 min, operator does monitoring, and takes over if notified by automation.	NA	NA	Direct control if no lidar for local positioning	Direct control by operator needed if wind > 10 m/s	Deberthing
A. Leaving port, Horten	Autonomous control (AC)	1 min, operator	Medium traffic	NA	Direct control if camera detects	Direct control by	Port Navigation

Voyage Phases	Degree of autonomy	Operator response time T_{DL}	Traffic condition	Geographic conditions	Operational status	Weather	Voyage Phase Pattern
		available, and close monitoring	density, high traffic complexity		unidentified objects	operator needed if wind > 10 m/s	
B. Easy sailing	Autonomous control (AC)	5 min, operator available, but monitoring not needed, automation can be accountable party	Low traffic density, low traffic complexity	NA	Tactical control if CPA must be changed	Direct control by operator needed if wind > 18 m/s	Easy sailing
C. Complex sailing	Autonomous control (AC)	2 min, operator monitoring and is always the accountable party	Medium traffic density, low traffic complexity	NA	Direct control in case evasive manoeuvre is needed	Direct control by operator needed if wind > 18 m/s	Complex sailing
D. Easy Sailing	Autonomous control (AC)	5 min, operator available, but monitoring not needed	Low traffic density, low traffic complexity	NA	Tactical control if CPA must be changed	Direct control by operator needed if wind > 18 m/s	Easy sailing
E.Approaching Port, Moss	Autonomous control (AC)	1 min, operator available, and close monitoring	Medium traffic density, high traffic complexity	NA	Direct control if camera detects unidentified objects	Direct control by operator needed if wind > 10 m/s	Port Navigation
Automatic berthing, Moss	Autonomous control (AC)	1 min, operator does monitoring, and taking over if notified by automation.	NA	NA	Direct control if no lidar for local positioning	Direct control by operator needed if wind > 10 m/s	Berthing
Automatic cargo unloading, Moss	Autonomous control (AC)	1 min, operator available, and taking over if notified by automation.	NA	NA	Check if cargo and autonomous trucks are available for unloading	NA	Automatic Cargo Handling

Fig.8: Example state space for ASKO ferries

3.3.2 Voyage Phase Patterns

After specifying each of the voyage phases that the voyage from Horten to Moss consists of, generalizations may be done into voyage phase patterns covering two or more of the voyage phases. This will be based on the actual voyage phases described and also the state space for each voyage phase and ship process. The rightmost column in Fig.8 lists the voyage phase pattern that each voyage phase in the Horten-Moss crossing can be generalized into.

3.3.3 Ship Control Tasks

The ship processes described in Section 3.2.3 and the voyage phase patterns from Section 3.3.2 give us the five Ship Control Tasks (SCTs) as shown in Fig.9.

		Voyage Phase Patterns					
		Automatic Cargo Loading/Unloading	Deberthing	Berthing	Easy sailing	Complex sailing	Port Navigation
Ship Processes	Navigation		UCS1 Navigation during berthing/deberthing		USC2 Navigation during easy sailing	UCS3 Navigation during complex sailing	UCS4 Navigation during port approach and leave
	Cargo Handling	UCS5 Autonomous cargo handling					

Fig.9 Example Ship Control Tasks for ASKO ferries crossing the Oslofjord

Fig.9 gives an overview of the different use cases that realize the ship control tasks for each ship process and voyage phase pattern. In this example, we have selected navigation and cargo handling as the most relevant processes. The rest of this paper shows example UML diagrams to describe the Ship Control Task for navigation during automatic berthing and deberthing (UCS1 in Fig.9).

Fig.10 shows the overall UML activity diagram for the ASKO autonomous ship system for the navigation process during automatic berthing and deberthing where the RCC operator is available. This diagram shows that the berthing/deberthing starts in an automatic mode by checking the connection to the auto-mooring system, checking the physical mooring conditions and by validating the position by the local positioning system. When initialization is OK, the automation onboard will keep track, speed and heading to/from quay until finished. If problems are encountered that cannot be solved by the automation onboard, the RCC operator is requested to take direct control.

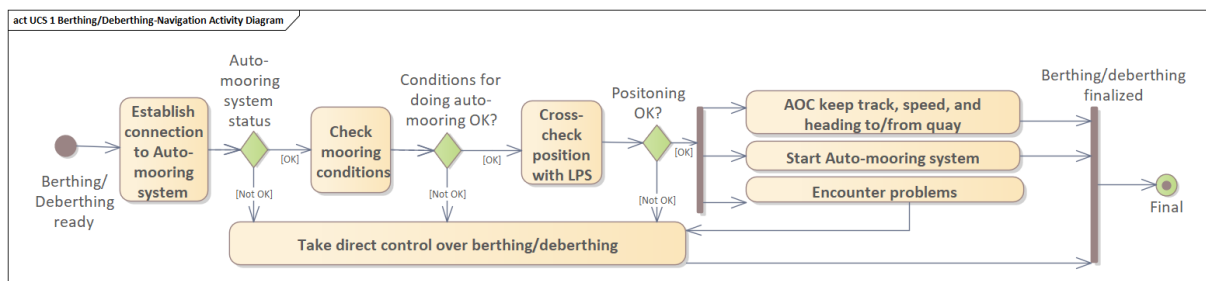


Fig.10: UML Activity diagram for UCS1 Navigation during berthing/deberthing

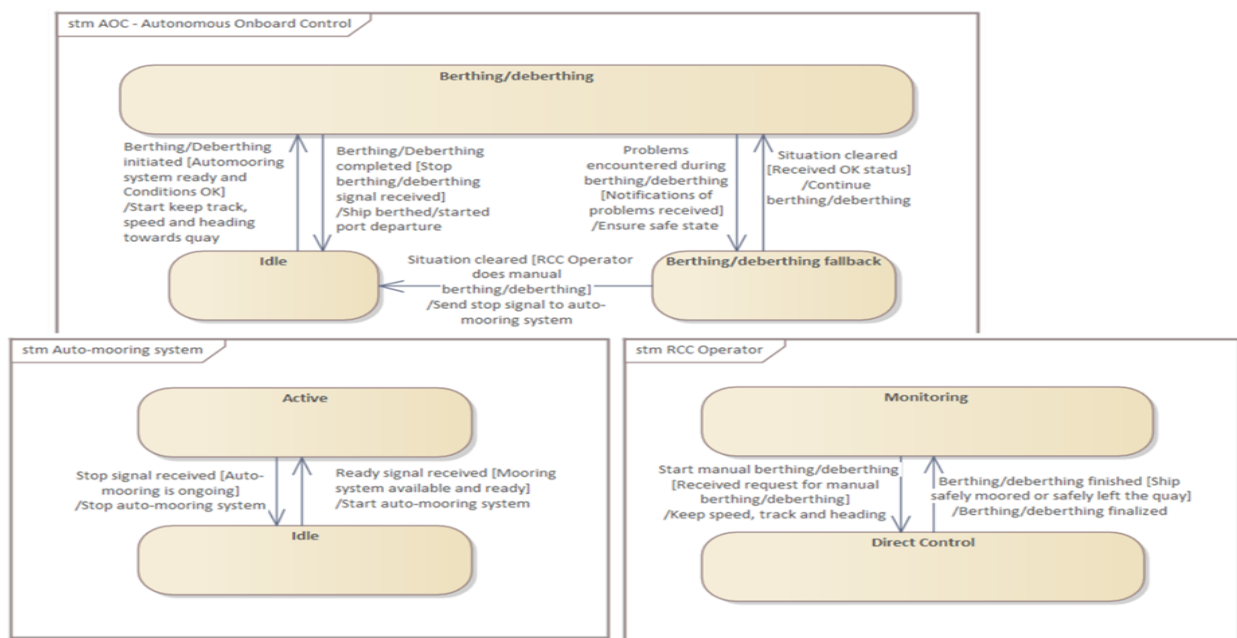


Fig.11: UML State diagram for UCS1 Navigation during berthing/deberthing

Fig.11 shows the UML state diagrams for the AOC, the auto-mooring system and the RCC operator during navigation to and from the quay. The AOC is in state berthing/deberthing until the ferry is safely moored or has left the quay, or until some problems have occurred which may trigger a fallback state. Further the AOC goes in idle state when the berthing/deberthing is finished or when the RCC operator has taken direct control. The fallback situation is solved either by the RCC operator taking direct control or the problem has been solved by the AOC itself or the auto-mooring system.

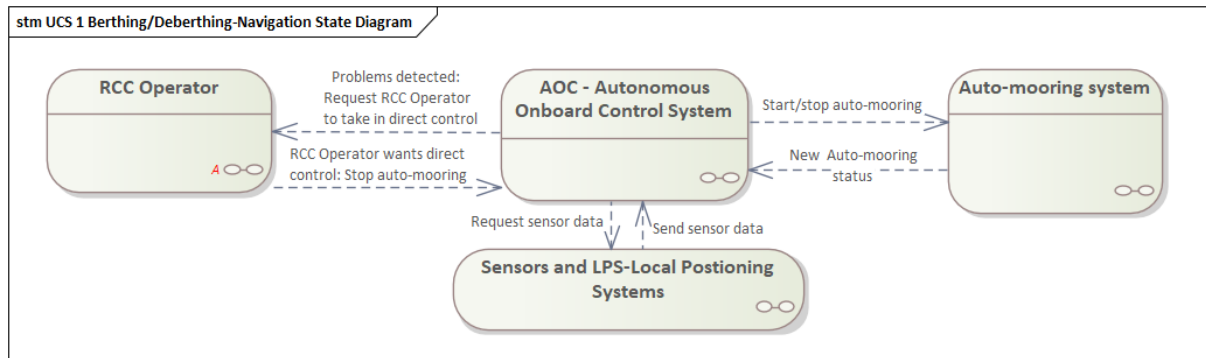


Fig.12: UML Collaboration diagram for UCS1 Navigation during berthing/deberthing

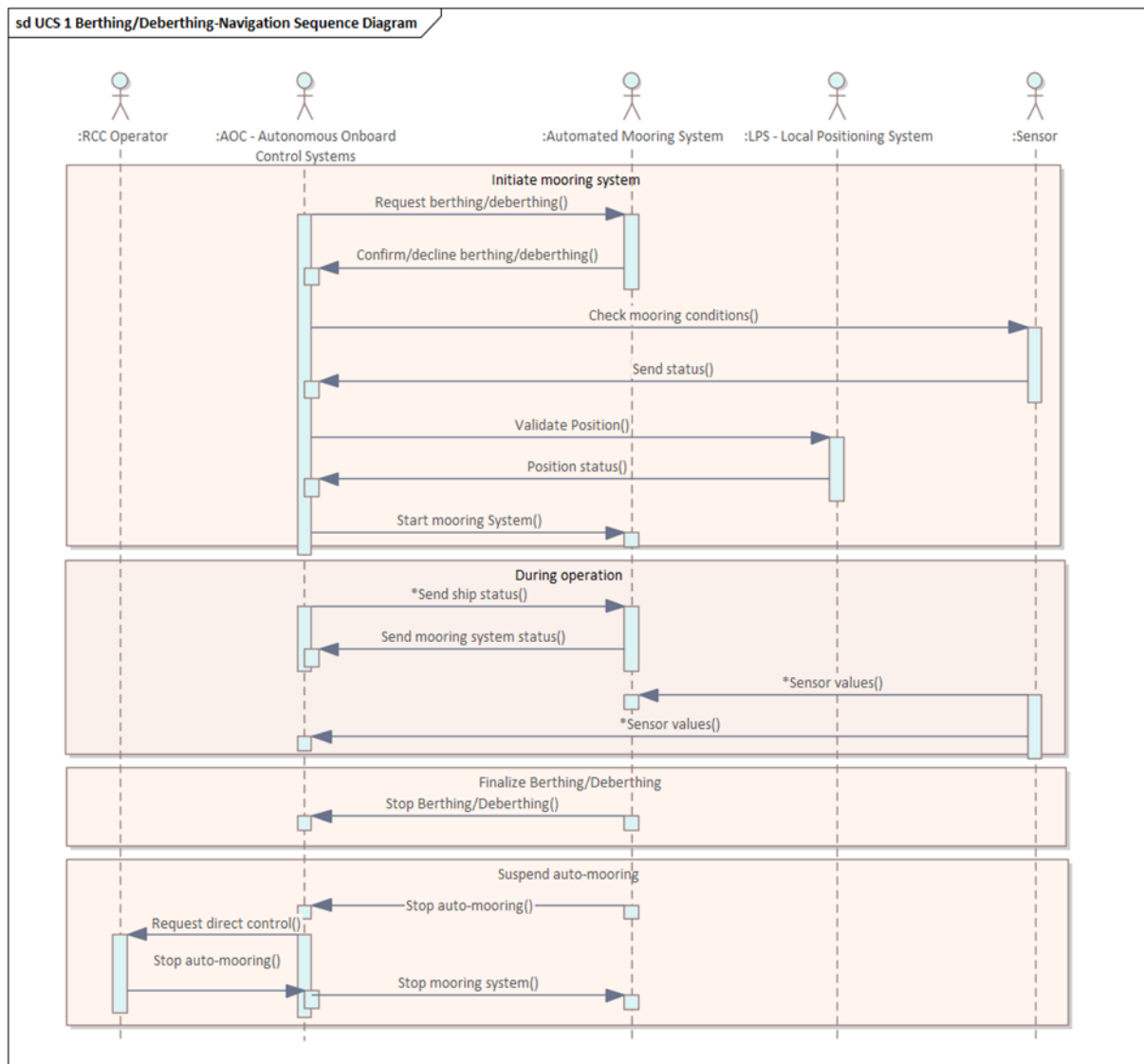


Fig.13: UML Sequence diagram for UCS1 Navigation during berthing/deberthing

Fig.12 shows a simple UML Collaboration diagram for the interaction between the state machines for the RCC Operator, the AOC, the auto-mooring system and external sensors. This diagram shows that the berthing/deberthing is initiated by the AOC, but also that the AOC is dependent of the clearance from the auto-mooring system to start and continue the operation. The RCC operator can at any time take direct control without asking the AOC, however, the AOC must be notified about this. Also, the AOC can request the RCC operator to take direct control in cases where problems have occurred.

Fig.13 shows an UML sequence diagram describing the interaction between the RCC operator, the AOC, the auto-mooring system, the Local Positioning System and some external sensors during navigation to and from the quay. This diagram can be used as a starting point for describing possible vulnerabilities of the communication between the various actors and the effect of this. This sequence diagram is divided into the following: Initialization of the auto-mooring system, message exchanges during operation, finalization of the berthing/deberthing, and handling of error conditions.

4. Conclusion and Further Work

This paper has given an example of how our proposed methodology can be applied on a relatively simple ferry operation. The method is still under development and results from applications on several projects, including VesselAI, will be used to improve it.

A main purpose of the methodology is that the use of UML in the design process also can be used in analysis, verification and approval of the systems. As was mentioned earlier in the paper, the methodology also emphasizes generalization of ship control tasks and their capability envelope, so that reuse of already approved ship control tasks in new scenarios can be greatly simplified.

Acknowledgements

This work has been performed as part of the VesselAI (<https://vessel-ai.eu/>) and AEGIS (<https://aegis.autonomous-ship.org/>) projects, that have received funding from the European Union's Horizon 2020 research and innovation program under Grant Agreements 957237 and 859992.

References

- DNV (2021), *Competence of remote control centre operators*, DNV-ST-0324, <https://rules.dnv.com/docs/pdf/DNV/ST/2021-08/DNV-ST-0324.pdf>
- IMO (2013), *Guidelines for the approval of alternatives and equivalents as provided for in various IMO instruments*, MSC.1/Circ.1455, Int. Maritime Org., London
- IMO (2021), *Outcome of the Regulatory Scoping Exercise for the Use of Maritime Autonomous Surface Ships (MASS)*, Int. Maritime Org., London, [https://wwwcdn.imo.org/localresources/en/MediaCentre/PressBriefings/Documents/MS.1-Circ.1638%20-%20Outcome%20Of%20The%20Regulatory%20Scoping%20ExerciseFor%20The%20Use%20Of%20Maritime%20Autonomous%20Surface%20Ship%20s...%20\(Secretariat\).pdf](https://wwwcdn.imo.org/localresources/en/MediaCentre/PressBriefings/Documents/MS.1-Circ.1638%20-%20Outcome%20Of%20The%20Regulatory%20Scoping%20ExerciseFor%20The%20Use%20Of%20Maritime%20Autonomous%20Surface%20Ship%20s...%20(Secretariat).pdf)
- ISO (2021), *ISO/TS 23860 - Ships and marine technology - Vocabulary related to Autonomous Ship Systems*, Int. Standard org., Geneva
- MYHRE, B.; RØDSETH, Ø.J.; PETERSEN, S. (2020), *Integrating accountability in the systems design of autonomous and remote-controlled operations*, IOP Conf. Series: Materials Science and Engineering 929
- RØDSETH, Ø.J. (2021), *Constrained Autonomy for a Better Human–Automation Interface*, Sensemaking in Safety Critical and Complex Situations, CRC Press, pp.235-247

RØDSETH, Ø.J.; WENNERSBERG, L.A.L.; NORDAHL, H. (2021a), *Towards approval of autonomous ship systems by their operational envelope*, J. Marine Science and Technology, pp.1-10

RØDSETH, Ø.J.; FAIVRE, J.; SIV RANDI HJØRUNGNES, S.R.; PÅL ANDERSEN, P.; BOLBOT, V.; PAUWELYN, A.S.; WENNERSBERG, L.A.L. (2021b), *D3.1 - Autonomous ship design standards*, Report from AUTOSHIP project on Autonomous Shipping Initiative for European Waters

WENNERSBERG, L.A.L.; NORDAHL, H.; RØDSETH, Ø.J.; FJØRTOFT, K.; HOLTE, E.A. (2020), *A framework for description of autonomous ship systems and operations*, 3rd Int. Conf. Maritime Autonomous Surface Ship (ICMASS)

Meteorological Navigation by an ECDIS-Like System: Discussing the Algorithms and Demonstrating the Functionalities for Conventional Propulsion and for Sail-Assisted Ships

Andrea Orlandi, Consorzio LaMMA, Florence/Italy, orlandi@lamma.toscana.it

Andrea Cappugi, Tate, Florence/Italy, andrea@tate.it

Riccardo Mari, CNR-IBE and Consorzio LaMMA, Florence/Italy, mari@lamma.toscana.it

Francesco Pasi, CNR-IBE and Consorzio LaMMA, Florence/Italy, pasi@lamma.toscana.it

Alberto Ortolani, CNR-IBE and Consorzio LaMMA, Florence/Italy, ortolani@lamma.toscana.it

Abstract

A meteorological navigation system has been implemented by integrating MetOcean data in an open-source ECDIS-like system. Several novel functionalities have been added, based on different MetOcean data layers. These are accessed by GIS standard approaches. Wave spectral data are also included, by adopting the spectral partitions synthesis and adding an effective graphical representation for directional polar diagrams. Some of the implemented seakeeping and powering computational approaches are discussed. These are based on the definition of a decoupling scheme where part of the ship-specific dataset is “off-line” precomputed, by the heaviest part of algorithms, leaving only the cheapest and fast ones to the “on-line” phase, under the routing operator control. Different approaches to seakeeping and powering computations have been considered, also including approximations for wave spectral partitions and for the effect of auxiliary sails, allowing for different sail settings. In further developments, the ship specific pre-computed dataset could be fine-tuned by data-driven system identification techniques exploiting tank measurements or in-service recorded performance data. Numerical benchmark tests are shown in order to demonstrate the potentialities of the present prototype system, both for conventionally propelled, and for sail assisted ships.

1. Introduction

Navigation tasks have always required the clever and efficient integration of many different elements and knowledge areas, Bull (2021), going from ship positioning techniques and nautical cartography, passing through general and area specific navigation and safety regulations, till to the current and the (predicted) forthcoming en-route MetOcean conditions, along with own ship responses and performance in such environmental conditions, Chen and Chesneau (2008). To accomplish these tasks, modern technologies offer relevant and valuable navigational instruments and aids, today available on-board through Integrated Bridge Systems (IBS) and Integrated Navigation Systems (INS). A further and wider level of integration is being developed under the e-Navigation concept framework, that has been developed under the auspices of IMO, <https://www.imo.org/en/OurWork/Safety/Pages/eNavigation.aspx>, and is finalized to increase safety and security in commercial shipping through better organization of data on ships and on-shore, and better data exchange and communication between the two and among ships, www.iala-aism.org/technical/e-navigation, Lind et al. (2018).

This paper focuses on the “meteorological navigation” component of the navigational tasks, that is on the complex activity of route planning and voyage profile selection, keeping into account the interplay between ship responses and environmental MetOcean conditions. Also en-route voyage monitoring and post-voyage analysis can be considered as part of meteorological navigation. In all this matter the key element is the capability of making a clever and effective synthesis of the available MetOcean data with the knowledge on how a ship specifically responds to the encountered environmental conditions. In this context the interplay between data on MetOcean conditions and weather routing software tools Perera et al. (2017) play a relevant role, not only in relation with offshore and oceanic navigation, but also for coastal navigation and Short Sea Shipping, e.g. López et al. (2020).

This paper has the goal of describing OrCa_EPD, a prototype meteorological navigation system that, starting from EPD (e-Navigation Prototype Display, by Danish Maritime Authority) open source

ECDIS-like system, *Brinkmann et al. (2017)*, has been implemented in order to dynamically merge data from numerical models for atmospheric and oceanographic forecasts, with ship specific data and ship performance models. Several features have been added to the EPD system and the resulting OrCa_EPD prototype system has a wider set of functionalities that, starting from the uploading and effective visualization of MetOcean data, enable the computation of fuel consumption along any selected route, the detailed examination of the encountered meteo-marine conditions on any route way point and the comparison of the results obtained for different routes.

The different approaches adopted for the implementation of the new functionalities in OrCa_EPD are illustrated and discussed also by reporting example results of numerical benchmark tests on ships with conventional propulsion and with auxiliary sails. This latter topic is treated with a heuristic approach, by adopting a quite simple first approximation computational scheme. The main goal here is to put in evidence the implemented framework potentialities to include details of different propulsion systems in a simple and straightforward way. The capability to deal with non-conventional and hybrid propulsion systems is becoming more and more relevant if one considers the strong impetus of the decarbonisation trends in shipping, *DNV (2021)*, *Mallouppas et al. (2021)*. In this scenario Wind-Assisted Propulsion Systems, *DNV (2019)*, are candidate to play a relevant role, <https://www.decadeofwindpropulsion.org/>, and for their best effectiveness they require specific optimal planning to match ship performance with MetOcean conditions and mission requirements, *van der Kolk et al. (2019)*, *Hagemeister et al. (2020)*, <https://www.napa.fi/the-role-of-data-in-harnessing-the-power-of-the-wind/>, <https://marine.copernicus.eu/it/node/4901>.

2. MetOcean data

The basic most relevant dataset for meteorological navigation is composed by atmospheric surface wind and marine surface waves and currents. These data are produced at forecasting centers by software chains composed of meteorological forecast models, whose wind data are used to drive marine waves forecasting models. Moreover forecast for wind and other atmospheric variables, characterizing atmosphere-sea fluxes through the atmosphere-ocean interface, are used to force marine hydrodynamics models. Such a basically relevant MetOcean dataset is synergistically integrated in the here described first version of the OrCa_EPD prototype system for visualization and for ship performance evaluations. The OrCa_EPD system requires that input MetOcean data be in netcdf or grib format, that are the standard and commonly adopted formats by most of the forecasting centres.

The OrCa_EPD prototype interface has the same ECDIS basic functions available in the original EPD, hence through them it is possible to graphically construct routes, and then edit and modify them, setting the time of departure and creating speed profiles, by defining different ship speed values for each route leg. Consequently a specific voyage timing is available for each defined route. Considering a specific route, based on its geographical details of (lat, lon position of each route way point) and on the voyage timing, it is possible to interrogate the available MetOcean data in order to grasp the predicted environmental conditions for the whole voyage and to variate the route for searching better voyage conditions. Here below the several modes of MetOcean data visualization are schematically described with the help of some figures.

2.1. Along route MetOcean data visualization and MetOcean maps display

A first way to visualize MetOcean data through the prototype interface is the “along route metoc” mode, which is common to the original EPD interface and to all ECDIS interfaces. In such a mode, MetOcean data can be visualized in terms of vectors for Wind and marine Current, Average Direction and SWH for waves, for a set of points spaced by regular time intervals (15, 30, 60 minutes) along any route in accordance with voyage timing. Arrow symbols typically adopted in ECDIS terminals are used, i.e. arrows with barbs: for wind; bold arrows: for waves; curvy arrows: for current. MetOcean data are loaded from files in standard grib or netcdf format, by accessing them in a local folder or by accessing remote files through connection to an OPeNDap server, <https://www.opendap.org/>. Fig.1

shows an example of the graphics, where a typical screen of the prototype shows a short Mediterranean route in the North Tyrrhenian Sea, from Savona to Giglio Island, in the Tuscany Archipelago. The data there shown are from the MetOcean forecasting system of Consorzio LaMMA, <http://www.lamma.rete.toscana.it/mare/modelli/vento-e-mare>, and are loaded for a voyage starting on 06/03/2022 at 12:00 UTC to be performed at a constant ship speed (Speed Over Ground, SOG) of 10 kn.

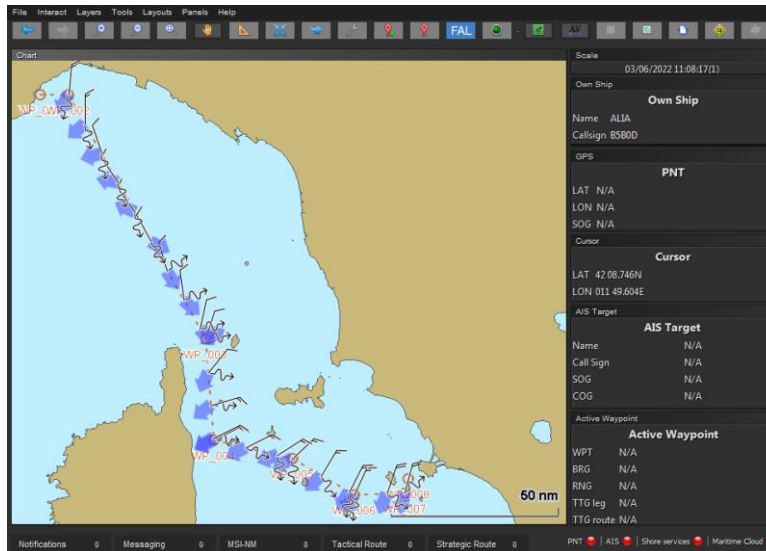


Fig.1: Example of along route metoc visualization mode by the prototype interface, corresponding to a route from Savona to Giglio Island, in the Tuscany Archipelago. The voyage starts on 06/03/2022 at 12:00 UTC, is performed at a constant ship speed (over ground, SOG) of 10 kn. The shown data are from the MetOcean forecasting system of Consorzio LaMMA.

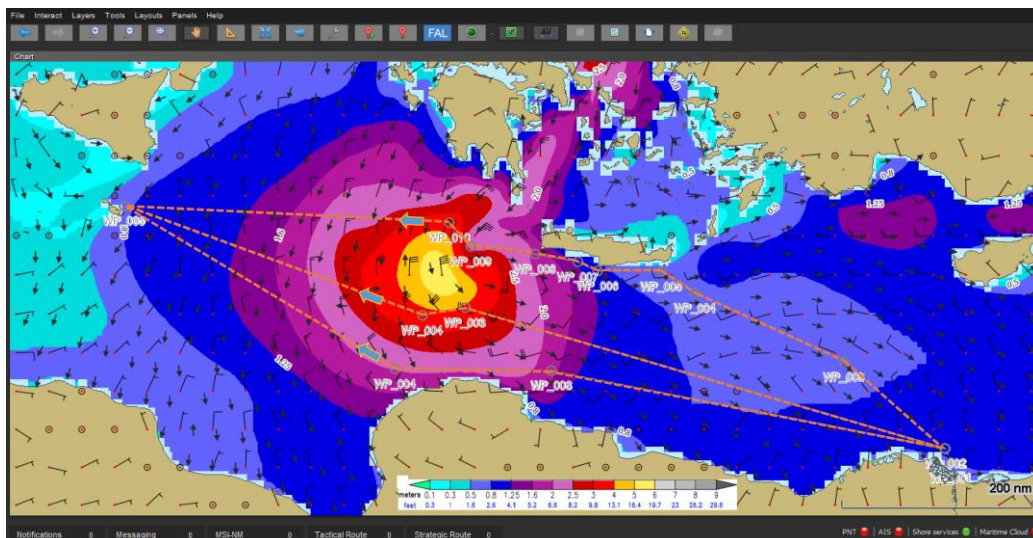


Fig.2: Example of “metoc maps” visualization of the fields of SWH, Mean Wave Direction and Wind Barbs, from Consorzio LaMMA Wind-Wave forecast data for 18/09/2020 at 01:00 UTC. Three alternative routes are shown from Port Said, Egypt, to La Valletta, Malta.

In the OrCa_EPD prototype system some novel functionalities have been introduced through the “metoc maps” visualization mode, that exploits GIS standards supported in the original version of prototype system to access MetOcean data through a Web Map Service (WMS), www.ogc.org/about. The added novel functionalities allow a higher level of integration of the MetOcean data analysis with the related process of route evaluation and variation. In this mode, MetOcean maps are loaded by selecting a given point on the route (by mouse clicking) and data are shown for the time nearest to the one at which the ship reaches the selected point. It is possible to select the MetOcean variables to be

visualized among: Wind Speed, or Current Speed, or Significant Wave Height (SWH) fields with the superposition of the respective direction arrows. An example of such a visualization is shown in Fig.2, the SWH field is shown together with Mean Wave Direction (little black arrows) and Wind Barbs, showing Wind Speed (with barbs standard coding) and Wind Direction (barbs on the tail and a little red dot on the head). Once the map has been loaded at the selected way point time, it is possible to load and show MetOcean data at the same time, but for different points (still by mouse clicking), also out from the route track. The example reported in Fig.2, shows also three alternative Mediterranean routes from Port Said, Egypt, to La Valletta, Malta. The Time of Departure (TOD) is 18/09/2020 at 01:00 UTC, the ship SOG is 14 kn. MetOcean data from consorzio LaMMA, visualized on the map are valid for 22:00 UTC 19/09/2020, when the ship position on the three routes is in correspondence of the blue bold arrows.

In the example of Fig.2, a relevant heavy weather condition, related to the dynamical evolution of a Mediterranean Tropical Like Cyclon (TLC), that formed in the Ionian Sea and, after an intermediate phase of lower intensity due to the passage over the Greek land area, re-intensified moving over the sea towards South and then towards South-East. Fig.3 shows a zoom of the same map focused on the area of the TLC center. (On the right, the selection panel for the variables from the LaMMA WMS server and visualized in the “metoc map” is shown.) In addition “along route metoc” visualization has been activated for each one of the three routes. In this quite extreme case, different MetOcean data visualization tools of the prototype interface can be effectively exploited in an integrated process to design route variations avoiding the encounter of the worst heavy weather conditions. Moreover the capability to estimate the ship fuel consumption along each one of the analyzed routes (through the computational schemes described below), allows also to check the fuel consumption increment and to select route variations with not excessive fuel consumption increments. On this point, it must be added that the integrated capability to trigger the execution of route optimization algorithms is a relevant step of improvement on which the work of development and integration is still ongoing.

2.2. Wave spectra trough partitions visualization

For deeper analyses of the seaway conditions, the “spectral partitions visualization” mode has been added in the OrCa_EPD prototype interface. This mode of visualization is possible because most current third-generation wave prediction models have built-in wave portioning algorithms, e.g. *Tracy et al. (2009)*. Fig.3 shows an example where the “spectral partitions visualization” is activated for a point evidenced by the cyan circle on the map and shown by the polar diagram in the white panel on the right side of the interface.

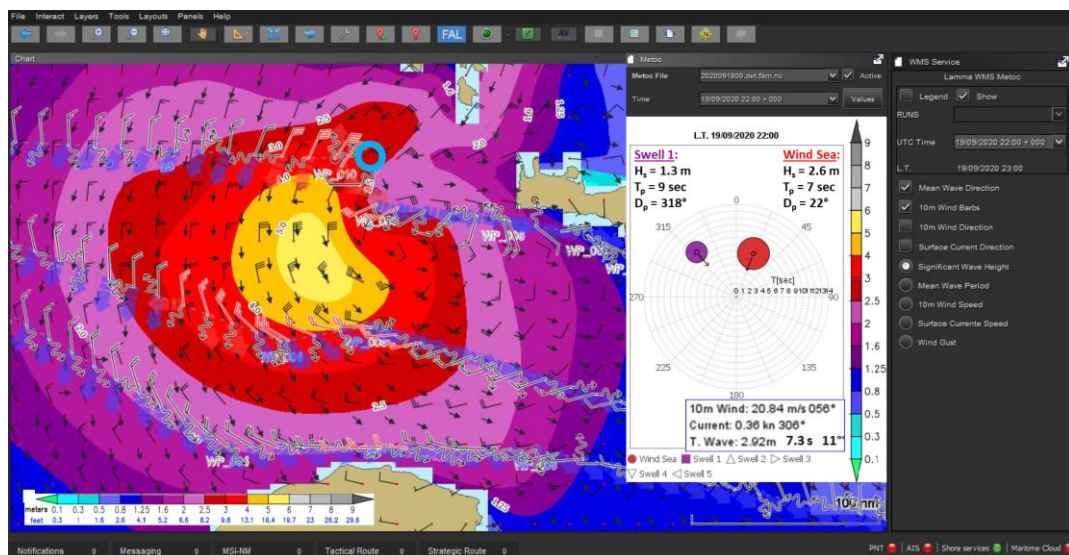


Fig.3: Zoom of Figure 2, with “along route metoc” for the three routes in the area of the Tropical Like Cyclon centre. On the white panel in the right the wave spectral partitions are shown for a point

inside the cyan little circle, at the same date and hour.

Such a polar diagram describes in this case a bimodal seaway (total SWH of 2.92 m), composed of a wind sea dominant component from NE (red big circle: partial SWH 2.6 m, Peak Period 7 s, Peak Direction from 22°) and a secondary component of swell from NW (violet small circle: partial SWH 1.3 m, Peak Period 9 s, Peak Direction from 318°). Each component is indicated by the respective circle symbol, whose centre is positioned in the polar diagram in accordance with the respective values of the Peak Period (radial polar coordinate) and Peak Direction of provenience (angular polar coordinate). The intensity of each component is rendered by the colour of the respective circle symbol. The operator is also helped to perceive the relative importance of each component by the respective circle symbol dimension, that grows with the SWH value. In order to facilitate the estimate the effects on the ship dynamics, the prototype interface allows to compute the Encounter Period for each one of the different wave components of the seaway, after having defined the ship SOG and HeadinG (HDG). Such SOG and HDG data can be taken from the route definition dataset, or by manual insertion, in order to check changes induced by route kinematics variations, or in order to check points outside the actual route, but that could be included in eventual varied routes.

In Fig.4 a further example is shown to better clarify the details of the graphics of the “spectral partitions visualization” mode. In this case, the sea state is characterized by a multimodal wave spectrum as shown by the left panel that shows the polar diagram for the complete numerical directional wave spectrum, as computed by the Consorzio LaMMA implementation of WW3 model.

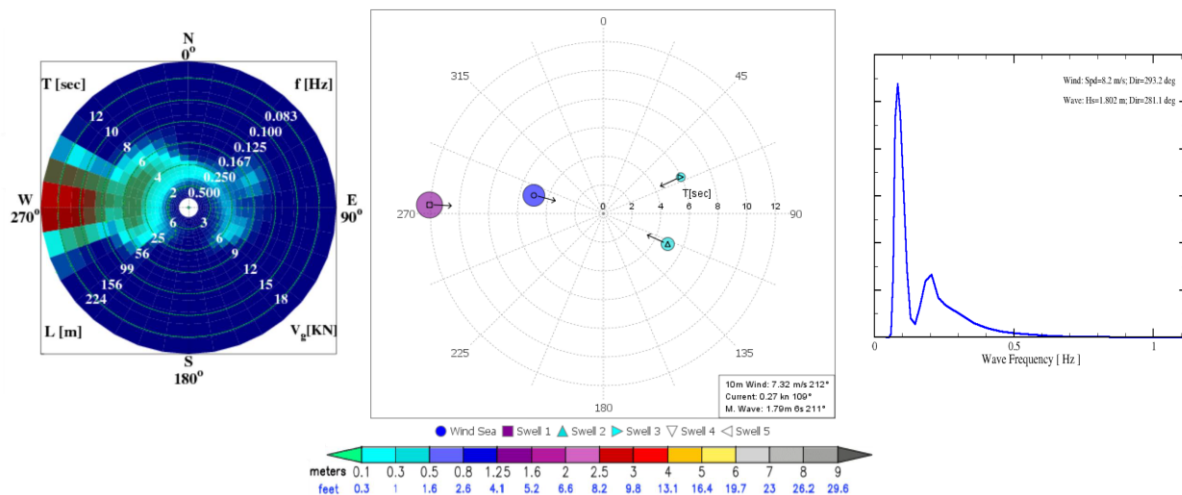


Fig.4: Different representations of the same wave spectrum. Left side: 2D discretized directional polar plot spectrum. Right: 1D spectrum, versus frequency. Center: schematic polar diagram of the directional spectrum through wave partitions.

The value of the total SWH corresponding to that spectrum is about 1.8 m. The directional spectrum shows that the total wave energy is mainly due to the presence of a very long and very tuned and collimated swell component coming from W, with a peak period of about 12 s. Another wave component is present, with a peak period of ~5 s, nearly collinear with respect to the dominant swell. It is the wind sea component and is characterized by a wide directional spreading. Other two very weak swell components are present, coming from the NE and SE quadrants, with peak periods in the range 5-6 s. The one-dimensional spectrum is shown on the right panel of Fig.4. The polar diagram in the central panel shows the spectral partitioning synthesis of the same multimodal wave spectrum.

3. Ship modelling

As anticipated above, a relevant aid in route evaluation comes from the capability to estimate the fuel consumption expected from each analyzed route, given the own ship technical data, the selected speed profile along the route and the consequently encountered MetOcean conditions, so as from the fore-

cast data. The ship modelling functionalities added to the prototype interface allow OrCA_EPD to guide deck officers to reliably perform, with minimal effort, a computational process that approximates the inherent complex bundle of kinematical and dynamical interrelationships till to obtain estimates of fuel consumption along the route. The inner computing core of this functionality has been implemented by decoupling the heaviest powering and aero-hydrodynamic computational tasks from the along-route meteo-dependent fuel consumption rate evaluations. This requires some approximations to be made, but the resulting computational framework remains sound, and allows improvements to be easily made if and where needed. Ship specific data are pre-computed and stored in Look-Up Tables (LUTs), to be quickly accessed and combined with MetOcean data through simple algebra. This allows to obtain (through a numerical time integration) fuel consumption estimates with a fast and quickly repeatable procedure, as required by an effective meteorological navigation GUI. The main steps of the computational process and the roles of the specific look up tables are described in what follows. A wider discussion can be found in *Orlandi et al. (2020)*.

The key quantity to be computed is the fuel consumption rate FC , to be then numerically integrated in time along the studied route. A relevant feature to be accounted for is the dependence of FC on MetOcean conditions, which in turn is determined by dynamic balance between propeller(s) thrust and ship's total resistance R_{tot} , that represents the propulsive engine load and depends on MetOcean conditions. In this process, the total resistance of the ship is evaluated by considering it as composed of two relevant terms:

$$R_{tot} = R_{hull} + \Delta R \quad (1)$$

R_{hull} is the calm-water resistance that depends on ship hull form, loading and trim conditions, and Speed Trough Water (STW). The added resistance term ΔR is considered as being composed of all the other relevant terms that need to be added to R_{hull} in order to reliably estimate R_{tot} . The main terms of ΔR are strongly dependent on meteo-marine conditions. The dependence of R_{hull} on STW can be computed by numerical approaches, or estimated by empirical measurements (in model test basins or from in-service measurements), or also from a suitable mix of the two. Once it is known, the propulsion powering problem can be solved by pre-computing the fuel consumption rate FR for several values of STW in the range of interest, and for several values of ΔR , in a suitable range. For the completion of such computations, propeller-hull characteristics and engine data are needed. In order to span all the main alternatives, the computations should be repeated for the different propulsive settings adopted in the conduction of the given ship (e.g. number of active main engines, eventually active shaft generators, combinator settings in the case of CPP). Fouling growth on hull and propeller could be accounted for by repeating the computations with growing hull resistance curves. The resulting dependence of the computed Fuel Rate LUTs on the main discretized variables can be indicated as follows:

$$FR(i,j) = FR(STW_i, \Delta R_j) \quad (2)$$

where the (i, j) dependence corresponds to the ship speed and added resistance discretized values (with suitable discretization steps). In addition (but not explicitly shown in Eq.(2)) the dataset structure depends also on “ship-voyage configuration parameters” defining the different ship loading conditions and propulsive configurations. Once these latter have been selected, the precomputed LUTs allow to simply pick-up the pre-estimated fuel consumption rate value FR for each desired STW, after the corresponding value of ΔR is estimated according to the encountered meteo-marine conditions.

In the approximation adopted in the present version of OrCa_EPD, the added resistance term is written as follows:

$$\Delta R = R_{wi} + R_{aw} \quad (3)$$

R_{wi} is the wind added resistance, due to the interaction of ship superstructures with the surrounding air, R_{aw} the added resistance in waves, due to the hydrodynamic interaction of the ship with the field of the encountered marine surface waves. The wind added resistance term depends on the total ship-relative wind, resulting from the vector composition of the ship SOG with the wind due to meteo-

logical conditions. In idealized, completely calm environmental conditions, no wind nor sea waves of “meteorological origin” are present and the total resistance is well approximated by the sum of R_{hull} and the R_{wi} term due to the SOG only. It is evaluated by the expression:

$$R_{wi} = 0.5 \rho_{air} A_T U_r^2 C_x(\theta_{rwi}) \quad (4)$$

ρ_{air} is air density, A_T is the ship frontal area, U_r is the modulus of the ship-relative total wind vector. The longitudinal wind resistance coefficient $C_x = C_x(\theta_{rwi})$ depends on ship above waterline structures and is function of the ship-relative wind angle θ_{rwi} . It can be computed with a suitable discretization step, in the 0° - 360° (or 0° - 180° , for symmetrical configurations) interval and stored as wind added resistance LUT. Differing functional shapes $C_x(\theta_{rwi})$ can be stored in the wind resistance LUTs, depending on the ship configuration or loading condition (e.g. accounting for different loading conditions, or for different containers arrangement and filling factor). The specific details of R_{wi} could be accounted for by ship specific C_x coefficients, from wind tunnel or/and from CFD. Also other wind-related added resistance terms could be included through transverse forces and moments coefficients (C_y and C_N , respectively) and corresponding “passive rudder” terms.

The added resistance in waves term R_{aw} in general confused seaways can be evaluated in terms of the spectral significant value integral:

$$R_{aw} = 2 \int_0^\infty \int_0^{2\pi} ARO(\omega, \theta_{raw}) S_\zeta(\omega, \theta_{raw}) d\theta_{raw} d\omega \quad (5)$$

$ARO(\omega, \theta_{raw})$ is the Added Resistance Operator, i.e. the longitudinal component of the drift force in regular waves per (regular) wave amplitude squared, while $S_\zeta(\omega, \theta_{raw})$ is the directional wave spectrum, and the integration variables (ω, θ_{raw}) are the wave “angular” frequency and the ship-relative (i.e. w.r.t. ship bow) wave direction. Computational approaches based on the full directional spectrum, *Orlandi et al. (2015)*, *Spentza et al. (2017)*, have the potential of a high accuracy, but are computationally intensive and imply huge memory occupation for storing full spectra for the whole marine area and forecast time horizon. A less accurate, but strongly lighter approach, which allows to pre-compute LUTs for R_{aw} , has been experimented in the present study. As a first step the following wave spectrum factorization is introduced:

$$S_\zeta(\omega, \theta_{raw}) = H_s^2 \Sigma_\zeta(\omega, \theta_{raw}) \quad (6)$$

H_s is the SWH, whose square value is linked to the energy content of the sea state described by the spectrum, and $\Sigma_\zeta(\omega, \theta_{raw})$ is the “unitary directional wave spectrum, *Orlandi and Bruzzone (2011)*, i.e. a spectrum with the same frequency-directional shape of $S_\zeta(\omega, \theta_{raw})$, but with unitary SWH. As a result R_{aw} can be re-written as:

$$R_{aw} = H_s^2 C_{aw} \quad (7)$$

$$C_{aw} = 2 \int_0^\infty \int_0^{2\pi} ARO(\omega, \theta_{raw}) \Sigma_\zeta(\omega, \theta_{raw}) d\theta_{raw} d\omega \quad (8)$$

If a family of parametric spectra is introduced for approximating the shape of the “unitary” spectrum in Eq.(8), a dataset of C_{aw} values can be computed by allowing the relevant parameters to vary in suitable intervals, with suitable discretization steps. As an example, once fixed the spectral shape, its mean wave direction (w.r.t. ship bow) and period can be appropriately varied in order to obtain a sufficiently detailed representation of all the possible encounter conditions. The Added Resistance Operator functions $ARO(\omega, \theta_{raw})$ needed for evaluating the numerical integral have to be computed by appropriate seakeeping hydrodynamic approaches, *Reed (2004)*, *Bertram and Couser (2014)*. A reasonably good approximation that can be adopted here is the Strip Theory, *Bertram (2011)*, whose general framework is compliant with the spectral approach, *Price and Bishop (1974)*, *Dern et al.*

(2015). More accurate approaches, e.g. *Liu et al. (2011)*, capable of accounting for the nonlinearities of added resistance in waves, could be utilized, or on the other extreme, much simpler approaches could be inspired by the adoption of the JIP STAWAVE-1,2 approaches, *Van den Boom et al. (2013)*, *Kim and Roh (2020)*. Also novel applications of machine learning techniques could be employed, e.g. see *Yang et al. (2021)*. The ARO functions are obviously strongly ship dependent and for each ship, they must be computed for the relevant loading conditions and for various values of the ship speed STW in the speed range of interest, as for R_{hull} . The ship specific dataset to be precomputed and archived in the C_{aw} LUTs have a functional dependence on the main discretized variables as follows:

$$C_{aw} = C_{aw}(STW_i, T_{mk}, D_{rmh}) \quad (9)$$

where the integers (i, k, h) are the discretization indices for STW, mean wave period T_m and mean wave direction D_{rm} (the subscript r stands for ship-relative) respectively. After the C_{aw} coefficients precomputing task have been completed for a given ship, its added resistance in waves can be estimated by the application of Eq.(7), picking the right values of H_s and of the C_{aw} coefficient.

A further level of detail could be obtained by using different parametric spectra for wind sea and swell and pre-computing the respective C_{aw} datasets. In this approach Eq.(7) should be generalized by a sum extended to all the spectral partitions in the spectrum with a similar form for each term, but with the total SWH substituted by the corresponding partition value multiplied by the respective C_{aw} . An approach of this kind could, also if in a simplified LUTs based approximation, account for the effects of spectra multimodality in fuel consumption computations. In the present version of OrCa_EPD a first implementation of this approach has been included and preliminary tests have been performed.

Finally, the effects of marine currents can be included in the above treatment by introducing the implied kinematics, where needed.

In the following sub-chapters the results of some preliminary applications of the version OrCa_EPD are presented as heuristic, simplified examples of meteorological navigation, to illustrate the functionalities of the prototype interface. The characterization of meteo-marine conditions for the reported numerical tests is through MetOcean data from Consorzio LaMMA operational forecasting models for wind and waves, <http://www.lamma.rete.toscana.it/mare/modelli/vento-e-mare>, while current data are from <https://marine.copernicus.eu>.

3.1. Numerical tests for conventional ship propulsion

Numerical tests have been performed by considering a typical, real fast RoPax ship in Mediterranean navigation, whose principal particulars are reported in Table I. It has been designed for 1700 passengers, 500 cars, with a cruise speed of 28 knots at 80% MCR. It is equipped with two shaft lines, with CPP propellers, driven by a total of four Wartsila 12V46C (11700 kW each) medium speed four stroke diesel engines. Ship specific data processed in *Orlandi et al. (2015)* were reprocessed and the FC (Fuel Rate, as in Eq.(2)) LUTs have been built for a single loading condition (indicated as ldcnd01 in the filenames containing the ship specific LUTs) with two different “Propulsion Configurations”. Using the ship definition functions of OrCa_EPD two propulsion configurations have been defined to study the voyages of this ship, as shown in Fig.5.

Table I: Principal particulars of RoPax ship

Ship	RoPax
Full load displacement Δ	15470 t
Length between the perp.s L_{pp}	160.00 m
Beam B	25.00 m
Mean draft T	6.70 m

The corresponding “Fuel Consumption Settings” is shown in Fig.5, bottom right panel, where the ship name assigned for our numerical tests has been RoPax, and its specific LUTs configuration is named RoPax2S2E, for which two possible “Propulsion Configurations” can be selected: RoPax2ENG and RoPax4ENG. For the first one a FC LUTs computed with only two engines active (one for each shaft line). This can be activated only at quite low speed and with fair weather conditions allowing slight, but not negligible, fuel consumption reductions. With not calm wind and waves or/and at medium/high speeds only the second one, with all four engines, can be activated. In the “Ships Data Manager” panel reported in the left side of Fig.5 ship configuration buttons are visible, through which the files containing the wind resistance (windres, as from Eq.(4)) and the added resistance in waves (waveres, as from Eqs.(5)-(9)) LUTs can be loaded. For the tests here reported the C_x coefficient stored in the windres LUT have been estimated by a simplified approach, trough data and models from *Fujiwara et al. (2006)*, while the C_{aw} coefficients stored in the waveres LUTs have been computed by utilizing the PDSTRIP strip theory code, *Bertram et al. (2006)*, adopting a family of parametric spectra based on the JONSWAP spectrum, with a cosn directional spreading function, and following the recommendations of *DNV (2017)* for parameter selection for the generic total spectrum (waveres_Generic). The same has been adopted also for defining specific C_{aw} LUTs for swell waves (waveres_Swell) and wind waves (waveres_Wind), to be used in some preliminary test computations with the spectral partitions forecast data.

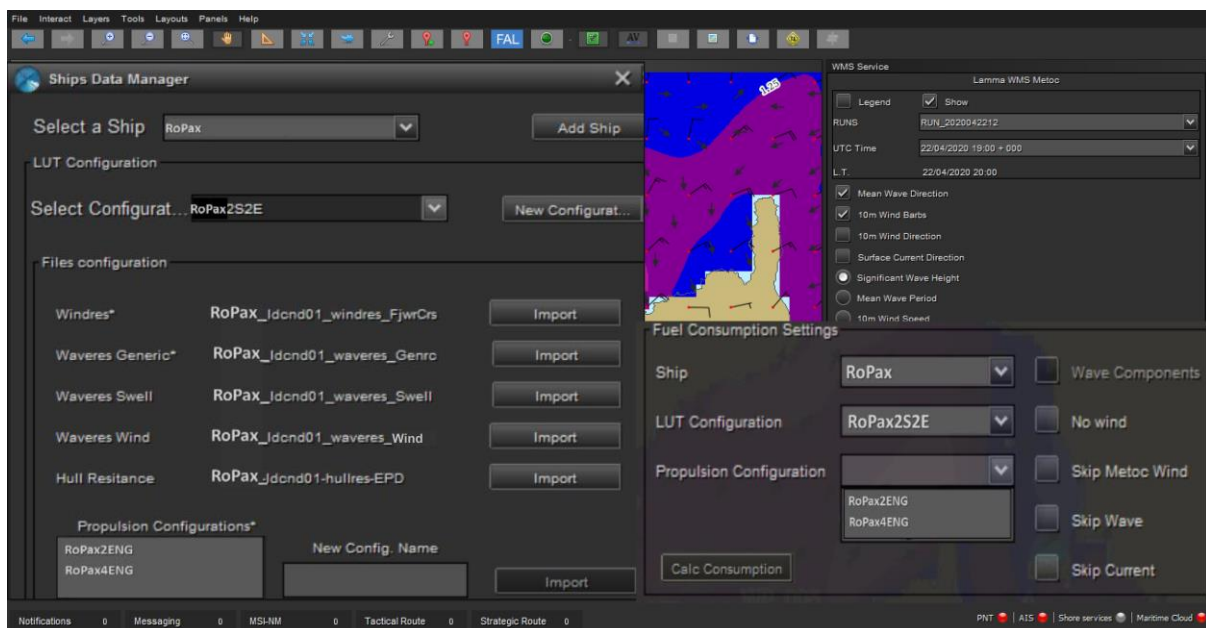


Fig.5: Example of OrCa_EPD display with “Ship Data Manager” (left) and “Fuel Consumption Settings” (right) panels activated, for ship data LUTs loading and fuel consumption evaluation settings, respectively.

The processing steps in OrCa_EPD, begin with a preliminary phase through the “Ships Data Manager”, where the ship specific LUTs are loaded and different configurations are defined, by. Then the route definition process (common to all ECDIS systems interfaces) must be performed, followed by the the MetOcean data loading and analysis (through the “along route metoc” and “metoc maps” functionalities described above). The process is completed, in the “Fuel Consumption Settings” panel, where the loading conditions and propulsion configuration are selected, among those configured in the preliminary phase, and fuel consumption can be estimated. All the steps of route definition, MetOcean data loading and propulsion configuration can be very rapidly repeated several times in order to evaluate the consumptions for different route shapes and timing, different ship speed profiles and powering conditions. For this, it is possible to edit the details of each route leg for the analysed route, and to change the ship speed and the propulsion configuration per leg. All the tested route variants can be stored and compared through the “Routes Sorting” panel, that allows to sort all of them in relation to the fuel consumption, or the voyage length, or the voyage duration.

As visible in the bottom extreme right of Fig.5, the “Fuel Consumption Settings” panel allows also to select the spectral partition computational mode, by ticking “Wave Components”, or to differentially evaluate the effects of the single resistance components by switching off from the computation the effects of the wind, of the waves and of the currents, by ticking on the corresponding “Skip” selector.

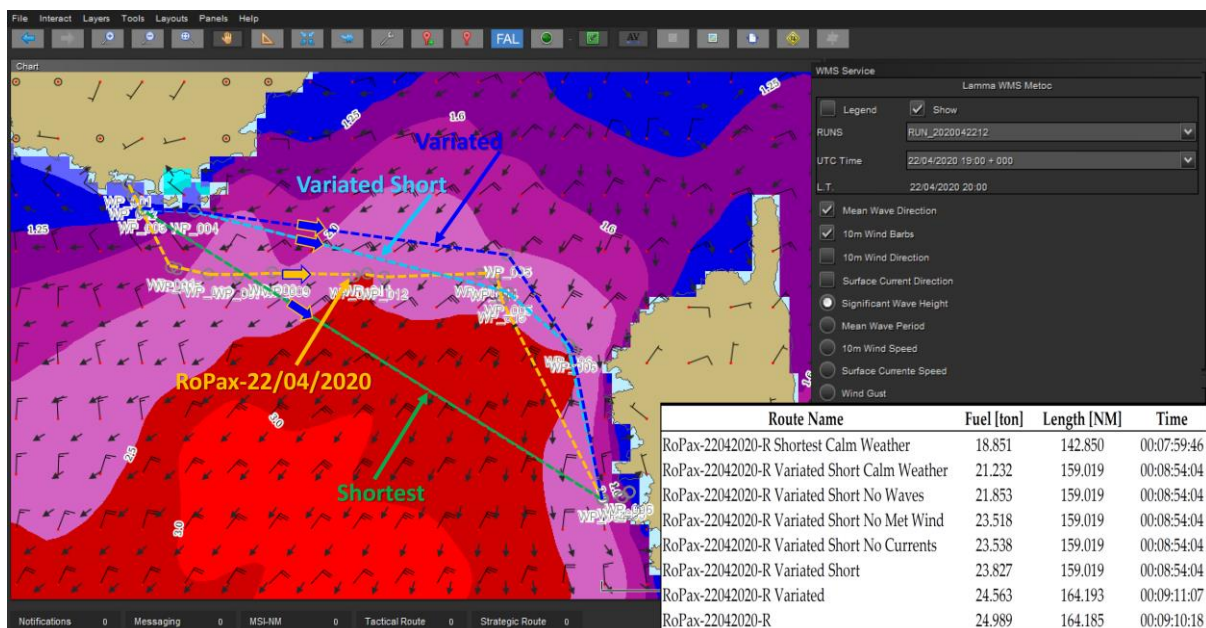


Fig.6: Alternative routes display for the RoPax voyage analysis, with “metoc map” visualization for SWH, MWD and Wind Barbs from Consorzio LaMMA wind-wave data, for 22/04/2020 at 19:00 UTC. Bottom right: alternative routes sorting based on fuel consumption estimations.

In Fig.6 an example is reported, by showing some details of a series numerical tests performed by analysing a real voyage of the studied RoPax from Toulon, France, to Ajaccio, Corse, on 22/04/2020 with Time Of Departure (TOD) in late afternoon. The route really followed is indicated as RoPax-22/04/2020, and is in yellow in Figure. Some alternative routes are also shown. For all the same TOD has been selected and the speed profile (with SOG the range 18-20 kn) has been defined quite similar to the real one. The shortest route is in green, and was not available because it entered too deeply in areas affected by heavy weather. The first of the tested variations is shown in blue (“Variated”), and has been defined by escaping the worst weather by sailing north-westward of it, with about the same route length. The second variation is shown in cyan (“Variated Short”) and has been defined trying to shorten the voyage, by bordering more closely bordering the bad weather area. The variated routes have been defined by exploiting the dynamic visualization tools for MetOcean data maps in accordance with voyage timing. As an example, the map shown in Fig.6 is valid when the ship is where indicated by the blue bold arrows, on each route. Some of the results of the fuel consumption computations are shown in the bottom right white table in Fig.6. The results for the three studied routes are sorted by the fuel consumption. The Variated Short resulted to be the least fuel consuming. In addition, for this route, the fuel estimation has been repeated by alternatively switching off all MetOcean factors and one by one wind, wave and currents, to somehow evaluate the separate effects on fuel consumption of the different environmental factors. As a basic term of comparison, the fuel has also been estimated for the shortest route, with no MetOcean conditions. A further, but here not reported, analysis can be performed by introducing speed profile variations. From another perspective, it is also possible to evaluate the reliability of the forecast data by repeating the same computations, on the same routes, but with MetOcean data with different forecast initialization times or from different forecasting centres.

3.2. Numerical modeling for sail assisted ships

The potentialities of OrCa_EPD have also been investigated by considering a heuristic and very preliminary approach to sail assisted propulsion. The adopted modelling approximations are at the moment quite rough, and have been considered as a way to demonstrate the capability of OrCa_EPD framework to treat different propulsion configuration depending on the encountered MetOcean conditions. In particular a numerical benchmark model has been constructed considering the S175 containership, Table II, equipped with auxiliary sails. The engine-hull-propeller matching has been performed associating a single shaft line FPP propeller and a single engine of the type MAN B&W 6S50MC-C8 low speed two stroke diesel. The resulting ship model is not strictly realistic, has quite a poor weather margin, with top speed of 20 kn reachable in completely calm conditions. On the other hand, with such an undersized engine the dependence of ship powering performance on the encountered MetOcean conditions and consequently the potential for the auxiliary sails is more evident. It must be pointed out here that the implication of the introduction of limits to ship powering for GHG emissions reduction have been recently studied and IMO adopted specific guidelines through the IMO-MEPC76, as reviewed in *Liu et al. (2022)*.

Table II: Principal particulars of the S175 containership

Ship	S175
Full load displacement Δ	24609 t
Length between the perp.s L_{pp}	175.00 m
Beam B	25.00 m
Mean draft T	9.50 m

In this study, the effect of an auxiliary sail on powering have been accounted for by the following expression for the sail induced longitudinal thrust:

$$R_{sail} = 0.5 \rho_{air} A_{sail} U_r^2 C_{x^{sail}}(\theta_{rwi}) \quad (10)$$

A_{sail} is the sail area and $C_{x^{sail}}(\theta_{rwi})$ is the longitudinal sail thrust coefficient. The sign of this latter has been defined in such a way to have a negative R_{sail} when the longitudinal thrust is positive (i.e. when the sail pushes the ship forward). In this way it can be summed to the meteo-dependent added resistance term ΔR in Eq.(1). This approach has been adopted being aware that it is only a rough approximation (albeit frequently adopted in literature) and that it does not allow to account for the complex dynamical balance induced by the transverse force and moment terms C_y and C_N , *Reche-Vilanova et al. (2021)*. All this is the object of further investigations and will be included in forthcoming developments.

Based on such a first approximation, the present version of OrCa_EPD allows defining several “Sails Configurations”, each defined by the presence of one or more active sails. For each active sail in a “Sails Configuration” a LUT is loaded containing data for A_{sail} and $C_{x^{sail}}(\theta_{rwi})$ as for the wind resistance of the ship superstructure. In the numerical tests here described three “Sails Configurations” were defined: “Full Sail”, “Half Sail” and “Min Sail”. The “Full Sail” configuration is composed of two identical sails, whose A_{sail} and $C_{x^{sail}}$ in the LUTs have been determined by reprocessing the technical data from *Hagiwara (1989)* for the Walker Wingsails Triplane System. The “Half Sail” configuration has been defined to heuristically model the possibility to somehow reduce the sails extent, as an example telescopically retractable sail systems can be found in literature, e.g. <https://www.walleniusmarine.com/our-services/ship-design-newbuilding/ship-design/wind-powered-vessels>. Consequently the “Half Sail” configuration is composed of two identical sails, whose A_{sail} surface is half the “Full Sail” surface, and $C_{x^{sail}}(\theta_{rwi})$ has a similar angular dependence, but with lower values in the directions of maximum thrust, in order to account for some loss of lifting efficiency of the wingsails in the partially “retracted” configuration. The “Min Sail” configuration has been defined to simulate the possibility to completely “close” the sails, hence it is composed of two identical sails, with A_{sail} surface amounting to 15% of “Full Sail” surface, and $C_{x^{sail}}(\theta_{rwi})$ is more similar to that of a ship superstructure, simulating the complete absence of lifting effects.

As a practical example, Fig.8 shows the definition of a possible route for the voyage from Toulon, France, to La Valletta, Malta. The “Fuel Consumption Settings” panel on the top right shows the powering settings defined by loading the LUTs for the S175 model with auxiliary sails, as described above. The voyage has been studied with TOD on 11/05/2020 at 13:00 UTC, with a constant ship speed profile of 15 kn. Different routes have been defined varying the sail settings, but maintaining the same TOD and the same route shape as shown in Fig.8. Two routes with constant sail settings have been tested: the “ToVa Full Sail” and the “ToVa Min Sail”. For the sake of comparison also the voyage of the S175 without auxiliary sails has been analysed, and this is the “ToVa No Sail Route”. Finally the possibility to select a different “Sail Configuration” for each route leg has been exploited and the “ToVa Profile Sail” has been defined by activating the “Min Sail” configuration on all the route legs with head wind, while on all the other legs the “Full Sail” configuration has been activated.

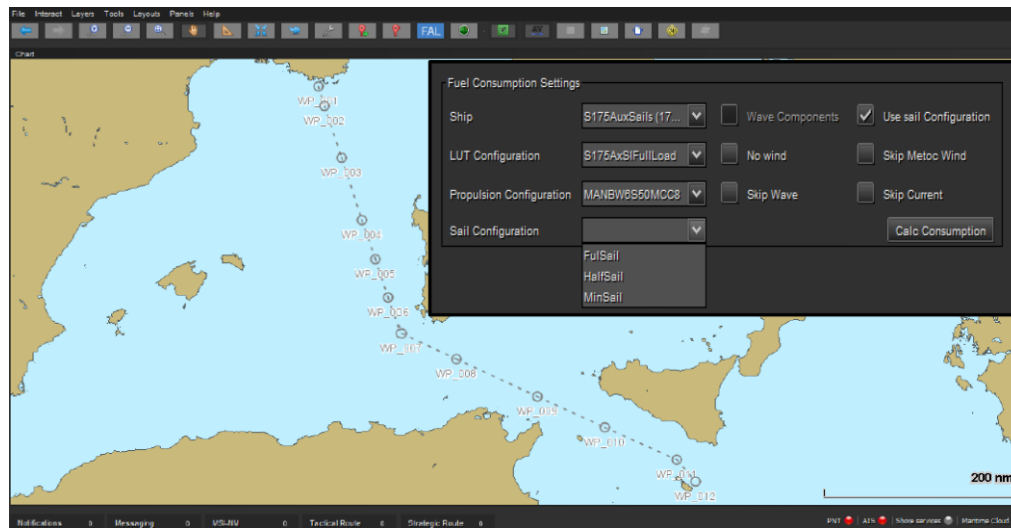


Fig.8: Display of the analysed route shape for the voyage from Toulon, France, to La Valletta, Malta. The “Fuel Consumption Settings” panel on the top right shows the powering settings defined by loading the LUTs for the S175 model with auxiliary sails, as described in the text.

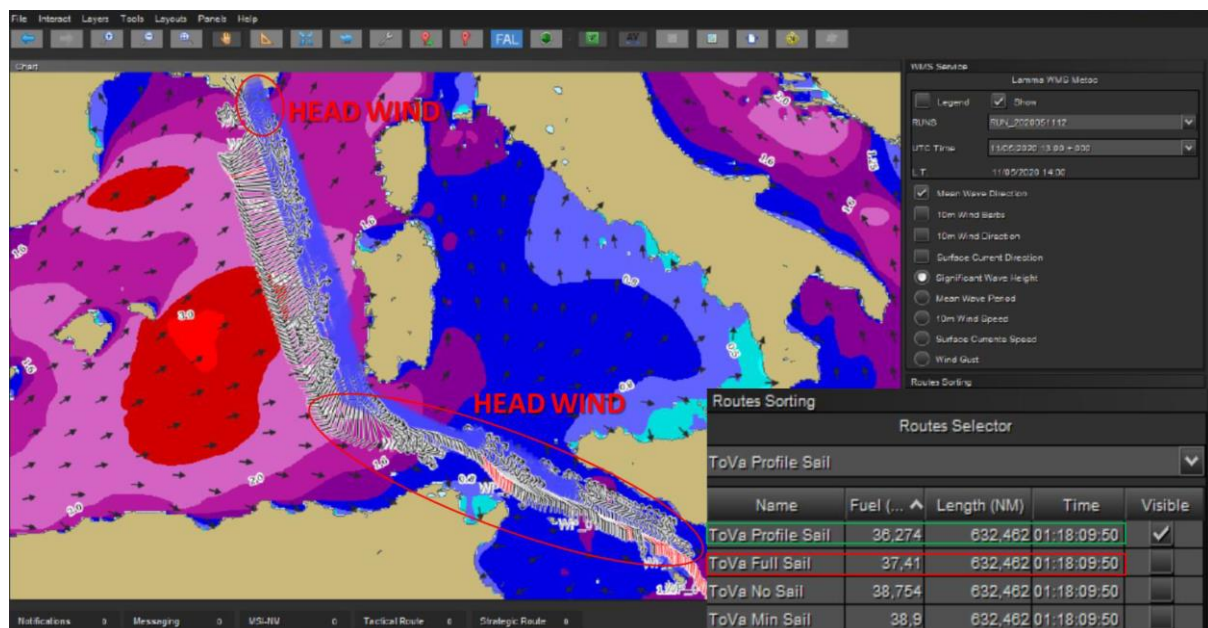


Fig.9: Display of “along route metoc” data for the analysed voyage along route for the voyage from Toulon, France, to La Valletta, Malta of the sail assisted S175 containership numerical model. Also “metoc map” data at TOD are shown (SWH and MWD). At the bottom right the “Route Sorting” panel is shown, reporting the results of fuel consumption estimations obtained for the different sail settings analysed in the example described in the text.

In Fig.9 some details of this example are shown: the “along route metoc” visualization is active and the route legs affected by head wind conditions have been highlighted in red. The map of SWH and Mean Wave Direction (MWD) is shown at TOD. In the “Route Sorting” panel present on the bottom right a comparison of the tested routes is present, with sorting based on fuel consumption. It emerges that “No Sail” or “Min Sail” constant sail setting determine the higher fuel consumption. The “Min Sail” configuration is slightly worst, because it is also affected by the wind resistance due to the “closed” auxiliary sails, modelled on the ship superstructure. The “Full Sail” constant sail setting is better because it exploits the sail thrust in all the legs with favourable wind, but pays some more fuel along the legs with head wind conditions. This detrimental effect can be minimized by activating the “Min Sail” configuration on the legs with head wind conditions, and consequently the fuel consumption for the “ToVa Profile Route” is even smaller.

4. Conclusions and further developments

The implementation of meteorological navigation functionalities in an ECDIS-like prototype display system has been described. Various MetOcean data visualization functionalities have been connected with a computational framework for ship fuel consumption evaluation along several routes and results sorting and comparison. The implemented algorithms are based on a decoupling scheme, that allows to pre-compute the quantities requiring heavy aero-hydrodynamics computations and store them in Look-Up Tables (LUTs). Based on these latter, the prototype display allows quick evaluations of fuel consumption along different routes with different powering settings. The modularity of the LUTs based implemented scheme allows different powering and sailing configurations to be simply defined, and also Wind-Assisted Propulsion Systems (WAPS) can be accounted for. These functionalities have been illustrated with examples of Mediterranean navigation, considering a realistic RoPax ship with conventional propulsion and a numerical benchmark model for the S175 containership, with auxiliary sails modelled in a heuristic first approximation scheme.

The approach can be extended also to other ship responses, besides the fuel consumption, studies are being performed considering seakeeping performance, comfort, structural stresses and safety indicators, and ship pollutant emissions.

Further developments are expected from the interplay in-service data recording systems and big-data analysis techniques to improve and validate the numerical approaches to be applied in the pre-computing phase and to correct the decoupling scheme and to devise consequent better computational schemes. A possible outcome of these studies is the implementation of a continuous data driven tuning of ship specific LUTs, with relevant synergies with the emerging trends in holistic ship design, machine learning and data driven surrogate models and the ample world of digital twins, whose role is strongly growing also in the maritime field.

Through the inclusion of different algorithms for automatic route optimization, the prototype system could allow to perform route optimizations with different approaches and then to evaluate and compare the different optimized routes by further exploiting the integrated graphical capabilities of the interface in a totally “ECDIS compliant” framework.

Acknowledgements

This work has been partially developed under the PROFUMO Demonstration project, funded by the ESA Artes IAP programme.

References

BERTRAM, V.; VEELO, B.; SÖDING, H. (2006), *Program PDSTRIP: Public Domain Strip Method*, Software Documentation

- BERTRAM, V. (2011), *Practical Ship Hydrodynamics*, Butterworth-Heinemann
- BERTRAM, V.; COUSER, P. (2014), *Computational methods for seakeeping and added resistance in waves*, 13th COMPIT Conf., Redworth
- BRINKMANN, M.; HAHN, A.; HJØLLO, B.A. (2017), *Physical Testbed for Highly Automated and Autonomous Vessels*, 16th COMPIT Conf., Cardiff
- BOUKHANOVSKY, A.V.; GUEDES SOARES, C. (2009), *Modelling of multipeaked directional wave spectra*, Applied Ocean Research 31, pp. 132-141
- BULL, M. (2021), *Bridge watchkeeping*, The Nautical Institute
- CHEN, M.L.; CHESNEAU, L.S. (2008), *Heavy Weather Avoidance and Route Design*, Paradise Cay Publ.
- DERN, J.C.; QUENEZ, J.M.; WILSON, P. (2015), *Compendium of Ship Hydrodynamics. Practical Tools and Applications*, Les Presses de l'ENSTA
- DNV (2017), *Recommended Practice. Modelling and Analysis of Marine Operations*, DNV-RP-H103, DNV
- DNV (2021), *Energy Transition Outlook 2021. A global and regional forecast to 2050*, DNV
- DNV (2019), *Wind-Assisted Propulsion Systems*, DNVGL-ST-0511, DNV
- FUJIWARA, T.; UENO, T.; IKEDA, Y. (2006), *Cruising performance of a large passenger ship in heavy sea*, 6th Int. Offshore and Polar Engineering Conf., San Francisco
- HAGEMEISTER, N.; HENSEL, T.; JAHN, C. (2020), *Performance Prediction and Weather Routing of Wind Assisted Ships*, 12th HIPER Conf., Cortona
- HAGIWARA, H. (1989), *Weather Routing of (Sail-Assisted) Motor Ships*, Ph.D. Thesis, TU Delft
- KIM, K.S.; ROH, M.I. (2020), *ISO 15016:2015-based method for estimating the fuel oil consumption of a ship*, J. Mar. Sci. Eng. 8/791
- LIND, M.; BERGMANN, M.; HÄGG, M.; KARLSSON, F.; SIWE, U.; WATSON, R. (2018), *Sea Traffic Management – The Route to the Future*, 17th COMPIT Conf., Pavone
- LIU, S.; PAPANIKOLAOU, A.; ZARAPHONITIS, G. (2011), *Prediction of added resistance of ships in waves*, Ocean Eng. 38, pp.641-650
- LIU, S.; PAPANIKOLAOU, A.; SHANG, B. (2022), *Regulating the safe navigation of energy-efficient ships: A critical review of the finalized IMO guidelines for assessing the minimum propulsion power of ships in adverse conditions*, Ocean Eng. 249/1
- LÓPEZA, J.M.L.; CALABRIAA, L.; TANNERA, M.; MARTÍNEZA, J.; GIMÉNEZA, J.A. (2020), *VESSL as a tool for macro-analyses at European level. STM Validation Project results calculated by the use of Short Sea Shipping data mining*, 8th Transport Research Arena, Helsinki
- MALLOUPPAS, G.; YFANTIS, A.Y. (2021), *Decarbonization in Shipping Industry: A Review of Research, Technology Development, and Innovation Proposals*, J. Mar. Sci. Eng. 9/415, <https://doi.org/10.3390/jmse9040415>

ORLANDI, A.; BRUZZONE, D. (2011), *Numerical Weather and Wave Prediction Models for Weather Routing, Operation Planning and Ship Design: The Relevance of Multimodal Wave Spectra*, IMAM Conf., Genova

ORLANDI, A.; PASI, F.; CAPECCHI, V.; CORADDU, A.; VILLA, D. (2015), *Powering and seakeeping forecasting for energy efficiency: Assessment of the fuel savings potential for weather routing by in-service data and ensemble prediction*, IMAM Conf., Pula

ORLANDI, A.; CAPPUGI, A.; MARI, R.; PASI, F.; ORTOLANI, A. (2021), *Meteorological Navigation by Integrating MetOcean Forecast Data and Ship Performance Models into an ECDIS-like e-Navigation Prototype Interface*. J. Mar. Sci. Eng. 9/502

PERERA, L.P.; GUEDES SOARES, C. (2017), *Weather routing and safe ship handling in the future of shipping*, Ocean Eng. 130, pp.684-695

PRICE, W.G.; BISHOP, R.E.D. (1974), *Probabilistic theory of Ship Dynamics*, Chapman and Hall

RECHE-VILANOVA, M.; HANSEN, H.; BINGHAM, H.B. (2021), *Performance Prediction Program for Wind-Assisted Cargo Ships*, J. Sailing Technology 6/1, pp.91-117

REED, M. (2004), *The Second Order Steady Force and Moment on a Ship Moving in an Oblique Seaway - Revisited*, Internal Report, David Taylor Research Center, Bethesda

SPENTZA, E.; BESIO, G.; MAZZINO, A.; GAGGERO, T.; VILLA, D. (2017), *A Ship Weather Routing Tool for Route Evaluation and Selection: Influence of the Wave Spectrum*, IMAM Conf., Lisbon

TRACY, B.E.M.; DEVALIERE, J.L.; HANSON, T.; NICOLINI, T.; TOLMAN, H.L. (2007), *Wind sea and swell delineation for numerical wave modeling*, 10th Int. Workshop on Wave Hindcasting and Forecasting, Oahu

VAN DEN BOOM, H.; HUISMAN, H.; MENNEN, F. (2013), *New Guidelines for Speed/Power Trials: Level Playing Field Established for IMO EEDI*, SWZ/Maritime, MARIN, Wageningen, pp.1-11

VAN DER KOLK, N.; BORDOGNA, G.; MASON, J.C.; DESPRAIRIES, P.; VRIJDAG, A. (2019), *Case Study: Wind-Assisted Ship Propulsion Performance Prediction, Routing, and Economic Modelling*, Power & Propulsion Alternatives for Ships, London

YANG, Y.; TU, H.; SONG, L.; CHEN, L.; XIE, D.; SUN, J. (2021), *Research on Accurate Prediction of the Container Ship Resistance by RBFNN and Other Machine Learning Algorithms*. J. Mar. Sci. Eng. 9/376

Exploiting Digital Point Clouds in Design E3D

Marius Blom, Blom Maritime AS, Lysaker/Norway, marius.blom@blommaritime.com
Gauthier Stonestreet, AVEVA GmbH, Hamburg/Germany, gauthier.stonestreet@aveva.com

Abstract

This paper describes how 3D laser scans can be incorporated in AVEVA's E3D software. A prime application is for retrofit projects where the point cloud technology saves time and money and allows rapid, intuitive visualization during retrofit projects.

1. Introduction

The Digital Twin concept has evolved to one of the big IT buzzwords in the engineering world, including the maritime industries. Numerous papers give testimony of this, e.g. *Cabos and Rostock (2018)* and *Erikstad (2018)*. At the core of any Digital Twin will be a 3D geometrical representation, which opens the door for numerous applications in simulating physical behaviour and Virtual Reality interaction. As such, this is old hat, *Aarnio (2000)*. But how do we get a 3D model and how do we ensure that the Digital Twin evolves as its physical counterpart?

For hull geometry, *Bole (2014,2015)* discussed 3D ship hull scans to be imported to (re-)design software, namely the AVEVA design world. Here, smooth CAD surfaces are fitted to the (coarsely) scanned ship hull. For equipment and internal arrangement, the situation is more complex. Designs are frequently changed ad-hoc in the outfitting phase, and retrofitted equipment is often not reflected in the (supposed) Digital Twin model, e.g. of an engine room. This became blatantly apparent in recent years, when IMO regulations forced many ship owners to retrofit ballast water treatment systems (BWTS) and exhaust gas cleaning systems (EGCS) (= 'scrubbers'). Similar issues appear when considering retrofitting energy saving equipment, e.g. exhaust heat recovery systems.

The available resolution of 3D laser scanning has increased, while cost and portability of 3D scanners have decreased. As often in IT applications, a key issue is the interfacing between different software solutions and the art of creating not just a 3D model, but creating it efficiently and to the appropriate level of detail needed for the customer's purpose.

2. Using 3D point clouds in CAD systems

2.1. 3D scan technology

High-resolution 3D scanning results in point clouds that can be integrated in CAD and VR (Virtual reality) software for a multitude of industry applications, *Blom (2021)*:

- Survey and 3D laser scanning
 - Retrofit surveys
 - 3D laser scanning
 - Virtual representation
 - Cloud data with an accuracy of ± 2 mm is achieved.
 - No interruption to the assets' operations, while scanning, Fig.1
- 3D conceptual (re-)design
 - Conceptual design, Fig.2
 - Virtual merging existing systems with new design
 - Alternative solutions discussed
 - Multiple systems could be modelled to verify their suitability on board
 - Conceptual design freeze

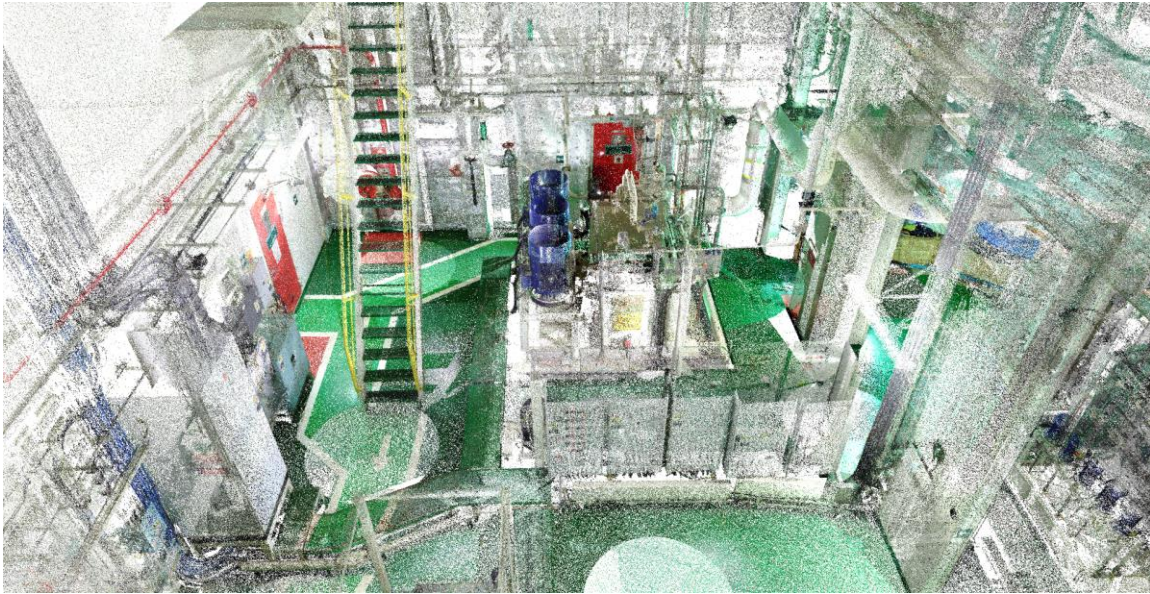


Fig.1: Assets can be scanned while in usual operation

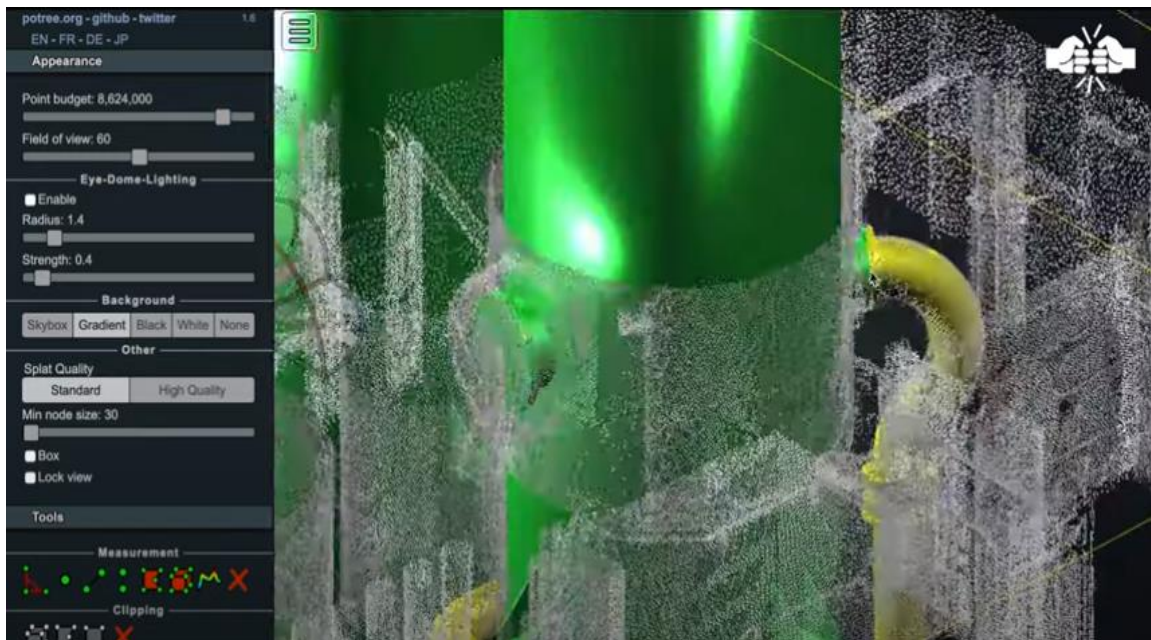


Fig.2: Concept design fitted to point-cloud presentation

- Detailed design
 - Multi-disciplinary concurrent engineering
 - Pipe, Structure and electrical design, Fig.3
 - ISO and Updated CAD drawings
 - Flow/Stress calculations
 - Drawings & documents
 - Design validation
 - Material takeoff
- Class approval
 - All deliverables submitted to class authorities
 - Criteria of class rules are followed while design
 - Minimal changes to deliverables after class comments
 - Class comments are addressed diligently

- Smooth class approval process
- Class approval process will go on till Installation and commissioning phase

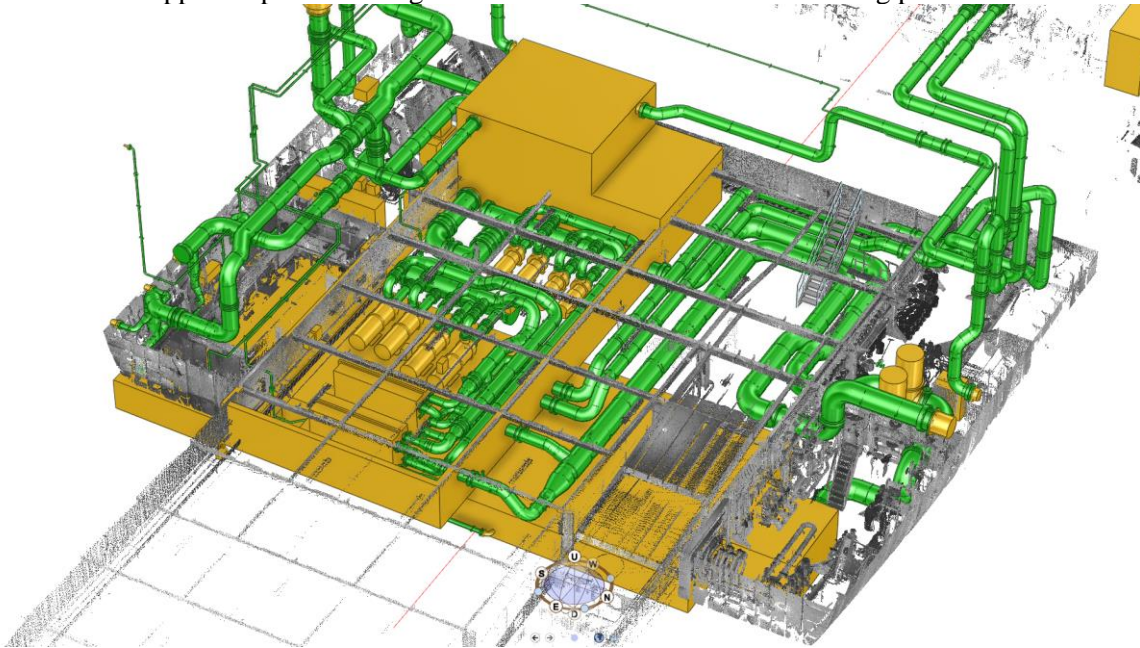


Fig.3: Detail design from AVEVA software created according to as-is point-cloud

2.2. E3D Design

E3D Design is AVEVA's 3D design solution for accurate and clash-free hull and outfitting basic design of ships and offshore vessels, Fig.4. E3D Design capabilities for marine include the Hull Basic Design Module, used for the preliminary design of a ship's hull structure, and supporting key decisions regarding naval architectural characteristics, Space Management, Outfitting Design and Drawings.

Of course, E3D Design integrates seamlessly with other AVEVA solutions, providing extensive functionality. The integrated design also facilitates information exchange with many third-party systems, such as Blom Maritime's dedicated 3D scan software.

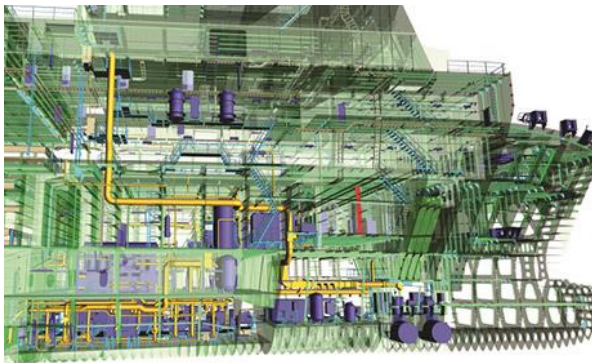


Fig.4: E3D Design model with outfitting

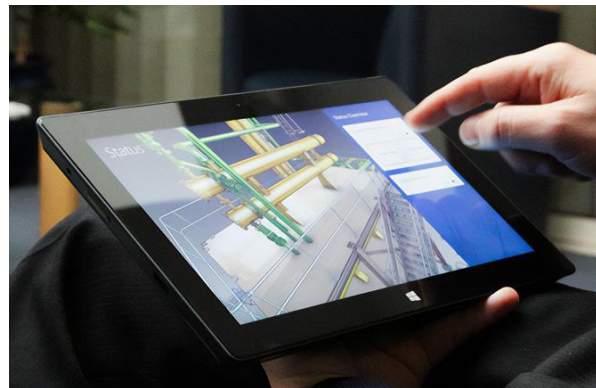


Fig.5: E3D design viewing on tablet

E3D Design is particularly suited for Hull and Outfitting basic design enabling the creation of complete, error-free, production-oriented 3D modelling of the vessel, with remote design synchronization capabilities. Key benefits include:

- Enabling clash-free, multi-discipline 3D design and rapid generation of accurate drawings and reports to meet demanding project schedules

- Quickly developing hull basic design models to serve design certification and preliminary analysis
- Reducing costs, timescales, and commercial risks for both new-build and retrofitting projects
- Automatically dividing a ship's hull design into spaces, enabling the efficient design of even very complex ships. Logical dependencies between designed objects and the space attributes retain design intent while the hull layout evolves.

An extensive catalogue enables predefined parametric components and objects to be quickly selected and positioned within the model, then automatically checked for clashes and for compliance with configurable design rules. The Space Management module enables more efficient collaboration as it facilitates work distribution, design review, reporting and design analysis. As the design evolves, changes can be highlighted and tracked which make it easier to identify, manage and communicate the change across different disciplines.

The “insight in action” feature allows viewing the 3D models anytime, anywhere, also on mobile devices, such as tablets, Fig.5.

2.3. Integration of 3D scans in E3D

As a particular feature of E3D Design, photorealistic laser scan data integrated into the design environment enables rapid, intuitive and accurate design of vessel modifications, and verification of construction status against the design intent as constructions progresses, Fig.6.



Fig.6: Laser data integrated with 3D model in E3D Design

3. Conclusion

For ships without appropriate digital representation of the as-built status, 3D laser scanning has been found to be a viable solution. In our experience, “data at your fingertips” have saved up to 30% on material cost and up to 35% on manhours in retrofit projects. Initially motivated for retrofits, the geometrical digital twin created by advanced 3D laser scanning has been found to be very versatile also for other applications, such as preventive maintenance or training.

Integration of 3D scan point clouds in CAD software has been streamlined and is drifting into best business practice also in the maritime world.

Acknowledgements

We are grateful for Volker Bertram's help in shaping this paper and his guidance during the writing process.

References

AARNIO, M. (2000), *Early 3-D ship model enables new design principles and simulations*, 1st COMPIT Conf., Potsdam pp.5-17, http://data.hiper-conf.info/compit2000_potsdam.pdf

BOLE, M. (2014), *Regenerating Hull Design Definition from Poor Surface Definitions and other Geometric Representations*, 13th COMPIT Conf., Redworth, pp.193-208, http://data.hiper-conf.info/compit2014_redworth.pdf

BOLE, M. (2015), *Regenerating Hull Surface Definition from Laser Point Clouds*, 17th ICCAS Conf., Bremen

BLOM, M.; CZAPLA, M. (2021), *Direct Integration of 3D Laser Scanning in CAD*, 20th COMPIT Conf., Mülheim, pp.24-29, http://data.hiper-conf.info/compit2021_muelheim.pdf

CABOS, C.; ROSTOCK, C. (2018), *Digital Model or Digital Twin?*, 17th COMPIT Conf., Pavone, pp.403-411, http://data.hiper-conf.info/compit2018_pavone.pdf

ERIKSTAD, S.O. (2018), *Design Patterns for Digital Twin Solutions in Marine Systems Design and Operations*, 17th COMPIT Conf, Pavone, pp.354-363, http://data.hiper-conf.info/compit2018_pavone.pdf

A Novel Integrated Multi-System Approach for Situational Awareness in Maritime Environment

Luisa Mancarella, Apphia, Lecce/Italy, luisa.mancarella@apphia.it

Francesca Calabrese, Apphia, Lecce/Italy, francesca.calabrese@apphia.it

Marco Cataldo, Apphia, Lecce/Italy, marco.cataldo@apphia.it

Gabriele Serafino, Apphia, Lecce/Italy, gabriele.serafino@apphia.it

Luigi Paiano, Apphia, Lecce/Italy, luigi.paiano@apphia.it

Luca Carlino, Fincantieri NexTech, Lecce/Italy, l.carlino@fincantierinxt.it

Angelo Cirigliano, Fincantieri NexTech, Lecce/Italy, angelo.cirigliano@fincantierinxt.it

Nicola Leonardi, Fincantieri NexTech, Lucca/Italy, nicola.leonardi@fincantierinxt.it

Emanuele Sansebastiano, Fincantieri NexTech, Lecce/Italy, emanuele.sansebastiano@fincantierinxt.it

Luca Sebastiani, Fincantieri NexTech, Lecce/Italy, luca.sebastiani@fincantierinxt.it

Abstract

This paper describes an autonomous vessel's situational awareness system, which allows automatic operations in autonomous navigation and shore operations personnel to have the same perception of the surrounding environment as they would be on the vessel. The proposed approach fuses the data coming from different systems: AIS, ARPA and camera on UAV for target detection finalized to motion replanning, LiDAR and six Optical Systems for the reconstruction of a panorama and a 3D virtual view as support for the Ground Control Station.

1. Introduction

Situational awareness is a key aspect of decision management in complex and dynamic areas, such as air travel, air traffic control, navigation, power plant operations, military command and control, and emergency services. It consists in the perception of elements and events of the surrounding environment, the understanding of their meaning and their projection into the future, with the aim of understanding the impact that they will have in the immediate and near future on the specific objectives of the individual operations to be carried out.

The sea transport sector is becoming increasingly important in modern life. The constant effort of the scientific community in the sector is aimed at allowing, in whole or in part, autonomous navigation. The detection of nearby objects and boats is essential for the development of systems for safety in navigation. Collision avoidance, in fact, is one of the high-level safety objectives and requires a complete and reliable description of the surrounding maritime traffic situation.

In recent years, more and more sensors have been developed to support surveillance operations in general. Data Fusion techniques allow combining data and information from multiple sensors, for obtaining more specific assessments than those obtainable using a single and independent sensor, and to meet the needs related to Situational Awareness. Developing more efficient fusion strategies and improving the design of advanced and microprocessor-based sensors that are fast in processing and calculating distributed data can provide significant aid to naval surveillance operations and can reduce computational load of global surveillance.

Multisensor data fusion techniques are based on collecting datasets from multiple sensors and merging them to create a more accurate dataset. It improves the ability to obtain information from the raw data by increasing the overall statistical accuracy of the datasets. The robustness of a system that adopts a data-fusion framework, in fact, is greater due to the contribution of different sources.

Moreover, having more than one data sources compensates the temporary failure of some of those data sources. Statistically, the system is never blind. The integration of sensors and the collaboration between them can be effectively employed for different military and civil applications to aggregate

data from multiple sources, ensure complete and reliable coverage of the observed area, provide timely information on potential threats and improve the overall accuracy of event tracking.

Heymann et al. (2013) propose an approach to improve the accuracy and integrity of traffic situation related information by a combined use of data provided by independent data sources.

Lee et al. (2021) propose detection, location and tracking methods applied to videos taken from real boats. The results obtained were compared with AIS data and showed that the proposed algorithm could be used effectively for the awareness of the surrounding environment. An approach aimed at identifying and tracking objects in the maritime environment by association of probabilistic data is reported in the study proposed by *Haghighyan et al. (2018)*.

In the literature, there are several studies conducted on ship detection and tracking in maritime environments. The application areas of AI methods in maritime navigation and vessel situational awareness are identified as object identification, localization, and trajectory analysis, *Thombre et al. (2022)*.

Multisensor fusion has always been essential to robotics and self-driving systems, for accurate perception of the surrounding environment. Among different types of fusion, the most common one is the combination of LiDAR (Light Detection And Ranging) and optical camera, especially in the tasks of vision-based odometry and mapping, object detection and tracking tasks. In fusing the multi-modal data from LiDAR-camera systems, the first and most critical step is the accurate extrinsic calibration, *Cui et al. (2020)*. The general calibration process is to detect the multiple corresponding 3D-2D corners, and then solve the relative pose between LiDAR and the camera by utilizing the PnP (Perspective-N-Point) method. Thus, it is essential to find the corresponding features accurately by geometric and texture constraints from point clouds and images. *Wang et al. (2017)* propose a method to execute an extrinsic calibration between a LiDAR and a 360° panoramic camera using a printed chessboard, and the correlation between the reflectance intensity of the LiDAR laser and the colour of the chessboard's patterns. *Cui et al. (2020)* propose an improved approach for the 3D corners estimation based on the same laser intensity-colour correlation. The proposed solution in the present work aims at implementing this calibration approach in an operative-like scenario to provide an always updating 3D virtual view reconstruction of the surroundings by LiDAR and Optical Systems fusion.

1.1. Contributions

Multisensor Integration allows making more reliable decisions than those that could be taken if the information sources were analysed individually. This work proposes multisensor data fusion focusing on situational awareness aspects in maritime environment. The research activities focus on aspects of target association aimed at automatic obstacle avoidance and motion replanning of an unmanned naval platform and on the reconstruction of panorama view and a virtual view to support Ground Control Station.

We present the results of research activities on the fusion of data coming from an unmanned surface ship and the following systems: AIS (Automatic Identification System), ARPA (Automatic Radar Plotting Aid) system, camera installed on a drone operating near the vessel, LiDAR system and six video sources installed on unmanned platform mast.

The need to create a precise, accurate and reliable system has prompted us to identify processes and methodologies for the correct management of measurement errors which are inevitably affected by the data coming from the involved systems. Initially, the main problems related to data fusion, deriving from the heterogeneity of sources, the synchronization of needs of information and the accuracy of data are described.

The main objective of this work is to analyse the targets identified by the various systems, evaluate their reliability and improve, where possible, the accuracy of the information by analysing a particular

aspect of the multisensor data fusion process, namely the target association. We describe the problems arising from the difficulties of the marine environment and from the specific needs of the project, comparing the proposed approach respect to previous works in ship detection and data fusion in maritime environment, *Heymann et al. (2013)*, *Haghbayan et al. (2018)*.

Particular attention is paid to the logic and processes of target association carried out on the various subsystems available. The data coming from the LiDAR and six video sources are used for the reconstruction of a panorama view and a 3D virtual view of the area around the unmanned platform, with the aim of creating an innovative support tool to improve situational awareness on terrestrial station. The experimental results obtained in marine scenarios are presented.

1.2. MARIN project

In this paper, we focus on the autonomous vessel's situational awareness system, which allows shore operations personnel to have the same perception of the surrounding environment as they would be on the vessel. The work presented in this paper is part of the research and development activities of the “MARIN – Monitoraggio Ambientale Remoto Integrato su piattaforma Navale” project (project Code: KATGSO3 – “Programma operativo FESR 2014-2020 Obiettivo Convergenza” – Regolamento Regionale n. 17/2014 – Titolo II Capo 1 – “Aiuti ai programmi di investimento delle grandi imprese”), co-funded by Regione Puglia within the framework of “Contratti di Programma”. Project beneficiaries are Fincantieri NexTech S.p.A., RINA Consulting S.p.A. and Co.M.Media s.r.l.. The objective of MARIN project is to set-up and sea-test a technological demonstrator of the enabling technologies for autonomous navigation. The demonstrator platform is the TESEO I, an experimental vessel jointly developed by NAVTEC and Tringali Shipyard as part of a previous research project, with subsequent proper adaptation to the needs of the MARIN project.

2. Multisensor fusion and critical aspects

Each multisensor data fusion process is characterized by a set of problems intrinsic to the very nature of the process, which fall into the following main aspects: sources heterogeneity, needs of time and spatial synchronization of information, data accuracy.

- Sources heterogeneity - Multisensor fusion needs the unified management of data from heterogeneous sources, such as sensors of different types, systems and on-board instrumentation. The different technologies, standards and protocols used by each of them highlight the need to carry out specific, and in some cases complex, information processing with the aim of ensuring data uniformity.
- Time synchronization of information - Each sensor or subsystem involved in the data fusion process is also characterized by different data acquisition intervals and frequencies. From a data fusion perspective, the information must refer to the same instant in time, and this entails the need to synchronize it.
- Spatial synchronization of information - Another of the problems that usually characterize multiple sensor data fusion process concerns the different reference systems used for indicating the coordinates of the identified targets. For a correct evaluation of the information of the various sensors and/or systems, with the aim of improving the accuracy of the detections, it is necessary to standardize the data, making one or more conversions from the starting reference system to a single frame of reference valid for all sources and suitable for subsequent processing. The uniformity of the reference systems can be achieved through the application of dedicated techniques and methods, already existing in the literature.
- Data accuracy - Due to the different technologies used and the hardware used, the sensors and systems involved in the process are characterized by different levels of accuracy in the acquisition and representation of data. This aspect can significantly affect data fusion operations.

The multiplicity of sensors and measuring instruments available, together with the diversity of technologies used by each of them, can also represent an important opportunity. As part of the design of the decision support model based on the data fusion process, particular importance was given to the possibility of optimizing the potential of some sources compared to others, based on the different situations, possible scenarios, and data availability.

3. Proposed Approach

A crucial part of an autonomous system is the ability to perceive and understand the surrounding environment. This study explored the possibility of using systems and sensors to help autonomous naval platforms to generate information about the surrounding environment.

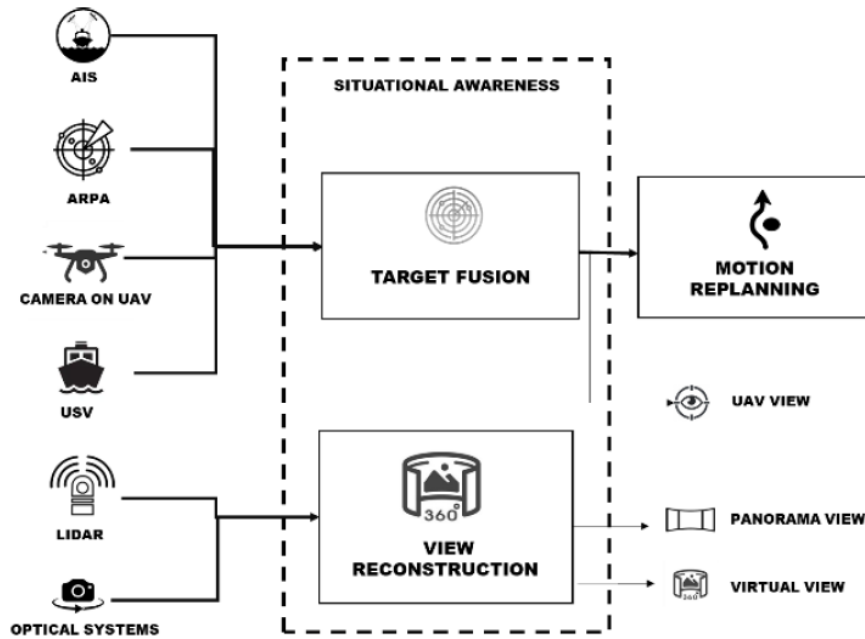


Fig.1: Proposed approach

The study focused on an USV (Unmanned Surface Vessel) and on the use of data from:

- AIS, ARPA, a video camera installed on an UAV (Unmanned Aerial Vehicle) for target fusion finalized to motion replanning
- LIDAR and six Optical Systems installed on the unmanned platform mast for the reconstruction of view around the unmanned platform as support for Ground Control Station.

The aim of Target Fusion is the identification of a set of targets within the operating scenario that represents the set of external objects (fixed or mobile) that can be assimilated to obstacles to avoid, as they are subject to possible collision with the unmanned platform. The information extracted from elaboration on UAV data, together with the data coming from other systems, could contribute to the multisensor data fusion process aimed at avoiding collisions.

4. Target fusion for motion replanning

The main objective is to create a system capable of identifying the targets present nearby the platform and providing an overview of the navigation area, to obtain situational awareness that can allow the navigation modules to re-plan the route to avoid possible collisions. The Target Fusion process involves following systems:

- ARPA, a navigation support system based on radar technology installed on the platform.

- AIS, an automatic identification system used for sharing information, for which the autonomous vessel is equipped.
- Optical sensor installed on an aerial drone that provides information on the environment around the unmanned platform.

In target fusion process it is essential to consider that the different systems used for detecting targets near the boat have very different hardware and software characteristics, which significantly influence the accuracy of the data provided by each of them. Each system, in fact, is characterized by different measurement errors.

We therefore considered it necessary to develop a target association process that managed appropriately the different levels of accuracy of the processed data.

The dynamic, parametric and specific handling of measurement errors of the various information used for each of the systems involved reduces the possibility of false associations to a minimum, allowing high-precision outputs to be obtained.

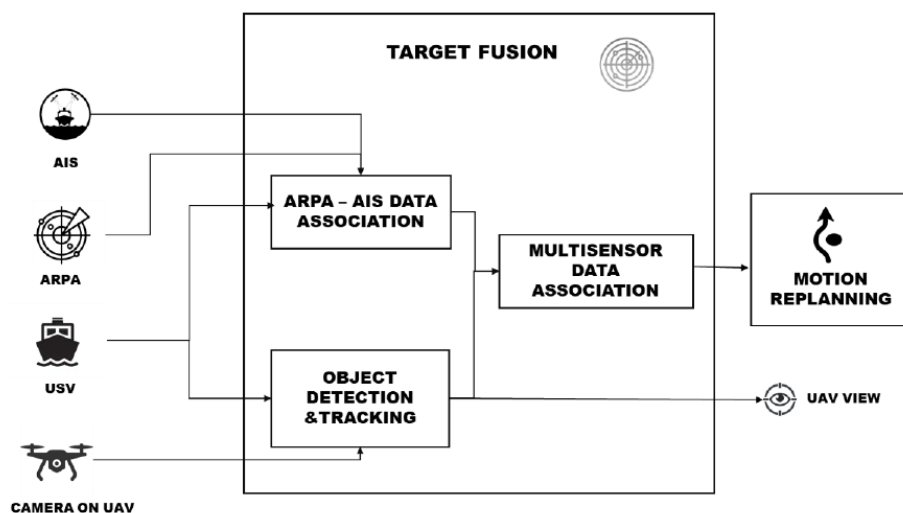


Fig.2: Target Fusion schema

Target Fusion includes three processes: ARPA-AIS Data Association, Object Detection & Tracking and Multisensor Data Association.

The first step consists in the process of associating targets detected by AIS and targets detected by ARPA. The output of ARPA-AIS Data Association process constitutes the input of the next process, Multisensor Data Association, which deals with the association with the targets detected by “Object Detection & Tracking” process on data coming from the video system installed on the drone. So, Multisensor Data Association inputs consist of the AIS-ARPA target association process outputs and of the targets identified by means of object detection techniques applied to the images extracted by the camera installed on the drone.

Data Association processes provide that the association is defined through the processing of different phases, based, respectively, on various criteria (temporal, position, motion and previous history, described in detail in the following sections). The output of the Multisensor Data Association process consists of the targets detected by the various subsystems. If the association is successful, only one of the targets involved is shown, selected by means of specific rules. A hierarchy has been defined between the three subsystems based on the level of accuracy of each of them:

1. AIS
2. ARPA
3. UAV Camera

In the case of association of targets coming from all three subsystems, therefore, the output consists only of the target coming from the AIS, while in the case in which the association has occurred between targets coming from ARPA and UAV Camera, in output only ARPA output is reported. The same logic is followed in all the different possible associations.

4.1. ARPA-AIS Data Association

The initial process of the fusion involves the AIS and ARPA systems. The information on the AIS targets is encoded within specific NMEA messages sent by the vessels near the unmanned platform and received by the AIS receiver, while the data on the ARPA targets and on the position of the platform itself are made available, in the form of NMEA messages, directly from on-board systems. There are some substantial differences, of particular interest in the context of the activities covered by this document, regarding the tracking of targets carried out by the two ARPA and AIS systems, *Chang and Xiaofei (2009)*:

- Reliability in target monitoring - Radar target data is affected by disturbances caused by sea state, false echo and low tracking resolution. These disturbances cause some problems in tracking the target, such as false-tracking, non-tracking, loss of tracking and cross-tracking. In the tracking performed by AIS systems, these conditions do not exist.
- Target tracking range - Within the radar detection range, all targets can be detected, while in the AIS coverage area only AIS-equipped targets can be tracked.

The reasons behind the data fusion on AIS and ARPA data mainly lie in the difference in accuracy and reference target of the two systems. In ARPA systems the targets can be of different types, but the precision of the detections is not high, and the information on the targets is poor. On the contrary, the information received by the AIS system is very accurate but limited only to the boats that are equipped with it. The AIS system, at certain intervals, automatically transmits, receives and displays, among other things, the information of the devices connected to it, such as the gyro, the speed and distance measuring device, the GPS. Furthermore, it can calculate and indicate, based on the knowledge of the geographical positions and motion vectors of its own vessel and of the vessel from which it receives the AIS messages, a series of data, such as the Closest Point of Approach (CPA) and the Time to the Closest Point of Approach (TCPA). The ARPA system, on the other hand, calculates the real vector, the CPA and the TCPA of the object detected and tracked exclusively on the basis of radar measurements of its distance and its bearing.

Therefore, the radar system has a lower accuracy and a certain time delay in the presentation of data, but, unlike AIS, it is an independent source of information about the surface objects present near the vessel, *Wawruch (2018)*. The main objective of data fusion between the data of the two systems is to increase the types of detectable targets and the accuracy of the information.

The main problems encountered in the data fusion process are attributable to some characteristics and substantial differences in the data collected by the two systems. One of the preliminary aspects to pay attention to is the time synchronization of the information coming from the two systems, as both the time slot and the data acquisition frequency are different. To carry out a correct fusion of the data it is necessary that the surveys refer to very close instants in time.

Another important difference, moreover, is represented by the inconsistency of speed and course of the same target detected, due to the different reference systems used by the two systems. Often, in fact, the data coming from the two systems are expressed in different units of measurement and/or reference systems. In these cases, it is evident the need for a preliminary conversion of the information to allow its correct processing.

Finally, further aspects to consider are the possible lack of identification of the radar target, the intrinsic error of information from both systems and the error in the size of the radar echo in relation to the AIS target of the point. The logic behind the data fusion process of ARPA and AIS data were

developed according to the literature currently available in the field of data fusion in the maritime field. The system inputs consist of messages received from the AIS system and data from the ARPA system and the vessel's positioning system.

The preliminary phases of the process are mainly two:

- Verification of the consistency of AIS targets (AIS Target Validation)
- Temporal association of ARPA targets to AIS targets.

The core of the data association process has the objective of associating each of the validated AIS targets with the corresponding target detected by the ARPA system, if any. It mainly consists of the following two phases:

- Uniformity in the definition of coordinates (Spatial Association)
- Association of the single ARPA target to the single AIS target (Target Association)

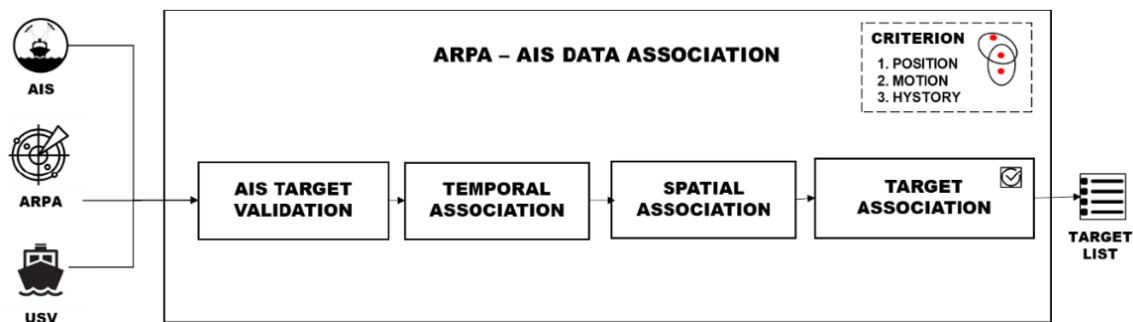


Fig.3: ARPA-AIS Target Association schema

4.1.1. AIS Target validation

The verification of the consistency of the AIS targets is carried out by verifying that there are no two targets with different IDs, detected in very close instants (within a specific time interval), and whose distance is less than a certain threshold value. If these conditions occur, both targets are eliminated, as they are deemed to come from unreliable surveys (based on what is presented in *Heymann et al. (2013)*). The input of the sub-process is represented by the pair of AIS targets to be compared and by two threshold values, one relating to time, and another relating to distance. The final goal is to obtain a list containing only the targets whose validation has been successful, and on which to subsequently proceed with further processing.

4.1.2. Temporal association

The temporal association of the ARPA targets to the AIS targets is carried out through the selection, for each AIS target validated in the previous phase, of the ARPA targets detected in a specific time around the instant of detection of the AIS target. According to the different data acquisition frequencies of the systems and the specific configured time threshold, each AIS target can therefore be associated with a single ARPA target, multiple ARPA targets or none.

The core of the data association process has the objective of associating each of the validated AIS targets with the corresponding target detected by the ARPA system, if any. It mainly consists of the following two phases:

- Uniformity in the definition of coordinates (Spatial Association)
- Association of the single ARPA target to the single AIS target (Target Association)

4.1.3. Spatial association

To ensure uniformity in the expression of the coordinates of the two systems involved, necessary to ensure a correct comparison and evaluation of the distances, the conversion of the ARPA polar coordinates into geographic coordinates expressed in latitude and longitude is carried out. The input of the conversion process is represented not only by the polar coordinates of the ARPA target, but also by the data from the vessel's positioning system, detected at the same reference instant as the target data. The selection, for each AIS target, of the ARPA targets to be associated is made by identifying, among those already temporally associated, the ARPA targets which satisfies the condition that the distance is less than a specific threshold value.

4.1.4. Target association

The selection, for each AIS target, of the ARPA target to be associated is made by identifying, among those already temporally and spatially associated, the ARPA target closest to it. To prevent incorrect associations, possible in extreme situations, definitive association is made only if the selected ARPA target satisfies further two conditions, related to the motion and to the previous association history. The output of the entire data fusion process consists of a series of targets, which can be, in detail:

- AIS target, in the case of pairs of AIS targets and associated ARPA targets
- AIS target for which there is no ARPA target to be associated
- ARPA target for which there is no AIS target to associate.

4.1.5. Measurement errors

Throughout the association process, we paid particular attention to the management of the aspects related to measurement errors. *Lenart (1989)* and *Kazimierski (2015)* report indications on accuracy requirements according to IMO. The information relating to the measurement uncertainty of the systems involved was incorporated directly into the core of the Data Association process. *Kazimierski (2010)* proposed an association process of ARPA and AIS targets which involves the cascade use of different association criteria based on the measurement uncertainties of the two systems. In particular, the proposed criteria are based, respectively, on data relating to:

- Position of the targets
- Motion of targets
- History of the associations

To simplify the calculations, in the proposed study the dimensions of the target boats are not considered, and it is assumed that the positions detected by the ARPA and the AIS refer to the same point of the target itself. The first step of the proposed process consists in defining a general condition of association, which forms the basis of the first two proposed criteria:

$$|X_{\text{ARPA}} - X_{\text{AIS}}| \leq B$$

where X represents the value calculated according to the specific criterion used, and B is the association threshold.

- Position-based criterion
The first criterion used in the association process is the one on the distance between the targets. Under the assumption that the positions expressed by AIS and ARPA refer to the same point of the target, and that the data refer to the same instant in time, the association criterion is as follows:

$$|POS_{\text{ARPA}} - POS_{\text{AIS}}| \leq B_P$$

Pos_{ARPA} and Pos_{AIS} are, respectively, the positions detected by the ARPA system and the AIS, B_P the association threshold of the position criterion, defined as:

$$B_P = d_1 + d_2$$

d_1 and d_2 are the position detection errors by ARPA and AIS. The value of d_2 derives directly from the accuracy of the position detection system of the AIS system (probably GPS). The value of d_1 depends on the distance to the target and the specifications of the ARPA system itself. It can be calculated by:

$$d_1 = d_0 + d_D + (2\pi/360) \cdot D \cdot d_N$$

d_1 is the radar detection error expressed in [m], d_0 the error [m] in determining the position of the radar itself, d_D the error [m] in determining the distance to the target, d_N [°] the one in determining its bearing, and D the value of the distance to the target.

- Motion-based criterion

Since sometimes the association based on the position may not be sufficient to ensure a correct association, the study proposes a further step, using a criterion based on the data relating to the motion of the targets. Assuming that the COG (Course Over Ground) and SOG (Speed Over Ground) values of the AIS and ARPA targets are known, the association criterion can be expressed according to the same principle as the association by position, with the following formulas:

$$B_C = d_{C1} + d_{C2}$$

where d_{C1} is the radar COG detection error [°], d_{C2} the AIS COG detection error [°], and

$$B_V = d_{V1} + d_{V2}$$

where d_{V1} and d_{V2} are the errors [kn] on SOG of radar and AIS, respectively.

- Association history-based criterion

The target association based on the precise verification of the presented association criteria may not always be sufficient, and in some cases, it could lead to incorrect associations. The association, in fact, could be the result of a temporary and occasional similarity of the movement parameters in a close position. Therefore, the history of associations should also be considered as the third stage of the general algorithm. The aim should be to verify if the association of the targets is maintained over a certain period, thus confirming the associative trend in a few consecutive steps, and eliminating the random association. The approach consists in establishing that if an objective satisfies the criterion in N of M consecutive steps, the trend is considered stable, and the association is considered valid.

4.2. Object Detection & Tracking

In this context, the work focuses on elaboration of data coming from the optical system on an aerial drone for supporting an unmanned platform in obstacle identification.

The Object Detection & Tracking process deals with the detection and tracking of objects around the unmanned platform. The use of UAV enhances the capabilities of the USV, extending the monitored area of the drone's range of action. Systems of this type make it possible to have video footage taken from a very high point of view in real time, thus obtaining an almost perfectly flat view, allowing a 360° Bird Eye View (BEV) view of the environment surrounding the USV in all visibility conditions.

The operational hypotheses provide that the drone shoots by positioning itself in a predetermined area over the boat, at a specified height and that the unmanned platform is present in the images so that objects can be referenced with respect to it. The use of the camera on the drone facing downwards with a fixed zoom level and non-modifiable angle of view is envisaged.

The video stream from the camera on the drone is the input for a preliminary phase of processing the detected images. The main objective is to detect and identify the targets of interest.

In this project, we propose an approach based on machine learning techniques for detection and tracking ship in marine environment monitoring, with focus on a custom large data set based on aerial images. *Paiano et al. (2022)* present ship detection and tracking based on YOLOv4 and Deep Sort algorithms focusing on the need of large amounts of data for the training stage to perform robust detections and tracking even in critical glare and waves variations. The work is according to a data-centric Artificial Intelligence (AI) approach, which involves building AI systems with quality data with a focus on ensuring that the data clearly conveys what the AI must learn.

The Bounding Boxes of the various identified objects in the video acquired by the drone and the position information of the drone are used to estimate the position of the targets. Fig.4 shows ship detection examples on data acquired on the field in different marine scenarios. This information is used for the Multisensor Data Association process.

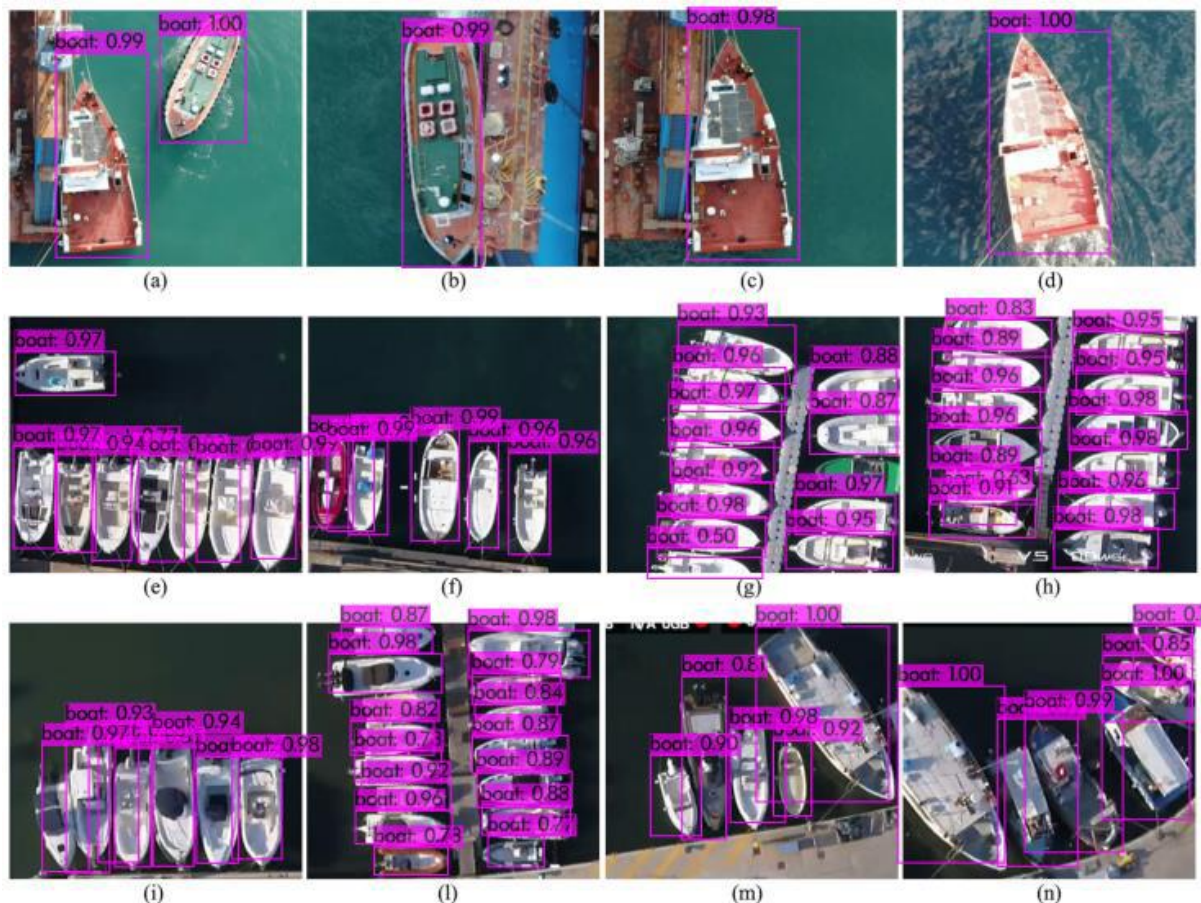


Fig.4: Example of ship detection (by Object & Tracking process)

5. View reconstruction

The data from the LiDAR and the six Optical Systems are used with the aim of providing useful support for situational awareness by the generation of a Panorama View and a 3D Virtual View. Both the LiDAR and the Optical Systems were installed on the mast of the ship, at different heights.

5.1. Panorama View

In MARIN Project it is integrated on the demonstrator vessel a video perimeter monitoring system which includes two pods with three high-definition video-cameras each, to guarantee 360° optical coverage and support navigation.

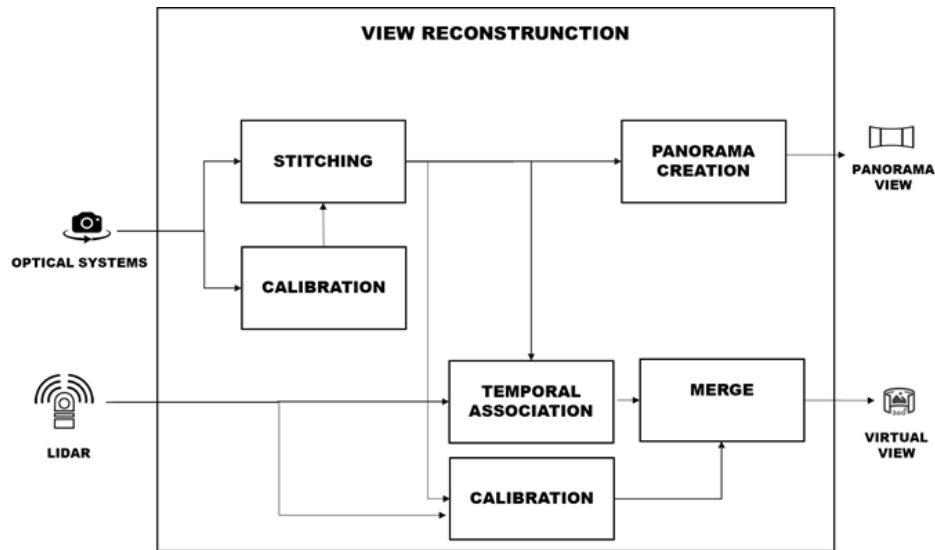


Fig.5: View Reconstruction schema

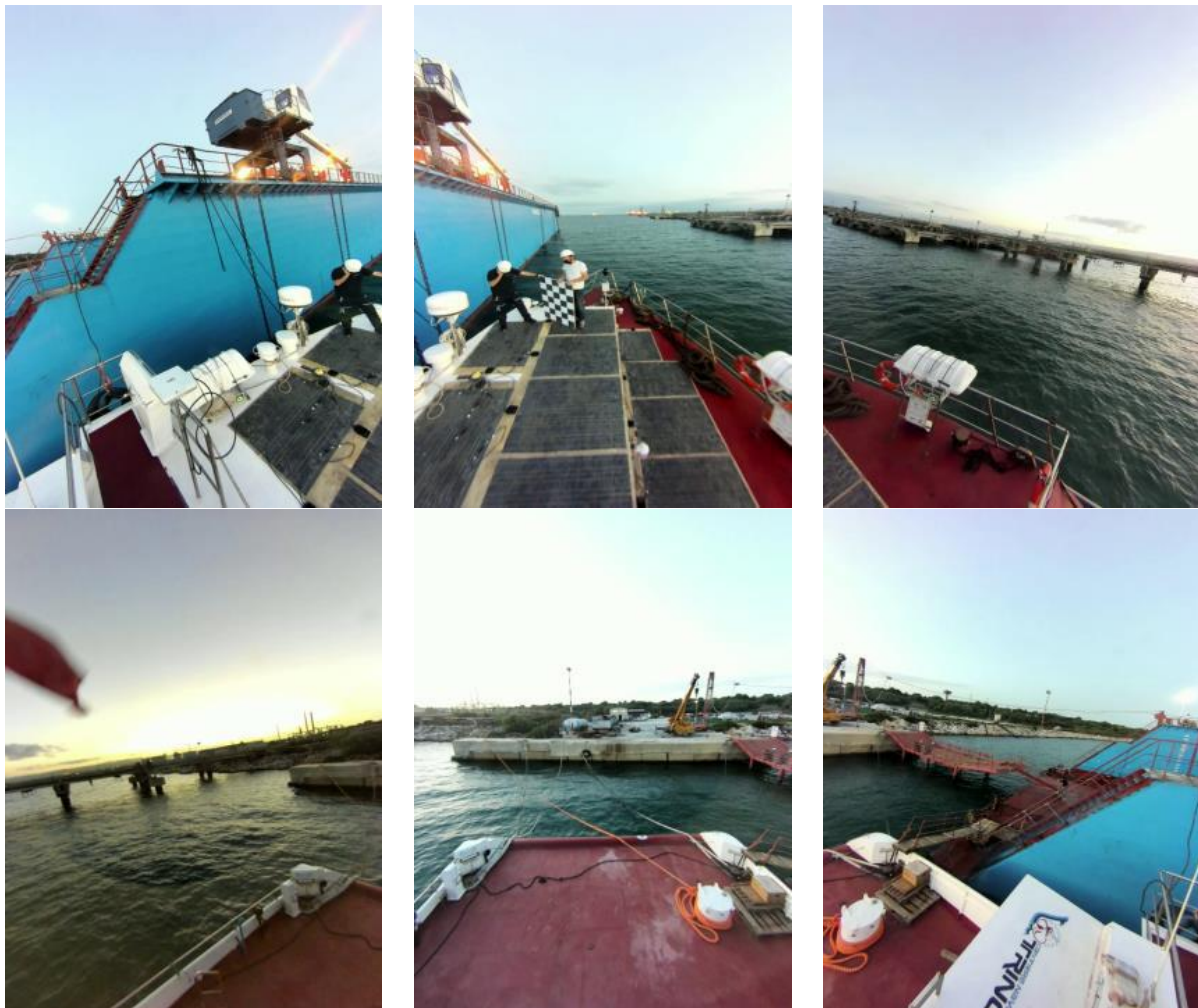


Fig.6: Example of frames extracted by Optical Systems



Fig.7: Examples of panorama view (AFT/FWD)

The research activities aim at verifying the feasibility of panorama coverage through images stitching. We explored temporal synchronization problem, calibration and stitching for generating the panorama view. The achieved results were two distinct stitched panorama images, each showing 180° of horizontal field of view.

5.2. 3D Virtual View

The data coming from the Optical Systems constitute one of the inputs of the View Reconstruction process. The design idea involves the use of images from the video system together with LiDAR data to generate a three-dimensional virtual view for Situational Awareness.

Optical Systems are limited to providing two-dimensional images, which means that depth and distances are difficult to estimate while they are certainly relevant for Situational Understanding: the lack of direct three-dimensional vision can be compensated for through additional instrumental supports, e.g. using additional distance sensors and merging a graphical presentation of this information into the image presentation. For a complete and continuous 3D spatial representation of the surrounding environment, it is therefore considered necessary to include a 360° LiDAR sensor, whose measurements can be combined with the corresponding optical images of the video system.

The images of the video system, after the stitching process, and the data from the LiDAR system are managed in the View Reconstruction process with the aim of providing useful information for a confirmation of the Target Association process outputs at the Ground Control Station on land.

The Temporal Synchronization process allows to manage in an appropriate way the temporal synchro-

nization of the information coming from the stitching process of the Optical Systems and the data acquired by the LiDAR, a fundamental operation for the calibration and merge processes.

Before the merge process, it is necessary to execute the extrinsic calibration process of the systems using a printed chessboard. The calibration process was split in two distinct steps used to correlate the spatial correspondence between the LiDAR and each camera pod. The chessboard used in this work in experimental environment is constructed by 5×7 cells with a side length of 16.6 cm, Fig.8. We use the corner information of the chessboard's point cloud instead of the edge information. Corners of the sparse and noisy chessboard's point cloud are estimated by solving the optimization problem with the intensity information. After the correspondence of corners both on the image and in the point cloud, the extrinsic transformation matrix is generated by solving the nonlinear optimization problem.

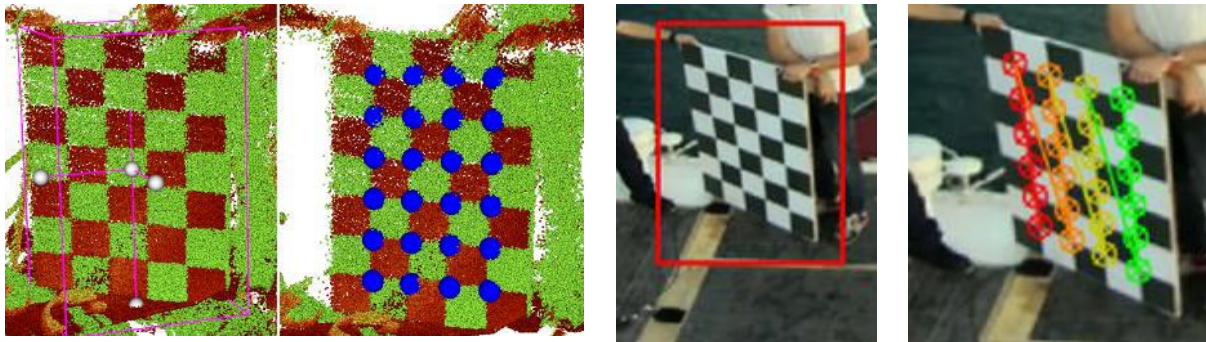


Fig.8: Example of Calibration by chessboard

The Merge process was also applied to the LiDAR and the two pods individually; each merge used the calibration results for the LiDAR system and the corresponding pod. Both steps, applied to the same point cloud from the LiDAR, result in a complete 360° virtual view. Each step includes the following phases:

1. Spatial synchronization: it is necessary to execute 3D cloud points rotation and translation and change of coordinate system. The calibration parameters are used to perform a transformation of the points present in the cloud according to the reference system of the Optical Systems. Each cloud point position is converted from the Cartesian to the spherical coordinate system.
2. 3D point coordinates to pixel image mapping: Using the information of the stitched image (dimensions in pixels and field of view), the positions expressed in spherical coordinates are converted into coordinates on the plane (in pixels on the image canvas).
3. Pixel coordinates RGB selection: For each coordinate, the RGB information relating to the pixel present in that position is extrapolated from the image (an arbitrary colour was given to the LiDAR points mapped outside of the image canvas).
4. 3D points coordinates and RGB values juxtapose: The set of points of the cloud input and the set of RGB data have the same size. The i -th RGB information is associated with the i -th coordinate (xyz) of the point cloud.



Fig.9: Example of point clouds by LiDAR acquisition and stitched image by elaborating bow pod data

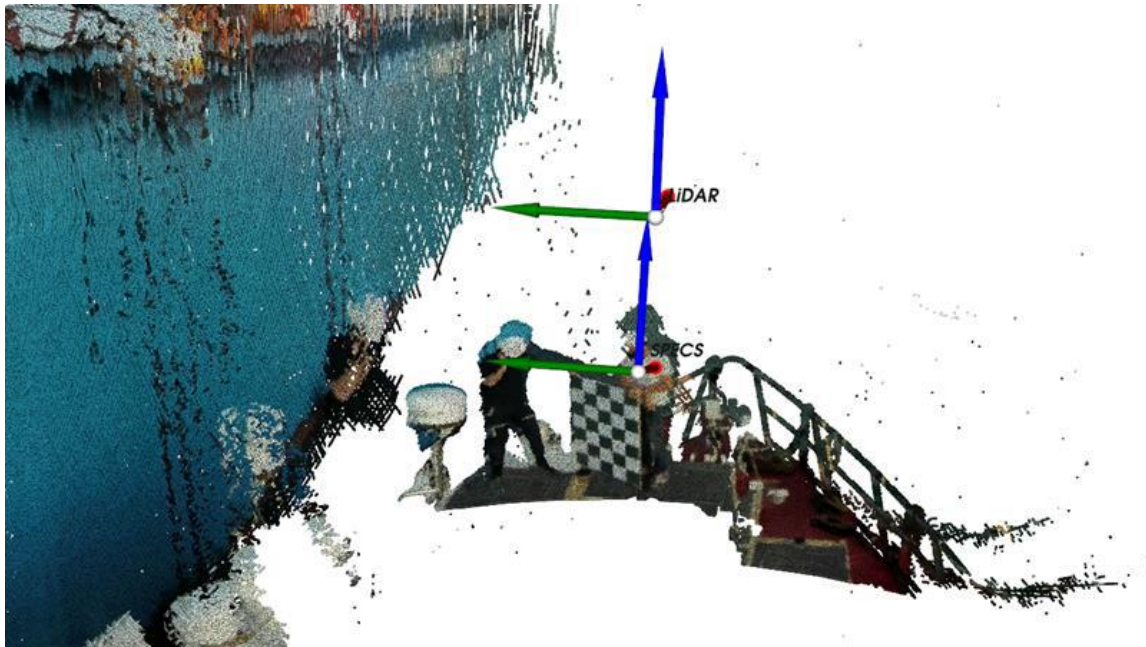


Fig.10: Example of 3D Virtual View by Merge

One of the problems that we encountered in the temporal synchronization management was due to the different acquisition methods used by the Optical Systems and the LiDAR: the former acquires complete frames tens of times each second, the latter acquires a continuous stream of points evenly distributed on its 360° horizontal field of view (the longer the acquisition, the denser the resulting point cloud). The proposed solution was to treat the point cloud acquired by the LiDAR in a relatively small timeframe (~ 1 s) as a “Point cloud frame” that would then be merged with the closest stitched images in terms of acquisition timestamp. Multiple small merges are then stacked to create a denser coloured point cloud as the 3D Virtual View.

The software modules for the View Reconstruction were developed in a combination of Python and C++ and based on the OpenCV library to perform image manipulation.

6. Conclusions

This study proposed an approach for fusing information from multiple target identification systems, to improve situational awareness of an autonomous ship. The main objective of the system is to improve the accuracy and integrity of the information relating to the traffic situation with a view to motion replanning aimed at obstacle avoidance.

The systems involved in the fusion process are AIS, ARPA system, camera installed on a drone operating near the vessel, LiDAR system and Optical Systems installed on the mast of the unmanned ship. The intrinsic critical aspects of data fusion processes have been addressed, and particular attention has been paid to the aspect relating to measurement errors of the various systems involved, with the aim of improving the accuracy and reliability of the association processes of the target identified by the available systems.

The developed algorithms are part of a modular system that allows the management of data coming from the involved systems in an independent and optimized way. The system, thanks to hierarchical rules established based on the performance characteristics of the different systems, identifies the most reliable information for each target and proposes it as output.

The experimental results obtained on data acquired in marine scenarios are presented. One of the future tasks that we might carry out is to perform further analysis on other real data in different scenarios to verify the adequacy and the correct behaviour of the proposed approach.

Acknowledgements

This study is sponsored by the “MARIN – Monitoraggio Ambientale Remoto Integrato su piattaforma Navale” project (project Code:KATGSO3, found by “Programma operativo FESR 2014-2020 Obiettivo Con-vergenza” – Regolamento Regionale n. 17/2014 – Titolo II Capo 1 – “Aiuti ai programmi di investimento delle grandi imprese”), co-funded by Regione Puglia within the framework of “Contratti di Programma”. Project beneficiaries are Fincantieri NexTech S.p.A., RINA Consulting S.p.A. and Co.M.Media s.r.l..

References

- CHANG, L.; XIAOFEI, S. (2009), *Study of Data Fusion of AIS and Radar*, Int. Conf. Soft Computing and Pattern Recognition, Malacca, pp.674-677
- CUI, J.; NIU, J.; OUYANG Z.; HE, Y.; LIU, D. (2020), *ACSC: Automatic Calibration for Non-repetitive Scanning Solid-State LiDAR and Camera Systems*, <https://arxiv.org/pdf/2011.08516.pdf>
- GIOMPAPA, S.; FARINA, A.; FINI, G.; GRAZIANO, A.; CROCI, R.; DI STEFANO, R.D. (2008), *Study of the classification task into an integrated multisensor system for maritime border control*, IEEE
- HAGHBAYAN, M.-H; FARAHNAKIAN, F.; POIKONEN, J.; LAURINEN, M.; NEVALAINEN, P.; PLOSILA, J.; HEIKKONEN, J. (2018), *An Efficient Multisensor Fusion Approach for Object Detection in Maritime Environments*, 21st Int. Conf. Intelligent Transportation Systems, Maui
- HEYMANN, F.; NOACK, T.; BANYIS, P.; ENGLER, E. (2013), *Is ARPA Suitable for Automatic Assessment of AIS Targets?* 10.1201/b14961-40
- ITU-R M.1371-5 (02/2014) - *Technical characteristics for an automatic identification system using time division multiple access in the VHF maritime mobile frequency band*, https://www.itu.int/dms_pubrec/itu-r/rec/m/R-REC-M.1371-5-201402-I!!PDF-E.pdf
- KAZIMIERSKI, W. (2010), *Target association in the process of tracking radar and AIS integration*, Computer Science
- KAZIMIERSKI, W.; STATECZNY, A. (2013), *Fusion of data from AIS and tracking radar for the needs of ECDIS*, Signal Processing Symposium, SPS 2013, pp.1-6.
- KAZIMIERSKI, W.; STATECZNY, A. (2015), *Radar and Automatic Identification System Track Fusion in an Electronic Chart Display and Information System*, J. Navigation 68, pp.1141–1154
- KHALEGHI, B.; KHAMIS, A.; KARRAY, F.O. (2011), *Multisensor data fusion: A review of the state-of-the-art*, Information Fusion
- KIM, D.J.; AHN, K.S.; SHIM, S.B.; OH, K.S.; KIM, Y.S. (2015), *A study on the verification of collision avoidance support system in real voyages*, Int. Assoc. Institutes of Navigation World Congress (IAIN), Prague, pp.1-6
- LEE, W.J.; ROH, M.I.; LEE, H.W.; HA, J.S.; CHO, Y.M.; LEE, S.J.; SON, N.S. (2021), *Detection and tracking for the awareness of surroundings of a ship based on deep learning*, J. Computational Design and Engineering 8/5, pp.1407-1430
- LENART, A.A. (1989), *ARPA accuracy testing*, J. Navigation 42, pp.117-123

- NAKAMURA, E.F.; LOUREIRO A.A.F.; FRERY A.C. (2007), *Information Fusion for Wireless Sensor Networks: Methods, Models, and Classifications*, ACM Comput. Surv. 3, p. XXXIX
- PAIANO L.; CALABRESE F.; CATALDO M.; SEBASTIANI L.; LEONARDI N. (2022), *Ship Detection and Tracking based on a custom aerial Dataset*, 21st Int. Conf. on Image Analysis and Processing, Lecce
- QIN, X.; YAN, M.; ZHU, D. (2018), *Research on information fusion structure of radar and AIS*, Chinese Control and Decision Conf, Shenyang, pp.3316-3322
- SHIJUN, Y.; JINBIAO, C.; CHAOJIAN, S. (2009), *A Data Fusion Algorithm for Marine Radar Tracking*, 2009 WRI Global Congress on Intelligent Systems, Xiamen, pp.234-238
- STATECZNY, A.; LISAY, A. (2006), *Radar and AIS Data Fusion for the Needs of the Maritime Navigation*, pp.1-4, 10.1109/IRS.2006.4338063
- THOMBRE, S.; ZHAO, Z.; RAMN-SCHMIDT, H.; VALLET GARCIA, J.M.; MALKAMAKI, T.; NIKOLSKIY, S.; HAMMARBERG, T.; NUORTIE, H.; H. BHUIYAN, M.Z.; SARKKA, S.; LEHTOLA, V. (2022), *Sensors and AI Techniques for Situational Awareness in Autonomous Ships: A Review*, IEEE Trans. Intelligent Transportation Systems 23/1
- WANG, W.; SAKURADA, K.; KAWAGUCHI, N. (2017), *Reflectance Intensity Assisted Automatic and Accurate Extrinsic Calibration of 3D LiDAR and Panoramic Camera Using a Printed Chessboard*, Remote Sensing 9/8
- WAWRUCH, R. (2018), *Tests of the Accuracy of Indications by ARPA and AIS of the Opposite Vessel True Course, True Speed and CPA*, 19th Int. Radar Symp. (IRS), Bonn, pp.1-10

Standalone Intelligent General Arrangement Tool for Holistic Basic Design

Madalina Florean, CADMATIC, Groningen/The Netherlands, madalina.florean@cadmatic.com

Verónica Alonso de los Ríos, CADMATIC, Madrid/Spain, veronica.alonso@cadmatic.com

Juan Prieto, CADMATIC, Groningen/The Netherlands, juan.prieto@cadmatic.com

Ludmila Seppälä, CADMATIC, Turku/Finland, ludmila.seppala@cadmatic.com

Abstract

The paper describes a standalone intelligent and adaptive General Arrangement tool for holistic improvement of the basic design process in shipbuilding. The approach generates high topology 3D hull structure layouts based on 2D sketches. Furthermore, it uses an open standard format to interact with scantling tools that facilitates the hull definition process and approval. The tool connects hull shape optimization tools, hull design, and outfitting layout, leading to the overall optimized design of vessels. The key features of this new approach are 1) the option to define different design alternatives, specifically in the hull structure, allowing more flexibility in the designing process, 2) the feasibility to manage changes in a more straightforward manner, and 3) the interoperability to exchange data in standard formats to analyze the impact on other aspects of the basic design.

1. Introduction

The basic design stage is a relatively fast process but an essential part of the ship's lifecycle. It is not straightforward to measure the downstream impact of the quality of basic design. Errors in the detail engineering stage, costly changes in production, lack of efficiency, predictability, and profitability in operation are all aspects that are not easy to consider when an experienced naval architect defines the configuration of a new ship. These aspects have an immediate impact on the ship cost, performance, weight, stability, safety, and manufacturability. The challenge is how design authorities, regulatory bodies, shipyards, engineering companies, and suppliers can improve the simultaneous set of tasks and manage data in diverse software applications.

This paper describes an approach for a standalone software solution that generates the basic design documentation for any type of vessel in a multi-company and multi-software environment. The presumed situation reflects real-life cooperation between naval design and engineering companies, shipyards, shipowners, and regulatory bodies such as classification societies. Often, each participant uses different tools and software solutions focused on specific tasks and presents output documentation in an agreed format. This results in an enhanced need for an overall project follow-up process and impacts the overall shipbuilding management process, *Bruce (2021)*.

Critical aspects covered in this paper include the flexibility to define different design alternatives, specifically in the hull structure and in the main equipment layout configuration, the feasibility to manage simultaneous changes, and the interoperability to exchange data to analyze the impact on other design phases, while ensuring that the requirements and rules and regulations are met.

The general arrangement is the central document for the initial and basic design stages. It is critical to consider requirements for the ship performance specification, hull shape and deck arrangement, definition of fire zones, the layout of the main equipment and the preliminary arrangement of large piping, HVAC, and electrical connections, as well as accommodation areas. A typical general arrangement from a previous similar project is often used. This way, it is possible to get a head start and use it as a basis for further modification and adjustments.

The paper presents a solution that considers the importance of general arrangement preparation and a realistic scenario of fragmented stakeholders and software tools involved in different stages. In the suggested approach for the definition of general arrangements, an entire system of parameters that influences the main dimensions of the vessel can be defined and modified in the whole project, even

with external software. As a result, modifying any parameter changes every key construction in the ship and automatically adjusts the stiffening.

The weight estimation and repositioning of the heavy machinery are improved based on the mainframe distribution while all the conditions are automatically considered. The interaction with other scantling tools using a standard format improves a process that usually involves many changes. Finally, the basic design definition can be optimized by connecting the general arrangement tool with optimization tools that ensure the automatic iteration of hull structure parametric values.

All participants benefit in the short term and during the project life cycle via a project that is engineered better with a more holistic view.

2. Adaptive general arrangement

Traditionally ship design has been done according to Evans' design spiral, *Evans (1959)*. Processes do not always follow theory; there are many interdependencies, some stages start already while previous stages are still ongoing, and changes occur all the time. How can we be agile and adapt accordingly to shipbuilding design?

The General Arrangement preparation tool must be enhanced with functionality that ensures the fast definition of different ship design alternatives based on a high level of topology, parameters, and reference planes. The solution proposed in this article is innovative as it allows the definition of the layout in 3D, based on 2D sketches, with automatic stiffener positioning and pillar definition.

The proposed tool is currently implemented as a part of CADMATIC software applications. It can be linked with other external tools for scantling calculations via a standard format in a bidirectional way. Also, it is possible to connect it with optimization tools for design optimization based on parametric hull values to achieve a more qualified design in less time.

2.1. High level of topology in hull design

Ideally, the 3D model of a vessel is defined so that any changes to the main dimensions or any item in the model at any time triggers the system to update the whole model accordingly. This relieves specialists of the burden of manually changing and checking the model.

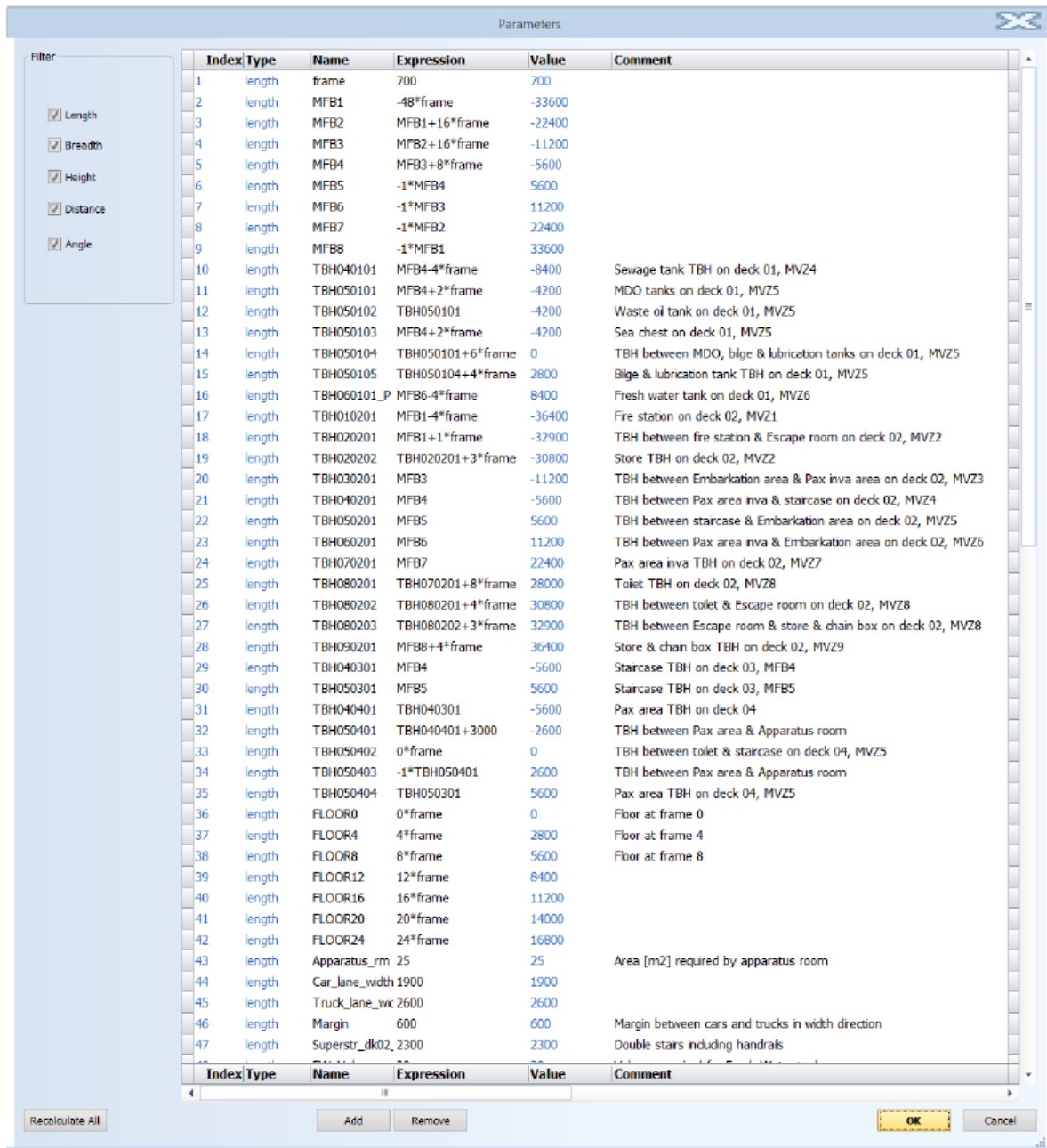
During the basic design stage, several dimensions influence the main dimensions of the vessel. They affect, for instance, the ship weight, stability, and damage characteristics. The ability to modify these dimensions at any time throughout the entire project ensures a high level of model malleability. Furthermore, automatic model recalculation gives the naval architect the workspace necessary to optimize the model iteratively.

A high level of topology must be provided to assist the naval architect in the creative process to ensure that the whole model is updated accordingly whenever the main dimensions change. This allows changes to be considered at any stage of the initial design. The required iterations involving assessment from different stakeholders and transformations are triggered by significant equipment adjustments by suppliers or similar parties.

The design solution proposed incorporates a solution with a high level of topology. The designer can create the complete hull structure with a flexible approach using parameters and reference planes in a topological model from hull surfaces imported from third-party software. The design process is thus not locked inside a specific design solution. It also provides shipyards with the flexibility to use design subcontractors of their choice, which allows the involvement of the best expertise in each area in the design project.

2.1.1. Parameters

The main dimensions can be represented using parameters in the Adaptive General Arrangement tool. These parameters are defined once conceptually and are used throughout the project. The parameters can be defined as fixed values, such as the main dimensions, or mathematical formulas. Other parameters can be used in the mathematical formulas, for instance, to define dimensions dependent on the main dimensions, creating an inter-dependency between these values. One can, for example, define a reference distance between decks dependent on the fixed value parameters for the deck positions. An example of parameter definition can be seen in Fig.1.



Index	Type	Name	Expression	Value	Comment
1	length	frame	700	700	
2	length	MFB1	-48*frame	-33600	
3	length	MFB2	MFB1+16*frame	-22400	
4	length	MFB3	MFB2+16*frame	-11200	
5	length	MFB4	MFB3+8*frame	-5600	
6	length	MFB5	-1*MFB4	5600	
7	length	MFB6	-1*MFB3	11200	
8	length	MFB7	-1*MFB2	22400	
9	length	MFB8	-1*MFB1	33600	
10	length	TBH040101	MFB4-4*frame	-8400	Sewage tank TBH on deck 01, MVZ4
11	length	TBH050101	MFB4+2*frame	-4200	MDO tanks on deck 01, MVZ5
12	length	TBH050102	TBH050101	-4200	Waste oil tank on deck 01, MVZ5
13	length	TBH050103	MFB4+2*frame	-4200	Sea chest on deck 01, MVZ5
14	length	TBH050104	TBH050101+6*frame	0	TBH between MDO, bilge & lubrication tanks on deck 01, MVZ5
15	length	TBH050105	TBH050104+4*frame	2800	Bilge & lubrication tank TBH on deck 01, MVZ5
16	length	TBH060101_P	MFB6-4*frame	8400	Fresh water tank on deck 01, MVZ6
17	length	TBH010201	MFB1-4*frame	-36400	Fire station on deck 02, MVZ1
18	length	TBH020201	MFB1+1*frame	-32900	TBH between fire station & Escape room on deck 02, MVZ2
19	length	TBH020202	TBH020201+3*frame	-30800	Store TBH on deck 02, MVZ2
20	length	TBH030201	MFB3	-11200	TBH between Embarkation area & Pax inva area on deck 02, MVZ3
21	length	TBH040201	MFB4	-5600	TBH between Pax area inva & staircase on deck 02, MVZ4
22	length	TBH050201	MFB5	5600	TBH between staircase & Embarkation area on deck 02, MVZ5
23	length	TBH060201	MFB6	11200	TBH between Pax area inva & Embarkation area on deck 02, MVZ6
24	length	TBH070201	MFB7	22400	Pax area inva TBH on deck 02, MVZ7
25	length	TBH080201	TBH070201+8*frame	28000	Toilet TBH on deck 02, MVZ8
26	length	TBH080202	TBH080201+4*frame	30800	TBH between toilet & Escape room on deck 02, MVZ8
27	length	TBH080203	TBH080202+3*frame	32900	TBH between Escape room & store & chain box on deck 02, MVZ8
28	length	TBH090201	MFB8+4*frame	36400	Store & chain box TBH on deck 02, MVZ9
29	length	TBH040301	MFB4	-5600	Staircase TBH on deck 03, MFB4
30	length	TBH050301	MFB5	5600	Staircase TBH on deck 03, MFB5
31	length	TBH040401	TBH040301	-5600	Pax area TBH on deck 04
32	length	TBH050401	TBH040401+3000	-2600	TBH between Pax area & Apparatus room
33	length	TBH050402	0*frame	0	TBH between toilet & staircase on deck 04, MVZ5
34	length	TBH050403	-1*TBH050401	2600	TBH between Pax area & Apparatus room
35	length	TBH050404	TBH050301	5600	Pax area TBH on deck 04, MVZ5
36	length	FLOOR0	0*frame	0	Floor at frame 0
37	length	FLOOR4	4*frame	2800	Floor at frame 4
38	length	FLOOR8	8*frame	5600	Floor at frame 8
39	length	FLOOR12	12*frame	8400	
40	length	FLOOR16	16*frame	11200	
41	length	FLOOR20	20*frame	14000	
42	length	FLOOR24	24*frame	16800	
43	length	Apparatus_rm	25	25	Area [m2] required by apparatus room
44	length	Car_lane_width	1900	1900	
45	length	Truck_lane_wic	2600	2600	
46	length	Margin	600	600	Margin between cars and trucks in width direction
47	length	Superstr_dk02	2300	2300	Double stairs including handrails

Fig.1: Example of parameters based on fixed values or other parameters via mathematical formulas

Therefore, all parameters are defined once and referenced throughout the entire project and can be modified at any point during the project's life and are automatically recalculated. Changing these parameters, results in a vessel with different characteristics.

2.1.2. Reference surfaces

Further refining of the theoretical model can be done by using the parameters to define conceptual surfaces with properties named reference surfaces. These surfaces are concealed flat surfaces with properties such as thickness and material type, which are used as the topological basis of the plate definition. The actual steel structures cross-refer the reference surfaces and are given the same properties. They are updated accordingly when changes are made to the linked reference surface.

Besides the high degree of malleability, detailed engineering in the following design stage is also much faster because the plane and the properties are predefined in the reference surface.

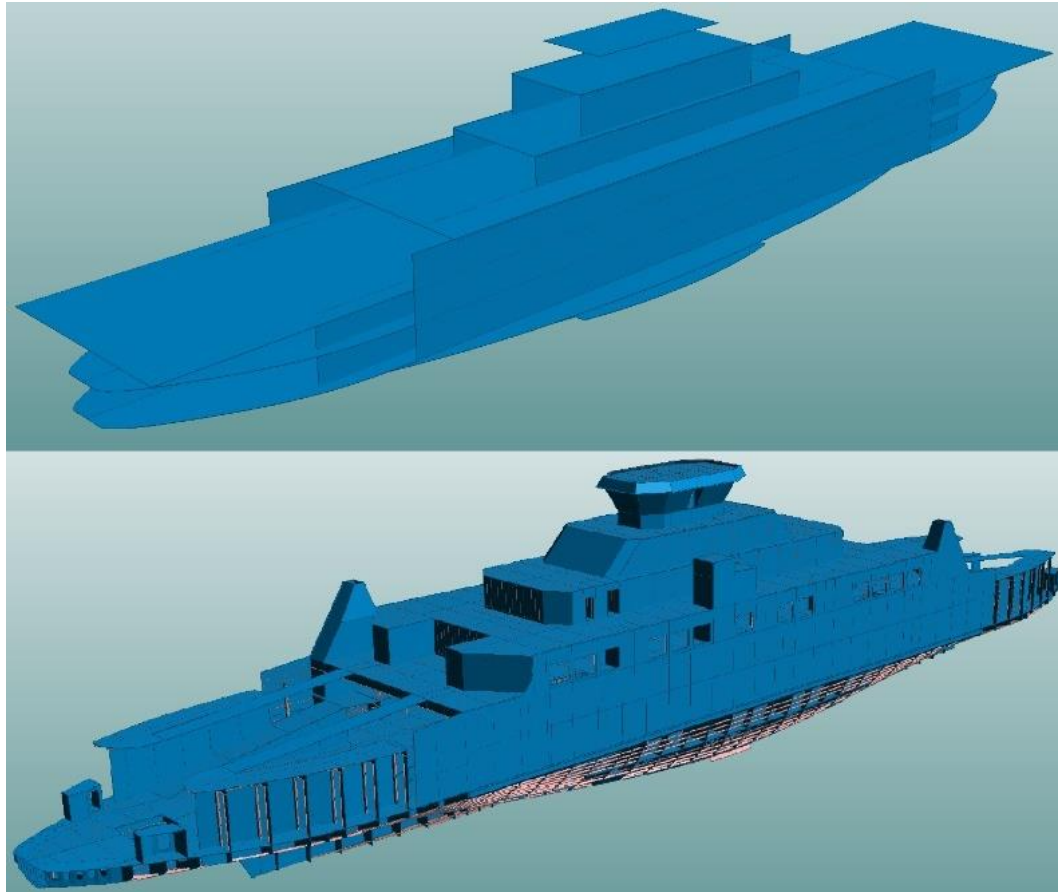


Fig.2: Reference surface model (top) and steel model (bottom) of a Ropax

Consequently, it is possible to define a whole topological system where altering a single parameter modifies every key construction in the ship, taking all the conditions into account.

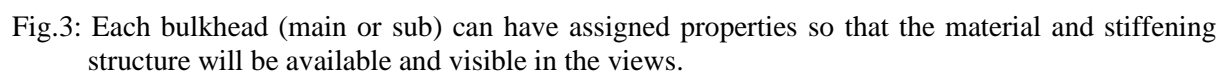
2.2. Layout definition

How should one sketch the main layout of a ship once the main dimensions of the vessel are defined? Ideally, the creative process of the naval architect is supported by the design system. Drawing the vessel's layout in the simplest and fastest way must be the focus of an intelligent general arrangement tool.

2.2.1. Bulkheads

To capture a complex vessel, naval architects break the design into pieces, designing on the floor and deck level. They try to create a sufficiently complete design quickly, so that all relevant requirements can be checked against the design. Designing in 2D is the best option when faced with tight deadlines.

New functionality for fast design lets naval architects promptly generate a ship layout by selecting multiple drawing lines or a fixed value with step sizes. Sub-bulkheads and longitudinal bulkheads can be created by converting drawn lines at the floor or deck level to steel plates; the system builds the 3D model automatically and searches for the 3D boundaries of the steel plates to be created, as is illustrated in Fig.3.



407

The generated 3D model is used directly in later stages of the design for complex changes. Because the 3D model is simultaneously created during sketching, there is a direct connection between the 3D model and the sectional views. When the 3D model is changed, these views are automatically updated, thereby saving time and avoiding errors.

2.2.2. Profiles as properties

After the main layout has been defined, the naval architect can speed up the design by stiffening the designed structure with automatic stiffening functions. The profiles as properties functionality enables the maritime architect to strengthen the bulkheads automatically in one go. The software tool automatically places stiffeners on each grid position on the selected bulkheads. When a stiffened bulkhead size changes, the system automatically adds or removes stiffeners to it depending on the new size of the bulkhead.

Besides the obvious speed gain by automatically stiffening the bulkheads, the design is further sped up due to faster model calculation, since these automatic stiffeners are considered one 3D model, not separate ones. After the general arrangement has been approved, the stiffeners can be converted into regular stiffeners for production.

2.2.3. Pillars

A naval architect can define pillars in a matrix, and the system automatically determines the end relations. For example, the maritime architect can establish a series of pillars in length and a series of pillars in breadth on a deck level all in one go by providing the direction and distance. The system automatically searches for the end limitations, like the deck below. When a girder is present, the pillar is automatically connected to it, Fig.4.

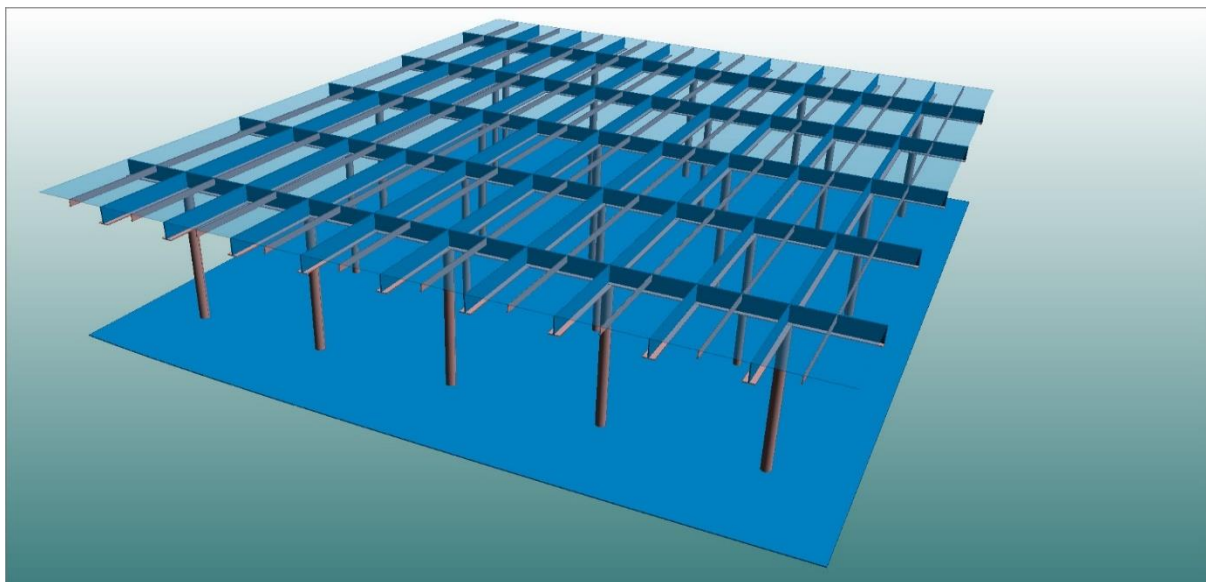


Fig.4: Example of pillars in a matrix with automatic connections to girders and the deck below

2.3. Weight estimation

Commonly, the steel weight in ship design software is based on adding together the data of all parts. At the initial and basic design stage, however, the naval architect creates a minimalistic design in order to deliver the proposed solution in time. The weight of the vessel is a major factor in optimizing the design. As a consequence, an intelligent general arrangement tool should assist the naval architect with a solution to estimate the weight of the vessel even if the design is not yet complete. This research paper describes a novel way to estimate the weight on the ship based on the main layout.

The midship section and the main layout are mandatory to define the basic design and general arrangement. With this information, the scantlings are determined so that the ship follows the rules. The solution for weight calculation has been extended not only to do the addition, but also to estimate the weight and center of gravity (COG) of the ship based on “reference” frames. After the naval architect has designed the mainframe, a parallel mid-ship section can be created as a fully loaded 3D space.

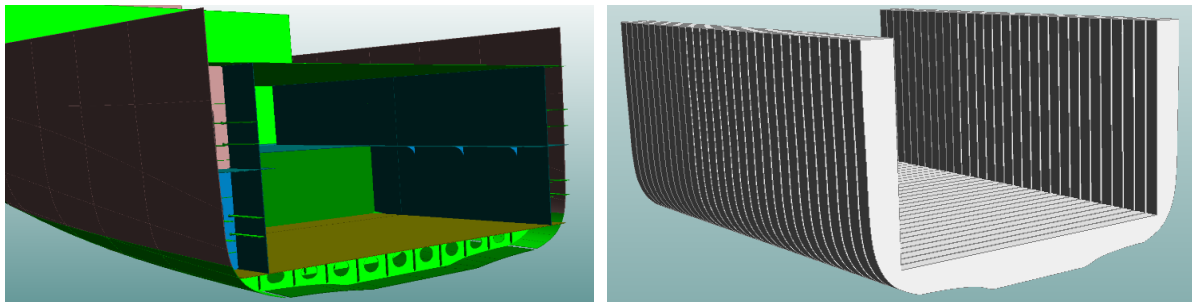


Fig.5: Example of a mid-ship section (left) and the corresponding fully loaded 3D space (right)

It is possible to calculate the actual steel weight and COG of the mid-ship section, the volume, and the weight of the fully loaded space, Fig.6. Based on this information, it is possible to extract the ship shape's weight per volume ratio [kg/m^3]. This weight is used for other frames similar to the mid-ship.

Sets/Boxes	Based On	Est. Weight	Weight	COG Length	COG Trans...	COG Vertical	Surface	Min. Length	Max. Length	Min. Breadth	Max.
29	29	4811	4811	18451	1965	5181	118	FR28.5	FR29+350	-8016.8	8016
30	30	5137	5137	19151	2152	5190	126	FR29+350	FR30+350	-8016.8	8016
31	31	4985	4985	19850	2072	5049	122	FR30+350	FR31+350	-8016.8	8016
32	32	9180	9180	20553	2467	4217	209	FR31+350	FR32+350	-8016.8	8016
33	32	9345	4670	21253	2542	4169	118	FR32+350	FR33+350	-8016.8	8016
34	32	9515	4169	21953	2612	4121	108	FR33+350	FR34+350	-8016.8	8016
35	32	9993	4144	22653	2677	3986	108	FR34+350	FR35+350	-8016.8	8016
36	36	11289	11289	23360	300	3681	268	FR35+350	FR36+350	-8016.8	8016
37	37	4267	4267	24050	797	4058	105	FR36+350	FR37+350	-8016.8	8016
Total		68523	52653	21379	1357	4387	1282				

Fig.6: Example of weight and COG estimation based on mid-ship reference frames

The tool is not limited to the mid-ship section. Several reference frames can be utilized concurrently for weight estimation to achieve a more accurate estimation. The more reference frames are used, the better the results. An analysis performed on the accuracy of the results showed that the estimates provided by the tool are within a 2% difference margin compared to the actual weight of benchmark vessels. This allows us to conclude that the weight estimation method can be safely used for quick weight estimation.

2.4. Scantling analysis

To create sound and consistent structures to ensure safety and economic viability, the design must be checked against well-known rules and regulations. Several classification societies can calculate the feasibility of the design in terms of scantling choices, plate and panel thickness, and the spacing of internal frames, bulkheads, and longitudinal stringers. The solution proposed is linked to different unidirectional or bidirectional scantling tools, which reduces the time needed for the iterative early design process.

2.4.1. Cross-section approach

Traditionally, scantling calculations are done based on data from frame views. The primary data passed on to the scantling calculation software contains the description of the inner construction of the vessel and its variation along with the ship, translated to the calculator's specific protocol. A schematic of the proposed hull structure tool and the scantling analysis tool is shown in Fig.7.

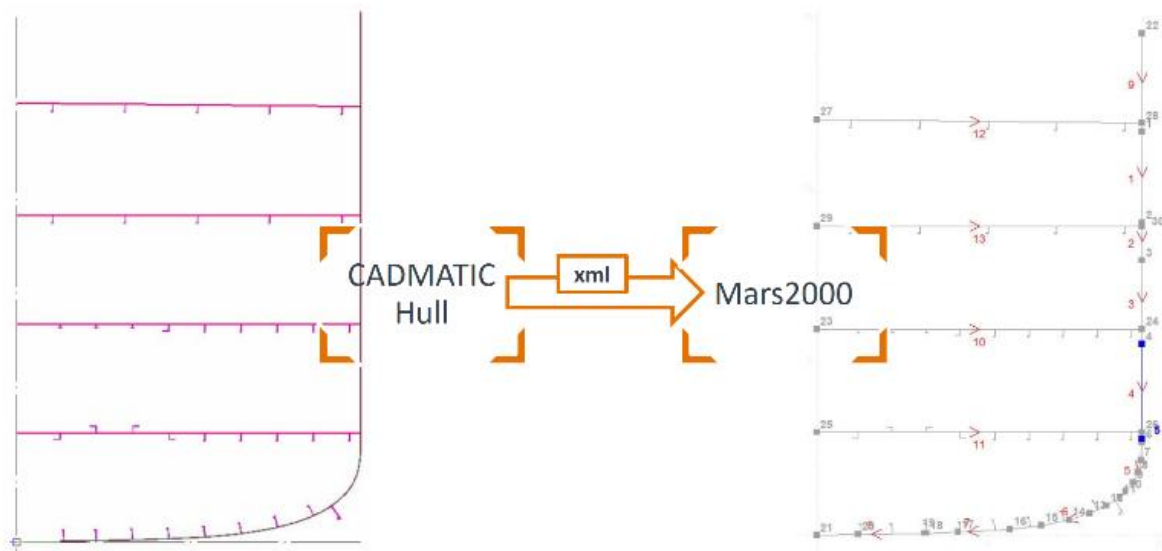


Fig.7: Schematic of hull design software and scantling analysis tool interface

Data exported from the design system to the frame-based scantling calculator consists of basic ship information, such as the name, class notation, main dimensions, material, and relevant ship drafts. In addition, the data includes bending moments and shear force distributions. The data transfer is file-based, for example, in XML format and other standard formats such as OCX that are covered under 3D scantling calculation below. Research has been conducted with Bureau Veritas's Mars2000 software, an example of a frame-based rules calculator tool. The data from the proposed CAD system is exported in an XML file, which is opened in Mars2000. The cross-section appears in the project window. Primary ship data can be manually modified, and the transferred values of bending moments and materials can also be corrected, if needed. In Mars2000, the user can adjust the plates and stiffeners of the cross-section of the resulting midship section that does not comply with classification rules. Possible changes in plate thicknesses and stiffener profiles are then shown to the user, who can modify the model in the CAD system accordingly. The same process interface can be used between the CAD and similar scantling tools.

2.4.2. 3D scantling calculation

To enhance the classification process, a switch from a 2D drawing-based to 3D model-based process has been researched and defined in the Open Class 3D Model Exchange (OCX), Fig.8. As described by *Astrup (2019)*, OCX specifically addresses the needs of classification societies and shipbuilders for fully digital information exchange.

This OCX format is intended to become an open industry standard for exchanging design information between designers/yards and classification societies. In addition to optimizing the calculation process by directly interfacing with the 3D design model, all parties involved in the vessel design have direct access to the model by directly interfacing with the 3D design model. This ensures transparency and reduces the amount of work by eliminating unnecessary drawings. Having direct access to the 3D model also improves the understanding of the design.

The application of such a universal format goes beyond 3D scantling calculations. We are studying the possibility of using the model in the OCX format to perform FEM calculations. Presently, the naval architect needs to prepare a meshed model of the vessel to study the steel stresses. The Adaptive General Arrangement tool eliminates this cumbersome step by expanding the standard OCXformat for FEM analysis. Preliminary results have confirmed great potential in directly sharing the vessel 3D model via the OCX format with the FEM software, eliminating the need of meshing the model inside the CAD software.

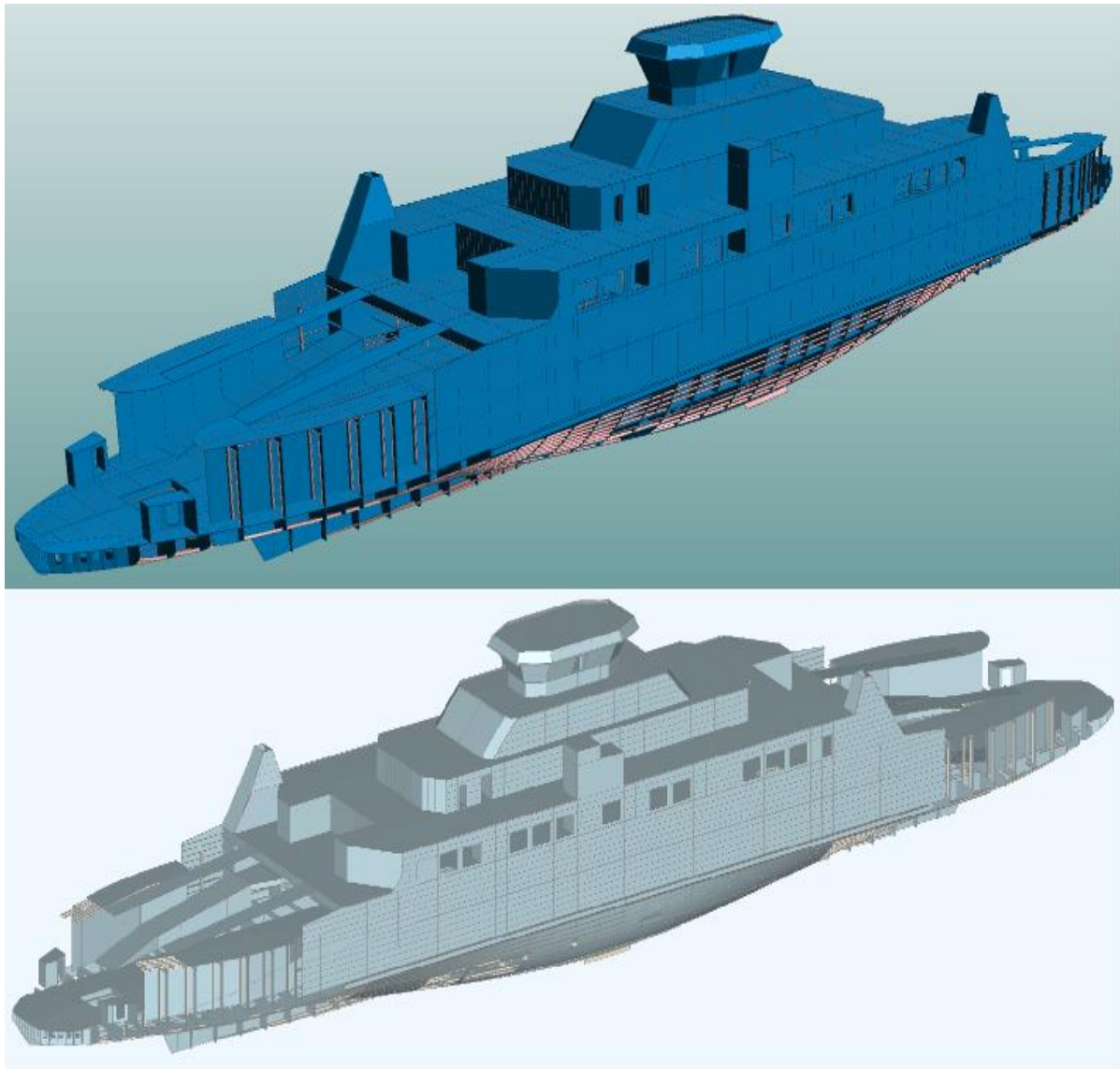


Fig.8: Ropax CAD model (top) imported in classification software via OCX format for 3D scantling calculations (bottom)

The proposed adaptative general arrangement software ensures access to the 3D model and can read back information. With the traditional method, the design must begin with structural design software, such as the design tool mentioned, after which the model is exported to the approval software. With this bidirectional solution, the procedure could start in the scantling software and continue to the structural design software.

Furthermore, when the classification society requires changes to the model, these changes must be made manually in traditional approaches. With a bidirectional connection, such modifications can be automatically done in the adaptative design tool by importing 3D models from an OCX file.

The process described improves the drawingless strategy in shipbuilding. *Seppälä (2020)* proposed that there are possible scenarios for drawingless production in shipbuilding. Considering the primary driver of intelligent IT, drawings are already being gradually substituted with 3D viewers and with direct data transfer to production or manufacturing control systems. CAD plays a vital role in the substitution process by providing interactivity with data and faster access to it within change management. Design application functionality will impact how regulatory bodies classify vessels, and it would represent a significant change if drawings were eliminated.

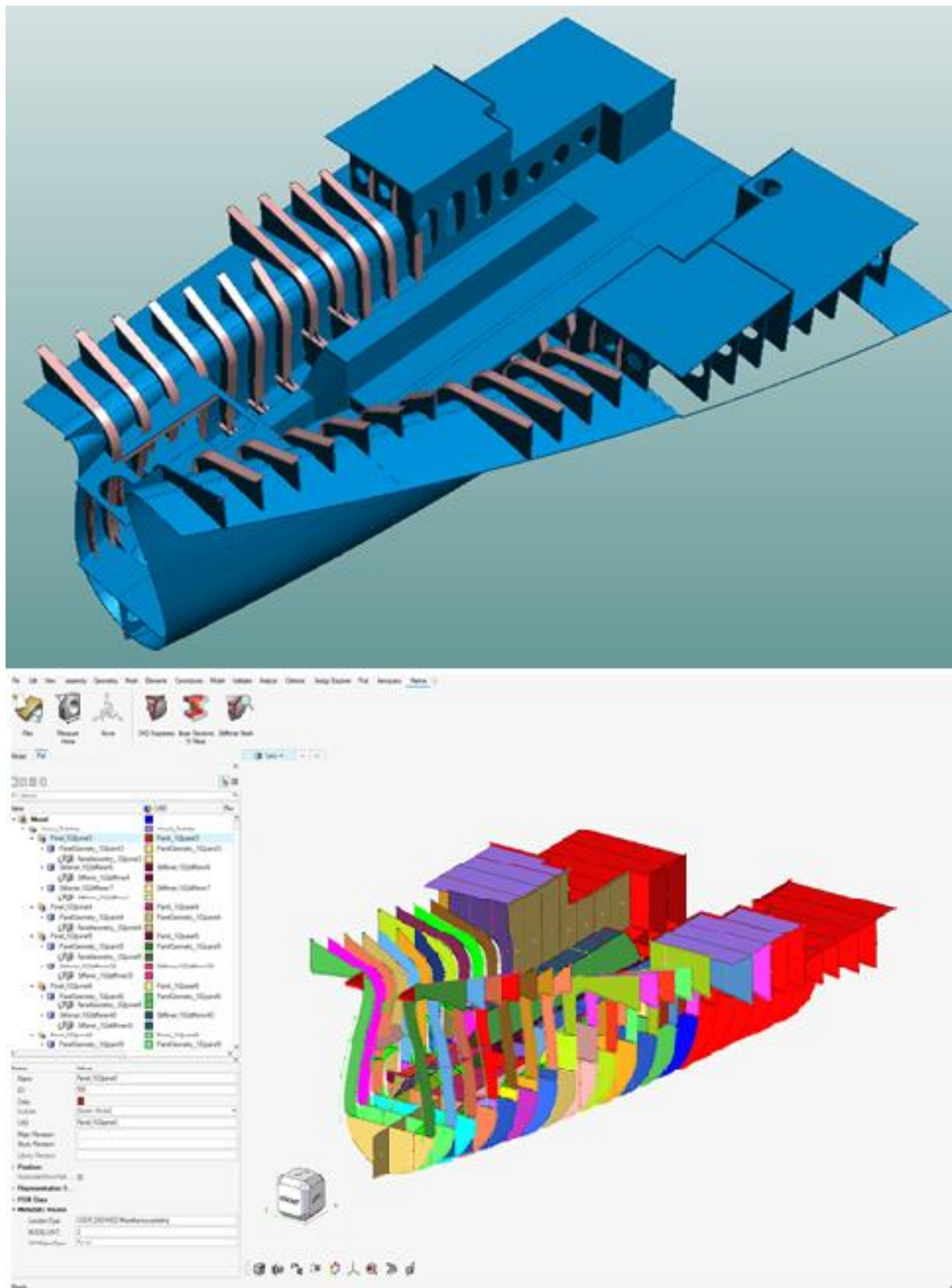


Fig.9: CAD vessel section (top) imported via OCX in FEM software (bottom)

2.5. Layout of equipment in general arrangement

During the basic design phase, heavy machinery layout significantly influences the ship's weight. Therefore, adaptability to new designs must be extended to outfitting elements. Outfitting elements,

such as power, propulsion, and ship system equipment, platforms, and other outfitting steel constructions are usually added in the outfitting module. The solution proposed integrates the design disciplines so that the hull application has access to these elements via an equipment library which provides access to the outfitting database. This allows the model to be equipped with components from libraries that can be reused whenever necessary.

With the elaborated “Equipment Layout” function in the hull application tool, the user can insert heavy machinery, for instance, by opening the component library and selecting equipment. The equipment is displayed in the hull view and can be positioned as required. Outfitting and piping disciplines can access the same model, making adjustments or changes according to machinery requirements.

Since topology is the main factor that speeds up and automates steel creation, this property is also added to the equipment via the “Connect to view plane” function. This ensures that the circle of automatic topological behavior triggered by the parameters is applied to close the loop. The equipment is connected to the level view (i.e., level drawing) in which the equipment is added to the equipment data. Level views are related to reference planes and are thus updated when the reference surface changes, thereby updating the equipment.

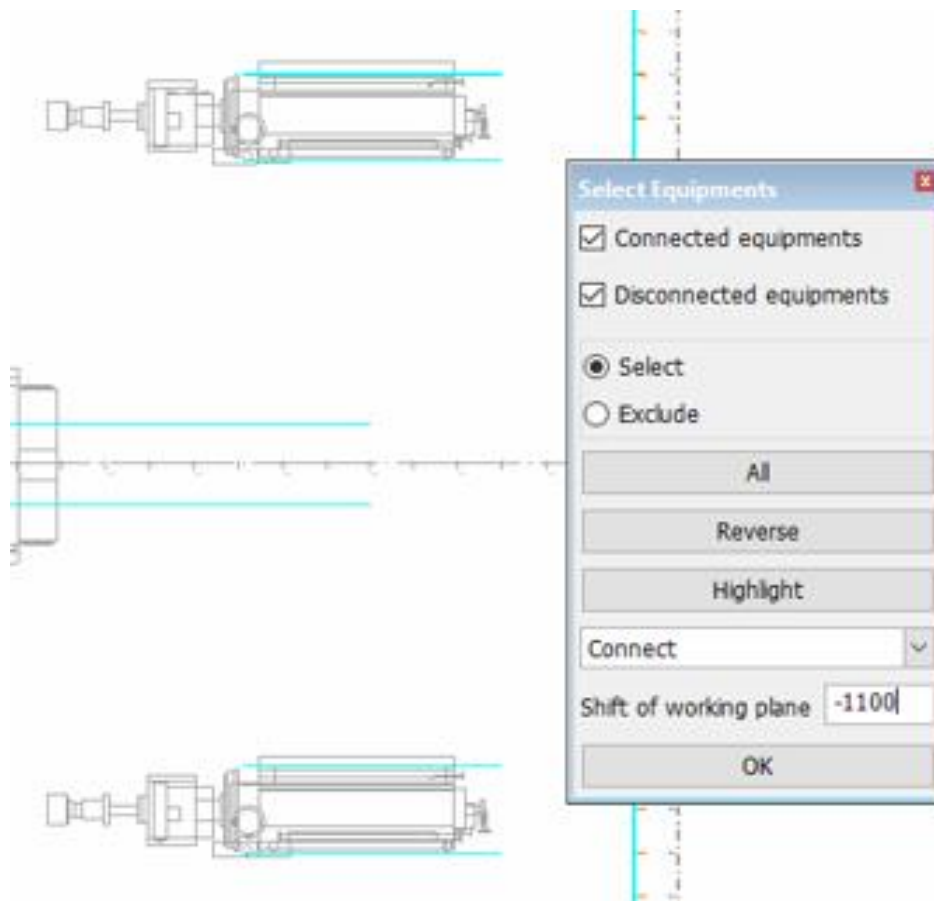


Fig.10: Example of equipment layout topologically connected with hull structures

3. Optimization

The design of a ship is complex, with several variables that need to be considered. In addition to traditional design factors such as efficiency, cost, ease of production, a sound and safe structure with a long life cycle, new variables are constantly introduced to achieve updated goals. Currently, an important goal is the achievement of green ships as an environmental responsibility and a sound economic investment. This requires several factors to be considered, such as low emissions, eco-friendly hull design, zero discharge, or a low acoustic signature.

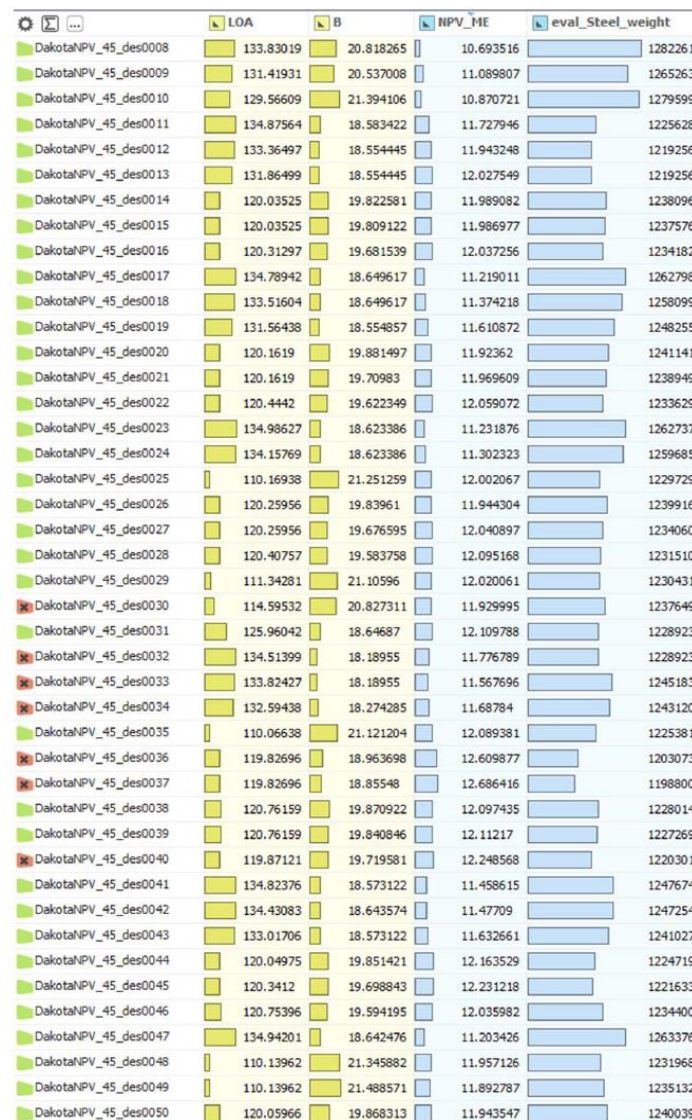
Several methods to optimize ship design have been introduced, such as optimizing parametric models, simulations, or surrogates. The adaptative general arrangement tool is linked with optimization tools. A high level of integration between the design system and optimization system facilitates the iterative early design work by coupling the design of a skilled naval architect with an optimization package that carries out the optimization in batch-mode without manual intervention.

3.1. Shape optimization

Shape optimization is a factor when optimizing a vessel due to its significant impact on hydrodynamic performance and structural behavior. Changes in the shape lead to changes in length and beam, which influence the weight and resistance.

3.2. Example of CAESES

Parameter-based modelling is not confined to the CAD model but also extended to geometry modelling. Therefore, the vessel's shape is represented by a set of variables that trigger changes in the shape when the variables are modified. Thus, due to the possibility of parametrizing both the shape and the model, one can encapsulate the most critical constraints and pass on the corresponding parameters to optimization algorithms to optimize the whole ship design.



	LOA	B	NPV_ME	eval_Steel_weight
DakotaNPV_45_des0008	133.83019	20.818265	10.693516	1282261
DakotaNPV_45_des0009	131.41931	20.537008	11.089807	1265263
DakotaNPV_45_des0010	129.56609	21.394106	10.870721	1279599
DakotaNPV_45_des0011	134.87564	18.583422	11.727946	1225628
DakotaNPV_45_des0012	133.36497	18.554445	11.943248	1219256
DakotaNPV_45_des0013	131.86499	18.554445	12.027549	1219256
DakotaNPV_45_des0014	120.03525	19.822581	11.989082	1238096
DakotaNPV_45_des0015	120.03525	19.809122	11.986977	1237576
DakotaNPV_45_des0016	120.31297	19.681539	12.037256	1234182
DakotaNPV_45_des0017	134.78942	18.649617	11.219011	1262798
DakotaNPV_45_des0018	133.51604	18.649617	11.374218	1258099
DakotaNPV_45_des0019	131.56438	18.554857	11.610872	1248255
DakotaNPV_45_des0020	120.1619	19.881497	11.92362	1241141
DakotaNPV_45_des0021	120.1619	19.70983	11.969609	1238949
DakotaNPV_45_des0022	120.4442	19.622349	12.059072	1233629
DakotaNPV_45_des0023	134.98627	18.623386	11.231876	1262737
DakotaNPV_45_des0024	134.15769	18.623386	11.302323	1259685
DakotaNPV_45_des0025	110.16938	21.251259	12.002067	1229729
DakotaNPV_45_des0026	120.25956	19.83961	11.944304	1239916
DakotaNPV_45_des0027	120.25956	19.676595	12.040897	1234060
DakotaNPV_45_des0028	120.40757	19.583758	12.095168	1231510
DakotaNPV_45_des0029	111.34281	21.10596	12.020061	1230431
DakotaNPV_45_des0030	114.59532	20.827311	11.929995	1237649
DakotaNPV_45_des0031	125.96042	18.64687	12.109788	1228923
DakotaNPV_45_des0032	134.51399	18.18955	11.776789	1228923
DakotaNPV_45_des0033	133.82427	18.18955	11.567696	1245183
DakotaNPV_45_des0034	132.59438	18.274285	11.68784	1243120
DakotaNPV_45_des0035	110.06638	21.121204	12.089381	1225381
DakotaNPV_45_des0036	119.82696	18.963698	12.609877	1203073
DakotaNPV_45_des0037	119.82696	18.85548	12.686416	1198800
DakotaNPV_45_des0038	120.76159	19.870922	12.097435	1228014
DakotaNPV_45_des0039	120.76159	19.840846	12.11217	1227269
DakotaNPV_45_des0040	119.87121	19.719581	12.248568	1220301
DakotaNPV_45_des0041	134.82376	18.573122	11.458615	1247674
DakotaNPV_45_des0042	134.43083	18.643574	11.47709	1247254
DakotaNPV_45_des0043	133.01706	18.573122	11.632661	1241027
DakotaNPV_45_des0044	120.04975	19.851421	12.163529	1224719
DakotaNPV_45_des0045	120.3412	19.698843	12.231218	1221633
DakotaNPV_45_des0046	120.75396	19.594195	12.035982	1234400
DakotaNPV_45_des0047	134.94201	18.642476	11.203426	1263376
DakotaNPV_45_des0048	110.13962	21.345882	11.957126	1231968
DakotaNPV_45_des0049	110.13962	21.488571	11.892787	1235132
DakotaNPV_45_des0050	120.05966	19.868313	11.943547	1240039

Fig.11: Example of optimization using the Dakota algorithm

The intelligent hull general arrangement tool can be directly connected to any optimization software. CAESES software has conducted research that provides a new hull shape for every optimization variant, *Harries and Abt (2019)*. In addition to the unique shape, the primary dimension parameters such as length and beam are updated, and the CAD system recalculates the 3D model. It is subsequently checked whether the scantlings are acceptable, and a new weight is provided based on the updated 3D model. The optimization software then calculates the resistance of the current hull form and the CAPEX and OPEX. The cycle continues until the optimization software finds the optimal parameters corresponding to an optimal vessel design, *Harries et al. (2019)*.

4. Conclusions

The main conclusion of this research is that there is a possibility for ship basic design optimization with a holistic approach using an adaptative general arrangement tool and integrating different tools and processes (design applications with calculation, scantling, and optimization tools). Using an adaptative available arrangement tool, a naval architect can generate various design alternatives in less time. The process is unidirectionally or bidirectionally integrated with scantlings and approval via standard formats accepted in the shipbuilding industry.

The adaptative intelligent general arrangement tool improves the design layout with the definition of the hull structure based on high topology, parametric values, and reference planes. This allows the brief description and propagation of changes, which are very common during early design. The designer leverages the generation of the 3D layout from a 2D drawing sketch while the boundaries of the hull structure elements are automatically calculated. Stiffeners are added to the model automatically as well. Changes are propagated easily, with the ability to analyze their impact on weight estimation. The iterative approval process improves the ability to interchange 3D data with scantling tools via a standard format. Finally, the adaptative general arrangement tool is linked with optimization software for simulation-driven optimization based on parametric values. Further developments and new processes will ensure a fully drawingless approval process.

Further research should include aspects of equipment layout and topology of the 3D arrangement of equipment and the accommodation of hull structure and other interoperability questions for independent design evaluation.

References

- ASTRUP, O.C. (2019), *APPROVED redraws requirements for class verification*, https://www.rina.org.uk/APPROVED_redraws_requirements_for_class_verification.html
- BRUCE, G. (2021), *Shipbuilding Management*, Springer Singapore, 2021
- EVANS, J.H. (1959), *Basic Design Concepts*, J. American Society for Naval Eng. 71/4, pp.671-678
- HARRIES, S.; ABT, C. (2019), *CAESES – The HOLISHIP Platform for Process Integration and Design Optimization*; A Holistic Approach to Ship Design Vol. 1, Springer, pp.247-293
- HARRIES, S.; DAFERMOS, G.; KANELLOPOULOU, A.; FLOREAN, M.; GATCHELL, S., KAHVA, E.; MACEDO, P. (2019), *Approach to Holistic Ship Design – Methods and Examples*, 18th COMPIT Conf., Tullamore, pp.224-245, http://data.hiper-conf.info/compit2019_tullamore.pdf
- SEPPÄLÄ, L. (2019), *Drawingless production in digital and data-driven shipbuilding*, CADMATIC, <https://www.cadmatic.com/en/resources/articles/drawingless-production-in-digital-and-data-driven-shipbuilding/>

Open and Collaborative Ship Design

Henrique Gaspar, Norwegian Univ. of Science and Technology (NTNU), Ålesund/Norway,
henrique.gaspar@ntnu.no

Abstract

Openness and collaboration are words rarely associated to the maritime area, especially in the narrow, competitive, traditional and averse-to-drastic-changes-world of ship design. It is understandable (even though unfounded) the fear that, by making knowledge available one can lose its position in the market. It is my belief, however, that such fears underestimate drastically the complexity and difficulty of the ship design task, acting as key factors that constrain and undermine the opportunity for innovation and profit in our beloved marine design field. This year's COMPIT contribution is an argumentative sparkle aimed at the ship design community towards facilitating the availability of processed marine design knowledge (open), as well as developing this knowledge in a way that facilitate peers to re-use, contribute, and develop further (collaborative). The paper will be divided in an introduction to the concept of openness and collaboration for the maritime community, followed by a discussion on the fears and obstacles that openness face. A description for a basic toolbox for collaboration is done, commenting on shared folders, versioning systems, and library/catalogue concept. Later, it is presented some examples of open software applied for maritime engineering as well a selected successful case, the simulation of a ship manoeuvring in the fjords, where collaboration and openness were essential. The paper concludes with a call for open and collaborative approach in the academia, software firms, design offices and shipyards.

1. Openness and Collaboration

Rather than a purely traditional article, what is here attempted is an essay towards openness and collaboration in the maritime engineering field. The ideas discussed are based (and biased) on my experience developing and working with open software for ship design in the last decade. Emphasis is given to the rather informal 1st Symposium in Open and Collaborative Ship Design, Fig.1, organized in 2019 at University College London (UCL, UK). The initiative was support by myself (NTNU), Prof. Giles Thomas (UCL) and Prof. Gabriel Weymouth (University of Southampton). Many of the ideas commented on this paper were discussed orally in that symposium, and here presented with almost three years delay, <https://open.ntnu.co/>.



Fig.1: Poster for the 1st Symposium on Open and Collaborative Ship Design, <https://open.ntnu.co/>

The concept of open and collaboration is here associated to the broad sense of the open source / software philosophy, that is, that the core of the data, information, knowledge, and wisdom (DIKW) is available to be accessed, modified, and re-used by a community. The data and methods there are therefore transparent and can be tested and scrutinized. Comparing to the general scientific method of sharing knowledge, open and collaborative means, for instance, to use the current digital toolbox (e.g. online servers, databases) to provide quickly access to the information. As defended earlier in COMPIT,

Gaspar (2017,2018a), computer science seems to have understood the lack of compatibility problem among data well, and the high pace development of internet tools just accelerated the need for common standards and practices, with a pressure to move faster without sacrificing reliability.

In the rest of this essay, thus, open is understood as a piece of DIKW that the original code/algorithm/formula/process/method is made available and may be redistributed and modified. Collaborative is understood as the process of developing this piece in a way that facilitate peers to re-use, contribute, and develop further. Pretty much the idea of an academia, but for everyone and here applied to the activities in the ship design value chain, Fig.2.

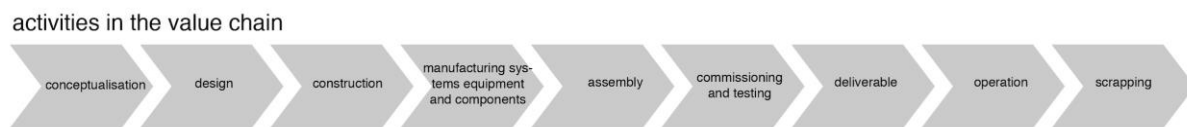


Fig.2: Activities in the ship design value chain, from conceptualization to scrapping

This essay is structured by compiling a list of fears and obstacles that affects openness and collaboration in the maritime sector, followed by a suggested toolbox for collaboration (shared folders, versioning systems, and a library of components). Later, a short list of open initiatives in maritime engineering is described, closing the paper with a simulation of a ship sailing in the fjords, joint work between Vessel.JS, <https://vesseljs.org/>, and OpenBridge, <http://www.openbridge.no/> initiatives, concluding with a call for more open and collaborative methods.

2. Fears and Obstacles for Openness in the Ship Design Community

2.1. Compiling Fears in a Traditional Industry

Openness and collaboration are words rarely associated to the maritime area, especially in the narrow, competitive, traditional and averse-to-drastic-changes-world of ship design. The ship design data, the way it is today, is not meant to be reused, *Chaves et al. (2018)*, *Erikstad (2009)*. Traditionally, vessels are quite unique, and shipyards try their most to attend every requirement imposed by shipowners, preventing the industry to develop itself towards standardization, modularization and reuse, as other industries (e.g., automotive) had done decades ago. The fear is understandable (even though unfounded) that, by making knowledge available, one can lose its position in the market. It is my belief, however, that such fears underestimate drastically the complexity and difficulty of the ship design task, acting as key factors that constrain and undermine the opportunity for innovation in the marine design field.

Over the years, when suggesting to my peers that their work should be made openly available, many were the arguments against, for instance ‘And if someone copies it?’ or ‘It took me a lot of time to do it, I will not provide it for free!’, and also ‘But this code/method/procedure is not ready yet!’ What at the end leads to high-quality work lost, rarely re-used, given the difficulty to access and modify its content. Worse, much of this work is publicly funded, and should be available outside the restricted article format.

Moreover, when we have understood how complex the ship design value chain is and all its tasks, is this fear really appropriate? Is one piece of information so valuable that sharing it means losing money, advantage or shows weakness? Is not the know-how strongly connected to experience, constructing and operating the ship efficiently rather than keeping information hidden?

These conversations over the years have led me to classify the fears into three categories, namely: a) copying intellectual property; b) the high cost of acquiring valuable data; and c) reputation damage (weakness) on showing non-rational decisions. The following subsections discuss these fears, as well as some obstacles intrinsic to the ship design activity.

2.2. Fear of Copying Intellectual Property

Probably the most common fear lies on the idea that sharing information means to share intellectual property that can be copied and re-used by a competitor, or that the client can use without paying for it. I can see how this can be true in some cases, for instance when preparing a tender package to get a contract, as the time is short and any information about an advantage seems to be a factor in favour of secrecy. In the academic side, this can also be observed when a key part of data is missing to solve a known problem and sharing means not receiving the credits. On the software side, sharing a program or algorithm means have a potential client to just not paying, as if one can get for free, then why to pay? At the end of the spectrum, the pessimistic view about this fear means a company that is not able to sell ship, a researcher that is not able to publish the new idea or a software company that will not get paid for someone using their software. Security issues are also raised, as weakness of an open code/design could be exploited in the wrong way.

To tackle this fear, we need to acknowledge that the definition of ‘open’ previously mentioned is not necessarily synonymous to ‘free’, neither that the DIKW means the totality of the data. In other words, not every data or information should be shared for free all the time. I can see that this is an approach in some software development, especially with the multitude of different software licenses, <https://opensource.org/licenses>, and that some are very open. This extreme is not advocated here.

First, open standard of data seems to benefit us all. It means that software can communicate and contribute. Making a tool with open inputs and outputs, well documented, with modern application programming interface (API) principles is a great step towards keeping the intellectual property while sharing data. Such type of openness also speeds up development, as many standards are already maintained by a community, and the workload is shared. Regarding algorithms and libraries, there are already plenty of good libraries that also saves time for many developers, and contributing one piece on this does not mean giving all the IP of a software for free but, again, sharing the burden of maintaining a common used part of your tool. On the safety aspect, openness seems to be only way to provide great security, as open standards are the ones most secure, given that weakness are rapidly found and fixed by the community. No wonder 71.5% of all servers (and +95% of the top servers) in the world run Linux, *Ackermann and Greenstein (2018)*.

Studies on the economic benefits of opening suggests that an open model may be profitable as well as discussed in *Casadesus-Masanell and Llanes (2010)*. They present a profit-maximizing model for firms that sells software and complementary goods (such as training or support services) and have the option whether to open all or part of its software and the price at which to sell its product. Software in their models is composed of two modules: a base program (the core code) and a set of extensions (the edge code). The base may be used without the extensions. The extensions, on the other hand, are valueless unless used in conjunction with a base, i.e. the base is a one-way essential complement to the extensions, and firms may open the base, the extensions, or both. They also conclude that there may be no trade-off between value creation and value capture when comparing business models with different degrees of openness.

2.3. Fear of Sharing Valuable Data

The second fear is that the information that one already has was acquired under a cost, and sharing it freely means to give for free something that was paid for. A database of ships or AIS information, for instance, we do know that it requires either time or money to get this data, to clean, filter and apply to a design project. And design after design we ended up doing the same process. The same applies for structural and hydrodynamic analysis made during conceptual design: not much information from previous analyses are used in new one, it is almost as the process starts from scratch again.

It seems that this type of data is expensive because it is time consuming to gather and maintain, as databases need to be paid for, cleaned, checked. The contradiction lies in the fact that, instead of every company have their own database, it makes more sense to have an online database, where all users can

access, feed, correct and edit the data. Some sort of Wikipedia of relevant maritime data, such as regressions, formulas and rules. Take the classical exercise of requirements elucidation and analyses of similar vessels. The steps in looking for what is already available in the market is somehow universal to all competitors. A common base to start from seems, in the long term, a win-win situation, as the additional cost for maintaining and feeding these large databases is shared among all users. An example of a library/catalogue of designs and its components is later described in Section 3.3.

Specially to the academic environment, the concept of open science is paramount. Open science adheres to the scientific ideals of knowledge as a public good, independence of research, universalism, and systematic critical appraisal of sources. Research data which is public funded should be shared and reused more widely. Public funded refers to: (i) data collected or generated for use for or as a result of publicly funded research, and (ii) data underpinning publications that are the result of publicly funded research, regardless of the source of the data, *Norwegian Ministry of Education and Research (2018)*. NTNU has a quite comprehensive policy for open science, where the reading is suggested, <https://www.ntnu.edu/policy-for-open-science>.

2.3. Fear of Acknowledge Uncertain / Non-Rational Choices

The third aspect lies in the high uncertainty of the ship design task, and the real fact that many important decisions, when not taken forced by rules and regulations, are taking by experienced and educated guesses, inspiration, gut feeling. Therefore, to share data and information that some of the decisions were made stylistic rather than purely scientific may seem like weakness in the quality of the project. I believe *Andrews (2018)* turns this argument around quite elegantly on affirming that much of the decision during early stages is stylistic by definition and, even if we may not ever find a number to measure how many percentages of a design is really decided by style, sharing this stylistic information is key to understand the decisions and trade-offs. It is, however, a hard exercise to formalize what cannot be formalized, therefore another argument to not be open about it.

Related to this are the fears of damage reputation ('airing dirty laundry', as said by Prof. Weymouth during our symposium) and the fear of associating open to poor compatibility and reliability. Recent studies show, luckily, the opposite, as quality usually increases when openness is a factor.

Open source and proprietary software development used to be competing strategies but in the last decade software companies are taking a best-of-both-worlds approach by creating products that use a combination of open and proprietary software code, as described by *Casadesus-Masanell and Llanes (2010)*. When a component is open, the authors concluded, users can access and improve the code, which increases quality and value creation. The trade-off they discuss is the following: "When a module is opened, users can access and improve the source code, which increases quality and value creation. Opened modules, however, are available for others to use free of charge. Thus, when opening a module, the firm must consider that it may be adopted by other players which may strengthen competitive pressure. As competitive pressure intensifies, the firm must lower prices which hampers its ability to capture value." Besides discussing profit, their model took in consideration quality. They found that that compatibility (i.e. open standards) provides higher value creation, but may not be optimal for the firm from a profit standpoint, while that incompatibility is optimal when the firm's modules are of substantially higher quality. When the firm has only one module of higher quality, then compatibility is generally best because business models that combine modules from different developers are possible. Finally, when the firm's modules are both of lower quality, both compatibility regimes lead to the same profitability, meaning that improving quality is key to maximize profit, rather than purely IP protection.

2.4 Obstacles: Academia, Low Volume and One-of-a-kind

Added to our fears, we have the causes that lead us to thinking and acting little in terms of open data for the maritime, here summarized in three obstacles: choices from the academia when teaching and researching; not enough volume on the ship design market to justify the investment in an open standard; and too many one-of-a-kind projects that makes it difficult to re-use previously projects.

First, us at the academy to blame, as engineers are trained usually in proprietary tools. My experience shows that we have pretty good consensus when teaching the classical authors, books, and references. Most of us teachers have a favourite text on ship design, propulsion, structure or hydrodynamics, and we do know the main sources available, as authors like Bertram, Faltinsen, Tupper, Andrews, Biran, Hughes, among others, are overall familiar. The same is not observed in terms of software. There is no unique design software taught at every school, except maybe for AutoCad, which is used for general arrangement only, and not specific a ship design software. Each university selects what the teachers are used to or get feedback from companies that either use or develop the software, to train the students on it. Most of it is copyrighted and not freely available outside the academic environment.

On the other side of the spectrum, we have the codes and routines developed at each institution, usually a smart-spreadsheet, or many examples over the years of Matlab routines and, more recently python language via Jupiter notebooks. These are generally open, in the sense that each student can get and modify the code. But very few of them are accessible to a larger audience outside the classroom, neither available online.

The second bottleneck lies in the software companies that develop for the maritime market and could benefit from an open standard/interface between the available software. A parametric CFD analysis, for instance, direct from the 3D model software, without the need of cleaning the mesh would be a dream. Many developers are indeed positive towards this type of openness, as this would merge capabilities, corroborated by the findings of *Casadesus-Masanell and Llanes (2010)* that, when a firm has one piece of high-quality product, which is usually the case in small and medium size maritime software firms, it is more profitable in the long term to open standards and collaborate with others. The obstacle here is the cost of developing the APIs and open interfaces, filtering, cleaning, and adapting one model/code to the standards of other's model code.

As the development cost cannot be shared among many users, developers see the option of innovate in opened as a trade-off similar as the ones studied by *Casadesus-Masanell and Llanes (2010)* between will the cost to develop interface to model/standard X pays itself? Does it worth the risk? Such trade-offs usually converges to profit when openness is selected (but not always), and it is observed in few custom cases, usually in an agreement that a client and the software company would have to connect one type of data to the other. I have witnessed some examples of design offices and shipyards paying for an extra feature or add-ons from a software that they use, but this is unusual, and the low selling volume of our niche market does not justify the same type of open interfaces that we see in other technical software.

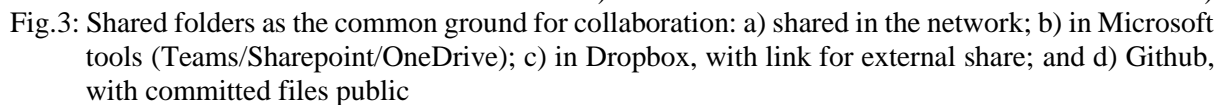
Erichsen (1994) has a good study on how breaking a series of sister ships construction in a shipyard environment reflects in longer time (and consequently costs), and that the best would just construct all sister ships in series. This argument here is extended to justify our third obstacle. At the design offices and shipyards, especially in the European market, long series are not common, *Erikstad (1996)*, with our designs and constructions predominantly one-of-a-kind. In this sense not much is re-used from one project to another, and the data shared is more in terms of known-how and less in practical terms of re-using models, drawings, analyses, and calculations. To overcome this obstacle, it is suggested in the next section a toolbox for collaboration, aimed mainly at the re-use of one-of-a-kind data. The modern idea of shared folders, versioning system, tags and design libraries/catalogues may facilitate the re-use of data in the office / shipyard routine.

3. Toolbox for Collaboration

3.1. Shared Folders

Probably a common ground for a collaborative toolbox is a shared folder. The practice is as old as computers in network and got momentum in the late 90s. Usually they mean collaboration in a restricted environment: inside a department, company. Rarely we see shared folders open for the generic public. This is a good start, if properly used. My experience says that this, as other similar practices, are really

Shared folders in the network, followed by Microsoft solutions (Sharepoint, Teams, One Drive) are currently the most common tools. Particularly, I am very satisfied with the administrative tools from Dropbox, as the shared folder is combined with easy share with external people without the need of logging in as the Microsoft solution requires, as well as a good versioning control. For open to the general public, Github like option can also be used as shared folder, with the limitation of the license (e.g. document size). Fig.3 compiles a screenshot from these options.



Version control of files and infrastructure enables collaboration and rollbacks, *Gaspar (2018a)*, and is here understood in the general terms of collaborative storage and editing capabilities, in line with modern repositories, with features such as versioning, track of changes, reviews, ownership levels, task assignments, automatic documentation, web interface, intelligent search algorithms. Git, and consequently Github, are probably the most popular, and most of its features are also available by PLM/PDM suites.

421

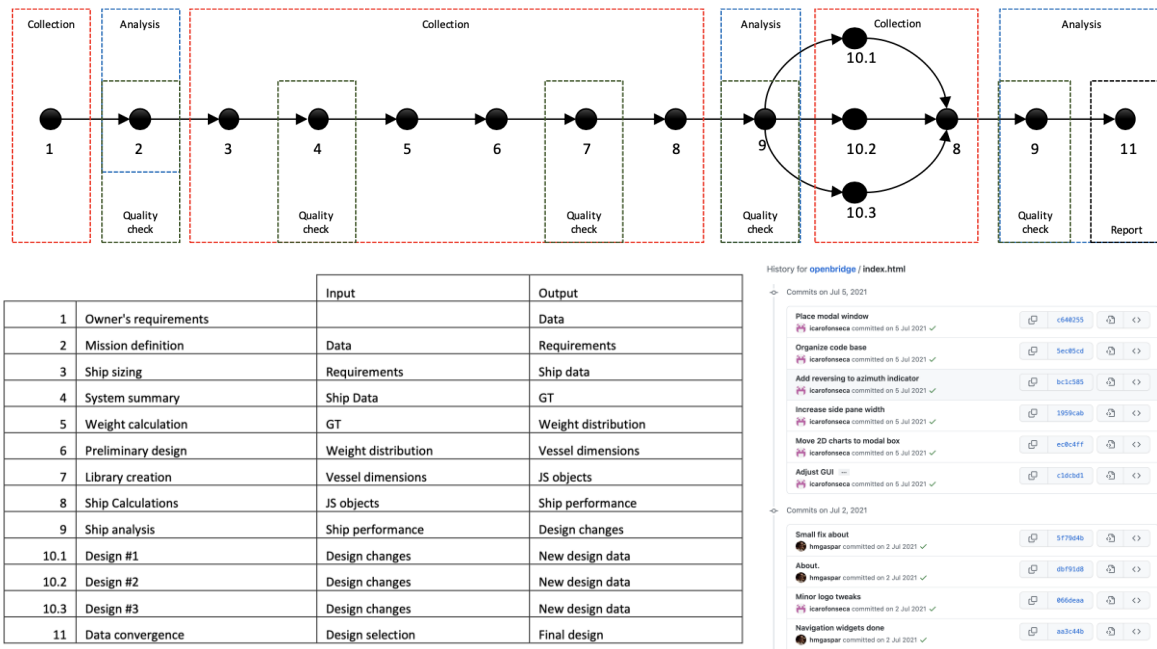


Fig.4: Versioning allows track changes in the document, understanding the design process as a thread, with each new version connected to a task, with a definitive input and output for serial and parallel tasks during the ship design process.

Initially, a timeline of the process and its associated Gantt diagram are showed. The inputs and outputs of each step are defined and all of them represent different types of data. Consecutively, a document is followed through these tasks, with each change noted in the version control system (Git style). Basic elements of data-driven methods, such as data quality, collection and analysis, *Gaspar (2018a)*, are incorporated in the design process, until the final report is concluded.

3.3. Library of Components (Catalogue)

While versioning takes care of each individual file, a whole project must be organized withing a library. This is a more complicate task than the previous, as the organization is not only in term of serial or parallel tasks, but also follows multiple components part of multiple hierarchies, such as commercial, physical, functional, construction, operational, where each component, in each phase of the lifecycle, is associated with multiple files and hierarchies that has its own path over time.

Again, we look at computer science and large software development as example of good practices on how to handle it. There, we see that taxonomies are not necessarily rigid, and the structure of a large project is fluid, constructed by its elements. Modern development moved outside the idea of purely class-instances of traditional object-oriented approach, to a wider idea of object and its multi-hierarchical data, *Gaspar (2017,2018a)*, where the structure is constructed by the tags that an object has, rather than purely a pre-defined scheme, a set of attributes that can be added, nested and quarriable. In other words, collaboration does not require that a new or updated element must fit exactly a place in the hierarchy but requires that this element has the necessary information to be allocated, searched, and edited. In other words, tags or #hashtags for each individual part, while a set of rules investigates the whole library for the needed set of tags, to create a view of the system according to the desired taxonomy.

In this way, a propeller, for instance, would be allocated in the Astern portion of the physical taxonomy, while it also would be part to the Propulsion System in the functional taxonomy, Factory XYZ in the supplier (geographical) taxonomy and Budget ABC in the economic hierarchy. Any change on the original component would add or edit the current tags, rather than create duplicated components for different taxonomies.

Note that this #hastag concept is not in practice in ship design, especially when looking into fixed taxonomies such as the SFI, which focus mainly in the physical and economical aspects of a components and was developed mainly to be used by cost and document control in shipyards. SFI is, however, a great start to organize its elements into tags, as the structural tag has a consistent rule among many actors, and can be used as a common ground in many cases.

Electrical Components for 2017 Nissan Leaf

VEHICLE
2017 Nissan Leaf
[Change Vehicle](#)

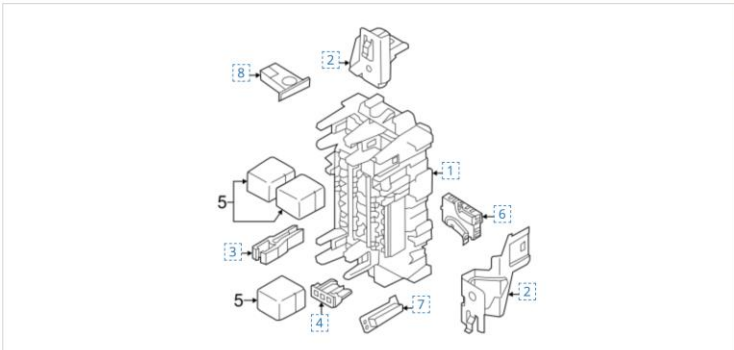
Categories

All
Parts
Accessories

Body
Brake
Brakes
Cooling System
Electric Propulsion System


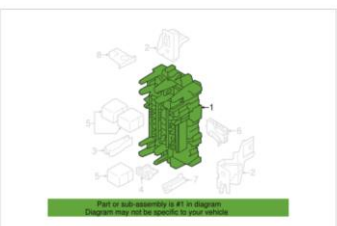
Electrical

ABS Components
Air Bag Components
Antenna & Radio
Anti-Theft Components
Battery
Bulbs - Chassis
Communication System Components
Controls
Electrical Components
Fog Lamps
Front Door
Front Seat Belts
Headlamp Components
Heated Seats
High Mounted Stop Lamp
Horn



No.	Part # / Description	Price
1	Fuse & Relay Box 24311-1HA0A Instrument panel.	M5RP-\$143.76 \$94.88 ADD TO CART
2	Fuse & Relay Box Upper Bracket 24317-3DA0A Mount Bracket Instrument panel, upper. Fuse & relay components, instrument panel.	M5RP-\$17.95 \$11.26 ADD TO CART
2	Fuse & Relay Box Lower Bracket 24317-3DA0B Mount Bracket Instrument panel, lower. Fuse & relay components, instrument panel.	M5RP-\$17.95 \$11.26 ADD TO CART
3	Fuse Puller 24321-79903 Instrument panel & body.	M5RP-\$11.49 \$7.58 ADD TO CART

Fuse & Relay Box - Nissan (24311-1HA0A)
Warranty provided by Nissan North America

VEHICLE FITMENT

Year	Make	Model	Body & Trim	Engine & Transmission
2019	Nissan	Sentra	Nismo, S, SL, SR, SR Turbo, SV	1.6L L4 - Gas, 1.8L L4 - Gas
2019	Nissan	Versa	1.6 S, 1.6 S Plus, 1.6 SV, S, S Plus, SV	1.6L L4 - Gas
2019	Nissan	Versa Note	S, SR, SV	1.6L L4 - Gas
2018	Nissan	Sentra	Nismo, S, SL, SR, SR Turbo, SV	1.6L L4 - Gas, 1.8L L4 - Gas
2018	Nissan	Versa	1.6 S, 1.6 S Plus, 1.6 SV	1.6L L4 - Gas

▼ (23 more fitments)

Fig.5: An automotive catalogue organized with tags, where one components is able to be part of multiple instances and taxonomies, <https://www.nissanpartsusa.com/>.

An example from the automotive industry can illustrate this library/catalogue concept in practice. Fig.5 shows a supplier website with the catalogue of components for Nissan cars in the USA, <https://www.nissanpartsusa.com/>. The library is presented in terms of type of vehicle, model and year. When one instance is selected, the physical taxonomy is presented, where the final component is a part that can be linked to a drawing, supplier, and price. When filtering by components, the tags connect a component leads to a list of other models that use the same part, as well as specific conditions (e.g. supplier, warranty, geographical constraints).

Imagine if we could browse through the design, components, and drawings in ship design in the same way? With this wish in mind a prototype was developed by myself in cooperation with Ulstein Group

some years ago. Components were analysed for a three-dimensional taxonomy: commercial, physical (modules) and functional (systems). Much of the features were inspired by the automotive industry case described. The result of this work is illustrated in Fig.6. There, the same principle of components and tags were used, where a unique library was able to link drawings, suppliers, and customer's requirements for multiple taxonomies.

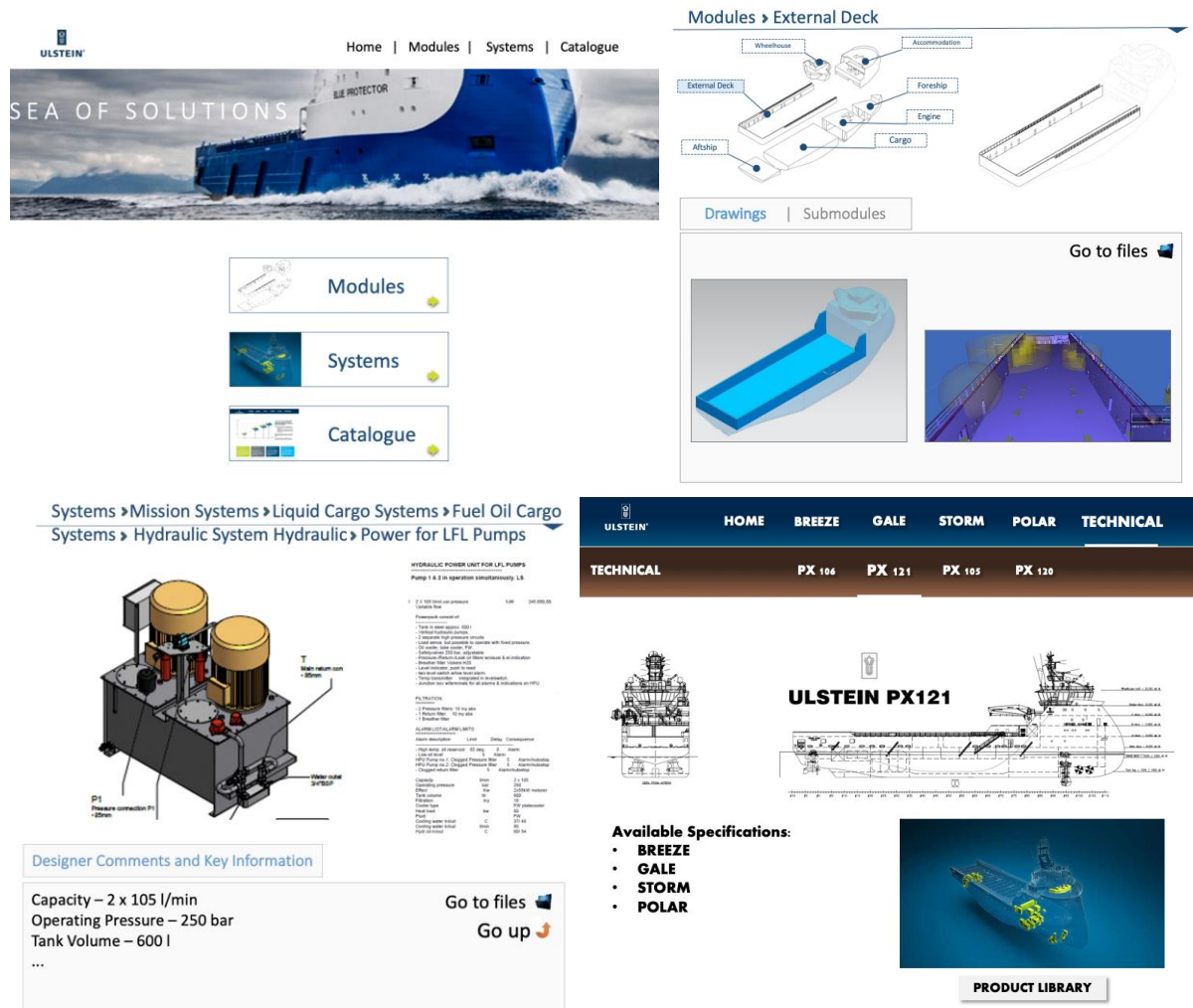


Fig.6: Prototype of a catalogue of designs from Ulstein Group, combining components into modules, systems and commercial taxonomies.

4. Open Engineering Toolbox for Marine Engineering (Executables, Web-apps, Libraries)

There is no real open source / software toolbox commonly used in marine engineering, as the price of a developer to work on the creation of a state-of-the-art tool, that is able to be reliable, maintainable and at the end construct efficient and safe ships, must be paid to justify the risks and benefits for this developer. As commented, the low volume of our market is one reason to it. In this section I will only mention few examples as to show that this is a possibility, even if far from a rule.

We can see a first wave of motivation in the 2000s, with executables shared in pre-Github platforms (such as Source Forge). Two notable examples are yet available and functional: PDStrip, <https://sourceforge.net/projects/pdstrip/>, and FreeShip, <https://sourceforge.net/projects/freeship/>. The first is a hydrodynamic strip code for seakeeping, which computes ship motions for monohulls including sailing boats. The second is a subdivision surface modeling program for designing hulls. Widening the spectrum, we see OpenFOAM as a popular alternative to CFD, <https://www.openfoam.com/>. Code Aster is gaining momentum as a finite element option for structures and thermomechanics analysis, but

its documentation majoritarian in French is not helping the spread of the tool to an international audience, <https://www.code-aster.org/>.

The possibilities of Webapps are gaining momentum in the last years, with me advocating the use of software development practices and JavaScript as a serious tool in engineering in previous COMPITs, *Gaspar (2017,2018a)*. Most of the examples that our group have been working with are available online, and we are (trying to) converging to a library of examples that can be accessed, edited and copied, exemplified by the Vessel.JS, <https://vesseljs.org/>, *Gaspar (2018b)*. Fig.7a shows a part of this library. Each of the examples is a piece that follows similar structure as described previous, regarding versioning, re-use of code and online repositories. Similar compilation of codes and web-application is also practice in other research groups. Fig.7b presents the screenshot from the group of Gabriel Weymouth, at University of Southampton, <https://weymouth.github.io/>.

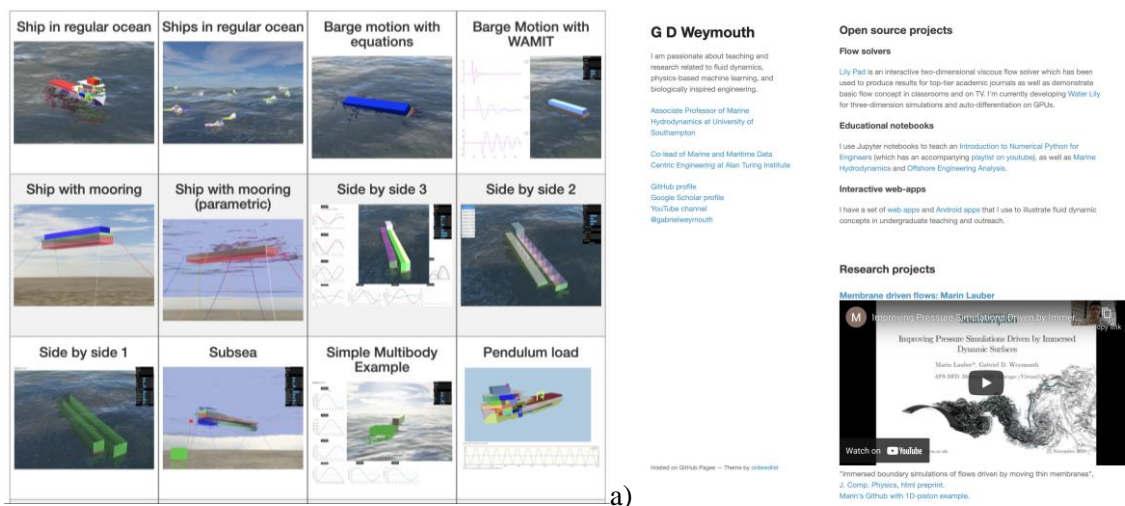
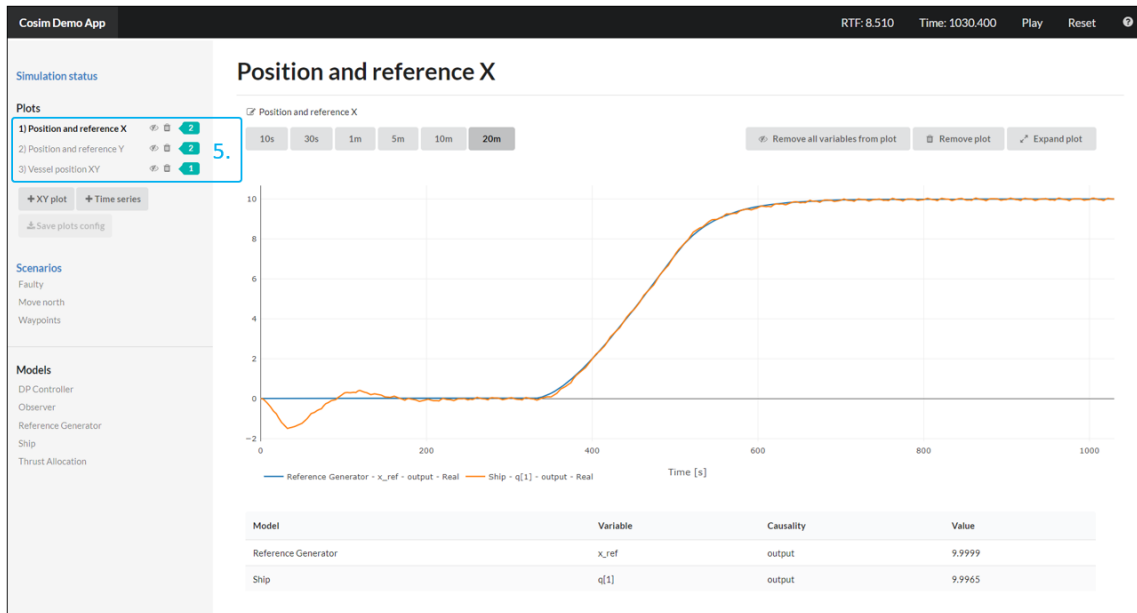


Fig.7: a) Examples from online apps from Vessel.JS (<https://vesseljs.org/>), maintained by myself; and b) Compilation of Open Source projects by Gabriel Weymouth at Univ. of Southampton, <https://weymouth.github.io/>.

Synergy between academia and industry in open initiatives is exemplified by two ongoing projects: OpenBridge and Open Simulation Platform (OSP), <https://opensimulationplatform.com/>. The first is a joint industry effort between Oslo School and Architecture (AHO) and maritime partners to develop open standards to user interface (UI) and user experience (UX) to operate maritime structures. The parts of the library are free for all to use, while the client's identity and knowledge is protected, as the client has the actual domain knowledge of their specific maritime sector. The second is an initiative was started by DNV, NTNU, Kongsberg and SINTEF, towards a maritime ecosystem for co-simulation of black-box simulation models and plug and play configuration of systems. OSP relies on the Functional Mock-up Interface (FMI) standard and their own OSP interface specification (OSP-IS) for the simulation models interfaces. Both initiatives make demos and examples online for public use. Fig.8 exemplifies both initiatives.

4. Ship Simulator – An example of merging two open libraries (Vessel.JS + OpenBrigde)

A last example is presented, developed last year by the Ship Design and Operations Lab at NTNU, <https://www.ntnu.edu/ihb/ship-lab>, which I coordinate, and the AHO OpenBridge group, coordinated by Prof. Kjetil Nordby. The key objective of the example is to combine the work of both open libraries, Vessel.JS and OpenBridge, into a functional and illustrative online app. The target was to combine the 3D elements and propulsion model current developed at Vessle.JS with the bridge and control and UI/UX elements from OpenBridge. The final web application is presented in Fig.9, <https://shiplab.github.io/openbridge/>. The elements from the Vessel.JS library are the 3D models (ship, sea, sky and city), as well as the propulsion and manoeuvring model.



a)



b)

Fig.8: a) Screenshot from a demo by the OSP initiative, <https://opensimulationplatform.com/>; and b) Showcase with the UI/UX elements from the OpenBridge platform, <http://www.openbridge.no/>

OpenBridge elements are the control instruments at the right side of the window, exemplified by the azimuth and compass elements, as well as the multi-view tab in the bottom. The app has the simple feature of controlling the ship in the Trondheim fjord, with the objective of passing by three checkpoints. An alert is given when the pilot manages to fulfil the three checkpoints. Such development was paramount to both groups, to show the potential of combining two initiatives into a new open, available and editable delivery, able to be scrutinized by students and peers.

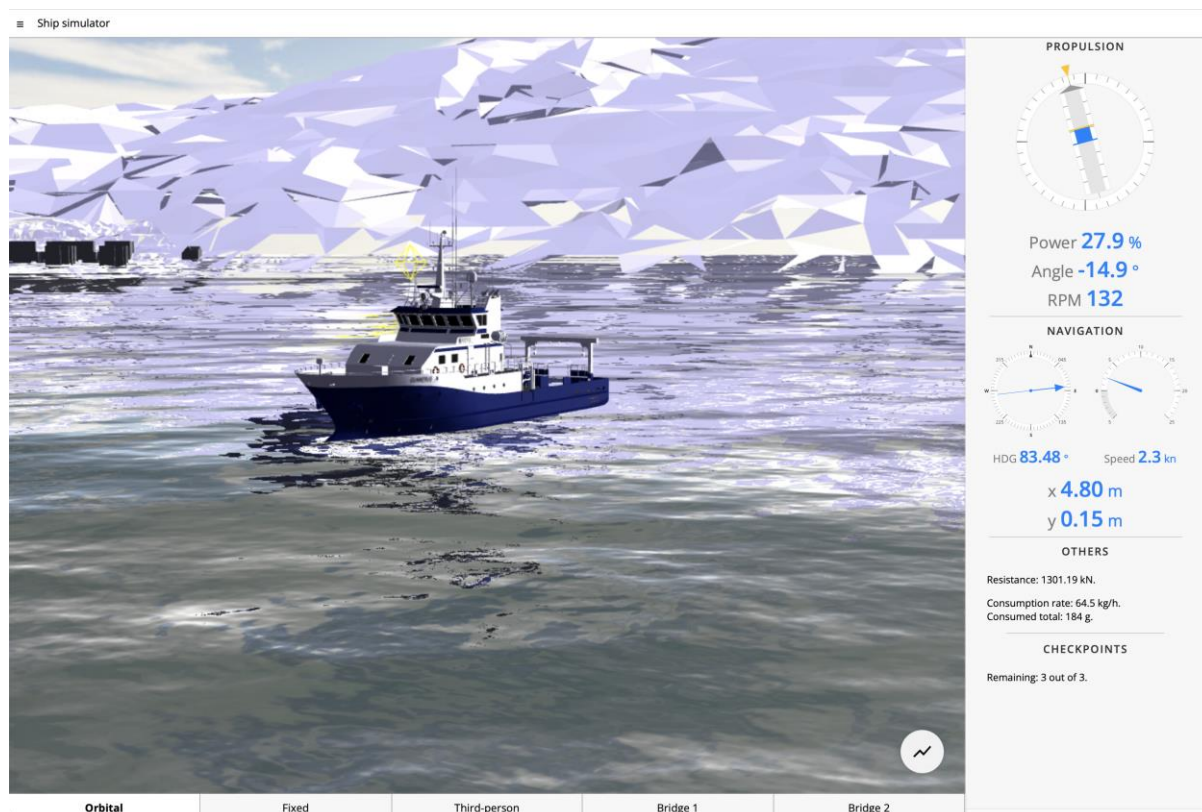


Fig.9: Simulation of a ship manoeuvring in a fjord, merging capabilities from Vessel.JS and OpenBridge libraries (<https://shiplab.github.io/openbridge/>).

5. A Call for Openness and Collaboration in Ship Design

I close this paper with a call for my colleagues and students to consider implementing open and collaborative methods in the everyday design tasks, both at academic and industrial environments. Simple practices for versioning, tagging and library concepts, discussed in Section 3, seems a good start. A Github page for a project – either public or private (paid) is also an experience highly recommended. As this is used to manage large software projects, it has functions like allocating tasks, discussions a traceability in pair (or even better) than most of PDM/PLM solutions. Giving up proprietary data-files in exchange of a standard among all tools seems to be a feasible (and lucrative) path.

The open examples here discussed, like the simulator from Section 4, are a working in process, and much of the libraries and methods intends to be improved in the years to come. The main point defended in this paper is that technology is not a bottleneck for open and collaborative data-driven ship design, exemplified by the current fast-paced stage of online web-development, neither the speed of the computer processors and memory size, but rather how efficient ship design data is able to be transferred from books and experience to useful reusable models. As for the development of real ship design engineering in an open library, I recognize the value of current engineering tools and PLM suites; no doubt, they are responsive for the visible gain in productivity that the maritime industry faced in the last decade. Industry 5.0, with an open digital thread that all actors may follow is thus the next step.

As a final call, it would be nice to see academia really incorporating the open science concept, where the data from public funded projects is not only find in hidden papers, but in a repository, able to be accessed, scrutinized and re-used. For software developments, many models suggests that an open standards and interfaces is key to grow in the market, and may be a lucrative approach. For ship design offices and shipyards, an urgent investment in the *#hashtag* concept of tagging documents according to multiple taxonomies tags, as well as a construction of a library / catalogue that, when proprietary, can be reused internally for the next project and, when public, may be accessed by clients and suppliers.

Acknowledgements

Appreciation is given to all the colleagues that attended our informal, fun and educative symposium on Open and Collaborative Ship Design in a distant Covid-free June 2019, at UCL (London, UK). Special thanks to Prof. Giles Thomas (UCL) and Prof. Gabriel Weymouth (Univ. of Southampton) for their teams input in the symposium. Many of the arguments here presented are inspired by the discussion in that event.

Aside, holding an associated professor position at the Department of Ocean Operations and Civil Engineering at NTNU (Ålesund, Norway), I have no commercial or professional connection with the software and companies cited. Statements on usability and performance reflects solely my opinion, based on personal experience, with no intention to harm or diminish the importance of past or current commercial digital tools. This research is connected to the Ship Design and Operations Lab at NTNU in Ålesund, which is partly supported by funding from the cooperation with Ulstein International AS (Norway) and the Research Council of Norway.

References

- ACKERMANN, K.; GREENSTEIN, S. (2018), *The State of Open Source Server Software*, Harvard Business School, Boston, 40pp.
- ANDREWS, D. (2018), *The Sophistication of Early Stage Design for Complex Vessels*, Trans RINA, Special Edition, Intl J Maritime Eng. 10.3940/rina.ijme.2018.SE.472
- CASADESUS-MASANELL, R.; LLANES, G. (2010), *Mixed Sources*, Harvard Business School, Boston, <https://hbswk.hbs.edu/item/mixing-open-source-and-proprietary-software-strategies>
- CHAVES, O.S.; GASPAR, H.M.; BORGES, H. (2018), *An Open and Collaborative Knowledge-Based Approach for Automated Design of Hull Scantlings*, Int. Conf. Ships and Offshore Structures ICSOS, Gothenburg
- ENCINAS, V.A.I. (2018), *Data-Driven Methods applied to Conceptual Ship Design*, NTNU, 11pp.
- ERICHSEN, S. (1994), *The Effect of Learning When Building Ships*, J. Ship Production 10/3, pp.141-145
- ERIKSTAD, S.O. (1996), *A decision support model for preliminary ship design*, NTNU, MTA report 1996:114, 245pp
- ERIKSTAD, S.O. (2009), *Modularisation in Shipbuilding and Modular Production*, NTNU, Trondheim, s.n.
- GASPAR, H.M. (2017), *Javascript applied to maritime design and engineering*, 16th COMPIT Conf., Cardiff, pp.428-443
- GASPAR, H.M. (2018a), *Data-Driven Ship Design*, 17th COMPIT Conf., Pavone, pp.426-439
- GASPAR, H.M. (2018b), *Vessel.js: an open and collaborative ship design object-oriented library*, Int. Marine Design Conference (IMDC), Helsinki
- NORWEGIAN MINISTRY OF EDUCATION AND RESEARCH (2018), *National strategy on access to and sharing of research data*, https://www.regjeringen.no/contentassets/3a0ceaa1c9b4611a1b86fc5616abde7/en-gb/pdfs/national-strategy-on-access_summary.pdf

OCX Revisited: The New Data Exchange Standard?

Jan Bitomsky, PROSTEP, Hamburg/Germany, Jan.Bitomsky@PROSTEP.com
Alexander Danetzky, PROSTEP, Hamburg/Germany, Alexander.Danetzky@PROSTEP.com
Carsten Zerbst, PROSTEP, Hamburg/Germany, Carsten.Zerbst@PROSTEP.com

Abstract

The OCX standard developed in the APPROVE research project run now available. In this paper, we have a closer look at the format specification itself and the available implementations in real-world CAD tools. We also check the applicability of OCX for common data exchange use-cases in the maritime industry.

1. Introduction

The OCX exchange format was developed to transfer information about ship compartmentation and the hull structure. This information is needed to check a ship's design concerning its hydrostatic and flooding layout as well as the scantlings by classification societies. OCX is not the first format for this purpose, as there are numerous predecessors for the same purpose. Among these are neutral STEP formats defined in the late 1990' and early 2000 (ISO AP215—218) as well as tool-specific formats tied to either a specific classification tool (e.g. ABS Safehull, DNV Nauticus Hull, RINA Leonardo Hull) or a design package like AVEVA Marine.

But none of these formats gained the status of a standard format used in the shipbuilding industry. Despite the huge research funding the STEP formats were never implemented in all relevant shipbuilding tools nor used productively by design offices, yards, or classification societies. The tool-specific formats on the other side are tied to a specific classification society or design tool. As a result, design systems that want to transfer information to classification society need to support writing numerous specific file formats. When implementing a specific tool e.g. to estimate a vessel's production costs based on initial design data, or applying a new method to calculate seakeeping is hindered by the lack of a common input format.

The OCX format is a new attempt to fill the gap of a common, shipbuilding specific data format. It was developed to serve as a replacement for the existing formats and hopefully find widespread use in shipbuilding tools. As such it must support common use cases in the communication between ship design and classification society and should be easily implemented.

For historical interest: OCX is not the first attempt to replace traditional drawings in classification societies. In 2008 we developed the prototype for Germanischer Lloyd based on neutral 3D PDF files, *Grau et al. (2008)*. That format supports the business case with out-of-the-box capabilities like redlining and signatures. The files were created based on the AVEVA specific hull export file rendered into 3D geometry for viewing purposes. In 2017 we provided a similar solution to Meyer Werft as part of their paperless initiative. The yard started providing 3D models with metadata like material quality and thickness in addition to the drawings. DNV GL used this information to assess the ship's structure and to provide digital comments, Fig.6). Both solutions proved to be useful but were not applied to bigger scope due to their singular nature. With several tool vendors, classification societies and yards on board of the OCX consortium we see a much better chance that this attempt becomes successful.

In this paper, we have a closer look at the format itself, the existing example files and possible use cases. Those findings are based on the schema and example file publicly available at the OCX Consortium, <https://3docx.org>.

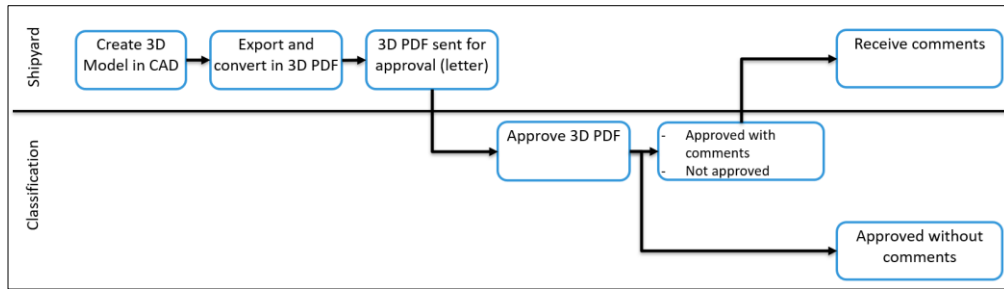


Fig.1: Workflow implemented at Meyer Werft for digital approval in 2017

2. OCX Format

OCX is an XML based format with the namespace <http://data.dnvgl.com/Schemas/ocxXMLSchema> and defined in the file OCX_Schema_V286.xsd. At the time of writing this paper, the schema was not available for download using the schemas URL, which requires having a local copy for validation and reference purposes. As shown in Fig.1, the overall layout is pretty straightforward: documents contain a header section with sender information, a vessel section containing design information, and finally a catalogue section with reusable information like material properties, profile cross-sections, or parametric holes.

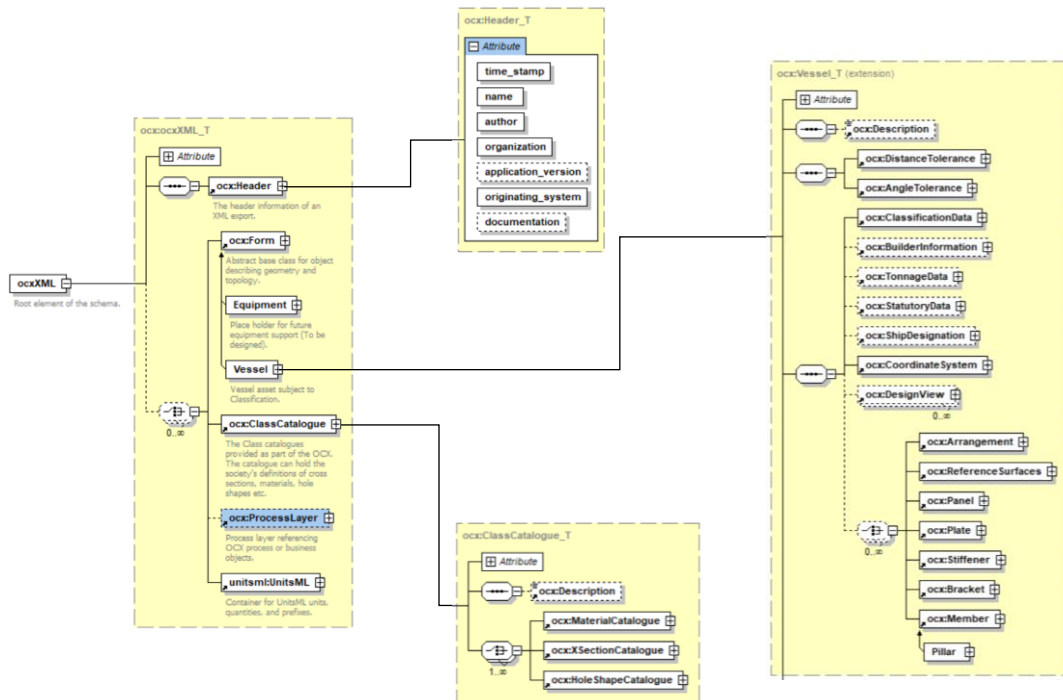


Fig.2: Overall layout of OCX format

```

<ocx:CompartmentProperties>
  <ocx:CenterOfGravity>
    <ocx:X numericvalue="176.1" unit="Um" />
    <ocx:Y numericvalue="0" unit="Um" />
    <ocx:Z numericvalue="16.7" unit="Um" />
  </ocx:CenterOfGravity>
  <ocx:Volume numericvalue="33586.5557" unit="Um3" />
</ocx:CompartmentProperties>

```

Fig.3: Measurable information has directly associated units based on UnitsML schema

Most elements share a common base type with attributes like name, ID, GUID and description. This allows preserving references to entities in the source system. Measurable information (length, volume, etc.) is contained as defined by the UnitsML scheme, <https://www.unitsml.org>. Unlike other formats sporting a default unit system, all information is given with a direct reference to the used unit, Fig.3.

This adds a bit of extra effort for the reader implementation but enables transferring information in their native values (1/2" vs. 12.7 mm plate thickness).

The OCX format supports all the geometry primitives used by today's ship design tools. Curve definition is based on line, circle, ellipse, poly-lines, NURBS, and combination of them, the surface definition is based on either plane, cylinder, cone, sphere, ruled surface from base and sweep curve, NURBS, or combination of them. Implementing an OCX reader is a nice exercise in geometry or requires using a CAD kernel provided by a commercial provider or an open-source alternative like OPEN CASCADE, <https://www.opencascade.com>.

All vessel-specific data is contained in the `Vessel` element and its children. This covers several areas, e.g. initial design values like LPP and block coefficient over IMO number and ship name to the two areas covering detailed design information: arrangement and hull structure. The `Arrangement` element contains data used for hydrostatic calculation, e.g. the compartments with summary information like centre-of-gravity and volume as well as the detailed geometric description.

The hull structure is covered by the elements found in the lower right corner of Fig.4. It follows the usual Panel→Plate→Stiffener breakdown found in most shipbuilding tools. Items that are used outside this breakdown like pillars or brackets are also supported by the OCX format. The level of detail for those items is pretty exhaustive, it contains information down to applied holes, cut-outs, or end cuts. These design features as well as the stiffener or pillar cross-section are providing the *raison d'être* for the catalogue: information on these repeated items is referenced from there instead of duplicating it over and over again.

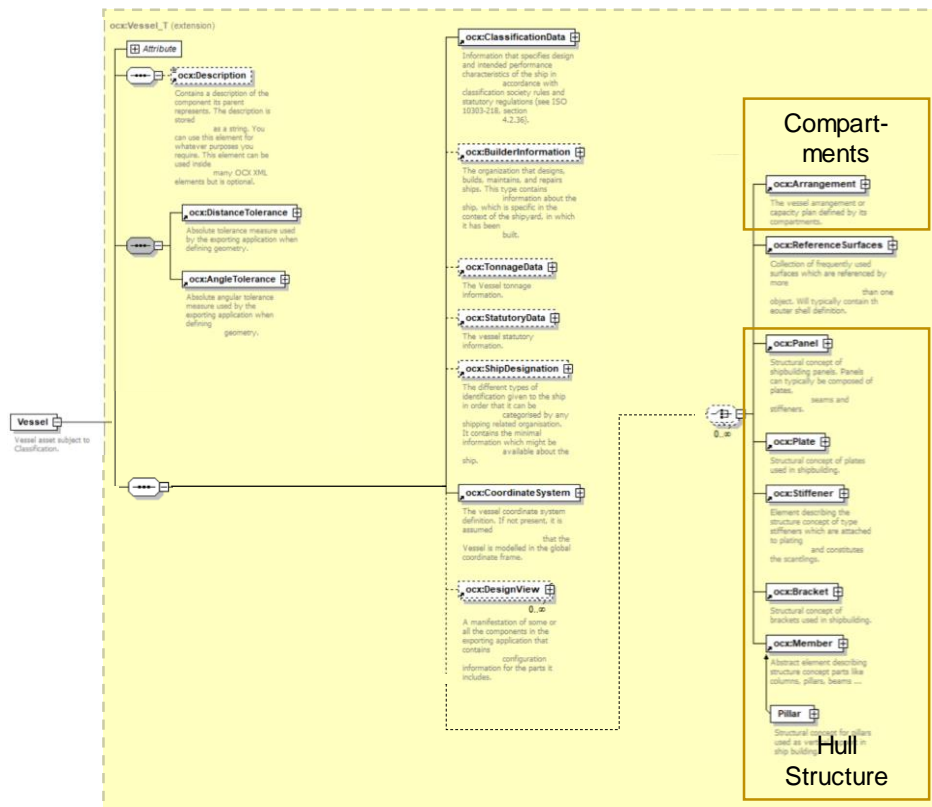


Fig.4: Vessel Data in OCX

The `ClassCatalogue` element is the top-level item containing information that is used in several places of the vessel-specific data. These are most notably catalogues for material qualities, profile cross-sections as well as hole-sections used by holes, cut-outs, or notches.

Overall the schema looks quite reasonable and is pretty close to vendor-specific formats. A nice touch is reusing the data by references e.g. cross-section or surface definitions are contained only once. This allows the result files to stay relatively compact, even though the format is based on the notoriously chatty XML format. On the other side, the schema has two technical issues which are worth changing. The first is the namespace, it references the URL <http://data.dnvgl.com/Schemas/ocxXMLSchema>. But the actual location of the current schema file is https://3docx.org/fileadmin/ocx_schema/OCX_Schema_V286.xsd, so any tool trying to download the schema for e.g. validation purpose fails. Adding a forward to the DNV homepage or changing the namespace to the <https://3docx.org/> domain would solve this problem. The second problem is the existence of two elements called `Length` in the schema. This breaks tools used to automatically generate code from the schema. Listing 1 contains a simple fix for Java users, it hints JAXB to use a different class name on one of the two `Length` elements.

Sample OCX files are available for download from the *OCX Consortium* site. This includes examples written from the tools AVEVA E3D, HEXAGON S3D, NAPA Designer, and SIEMENS NX. If you have access to one of these tools, you could generate them from your ship designs. The example files cover both the definition of compartments by their boundary surfaces (see Fig.5) as well as the hull structure definition by panels (see Fig.6) displayed by our internal OCX Viewer.

In the positive sense, those files do not contain any surprises for experienced developers. As the OCX schema is still in a pre-1.0 version and OCX support was added only last year to some tools, this is much better than we'd normally expect in such an early stage of the development.

Listing 1: JAXB annotation needed to map duplicate `Length` element name

```
<?xml version="1.0" encoding="UTF-8"?>
<xs:schema xmlns:xs=http://www.w3.org/2001/XMLSchema
  xmlns:vc=http://www.w3.org/2007/XMLSchema-versioning
  xmlns:ocx="http://data.dnvgl.com/Schemas/ocxXMLSchema"
  xmlns:unitsml="urn:osis:names:tc:unitsml:schema:xsd:UnitsMLSchema_lite-0.9.18"
  xmlns:jaxb="http://java.sun.com/xml/ns/jaxb"
  xmlns:xjc="http://java.sun.com/xml/ns/xjc"
  targetNamespace="http://data.dnvgl.com/Schemas/ocxXMLSchema"
  elementFormDefault="qualified" attributeFormDefault="unqualified"
  vc:minVersion="1.1" jaxb:version="2.0">
  <!-- CZ Import the NIST unitsML lite schema from local file -->
  <xs:import namespace="urn:osis:names:tc:unitsml:schema:xsd:UnitsMLSchema_lite-0.9.18"
    schemaLocation="unitsmlSchema_lite-0.9.18.xsd"/>
  ...

  <xs:element name="Length" type="ocx:Quantity_T">
    <xs:annotation>
      <xs:documentation>The curve length computed by the ...
    </xs:documentation>
    <!-- CZ Rename classname to OCXLength to avoid name clash -->
    <xs:appinfo>
      <jaxb:class name="OCXLength"/>
    </xs:appinfo>
    </xs:annotation>
  </xs:element>
```

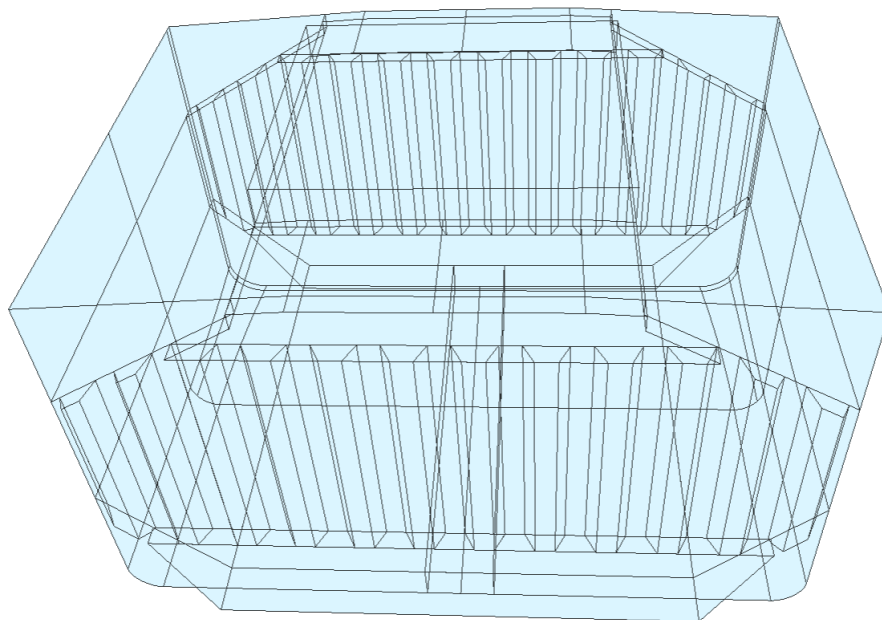


Fig.5: Compartment definition by faces

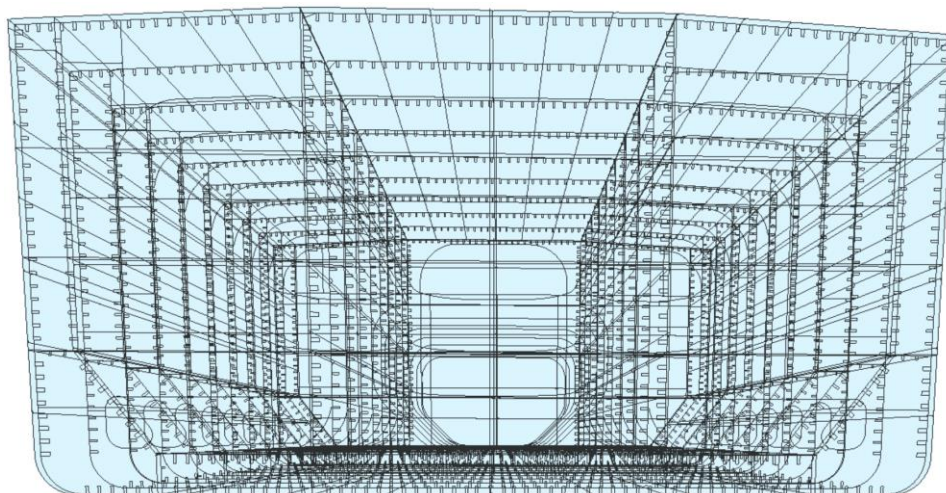


Fig.6: Hull Structure definition by panels

3. OCX Enabled Use Cases

PROSTEP's day to day business is providing consulting services and IT tools for the maritime sector. We implemented several data transfer processes used on daily basis or as migration tools either as a custom-specific solution or as commercial of the shelf product, *Sieranski and Zerbst (2019)*. In many cases, these transfers do not simply transfer geometry from A to B but provided a semantic data exchange where the target tool requires real shipbuilding information, *Gresens and Zerbst (2020)*. The basis for these tools is our own XML format ShipXML, supporting semantic data exchange for both hull structure and outfitting including full parametric and topologic information. This allows us to create a native model in the target system enabling users in the yard or classification society to work seamlessly with the imported data. For these reasons, we see ourselves as experts in the field of shipbuilding data transfer and are quite interested in the OCX format definition.

As we see in the work with our customers, every “solution” requires a process-related and a technical component. Or in other words, the business department's requirements must be aligned with the technology implementation part. At many shipyards, we saw that there is a certain discrepancy between business and IT. In some shipyards the business is not open to adapting existing processes to a new

technical component, on others solution is primarily driven by IT with little regard for business requirements.

As said, OCX is not the first attempt to replace traditional drawings in classification societies. Two real-world use-cases from the shipbuilding industry are already mentioned in chapter 1. Based on this experience, a general classification process between shipyards and classification societies can be represented by the process in Fig.7.

Let's take this generic and simplified process as a reference and overlay the OCX schema as a technical solution for the moment. In this context and based on our experiences, we want to investigate the indicated OCX use cases (ASTRUP 2019). Figure 1(A digital information flow between yard/designer and the classification society) in that paper illustrates the intended design-centric work process. It mentions the following workflow: the yard/designer uploads a 3D model to the classification society, which verifies the model and provides feedback back to the yard/designer. They make modifications and revisions to send an updated model back to the classification society.

This could be broken down into the following three use cases:

- Use Case 1 – Yard/Designer to Classification society
- Use Case 2 – Classification society to Yard/Designer
- Use Case 3 – Combined Use Cases 1 and 2 as full round trip

3.1. Use Case 1 – Yard/Designer to Classification society

This intended use case is described with some details in Fig.3 by Astrup *et al.* (2019). It is defined as the retrieval of the shipyard's design information required by the classification society. This use case also covers visualisation, comment, and red-marking to focus on the currently discussed topic. It was demanded that the OCX file contains all the model information needed by the classification society to perform necessary calculations or checks to verify the design. Within our generic and simplified classification process in Fig.7, these steps are represented by boxes 1 to 5.

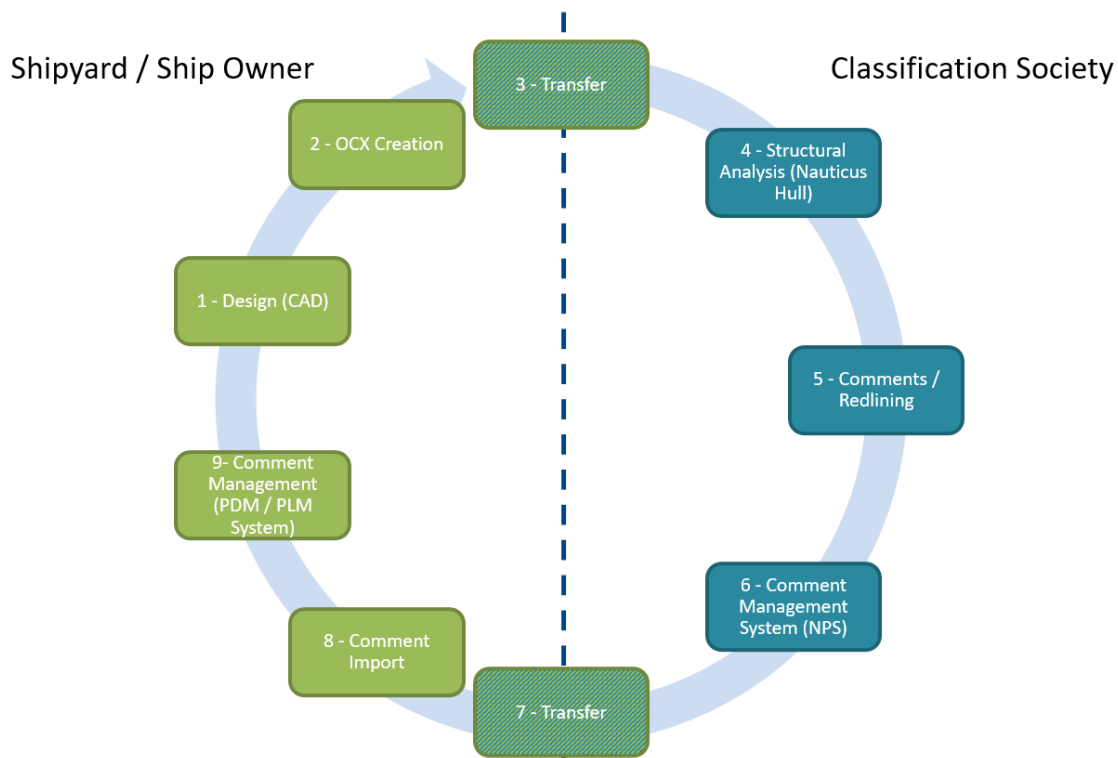


Fig.7: Generic and simplified classification process (OCX context)

Reviewing this demand against the current definition of the OCX format, we see it pretty capable of transferring the vessel's design for both the arrangements as well as the hull structure. But there is more to a process than just transferring the vessel's design itself. Within the currently used drawing-based classification process, red-lining is added to the drawings, and additional comments are added to the classification societies' comment management system in the scope of a specific drawing.

This is quite difficult if the comments have only an OCX file containing the complete vessel as an anchor. That's why we see an immediate need to enhance the OCX format by workflow related entities like comments and redlining and viewports. This would allow the yard to transfer that information in the very same file and thus with fewer ambiguities in communication.

3.2. Use Case 2 – Classification society to Yard/Designer

Within the second use case, the classification society provides feedback to the shipyard or design office. Our generic and simplified classification process represents this use case in boxes 6 to 9 (Fig.7). The feedback must contain information about the referenced design entity, the comment itself and perhaps some severity.

Comparing this demand with the OCX format, one could start with transferring only individual comments in a text form like an email. But referencing the afflicted item is a problem for humans. Technically one could transfer the OCX GUID to find the item on the yard, but this implies that the shipyard's CAD model provides the same set of GUIDs as used during OCX export. This sounds easy, in reality, it is not always that case. Often, a CAD user is faster by deleting a couple of panels to copy a modified panel along the frame grid and thus losing the identifiers. At this point, the shipyard and the classification society must have a common understanding of how an object reference is defined and this must work for both sides.

A second topic is approval granularity. In the past, a complete drawing was approved. This means that all the shown structures within a specific drawing are accepted. With an OCX model containing the complete vessel, we will have a mix of approved and rejected items and need to keep them apart.

As a result, we see the need to use the OCX format also for the way back from classification society to the yard. This would allow to unambiguously transfer comments, redlining and approval status associated to design items. In the ideal world, design tools would then read in this information, e.g., highlight entities based on their approval status or show comments.

3.3. Use Case 3 – Use Cases 1 + 2 as Full Round Trip

Use case 3 describes the combination of use cases 1 and 2, defining the full round trip. This use case applies, for example, when a shipyard needs to send a model a second time for the approval to the classification society, e.g., the model is updated based on some comments. Here, the classification society must be able to link the new OCX model in the previously captured comments (e.g., same GUID as previous transfers).

This use case is also valid for shipyards, for example, when an updated OCX model was reviewed by the classification society. Of course, for a shipyard, it is important to identify which comments are closed or not closed. At the same time, it is also important for a shipyard to identify new comments, especially when the affected objects were not commented on by a previous class review. In the past, a drawing had different revisions to keep track of, and today with OCX, the 3D model must be revised. This use case 3 represents some of the core topics of model-based engineering.

A full round trip requires that comments and approval status with OCX support some kind of lifecycle information.

4. Conclusions

We investigated the OCX format both from the technical perspective as well as from the business perspective. Despite the two minor issues in the schema definition mentioned above, we are confident it is technically able to transfer vessel information needed on an initial design level. If you are looking beyond the initial design, into a fully topological and parametric transfer and native import into e.g. AVEVA Marine, OCX is not a valid choice. But to be fair, this was not a design goal for the format. The tool support to export OCX is also quite a descent for this early stage, NAPA even added OCX Import with NAPA Designer 2020.2.

From the business perspective, we see a lot of potential for a widespread shipbuilding specific data exchange format. The usual suspect's design office, yard and classification society would benefit if they could rely on one common format instead of supporting a plethora of different formats. When working on hydrostatics or scantlings this is no far-fetched goal.

But an exchange format and tool support alone does not guarantee, that potential benefits are applied in daily practice. To fully support the development cycle between the design office and classification minor enhancements to cover commenting, redlining and approval status would add a lot. In the long run, one would need some tooling support to merge changes applied to the design with information flowing back from the classification society. Otherwise, it needs a lot of manual effort to merge changes required by a classification society and those applied until feedback arrives. Only a few shipbuilding tools offer such a PDM layer.

Overall, we see the OCX format as a step forward to enable initial design data exchange. It could help the shipbuilding industry to become more efficient in that part of the life cycle. But it requires yards to embrace the idea of handing out a (subset) digital model of their vessel. Compared to this change of mind, enhancing the OCX format and tooling is the lesser challenge.

References

- ASTRUP, O.C.; AAE, O.; KUS, T.; UYANIK, O.; BITERLING, B.; BARS, T.; POLINI, M.; VIJAYA, G.; YU, K.; JUTTU, L. (2019), *Model-Based Approval – The Open Class 3D Exchange (OCX) Standard*, ICCAS Vol. 3, Rotterdam, pp.27-40
- GRAU, M.; ZERBST, C.; SACHERS, M. (2008), *Building the Business Process View into Shipbuilding Data Exchange*, COMPIT Conf., Liege, pp.282-290, http://data.hiper-conf.info/compit2008_liege.pdf
- GRESENS, C.A.; ZERBST, C. (2020), *How to Achieve Data Integrity in Ship Design through Unified Data Models*, COMPIT Conf., Pontignano, pp.82-88, http://data.hiper-conf.info/compit2020_pontignano.pdf
- SIERANSKI, J.; ZERBST, C. (2019), *Automatic Geometry and Metadata Conversion in Ship Design Process*, COMPIT Conf., Tullamore, pp.146-155, http://data.hiper-conf.info/compit2019_tullamore.pdf

Using Deep Reinforcement Learning for Energy Efficient Automatized Berthing Maneuvers in Inland Navigation

Carsten Genschorek, TU Berlin, Berlin/Germany, carsten.genschorek@tu-berlin.de

Tim Holzki, TU Berlin, Berlin/Germany, tim.holzki@tu-berlin.de

Abstract

This paper presents an approach to utilize deep reinforcement learning to train algorithms for the energy efficient and automatized control for berthing maneuver of inland navigation vessels. Towards the necessary modernization of inland navigation, two technological aspects are inevitable: automation and decarbonization. The matter of this paper lies in the midst of these aspects, as the berthing maneuver of a ship is eminently energy intensive and intelligent automation can help preserving the limited energy storage of ships powered by alternative energies. Deep reinforcement learning is utilized to train algorithms, that combine the path finding and drive control processes with the objective energy efficiency and duration of the berthing maneuver. The algorithms are applied for different - conventional and unconventional - drive systems and configurations.

1. Introduction

European inland navigation is at a crossroads. As part of the transport sector whose greenhouse gas emissions continue to increase, it faces the massive challenge of switching to alternative propulsion energies. On the other hand, the transport of goods on waterways is particularly low in energy, encouraging a shift from road transport to waterways. This leads to the goal of emission savings while increasing transport volumes. The operation of inland waterway vessels with alternative drive energies requires strict conservation of energy in reference to the individual ship unit, as energy is a limited source onboard.

On the other hand, there is a tense personnel situation and increasing demands on navigation tasks in inland navigation. Among other things, increasing shallow water periods have an influence on the constantly changing dynamic behavior of the ships. For transports on waterways in metropolitan regions, small ship units are becoming more and more important, *Kreidel et al. (2022)*. These additionally have a special maneuvering behavior and are exposed to large interactions due to environmental influences and e.g. passing ships of conventional size. Smaller vessel units also offer potentials for the use of unconventional propulsion configurations in order to be particularly maneuverable or to be able to interact as well as possible with other vessels. Automation of inland navigation is addressing these developments and can help in the first steps to cope with difficult maneuvers and save energy, and in the future, it can take over the control completely. Ultimately, berthing maneuvers are particularly energy-intensive due to high thrusts to be applied and thus offer special savings potential for assistance systems and automated maneuvers.

Machine learning plays a significant role in automating complex navigation operations. The work carried out here is based on the premise of an efficient approach using a deep learning approach to combine the path finding and drive control processes with the objective energy efficiency and duration of the berthing maneuver.

The investigations described here took place in the context of the joint research project A-SWARM: Autonomous Electric Shipping in Metropolitan Areas, funded by the German Federal Ministry for Economic Affairs and Climate Control.

2. Fundamentals

2.1. Unity

Unity is originally a game engine, but it finds more and more applications outside this original area of use, popular fields are film, architecture, VR and as in this case the training of artificial intelligence. For this purpose, a machine learning toolkit is used which can interact directly with the Unity engine. Such an integration allows for rapid development and customization of the simulation and training environment. Thus, as in our application, the position of targets, starting points, obstacles as well as the position of actuators and their parameters can be changed with little effort.

Unity Machine Learning lends itself to both deep reinforcement learning and imitation learning. For our task, we chose deep reinforcement learning. ‘Deep’ in the machine learning context means that multiple layers of artificial neuron exist, these together with the connections between them form the actual artificial network. Large amounts of data are fed into the input layer of the network, the result of the computation is available in the output layer after passing through the hidden layers. During the learning process, the connections between the neurons are strengthened or weakened depending on the result of the learning process. In reinforcement learning, desired behavior is positively rewarded and undesired behavior is negatively rewarded. During learning, the algorithm aims to determine ways to maximize the reward. The advantage of deep reinforcement learning is that the data sets needed for deep learning are generated by the AI itself. This learning method is particularly suitable for dynamic environments such as harbor areas.

2.2. Simulation environment

The simulation environment consists of a square area limited by walls. Within the simulation environment are areas that are used for the placement of various objects at the start of training. Since the Unity Engine works unitless, the units and scale can be freely chosen. Therefore, in our scenario, the side length is 100 m.

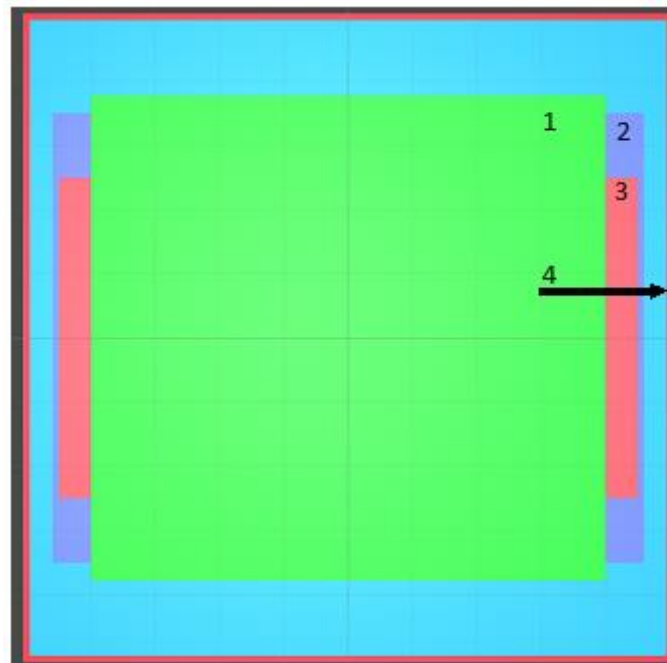


Fig.1: Layout of the simulation environment for training of the agent. 1: Positioning area for the target. 2: Positioning area for the agent. 3: Positioning area of the obstacles. 4: Boundaries of the simulation environment

Our vehicle has a length of 6 m and a width of 3 m. With the existing algorithm 4 propulsion concepts were trained, Fig.4:

- one thruster in the starboard stern, one thruster in the port bow (skewed)
- one thruster in the stern (conventional)
- one thruster at the stern and one thruster at the bow in one line (line)
- two thrusters side-by-side in the stern (side-by-side)

Each thruster can be rotated 360° and can therefore provide thrust in all directions.



Fig.2: Simulation environment during training. 1: randomly placed agent. 2: randomly placed target

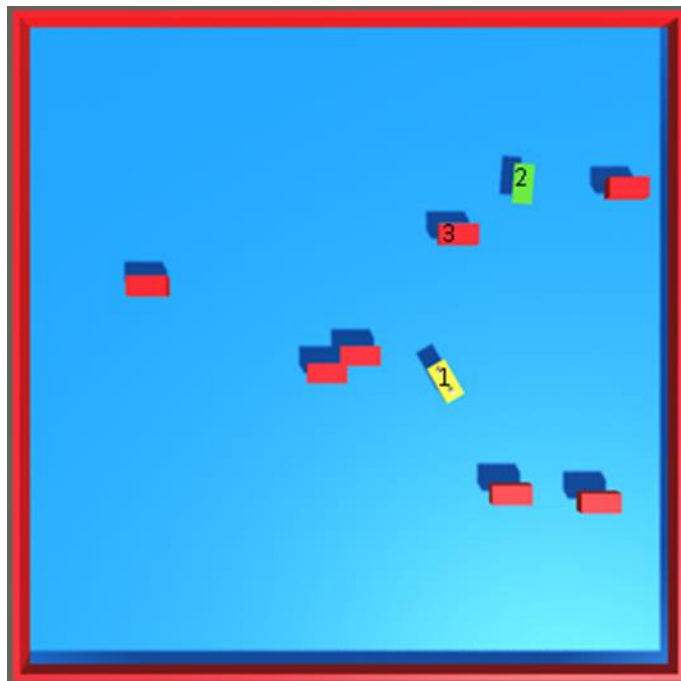


Fig.3: Simulation environment during training with obstacles. 1: randomly placed agent. 2: randomly placed target point 3: seven randomly placed obstacles.

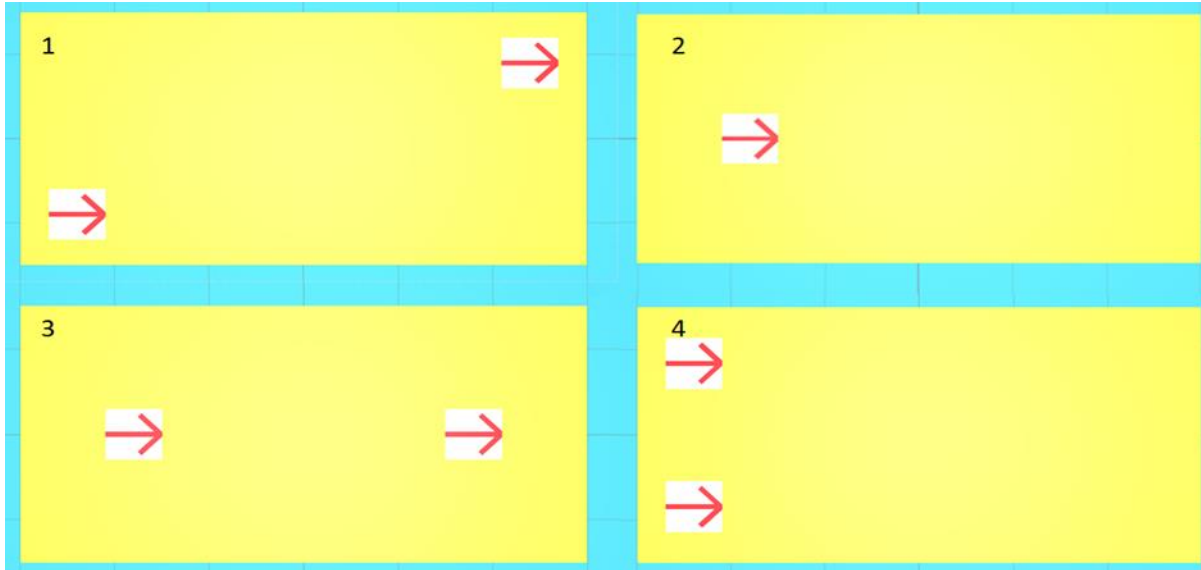


Fig.4: Drive arrangements (red arrows) of the trained agents (yellow rectangles). 1: Skew arrangement. 2: Single drive. 3: Line arrangement. 4: Side by side arrangement.

2.3. Inputs

The inputs for the neural network are defined as observations or sensors that represent variables of the agent in the simulation environment. These sensors form the first layer of the artificial neural network, the output layer forms the control commands for our vehicle. The more variables there are at the input of the network, the more comprehensive the image of the environment the agent can form. This increases the possibility of finding patterns that are necessary for an optimal solution strategy. Another factor for the selection of sensors is the desired behavior that the agent should exhibit. In our simulation we observe the following sensors, the syntax is determined by the Unity Engine and C#:

Table I: Sensors observed and evaluated by the agent during training

localVelocity.x	Speed in X direction
localVelocity.z	Speed in Z-direction
m_BoatRb.angularVelocity.y	Rotation speed around the Y-axis
m_BoatRb.transform.localPosition	Position of the agent
parkingSpot.transform.localPosition	Position of the target
parkingSpot.position - m_BoatRb.transform.position	Distance between the two points in X and Y
m_BoatRb.transform. InverseTransformPoint(parkingSpot.position)	Direction of the target seen from the agent
Vector3.SignedAngle(m_BoatRb.transform.right, parkingSpot.transform.right, Vector3.up	Deviation of the orientation of the agent from the orientation of the target
Vector3.SignedAngle(ThrusterFront.transform.right, m_BoatRb.transform.right, Vector3.up	Angle of the front thruster relative to the orientation of the agent
Vector3.SignedAngle(ThrusterBack.transform.right, m_BoatRb.transform.right, Vector3.up	Angle of the rear thruster relative to the orientation of the agent
ThrustFront	Thrust of the front thruster
ThrustBack	Thrust of the rear
Energy	Current energy consumption
Energy_total	Energy consumption during the episode

In addition to the sensors that are integrated via a script, an engine's own Ray Perception Sensor is used to detect obstacles and the walls of the simulation environment. This sensor acts like a lidar (light detection and ranging) and provides information about the distance to the obstacle as soon as a ray

touches an object. The vehicle thus has a total of 16 rays that provide information around the vehicle in 360°, Fig.5.

What should be considered especially with the inputs is that they should be normalized to values between zero and one. This is particularly important for inputs with very different magnitudes, as otherwise there may be a strong distortion due to the input values inside the hidden layer. Under certain circumstances, this may cause the training to fail.

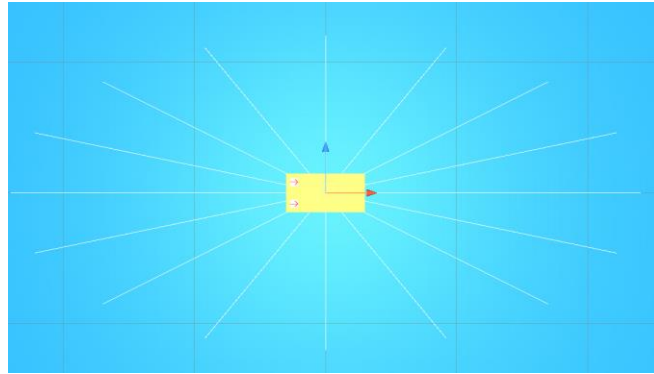


Fig.1: Arrangement of the rays (white lines) of the Ray Perception Sensor around the vehicle (yellow rectangle)

2.4. Outputs

The output layer of the neural network provides the control commands for our vehicle. For each drive there are two outputs: one to change the orientation of the actuator and one for the power of the thruster.

2.5. Reward function

Before increasing the complexity of the simulation, it was necessary to ensure that the training was stable and successful. Crucial here is how and at what time the positive and negative rewards are distributed.

A rare distribution of the reward, usually at the end of a training episode, gives the model the greatest freedom to explore the environment and develop solution strategies. In complex environments, however, an infrequent reward may lead to slow or unsuccessful training.

A frequent reward can increase the learning speed or make a successful training first possible. Note, however, that the reward function directly influences both learning and the solution strategy and thus, in the worst case, stands in the way of the, for this scenario, optimal solution. Therefore, for the design of the reward in a dense reward environment, the scenario must be well known *Larsen et al. (2021)*.

For our training, a dense reward environment was chosen to speed up the training and reward desired or required behavior. Small rewards were distributed at each simulation step as well as larger positive and negative rewards at the end of the episode.

To successfully complete an episode in our simulation, the vehicle had to reach a certain point while adhering to specified parameters:

- velocity in X and Z below 0.5 m/s
- rotation speed around Y-Axis below 0.1 °/s
- deviation from position less than 1.5 m
- deviation from orientation of less than 10°

2.5.1. Positive reward

At each time step, the agent receives a small positive reward that is larger the closer the vehicle is to the target point while moving toward it. On successful completion of an episode, the agent receives a larger reward, which is further increased by an amount that becomes larger the closer the orientation of the vehicle matches the orientation of the target point.

2.5.2. Negative reward

To motivate the agent to move, a negative reward is distributed for each simulation step. In addition, the reward function also becomes negative as soon as the vehicle moves away from the target point. The closer the vehicle is to the target point and the faster it moves away from it, the greater the negative reward. Energy consideration and optimization is reflected in the negative reward, the total energy used is multiplied by a factor and awarded at the end of an episode. Should the vehicle touch an object in the simulation environment, the episode will end and a large negative reward will be distributed.

2.6. Implementation of the training

In the simulation environment, the vehicle, or agent, is supposed to navigate to a point. Both the starting point and the target point change with each new attempt, this has the advantage of ensuring that the algorithm learns to guide the vehicle to an arbitrary target and not, as in a static environment, to always navigate to the same point.

The destination, starting point and any obstacles are randomly positioned in a fixed area at the beginning of the training episode, Fig.1.

After the first simulation converged reliably and successfully, another advantage of the Unity Engine could be used to increase the complexity of the simulation. With the help of C# scripts, Unity's own physics can be better adapted to reality within the simulation.

Especially the drag is kept very simple in the Unity Engine and only depends on the velocity and the mass, but not on the shape or area nor on the drag coefficient.

Therefore, for the next simulations, we included our own simple drag forces acting on the vehicle. Since no real drag curves were available for a model at the time of the paper, the velocities in X and Y and rotational velocities around the Z axis were squared and each was assigned a factor to account for the different drag coefficients.

In the last progression stage of the simulation, the energy consideration was included as a negative reward. The higher the consumption during a session, the greater the negative reward.

In each training, 100 million simulation steps were calculated before the simulation was terminated. Initially, the algorithm and training were only designed for the propulsion arrangement: one thruster at the stern and one thruster at the bow and were optimized to ensure that the training was performed reliably and successfully.

To check the robustness and flexibility of the training, the other drive arrangements were trained with the same parameters and the results were compared with the successful training of the line arrangement. In addition to varying the actuator arrangement, the conditions of the simulation environment were also changed for two calculations.

In one environment, to successfully complete an episode, a randomly re-placed point had to be approached five times in succession.

In the second modified environment, training was performed with seven randomly placed obstacles in the environment that were repositioned for each episode, **Error! Reference source not found..**

To take advantage of the parallelization capability of the ML-Agent framework to speed up the training, parallel computation was performed in 160 simulation environments.

Overview of trainings:

- Line arrangement
 - Standard training
 - Modified environment with obstacle
- two thrusters side by side in the rear (side by side)
 - Standard training
 - Modified environment with five consecutive targets
- one thruster starboard stern, one thruster port bow (skewed)
 - Standard training
- one thruster in the stern (conventional)
 - Standard training

3. Evaluation

To validate the training, the ratio of successful and unsuccessful training episodes was examined. Once this ratio reaches one, only successful trainings have been completed in the measured period, 500000 simulation steps. Since the focus is on energy optimization the training is considered successful only when both the energy consumption and the episode length reach a minimum and the cumulative reward reaches a maximum.

All actuator configurations with two actuators, except for the simulation environment with obstacles, show very similar learning behavior. After about 5 million computational steps, the learning effect sets in, the success rate increases, and at the same time the energy consumption and the episode length decrease for the standard trainings. Between 30 and 50 million simulation steps, more than 95% of all episodes are successful. During this period, episode length and energy consumption fall. Between 45 million and 72 million steps, there is a short-term degradation in the standard training of the actuator configurations with two motors. After 70 million steps, all episodes are successful and little or no improvement in episode length, reward, or energy consumed occurs, Figs.6 to 10.



Fig.6: Success ratio of different actuator configurations during training. Duration 100 million steps. Zero means no episode was successfully completed, one means all episodes were successfully completed. 1: Side by side arrangement with 5 target points. 2: Skew arrangement. 3: Line arrangement. 4: Side by Side arrangement Standard Training.

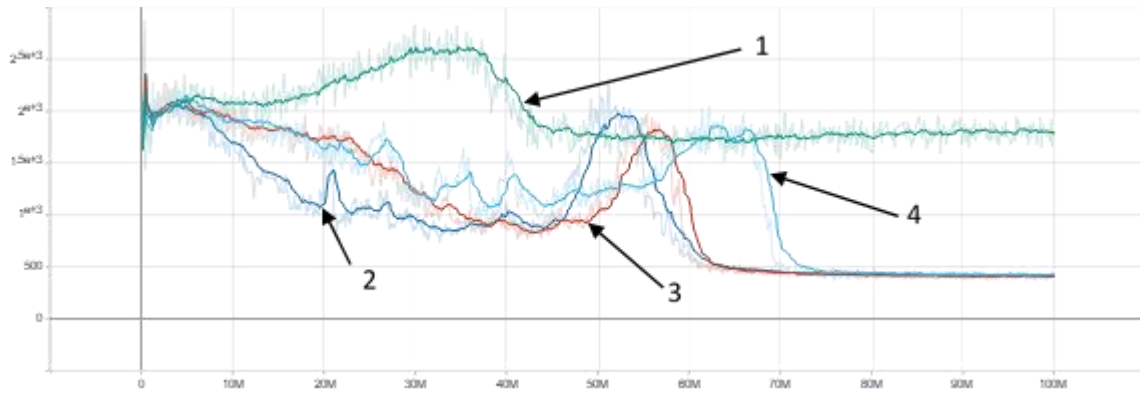


Fig.2: Energy consumption of different actuator configurations during exercise. Duration 100 million steps. 1: Side by side arrangement with 5 target points. 2: Skew arrangement. 3: Line arrangement. 4: Side by Side arrangement Standard Training.

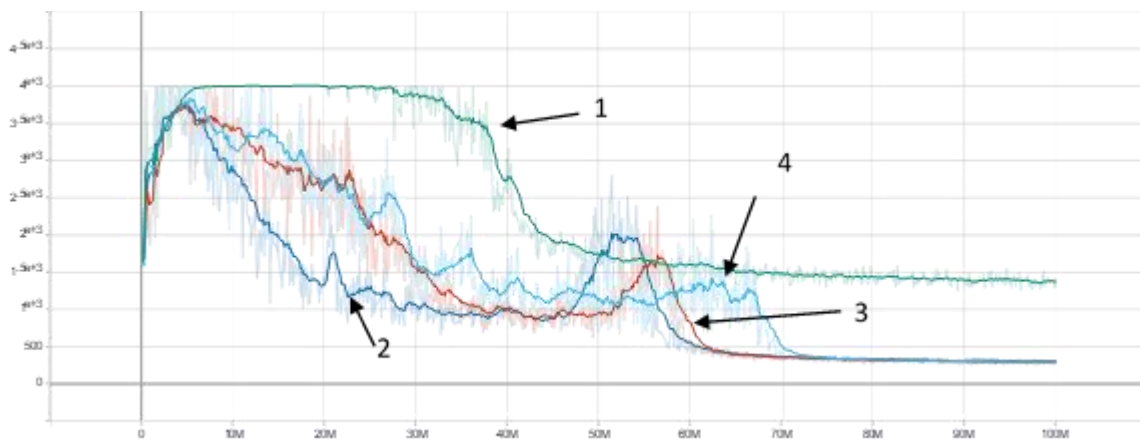


Fig.8: Episode length in calculation steps of different actuator configurations during training. Duration 100 million steps. 1: Side by side arrangement with 5 target points. 2: Skew arrangement. 3: Line arrangement. 4: Side by Side arrangement Standard Training.

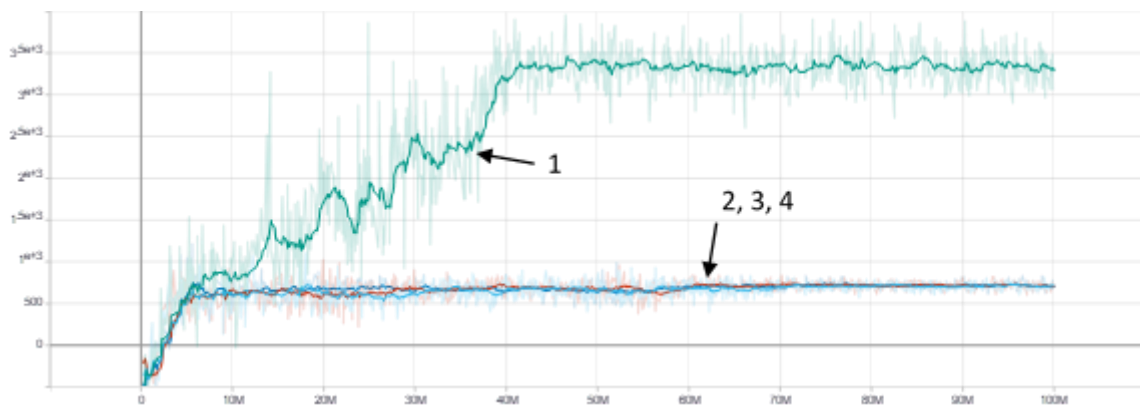


Fig.9: Received reward of different actuator configurations during training. Duration 100 million steps. 1: Side by side arrangement with 5 target points. 2: Skew arrangement. 3: Line arrangement. 4: Side by Side arrangement Standard Training.

The conventional single drive and line arrangement with obstacles showed no significant improvement in success rate up to 100 million steps. Therefore, the training period was extended. From 180 million steps, the single propulsion arrangement improved to over 90% success rate. In the same time, the training with obstacles could only improve to about 60%.

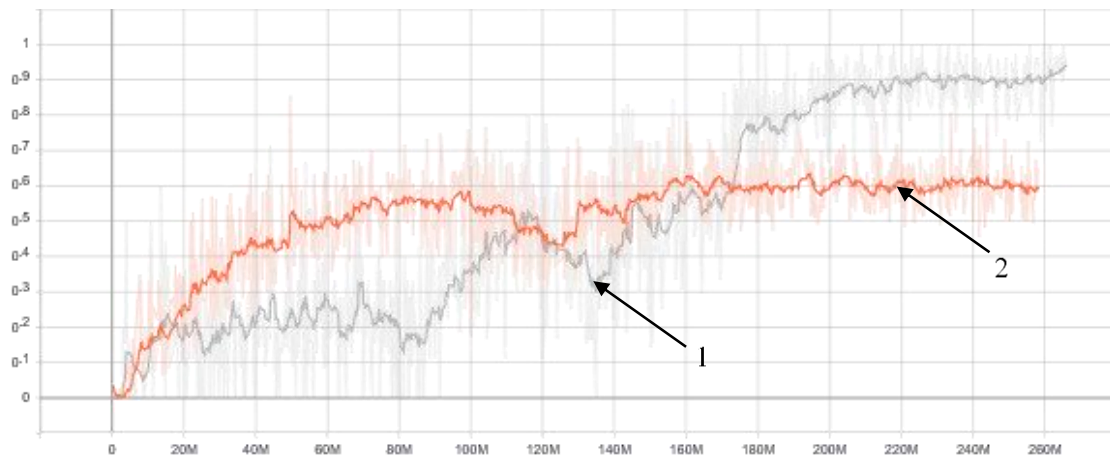


Fig.10: Success ratio of different actuator configurations during training. Duration 250 million steps. Zero means no episode was successfully completed, one means all episodes were successfully completed. 1: one actuator conventional arrangement. 2: Line arrangement

It could be shown that within the scope of our simulation environment, different actuator concepts in combination with different environmental and success conditions could be trained quickly and easily. The training was particularly reliable for configurations with multiple drives and without obstacles.

5. Outlook

It was shown that the use of Unity and machine learning algorithms has the potential to reduce the complexity and effort required to generate conventional control algorithms. At the same time, the ease of programming allows for the exploration of interesting actuator concepts in advance and thus the identification of effective solutions. Nevertheless, there are areas that need additional consideration.

One aspect to be investigated further is how the trained algorithm can interact with a real vehicle. A promising candidate for this is ROS (Robot Operating System), since it already has interfaces that allow communication between a vehicle and Unity. This allows sensor data to be fed into Unity and control commands to be passed to a vehicle.

Another possibility are edge tensor processing units (TPU). These TPUs are specially designed for the deployment of neural networks.

For use on a real vehicle, however, real resistance values and engine characteristics must first be recorded in model tests in order to integrate them into the simulation environment. This allows the agent to be trained under more realistic conditions.

Furthermore, the complexity of the environment can be increased, or the target conditions can be changed. Moving obstacles are a possibility as well as adding external disturbances like wind or currents, as target conditions a path following behavior is imaginable.

References

KREIDEL, N.; ROUX, L.; ZARKOU, A.; MEISSNER, S.; FERRARI, M. (2022). *Thematic Report - An Assessment of New Market Opportunities for Inland Waterway Transport*, The Central Commission for the Navigation of the Rhine (CCNR)

LARSEN, T.N.; TEIGEN, H.Ø.; LAACHE, T.; VARAGNOLO, D.; RASHEED, A. (2021). *Comparing Deep Reinforcement Learning Algorithms' Ability to Safely Navigate Challenging Waters*, In *Frontiers in Robotics and AI* Vol. 8, <https://doi.org/10.3389/frobt.2021.738113>

A Modular Ship Design, Construction and Pre-Approval Approach

Antoine Rouhan, Bureau Veritas M&O, Nantes/France, Antoine.Rouhan@bureauveritas.com

Richard Audoire, Dassault Systèmes, Vélizy/France, Richard.Audoire@3ds.com

Baldassare Messina, Damen Shipyards, Gorinchem/ The Netherlands, Baldo.Messina@damen.com

Abstract

This paper presents the approach developed by the European NAVAIS research project for developing a modular ship design and construction approach, embedded within a digital platform. The overall process uses model-based system engineering (MBSE), helping shipyards to transition from an engineering to order (EtO) conventional ship design method to a configuration to order (CtO) business model. One of the cornerstones of such an approach is the ability for the Class society to pre-approve in advance the various pre-designed systems modules to ensure re-usability with a high level of confidence. The paper presents the research results that has been achieved on that topic and shows how it has been prototyped within a collaborative digital platform that can be used by all stakeholders.

1. Introduction

To maintain world leadership in complex, value-added and highly specialized vessels European shipbuilders must develop tailor-made innovative concepts that are efficient to design and build. Project NAVAIS (New, Advanced and Value-Added Innovative Ships) proposed solution is a platform-based modular product family approach supported by a numerical platform, the 3DExperience, integrated business platform. By sharing components and production across a platform of vessels, higher efficiency in vessel design and flexibility in production networks is achieved. NAVAIS uses system engineering approaches to develop the principles, procedures and a re-use component library for modular design and production.

A major aspect of the platform-based modular approach is the change in value chain management. The current class approval procedure of engineered-to-order designs will be replaced by a procedure where pre-engineered product modules are approved by class, stored in a re-use library and applied in new vessel modular designs. This transfer from an engineered-to-order business model to an configure-to-order business model allow shorter process lead-times, constant quality, reduced design and production costs and better integration of the SME supply chain. The NAVAIS partnership contains 16 partners from 5 EU and 1 associated countries and includes technology providers, technology integrators and technology users. The project duration is 4 years.

The proposed paper first introduces the concepts used on the model-based system engineering (MBSE), first introduced by Wymore (1993). In a second step, the paper presents the importance of using a software platform to handle and support the design process under MBSE. Finally, the paper presents a new process related to pre-approval of systems and sub-systems with the MBSE approach.

2. Model-Based System Engineering

The project takes a system engineering approach to the process of shipbuilding, which is traditionally phased and more or less sequential from design and proposal to basic engineering, detailed engineering, supply chain, hull construction, production, outfitting and commissioning. Applying those principles provides a structured framework for a modular design architecture of ships that can be produced in a configure-to-order (CtO) approach. Rather than an engineering-to-order approach, a CtO approach will significantly reduce lead time and cost, and by reusing information, quality will be enhanced, without compromising on options for customisation. Systems engineering is a proven approach to manage such complexity in products and projects.

Historically the ship design process follows a very consolidated step phased plan. These steps might

differ in title and content depending on business models and shipyard practices but can be generally clustered in three mayor steps:

- pre-contract,
- Contract,
- contract execution.

For each progressing step the design gains in accuracy and detail towards completion, Fig.1.



Fig.1: Steps of the ship design process

The various steps are further detailed:

- Concept design: captures the mission requirements specified by the ship owner based on market scenarios. The concept design includes the ship type, deadweight or payload, type of propulsion, service speed, service area, endurance at sea, position keeping (eventually), class society and class notation.
- Preliminary design: determines main hull dimensions and preliminary hull geometry, arrangement and compartmentation (sufficient to estimate stability and mission-critical capacities), first estimate of propulsive power, light ship weight.
- Contract design: specifies ship characteristics and main equipment, to be annexed to the contract: general arrangement, technical specification on functional level, diagrams of main piping systems.
- Basic design: finalizes the hull geometry suitable for model tests, class drawings, hydrodynamic calculations and component selection based on functional technical specification.
- Detail design: provides information for manufacture, assembly and testing such as fairing of the body plan, definition of all structural components, material specifications and production information for cutting, shaping, assembling, joining and surface preparation of structures, pipes and other outfit items, integration and installation information for all equipment, applicable standards and norms.

Current ship design procedures are the point-based design approach illustrated by the well-known Evans-Buxton-Andrews spiral, Fig.2, in which an initial idea is refined and modified. Each “turn” of the spiral towards the origin increases the accuracy of the ship’s properties, finally arriving at the desired degree of accuracy and reliability.

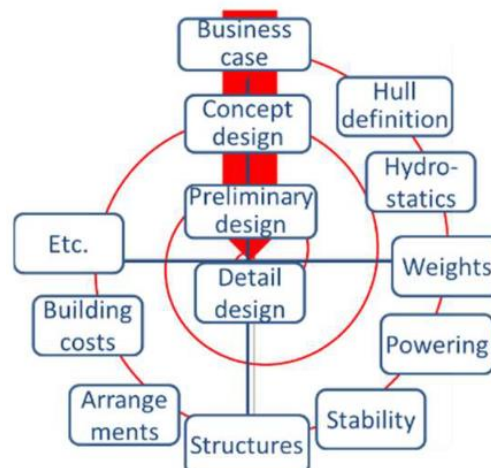


Fig.2: Evans-Buxton-Andrews spiral

The above explained design process is perfectly suited for an engineered-to-order business model suitable for market “specials” (one-offs) with high level of customization.

Within the framework of the above-described design procedure, a new ship design may benefit from past experiences by:

- Copying or scaling of similar solutions, usually of designs of comparable requirements that provide a starting point for the new design. Hereby non-optimal solutions might be introduced in the new design.
- Parametric design, i.e. the creation of a digital model based on a series of pre-programmed rules or algorithms derived from earlier analysis of existing solutions. The design is generated automatically by internal logic arguments rather than by manually manipulation.
- First principles tools which use analytical models to relate functional attributes to design parameters. Based on these attributes, merits are built in accordance to the design requirements in order to optimize the design.

The main limitations of this approaches are two:

- The first limitation is that even if a new design is entirely based on an existing (sister) vessel, the entire Class approval process is carried out for the new design,
- The second limitation is that the production preparation and process (purchasing, work breakdown, bill of materials, resources estimation, scheduling) is often a simple linear follow-up of the design.

Both limitations are quite heavily impacting the cost and lead time of the vessel as both of them will increase.

Differently from the engineered-to-order business model there are a number of markets where functional requirements can be “packed” in a limited number of ship classes e.g., tugboats and workboats. For these markets a slightly different business model, typically known as “Configure to Order”, is adopted.

Fig.3 shows the difference between the “Engineering to Order” (EtO) and the “Configure to Order” (CtO) processes.

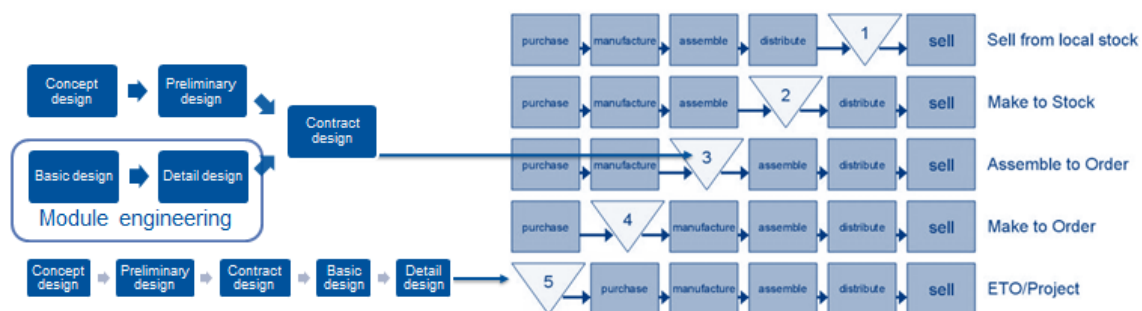


Fig.3: Different manufacturing processes

In order to increase the market competitiveness various ship designers and builders have to challenge themselves in finding the balance between customer requirements for engineered-to-order designs and cost and lead time efficiency.

For serving individual customer needs with minimum development, manufacturing and service efforts the manufacturing industry common solution is the adoption of the “Configure to Order” business model.

To successfully apply the “Configure to Order” business model the appropriate platform-based product family should be established together with a number of possible variants enabling a decent level of customization of the selected platform.

It follows that within the “Configure to Order” business model the pre-contract and contract steps are carried out by the ship designer prior the engagement with a specific ship-owner based on extensive market analysis.

As matter of fact, for such markets the vast majority of requirements are generally accepted by the ship-owners since they could be considered industry standards e.g., bollard pull of a harbour tug.

The above-described business model is relatively new to ship designing and building industries whereas is well established in automotive and aerospace ones.

Where applicable the “Configure to Order” business model will imply the need of defining the modular architecture for the platform-based product family.

Modular architecture products have a one-to-one correspondence between a component and its function so that the different functions of the product are, to the extent possible, allocated to separate product modules. In other words, the modular architecture allows decomposing a product into smaller blocks, i.e., modules, with specified interfaces. Modular architectures are flexible in structure, with highly standardized interoperability and standard connections for subsystems. Modular design identifies particular functions necessary to achieve the overall product purpose and standard assemblies are then used to undertake these individual functions. Subsequently, the assemblies or modules are brought together to form the complete product, which can then perform its complete function.

A practical division into module types is shown in Fig.4:

- Interchangeable modules can be used across multiple classes and sizes of ships, for example cabins for crew and passenger accommodation. The size of such facilities may vary because of different crew size but the basic tasks and the means to accomplish them are common across all ships.
- Independent modules provide plug-and-play capability with standard connections and interfaces within defined boundaries and are typically used for a specific type of system, such as integrated ship navigation bridge systems.
- Functional modules are the ones where different modules are connected to the ship “platform” so that the installation performs a different task, for example a diving support module that can be exchanged for a Hospital module

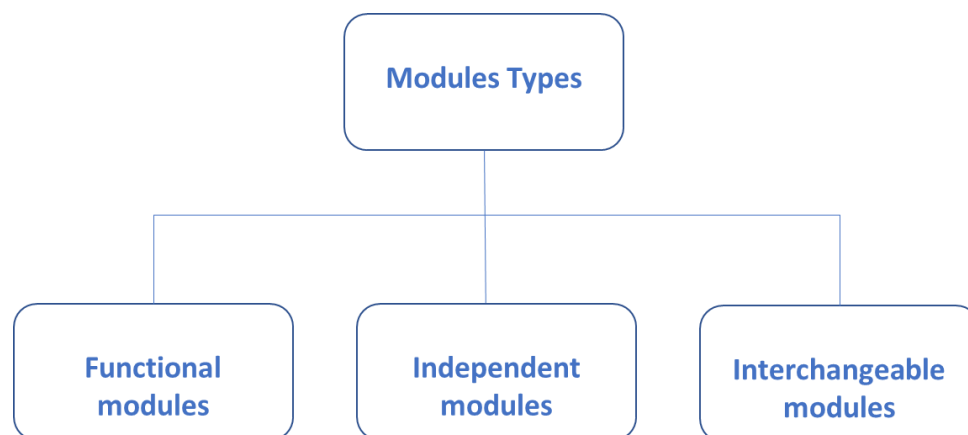


Fig.4: Different types of modules

With modular design, assemblies are treated like individual components.

The platform-based product family designed with a proper modular architecture makes it possible to select and purchase assemblies (i.e., modules) in the same way as components are procured; cost-wise, clearly this makes sense, as parts that make up an assembly can be purchased in greater numbers for less, as more are required.

Additionally, the design of platform-based product family will be approved only once at his creation avoiding the re-classification for each unit.

Thanks to the “Configure to Order” business model the cost or lead time of the vessel will decrease since:

- the pre-contractual and contractual steps are completed prior the engagement with the ship-owner,
- the classification review process is restricted to the variants of the products selected by the ship-owner and not on the entire vessel,
- a large number of components and submodule can be purchased and assembled independently from the vessel to be built.

3. How the MBSE can be implemented in a digital world?

3.1. The context

The main objectives for Dassault Systèmes are to help develop NAVAIS principles and guidelines moving from ETO traditional shipbuilding method to the CtO one. Thus, the modularization approach at the early stage of design is the focus (design process and re-use library), for platform-based product families’ definition, for modular production concept and scheduling simulation and finally for approval procedure using the 3DEXPERIENCE platform benefit. The objective of modularization is to define groups of related products that share common features, components, subsystems, interfaces and manufacturing processes that satisfy a wide range of customer requirements. Then, to ensure that each requirement is taken into account from the initial design phase, the Model-Based System Engineering (MBSE) method has become obvious.

3.2. The Model-Based System Engineering approach

The MBSE is an approach based on the visual representation (model) of the system to be developed, rather than a text document whose interpretation usually leads to errors whose consequences often have repercussions on the entire design and production chain.

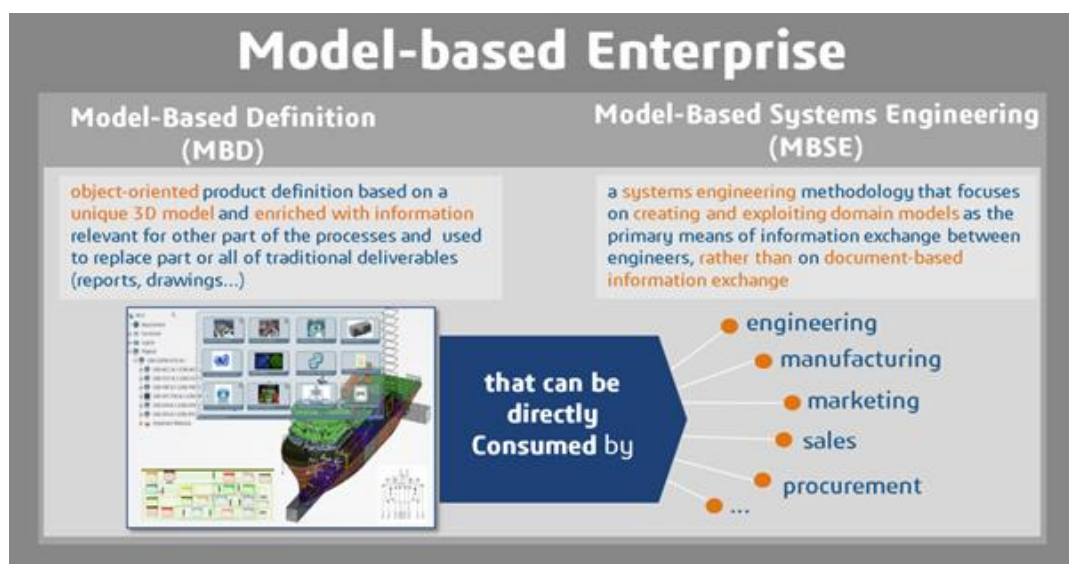


Fig.5: The Model-Based: a unique object-oriented product definition

Model-Based System Engineering is therefore a solution aimed at simplifying the processes of design and production of technological tools, Fig.5.

In fact, product development systems are often complex (incorporating embedded software), because they include mechanical components as well as fluidic, electrical, electronic components and software. Therefore, in order to achieve an optimal result, it is essential that all these components work in full coherence. That is when system-engineering processes come into play because they allow system engineers to share information seamlessly. Indeed, the interdependence between the resources and the components mentioned above requires a perfect understanding of the requirements, so that the updating is carried out automatically at the level of all the departments involved of the company.

In a glance, the main advantages of model-based systems engineering are threefold: rigorous design based on requirements, management of product lines and reuse and simplification of manufacturing processes.

3.3. Model-Based System Engineering supported by a platform

The NAVAIS modular design process is guided by the Model-Based System Engineering (MBSE) approach to support system requirements, design, analysis, verification and validation activities beginning in the conceptual design phase and continuing throughout development and later life cycle phases. The native MBSE approach delivered by the 3DEXPERIENCE platform follows a « V » model-based on a sequential mode easy to understand and to apply. The V-model demonstrates the relationships between each phase of the development life cycle and its associated phase of testing. The horizontal and vertical axes represent time or project completeness (left-to-right) and level of abstraction (coarsest-grain abstraction uppermost), respectively, Fig.6.

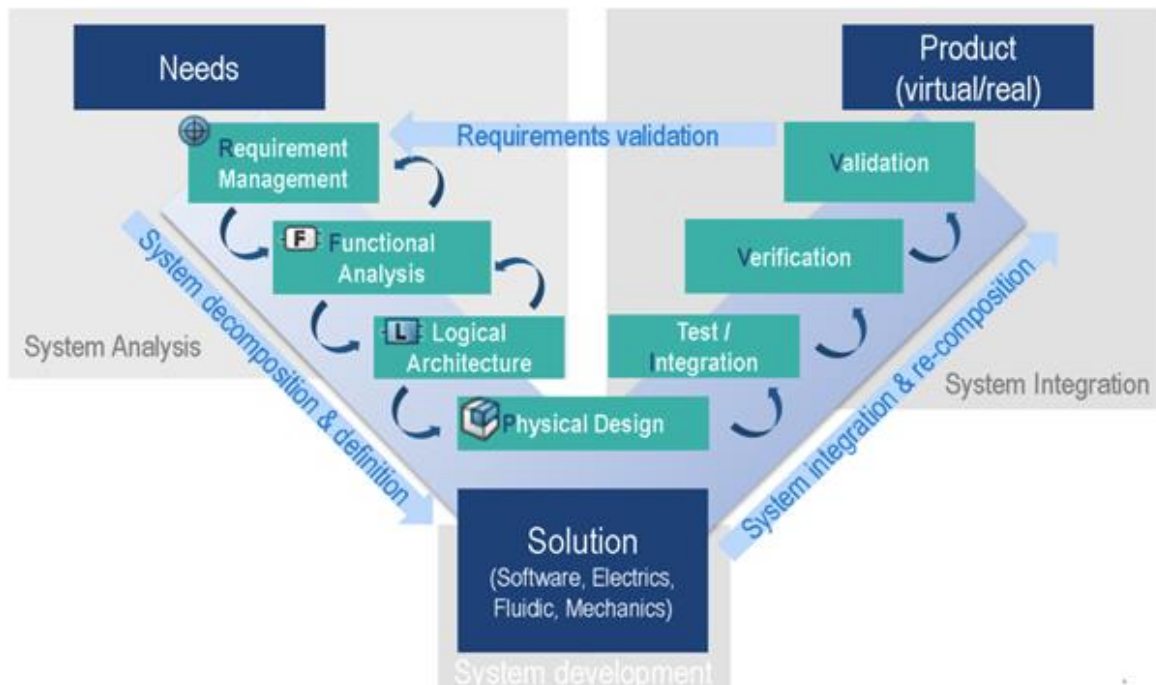


Fig.6: MBSE approach of the 3DEXPERIENCE platform based on a “V” model

The platform is managing one single digital model that includes Requirements (R), Functional (F), Logical (L), and Physical (P) on the upstream decomposition side (left side of the V-model) and Integration (I), (V) Validation, Verification (V) on the downstream integration side (right side of the V-model). It is mainly a top-down process starting from the stakeholders’ needs to a system design and implementation.

3.4. “Requirements-Functional-Logical-Physical” (RFLP) framework

The RFLP is a framework to engage on the MBSE approach within the 3DEXPERIENCE platform. The RFLP decomposition of systems, which initially grew popular among embedded software development teams, has now become more widely adopted across other industries (automotive, aerospace...). The benefit of the RFLP approach is that it enables product teams to analyze design elements independently, opening the possibility for reuse, and providing a logical path for integration to gain a holistic view of the product definition.

The RFLP framework supports a Model-Based Systems Engineering process. It is a unified system definition with four fundamentals facets, Fig.7.

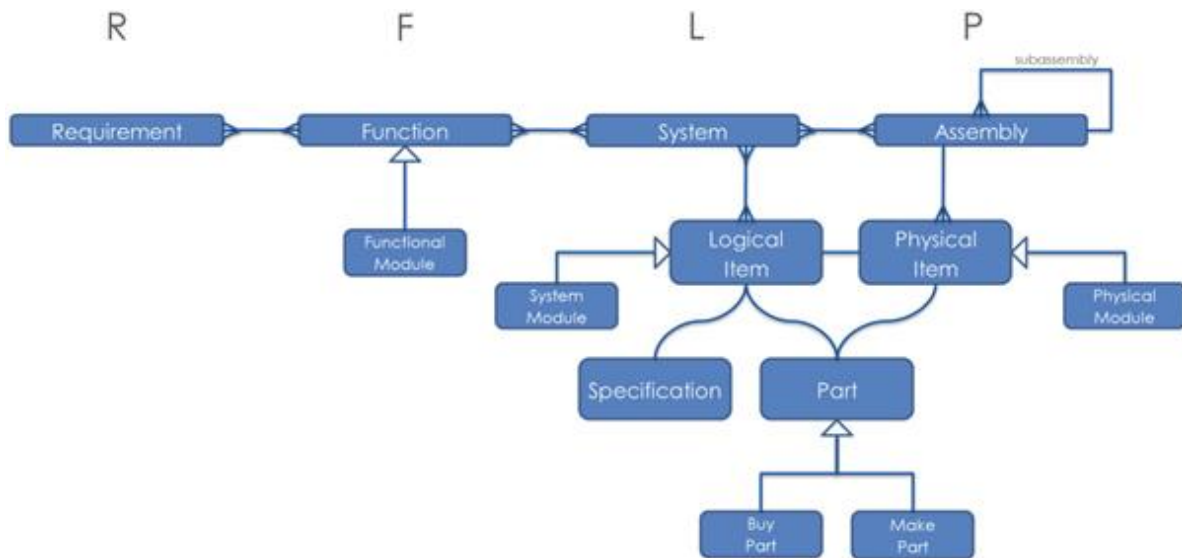


Fig.7: Module structure mapped with RFLP framework

- **Requirements (R):** describes all the requirements that a system has to fulfill, from stakeholders' requirements to system and design requirements. "What the system or the product should satisfy?"
- **Functional (F):** describes the system services and the functional architecture with functions and flows that the components of the system must provide. "What the system or the product should do?"
- **Logical (L):** describes the components architecture with components of the system, their interfaces and the allocated functions and flows. "What technology should be used (how the system or the product will be constituted)?"
- **Physical (P):** defines the life-like system components, including the disciplines 3D Modeling (Mechanical, Electrical, Fluidics...). "How the real system will be realized?"

The IVV (or some time IVVQ for Qualification aspect) re-composition of systems is a set of domains and processes that implement strategies for the design/validation stages of systems. These strategies aim at guaranteeing a level of quality and robustness. It is a multi-disciplinary approach to compliance and system quality.

- **Integration (I):** is a decision-making procedure between hypotheses, based on a dataset (sample). "Is it a choice that is compatible with the entire product or system?"
- **Verification (V):** is the confirmation that the specified requirements are met. "Do we make the product right?"
- **Validation (V):** is the confirmation that the requirements for a specific use or intended application are met. "Are we making the right product?"

The RFLP loops and the IVVQ feedback loops are important steps towards achieving the traceability that is essential for platform engineering because of the way it decomposes the product definition, in our case the module definition, Fig.8.

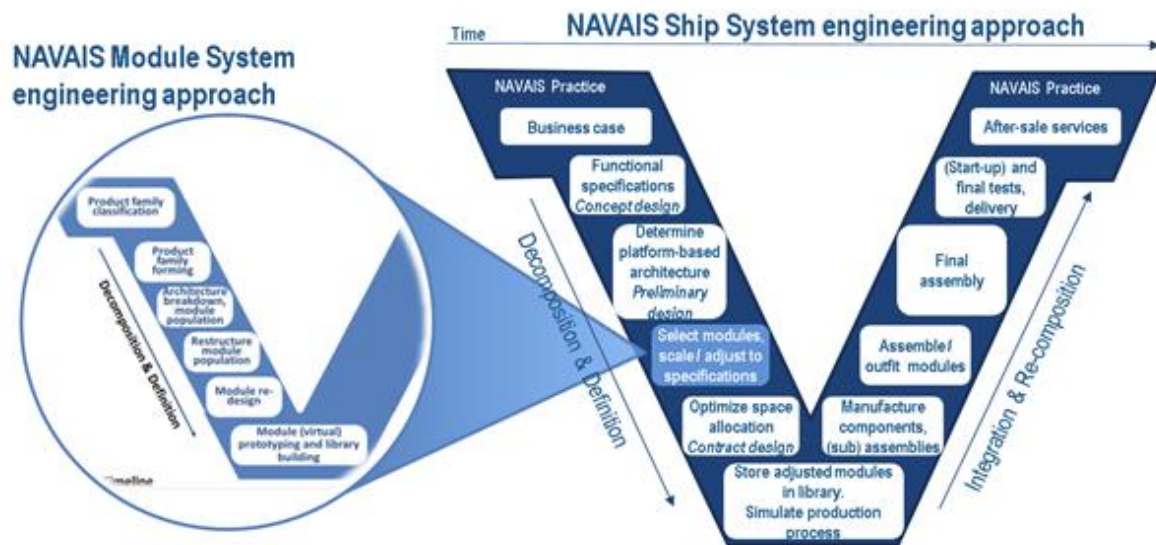


Fig.8: MBSE approach apply to build module

3.5. The RFLP framework apply to a workboat platform-based product family

The choice for a platform-based product family approach has implications for the product architecture meaning how the function of any product is organized. We start from the customer requirements (then later we will integrate the requirements of the class and some specific to the study process of DAMEN). The number of sub-requirements (light blue blocks in Fig.9) is a first attempt of characterization of the workboat to be designed. Then, each sub-requirement (light blue block) will be decomposed in primary functions (orange blocks) to which a measure of performance will be attached, Fig.9.

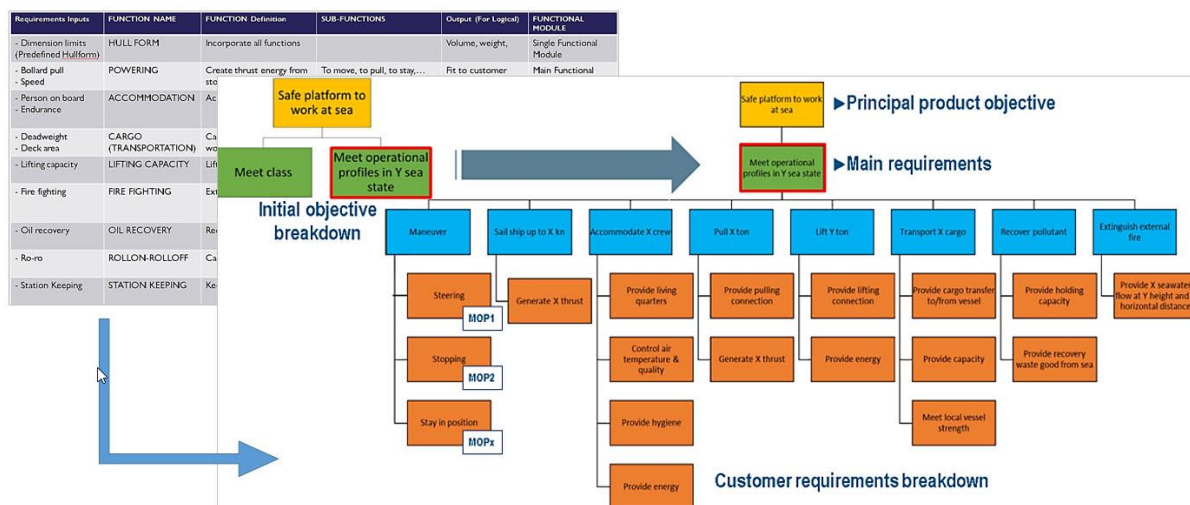


Fig.9: From requirements to Functional decomposition

The introduction of the measure of performance for every function is a necessary step, which enables the constant verification and validation along the complete life cycle of the design and building process. Meany that each function will be linked to a defined range of measure of performance and to a certain number of ship systems able to fulfil the reference function, and hence the requirement, itself.

Then the functionalities are decomposed into several logical modules mainly represented by a Piping & Instrumentation Diagrams (P&ID). Each P&ID is associated to a platform algorithm to perform calculations and simulate the behavior of the system to properly size the components. Once the components are sized, they can be instantiated in the 3D virtual digital twin, (i.e. Physical objects), Fig.10.

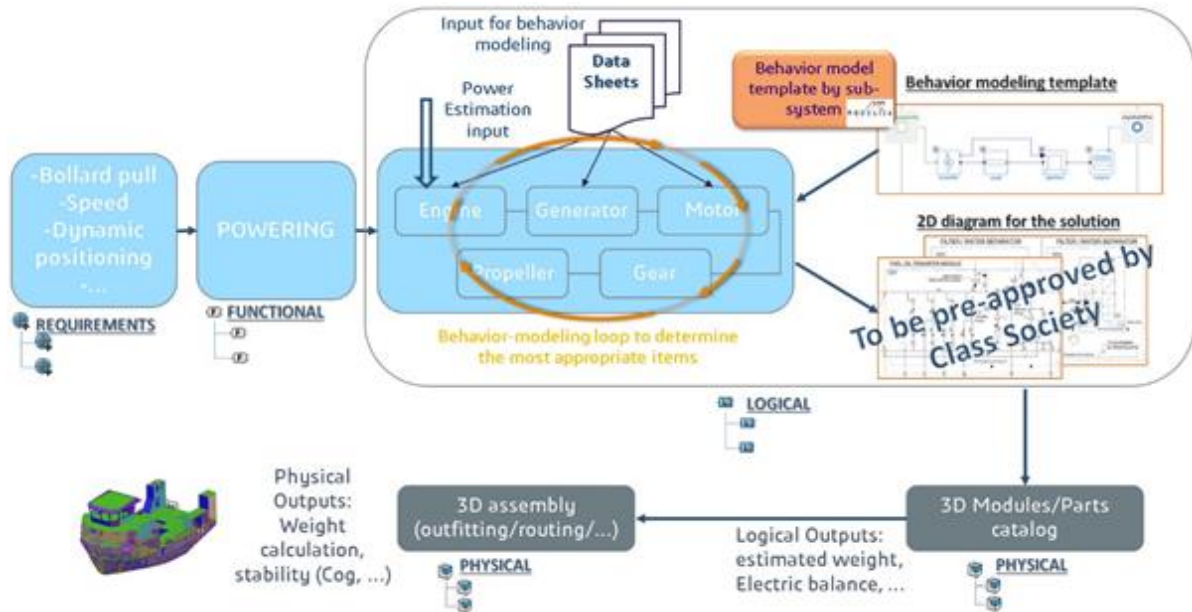


Fig.10: Propulsion function module decomposition into logical sub-systems

3.6. Requirements traceability and relationships

One of the most important aspects of the MBSE approach is traceability to sources, to steps in the engineering process, and to elements of the system architecture. Meaning that all RFLP facets are linked by implementation links to allow the systems engineer to retrieve the exact path of a requirement from R to P fact. The diagram maps the provenance of the requirement, Fig.11.

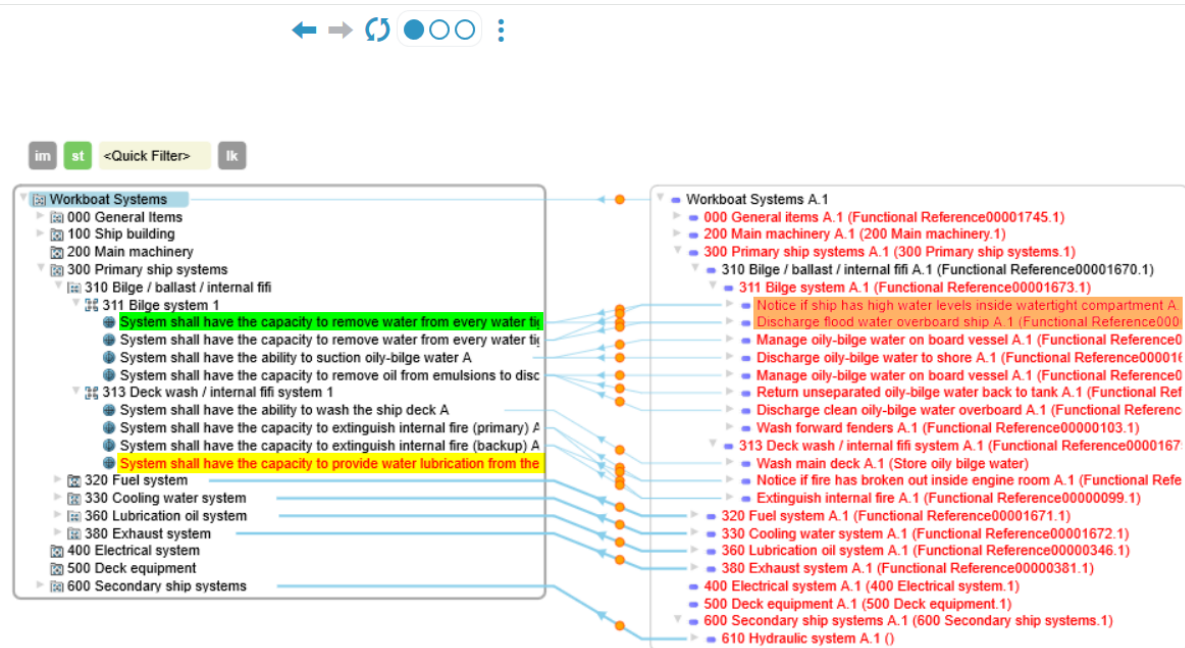


Fig.11: 3DEXPERIENCE diagram from traceability widget relative to the workboat bilge system

The advantage of the MBSE approach of the platform is the capability to centralize all the RFLP data set that can be then directly exploited by the class approval society starting from the initial design phase (Requirements and Logical objects). Thus, a procedure for pre-approval the logic modules was defined, tested and demonstrated on the platform allowing a significant time saving at the final approval of the ship. It is the assurance that the modules are well designed from the initial design phase thanks to class society pre-endorsement. In the end, the logic module can be considered as a standard module for a given ship family.

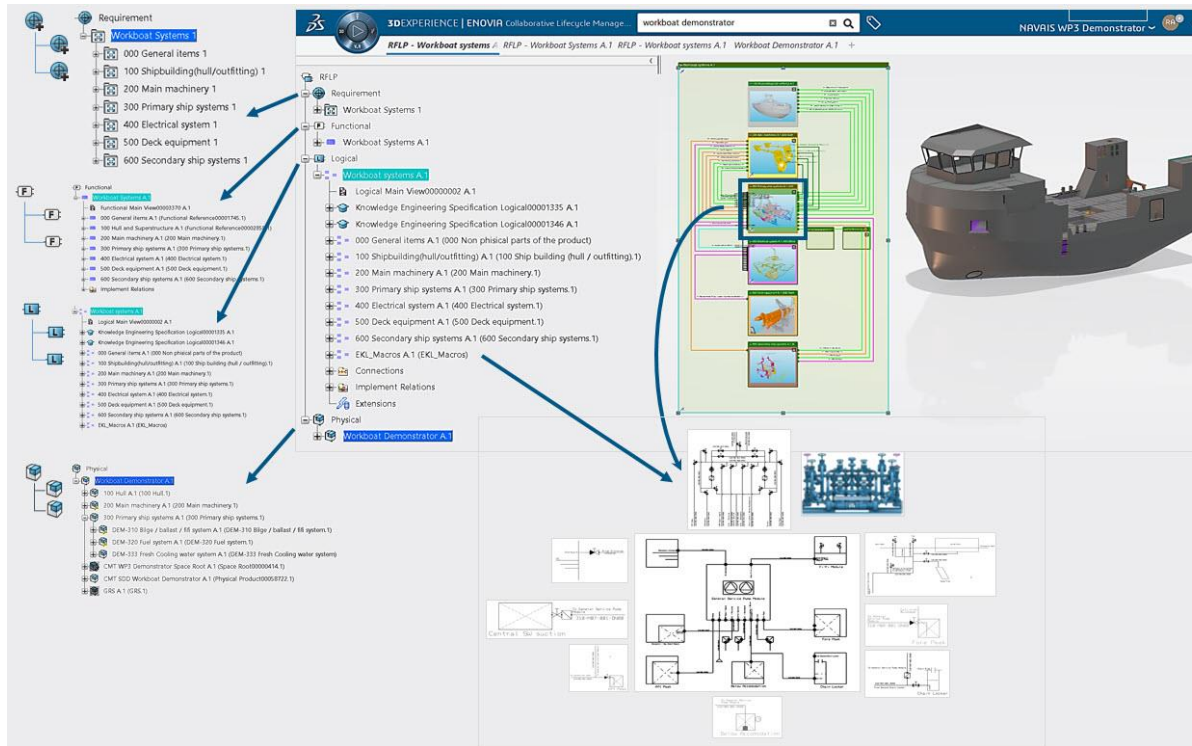


Fig.12: One of the final NAVAIS demonstrator using the MBSE approach of the 3DEXPERIENCE platform

4. Class approval

4.1. Current plan approval Practices

Let us presents the usual Class approval practice where a ship has been contracted to a shipyard and to be classed during design and construction with a given class society. Basically, the ship design is checked by Class society against class rules, as well as other regulations rules and/or requirements. The checking activity is related to detailed design for a specific ship contract. The detail design comes usually under the form of drawings issued by the ship designer and then checked against rules requirements by the Class society. Non conformities are then reported on the drawings and sent back to the ship designer for an update, until all non-conformities are cleared. At the final stage, the drawings are stamped as approved for construction. Let's stress again that this process is applied for an existing ship at detail design stage, hence, all required information for the approval of a system is available.

4.2. Changes required from EtO to CtO

When moving from engineering to order design method to configure to order design method, such approval process can still be applied, that is approval of the structure and system during detailed design. However, in the CtO design process, modules or systems are engineered at a logical level well in advance, as explained before. The use of a digital platform helps in storing the various systems and subsystems and ensure their re-usability in a final design. However, performing approval at final design

stage of a CtO design leads to almost no gain in the approval process. During the course of the NAVAIS project, partners have looked to gain advantage of the existing pre-design of systems and find a means to secure those systems in advance, so that when the detail design is sent for approval to the Class society, the uncertainty regarding the time for approval of systems are reduced to its minimum.

This new process requires a pre-approval approach, that is, each sub-system is analysed by Class society prior being part of the library of modules available for detail design under CtO.

Of course, as each system analysed is not part of an existing ship design, not all part can be checked against the class and regulatory rules, which means only part of the rules can be verified. All main elements that cannot be verified are stated and part of an exclusion list which provides a comprehensive list of the various areas for which the system has not been checked against the rules. All other elements are covered, which means that this system is pre-checked. When using such a module in a detail design, the system designer can use the exclusion list to verify in advance the various areas to be checked prior sending to Class society for approval. When the detail design is then sent for approval to Class society, much of the systems and sub-systems have already been pre-approved, meaning that the full approval of a system has a much-reduced non-conformities levels thereby reducing the whole approval process-design time.

4.3. Pre-approval process

Mainly four actors or identified responsibilities are part of the process: on ship designer side: the system engineer that design the system under MBSE, the lead system engineer that approves work of system engineer, on Class society side: the plan approval system engineer reviews, checks and establishes non conformities and exclusion list, and the lead plan approval system engineer that approves its work.

The defined pre-approval process can be roughly described as follows:

- Given a logical system design, the system designer gets approval from lead system designer prior handover to Class of the drawings to be pre-reviewed.
- Once notified, the plan approval system engineer start reviewing and checking the provided drawings against the applicable rules. If necessary, small exchanges with the ship system designer are possible, for example to clarify elements of the design. He reports non-conformities on the drawings. After approval by the lead plan approval system engineer, the drawings and non-conformities are handover to system engineer.
- The system engineer, once notified of the reviewed drawings, update its design until all non-conformities are cleared.
- Once all non-conformities cleared, the plan approval system engineer establish a list of exclusions, which states elements of the rules that where not checked as part of the pre-approval process. The final system drawings are marked as 'pre-approved' for the specific set of rules used. After approval by the plan approval system engineer, the set of drawings are handover to ship designer.
- The ship designer stores the pre-approved drawings in a library of system modules available for use during basic and detail design phase.

4.4. Support of digital solution in Class pre-approval process

This proposed pre-approval benefits strongly from the support of the accompanying software platform in which system design is perform. The pre-approval process requires validation steps both on ship designer side and Class society side as part of quality assurance processes. It also requires as well exchanges between Class and ship designer in terms of notifications, statuses and responsibilities definitions of the work to be done, comments and their statuses until final pre-approval is stated. It should also be linked with the systems already designed at Logical (L) level, and keep track of the work and exchanges between parties.

During the course of the NAVAIS project, a set of existing components of the 3DEXperience Platform have been configured so to as allow running of the defined pre-approval process. Fig.13 presents part of the interface of the configured components of the 3DEXperience platform for the pre-approval process. Window (1) shows the documents and their statuses in the whole pre-approval process, window (2) shows the life-cycle of the drawings, window (3) shows one of the drawings used in the pre-approval process and window (4) shows results of the search engine showing the various drawings and their attributes and statuses.

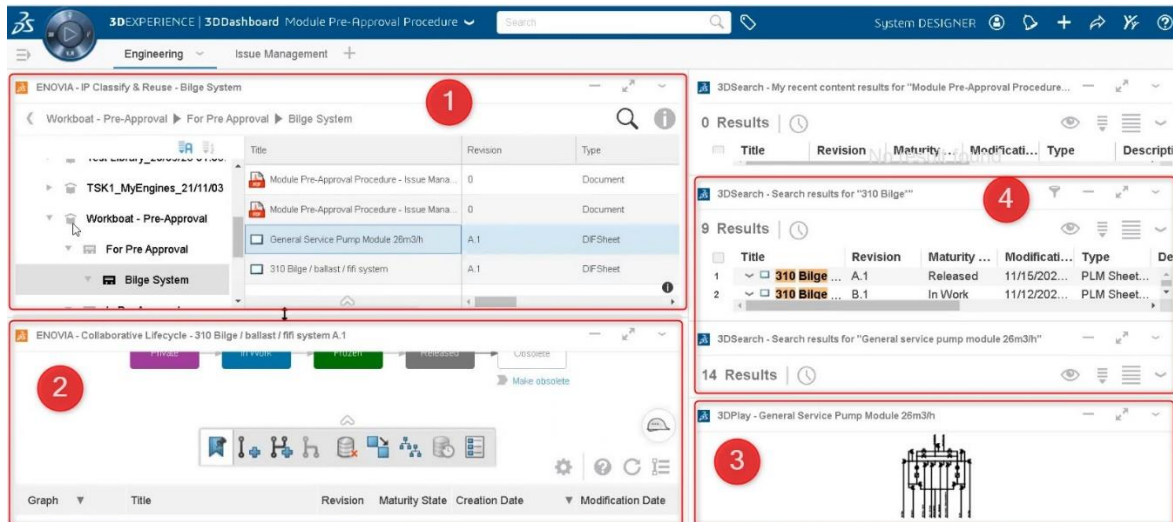


Fig.13: pre-approval module configured in the 3DEXperience platform

5. Conclusions

This paper presented some of the results of the EU-funded NAVAIS project. It focuses in particular on the modularity approach in ship design using the Model-Based System Engineering approach, the accompanying software platform that support such a design approach, and finally describes the pre-approval concept that has been developed. The move from EtO to CtO requires changes in the usual design, software and Class approval practices to benefit the gain such a move is expected to provide.

Acknowledgments

The authors want to thank all contributors of the NAVAIS project to this paper and to research that lead to its results. We also want to recall that the project been performed within the H2020 frame and has received funding from the European Union Horizon 2020 research and innovation programme (Contract No.: 769419).

References

WYMORE, A.W. (1993), *Model-based systems engineering: an introduction to the mathematical theory of discrete systems and to the tricotyledon theory of system design*, Taylor & Francis

Index by Authors

Aae	258	Harries	169	Sandvik	201
Abels	34	Hauschulz	169	Schäfer	110
Adlon	110	Hildebrandt	7	Sansebastiano	387
Alessi	7	Hirsch	7	Sebastiani	387
Alonso	403	Holzki	437	Seppälä	258,403
Amadori	7	Ichinose	43	Serafino	387
Andrews	231	Jabary	153	Serani	221
Aracri	120	Jørgensen	201,311	Settler	323
Astrup	258	Jiang	153	Son	258
Audoire	446	Kana	76,273	Sprenger	153
Baumfalk	153	Klausen	212	Stensrud	212
Bellingmo	311	Kleinsorge	153	Stochholm	53,63
Berge	311	Leonardi	387	Stonestreet	382
Bernhardt	16	Lödding	323	Takezawa	137
Beyer	110	Lutz	336	Tani	24
Bibuli	120	Maccatrozzo	95	Taniguchi	43
Bitomsky	429	Mallol	7	Terün	76
Blom	382	Mancarella	387	Thies	169
Brahan	187	Mari	367	Van Den Boogard	7
Bresciani	24	Marzi	169	Van Den Broek	95
Bronkhorst	273	Matsuo	137	Van Der Waa	95
Brug	95	Meland	352	Velner	273
Burggräf	110	Meling	352	Wille	352
Caccia	120	Merikanto	258	Wunsch	7
Caiti	24	Messina	446	Zampieri	7
Calabrese	387	Mewes	153	Zerbst	336,429
Cappugi	367	Mikkelsen	53,63		
Carlino	387	Milat	343		
Cataldo	387	Mukti	231		
Cirigliano	387	Murray	311,352		
Clero	7	Neugebauer	153		
Costanzi	24	Odetti	120		
Daehlen	201	Orlandi	367		
Danetzky	336,429	Ortolani	367		
Dekker	76	Paiano	387		
De Nucci	187	Pasi	367		
De Winter	273	Pawling	231		
Diez	221	Perez	131		
El Moctar	153	Pinskiy	299		
Elzalabany	323	Plowman	16		
Floean	403	Pobitzer	311		
Frank	343	Presicci	120		
Fujimoto	137	Prieto	403		
Fulterer	110	Procee	288		
Gaspar	416	Rødseth	249,352		
Gatchell	169	Rørhus	311		
Genschorek	437	Rost	323		
Gorris	34	Rouhan	446		
Hagaseth	249,352	Ruscio	24		

22nd Conference on
Computer Applications and Information Technology in the Maritime Industries
COMPIT'23
Drübeck / Germany, 23-25 May 2023

Topics: Artificial Intelligence / Big Data / CAX Techniques / Digital Twin / Simulations /
Virtual & Augmented Reality / Robotics / Autonomous Technology
In Design, Production and Operation of Maritime Systems

Organiser: Volker Bertram (volker.bertram@dnv.com or volker@vb-conferences.com)

Advisory Committee:

Marco Bibulii	CNR, Italy	Ken Goh	Knud E. Hansen, Australia	Jialun Liu	WUT, China
Jean-David Caprace	COPPE, Brazil	Stefan Harries	Friendship Systems, Germany	Kohei Matsuo	NMRI, Japan
Nick Danese	NDAR, France	Woo-Sung Kil	Korean Register, S. Korea	Rodrigo Perez	Siemens, Spain
Henrique Gaspar	NTNU, Norway	Herbert Koelman	SARC, Netherlands	Ulf Siwe	Swed. Mar. Adm., Sweden

Venue: The conference will be held in the Abbey Drübeck in Drübeck near Wernigerode



Format: Papers to the above topics are invited and will be selected by a committee.

Deadlines:	anytime	Optional "early warning" of intent to submit paper
	22.1.2023	First round of abstract selection (1/3 of available slots)
	22.2.2023	Final round of abstract selection (remaining 2/3 of slots)
	22.3.2022	Payment due for authors
	20.4.2022	Final papers due (50 € surcharge for late submission)

Fees:	650 € / 325 €	regular / PhD student – early registration (by 30.2.2023)
	750 € / 375 €	regular / PhD student – late registration

Fees are subject to German VAT
Fees include proceedings, lunches, coffee breaks and conference dinner

Sponsors: Tutech Innovation (further sponsors to be announced)

Media partners: Hansa, RINA

Information: www.compit.info